frontiers | Research Topics

Molecular diagnosis and epidemiology of human pathogens

Edited by
Wafa Achour, Ons Bouchami and Arabella Touati

Published in
Frontiers in Microbiology
Frontiers in Immunology

ISSN 1664-8714
ISBN 978-2-8325-4065-7
DOI 10.3389/978-2-8325-4065-7

About Frontiers

Frontiers is more than just an open access publisher of scholarly articles: it is a pioneering approach to the world of academia, radically improving the way scholarly research is managed. The grand vision of Frontiers is a world where all people have an equal opportunity to seek, share and generate knowledge. Frontiers provides immediate and permanent online open access to all its publications, but this alone is not enough to realize our grand goals.

Frontiers journal series

The Frontiers journal series is a multi-tier and interdisciplinary set of open-access, online journals, promising a paradigm shift from the current review, selection and dissemination processes in academic publishing. All Frontiers journals are driven by researchers for researchers; therefore, they constitute a service to the scholarly community. At the same time, the *Frontiers journal series* operates on a revolutionary invention, the tiered publishing system, initially addressing specific communities of scholars, and gradually climbing up to broader public understanding, thus serving the interests of the lay society, too.

Dedication to quality

Each Frontiers article is a landmark of the highest quality, thanks to genuinely collaborative interactions between authors and review editors, who include some of the world's best academicians. Research must be certified by peers before entering a stream of knowledge that may eventually reach the public - and shape society; therefore, Frontiers only applies the most rigorous and unbiased reviews. Frontiers revolutionizes research publishing by freely delivering the most outstanding research, evaluated with no bias from both the academic and social point of view. By applying the most advanced information technologies, Frontiers is catapulting scholarly publishing into a new generation.

What are Frontiers Research Topics?

Frontiers Research Topics are very popular trademarks of the *Frontiers journals series*: they are collections of at least ten articles, all centered on a particular subject. With their unique mix of varied contributions from Original Research to Review Articles, Frontiers Research Topics unify the most influential researchers, the latest key findings and historical advances in a hot research area.

Find out more on how to host your own Frontiers Research Topic or contribute to one as an author by contacting the Frontiers editorial office: frontiersin.org/about/contact

Molecular diagnosis and epidemiology of human pathogens

Topic editors

Wafa Achour — Centre National de Greffe de Moelle Osseuse, Tunisia

Ons Bouchami — Universidade Nova de Lisboa, Portugal

Arabella Touati — Centre Hospitalier Universitaire de Bordeaux, France

Citation

Achour, W., Bouchami, O., Touati, A., eds. (2023). *Molecular diagnosis and epidemiology of human pathogens*. Lausanne: Frontiers Media SA.

doi: 10.3389/978-2-8325-4065-7

Table of contents

frontiers | Frontiers in Microbiology

TYPE Editorial
PUBLISHED 20 November 2023
DOI 10.3389/fmicb.2023.1329115

OPEN ACCESS

EDITED AND REVIEWED BY
Axel Cloeckaert,
Institut national de recherche pour l'agriculture, l'alimentation et l'environnement (INRAE), France

*CORRESPONDENCE
Wafa Achour
✉ wafaachour@gmail.com

RECEIVED 28 October 2023
ACCEPTED 06 November 2023
PUBLISHED 20 November 2023

CITATION
Achour W, Bouchami O and Touati A (2023) Editorial: Molecular diagnosis and epidemiology of human pathogens. *Front. Microbiol.* 14:1329115. doi: 10.3389/fmicb.2023.1329115

Editorial: Molecular diagnosis and epidemiology of human pathogens

Wafa Achour[1,2]*, Ons Bouchami[3] and Arabella Touati[4]

[1]Laboratory Department, Centre National de Greffe de Moelle Osseuse, Tunis, Tunisia, [2]Research Laboratory, Microbiology of Children and Immunocompromised, (LR18ES39), Faculty of Medicine of Tunis, University Tunis El Manar, Tunis, Tunisia, [3]Laboratory of Human Microbiota – Xenobiotics Interactions, Instituto de Tecnologia Química e Biológica António Xavier, Universidade Nova de Lisboa (ITQB-NOVA), Oeiras, Portugal, [4]CHU de Bordeaux, Bacteriology Department, National Reference Center for Bacterial Sexually Transmitted Infections, F-33000, Bordeaux, France

KEYWORDS

clinical medicine, infectious diseases, molecular diagnostics, molecular epidemiology, microbiology

Editorial on the Research Topic
Molecular diagnosis and epidemiology of human pathogens

In the past two decades, the expansion of Medical Microbiology is essentially due to the great advances in related fields such as immunology, genetics, bioinformatics, science, technology, engineering, and mathematics. This Research Topic provides an updated core of basic knowledge critical to clinical practice in medicine. Each article deals with an important human pathogen. It provides an update of the current state-of-the-art scientific knowledge applied to molecular diagnosis and epidemiology of human pathogens.

Integrative review, which highlights advances in molecular diagnosis of human pathogens, helps researchers, and practitioners to access and scrutinize the fast expanding knowledge. Cao et al. exposed microbiological and molecular biological diagnostics for tuberculous meningitis. Xiang et al., demonstrated, in a meta-analysis, that metagenomic next-generation sequencing had good specificity but moderate sensitivity for the early diagnosis of tuberculous meningitis. These articles deal with the difficult microbiological diagnosis of tuberculous meningitis, the most severe form of extra-pulmonary tuberculosis.

New scientific knowledge and understanding make new applications possible. Zheng et al. confirmed that hepatocyte growth factor plus adenosine deaminase is an excellent biomarker in tuberculous pleural effusion patients. In the field of tuberculosis, the World Health Organization has proposed the development of a diagnostic biomarker or triage biomarker among the high-priority target product. However, the development of a universal biomarker that diagnoses tuberculosis disease in both adults and children, pulmonary and extrapulmonary tuberculosis, and in varying stages of immunosuppression is challenging. Zhao et al. proposed a sensitive and specific digital droplet Polymerase Chain Reaction (PCR) assay for the detection of *Mycoplasma pneumoniae*. Digital Droplet PCR, known as the third generation of quantitative PCR, enables the exact quantification of nucleic acid targets within a sample. In contrast to real-time PCR, it relies on analysis of the endpoint of the PCR. Its capability to accurately detect and quantify low abundant targets has led to its fast-growing applications in detection of different pathogens. Chen et al. reported a novel molecular diagnostic assay named reverse transcription loop-mediated isothermal amplification combined with a visual gold nanoparticle-based lateral flow assay that can be eventually used as a point-of-care diagnostic tool for HIV-1 detection in clinical settings. Pollak et al. developed three rapid Nipah virus molecular diagnostic tests based on

reverse transcription recombinase-based isothermal amplification coupled with lateral flow detection. In the last decade, many methods for the sequence-specific detection of Loop-mediated isothermal amplification have emerged as an important diagnostic tool. Indeed, rapid, and inexpensive diagnostic tests are necessary to control spread of disease in endemic settings where sophisticated laboratories may not be available.

Next-generation sequencing technologies are increasingly available in clinical microbiology laboratories. Their main applications are: whole genome sequencing, targeted metagenomics sequencing, and shotgun metagenomics sequencing. These applications are used for microbial identification, antimicrobial resistance genes detection and epidemiologic tracking of organisms. Yao et al. found that blood nanopore targeted sequencing can detect infection in deceased donors earlier and more accurately than bloodculture, which could raise the donation conversion rate. Sun et al. suggested that 16S *rRNA* gene next-generation sequencing is more suitable than aerobic culture for identification of polymicrobial pancreatic infections in severe and critical acute pancreatitis patients. Huang et al. concluded that PCR-based targeted next-generation sequencing can effectively identify periprosthetic joint infection pathogens and may provide information on drug resistance, while it is superior to metagenomic next-generation sequencing in terms of cost and turnaround time. Jaworska et al. found that urobiome composition in patients undergoing dialysis and in kidney transplanted patients is better characterized by amplicon sequencing than classical microbiology methods. Currently, the application of next-generation sequencing is mainly limited to academic or reference laboratories. Major decision-making regarding technologies, operational models, infrastructure, human resources, and professional expertise is needed before the widespread implementation of next-generation sequencing in clinical laboratories.

Nucleic acid amplification and next generation sequencing techniques are the most widely used methods in pathogen detection. These methods have become the gold standard as they detect even a few nucleic acid copies. However, they have numerous limitations such as complex thermal cycle process, complex primer design of PCR, unstable single base resolution of loop-mediated amplification and deep knowledge of biology to analyze data generated by next-generation sequencing. CRISPR-Cas-based method, a new generation of gene editing technology, may be an interesting approach. Ren et al. developed a sensitive and specific PCR-CRISPR/Cas13a method for *Mycobacterium tuberculosis* detection in sputum, bronchoalveolar lavage fluid and pus samples. Wang et al. developed a Cas12b-based one-pot platform by integrating isothermal amplification and CRISPR detection into one step, named CDetection.v2, enabljng the detection of SARS-CoV-2 in 30 min. Zhu et al. described latest advances in nucleic acid detection methods for SARS-CoV-2, in particular, biosensors and clustered regularly interspaced short palindromic repeats (CRISPRs)-based diagnostic systems. Emerging CRISPR technologies have been widely applied in combination with isothermal amplifications for SARS-CoV-2 detection. Their applications are still limited due to many reasons: immaturity of the CRISPR technology, incomplete auxiliary instruments and reagents, unconfirmed advantages over PCR (such as cost, stability, and convenience).

The pathogenesis and the epidemiology of microorganisms that colonize or infect humans had practical applications in treatment and prevention of diseases (infectious diseases, infection-related cancer, dysbiosis related diseases, etc.). Regarding infection-related cancer, Burassakarn et al. reported that the overall prevalence of HPV DNA was statistically associated with an increased risk of esophageal cancers. Seyoum et al., found that the presence of high-risk HPV, irrespective of genotypes, is highly correlated with cervical cell abnormalities. The distribution of HPV genotypes varies across continents, countries, and even within a single country. Morover, the current vaccines confer a limited cross-protection. Therefore, it is essential to generate scientific data concerning HPV prevalence, genotype distribution, cytological profile and associated factors in different populations in order to predict the efficacy of current vaccines and to develop a new vaccine strategy. Concerning dysbiosis related diseases, Li et al., based on 16S rRNA gene sequencing, had preliminary confirmed that dysbiosis occurs in patients susceptible to pathological scars. Growing evidence supports that gut microbial dysbiosis can promote the development and progression of different diseases via the interaction between gut microbiota and host. Deciphering the functional relationships in this symbiotic ecosystem, beyond the microbial DNA contents, permits a more comprehensive analysis.

Typing of causative pathogens is important to trace pathogens and to study microbial population dynamics which are necessary in infection prevention and control. Miellet et al. concluded that molecular testing of culture-enriched saliva samples improves the sensitivity of overall surveillance of pneumococcal carriage in children and adults. Jacqueline et al. recommended the analysis of the non-coding region MF-NCR to be added to N450 sequencing for measles molecular surveillance during post-elimination phase. Shin et al. provided a genotype fingerprinting method for recurrence tracing of heterogeneous *Mycobacterium intracellulare*. Although sequence-based typing methods offer new prospects for improving the resolution and comparability of typing systems for public health applications, the typing process in diagnostic laboratories remains laborious and time-consuming.

Genomic microbial identification is used in the diagnosis and monitoring of infectious diseases within the One Health concept. Ergunay et al. found that, in field-collected ticks, metagenomic nanopore sequencing is better than broad-range and nested amplification in virus detection and diversity investigation. Indeed, metagenome sequencing can be employed for bio- or xeno-surveillance, where blood-sucking arthropods are used as sentinels to screen pathogens, that may threaten the health of wildlife, livestock, and humans. Nemati et al. described rapid, selective, and easy-to-use biosensor and nanobiosensor technology, developed for early detection of common waterborne protozoa. Smart biosensing platforms play an extremely significant role. Electrochemical biosensors and electroanalytical techniques are adapted to point-of-care testing. Therefore, they are very useful in diagnosing, predicting and controlling infectious diseases epidemics or pandemic.

The pace and sophistication of advances in all scientific disciplines applied to medical microbiology become a challenge due

to lack of expertise to analyze fast-growing data and to translate them in clinical practice and medical education. They call for a comprehensive and integrative understanding of the overall knowledge development in the different related fields.

In summary, this Research Topic deals with epidemiology, pathophysiology and diagnosis of important human pathogens. These pathogens have been investigated essentially in humans but also in vectors and in water. Adopting the One Health offers a powerful approach for improving human, animal, and environmental health and developing multi-level resilience across countries. Moreover, this topic presented affordable techniques for the diagnosis of epidemic pathogens (SARS-CoV-2, Nipah virus, *Mycobacterium tuberculosis*). Sustainable global and regional research and development networks are essential for pandemic preparedness efforts including strategies for sharing technology, data and knowledge to facilitate better access to affordable diagnostic, therapeutics and vaccines worldwide, particularly in developing countries for future pandemics.

Author contributions

WA: Writing—original draft, Writing—review & editing. OB: Writing—review & editing. AT: Writing—review & editing.

Funding

The author(s) declare that no financial support was received for the research, authorship, and/or publication of this article.

Conflict of interest

The authors declare that the research was conducted in the absence of any commercial or financial relationships that could be construed as a potential conflict of interest.

Publisher's note

frontiers | Frontiers in Microbiology

TYPE Review
PUBLISHED 09 December 2022
DOI 10.3389/fmicb.2022.1074289

OPEN ACCESS

EDITED BY
Sanket J. Joshi,
Sultan Qaboos University, Oman

REVIEWED BY
Guoliang Zhang,
Shenzhen Third People's Hospital, China
Seil Kim,
Korea Research Institute of Standards and Science, South Korea

*CORRESPONDENCE
Zhijun Jie
jiezjlxh@163.com
Shengce Tao
taosc@sjtu.edu.cn

†These authors have contributed equally to this work

SPECIALTY SECTION
This article was submitted to Infectious Agents and Disease, a section of the journal Frontiers in Microbiology

RECEIVED 19 October 2022
ACCEPTED 25 November 2022
PUBLISHED 09 December 2022

CITATION
Zhu Y, Zhang M, Jie Z and Tao S (2022) Nucleic acid testing of SARS-CoV-2: A review of current methods, challenges, and prospects. *Front. Microbiol.* 13:1074289. doi: 10.3389/fmicb.2022.1074289

Nucleic acid testing of SARS-CoV-2: A review of current methods, challenges, and prospects

Yuanshou Zhu[1,2†], Meng Zhang[3†], Zhijun Jie[3,4*] and Shengce Tao[1,2*]

[1]Key Laboratory of Systems Biomedicine (Ministry of Education), Shanghai Center for Systems Biomedicine, Shanghai Jiao Tong University, Shanghai, China, [2]School of Biomedical Engineering, Shanghai Jiao Tong University, Shanghai, China, [3]Department of Pulmonary and Critical Care Medicine, Shanghai Fifth People's Hospital, Fudan University, Shanghai, China, [4]Center of Community-Based Health Research, Fudan University, Shanghai, China

Coronavirus disease 2019 (COVID-19) is caused by severe acute respiratory syndrome coronavirus 2 (SARS-CoV-2) and has brought a huge threat to public health and the global economy. Rapid identification and isolation of SARS-CoV-2-infected individuals are regarded as one of the most effective measures to control the pandemic. Because of its high sensitivity and specificity, nucleic acid testing has become the major method of SARS-CoV-2 detection. A deep understanding of different diagnosis methods for COVID-19 could help researchers make an optimal choice in detecting COVID-19 at different symptom stages. In this review, we summarize and evaluate the latest developments in current nucleic acid detection methods for SARS-CoV-2. In particular, we discuss biosensors and CRISPR-based diagnostic systems and their characteristics and challenges. Furthermore, the emerging COVID-19 variants and their impact on SARS-CoV-2 diagnosis are systematically introduced and discussed. Considering the disease dynamics, we also recommend optional diagnostic tests for different symptom stages. From sample preparation to results readout, we conclude by pointing out the pain points and future directions of COVID-19 detection.

KEYWORDS

SARS-CoV-2, nucleic acid testing, biosensor, CRISPR-based diagnostic, COVID-19 variants

Introduction

Coronavirus disease 2019 (COVID-19), caused by severe acute respiratory syndrome coronavirus 2 (SARS-CoV-2), is a highly contagious and lethal disease. As of July 7, 2022, there have been over 548 million diagnosed cases and 6.3 million deaths.[1] Rapid and accurate diagnosis and the immediate isolation of infected individuals are crucial for controlling outbreaks. Serological tests are usually not able to detect early infections due to late seroconversion after infection, so they usually serve as complementary detection methods. Because of its high sensitivity and specificity, nucleic acid testing (NAT) is regarded as the first choice for SARS-CoV-2 detection. The basic requirements for NAT include high accuracy, high specificity, high sensitivity, high speed, and low cost. Furthermore, the SARS-CoV-2 outbreak may coincide with seasonal influenza, which causes similar symptoms. The visits of influenza patients to hospitals also contributed to the increasing spread of SARS-CoV-2 infection (Wolfel et al., 2020), which puts forward higher requirements for detection, including detection throughput, multiplicity, and portability.

Severe acute respiratory syndrome coronavirus 2 is an enveloped single-stranded RNA virus that belongs to the genus β-coronavirus (Harvey et al., 2021). The genome of SARS-CoV-2 is approximately 30 kb and encodes four major structural proteins [spike (S), envelope (E), membrane (M), and nucleocapsid (N)], 16 non-structural proteins, and 8 accessory proteins (**Figure 1**). It has been reported that SARS-CoV-2 evolves at a rate of approximately 1.1×10^{-3} substitutions per site per year, which corresponds to nearly one substitution every ∼11 days (Rambaut et al., 2020). For current high-risk variants of SARS-CoV-2, the WHO prompted their classification as Variants of Concern (VOCs) and Variants of Interest (VOIs) (World Health Organization, 2022a). The emergence of novel variants of SARS-CoV-2, especially for Omicron variants, further highlights the challenges of diagnosis and treatment when we are facing this pandemic. To further group these variants, many research organizations and WHO are working on the identification and classification of SARS-CoV-2. Although various nomenclature, such as country and Greek names, have been tried, a greater grouping, such as lineages and clades, is indispensable. One of the most accepted proposals is put up by GISAID, which identified the variants into eight global clades (S, O, L, V, G, GH, GR, and GV) (Global Initiative on Sharing Avian Influenza Data, 2022). GISAID provides open access to genomic data of SARS-CoV-2, and based on the data, the ARTIC Network provides a common resource of PCR primer sequences and recommendations for amplifying SARS-CoV-2 genomes (Artic network, 2022). Real-time tracking later was used for tracking SARS-CoV-2. As of June 2021, Nextstrain has identified 13 major clades (19A–B, 20A–20J and 21A) (Hadfield et al., 2018; Nextstrain, 2022). The other well-known nomenclature is PANGOLIN proposed by Rambaut et al. in the Phylogenetic Assignment of Named Global Outbreak Lineages (PANGOLIN) (Rambaut et al., 2020; Github, 2022; World Health Organization, 2022b). As of August 2021, 1,340 lineages had been designated (Rambaut et al., 2021; Cov-lineages, 2022). Therefore, a rapid (high detection throughput and less time-consuming), accurate (high sensitivity, specificity, and multiplicity), and low-cost POCT (point-of-care testing) method is in high demand for the timely identification of positive cases and effective tracing of potential SARS-CoV-2-infected individuals.

This review aims to present a comprehensive view of different nucleic acid testing methods for COVID-19 and help researchers make an optimal choice in detecting COVID-19 at different symptom stages. Here, we first outline the general workflow of SARS-CoV-2 detection and describe it in three steps: sample preparation, amplification, and nucleic acid testing (**Figure 2**). Then, we systematically summarize the current nucleic acid methods by emphasizing their pros and cons (**Table 2**). The unique selling points of this review are to introduce emerging biosensors and CRISPR-based diagnostic systems and specifically discuss the impact of COVID-19 variants on SARS-CoV-2 diagnosis. In view of the disease dynamics, we suggest choosing suitable diagnostic methods for different symptom stages. Moreover, the reasons related to false-negative and false-positive results in practice are also explained. Finally, we point out the pain points and future directions for the development of SARS-CoV-2 detection methods.

Workflow of severe acute respiratory syndrome coronavirus 2 detection

The diagnosis of COVID-19 mainly consists of three parts: sample preparation, amplification, and nucleic acid testing (**Figure 2**).

The sample preparation included sample collection and RNA extraction. For sample collection, specimens mainly come from people (such as nasal swabs and throat swabs) and the environment (such as the surface of packages). It has been reported that diverse samples from different parts of people show a great difference in positive rates. For example, Wang et al. (2020) collected 1,070 samples from 205 COVID-19 patients and found that bronchoalveolar perfusion fluid samples (93%), sputum (72%), and nasal swabs (63%) were the three sources with the highest positive rates. In practice, the World Health Organization (WHO) recommends sample collection from nasopharyngeal (NP) and oropharyngeal (OP) swabs and from the lower respiratory tract of patients on mechanical ventilation. NP swabs in the detection of SARS-CoV-2 are

1 https://covid19.who.int/

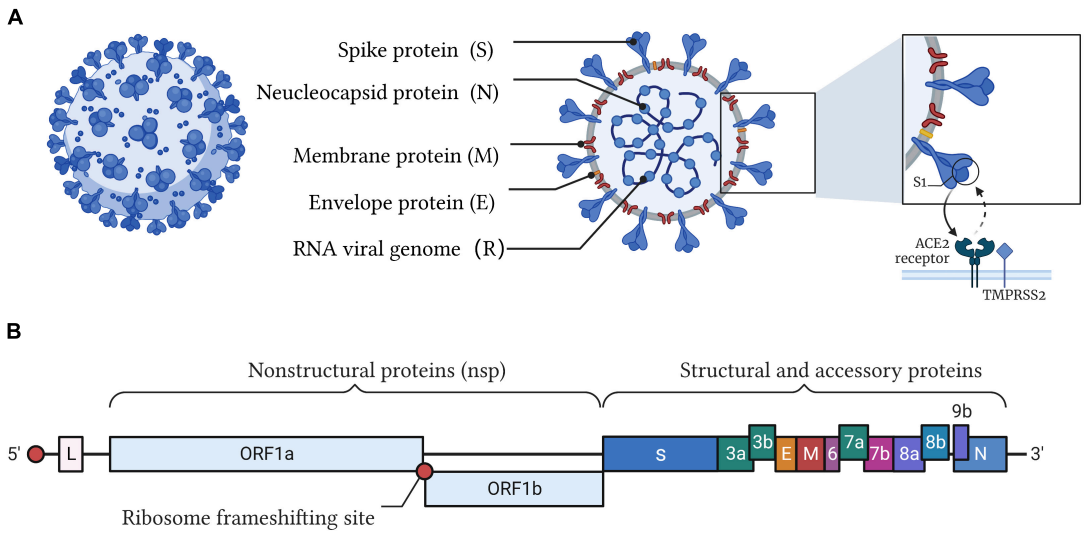

FIGURE 1
Illustration of the SARS-CoV-2 structure and genome. **(A)** SARS-CoV-2 belongs to the cluster of β-coronaviruses with spherically enveloped virions. Envelope glycoproteins such as spike protein (S), envelope protein (E), and membrane protein (M) are embedded in a lipid bilayer envelope. Nucleocapsid protein (N) coupled with single-stranded positive-sense viral RNA is inside the envelope. Through the interaction between the receptor-binding domain (RBD) of the spike protein and angiotensin converting enzyme 2 (ACE2), SARS-CoV-2 invades host cells. **(B)** The genome of SARS-CoV-2 encodes four major structural proteins (S, E, M, N), 16 non-structural proteins (nsp), and 8 accessory proteins.

superior to OP swabs, possibly because of the higher virus load in the nose (Tu et al., 2020; Wyllie et al., 2020; Lee et al., 2021). Apart from people, the environment, such as the surface of packages and wastewater, is also critical with an increasing chance of spreading infection in large-scale outbreaks. For example, Zhang et al. (2022) found that the increased confirmed cases on campus have a positive correlation with positive environmental samples. In sewage treatment plants and densely populated cities, wastewater is also related to active confirmed COVID-19 cases (Tandukar et al., 2022).

After sample collection, there are two main routes for treatment: RNA extraction for amplification and direct amplification without RNA extraction. The former would be more accurate with purified nucleic acids, which are often applied in clinical detection. RNA was extracted from deactivated samples, and cDNAs were synthesized based on reverse transcriptase for detection. Solid-phase extraction (SPE), relying on silica membranes or beads, filter papers, or polymer resins, is widely applied in clinical RNA purification with high accuracy. Incorporating SPE with a microfluidic chip makes nucleic acid testing more appropriate for patients with a high risk of viral transmission (Soares R. et al., 2021). Undoubtedly, detection performance can be greatly affected by the efficiency of different RNA extraction methods. Currently, several methods are used to extract RNA from samples, mainly including anion-exchange resin, magnetic bead-based methods, and guanidinium thiocyanate-phenol-chloroform extractions. Ambrosi et al. (2021) compared the efficiency of three different commercial kits (based on silica-gel affinity columns) and an in-house extraction protocol (based on EXTRAzol) for SARS-CoV-2 detection. They found that the Qiamp DSP Virus Spin kit (Qiagen, Cat. 61704) achieved the highest extraction efficiency, followed by the Viral Nucleic Acid (DNA/RNA) Extraction Kit I (Fisher Molecular Biology, Cat. DR-003), Total RNA Purification Kit (Norgen, Cat. # 17200), and EXTRAzol (BLIRT S.A., Cat. EM30-100). Therefore, caution should be exercised for the detection of SARS-CoV-2 with EXTRAzol, since in the presence of low or very low viral loads, it can go undetected. Nevertheless, purification will cause some loss of RNA and then decrease the sensitivity of detection. In contrast, direct amplification can avoid RNA loss and save considerable operation time. Some companies, such as Sansure Biotech (Banko et al., 2021; Wen et al., 2021) and Vazyme Biotech (Bruce et al., 2020; Qin et al., 2021), have launched lysis buffers for samples for direct amplification. Of course, unextracted samples may lead to the impurity of nucleic acids, inhibition of the reaction, and reduced sensitivity and accuracy. Therefore, nucleic acid extraction can be selected according to specific scenes and detection requirements.

Finally, various nucleic acid testing (NAT) methods, including sequencing, RT-PCR (reverse transcription polymerase chain reaction), isothermal amplification, CRISPR (clustered regularly interspaced short palindromic repeat), and biosensors, have been developed for SARS-CoV-2 detection. None of them is perfect, and different detection methods have their own strengths and weaknesses. We will introduce and evaluate these methods in detail below.

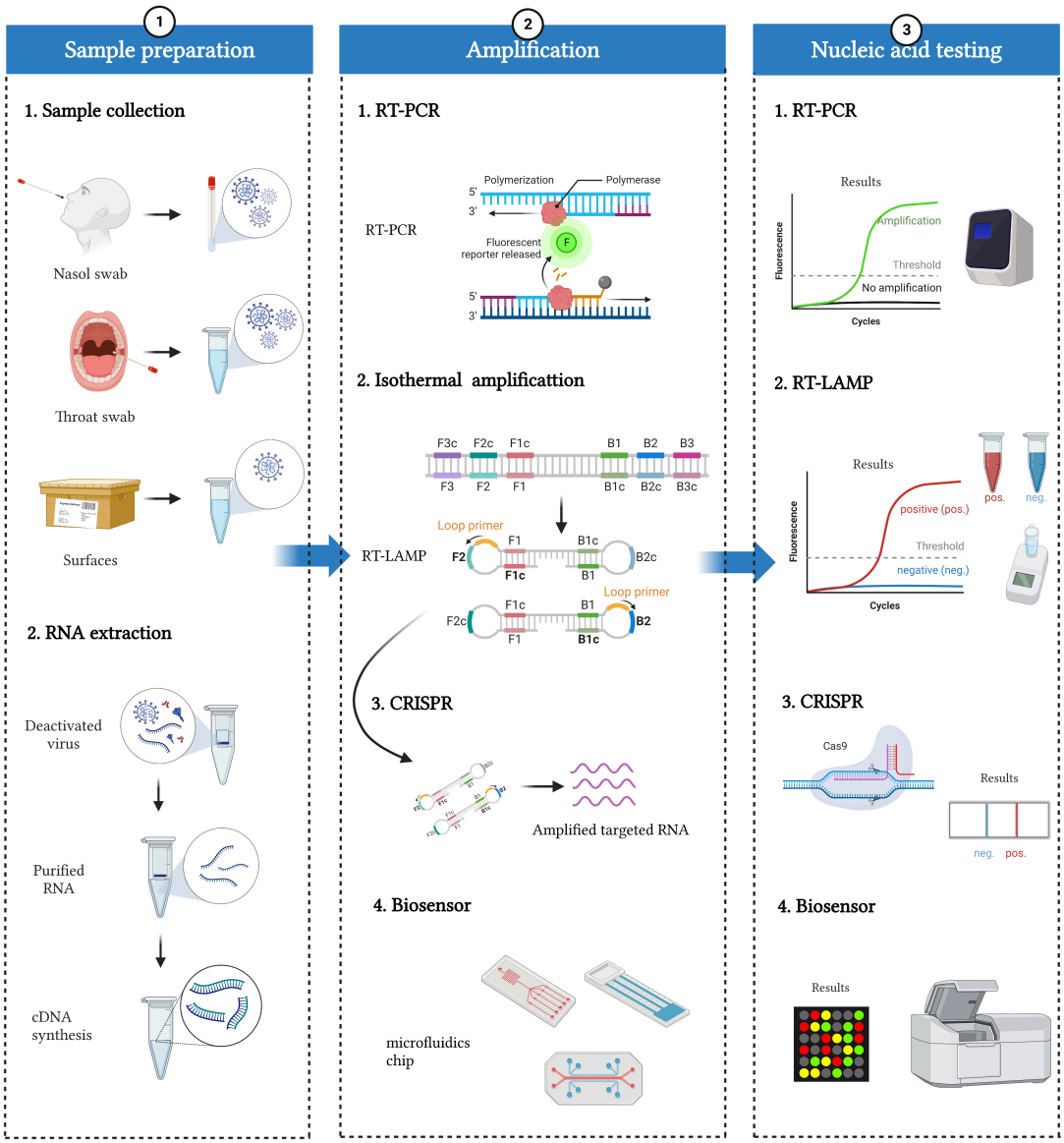

FIGURE 2
Workflow of SARS-CoV-2 nucleic acid detection. The whole detection process can be divided into three parts: sample preparation, amplification, and nucleic acid testing. Sample preparation included sample collection and RNA extraction. Specimens mainly come from people (such as nasal swabs and throat swabs) and the environment (such as the surface of packages). RNA can be extracted from deactivated virus, and then cDNAs are synthesized based on reverse transcriptase. Various nucleic acid amplification methods, including RT-PCR, isothermal amplification, CRISPR, and biosensors, can be applied to amplify and detect cDNAs.

Sequencing technology

High-throughput sequencing (HTS), also known as next-generation sequencing (NGS), can capture the pathogen from complex samples and analyze the complete information of its genome in detail, which is beneficial to the discovery of unknown pathogens. During the COVID-19 pandemic, NGS has been widely used in the comprehensive characterization and analysis of SARS-CoV-2 and surveillance of new variants. Chinese scientists were the first to extract viral RNA from bronchoalveolar lavage fluid (BALF) and complete the sequencing of SARS-COV-2 genomes and reported the emergence of this new virus (Wu et al., 2020). Apart from BALF, nasopharyngeal (NP) swabs are also used as an appropriate source of sequencing samples. Through metagenomics NGS (mNGS), we can also acquire information about the composition of the respiratory microbiome, SARS-CoV-2 coinfection, and the presence of other organisms that may influence infection progression. One of the greatest strengths

of NGS is to screen and identify viral pathogens without prior knowledge of the pathogen, while with high sensitivity and specificity. Currently, some commercial applications are under development, including BioCat, Arbor Biosciences and Swift testing based on NGS (Addetia et al., 2020).

To further improve the sample processing speed, portability, and read length, nanopore third-generation sequencing (NTS) has emerged. SARS-CoV-2 was sequenced through nanopore technology and the sequence-independent single primer amplification (SISPA) method (Chan J. F. et al., 2020), which did not require chemical labeling or PCR amplification of samples, thereby improving detection efficiency. Viehweger et al. (2019) used a direct RNA sequencing (DRS) method based on nanopores to detect viral RNA produced in SARS-COV-2-infected cells. They could map the longest (∼26 kb) continuous read to the viral reference genome, bypassing RNA reverse transcription and amplification to detect methylation sites in viral RNA. The specificity and sensitivity of NTS for SARS-CoV-2 detection are much higher than those of RT-PCR detection. However, it is necessary to strengthen research on improving sequencing accuracy and reducing background interference in the future.

Apart from the identification of pathogens, HTS has been applied for environmental and food safety monitoring, human and plant genome sequencing, and antibiotic resistance detection (Liu Y. X. et al., 2021; Maina et al., 2021). However, it is difficult to avoid the high cost, time consumption and need for highly professionals. Therefore, HTS is often used for unknown pathogen identification rather than routine nucleic acid testing.

Reverse transcription polymerase chain reaction

Reverse transcription polymerase chain reaction (RT-PCR) is currently regarded as the gold standard by the WHO for the diagnosis of COVID-19 (Mizumoto et al., 2020; Soares R. R. G. et al., 2021). Based on reverse transcriptase synthesizing complementary DNA (cDNA) from the viral RNA template, RT-PCR could generate double-stranded DNA, which can be detected using a TaqMan probe or DNA-embedded dye. The cyclic threshold (Ct) value could be used to evaluate the virus load. A Ct value below 35 is considered COVID-19 positive, and a Ct value above 35 is considered COVID-19 negative (Kampf et al., 2021). At present, the target genes detected by RT-PCR mainly include ORF1ab, E, N, and non-structural RNA-dependent RNA polymerase (RdRp), which are conserved or highly expressed (Kevadiya et al., 2021). Many commercial kits based on RT-PCR have been developed. For example, the United States has approved an Emergency Use Authorization (EUA) for RT-PCR kits for emergency use of diagnosing COVID-19, including Invitrogen SuperScript IV (Thermo Fisher, Waltham, MA, USA), Xpert Xpress SARS-CoV-2 Test (Cepheid, Sunnyvale, CA, USA), BioFire Respiratory Panel 2.1-EZ (BioFire Diagnostics, Salt Lake City, UT, USA), and other kits (Food and Drug Administration, 2022). The kits mentioned above are based on a one-step amplification method, reducing the risk of cross-contamination and artificial fault. In contrast, the two-step assay could improve the sensitivity and level of detection; however, there are some limitations, e.g., time consumption, aerosol contamination and requirements for optimizing parameters, that need to be solved.

It is necessary to note that the application of RT-PCR is limited by viral load. RT-PCR is not sensitive to excessively low viral loads in the very early stage of COVID-19 infection. In comparison, digital PCR (dPCR) can detect mutations as low as one copy, enabling the identification of SARS-CoV-2 in the very early infection period. Digital PCR, based on the principles of limited dilution, end-point PCR and Poisson statistics, has a broader dynamic range without external interference and robustness to variations in PCR efficiency. Additionally, an independent reaction system of dPCR can quantify the initial sample absolutely, which is much more beneficial for clinical analysis. Furthermore, droplet digital PCR (ddPCR) based on water-in-oil droplets displays greater superiority in clinical diagnosis along with a much higher dynamic detection range and accuracy than dPCR (Dong et al., 2021). However, ddPCR relies on much more expensive instruments and reagents, limiting its use in mass nucleic acid screening of SARS-CoV-2.

To further increase the detection efficiency and accuracy of PCR in the detection of multiple variants, multiplex PCR (mPCR) was developed, which can simultaneously amplify multiple target sequences in a single reaction. mPCR has been widely used in identifying mutations of SARS-CoV-2 and variants with the advantages of time savings, high sensitivity and accuracy, and high multiplicity. mPCR is also suitable for distinguishing between SARS-CoV-2 and other respiratory viruses. Using QIAstat-Dx Respiratory Panel V2 (Qiagen, Hilden, Germany), Bouzid et al. (2021) detected 22 respiratory viruses and bacteria within 1 h, which promotes the management of patients with similar respiratory symptoms.

In general, RT-PCR is suitable for large-scale nucleic acid screening and has played an important role in the COVID-19 pandemic. Nevertheless, RT-PCR also has some limitations, such as a long reaction time, sophisticated thermal cycling instruments, and skilled operators. With the emergence of isothermal amplification, microfluidics and CRISPR technologies, these problems have been solved to some extent.

Isothermal amplification

Although RT-PCR has been widely adopted in the diagnosis of COVID-19, it has some limitations. As opposed to RT-PCR, isothermal-based amplification, such as reverse transcription loop-medicated isothermal amplification (RT-LAMP) and reverse transcription recombinase polymerase amplification (RT-RPA), can be carried out at a constant temperature and only

requires minimal energy input. This feature enables them to be developed into potential point-of-care testing (POCT) methods.

Reverse transcription loop-medicated isothermal amplification

Reverse transcription loop-medicated isothermal amplification is currently one of the most common isothermal amplification methods, which was first reported in 2000 by Notomi et al. and can achieve 10^9∼10^{10}-fold amplification within 15∼60 min at 60∼65°C (Notomi et al., 2000). Two pairs of primers, known as inner primers and outer primers, are designed to recognize six specific regions of the target genes. To accelerate amplification, two loop primers are often added simultaneously to amplify the loop region of intermediate products. Due to its high sensitivity, specificity and convenience, RT-LAMP has been extensively applied in pathogen detection.

During the COVID-19 pandemic, a series of isothermal detection methods based on RT-LAMP have been developed, which can be divided into three categories. In the beginning of the outbreak of COVID-19, many researchers adopted conventional colorimetric RT-LAMP to establish similar SARS-CoV-2 detection methods in tubes and achieved good results (Dao Thi et al., 2020; Ludwig et al., 2021). If the sample is positive, the color of the reaction mixture will change from pink to yellow or intermediate orange. Second, to improve portability and multiplicity, Zhu et al. (2020) devised multiplex RT-LAMP (mRT-LAMP) coupled with a nanoparticle-based lateral flow biosensor (LFB) assay (mRT-LAMP-LFB) for COVID-19 diagnosis. They simultaneously amplified the ORF1ab and N genes of SARS-CoV-2 in a single-tube reaction and detected results with LFB. In contrast, Yang M. et al. (2021) applied a four-channel microfluidic chip to combine ultrasensitive RT-LAMP for SARS-CoV-2 detection, which can largely avoid contamination from aerosols. Third, some emerging technologies, including clustered regularly interspaced short palindromic repeat (CRISPR) and Argonaute (Ago), are also integrated with RT-LAMP for SARS-CoV-2 detection. For example, Broughton et al. (2020) reported a CRISPR-Cas12a-based lateral flow assay to detect SARS-CoV-2 from swab RNA extracts, which was called SARS-CoV-2 DNA Endonuclease-Targeted CRISPR Trans Reporter (DETECTR). Joung et al. (2020) applied Cas12b to establish an integrated viral detection platform named STOPCovid (SHERLOCK testing in one pot). Xun et al. (2021) developed a rapid scalable and portable testing (SPOT) system, which comprises one-pot RT-LAMP followed by PfAgo (Argonaute protein from Pyrococcus furiosus)-based target sequence detection. Ye et al. (2022) also reported a multiplex Argonaute (Ago)-based nucleic acid detection system (MULAN) to simultaneously detect SARS-CoV-2 and influenza viruses. Finally, molecular beacons were also adapted to detect RT-LAMP products of SARS-CoV-2 so that Sherrill-Mix et al. (2021) constructed the LAMP-BEAC platform.

Therefore, as a general isothermal amplification method, RT-LAMP can be integrated with different technologies to develop high-efficiency detection platforms. However, cross-reactivity can be an issue because of a higher number of primers. If we intend to realize multiplex detection in one tube, the design and optimization of the primers can be tedious and complex. Meanwhile, aerosol contamination is another common problem when we perform RT-LAMP. Hence, combining the strengths of other technologies is the future direction of RT-LAMP.

Reverse transcription recombinase polymerase amplification

Reverse transcription recombinase polymerase amplification (RT-RPA) is another promising isothermal amplification method, which was first reported in 2006 by Piepenburg et al. and can achieve ∼10^{12}-fold amplification within 20∼40 min at 37∼42°C (Piepenburg et al., 2006). Three key proteins, including recombinase (UvsX), strand-displacing polymerase (Bsu), and single-strand binding (SSB) protein (gp32), and other accessory proteins are in collaboration with two specific primers (between 30 and 36 bp) to amplify the target efficiently. Because of the low reaction temperature and high efficiency, RT-RPA enhances our ability to detect diverse pathogens.

Since the outbreak of COVID-19, researchers have made full use of RT-RPA to develop SARS-CoV-2 detection methods. They mostly combined SYBR Green I and/or lateral flow strips (LFS) with RT-RPA to construct the two-plex and visual detection platforms, but the amplification and detection were separate, which easily caused aerosol contamination and false-positive results. To address this problem, Liu D et al. (2021) integrated RT-RPA and a universal lateral flow (LF) dipstick detection system into a single microfluidic chip. The transfer of the RT-RPA mixture to the lateral flow strip is simple, and the chip device is inverted and simply shaken with no valving. To incorporate sample preparation, Tang et al. (2022) also developed a rapid integrated-RPA (I-RPA) system to detect SARS-CoV-2, which comprises a cartridge and an automatic nucleic acid detection device. No additional nucleic acid extraction processes are needed, so the whole time from adding the raw sample to obtaining the result is only 30 min. Moreover, to specifically detect the amplification products and amplify the signal, the CRISPR/Cas system is regarded as the ideal strategy. Lopez-Valls et al. (2022) combined RT-LAMP with CRISPR/Cas13 and gold nanoparticles (AuNPs) to establish a SARS-CoV-2 detection platform called CRISPR/CAS-based colorimetric nucleic acid detection (CASCADE). Upon target recognition, Cas13a cleaves ssRNA oligonucleotides conjugated to AuNPs, thus inducing their colloidal aggregation, which

can be easily visualized. In comparison, Guo et al. (2020) also presented a simple viral detection platform, CASdetec (CRISPR-assisted detection), to integrate Cas12b with RT-RAA (a modified version of RPA) for COVID-19 diagnosis. They executed the RT-RAA reaction within the tube while keeping the CDetection reagents within the cap of the tube for 30 min, after which the CDetection reagents were spun down into the tube for nucleic acid detection. Hence, a constant operating temperature near 37°C certainly has distinctive advantages over PCR-based viral detection.

Nevertheless, the weakness is that RT-RPA requires several proteins in the reaction, so it is not easy to directly integrate with other detection systems to develop a one-pot reaction. They often need to rely on specially designed tubes or microfluidic chips to realize physical isolation and mixing. Moreover, due to the smaller number of primers, RT-RPA often suffers from lower specificity than RT-LAMP. However, even so, low reaction temperature, lyophilized pellet format and high convenience make it popular in point-of-care testing (POCT) scenes. To clearly display the detection performance, we prepared **Table 1** to compare several isothermal amplification-based methods, including both domestic and foreign approved kits.

Clustered regularly interspaced short palindromic repeat-based diagnostic methods

The CRISPR (clustered regularly interspaced short palindromic repeat) system is an acquired immune system that exists in bacteria and archaea and is used to resist foreign invading bacteriophages or viruses (Broughton et al., 2020). In recent years, a variety of CRISPR-based nucleic acid detection technologies have been developed, represented by SHERLOCK (specific high-sensitivity enzymatic reporter unlocking), HOLMES (a 1-h low-cost multipurpose highly efficient system), and DETECTR (DNA endonuclease-targeted CRISPR transreporter), which are known as "next-generation molecular diagnostic technologies" (Safiabadi Tali et al., 2021). They mainly rely on the trans-cleavage activity of Cas proteins. When Cas proteins (Cas13a or Cas12a) bind to crRNA to form binary complexes, they scan the target RNA or DNA, recognize the protospacer adjacent motif (PAM) sequence, and form Cas13a-crRNA-ssRNA or Cas12a-crRNA-dsDNA ternary complexes (Abudayyeh et al., 2016; Li et al., 2018). Next, the ternary complexes will activate the *cis*-cleavage activity of Cas proteins (Cas13a or Cas12a) and specifically cleave the target RNA or DNA and then induce powerful trans-cleavage activity to non-specifically cleave ssRNA or ssDNA. Therefore, as long as we add the single-stranded fluorescent reporter (ssRNA or ssDNA reporter) into the system, the results can be visualized and amplified.

The ability to amplify the signal is the basis for highly sensitive CRISPR-mediated nucleic acid detection. For SARS-CoV-2 detection, most of the current CRISPR-based methods briefly include the following three steps (Broughton et al., 2020; Joung et al., 2020; Patchsung et al., 2020): (1) isothermal amplification of the sample for less than 60 min, such as RT-LAMP, RT-RPA, RCA, or NASBA; (2) CRISPR-based detection of the amplified SARS-CoV-2 RNA after incubation for

TABLE 1 Comparison of several isothermal amplification-based methods developed for SARS-CoV-2 detection.

Name of assay	Principle	Company	Target gene	Sensitivity	Time (min)	References
RT-LAMP assay	RT-LAMP	—	N	100 copies/rxn	30	Baek et al., 2020
mRT-LAMP-LFB	RT-LAMP	—	ORF1ab, N	12 copies/rxn	40	Zhu et al., 2020
COVID-19-LAMP	RT-LAMP	—	ORF3a, E	42 copies/rxn	60	Chow et al., 2020
Suitcase lab	RT-RPA	—	E, N	15 copies/rxn	15	El Wahed et al., 2021
—	RT-RPA	—	N	8 copies/rxn	20	Behrmann et al., 2020
Respiratory Virus Nucleic Acid Detection Kit	RT-LAMP	CapitalBio Technology	ORF1ab, N	150 copies/ml	90	CapitalBio coporation, 2022
Novel Coronavirus (2019-nCoV) Nucleic Acid Detection Kit	CPA	Ustar Biotechnologies	ORF1ab, N	200 copies/ml	80	USTAR, 2022
iAMP COVID-19 Detection Kit	RT-LAMP	Atila BioSystems	ORF1ab, N	4 copies/μl	<90	Rai et al., 2021
ID NOW COVID-19	NEAR	Abbott Diagnostics Scarborough	RdRp	125 copies/ml	15	Abbott Diagnostics, 2020
SHERLOCK CRISPR SARS-CoV-2 Kit	RT-LAMP, CRISPR-Cas13	Sherlock Biosciences	ORF1ab, N	4.5 copies/μl–ORF1ab; 0.9 copies/μl–N	60	Sherlock Biosciences, 2021
SARS-CoV-2 DETECTR Reagent Kit	RT-LAMP, CRISPR-Cas12	Mammoth Biosciences	E, N	10 copies/μl	45	Broughton et al., 2020

CPA, cross priming amplification; NEAR, nicking enzyme amplification reaction.

approximately 30 min; and (3) a lateral flow assay for displaying the results after 2 min of incubation. The SherlockTM CRISPR SARS-CoV-2 kit is the first FDA-authorized CRISPR-based diagnostic test for viral RNA detection (Joung et al., 2020). Nevertheless, the separation of amplification and detection easily causes aerosol contamination, which prompted Wang et al. (2021) to develop a one-pot visual reverse transcription (RT)-LAMP-CRISPR (opvCRISPR) method for SARS-CoV-2 detection. The RT-LAMP reagents are incubated at the bottom of the tube, while the CRISPR/Cas12a reagents are added to the lid. SARS-CoV-2 RNA templates are amplified by RT-LAMP, followed by mixing with Cas12a reagents for cleavage. In comparison, Ding et al. (2020)provided a true single reaction system named AIOD-CRISPR (All-In-One Dual CRISPR-Cas12a) for visual SARS-CoV-2 detection (Zhang et al., 2021). The components for both RT-RPA and CRISPR-12a were prepared in one pot, completely circumventing the separate preamplification of the target RNA or physical separation of Cas proteins. Furthermore, to realize point-of-care testing (POCT), de Puig et al. (2021) developed a minimally instrumented SHERLOCK (miSHERLOCK) device that combines built-in sample preparation from saliva, room temperature stable reagents, battery-powered incubation, and mobile phone-enabled results interpretation. Unlike Cas12/Cas13-based platforms, Cas9 is reported not to produce trans-cleavage activity on substrates, so it is not suitable for trans-cleavage signal output. To circumvent this, Azhar et al. (2021) constructed a platform called the FnCas9 Editor Linked Uniform Detection Assay (FELUDA) for COVID-19 diagnosis. They designed FELUDA as a direct, non-cleavage, affinity-based method of detection, working with single nucleotide mismatch sensitivity.

In summary, emerging CRISPR technologies have been widely applied in combination with isothermal amplifications for SARS-CoV-2 detection. Most of the methods regard it as a downstream means of amplifying the signal and further improving the sensitivity (Zhang et al., 2021). However, Cas proteins need to recognize a certain PAM sequence, which is still a rate-limiting step for widespread applications. Meanwhile, the possible reasons why CRISPR-based commercial products are still very few are as follows: First, the system and technology of CRISPR itself is not as mature as PCR; Second, the auxiliary instruments and reagents are not complete; Third, the advantages over PCR, such as cost, stability, and convenience, are not obvious now. Therefore, the real transformation of CRISPR technology requires joint efforts from academia and industry.

Biosensors and microfluidics

Microfluidics, such as microchannels, microchambers, and microdroplets, have the advantages of smaller reaction volumes, higher detection throughput, ease of integration, and portability compared to traditional detection methods. These characteristics endow microfluidics with the potential to become a powerful technology to meet nucleic acid detection demands. Currently, most microfluidic devices are made from polymer materials such as PDMS (polydimethylsiloxane) and PMMA (polymethyl methacrylate) (Chu et al., 2022). Centrifugal force is the most commonly used fluid manipulation method, followed by electrochemical pumping and capillary action.

With the progression of the COVID-19 pandemic, a variety of methods based on microfluidics have been developed. Combined with RT-PCR, Yang J. et al. (2021) presented a microfluidic cartridge-based sample-to-answer POC device adapted for SARS-CoV-2 detection directly from self-collected saliva specimens. Similarly, Ji et al. developed a centrifugal disc-direct RT-qPCR (dirRT-qPCR) assay for multiplex detection of SARS-CoV-2 and influenza A and B in pharyngeal swab samples in an automated manner (Ji et al., 2020). To displace the thermocycling process, microfluidic chips are also combined with isothermal amplification. Huang et al. (2021) provided a two-stage isothermal amplification method, which consists of a first-stage basic RPA and a second-stage fluorescence LAMP, as well as a microfluidic-chip-based portable system. Due to the ability to amplify the signal, emerging CRISPR has become another promising technology to combine with microfluidics. Chen et al. (2022c) developed a dual-CRISPR/Cas12a-assisted RT-RAA assay and a "sample-to-answer" centrifugal microfluidic platform that can automatically detect 1 copy/μl of SARS-CoV-2 within 30 min. To further fulfill the public health need for a clinically relevant surveillance technology that detects multiple pathogens quickly, Welch et al. (2022) combined the CRISPR/Cas13 system and microfluidics to establish a multiplex detection platform called microfluidic Combinatorial Arrayed Reactions for Multiplexed Evaluation of Nucleic acids (mCARMEN), which can simultaneously detect 21 viruses, including SARS-CoV-2, other coronaviruses, and influenza viruses.

However, all the aforementioned methods need the extraction and amplification of nucleic acids first, which is a complicated process and prolongs the overall detection time. Therefore, Chu et al. proposed an extraction-free, amplification-free, and ultrasensitive fluorescence-based SARS-CoV-2 detection method based on a nanomaterial hybrid microfluidic biochip including 15 parallel sensing units (Chu et al., 2022). The high signal-to-noise ratio of the biochip and the high-precision laser scanner enables accurate detection of target signals. Another method based on molecular nanostructures and automated microfluidics was developed by Zhao et al. (2021) and named after an electrochemical system integrating reconfigurable enzyme-DNA nanostructures (eSIREN). It leverages a molecular circuitry comprising catalytic enzyme-DNA nanostructures to directly recognize target RNA and automated microfluidics to interface the molecular circuitry

with the embedded electrodes to transduce the direct target recognition into an amplified electrical signal.

In addition to the literature, many companies have developed point-of-care (POC) testing systems for SARS-CoV-2 detection (Yang J. et al., 2021). For example, the Cepheid Xpert Xpress SARS-CoV-2/Flu/RSV system (CA, USA) can provide rapid detection of SARS-CoV-2 in 25 min and provide results for four pathogens in 36 min, with less than 1 min hands-on time. Moreover, the Abbott's ID NOWTM system (IL, USA) adopts isothermal amplification technology, and it can process

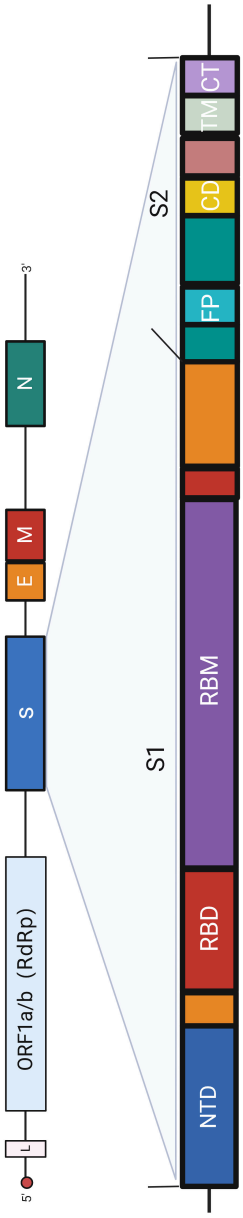

	Alpha variant	Beta variant	Gamma variant	Delta variant	Omicron variant
V1176				F	
D1118	H				
S982	N				
D950				N	
T716	I				
P681	H			R	H
A570	D				
T547					K
Y505					H
N501	Y	Y	Y		Y
Q498					R
G496					S
Q493					R
E484		K	K		A
T478				K	K
S477					N
L452				R	
G446					S
N440					K
K417		N	T		N
S375					F
S373					P
S371					K
D156/157				del	
Y144	del				
D144	del				
HV69/70	del				del
T19				R	

FIGURE 3
Schematic diagram of amino acid mutations in the S gene of SARS-CoV-2. The **left panel** shows the genome of SARS-CoV-2 and the detailed structure of the S gene. The S1 and S2 subunits and a transmembrane domain constitute the spike protein (S). RBD and RBM bind to the host cell receptor. S2 consists of FP, CD, and CT, contributing to membrane fusion. Substitutes of amino acids of mutations are presented on the **right panel**, and the colors correspond to the structure of the S gene. NTD, N-terminal domain; RBD, receptor-binding domain; RBM, receptor-binding motif; FP, fusion peptide; CD, connecting domain; TM, transmembrane domain; CT, cytoplasmic tail. Alpha (Berenger et al., 2021; Borsova et al., 2021; Hale et al., 2021; Fu et al., 2022; Oh et al., 2022; Ratcliff et al., 2022), beta (Hale et al., 2021; Dikdan et al., 2022; Fu et al., 2022), gamma (Hale et al., 2021; Ratcliff et al., 2022), delta (Berenger et al., 2021; Hale et al., 2021; Norz et al., 2021; Oh et al., 2022; Rosato et al., 2022), and omicron (Bloemen et al., 2022; Dachert et al., 2022; Rasmussen et al., 2022).

nasopharyngeal swabs and saliva samples and provide results in 15 min (Abbott, 2022). Although many POC devices for SARS-CoV-2 detection have been reported, there are several limitations, such as high cost and low throughput; furthermore, sample preparation cannot be easily incorporated into the detection process.

Overall, although research in microfluidics has been advancing for almost a half-century, its adoption into real-world applications has been slow and has encountered hurdles. The reasons include immature core technologies, poor compatibility of materials with biomolecules, difficulty in integration with peripheral devices, high production cost, and insufficient multidisciplinary talent. In recent decades, with advancements in material science and microfluidic device manufacturing techniques, great developments in microfluidics in diagnostics have been achieved.

The influences of severe acute respiratory syndrome coronavirus 2 variants on diagnostics

According to the level of virulence and risk, the World Health Organization (WHO) classified SARS-CoV-2 variants into variants of concern (VOCs), variants of interest (VOIs), and alerts for further monitoring (AFM) (World Health Organization, 2022a). VOCs include alpha, beta, gamma, delta, and micron variants, which are more infectious and can cause severe diseases with increased immune escape. The emergence of the variants makes it difficult to diagnose and reduce the effectiveness of treatments and vaccines. At present, the Omicron variant is the global-dominated strain with multiple subvariants. The Omicron variant (B.1.1.529) possesses more than 30 mutations and at least 15 amino acid changes in the receptor binding domain (RBD), which is a key structure for invasion (Barnes et al., 2020; Cui et al., 2022). It would be 2.8 times more infectious than the Delta variant, mainly because of RBD mutations N440K, T478K, and N501Y (Chen et al., 2022a). Currently, the Omicron variant BA.2 is the main focus of attention due to its widespread use in Europe, America, and China, with increased transmissibility and immune escape in people. Compared to BA.1, the effective reproduction number of the Omicron variant BA.2 is 1.4-fold higher (Yamasoba et al., 2022). A timely and effective diagnosis would cut the transmission chain and reduce excess mortality raised by overhigh transmissibility. However, variants pose new challenges to current detection methods, as shown below.

First, the accuracy of commonly used target genes becomes less reliable. Double-target (ORF1ab and N gene) reagents are widely used in the detection of SARS-CoV-2, while many

TABLE 2 Comparison of different SARS-CoV-2 nucleic acid detection methods.

Methods	Sample types	Absolute quantification	Sophisticated instrument	Time	LOD	Target gene	Advantages	Disadvantages
Sequencing	Nasopharyngeal swab	N	Y	2–3 days	—	—	More precise, genomic profiling, new mutations detection	Time-consuming, expensive, specialized operators
RT-PCR	Nasopharyngeal swab, sputum, bronchoalveolar lavage fluid, stool	Y	Y	70–120 min	100 copies/ml	ORF1ab, N	Mature technology, complete supporting reagents, absolute quantification, low cost	Thermal cycling, specialized operators, time-consuming
RT-LAMP	Nasopharyngeal swab, sputum, stool	N	N	30–60 min	1 copies/μl	ORF1ab, N	Isothermal, simple, rapid, highly sensitive	Non-specific amplification, too many primers, ladder band
RT-RPA	Nasopharyngeal swab, sputum, stool	N	N	20–40 min	0.25–2.5 copies/μl	N	Isothermal, simple, rapid, highly sensitive	Non-specific amplification, no primer design software, too many enzymes in system
CRISPR-based assay	Nasopharyngeal swab, bronchoalveolar lavage fluid	N	N	30–60 min	0.9–10 copies/μl	ORF1ab, N, E	Isothermal, amplify the signal, easy to combine with isothermal amplification	Immature technology, reaction system to be optimized
Biosensors and microfluidics	Nasopharyngeal swab, sputum, bronchoalveolar lavage fluid	N	N	60 min	0.5 copies/μl	N, M	Miniaturization, simple, real-time detection	Sensitive to surrounding environment, complex design, high cost

mutations of the Omicron variant exist in the N gene, triggering false negative results in the detection (Yu et al., 2020; Cui et al., 2022). Similar inaccuracy of the target gene also occurs in other SARS-CoV-2 variants. For example, Chen et al. (2022b) evaluated the influence of VOCs on commercial kits, suggesting that beta and delta variants adversely affected the sensitivity of ORF1ab gene analysis, and N gene analysis completely failed in the gamma variant. Therefore, the existing detection methods should be modified to detect new variants. More conserved mutations for the test should be considered, and mutations in the S gene are also suitable candidates. For the Omicron variant, the community track platform in Denmark developed and implemented the RT-PCR test using the L452R mutation, with an estimated specificity of 99.99% based on retrospective analysis (Spiess et al., 2021). Niu et al. (2022) developed a PCR-based CRISPR/Cas13a detection system (PCR-CRISPR) to improve the sensitivity and portability of SARS-CoV-2 HV69-70del mutant site detection.

Second, the mutations could limit the efficacy and sensitivity of the test. In the assay kit of Sansure Biotech (Changsha, China), the gamma variant affected the PCR amplification efficiency of ORF1ab (Chen et al., 2022b). Rajib et al. (2022) also reported that the Delta variant containing a mutation in the probe binding region of the E gene exhibited atypical PCR amplification and might induce false negative results. To improve the sensitivity and specificity, Liang et al. (2022) combined PCR with CRISPR technology to develop a CRISPR-Cas12a-based assay to detect and trace Omicron variants.

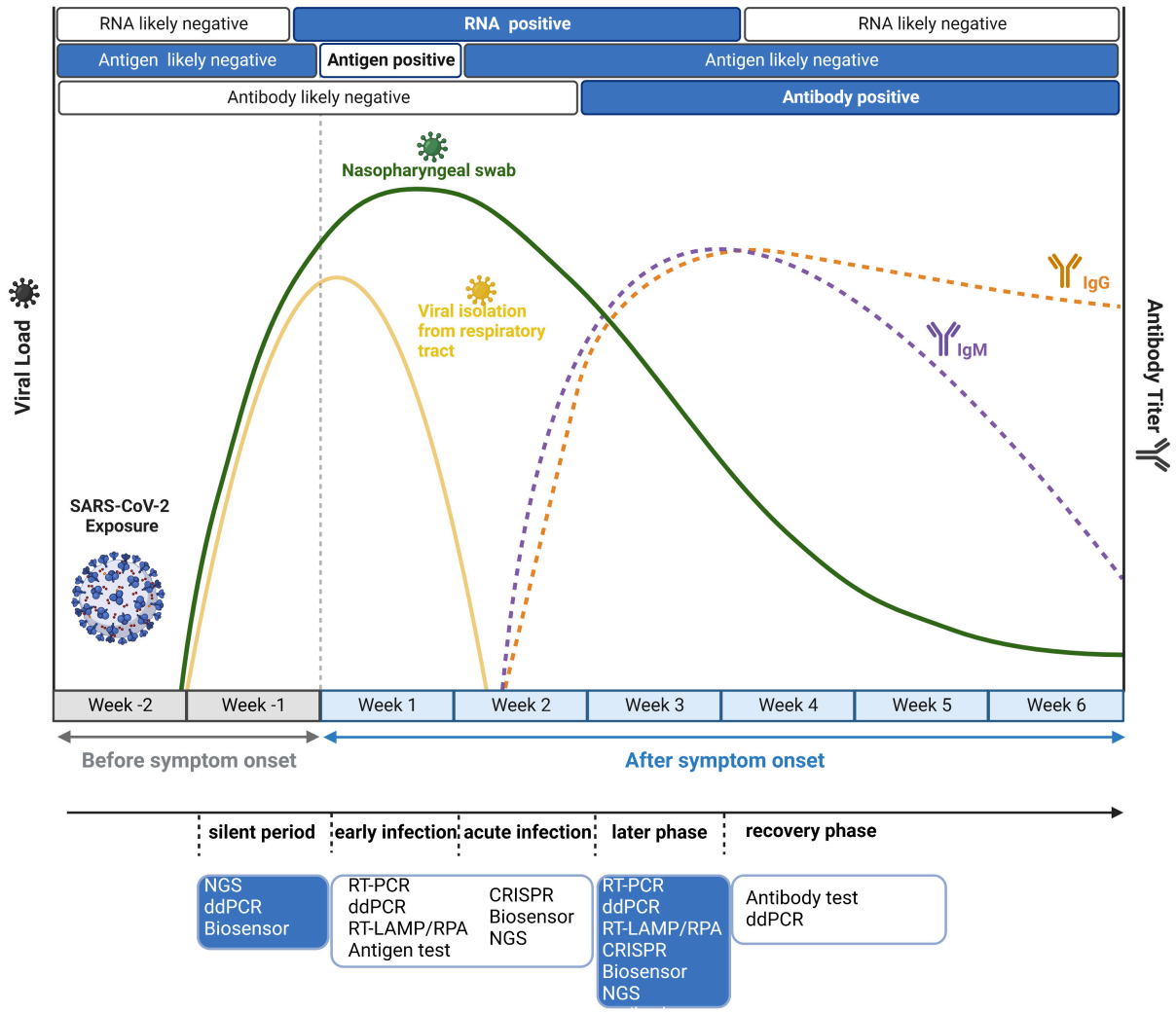

FIGURE 4
Disease dynamics and optional diagnostic tests for COVID-19. Because of virus load and antibody dynamics, it is necessary to adopt different detection strategies at different time points. Before symptom onset, the optimal choice is nucleic acid testing because its limit of detection (LOD) can reach 10^2–10^3 copies/ml. After symptom onset, antigen tests and viral RNA detection are all feasible in the first week, while antibody tests are positive later in the disease course.

They designed two sets of specific crRNAs based on Omicron mutations, including crRNA-S-37X (covering S371L, S373P, and S375F) and crRNA-S-49X (covering Q493R, G496S, and Q498R). Artificial introduction of additional mutations around the target mutation site into crRNAs could significantly improve identification efficacy. This quick test could be routinely implemented in resource-limited conditions to monitor and track the spread of Omicron variants.

On the other side of a double-edged sword, we can utilize these significant mutations to distinguish different SARS-CoV-2 variants (**Figure 3**). For example, Hale et al. (2021) used PCR to effectively distinguish alpha (HV69/70, N501Y), beta (N501Y, K417N, E484K, P681R), gamma (N501Y, E484K), and delta (P681R) variants through mutations HV69/70, N501Y, K417N, and E484K on the S gene, which showed 100% specificity and sensitivity. Similarly, Liang et al. (2021) developed a reliable and fast CRISPR-Cas12a system based on PCR to successfully utilize S gene mutations (K417N/T, L452R/Q, T478K, E484K/Q, N501Y, and D614G) to distinguish alpha, beta, gamma, and delta variants. This CRISPR-based approach can be used to screen emerging mutations and is immediately implemented in laboratories where nucleic acid tests are already performed or in resource-limited settings. Moreover, multiplex detection in a single reaction is a significant research direction for simultaneously monitoring multiple mutations and variants, in contrast to traditional tests.

Discussion and prospects

The COVID-19 pandemic highlights the need for diagnostic methods that can be rapidly adapted and deployed in a variety of settings. In this review, various SARS-CoV-2 nucleic acid detection methods, including sequencing, RT-PCR, isothermal amplification (LAMP and RPA), CRISPR, and biosensors, have been summarized and evaluated individually. To further clarify the strengths and weaknesses, we prepared a table to compare the above methods (**Table 2**). No method is perfect, and we need to choose a suitable method according to the specific application scenario and purpose.

Although these methods are robust and sensitive, their practical effect would be modified by different stages of individual-specific immune reactions and burdens of the virus. Therefore, it is important to adopt suitable detection strategies at different time points after infection. As shown in **Figure 4**, we also mark the distinct time points for antigen and antibody detection apart from nucleic acid detection. Because of the long incubation period of SARS-CoV-2, it is advisable to adopt several detection strategies. Based on the timeline, in the silent period of infection, most detection methods could not detect SARS-CoV-2 due to the very low virus load. In this case, NGS could realize real-time surveillance, while NGS is not suitable for large-scale screening. ddPCR is highly sensitive and suitable for detecting low viral load specimens that interfere with community transmission in the early stage of the epidemic (Dong et al., 2021). Suo et al. (2020) simultaneously compared the limit of detection (LOD) between ddPCR and RT-PCR and found that the LOD of ddPCR was 2.1 copies/reaction (ORF1ab gene) and 1.7 copies/reaction (N gene), much lower than that of RT-PCR (1,039 and 873.2 copies/reaction). Moreover, the combination of biosensors and rapid antigen testing can also be applied to detect asymptomatic infected patients, and the specificity is over 99% (Schuit et al., 2021). After symptom onset, both antigens and nucleic acids are suitable. Primary screening could use antigen testing, which is cost-effective and fast. Considering the high false positive rate of antigen detection, antigen testing alone is not recommended. Other nucleic acid tests, such as RT-PCR, RT-LAMP, and CRISPR, should be employed to further confirm the diagnosis. In the early, acute

TABLE 3 Possible reasons for false negative and positive results in nucleic acid detection.

	Factors	References
Sample preparation		
Sample collection	• Improper materials: the swap containing calcium alginate or a stick has inhibitors against PCR. • Source of sample: gastrointestinal symptoms are related to prolonged virus RNA in gastrointestinal when upper respiratory symptoms disappeared with undetected virus RNA in respiratory tract. • Time of sample: the longer the interval between symptoms and detection is, the higher the probability of false negative is.	Premraj et al., 2020; Natarajan et al., 2022
Sample store	• Improper store and transport sample: RNA might degrade due to inappropriate temperature.	
Detection technology		
Target gene	• Deletion of gene fragments and genome variation on target gene would affect the use of existing primers.	Su et al., 2020
Limiting of detection	• Reaction settings, amplification efficiency, reverse transcription efficiency, etc., could influence the range of limiting of detection.	Yang S. et al., 2021
Patients		
Drugs/Inhibitors	• heme and humic acid are common PCR inhibitors; drugs like Acyclovir also have been reported to inhibit Taq DNA polymerase	Yedidag et al., 1996
Infection dynamics and severity	• Infection severity and upper respiratory viral load of individual differences might contribute to false-negative results	

and later infection stages, nucleic acid testing can be used as the diagnostic choice for COVID-19. However, in the recovery period of infection, antibody testing is much more reliable. IgM is expressed 3–7 days after infection and can be detected in the second week after infection, whereas IgG antibody needs 8 days to reach a detectable level (Peeling et al., 2022). Overall, previous studies suggest that the right test at the right time is the key to correct the diagnosis of COVID-19.

False negative and false positive results have always been a concern for nucleic acid testing. Although the sensitivity and specificity of current detection methods such as RT-PCR have almost reached approximately 100% in diagnosing COVID-19, cases of false negatives and positives are continuously reported (Chan W. et al., 2020; Pokhrel et al., 2020; Kanji et al., 2021). Problems in every step from sample preparation to detection could influence the results, probably contributing to the false results. We summarized the possible reasons in **Table 3**. Of note, as mentioned in the table, new mutations would decrease the accuracy and sensitivity of nucleic acid testing from different aspects, especially the mutations in primers and the target region of the probe, giving rise to false negative results. Furthermore, the dynamics of virus load during infection would extend the limit of detection (LOD) of testing. The LODs of RT-PCR are reported as 5–7,740 copies/ml, and the LODs of RT-LAMP are 2–304 copies/reaction (Yang S. et al., 2021). Other factors, including RNA extraction, efficiency of reverse transcription and settings of reaction, cannot be ignored.

Last but not least, several pain points remain to be solved for current SARS-CoV-2 nucleic acid detection methods, which is also a future direction for development. First, integrated sample preparation is necessary, especially for POC diagnostic devices. Currently, most of the sample preparations are performed separately in the existing detection platforms, which increases the complexity of the test and reduces user friendliness. It is desirable to combine sample preparation with amplification and detection. Although some studies have developed sample preparation-free methods by utilizing RT-PCR and RT-LAMP, there is still a long way to go to improve the stability, sensitivity, throughput, and compatibility. A fully simplified process (raw sample-in-answer-out) is highly demanded.

Second, with the increasing number of targets and samples, nucleic acid detection raises higher requirements for detection throughput, multiplicity and portability. However, traditional RT-PCR and isothermal chips could hardly meet these requirements. Biochips and microfluidics can physically isolate different primer pairs through micropores or microchannels, enabling multiplex detection of targets in a closed space. For example, Xing et al. (2020) developed the RTisochipTM-W platform by combining isothermal amplification technology with a microfluidic disc chip, which can simultaneously detect 19 common viruses from 16 samples in a single run. Nevertheless, the design is actually to stack multiple chip devices together to realize high-throughput detection, and each instrument is expensive and not portable. Similarly, we also compared the international mainstream nucleic acid detection platforms based on microchips or microfluidics technology (**Table 4**) and found that they are basically portable and integrated. However, their detection throughput is also low, and only one sample can be detected at a time. To address this, Biofire has launched the FilmArray 2.0 platform, but in fact, it is also a combination of multiple FilmArray 1.0 devices, similar to the aforementioned RTisochipTM-W platform. Overall, there is still a lack of a detection platform simultaneously integrated with high detection throughput, multiplicity and portability.

Third, with the rapid spread of the COVID-19 pandemic, another major focus of future work is to develop POC and home tests that do not require specialized operations. In this way, people can acquire the detection results quickly and seek professional help instead of waiting longer for results from the laboratory. To increase the detection throughput and extensibility, POC tests can be combined with the automated sample processing system, allowing patients to be diagnosed sooner. Moreover, we should also develop more novel biosensors as POC diagnostic devices for SARS-CoV-2 detection, such as electrochemical sensors, field-effect transistor (FET)-based sensors, magnetic biosensors,

TABLE 4 Comparison of mainstream nucleic acid detection platforms.

Platforms	Company	Principle	Volume (cm)	Weight (kg)	Throughput	Target	Time (min)
FilmArray	Biofire	Nested PCR	39.3 × 25.4 × 16.5	7.3	1	24	60
GeneXpert Omni	Cepheid	Nested qPCR	8 × 11 × 23	1	1	1–2	30–60
io system	Atlas Genetics	PCR	27.7 × 27.5 × 38.4	10	1	24	30
Cobas Liat	IQuum	qPCR	19 × 11.4 × 24.1	3.76	1	1–2	20
ID Now	Abbott Molecular	NEAR	21 × 15 × 19	3	1	1–2	5–13
RTisochip-W system	CapitalBio	NASBA	58.6 × 69.0 × (17.5 × 4)	33 × 4	16	19	90
iPonatic	Sansure Biotech	qPCR	–	<10	1	1–2	15–45
Easy NET	USTAR Biotech	CPA	26 × 37 × 52	13	2	1–2	80–90

NEAR, nicking enzyme amplification reaction; CPA, crossing priming amplification.

enzyme-based sensors, and DNA biosensors. It is believed that through our joint efforts, nucleic acid detection methods will continue to innovate to better meet the detection needs of infectious diseases.

Author contributions

YZ and MZ contributed to the central idea and coordinated the writing of the manuscript. ZJ and ST read, discussed, and revised the manuscript. All authors contributed to the article and approved the submitted version.

Funding

This work was partially supported by the National Key Research and Development Program of China (Grant No. 2020YFE0202200), the National Natural Science Foundation of China (Nos. 31970130 and 82070024), Natural Science Foundation of Shanghai (No. 20ZR1443700), and Specialized Department Foundation of Minhang District (No. 2020MWTZB02).

Acknowledgments

We do appreciate the effort of Yifan Bao for the right to use the Biorender (Biorender.com) to create the Figures in this review.

Conflict of interest

The authors declare that the research was conducted in the absence of any commercial or financial relationships that could be construed as a potential conflict of interest.

Publisher's note

References

Abbott (2022). *Covid-19 response*. Available online at: https://www.abbott.com/coronavirus.html (accessed November 13, 2022).

Abbott Diagnostics (2020). *ID now Covid-19: Instructions for use*. Scarborough, ME: Abbott Diagnostics.

Abudayyeh, O. O., Gootenberg, J. S., Konermann, S., Joung, J., Slaymaker, I. M., Cox, D. B., et al. (2016). C2c2 is a single-component programmable RNA-guided RNA-targeting CRISPR effector. *Science* 353:aaf5573. doi: 10.1126/science.aaf5573

Addetia, A., Xie, H., Roychoudhury, P., Shrestha, L., Loprieno, M., Huang, M. L., et al. (2020). Identification of multiple large deletions in ORF7a resulting in in-frame gene fusions in clinical SARS-CoV-2 isolates. *J. Clin. Virol.* 129:104523. doi: 10.1016/j.jcv.2020.104523

Ambrosi, C., Prezioso, C., Checconi, P., Scribano, D., Sarshar, M., Capannari, M., et al. (2021). SARS-CoV-2: Comparative analysis of different RNA extraction methods. *J. Virol. Methods* 287:114008. doi: 10.1016/j.jviromet.2020.114008

Artic network (2022). *SARS-CoV-2*. Available online at: https://artic.network/ncov-2019 (accessed November 13, 2022).

Azhar, M., Phutela, R., Kumar, M., Ansari, A. H., Rauthan, R., Gulati, S., et al. (2021). Rapid and accurate nucleobase detection using FnCas9 and its application in Covid-19 diagnosis. *Biosens. Bioelectron.* 183:113207. doi: 10.1016/j.bios.2021.113207

Baek, Y., Um, J., Antigua, K., Park, J., Kim, Y., Oh, S., et al. (2020). Development of a reverse transcription-loop-mediated isothermal amplification as a rapid early-detection method for novel SARS-CoV-2. *Emerg. Microbes Infect.* 9, 998–1007. doi: 10.1080/22221751.2020.1756698

Banko, A., Petrovic, G., Miljanovic, D., Loncar, A., Vukcevic, M., Despot, D., et al. (2021). Comparison and sensitivity evaluation of three different commercial real-time quantitative PCR kits for SARS-CoV-2 detection. *Viruses* 13:1321. doi: 10.3390/v13071321

Barnes, C. O., Jette, C. A., Abernathy, M. E., Dam, K. A., Esswein, S. R., Gristick, H. B., et al. (2020). SARS-CoV-2 neutralizing antibody structures inform therapeutic strategies. *Nature* 588, 682–687. doi: 10.1038/s41586-020-2852-1

Behrmann, O., Bachmann, I., Spiegel, M., Schramm, M., Abd El Wahed, A., Dobler, G., et al. (2020). Rapid detection of SARS-CoV-2 by low volume real-time single tube reverse transcription recombinase polymerase amplification using an Exo probe with an internally linked quencher (Exo-IQ). *Clin. Chem.* 66, 1047–1054. doi: 10.1093/clinchem/hvaa116

Berenger, B., Stokes, W., Turnbull, L., Pabbaraju, K., Zelyas, N., Venner, A., et al. (2021). Save the Covid-19 point-of-care nucleic acid test swab after testing to identify variants of concern. *Clin. Chem.* 68, 249–251. doi: 10.1093/clinchem/hvab243

Bloemen, M., Rector, A., Swinnen, J., Ranst, M. V., Maes, P., Vanmechelen, B., et al. (2022). Fast detection of SARS-CoV-2 variants including omicron using one-step RT-PCR and Sanger sequencing. *J. Virol. Methods* 304:114512. doi: 10.1016/j.jviromet.2022.114512

Borsova, K., Paul, E., Kovacova, V., Radvanszka, M., Hajdu, R., Cabanova, V., et al. (2021). Surveillance of SARS-CoV-2 lineage B.1.1.7 in Slovakia using a novel, multiplexed RT-qPCR assay. *Sci. Rep.* 11:20494. doi: 10.1038/s41598-021-99661-7

Bouzid, D., Casalino, E., Mullaert, J., Laurent, O., Duval, X., Lescure, F. X., et al. (2021). Added value of rapid respiratory syndromic testing at point of care versus central laboratory testing: A controlled clinical trial. *J. Antimicrob. Chemother.* 76 (Suppl. 3), iii20–iii27. doi: 10.1093/jac/dkab241

Broughton, J. P., Deng, X., Yu, G., Fasching, C. L., Servellita, V., Singh, J., et al. (2020). CRISPR-Cas12-based detection of SARS-CoV-2. *Nat. Biotechnol.* 38, 870–874. doi: 10.1038/s41587-020-0513-4

Bruce, E. A., Huang, M. L., Perchetti, G. A., Tighe, S., Laaguiby, P., Hoffman, J. J., et al. (2020). Direct RT-qPCR detection of SARS-CoV-2 RNA from patient nasopharyngeal swabs without an RNA extraction step. *PLoS Biol.* 18:e3000896. doi: 10.1371/journal.pbio.3000896

CapitalBio coporation (2022). *SARS-CoV-2 nucleic acid detection kit (integrated isothermal amplification chip method)*. Available online at: https://www.capitalbio.com/gxba/xwzx/gsxw/2020nsjd/28883.shtml.htm (accessed November 13, 2022).

Chan, J. F., Yuan, S., Kok, K. H., To, K., Chu, H., Yang, J., et al. (2020). A familial cluster of pneumonia associated with the 2019 novel coronavirus indicating

person-to-person transmission: A study of a family cluster. *Lancet* 395, 514–523. doi: 10.1016/s0140-6736(20)30154-9

Chan, W., Ip, J., Chu, A., Yip, C., Lo, L., Chan, K., et al. (2020). Identification of nsp1 gene as the target of SARS-CoV-2 real-time RT-PCR using nanopore whole-genome sequencing. *J. Med. Virol.* 92, 2725–2734. doi: 10.1002/jmv.26140

Chen, Y., Zong, N., Ye, F., Mei, Y., Qu, J., and Jiang, X. (2022c). Dual-CRISPR/Cas12a-assisted RT-RAA for ultrasensitive SARS-CoV-2 detection on automated centrifugal microfluidics. *Anal. Chem.* 94, 9603–9609. doi: 10.1021/acs.analchem.2c00638

Chen, J., Wang, R., Gilby, N., and Wei, G. (2022a). Omicron variant (B.1.1.529): Infectivity, vaccine breakthrough, and antibody resistance. *J. Chem. Inf. Model.* 62, 412–422. doi: 10.1021/acs.jcim.1c01451

Chen, Y., Han, Y., Yang, J., Ma, Y., Li, J., and Zhang, R. (2022b). Impact of SARS-CoV-2 variants on the analytical sensitivity of rRT-PCR assays. *J. Clin. Microbiol.* 60:e0237421. doi: 10.1128/jcm.02374-21

Chow, F., Chan, T., Tam, A., Zhao, S., Yao, W., Fung, J., et al. (2020). A Rapid, simple, inexpensive, and mobile colorimetric assay Covid-19-LAMP for mass on-site screening of Covid-19. *Int. J. Mol. Sci.* 21:5380. doi: 10.3390/ijms21155380

Chu, Y., Qiu, J., Wang, Y., Wang, M., Zhang, Y., and Han, L. (2022). Rapid and high-throughput SARS-CoV-2 RNA detection without RNA extraction and amplification by using a microfluidic biochip. *Chemistry* 28:e202104054. doi: 10.1002/chem.202104054

Cov-lineages. (2022). *Pango lineages: Latest epidemiological lineages of SARS-CoV-2*. Available online at: https://nextstrain.org/ncov/gisaid/global/6 m (accessed November 13, 2022).

Cui, Z., Liu, P., Wang, N., Wang, L., Fan, K., Zhu, Q., et al. (2022). Structural and functional characterizations of infectivity and immune evasion of SARS-CoV-2 Omicron. *Cell* 185, 860–871.e13. doi: 10.1016/j.cell.2022.01.019

Dachert, C., Muenchhoff, M., Graf, A., Autenrieth, H., Bender, S., Mairhofer, H., et al. (2022). Rapid and sensitive identification of omicron by variant-specific PCR and nanopore sequencing: Paradigm for diagnostics of emerging SARS-CoV-2 variants. *Med. Microbiol. Immunol.* 211, 71–77. doi: 10.1007/s00430-022-00728-7

Dao Thi, V. L., Herbst, K., Boerner, K., Meurer, M., Kremer, L., Kirrmaier, D., et al. (2020). A colorimetric RT-LAMP assay and LAMP-sequencing for detecting SARS-CoV-2 RNA in clinical samples. *Sci. Transl. Med.* 12:eabc7075. doi: 10.1126/scitranslmed.abc7075

de Puig, H., Lee, R. A., Najjar, D., Tan, X., Soeknsen, L. R., Angenent-Mari, N. M., et al. (2021). Minimally instrumented SHERLOCK (miSHERLOCK) for CRISPR-based point-of-care diagnosis of SARS-CoV-2 and emerging variants. *Sci. Adv.* 7:eabh2944. doi: 10.1126/sciadv.abh2944

Ding, X., Yin, K., Li, Z., Lalla, R. V., Ballesteros, E., Sfeir, M. M., et al. (2020). Ultrasensitive and visual detection of SARS-CoV-2 using all-in-one dual CRISPR-Cas12a assay. *Nat. Commun.* 11:4711. doi: 10.1038/s41467-020-18575-6

Dikdan, R. J., Marras, S. A. E., Field, A. P., Brownlee, A., Cironi, A., Hill, D. A., et al. (2022). Multiplex PCR assays for identifying all major severe acute respiratory syndrome coronavirus 2 variants. *J. Mol. Diagn.* 24, 309–319. doi: 10.1016/j.jmoldx.2022.01.004

Dong, L., Zhou, J., Niu, C., Wang, Q., Pan, Y., Sheng, S., et al. (2021). Highly accurate and sensitive diagnostic detection of SARS-CoV-2 by digital PCR. *Talanta* 224:121726. doi: 10.1016/j.talanta.2020.121726

El Wahed, A. A., Patel, P., Maier, M., Pietsch, C., Rüster, D., Böhlken-Fascher, S., et al. (2021). Suitcase lab for rapid detection of SARS-CoV-2 based on recombinase polymerase amplification assay. *Anal. Chem.* 93, 2627–2634. doi: 10.1021/acs.analchem.0c04779

Food and Drug Administration (2022). *Medical devices*. Available online at: https://www.fda.gov/medical-devices (accessed November 13, 2022).

Fu, J. Y. L., Chong, Y. M., Sam, I. C., and Chan, Y. F. (2022). SARS-CoV-2 multiplex RT-PCR to detect variants of concern (VOCs) in Malaysia, between January to May 2021. *J. Virol. Methods* 301:114462. doi: 10.1016/j.jviromet.2022.114462

Github (2022). *Cov-lineages-pangolin*. Available online at: https://github.com/cov-lineages/pangolin (accessed November 13, 2022).

Global Initiative on Sharing Avian Influenza Data (2022). *Nextstrain*. Available online at: https://www.gisaid.org/phylodynamics/global/nextstrain/ (accessed November 13, 2022).

Guo, L., Sun, X., Wang, X., Liang, C., Jiang, H., Gao, Q., et al. (2020). SARS-CoV-2 detection with CRISPR diagnostics. *Cell Discov.* 6:34. doi: 10.1038/s41421-020-0174-y

Hadfield, J., Megill, C., Bell, S. M., Huddleston, J., Potter, B., Callender, C., et al. (2018). Nextstrain: Real-time tracking of pathogen evolution. *Bioinformatics* 34, 4121–4123. doi: 10.1093/bioinformatics/bty407

Hale, R., Crowley, P., Dervisevic, S., Coupland, L., Cliff, P. R., Ebie, S., et al. (2021). Development of a multiplex tandem PCR (MT-PCR) assay for the detection of emerging SARS-CoV-2 variants. *Viruses* 13:2028. doi: 10.3390/v13102028

Harvey, W. T., Carabelli, A. M., Jackson, B., Gupta, R. K., Thomson, E. C., Harrison, E. M., et al. (2021). SARS-CoV-2 variants, spike mutations and immune escape. *Nat. Rev. Microbiol.* 19, 409–424. doi: 10.1038/s41579-021-00573-0

Huang, Q., Shan, X., Cao, R., Jin, X., Lin, X., He, Q., et al. (2021). Microfluidic chip with two-stage isothermal amplification method for highly sensitive parallel detection of SARS-CoV-2 and measles virus. *Micromachines (Basel)* 12:1582. doi: 10.3390/mi12121582

Ji, M., Xia, Y., Loo, J. F., Li, L., Ho, H. P., He, J., et al. (2020). Automated multiplex nucleic acid tests for rapid detection of SARS-CoV-2, influenza A and B infection with direct reverse-transcription quantitative PCR (dirRT-qPCR) assay in a centrifugal microfluidic platform. *RSC Adv.* 10, 34088–34098. doi: 10.1039/d0ra04507a

Joung, J., Ladha, A., Saito, M., Kim, N., Woolley, A., Segel, M., et al. (2020). Detection of SARS-CoV-2 with SHERLOCK one-pot testing. *N. Engl. J. Med.* 383, 1492–1494. doi: 10.1056/NEJMc2026172

Kampf, G., Lemmen, S., and Suchomel, M. (2021). Ct values and infectivity of SARS-CoV-2 on surfaces. *Lancet Infect. Dis.* 21:e141. doi: 10.1016/S1473-3099(20)30883-5

Kanji, J. N., Zelyas, N., MacDonald, C., Pabbaraju, K., Khan, M. N., Prasad, A., et al. (2021). False negative rate of Covid-19 PCR testing: A discordant testing analysis. *Virol. J.* 18:13. doi: 10.1186/s12985-021-01489-0

Kevadiya, B. D., Machhi, J., Herskovitz, J., Oleynikov, M. D., Blomberg, W. R., Bajwa, N., et al. (2021). Diagnostics for SARS-CoV-2 infections. *Nat. Mater.* 20, 593–605. doi: 10.1038/s41563-020-00906-z

Lee, R., Herigon, J., Benedetti, A., Pollock, N., and Denkinger, C. (2021). Performance of Saliva, oropharyngeal swabs, and nasal swabs for SARS-CoV-2 molecular detection: A systematic review and meta-analysis. *J. Clin. Microbiol.* 59, e02881–20. doi: 10.1128/JCM.02881-20

Li, S., Cheng, Q., Liu, J., Nie, X., Zhao, G., and Wang, J. (2018). CRISPR-Cas12a has both cis- and trans-cleavage activities on single-stranded DNA. *Cell Res.* 28, 491–493. doi: 10.1038/s41422-018-0022-x

Liang, Y., Lin, H., Zou, L., Deng, X., and Tang, S. (2022). Rapid detection and tracking of omicron variant of SARS-CoV-2 using CRISPR-Cas12a-based assay. *Biosens. Bioelectron.* 205:114098. doi: 10.1016/j.bios.2022.114098

Liang, Y., Lin, H., Zou, L., Zhao, J., Li, B., Wang, H., et al. (2021). CRISPR-Cas12a-based detection for the major SARS-CoV-2 variants of concern. *Microbiol. Spectr.* 9:e0101721. doi: 10.1128/Spectrum.01017-21

Liu, D., Shen, H., Zhang, Y., Shen, D., Zhu, M., Song, Y., et al. (2021). A microfluidic-integrated lateral flow recombinase polymerase amplification (MI-IF-RPA) assay for rapid Covid-19 detection. *Lab Chip* 21, 2019–2026. doi: 10.1039/d0lc01222j

Liu, Y. X., Qin, Y., Chen, T., Lu, M., Qian, X., Guo, X., et al. (2021). A practical guide to amplicon and metagenomic analysis of microbiome data. *Protein Cell* 12, 315–330. doi: 10.1007/s13238-020-00724-8

Lopez-Valls, M., Escalona-Noguero, C., Rodriguez-Diaz, C., Pardo, D., Castellanos, M., Milan-Rois, P., et al. (2022). CASCADE: Naked eye-detection of SARS-CoV-2 using Cas13a and gold nanoparticles. *Anal. Chim. Acta* 1205:339749. doi: 10.1016/j.aca.2022.339749

Ludwig, K. U., Schmithausen, R. M., Li, D., Jacobs, M. L., Hollstein, R., Blumenstock, K., et al. (2021). LAMP-Seq enables sensitive, multiplexed COVID-19 diagnostics using molecular barcoding. *Nat. Biotechnol.* 39, 1556–1562. doi: 10.1038/s41587-021-00966-9

Maina, S., Zheng, L., and Rodoni, B. C. (2021). Targeted genome sequencing (TG-Seq) approaches to detect plant viruses. *Viruses* 13:583. doi: 10.3390/v13040583

Mizumoto, K., Kagaya, K., Zarebski, A., and Chowell, G. (2020). Estimating the asymptomatic proportion of coronavirus disease 2019 (Covid-19) cases on board the diamond princess cruise ship, Yokohama, Japan, 2020. *Euro Surveill.* 25:2000180. doi: 10.2807/1560-7917.ES.2020.25.10.2000180

Natarajan, A., Zlitni, S., Brooks, E. F., Vance, S. E., Dahlen, A., Hedlin, H., et al. (2022). Gastrointestinal symptoms and fecal shedding of SARS-CoV-2 RNA suggest prolonged gastrointestinal infection. *Med (N. Y.)* 3, 371–387.e9. doi: 10.1016/j.medj.2022.04.001

Nextstrain (2022). *Genomic epidemiology of SARS-CoV-2 with subsampling focused globally over the past 6 months*. Available online at: https://nextstrain.org/ncov/gisaid/global/6 m (accessed November 13, 2022).

Niu, M., Han, Y., Dong, X., Yang, L., Li, F., Zhang, Y., et al. (2022). Highly sensitive detection method for HV69-70del in SARS-CoV-2 alpha and omicron variants based on CRISPR/Cas13a. *Front. Bioeng. Biotechnol.* 10:831332. doi: 10.3389/fbioe.2022.831332

Norz, D., Grunwald, M., Tang, H. T., Olearo, F., Gunther, T., Robitaille, A., et al. (2021). Rapid automated screening for SARS-CoV-2 B.1.617 lineage variants (Delta/Kappa) through a versatile toolset of qPCR-Based SNP detection. *Diagnostics (Basel)* 11:1818. doi: 10.3390/diagnostics11101818

Notomi, T., Okayama, H., Masubuchi, H., Yonekawa, T., Watanabe, K., Amino, N., et al. (2000). Loop-mediated isothermal amplification of DNA. *Nucleic Acids Res.* 28:E63.

Oh, C., Sashittal, P., Zhou, A., Wang, L., El-Kebir, M., and Nguyen, T. H. (2022). Design of SARS-CoV-2 variant-specific PCR assays considering Regional and temporal characteristics. *Appl. Environ. Microbiol.* 88:e0228921. doi: 10.1128/aem.02289-21

Patchsung, M., Jantarug, K., Pattama, A., Aphicho, K., Suraritdechachai, S., Meesawat, P., et al. (2020). Clinical validation of a Cas13-based assay for the detection of SARS-CoV-2 RNA. *Nat. Biomed. Eng.* 4, 1140–1149. doi: 10.1038/s41551-020-00603-x

Peeling, R. W., Heymann, D. L., Y-Y, Teo, and Garcia, P. J. (2022). Diagnostics for Covid-19: Moving from pandemic response to control. *Lancet* 399, 757–768. doi: 10.1016/s0140-6736(21)02346-1

Piepenburg, O., Williams, C. H., Stemple, D. L., and Armes, N. A. (2006). DNA detection using recombination proteins. *PLoS Biol.* 4:e204. doi: 10.1371/journal.pbio.0040204

Pokhrel, P., Hu, C., and Mao, H. (2020). Detecting the coronavirus (Covid-19). *ACS Sens.* 5, 2283–2296. doi: 10.1021/acssensors.0c01153

Premraj, A., Aleyas, A. G., Nautiyal, B., and Rasool, T. J. (2020). Nucleic acid and immunological diagnostics for SARS-CoV-2: Processes, platforms and pitfalls. *Diagnostics (Basel)* 10:866. doi: 10.3390/diagnostics10110866

Qin, Y., Gao, S., Liu, Y., Wen, Y., Lu, C., Wang, F., et al. (2021). First report of dasheen mosaic virus infecting *Typhonium giganteum* Engl. (Baifuzi) in Henan Province of China. *Plant Dis.* 106:337. doi: 10.1094/PDIS-03-21-0589-PDN

Rai, P., Kumar, B., Deekshit, V., Karunasagar, I., and Karunasagar, I. (2021). Detection technologies and recent developments in the diagnosis of Covid-19 infection. *Appl. Microbiol. Biotechnol.* 105, 441–455. doi: 10.1007/s00253-020-11061-5

Rajib, S. A., Ogi, Y., Hossain, M. B., Ikeda, T., Tanaka, E., Kawaguchi, T., et al. (2022). A SARS-CoV-2 delta variant containing mutation in the probe binding region used for RT-qPCR test in Japan exhibited atypical PCR amplification and might induce false negative result. *J. Infect. Chemother.* 28, 669–677. doi: 10.1016/j.jiac.2022.01.019

Rambaut, A., Holmes, E. C., O'Toole, A., Hill, V., McCrone, J. T., Ruis, C., et al. (2020). A dynamic nomenclature proposal for SARS-CoV-2 lineages to assist genomic epidemiology. *Nat. Microbiol.* 5, 1403–1407. doi: 10.1038/s41564-020-0770-5

Rambaut, A., Holmes, E. C., O'Toole, A., Hill, V., McCrone, J. T., Ruis, C., et al. (2021). Addendum: A dynamic nomenclature proposal for SARS-CoV-2 lineages to assist genomic epidemiology. *Nat. Microbiol.* 6:415. doi: 10.1038/s41564-021-00872-5

Rasmussen, L. D., Richter, S. R., Midgley, S. E., and Franck, K. T. (2022). Detecting SARS-CoV-2 omicron B.1.1.529 variant in wastewater samples by using nanopore sequencing. *Emerging Infect. Dis.* 28, 1296–1298. doi: 10.3201/eid2806.220194

Ratcliff, J., Al-Beidh, F., Bibi, S., Bonsall, D., Costa, C. S., Estcourt, L., et al. (2022). Highly sensitive lineage discrimination of SARS-CoV-2 variants through allele-specific probe PCR. *J. Clin. Microbiol.* 60:e0228321. doi: 10.1128/jcm.02283-21

Rosato, A. E., Msiha, E., Weng, B., Mesisca, M., Gnass, R., Gnass, S., et al. (2022). Rapid detection of the widely circulating B.1.617.2 (Delta) SARS-CoV-2 variant. *Pathology* 54, 351–356. doi: 10.1016/j.pathol.2022.01.001

Safiabadi Tali, S., LeBlanc, J., Sadiq, Z., Oyewunmi, O., Camargo, C., Nikpour, B., et al. (2021). Tools and techniques for severe acute respiratory syndrome Coronavirus 2. *Clin. Microbiol. Rev.* 34, e00228–20. doi: 10.1128/CMR.00228

Schuit, E., Veldhuijzen, I., Veldhuijzen, R. P., van den Bijllaardt, W., Pas, S., Lodder, E., et al. (2021). Diagnostic accuracy of rapid antigen tests in asymptomatic and presymptomatic close contacts of individuals with confirmed SARS-CoV-2 infection: Cross sectional study. *BMJ* 374:n1676. doi: 10.1136/bmj.n1676

Sherlock Biosciences. (2021). *Sherlock CRISPR SARS-CoV-2 kit: Instructions for use*. Boston, MA: Sherlock Biosciences.

Sherrill-Mix, S., Hwang, Y., Roche, A. M., Glascock, A., Weiss, S. R., Li, Y., et al. (2021). Detection of SARS-CoV-2 RNA using RT-LAMP and molecular beacons. *Genome Biol.* 22:169. doi: 10.1186/s13059-021-02387-y

Soares, R. R. G., Madaboosi, N., and Nilsson, M. (2021). Rolling circle amplification in integrated microsystems: An uncut gem toward massively multiplexed pathogen diagnostics and genotyping. *Acc. Chem. Res.* 54, 3979–3990. doi: 10.1021/acs.accounts.1c00438

Soares, R., Akhtar, A., Pinto, I., Lapins, N., Barrett, D., Sandh, G., et al. (2021). Sample-to-answer Covid-19 nucleic acid testing using a low-cost centrifugal microfluidic platform with bead-based signal enhancement and smartphone read-out. *Lab Chip* 21, 2932–2944. doi: 10.1039/d1lc00266j

Spiess, K., Vithiagaran, G., Ellinor, M., Sofie Holdflod, N., Jørgensen, M. G. P., Fomsgaard, A. S., et al. (2021). Rapid surveillance platforms for key SARS-CoV-2 mutations in Denmark. *medRxiv* [Preprint]. doi: 10.1101/2021.10.25.21265484

Su, Y., Anderson, D., Young, B., Linster, M., Zhu, F., Jayakumar, J., et al. (2020). Discovery and genomic characterization of a 382-nucleotide deletion in ORF7b and ORF8 during the early evolution of SARS-CoV-2. *mBio* 11, e01610–e01620. doi: 10.1128/mBio.01610-20

Suo, T., Liu, X., Feng, J., Guo, M., Hu, W., Guo, D., et al. (2020). ddPCR: A more accurate tool for SARS-CoV-2 detection in low viral load specimens. *Emerg. Microbes Infect.* 9, 1259–1268. doi: 10.1080/22221751.2020.1772678

Tandukar, S., Sthapit, N., Thakali, O., Malla, B., Sherchan, S. P., Shakya, B. M., et al. (2022). Detection of SARS-CoV-2 RNA in wastewater, river water, and hospital wastewater of Nepal. *Sci. Total Environ.* 824:153816.

Tang, Y., Wang, Y., Li, Y., Zhao, H., Zhang, S., Zhang, Y., et al. (2022). An integrated rapid nucleic acid detection assay based on recombinant polymerase amplification for SARS-CoV-2. *Virol. Sin.* 37, 138–141. doi: 10.1016/j.virs.2022.01.006

Tu, Y., Jennings, R., Hart, B., Cangelosi, G., Wood, R., Wehber, K., et al. (2020). Swabs collected by patients or health care workers for SARS-CoV-2 testing. *N. Engl. J. Med.* 383, 494–496. doi: 10.1056/NEJMc2016321

USTAR (2022). *The novel coronavirus (2019-nCoV) real-time molecular diagnostic system*. Available online at: https://www.bioustar.com/intro/19.html (accessed November 13, 2022).

Viehweger, A., Krautwurst, S., Lamkiewicz, K., Madhugiri, R., Ziebuhr, J., Holzer, M., et al. (2019). Direct RNA nanopore sequencing of full-length coronavirus genomes provides novel insights into structural variants and enables modification analysis. *Genome Res.* 29, 1545–1554. doi: 10.1101/gr.247064.118

Wang, R., Qian, C., Pang, Y., Li, M., Yang, Y., Ma, H., et al. (2021). opvCRISPR: One-pot visual RT-LAMP-CRISPR platform for SARS-cov-2 detection. *Biosens. Bioelectron.* 172:112766. doi: 10.1016/j.bios.2020.112766

Wang, W., Xu, Y., Gao, R., Lu, R., Han, K., Wu, G., et al. (2020). Detection of SARS-CoV-2 in different types of clinical specimens. *JAMA* 323, 1843–1844. doi: 10.1001/jama.2020.3786

Welch, N. L., Zhu, M., Hua, C., Weller, J., Mirhashemi, M. E., Nguyen, T. G., et al. (2022). Multiplexed CRISPR-based microfluidic platform for clinical testing of respiratory viruses and identification of SARS-CoV-2 variants. *Nat. Med.* 28, 1083–1094. doi: 10.1038/s41591-022-01734-1

Wen, D., Yang, S., Li, G., Xuan, Q., Guo, W., and Wu, W. (2021). Sample-to-answer and routine real-time RT-PCR: A comparison of different platforms for SARS-CoV-2 detection. *J. Mol. Diagn.* 23, 665–670. doi: 10.1016/j.jmoldx.2021.02.010

Wolfel, R., Corman, V. M., Guggemos, W., Seilmaier, M., Zange, S., Muller, M. A., et al. (2020). Virological assessment of hospitalized patients with COVID-2019. *Nature* 581, 465–469. doi: 10.1038/s41586-020-2196-x

World Health Organization (2022a). *Tracking-SARS-CoV-2-variants*. Geneva: World Health Organization.

World Health Organization (2022b). *WHO-2019-nCoV-genomic_sequencing-2021.1*. Geneva: World Health Organization.

Wu, F., Zhao, S., Yu, B., Chen, Y. M., Wang, W., Song, Z. G., et al. (2020). A new coronavirus associated with human respiratory disease in China. *Nature* 579, 265–269. doi: 10.1038/s41586-020-2008-3

Wyllie, A., Fournier, J., Casanovas-Massana, A., Campbell, M., Tokuyama, M., Vijayakumar, P., et al. (2020). Saliva or nasopharyngeal swab specimens for detection of SARS-CoV-2. *N. Engl. J. Med.* 383, 1283–1286. doi: 10.1056/NEJMc2016359

Xing, W., Liu, Y., Wang, H., Li, S., Lin, Y., Chen, L., et al. (2020). A high-throughput, multi-index isothermal amplification platform for rapid detection of 19 types of common respiratory viruses including SARS-CoV-2. *Engineering (Beijing)* 6, 1130–1140. doi: 10.1016/j.eng.2020.07.015

Xun, G., Lane, S. T., Petrov, V. A., Pepa, B. E., and Zhao, H. (2021). A rapid, accurate, scalable, and portable testing system for COVID-19 diagnosis. *Nat. Commun.* 12:2905. doi: 10.1038/s41467-021-23185-x

Yamasoba, D., Kimura, I., Nasser, H., Morioka, Y., Nao, N., Ito, J., et al. (2022). Virological characteristics of the SARS-CoV-2 Omicron BA.2 spike. *Cell* 185, 2103–2115.e19. doi: 10.1016/j.cell.2022.04.035

Yang, J., Kidd, M., Nordquist, A. R., Smith, S. D., Hurth, C., Modlin, I. M., et al. (2021). A Sensitive, portable microfluidic device for SARS-CoV-2 detection from self-collected saliva. *Infect. Dis. Rep.* 13, 1061–1077. doi: 10.3390/idr13040097

Yang, M., Tang, Y., Qi, L., Zhang, S., Liu, Y., Lu, B., et al. (2021). SARS-CoV-2 point-of-care (POC) diagnosis based on commercial pregnancy test strips and a palm-size microfluidic device. *Anal. Chem.* 93, 11956–11964. doi: 10.1021/acs.analchem.1c01829

Yang, S., Pan, X., Yuan, D., Zeng, P., and Jia, P. (2021). Cross-disciplinary approaches to assist with nucleic acid testing for SARS-CoV-2. *Appl. Microbiol. Biotechnol.* 105, 6291–6299. doi: 10.1007/s00253-021-11498-2

Ye, X., Zhou, H., Guo, X., Liu, D., Li, Z., Sun, J., et al. (2022). Argonaute-integrated isothermal amplification for rapid, portable, multiplex detection of SARS-CoV-2 and influenza viruses. *Biosens. Bioelectron.* 207:114169. doi: 10.1016/j.bios.2022.114169

Yedidag, E. N., Koffron, A. J., Mueller, K. H., Kaplan, B., Kaufman, D. B., Fryer, J. P., et al. (1996). Acyclovir triphosphate inhibits the diagnostic polymerase chain reaction for cytomegalovirus. *Transplantation* 62, 238–242. doi: 10.1097/00007890-199607270-00015

Yu, F., Yan, L., Wang, N., Yang, S., Wang, L., Tang, Y., et al. (2020). Quantitative detection and viral load analysis of SARS-CoV-2 in infected patients. *Clin. Infect. Dis.* 71, 793–798. doi: 10.1093/cid/ciaa345

Zhang, W., Liu, K., Zhang, P., Cheng, W., Li, L., Zhang, F., et al. (2021). CRISPR-based approaches for efficient and accurate detection of SARS-CoV-2. *Lab. Med.* 52, 116–121. doi: 10.1093/labmed/lmaa101

Zhang, X., Wu, J., Smith, L. M., Li, X., Yancey, O., Franzblau, A., et al. (2022). Monitoring SARS-CoV-2 in air and on surfaces and estimating infection risk in buildings and buses on a university campus. *J. Expo. Sci. Environ. Epidemiol.* 32, 751–758. doi: 10.1038/s41370-022-00442-9

Zhao, H., Zhang, Y., Chen, Y., Ho, N. R. Y., Sundah, N. R., Natalia, A., et al. (2021). Accessible detection of SARS-CoV-2 through molecular nanostructures and automated microfluidics. *Biosens. Bioelectron.* 194:113629.

Zhu, X., Wang, X., Han, L., Chen, T., Wang, L., Li, H., et al. (2020). Multiplex reverse transcription loop-mediated isothermal amplification combined with nanoparticle-based lateral flow biosensor for the diagnosis of COVID-19. *Biosens. Bioelectron.* 166:112437. doi: 10.1016/j.bios.2020.112437

frontiers | Frontiers in Microbiology

TYPE Original Research
PUBLISHED 03 February 2023
DOI 10.3389/fmicb.2023.1117085

OPEN ACCESS

EDITED BY
Wafa Achour,
Centre National de Greffe de Moelle Osseuse, Tunisia

REVIEWED BY
Ruojun Wang,
Princeton University,
United States
Dharmendra Kumar Soni,
Uniformed Services University of the Health Sciences,
United States

*CORRESPONDENCE
Shanshan Li
✉ lss9011@126.com
Chuanyou Li
✉ lichuanyou6688@hotmail.com
Yu Pang
✉ pangyupound@163.com

†These authors have contributed equally to this work

SPECIALTY SECTION
This article was submitted to Infectious Agents and Disease, a section of the journal Frontiers in Microbiology

RECEIVED 06 December 2022
ACCEPTED 18 January 2023
PUBLISHED 03 February 2023

CITATION
Ren W, Zhou Y, Li H, Shang Y, Zhang X, Yuan J, Li S, Li C and Pang Y (2023) Development and clinical evaluation of a CRISPR/Cas13a-based diagnostic test to detect *Mycobacterium tuberculosis* in clinical specimens. *Front. Microbiol.* 14:1117085. doi: 10.3389/fmicb.2023.1117085

Development and clinical evaluation of a CRISPR/Cas13a-based diagnostic test to detect *Mycobacterium tuberculosis* in clinical specimens

Weicong Ren[1†], You Zhou[2†], Haoran Li[1†], Yuanyuan Shang[1], Xuxia Zhang[1], Jinfeng Yuan[1], Shanshan Li[1*], Chuanyou Li[1,3*] and Yu Pang[1*]

[1]Department of Bacteriology and Immunology, Beijing Chest Hospital, Beijing Tuberculosis and Thoracic Tumor Research Institute, Capital Medical University, Beijing, China, [2]Chest Hospital of Guangxi Zhuang Autonomous Region, Liuzhou, Guangxi, China, [3]Department of Tuberculosis, Beijing Center for Disease Prevention and Control, Beijing, China

Objective: Tuberculosis diagnosis requires rapid, simple and highly sensitive methods. Clustered regularly interspaced short palindromic repeats (CRISPRs) and associated protein (Cas) systems are increasingly being used for clinical diagnostic applications, due to their high flexibility, sensitivity and specificity. We developed a sensitive *Mycobacterium tuberculosis* (MTB) complex polymerase chain reaction (PCR)-CRISPR/Cas13a detection method (CRISPR-MTB) and then evaluated its performance in detecting MTB in clinical specimens.

Methods: The conserved MTB IS1081 sequence was used to design CRISPR-derived RNAs (crRNAs) and T7 promoter sequencing-containing PCR primers for use in the CRISPR-MTB assay, then assay performance was evaluated using 401 clinical specimens.

Results: The CRISPR-MTB assay provided a low limit of detection of 1 target sequence copy/μL and excellent specificity. Furthermore, use of the assay to detect MTB in bronchoalveolar lavage fluid (BALF), sputum and pus samples provided superior sensitivity (261/268, 97.4%) as compared to sensitivities of acid-fast bacilli (130/268, 48.5%) and mycobacterial culture (192/268, 71.6%) assays, and comparable or greater sensitivity to that of GeneXpert MTB/RIF (260/268, 97.0%).

Conclusion: The CRISPR-MTB assay, which provides excellent sensitivity and specificity for MTB detection in sputum, BALF and pus samples, is a viable alternative to conventional tests used to diagnose TB in resource-limited settings.

KEYWORDS

tuberculosis, *Mycobacterium tuberculosis* complex (MTB), GeneXpert MTB/RIF, CRISPR, PCR, diagnosis

Introduction

Tuberculosis (TB), caused by *Mycobacterium tuberculosis* (MTB) complex, remains one of the leading infectious causes of death worldwide, with an estimated 1.6 million TB deaths in 2021 (World Health Organization, 2022). Rapid and accurate TB diagnosis is critical to ensure timely initiation of anti-TB therapy (Walzl et al., 2018). Nevertheless, 58.89% of the estimated 9.9 million

new incident cases that emerge globally each year are undiagnosed. These undiagnosed cases act as a reservoir that fuels ongoing TB transmission that is hindering efforts towards meeting the ultimate goal of global TB eradication (Pai et al., 2016).

Currently, TB detection and diagnosis are based on clinical symptoms, radiologic abnormalities and laboratory test results. However, smear microscopy to detect tubercle bacilli, a century-old test that continues to be widely used for TB diagnosis worldwide, does not provide adequate sensitivity when used to test specimens obtained from children, HIV-infected individuals and extrapulmonary TB cases. Despite its status as a gold standard TB diagnostic test, mycobacterial culture testing of sputum specimens takes several weeks to complete, due to the intrinsic slow growth characteristics of tubercle bacilli (Miller et al., 1994). Hence, due to the abovementioned drawbacks of currently used tests, better tests are needed to facilitate early diagnosis of active TB cases. Recent technological advances have facilitated development of molecular diagnostic assays that have enabled more rapid, specific sensitive detection of *Mycobacterial tuberculosis* (MTB) bacilli in patient specimens. Several of these assays have been endorsed by the World Health Organization for use in initial diagnostic testing of suspected TB cases, such as Xpert MTB/RIF, Xpert MTB/RIF Ultra and loop-mediated isothermal amplification (TB-LAMP). However, the cost per test of such assays, which can be >20-times higher than that of smear microscopy, has hindered efforts to scale up such testing in low-income countries, warranting the development of less expensive and more accurate molecular diagnostic assays to identify active TB cases in resource-limited settings.

Clustered regularly interspaced short palindromic repeats (CRISPR) and associated protein (Cas) systems have been used increasingly for clinical diagnostic applications, due to their high flexibility, sensitivity and specificity (Yan et al., 2019). These novel methods can efficiently detect pathogens in human specimens by converting target nucleic acid sequences into fluorescent signals. For example, the CRISPR/Cas12a-based platform has already been used to diagnose TB and other infectious diseases (Xiao et al., 2020; Li et al., 2021; Qiu et al., 2021; Jiang et al., 2022; Lei et al., 2022). Meanwhile, another CRISPR/Cas system based on Cas13a, an RNA-guided RNA-targeting endonuclease, holds great promise as a molecular diagnostic platform. In fact, by combining Cas13a collateral RNase cleavage with molecular amplification, Zhang and colleagues established a CRISPR/Cas13a-based platform that has already been shown to detect specific viruses with attomolar-scale sensitivity and single-base specificity (Gootenberg et al., 2017; Kellner et al., 2019). However, to our knowledge, the diagnostic efficacy of this platform when used to detect tubercle bacilli has not yet been assessed in clinical practice.

In this study, we aimed to develop a CRISPR/Cas13-based diagnostic assay (hereafter referred to as CRISPR-MTB) for use in detecting MTB bacilli in TB patient specimens. The diagnostic performance of the proposed assay was then evaluated using multiple types of clinical specimens obtained from patients with TB and other respiratory diseases.

Methods

Study participants and collection of clinical specimens

A total of 401 participants, including 268 MTB patients (pulmonary TB and osseous TB) and 133 non-MTB group patients (lung cancer, non-TB infectious diseases of respiratory system) were recruited at Beijing Chest Hospital from August 2021 to May 2022. MTB group patients were diagnosed based on clinical symptoms suggestive of active TB plus positive evidence obtained from results of sputum smear testing that included acid-fast bacilli (AFB), GeneXpert MTB/RIF and mycobacterial culture assays and/or imaging findings. Meanwhile, samples were collected from enrolled patients with other respiratory diseases using the aforementioned assays or other microbiological tests. Genomic DNA was extracted from all clinical specimens and stored at −80°C for CRISPR-MTB testing.

Ethics statement

This study was conducted according to tenets specified in the Declaration of Helsinki of the World Medical Association and approved by the Ethics committee of Beijing Chest Hospital, Capital Medical University (approval number: YJS-2021-0926). Patients or surrogates signed informed consent forms.

Bacterial strains and human DNA

Mycobacterium tuberculosis H37Rv (ATCC27294), *M. bovis* Bacillus Calmette–Guérin (BCG), *M. kansasii, M. abscessus, M. avium, M. intracellulare, M. gordonae,* and *M. fortuitum* were maintained in our laboratory. *Escherichia coli* and *Streptomyces globisporus* were purchased from China General Microbiological Culture Collection Centre (CGMCC). Purified human DNA was purchased from Solarbio Co., Ltd. (Beijing, China) and dissolved in nuclease-free water.

Cas13a protein and other reagents

Primers and plasmids used to clone the MTB target sequence were synthesised by Sangon Co. Ltd. (Shanghai, China). The Cas13a protein used in this study, LwCas13a, was expressed and purified according to instructions provided by Professor Zhang of the Academy of Military Sciences Beijing, China (Gootenberg et al., 2017). LwCas13a protein was quantified according to instructions provided with the Bradford Protein Assay Kit (Beyotime Biotechnology, Shanghai, China). Aliquots of purified LwCas13a protein were stored at −80°C.

Nucleic acid and crRNAs preparation

The conserved MTB insertion element IS1081 that was selected for use as the target of the MTB-detection assay was cloned into the pUC57 vector to construct recombinant plasmids. After recombinant plasmids were confirmed as correct *via* sequencing, they were purified using an EasyPure® HiPure Plasmid MaxiPrep Kit (TransGen Biotech, China). Next, plasmid DNA was quantified based on optical density measurements conducted at 260 nm, then DNA copy number was calculated using the formula $(6.02\times10^{23})\times(\text{ng}/\mu\text{l}\times10^{-9})/(\text{DNA length}\times660)=\text{DNA copy number}/\mu\text{l}$. The crRNA template was an 84-base-pair single-stranded DNA (ssDNA) consisting of the T7 promoter sequence, repeat sequence and target sequence. To prepare crRNA, double-stranded DNA (dsDNA) was amplified using the 84-base-pair ssDNA template and its flanking primers

(Supplementary Table S1). After DNA was extracted with TRIzol Reagent (Invitrogen), the dsDNA product was transcribed overnight at 37°C to generate crRNA using the HiScribe® T7 Quick High Yield RNA Synthesis Kit (New England Biolabs). Thereafter, the transcription product was treated with DNase I at 37°C for 30 min to degrade the dsDNA template, then the final crRNA product was purified using an Agencourt RNAClean XP kit (Beckman Coulter) according to the manufacturer's instructions.

CRISPR-MTB assay

The CRISPR-MTB assay incorporated a PCR amplification step and a subsequent Cas13a detection step. The PCR mixture contained 25 µl 2× MightyAmp® Buffer Ver.3, 0.3 µM IS1081 sense (5′-ACAAAGCTTTCCAAGTCGCA-3′) and 0.3 µM IS1081 antisense (5′-AATTCTAATACGACTCACTATAGGGCCCA GGATCTCTCGG TAGC-3′) primers, 1 µl MightyAmp® DNA Polymerase Ver.3 and 2 µl of DNA sample in a total volume of 50 µl (adjusted with ddH_2O). The PCR amplification programme consisted of denaturation at 95°C for 5 min, followed by 36 cycles (98°C for 10 s, 68°C for 20 s and 1 cycle at 68°C for 5 min) and generated a 237-base-pair amplicon. Cas13a detection was conducted using a reaction mixture containing the following constituents: 0.5 µl of murine RNase inhibitor (New England Biolabs), 45 nM purified LwCas13a, 45 nM crRNA, 125 nM quenched fluorescent RNA reporter (RNAse Alert, Thermo Scientific, Waltham, MA, United States), 0.5 µl of T7 polymerase mix, 1 mM ATP, 1 mM GTP, 1 mM UTP, 1 mM CTP and 2 µl of PCR product in nuclease assay buffer (40 mM Tris–HCl, 60 mM NaCl, 6 mM MgCl2, pH 7.3). Assays were carried out at 37°C for 30 min and monitored for a fluorescent signal using an ABI 7500 instrument (Thermo Fisher, MA, United States). Fluorescein (FAM) fluorescence values were read every 1 min.

Genomic DNA extraction

Sputum was decontaminated with *N*-acetyl-L-cysteine (NALC)-NaOH and suspended as much as possible using a vortex mixer and then was incubated at 37°C for 30 min. Next, 1 ml of treated sputum or other type of sample was transferred to a nuclease-free, sterile 15-ml polypropylene tube. After centrifugation at 8,000 rpm for 10 min, the supernatant was removed and the pellet was washed twice in 2 ml of PBS buffer. Thereafter, the pellet was transferred to a new 1.5-ml tube and resuspended in 50 µl of PBS buffer. Next, tubes were heated at 100°C for 10 min and then were shaken at 1,500 rpm using a Thermo shaker followed by centrifugation for 10 min at 12,000 rpm. For PCR, 2 µl of extracted DNA of each sample served as template.

Statistical analysis

All statistical analyses were performed using SPSS version 20.0 (IBM Corp., Armonk, NY, United States). All figures were created using GraphPad Prism 8 (GraphPad Software, Inc., CA, United States). Continuous variables were expressed as median (range) and categorical variables were expressed as percent (%) values. Student's *t*-test, Mann–Whitney *U* test, Fisher's exact test and Chi-square test were used to evaluate continuous and binomial variables. Intergroup differences were declared significant if two-sided *p*-values were less than 0.05. Statistically significant differences were presented as $^{*}p < 0.05$, $^{**}p < 0.01$, $^{***}p < 0.001$, and $^{****}p < 0.0001$.

Results

Development of the CRISPR/Ca13a-MTB assay

We developed a highly sensitive and simple MTB-detection assay, with steps of this method presented in Figure 1. First, the target sequence (MTP IS1081) was amplified *via* PCR, during which the T7 promoter sequence was attached to 5′ ends of the PCR products. Next, the double-stranded DNA (dsDNA) amplicon was transcribed to generate single-stranded RNA (ssRNA) using T7 RNA polymerase. Thereafter, the ssRNA, under guidance of crRNA, was recognised and bound by Cas13a, which triggered collateral RNase cleavage of the reporter RNA molecule that resulted in release of fluorescent groups into the reaction solution. Significantly enhanced fluorescence indicated the presence of the target gene.

We selected the MTB-specific insertion sequence IS1081 as the target sequence, since this insertion sequence is present in multiple copies per genome, thus improving MTB-detection sensitivity. We then screened five candidate crRNAs (Supplementary Table S2) that targeted different rIS1081 sequences in order to select the crRNAs that produced the most intense fluorescence signal, as assessed using an ABI7500 fluorescence detector. The results (Figure 2A) revealed that the IS1081-b crRNA candidate provided greater fluorescence signal strength than signal strengths of the other four crRNAs.

In order to determine the analytical sensitivity of the CRISPR/Cas13a assay, a plasmid containing the IS1081 insertion sequence was used as a template, then the template was serially diluted to generate dilutions for limit of detection (LOD) evaluation. The results showed that an MTB DNA copy number as low as one copy per test could be detected after 10 min of PCR amplification using the IS1081-b crRNA (Figure 2B).

To confirm assay specificity, genomic DNA from human cells, *M. tuberculosis* (MTB) isolates and the MTB BCG strain, nontuberculous mycobacteria (NTM, including *M. kansasii, M. abscessus, M. avium, M. intracellulare, M. gordonae,* and *M. fortuitum*) or other bacteria (*E. coli*, *S. globisporus*) were tested using the CRISPR-MTB assay. As shown in Figure 2C, only MTB and BCG DNA contained the IS1081 target sequence; thus testing of samples containing only these organisms were the only samples that produced positive detection results. Altogether, these results suggest that CRISPR-MTB is a promising sensitive and specific molecular diagnostic assay for use in MTB detection.

Detection of clinical TB cases using CRISPR/Ca13a-MTB

In order to further evaluate the diagnostic potential of the CRISPR-MTB assay for testing of clinical samples, 401 clinical samples were obtained from 268 TB cases (112 BALF, 141 sputum, and 15 pus specimens) and 133 non-TB cases (114 BALF and 19 sputum specimens) (Supplementary Table S3). Statistical analysis of patient characteristics revealed age differences between patients with and without active TB infections (Supplementary Table S3).

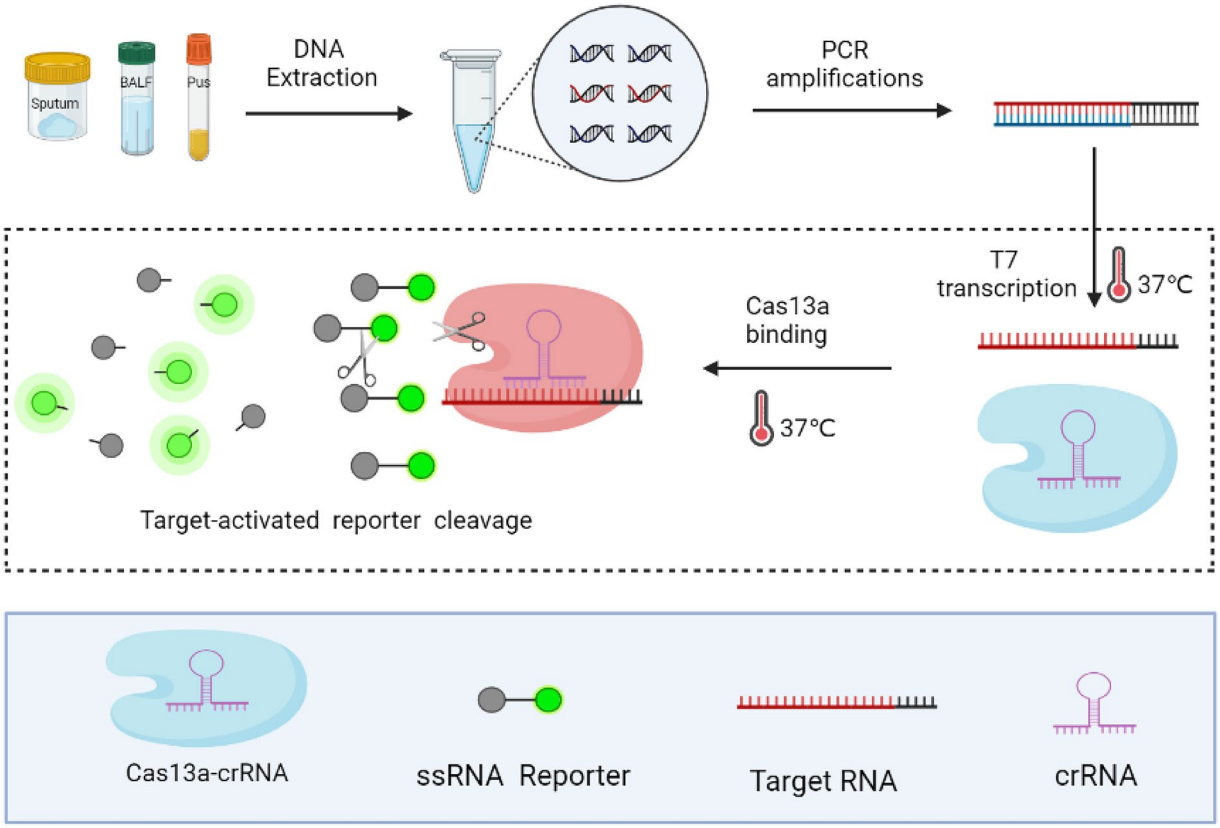

FIGURE 1
Schematic diagram of the CRISPR-MTB assay. Rapid DNA extraction from clinical specimens was performed followed by PCR amplification to increase the amount of target sequence, during which the T7 promoter sequence was attached to 5′ ends of PCR products. Next, PCR products were subjected to the CRISPR/Cas reaction, during which the collateral nuclease activity of Cas proteins was activated upon specific binding of crRNA to the MTB target gene sequence. Increased fluorescent signal produced by cleaved crRNA probes indicated the presence of MTB in clinical specimens.

CRISPR-MTB assay results of control samples containing no template or plasmid DNA containing the target sequence served as the negative control (NC) and positive control (PC), respectively (Figure 3). Based on the final clinical diagnoses of patients as a reference, we evaluated CRISPR-MTB TB diagnostic performance for all patients in our study cohort (Supplementary Tables S4, S5; Figures 3, 4), and then compared MTB-detection results obtained *via* Xpert, culture, AFB and CRISPR-MTB assays for all samples. The results revealed that CRISPR-MTB assay TB diagnostic sensitivity was as high as 97.4% (261/268), which was higher than sensitivities obtained for the mycobacterial culture assay (71.6%, 192/268) and the AFB assay (48.5%, 130/268), and was at least as sensitive as that obtained for GeneXpert MTB/RIF (97.0%, 260/268), Hence, these results suggest that CRISPR-MTB is a highly sensitive TB diagnostic assay.

After further analysis of the influence of clinical specimen type on assay diagnostic performance (Supplementary Tables S4, S5; Figure 4), it was found that CRISPR-MTB provided the highest sensitivity (97.2%, 137/141) when used to test sputum samples from pulmonary TB cases, which was significantly higher than that of AFB (58.9%, 83/141, $p<0.001$) and mycobacterial culture (79.4%, 112/141, $p<0.001$), and comparable to that of Xpert (95.0%, 134/141, $p=0.45$). Similarly, the detection results obtained for BALF samples collected from pulmonary TB cases showed that CRISPR-MTB sensitivity reached 97.3% (109/112), which was higher than that obtained *via* mycobacterial culture (64.3%, 72/112), significantly higher than that obtained *via* AFB (39.3%, 44/112, $p<0.001$) and statistically similar to that obtained *via* Xpert (99.1%, 111/112, $p=1.0$). Meanwhile, testing of pus samples obtained from osseous TB cases *via* both CRISPR-MTB and Xpert detected all TB cases and significantly outperformed both MTB culture (100% vs. 53.3%) and AFB (100% vs. 20.0%) (Figure 4). Interestingly, CRISPR-MTB testing identified six clinically verified TB patients who would not have otherwise received a TB diagnosis based solely on their AFB and mycobacterial culture test results (Figure 5).

In addition, it is noteworthy that the CRISPR-MTB assay produced false-positive results for samples from six patients without TB infections (specificity: 95.5%, 127/133), which included patients with malignancies, non-TB infections and non-infectious inflammatory diseases, as compared to specificities of Xpert and culture assays (97.7 and 99.2%, respectively) (Supplementary Tables S4, S6). Nevertheless, these results collectively suggest that CRISPR/Cas13a-MTB provides excellent sensitivity and specificity for MTB detection, warranting further development of the assay for use in clinical TB diagnosis.

Discussion

The discovery of CRISPR/Cas systems has generated a wave of development of innovative diagnostics that take advantage of both the sensitivity of PCR amplification and the specificity of the CRISPR system. In this study, we successfully developed a CRISPR/Cas13a-based diagnostic assay for use in diagnosing TB-based on clinical specimens.

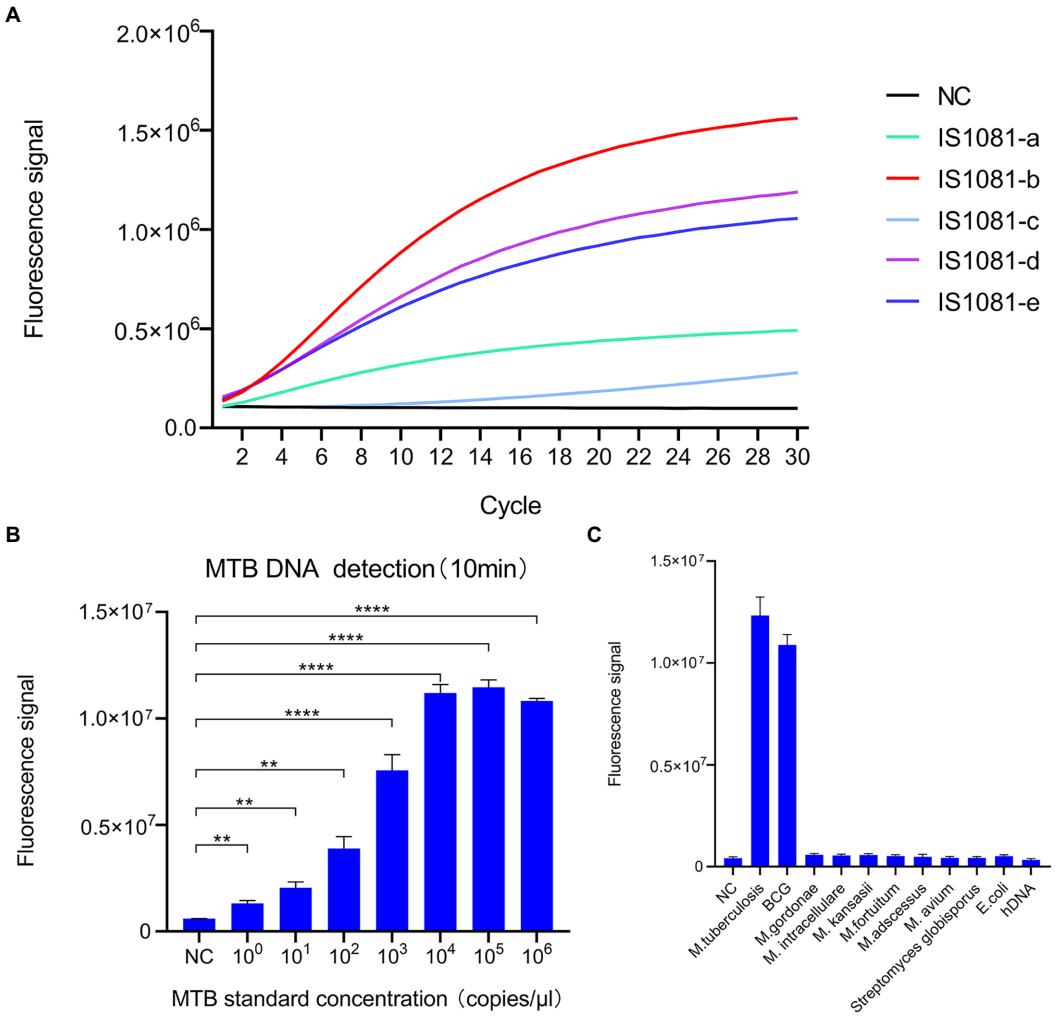

FIGURE 2
Development of the CRISPR-MTB assay. **(A)** Screening of crRNAs for MTB DNA detection ability based on Cas13a-induced detection. The signal obtained for the crRNA probe IS1081-b was greater than signals of all other crRNAs. **(B)** Analytical assessment of CRISPR-MTB sensitivity. CRISPR-MTB could detect one copy of MTB DNA in 10min (n =3 technical replicates; $^{**}p$ <0.01, $^{***}p$ <0.001, $^{****}p$ <0.0001; bars represent mean±standard error of the mean). **(C)** Analytical assessment of CRISPR-MTB specificity. Only genomic DNA of MTB and BCG were explicitly detected at 30 min, while genomic DNA samples without MTB or BCG produced no obvious signal (n =3 technical replicates; bars represent mean±standard error of the mean).

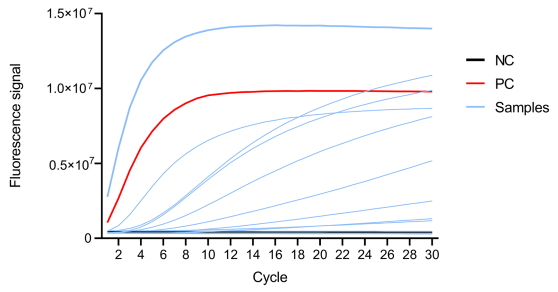

FIGURE 3
Fluorescence signal profile as detected using an ABI 7500 instrument. Black, red, and blue lines represent fluorescent signals from the negative control, positive control and samples, respectively.

The limit of detection (LOD) of our assay (1 copy/μL) was below that reported recently by Ai and colleagues for a CRISPR/Cas12a-based system of 5 copies/μL of MTB DNA, indicating slightly greater sensitivity of our approach (Ai et al., 2019). Additionally, the TB-QUICK MTB-detection assay, which is based on CRISPR-Cas12b and loop-mediated isothermal amplification (LAMP), had a LOD that was as low as 1.3 copies/μL within 2 h, although the exact explanation for this result is unclear. Nevertheless, we speculate that the lower LOD obtained for the CRISPR-MTB assay was mainly due to the production of more precisely targeted transcripts during the T7 RNA polymerase step. However, of greater concern is the greater rate of false-positive results obtained with our assay, which may have been due to its ultra-high sensitivity. Regardless, our primary results demonstrated that the CRISPR-MTB assay provided excellent specificity, since no false-positive results were obtained for any of the six NTM-containing samples or for samples containing *E. coli* and *S. globisporus* species, due to the excellent single-base mismatch specificity of Cas13a (Chen et al., 2019). According to a previous study, as compared with mycobacterial culture testing, the gold standard clinical diagnostic method, the CRISPR-MTB assay developed here provided diagnostic sensitivity of 97.4% and specificity of 95.5%, while the sensitivity and specificity of Xpert were 75.9 and 82.8%, respectively (Moussa et al., 2016), and the sensitivity

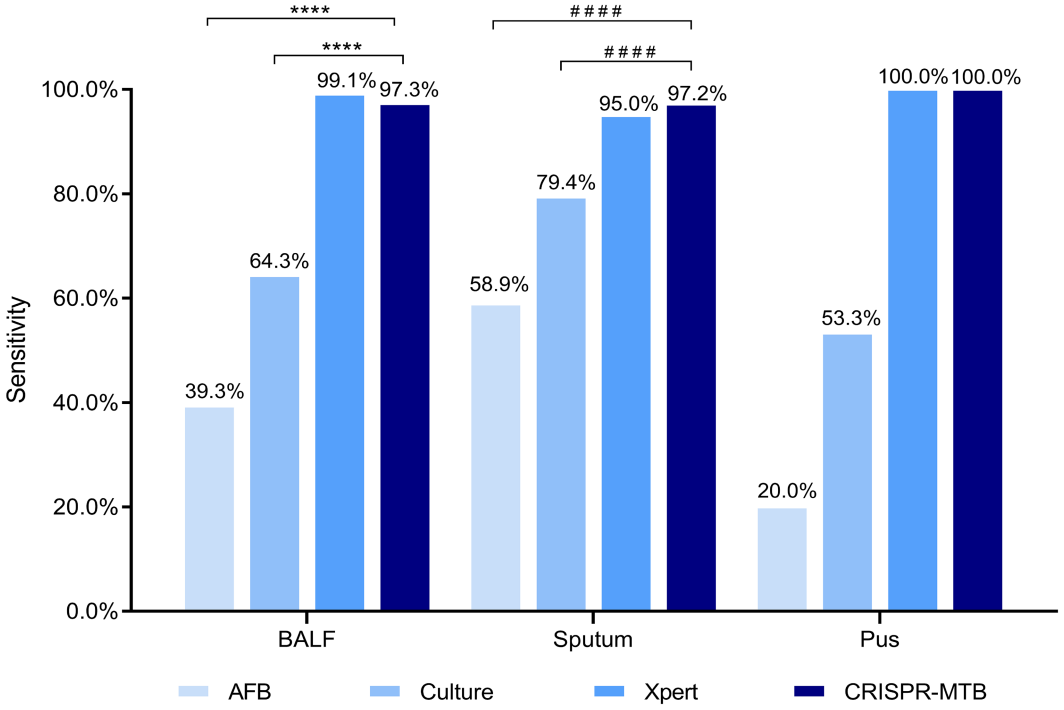

FIGURE 4
Evaluation of CRISPR-MTB sensitivity according to clinical sample type. Two hundred and twenty-six BALF, 160 sputum and 15 pus specimens were tested were detected *via* AFB, Culture, Xpert and CRISPR-MTB assays; ****McNemar test, $p<0.0001$; ####Fisher's exact test, $p<0.0001$.

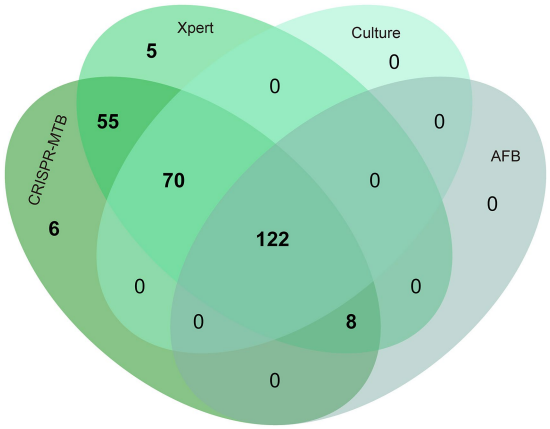

FIGURE 5
Venn diagram showing overlap in TB diagnostic test results obtained for different clinical MTB-detection assays.

and specificity of CRISPR/Cas12a-based test were 79.0 and 98.0%, respectively (Ai et al., 2019). Thus, the CRISPR/Cas13a-based diagnostic is a viable alternative to conventional assays for use in detecting MTB in clinical specimens with high sensitivity and specificity.

As consistent with our analytical test results, CRISPR-MTB assay sensitivity was significantly greater than assay sensitivities obtained using conventional microbiological methods (e.g., smear microscopy, mycobacterial culture). This distinction is particularly important when paucibacillary BALF and pus specimens from extrapulmonary TB cases are tested, thus highlighting CRISPR-MTB as an assay that may improve diagnosis of paucibacillary extrapulmonary TB. Specifically, the CRISPR-MTB assay required a much lower volume of body fluid (500 µl) than that required by conventional methods. Thus, this assay may be more appropriate for identifying tubercle bacilli in specimens obtained from paediatric TB and tuberculous meningitis cases. Our study also emphasises the advantages of CRISPR-based detection assays for use in detecting MTB in specimens with paucibacillary loads, since current molecular MTB-detection assays provide suboptimal results when used to test such specimens, warranting further study.

It is noteworthy that the CRISPR-MTB assay was at least as sensitive as Xpert when used to detect MTB in sputa and other specimens, a result that appears, at first glance, to contradict our results showing that CRISPR-MTB had a lower LOD than Xpert. However, diagnostic sensitivity greatly depends on both the efficiency of a molecular procedure and on sample preparation and DNA extraction efficiencies, such that the ostensibly better performance of the Xpert assay may reflect its more efficient standardized extraction protocol involving fractionation of mycobacteria *via* a pre-sonication step (Patel et al., 2013). This result is supported by results of previous clinical evaluations demonstrating that Xpert outperformed other molecular tests currently used for TB diagnosis. By contrast, the relatively low efficiency of the manual DNA extraction method used in our assay may have reduced CRISPR-MTB sensitivity, while Venter et al. reported that crude DNA extracted using the Xpert cartridge was suitable for MTBDRsl (*Mycobacterium Tuberculosis* Drug Resistance second line) assays and produced more accurate second-line DST results than other DNA extraction methods (Venter et al., 2017). Taken together, these results highlight the importance of using efficient DNA extraction procedures to boost sensitivity of molecular diagnostic assays.

When considering the clinical applicability of the CRISPR/Cas13a-MTB assay, all steps are easily implemented in most clinical settings, since they rely on routine PCR amplification procedures and

universal 'RNA reporter' probes that can be detected using common fluorescence detectors. Moreover, the assay can be completed in only 2 h using relatively inexpensive instrumentation and, as a critically important advantage, at low cost. In fact, in this pilot study the direct cost of each CRISPR/Cas13a-MTB test was less than $2 USD, a cost comparable to that of smear microscopy. However, the CRISPR-MTB assay provides dramatically greater diagnostic accuracy and thus is a superior alternative to routine TB diagnostic assays used currently in resource-limited settings.

We must acknowledge several limitations of the present study. First, the performance of CRISPR/Cas13a-MTB was only assessed based on a limited sample size, which may have weakened the significance of our conclusion, warranting further validation of the assay through testing of a greater number of specimens obtained from a larger patient cohort. Second, previous studies have demonstrated the potential role of LAMP in improving diagnostic sensitivity as compared with conventional real-time PCR (Sam et al., 2021). Thus, integration of LAMP amplification within the CRISPR-Cas13a system will be investigated in the future towards the development of a cost-effective point-of-care (POC) MTB detection assay (Kaminski et al., 2021). Finally, due to the intrinsic ability of Cas13a to target single-stranded RNA, an *in vitro* T7 transcription step was incorporated within the CRISPR-MTB diagnostic assay that undoubtedly increased the turnaround time as compared with DNA-targeting CRISPR-Cas systems.

In conclusion, we have successfully developed a CRISPR/Cas13a-based diagnostic test (CRISPR-MTB) to detect MTB in clinical specimens. Our data demonstrate that the CRISPR-MTB assay provides excellent sensitivity and specificity for rapid identification of MTB in sputum, BALF and pus samples and thus should be suitable for use as a TB diagnostic assay in resource-limited settings.

Data availability statement

The original contributions presented in the study are included in the article/Supplementary materials, further inquiries can be directed to the corresponding authors.

Ethics statement

This study was approved by the Ethics Committee of Beijing Chest Hospital, Capital Medical University. The patients/participants provided their written informed consent to participate in this study.

Author contributions

YP and CL: conceptualisation and methodology, writing — review and editing. WR, HL, YZ, and SL: formal analysis and investigation. YS, XZ, JY, and YZ: data curation. WR, YZ, and HL: writing — original draft preparation. YP and WR: funding acquisition. All authors contributed to the article and approved the submitted version.

Funding

This work was supported by the Beijing Key Clinical Specialty Project (20201214), the Beijing Hospitals Authority Ascent Plan (DFL20191601), the Beijing Hospitals Authority Clinical Medicine Development of Special Funding (ZYLX202122), and the Scientific Research Project of Beijing Educational Committee (KM202010025001). The funders had no role in the study design, data collection, analysis, interpretation or writing of the report.

Conflict of interest

The authors declare that the research was conducted in the absence of any commercial or financial relationships that could be construed as a potential conflict of interest.

Publisher's note

Supplementary material

The Supplementary material for this article can be found online at: https://www.frontiersin.org/articles/10.3389/fmicb.2023.1117085/full#supplementary-material

References

Ai, J. W., Zhou, X., Xu, T., Yang, M., Chen, Y., He, G. Q., et al. (2019). CRISPR-based rapid and ultra-sensitive diagnostic test for mycobacterium tuberculosis. *Emerg. Microbes Infect.* 8, 1361–1369. doi: 10.1080/22221751.2019.1664939

Chen, Y., Yang, S., Peng, S., Li, W., Wu, F., Yao, Q., et al. (2019). N1-Methyladenosine detection with CRISPR-Cas13a/C2c2. *Chem. Sci.* 10, 2975–2979. doi: 10.1039/c8sc03408g

Gootenberg, J. S., Abudayyeh, O. O., Lee, J. W., Essletzbichler, P., Dy, A. J., Joung, J., et al. (2017). Nucleic acid detection with CRISPR-Cas13a/C2c2. *Science* 356, 438–442. doi: 10.1126/science.aam9321

Jiang, C., Tao, D., Geng, Y., Yang, H., Xu, B., Chen, Y., et al. (2022). Sensitive and specific detection of lumpy skin disease virus in cattle by CRISPR-Cas12a fluorescent assay coupled with recombinase polymerase amplification. *Genes* 13:734. doi: 10.3390/genes13050734

Kaminski, M. M., Abudayyeh, O. O., Gootenberg, J. S., Zhang, F., and Collins, J. J. (2021). CRISPR-based diagnostics. *Nat. Biomed. Eng.* 5, 643–656. doi: 10.1038/s41551-021-00760-7

Kellner, M. J., Koob, J. G., Gootenberg, J. S., Abudayyeh, O. O., and Zhang, F. (2019). Sherlock: nucleic acid detection with CRISPR nucleases. *Nat. Protoc.* 14, 2986–3012. doi: 10.1038/s41596-019-0210-2

Lei, R., Li, L., Wu, P., Fei, X., Zhang, Y., Wang, J., et al. (2022). Rpa/CRISPR/Cas12a-based on-site and rapid nucleic acid detection of toxoplasma gondii in the environment. *ACS Synth. Biol.* 11, 1772–1781. doi: 10.1021/acssynbio.1c00620

Li, C., Lin, N., Feng, Z., Lin, M., Guan, B., Chen, K., et al. (2021). CRISPR/Cas12a based rapid molecular detection of acute Hepatopancreatic necrosis disease in shrimp. *Front. Vet. Sci.* 8:819681. doi: 10.3389/fvets.2021.819681

Miller, N., Hernandez, S. G., and Cleary, T. J. (1994). Evaluation of gen-probe amplified mycobacterium tuberculosis direct test and PCR for direct detection of *Mycobacterium tuberculosis* in clinical specimens. *J. Clin. Microbiol.* 32, 393–397. doi: 10.1128/jcm.32.2.393-397.1994

Moussa, H., Bayoumi, F. S., and Ali, A. M. (2016). Evaluation of Genexpert MTB/RIF assay for direct diagnosis of pulmonary tuberculosis. *Saudi Med. J.* 37, 1076–1081. doi: 10.15537/smj.2016.10.14998

Pai, M., Nicol, M. P., and Boehme, C. C. (2016). Tuberculosis diagnostics: state of the art and future directions. *Microbiol. Spectr.* 4. doi: 10.1128/microbiolspec.TBTB2-0019-2016

Patel, V. B., Theron, G., Lenders, L., Matinyena, B., Connolly, C., Singh, R., et al. (2013). Diagnostic accuracy of quantitative PCR (Xpert MTB/RIF) for tuberculous meningitis in a high burden setting: a prospective study. *PLoS Med.* 10:e1001536. doi: 10.1371/journal.pmed.1001536

Qiu, E., Jin, S., Xiao, Z., Chen, Q., Wang, Q., Liu, H., et al. (2021). CRISPR-based detection of helicobacter pylori in stool samples. *Helicobacter* 26:e12828. doi: 10.1111/hel.12828

Sam, I. K., Chen, Y. Y., Ma, J., Li, S. Y., Ying, R. Y., Li, L. X., et al. (2021). TB-QUICK: CRISPR-Cas12b-assisted rapid and sensitive detection of *Mycobacterium tuberculosis*. *J. Infect.* 83, 54–60. doi: 10.1016/j.jinf.2021.04.032

Venter, R., Derendinger, B., de Vos, M., Pillay, S., Dolby, T., Simpson, J., et al. (2017). Mycobacterial genomic DNA from used Xpert MTB/RIF cartridges can be utilised for accurate second-line genotypic drug susceptibility testing and Spoligotyping. *Sci. Rep.* 7:14854. doi: 10.1038/s41598-017-14385-x

Walzl, G., McNerney, R., du Plessis, N., Bates, M., McHugh, T. D., Chegou, N. N., et al. (2018). Tuberculosis: advances and challenges in development of new diagnostics and biomarkers. *Lancet Infect. Dis.* 18, e199–e210. Epub 2018/03/28. doi: 10.1016/s1473-3099(18)30111-7

World Health Organization (2022). *Global Tuberculosis Report 2022*. Geneva: World Health Organization

Xiao, G., He, X., Zhang, S., Liu, Y., Liang, Z., Liu, H., et al. (2020). Cas12a/guide RNA-based platform for rapid and accurate identification of major *Mycobacterium* species. *J. Clin. Microbiol.* 58:e01368-19. doi: 10.1128/jcm.01368-19

Yan, F., Wang, W., and Zhang, J. (2019). CRISPR-Cas12 and Cas13: the lesser known siblings of CRISPR-Cas9. *Cell Biol. Toxicol.* 35, 489–492. doi: 10.1007/s10565-019-09489-1

frontiers | Frontiers in Microbiology

TYPE Original Research
PUBLISHED 09 February 2023
DOI 10.3389/fmicb.2022.1101914

OPEN ACCESS

EDITED BY
Naveen Kumar,
ICAR-National Institute of High Security Animal Diseases (ICAR-NIHSAD), India

REVIEWED BY
Collette Bromhead,
Massey University, New Zealand
Beatriz Escudero Pérez,
Bernhard Nocht Institute for Tropical Medicine (BNITM), Germany
Anne Balkema-Buschmann,
Friedrich-Loeffler-Institut, Germany

*CORRESPONDENCE
Nina M. Pollak
✉ npollak@usc.edu.au
Joanne Macdonald
✉ jmacdon1@usc.edu.au
David McMillan
✉ dmcmill1@usc.edu.au

SPECIALTY SECTION
This article was submitted to Virology, a section of the journal Frontiers in Microbiology

RECEIVED 18 November 2022
ACCEPTED 13 December 2022
PUBLISHED 09 February 2023

CITATION
Pollak NM, Olsson M, Marsh GA, Macdonald J and McMillan D (2023) Evaluation of three rapid low-resource molecular tests for Nipah virus. *Front. Microbiol.* 13:1101914. doi: 10.3389/fmicb.2022.1101914

Evaluation of three rapid low-resource molecular tests for Nipah virus

Nina M. Pollak[1,2,3]*, Malin Olsson[1,2,3], Glenn A. Marsh[4], Joanne Macdonald[1,2,3,5]* and David McMillan[1,2,3]*

[1]Centre for Bioinnovation, University of the Sunshine Coast, Sippy Downs, QLD, Australia, [2]DMTC Limited, Kew, VIC, Australia, [3]School of Science, Technology and Engineering, University of the Sunshine Coast, Sippy Downs, QLD, Australia, [4]Commonwealth Scientific and Industrial Research Organisation Health and Biosecurity, Australian Centre for Disease Preparedness, Geelong, VIC, Australia, [5]BioCifer Pty Ltd., Brisbane, QLD, Australia

Accurate and timely diagnosis of Nipah virus (NiV) requires rapid, inexpensive, and robust diagnostic tests to control spread of disease. Current state of the art technologies are slow and require laboratory infrastructure that may not be available in all endemic settings. Here we report the development and comparison of three rapid NiV molecular diagnostic tests based on reverse transcription recombinase-based isothermal amplification coupled with lateral flow detection. These tests include a simple and fast one-step sample processing step that inactivates the BSL-4 pathogen, enabling safe testing without the need for multi-step RNA purification. The rapid NiV tests targeted the Nucleocapsid protein (N) gene with analytical sensitivity down to 1,000 copies/μL for synthetic NiV RNA and did not cross-react with RNA of other flaviviruses or Chikungunya virus, which can clinically present with similar febrile symptoms. Two tests detected 50,000–100,000 $TCID_{50}$/mL (100–200 RNA copies/reaction) of the two distinct strains of NiV, Bangladesh (NiV_B) and Malaysia (NiV_M), and took 30 min from sample to result, suggesting these tests are well suited for rapid diagnosis under resource-limited conditions due to rapidity, simplicity, and low equipment requirements. These Nipah tests represent a first step toward development of near-patient NiV diagnostics that are appropriately sensitive for first-line screening, sufficiently robust for a range of peripheral settings, with potential to be safely performed outside of biohazard containment facilities.

KEYWORDS

Nipah virus (NiV), rapid test, isothermal amplification, nucleic acid lateral flow, point of care, recombinase polymerase amplification (RPA), recombinase-aided amplification (RAA), nucleic acid extraction

1. Introduction

Nipah virus (NiV) is a zoonotic pathogen of the *Henipavirus* genus causing encephalitis and respiratory symptoms in humans with fatality rates of up to 75% (Eaton et al., 2006). Together with Hendra virus (HeV), they are the only paramyxoviruses that are classified as biosafety level 4 (BSL-4) pathogens. NiV has an exceptionally broad species tropism (Pernet et al., 2012). Transmission to humans can occur directly from *Pteropid* fruit bats (the reservoir host) or from contact with infected pigs (Luby et al., 2009; Clayton, 2017; Gurley et al., 2017), but also contaminated food. Interhuman transmission and nosocomial infections also contribute to Nipah dissemination (Weber and Rutala, 2001; Cleri et al., 2006; Sazzad et al., 2013). Cross-species transmissions of NiV have been reported as the causes of outbreaks in multiple South and Southeast Asia regions including Malaysia (Goh et al., 2000; Parashar et al., 2000), Singapore (Paton et al., 1999), India (Chadha et al., 2006; Arunkumar et al., 2019; Yadav et al., 2022), and Bangladesh (Sazzad et al., 2013). The range of the reservoir hosts has confined henipavirus spillover events to Asia and Australia, but detection of cross-reactive henipavirus antibodies in African bats (including West African fruit bats *Eidolon helvum*) and humans (Drexler et al., 2009; Pernet et al., 2014) markedly increased the number of people worldwide that live in regions at risk of henipavirus spillover events. There is no specific antiviral treatment for NiV infection, however, immunotherapeutic treatments (monoclonal antibody therapies) are currently under development (Playford et al., 2020). Nipah disease has been identified by WHO as a priority disease that poses a great public health risk due to its epidemic potential (World Health Organization [WHO], 2018).

Diagnostic tests with high sensitivity and specificity that enable early detection of NiV infection in humans are needed both for patient treatment and NiV disease control (Weber and Rutala, 2001; Cleri et al., 2006; Ahmed et al., 2009; Luby et al., 2009). Accurate diagnosis of NiV has traditionally relied on serological, molecular or virological analyses, which include western blotting, ELISA, plaque assay, immunofluorescence staining, genome detection by PCR and quantitative PCR, and virus isolation (Chua et al., 2000; Crameri et al., 2002; Drosten et al., 2003; Guillaume et al., 2004; Kashiwazaki et al., 2004; Wacharapluesadee and Hemachudha, 2007; Chiang et al., 2010; Kaku et al., 2012; Kulkarni et al., 2016; Fischer et al., 2018; Jensen et al., 2018; Schulz et al., 2020). Nucleic acid amplification tests (NAATs), such as reverse-transcriptase PCR (RT-PCR), are preferred for detection of active viral infection as they are highly sensitive and detect virus earlier in the infection cycle. However, the required laboratory infrastructure for NAATs may not be available in all endemic settings. For low-resource settings, isothermal amplification technologies offer highly sensitive and specific diagnosis of infectious diseases (Zhao et al., 2015; Zamani et al., 2021; Zheng et al., 2021). Combined with lateral flow detection (LFD), isothermal amplification offers a simple to use assay format that uses minimal equipment and is ideal for diagnostic point-of-care (POC) testing in resource-limited settings (James et al., 2018; Sadeghi et al., 2021; Ahmed et al., 2022). Of these, recombinase polymerase amplification (RPA) and recombinase-aided amplification (RAA) are two promising isothermal technologies. In RPA and RAA, double stranded DNA denaturation and strand invasion that is typically achieved by heat cycling in PCR is instead accomplished by a cocktail of recombinase enzymes, single-stranded binding proteins, and DNA polymerases (Piepenburg et al., 2006). Both methods have potential advantages over other technologies, such as loop-mediated isothermal amplification (LAMP), as they can be performed at near ambient temperature (37–42°C), are more rapid, require a less complex oligonucleotide design, and have higher tolerance to PCR inhibitors (Li et al., 2018, 2020).

Most isothermal approaches still require multiple nucleic acid extraction steps and/or two amplification steps to achieve high specificity (Zamani et al., 2021; Zheng et al., 2021). These additional steps increase workflow complexity, removing many of the benefits of the isothermal amplification for low-resource detection. Here we present a simple one-step method for NiV sample processing that requires only a single subsequent dilution step to enable processed samples to be directly used for nucleic acid amplification. The method uses a novel sample preparation reagent, TNA-Cifer Reagent E (BioCifer, Brisbane, QLD, Australia), which has been shown to process and inactivate dengue virus samples (Pollak et al., 2023). In this study, we trialed TNA-Cifer Reagent E for inactivation of NiV, and also trialed sample preparation testing in conjunction with three Nipah NAAT tests that were developed and characterized as part of our study. The three tests included RAA (Qitian, Jiangsu, China) and two formats of RPA (TwistDX, Cambridge, United Kingdom): the TwistAmp® nfo kit and the TwistAmp® exo kit (Li et al., 2018, 2020). Each test was trialed with LFD to provide a simple, low-resource results read-out. Our simple test format could improve the speed and ease of NiV point-of-care detection, providing vastly simplified workflows and improved laboratory safety that are greatly compatible with operation in low-resource settings.

2. Materials and methods

2.1. Plasmids, RNA transcripts and oligonucleotides

2.1.1. Plasmids

Plasmids (pBIC-A) containing a NiV Nucleocapsid protein (N) gene fragment (JN808863.1, 694-993 nt) and a HeV N gene fragment (MN062017.1, 694-993 nt) were obtained from Bioneer Pacific (Victoria, Australia).

2.1.2. RNA transcripts

Plasmids were linearized by restriction with Xho1 [New England Biolabs (Australia) Pty Ltd., Victoria, Australia], electrophoresed and purified (NucleoSpin® Gel and PCR Clean-up, Macherey-Nagel, Düren, Germany). RNA transcripts were generated by *in vitro* transcription according to manufacturer's instructions (MEGAscript® T7 transcription kit, Invitrogen by Thermo Fisher Scientific Australia Pty Ltd., Victoria, Australia) and RNA concentration was determined with a Qubit 4 Fluorometer (Invitrogen by Thermo Fisher Scientific Australia Pty Ltd., Victoria, Australia).

2.1.3. Oligonucleotides

Primers and probes for the recombinase-based isothermal amplification tests were designed from a consensus sequence of the highly conserved Nucleocapsid protein (N) gene coding region. A total of 100 published N gene sequences were first aligned to identify conserved regions within the gene. Primers and probes targeting these conserved regions were designed according to criteria described by the manufacturer (TwistDX). Primer-BLAST of NCBI was used to confirm the specificity of the primers and probes. The online OligoEvaluator software[1] was used to analyze the potential for primer dimers and hairpins. The primers (5′ biotin labeled reverse) and probes [5′ 6-FAM (fluorescein) labeled] were synthesized by Bioneer Pacific (Victoria, Australia) using HPLC and PAGE purification, respectively. A total of three forward and three reverse primers, as well as two probes were synthesized, and tested in various combinations using reverse transcribed RNA as template and the optimized combination used for testing. Optimized sequences are in **Table 1**.

2.2. Viruses

2.2.1. Virus strains

NiV strains were originally derived from two human isolates, Nipah/Bangladesh/Human/2004/Rajbari, R1 (GenBank accession no. AY988601; NiV_B) and Nipah virus/Malaysia/Human/99 (GenBank accession no. AF212302; NiV_M). Hendra virus was originally isolated from the lung of a horse (Hendra virus/Australia/Horse/2008/Redlands; GenBank accession no. HM044317; HeV). For inactivation, virus stocks were sent to a commercial gamma-irradiator where they were treated with 50 kGy gamma-irradiation. Flavivirus strains were originally derived from clinical isolates included Dengue virus serotypes 1–4 (DENV1 ET00.243 GenBank accession no. JN415499, DENV-2 ET00.300 GenBank accession no. JN568254, DENV-3 East Timor 2000 GenBank accession no. JN575566, and DENV-4 ET00.288 GenBank accession no. JN575585), Japanese encephalitis virus (JEV Nakayama strain GenBank accession no. EF571853), West Nile virus Kunjin strain (WNV_{KUNV} NSW2011 strain GenBank accession no. JN887352), Murray Valley encephalitis virus (MVEV 1-51 strain GenBank accession no. L48972), and Zika virus (ZIKV MR766 GenBank accession no. MW143022). Alphavirus strain originally derived from clinical isolate Chikungunya virus Mauritius 2006 (CHIKV GenBank accession no. MH229986).

2.2.2. Cell culture

Vero cells (Vero C1008) were obtained from ATCC. Vero cells were grown in Minimal Essential Medium (Gibco by Thermo Fisher Scientific Australia Pty Ltd., Victoria, Australia) containing 1× Antibiotic/Antimycotic solution (Gibco by Thermo Fisher Scientific Australia Pty Ltd., Victoria, Australia), and 10% fetal calf serum (Gibco by Thermo Fisher Scientific Australia Pty Ltd., Victoria, Australia), designated MEM-10), at 37°C and 5% CO_2. *Aedes albopictus* clone C6/36 (ATCC CRL-1660) were obtained from the American Type Culture Collection. C6/36 cells were cultured in RPMI 1640 (Thermo Fisher Scientific Australia Pty Ltd., Victoria, Australia) with 5% heat−inactivated fetal bovine serum (Sigma-Aldrich, New South Wales, Australia), 2 mmol/L L−glutamine (Gibco by Thermo Fisher Scientific Australia Pty Ltd., Victoria, Australia) and 100 U/mL Penicillin, 100 μg/mL Streptomycin and 0.25 μg/mL Amphotericin B (Sigma-Aldrich, New South Wales, Australia), at 28°C and 5% CO_2. Before reaching confluency, Vero and C6/36 cells were trypsinized with 0.25% trypsin solution (Gibco by Thermo Fisher Scientific Australia Pty Ltd., Victoria, Australia), and resuspended in fresh growth media before plating onto a new growth surface.

2.2.3. Virus culture

Hendra virus and NiV were propagated in Vero cells with a low MOI infection of T175 cm flask. Virus containing supernatant was harvested at approximately 72 h, when significant cytopathic effect (CPE) was visible, stock clarified by centrifugation at 5,000 g for 10 min and then stored at −80°C until needed. NiV_B, NiV_M, and HeV stock titers were 5.54×10^7 tissue culture infectious dose $(TCID)_{50}$/mL, 1.89×10^7 $TCID_{50}$/mL, and 9.5×10^7 $TCID_{50}$/mL. Flavivirus

1 http://www.oligoevaluator.com

TABLE 1 Primer and probe sequences for the rapid Nipah virus (NiV) tests.

Name	Sequence
NiV F6	ATTCTTCGCAACCATCAGATTYGGGTTGGAG
NiV P2	[5′ Biotin] ATTCCAGAGTGACCTCAACACCATCAARAGC [Internal dS spacer] TGATGCTACTCTACAG [3′ C3 spacer]
NiV R5[a]	[5′ FAM] TCAAGAAGCACCATATAAGGGGCTCTTGGG
NiV R6[b]	[5′ FAM] TTAGTCTGAATTGATTCTTCAAGAAGCACC

[a]$RT\text{-}RPA_{NFO}$ and $RT\text{-}RPA_{EXO}$.
[b]RT-RAA.

strains and CHIKV were propagated to a concentration of 10^5–10^7 $TCID_{50}$/mL in T25 culture flasks seeded with C6/36 cells in RPMI 1,640 growth media as described above, with the exception that 2% FBS was used. Seven days post infection, 2 mL of TRI Reagent (Sigma-Aldrich, New South Wales, Australia) was added to the flask preparation and swirled over the cell area for 1–2 min. To prepare the inactivated viruses for extraction the inoculum was separated into a tube and centrifuged at 3,000 rpm for 10 min at 4°C to separate supernatant from cell pellet. The total RNA for all flavivirus strains and CHIKV was extracted from the infected culture cell lysate stocks using the TRI Reagent extraction protocol, resuspended in nuclease-free water, quantified using a NanoDrop 2000 spectrophotometer (Thermo Fisher Scientific Australia Pty Ltd., Victoria, Australia) and stored at −80°C.

2.3. NiV and HeV RNA isolation and TaqMan PCR

RNA was extracted from NiV and HeV stocks using a MagMAX™ Viral RNA Isolation Kit (ThermoFisher) following manufacturer's instructions. RNA was eluted in a final volume of 60 μL. Samples were stored at −80°C prior to Taqman PCR analyses. TaqMan qPCR was performed using the AgPath-ID one-step reverse transcription-PCR kit (ThermoFisher), targeting the N gene of HeV or NiV as previously described (Feldman et al., 2009). Copy numbers were calculated using a previously derived formula from a standard curve.

2.4. Rapid NiV tests

2.4.1. NiV assay design

The rapid, low-resource NiV tests targeted the Nucleocapsid protein (N) gene of NiV (nt 910-1056 for RT-RPA_{NFO} and RT-RPA_{EXO}, nt 910-1047 for RT-RAA), as this region has previously been used for development of qPCR assays (Jensen et al., 2018). By analyzing multiple sequence alignments of NiV strains of the Malaysian and Bangladesh genotypes, a highly conserved region was chosen for primer and probe design suitable for use in recombinase-based isothermal amplification reactions adhering to the general rules for RPA primer and probe design provided by TwistDx (2018). Different combinations of forward and reverse primers, and probes were tested using reverse transcribed RNA as template to identify an optimized combination used for all further testing.

2.4.2. Sample processing

Gamma-irradiated NiV_B, NiV_M, and HeV isolates diluted in viral transport medium (VTM; Minimal Essential Medium containing 0.1% bovine serum albumin (Thermo Fisher Scientific Australia Pty Ltd., Victoria, Australia), 500 U/mL Penicillin (Gibco by Thermo Fisher Scientific Australia Pty Ltd., VIC, Australia), 500 μg/mL Streptomycin (Gibco by Thermo Fisher Scientific Australia Pty Ltd., Victoria, Australia) and 2,500 μg/mL Fungizone (Gibco by Thermo Fisher Scientific Australia Pty Ltd., Victoria, Australia) were mixed with TNA-Cifer Reagent E (BioCifer, Brisbane, QLD, Australia) at a ratio of 1:1 (4 μL sample to 4 μL TNA-Cifer Reagent E) and incubated for 2 min on ice. Processed samples were then diluted 1:6 (5 μL processed sample to 25 μL nuclease-free water) and immediately used as a template for either RT-nfoRPA (section "2.4.3 NiV RT-nfoRPA or RT-exoRPA tests"), RT-exoRPA (section "2.4.3 NiV RT-nfoRPA or RT-exoRPA tests"), or RT-RAA (section "2.4.4 NiV RT-RAA tests") reaction without further RNA purification.

2.4.3. NiV RT-nfoRPA or RT-exoRPA tests

Each test reaction was prepared using our developed primers and probe combined with either the TwistAmp™ nfo kit (TwistDX, Cambridge, United Kingdom) or the TwistAmp™ exo kit (TwistDX, Cambridge, United Kingdom), with final reaction conditions of 1× rehydration buffer and 1/5 rehydrated lyophilized pellet, forward primer (420 nM), reverse primer (420 nM), probe (120 nM), Ribolock (10 U), and Moloney Murine Leukemia virus reverse transcriptase (mMLV, 40 U) including 1 μL template (from section "2.4.2 Sample processing") and magnesium acetate (14 mM) to a final reaction volume of 10 μL. Reactions using the TwistAmp™ exo kit also contained Endonuclease IV (2 U; New England Biolabs, Victoria, Australia). Reactions were incubated at 39°C for 20 min before lateral flow detection.

2.4.4. NiV RT-RAA tests

Each test reaction was prepared using our developed primers and probe combined with the RAA kit (Qitian, Jiangsu, China), with final reaction conditions of 1.224× rehydration buffer and 1/5 rehydrated lyophilized pellet, forward primer (420 nM), reverse primer (420 nM), probe (240 nM), Moloney Murine Leukemia virus reverse transcriptase (mMLV, 40 U; Promega, New South Wales, Australia), SuperScriptIV (40 U; Invitrogen, Victoria, Australia), RNase H (0.4 U; Invitrogen, Victoria, Australia) and Endonuclease IV (2 U; New England Biolabs, Victoria, Australia) including 1 μL template (from section "2.4.2 Sample processing") and magnesium acetate (14 mM) to a final reaction volume of 10 μL. Reactions were incubated at 39°C for 20 min before lateral flow detection.

2.4.5. Lateral flow detection and analysis

Two microliters of the amplified test reaction mix (from sections "2.4.3 NiV RT-nfoRPA or RT-exoRPA tests or 2.4.4 NiV RT-RAA tests") was added to pre-activated HybriDetect lateral flow strips (Milenia Biotec, Giessen, Germany) (Rames and Macdonald, 2019), a universal dipstick for the detection of biotin- and fluorescein (FITC or FAM)-labeled analytes based

on lateral flow technology using gold particles. The strips were then placed for 5 min in 100 μL running buffer (Li et al., 2019), analyzed by eye and scanned with an Epson Perfection V39 Flatbed Scanner (Epson, NSouth Wales, Australia). On visual analysis, a single control line depicted the absence of NiV and the appearance of two lines i.e., a test line along with the control line indicated the presence of NiV. Lateral flow strips were analyzed as previously described (James et al., 2018; Li et al., 2019) using ImageJ software (National Institutes of Health, MD, USA).

2.5. Statistical data analyses

Diagnostic test evaluation and comparison was determined using the online MedCalc statistical software.[2]

3. Results

3.1. NiV isothermal assay analytical sensitivity

To test the analytical sensitivity of the three NiV assays (NiV RT-nfoRPA-LFD, RT-exoRPA-LFD, and RT-RAA-LFD), serial dilutions of a synthetic template RNA with known copy number were assessed. The analytical sensitivity ranged from the highest concentration tested (1×10^6 copies/μL) to as little as 1,000 copies/μL for all three tests (**Figures 1A–C**).

3.2. NiV isothermal assay analytical specificity

Since symptoms of NiV infection are similar to other febrile diseases, specific diagnosis is critical for containment of an outbreak and to facilitate appropriate patient care. To confirm our NiV assays were specific for NiV, we next trialed our three tests against synthetic HeV RNA transcripts and RNA extracts from Chikungunya virus (CHIKV), Dengue virus serotypes 1-4 (DENV 1-4), Japanese encephalitis virus (JEV), Murray Valley encephalitis virus (MVEV), West Nile virus Kunjin strain (WNV_{KUNJ}), Yellow fever virus (YFV), and Zika virus (ZIKV). Our Nipah tests did not detect CHIKV or any flaviviruses, however, HeV was detected at very high concentrations (10^6 copies/μL) showing faint positive test bands (**Figures 2A–C**). Testing HeV at lower concentration (10^5 copies/μL) revealed no positive test result with the RT-nfoRPA-LFD and RT-RAA-LFD. The RT-exoRPA-LFD resulted in a positive test result in one out of two replicates, suggesting more pronounced non-specific detection of synthetic HeV RNA compared to the other two test formats.

3.3. Inactivation of NiV using TNA-Cifer Reagent E

To develop a truly low-resource test, we wanted to trial the NAAT tests in conjunction with sample preparation using TNA-Cifer Reagent E. However, since NiV is a BSL-4 agent, we first had to determine the conditions in which TNA-Cifer Reagent E would inactivate NiV, before any processed samples could be used for NAAT detection. TNA-Cifer Reagent E was found to completely inactivate NiV_B (5.54×10^7 $TCID_{50}$/mL) in 2 min after mixing the sample and reagent in a 1:1 ratio, and this was confirmed by serial passaging of inactivated virus for a further two serial passages at 2, 5, and 10 min (**Figure 3A**). However, sample to reagent ratios of 5:1 and 9:1 failed to inactivate NiV_B during any of the tested incubation periods (2, 5, and 10 min, **Figure 3B**), and subsequent testing with NiV_B and NiV_M demonstrated that sample to reagent ratios of 2:1 also failed after both 5 and 10 min incubation (**Figure 3C**). These results suggested that equal parts of sample and TNA-Cifer Reagent E were required for successful NiV inactivation. Further investigation confirmed complete inactivation of both NiV_B (5.54×10^7 $TCID_{50}$/mL) and NiV_M (1.89×10^7 $TCID_{50}$/mL) at a 1:1 ratio after 2 min incubation, and this was confirmed by serially passaging culture supernatant through a further two serial passages (**Figure 3D**).

3.4. Sensitivity and specificity of rapid NiV tests using rapidly processed gamma-irradiated henipavirus isolate samples

By combining the rapid sample preparation method with our three isothermal NiV assays, we were able to develop three rapid NiV tests able to provide results in 30 min from sample to results. The rapid NiV_{NFO}, rapid NiV_{EXO}, and rapid NiV_{RAA} tests combined rapid sample preparation followed by RT-nfoRPA-LFD, RT-exoRPA-LFD, or RT-RAA-LFD, respectively. To assess strain-specific sensitivities, two distinct strains of gamma-irradiated NiV isolates, Bangladesh (NiV_B), and Malaysia (NiV_M), were serially diluted in viral transport medium and tested with each rapid NiV test. Using this approach, we detected both NiV_B and NiV_M with two of the three rapid NiV tests (NiV_{NFO} and NiV_{EXO}) in the range of 50,000–100,000 $TCID_{50}$/mL, the equivalent of approximately 50–100 infectious particles per microliter (**Figures 4A, B**). However, the rapid NiV_{RAA} test was shown to detect virus at only 1,000,000 $TCID_{50}$/mL (**Figure 4C**). All three NiV tests

2 https://www.medcalc.org/calc/diagnostic_test.php

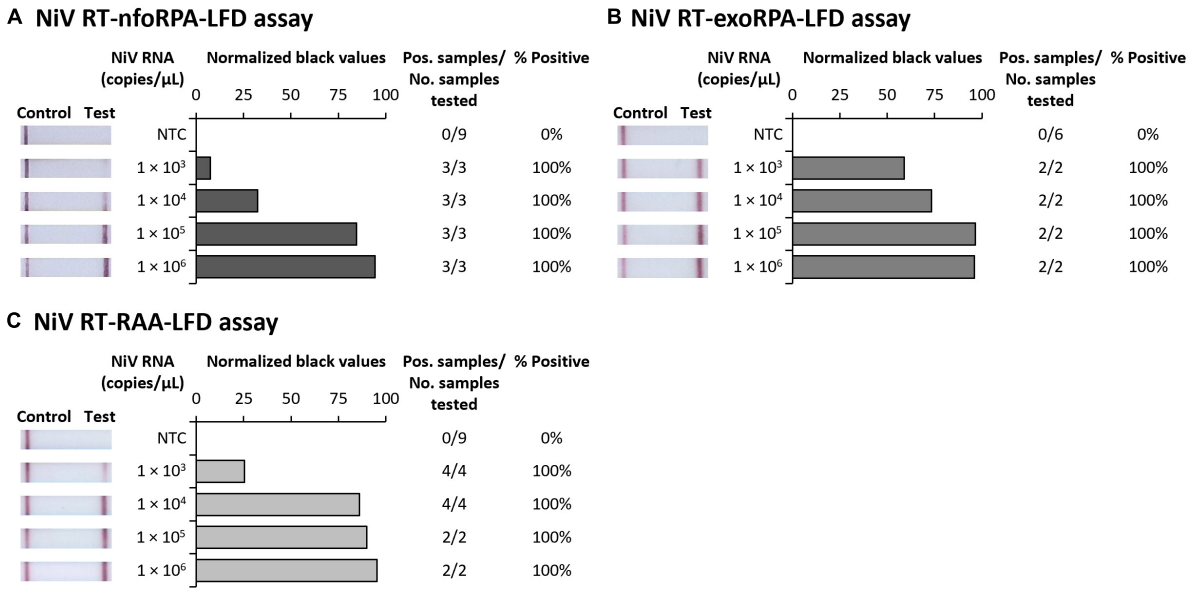

FIGURE 1
Analytical sensitivities of three Nipah virus recombinase-based isothermal amplification lateral flow detection assays with RNA transcripts. Sensitivity testing used Nucleoprotein (N) gene fragment RNA transcripts diluted 10-fold in water for RT-nfoRPA-LFD **(A)**, RT-exoRPA-LFD **(B)**, and RT-RAA-LFD **(C)**. Images of lateral flow strips with two bands (control and test band) indicates the sample is positive for NiV synthetic RNA transcript, and single control band indicates a valid reaction with negative sample. Photograph of lateral flow strips with control bands (all samples) and test bands (positive samples) compared to copy number of serially diluted NiV RNA (copies/µL) and no template control (NTC) (left). Normalized pixel density (normalized black values) from the lateral flow test strip displayed (middle). Positive samples compared to number of samples tested at that dilution was used to calculate the percentage of positive tests performed at that dilution (right).

did not detect HeV at very high concentrations (95,000,000 $TCID_{50}$/mL).

Combining all gamma-irradiated virus testing results from Figure 4 together, we assessed the diagnostic sensitivity and specificity of the test, for detection of henipavirus isolate samples at 100,000 $TCID_{50}$/mL or higher (n = 25, Table 2). The best performing test, the rapid NiV_{NFO} test, had 100.0% diagnostic sensitivity (95% CI: 79.4–100.0%) and 100.0% diagnostic specificity (95% CI: 29.24–100.0%). The other two Rapid NiV tests (NiV_{EXO} and NiV_{RAA}) demonstrated diagnostic sensitivities of 93.8% (95% CI: 69.8–99.8%) and 62.5% (95% CI: 35.4–84.8%), respectively, with both showing 100% diagnostic specificity (95% CI: 29.2–100.0%) (n = 25, Table 2).

4. Discussion

Given the often rural and remote NiV outbreak settings, NiV diagnostics should ideally be deployable for use in decentralized laboratories or field-based settings, and at the same time, still fulfill the need for sensitive and accurate detection of early NiV infection. Isothermal NAAT platforms have lower infrastructure requirements than laboratory-based diagnostics. If these could be combined with safe and simple sample preparation methods, they could be deployable for low-resource use, with fewer training requirements for healthcare workers. In this study, we developed and evaluated three rapid NiV tests in a simple low-resource format. These tests use a simple and rapid sample preparation protocol, a single-temperature isothermal amplification technology (RT-nfoRPA, RT-exoRPA, or RT-RAA), and are coupled with LFD for easy result interpretation within 30 min. The tests were shown to be specific for detection of NiV, and did not detect other viruses which can clinically present with similar febrile symptoms including flaviviruses, CHIKV. For the closely related HeV we note that synthetic HeV transcript was detected at very high concentrations (10^6 copies/µL), but gamma-irradiated HeV could not be detected at very high titers (9.5×10^7 $TCID_{50}$/mL) suggesting that the assays were specific for NiV. The tests can be used without expensive laboratory equipment, and could prevent extended waiting periods for NiV testing, by enabling on-site low-resource testing rather than delayed results due to sample shipment to central laboratory testing facilities.

The majority of previous studies have used RT-qPCR for the detection of NiV nucleic acids. Only one study has reported the development of an RT-LAMP assay targeting the N gene capable of detection of 100 pg (estimated approximately 10^7 copies/reaction) of total Nipah pseudovirus RNA, suggesting its detection limit was comparable to conventional RT-qPCR (Ma et al., 2019). The reported assay tested RNA prepared with a viral nucleic acid extraction kit and produced results

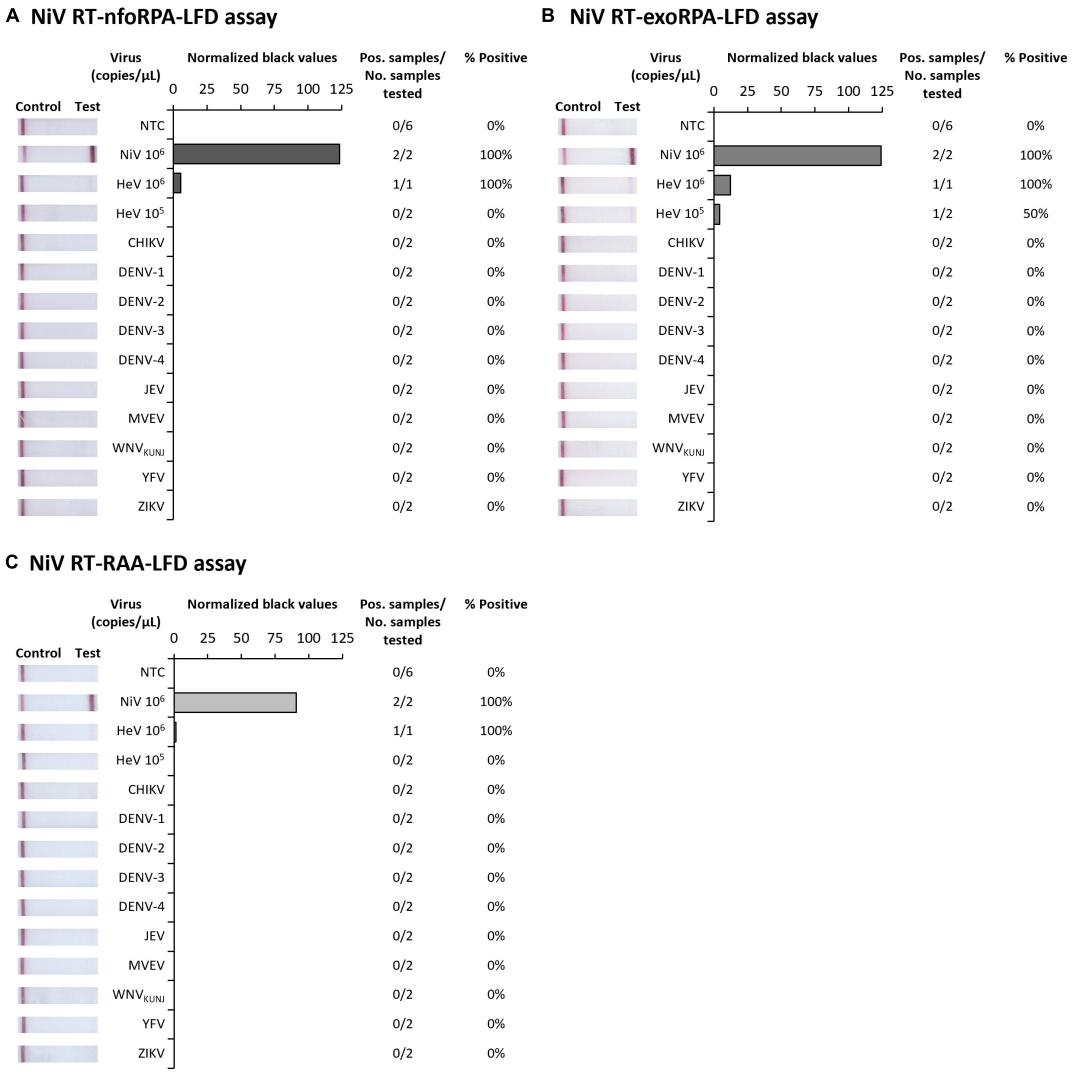

FIGURE 2
Analytical specificities of three Nipah virus recombinase-based isothermal amplification lateral flow detection tests. Specificity testing used synthetic RNA of NiV and Hendra virus (HeV), and viral RNA extracts from alphavirus Chikungunya virus (CHIKV), and flaviviruses DENV-1, DENV-2, DENV-3, DENV-4, JEV, MVEV, WNV_{KUNJ}, YFV, and ZIKV for RT-nfoRPA-LFD **(A)**, RT-exoRPA-LFD **(B)**, and RT-RAA-LFD **(C)**. Images of lateral flow strips with two bands (control and test band) indicates the sample is positive for respective viral RNA extract, and single control band indicates a valid reaction with negative sample. Nuclease-free water was tested as the no template control (NTC; left). Normalized pixel density (normalized black values) from the test displayed (middle). Positive samples compared to number of samples tested using different viral RNA transcripts and extracts were used to calculate percentage of positive samples (right).

in either 45 or 50 min with a Realtime Turbidimeter or a calcein dye detection method with a water bath (Ma et al., 2019). In comparison, two of our three rapid NiV tests (rapid sample processing followed by RT-nfoRPA-LFD or RT-exoRPA-LFD) had a detection limit ranging from 50,000 to 100,000 $TCID_{50}$/mL, equivalent to 20–263 infectious particles per microliter, or 20–250 RNA copies/reaction. The best performing rapid NiV test (rapid sample processing combined with RT-nfoRPA-LFD) showed 100.0% diagnostic sensitivity (95% CI: 79.4–100.0%) and 100.0% diagnostic specificity (95% CI: 29.24–100.0%) for detection of >100,000 $TCID_{50}$/mL virus (100–200 RNA copies/reaction). The rapid NiV test based on the exo product which required the addition of the enzyme endonucleases IV showed reduced diagnostic sensitivity (93.8, 95% CI: 69.8–99.8%; 200–250 RNA copies/reaction), but may represent a suitable alternative to the currently unavailable nfo product. In comparison, our rapid NiV test utilizing RAA kits only showed a diagnostic sensitivity of 62.5% (95% CI: 35.4–84.8%; 4,000–6,000 RNA copies/reaction), despite optimization which included slightly more rehydration buffer (1.224×) which slightly improved results. However, RT-RAA tests have previously been reported to reach high sensitivity (>95%) for

A

NiV_B to TNA-Cifer Reagent E	CPE positive wells/total number of wells								
	2 minutes			5 minutes			10 minutes		
	P1	P2	P3	P1	P2	P3	P1	P2	P3
1:1	0/3	0/3	0/3	0/3	0/3	0/3	0/3	0/3	0/3
5:1	3/3	-	-	3/3	-	-	3/3	-	-
9:1	3/3	-	-	3/3	-	-	3/3	-	-
1:1 PBS control	3/3	-	-	3/3	-	-	3/3	-	-

B

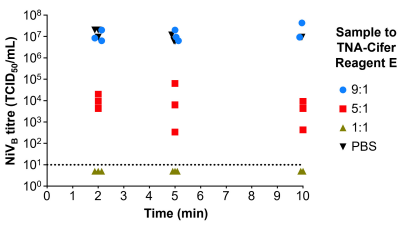

C

Sample to TNA-Cifer Reagent E	CPE positive wells/total number of wells								
	NiV_B			NiV_B			NiV_M		
	5 minutes			10 minutes			5 minutes		
	P1	P2	P3	P1	P2	P3	P1	P2	P3
1:1	0/3	0/3	0/3	0/3	0/3	0/3	0/3	0/3	0/3
2:1	3/3	-	-	3/3	-	-	1/2*	1/2*	1/2*
5:1	3/3	-	-	3/3	-	-	3/3	-	-
1:1 PBS control	3/3	-	-	3/3	-	-	3/3	-	-

D

Sample to TNA-Cifer Reagent E 1:1	CPE positive wells/total number of wells		
	2 minutes		
	P1	P2	P3
NiV_B	0/3	0/3	0/3
NiV_B PBS control	3/3	-	-
NiV_M	0/3	0/3	0/3
NiV_M PBS control	3/3	-	-

FIGURE 3
Rapid sample processing inactivates Nipah virus. **(A)** NiV_B recovery from samples (5.54×10^7 $TCID_{50}$/mL) incubated with and without TNA-Cifer Reagent E at a 1:1, 5:1 and 9:1 ratio, for 2, 5 or 10 min at room temperature. **(B)** NiV_B was incubated with TNA-Cifer Reagent E at 1:1, 5:1 and 9:1 ratio or PBS at 9:1 for the indicated times at room temperature and the virus titer determined by $TCID_{50}$ assays using Vero E6 cells. The dotted line indicates limit of detection of assays based on a starting 1/10 dilution of samples. This experiment was performed one time, with three samples taken per time point. **(C)** NiV recovery from samples (NiV_B 5.54×10^7 $TCID_{50}$/mL; NiV_M 1.89×10^7 $TCID_{50}$/mL) incubated with and without TNA-Cifer Reagent E at a 1:1, 2:1 and 5:1 ratio for 5 and/or 10 min at room temperature. **(D)** NiV recovery from samples (NiV_B 5.54×10^7 $TCID_{50}$/mL; NiV_M 1.89×10^7 $TCID_{50}$/mL) incubated with and without TNA-Cifer Reagent E at a 1:1 ratio and 2 min at room temperature. **(A, C, D)** Mixtures (100 μL) were added to individual wells of Vero E6 cells (approximately 70% confluent) on 6-well plate and incubated for 7 days. Individual wells were scored as either positive or negative for the presence of cytopathic effect (CPE) typical of Nipah virus (syncytia). Wells showing no evidence of NiV CPE had 200 μL supernatant removed and added to a new 6-well plate with fresh Vero cells (blind passage), again incubated for 7 days before scoring for NiV CPE. This blind passaging of negative samples was done for two additional passages (three 7 days incubations on Vero cells: P1, P2, and P3). Number of CPE positive wells compared to total number of wells for each condition. Green highlighted boxes show samples that were inactivated by TNA-Cifer Reagent E and showed no CPE. Orange highlighted boxes indicate samples that were not inactivated and showed CPE. Gray highlighted boxes mark where samples were not passaged due to the presence of CPE in the previous passage. Each experiment was performed in triplicate, except were indicated by * the experiment was performed in duplicate due to human error.

the detection of SARS-CoV-2 (Qian et al., 2020; Subsoontorn et al., 2020).

Preparing samples for nucleic acid testing is a critical step for any field-based diagnostic POC method, particularly for NAATs that traditionally require high purity of samples. Diagnosis of suspected Nipah cases could greatly benefit from the elimination of traditional RNA extraction kit use, particularly where a lack of infrastructure exists and excludes the use of automated costly robotics systems. Previously reported in house NAATs employed for NiV detection used commercial RNA extraction reagents and kits [reviewed in Mazzola and Kelly-Cirino (2019)], which require time consuming procedures or costly automated robotic systems, and cannot be performed if access to centralized well-equipped laboratories including robots, centrifuges and/or vacuum manifolds, is limited. One key advantage of our rapid NiV tests was the unique sample processing method that enabled rapid virus detection in NiV isolates, while inactivating the BSL-4 pathogen in the first step of the procedure. Our sample processing method reduced sample preparation time to only 2 min, involving the direct addition of a single reagent to the sample followed by dilution in nuclease-free water before subsequent isothermal amplification and did not require time-consuming multistep RNA extraction with a kit. Our simple sample processing method can provide a pathway for safer POC testing, or safer near-patient POC testing in low-resource environments that do not have full biohazard facilities. Additional work is required to clinically validate the performance and operational utility of our rapid NiV tests. Validation efforts for NiV tests have been limited due to the lack of NiV-positive human samples. This study limitation could be addressed by spiking gamma-irradiated NiV into blood, plasma, and serum, in an effort to show operational suitability with clinical samples. In addition, further analysis of NiV inactivation should consider the minimal TNA-Cifer Reagent E concentration, as well as the effect of serum, sub-optimal sample matrices, or other potential inhibitors of inactivation before field trialing tests.

NiV has both epidemic and pandemic potential (Gomez Roman et al., 2020). The virus has been shown to transmit

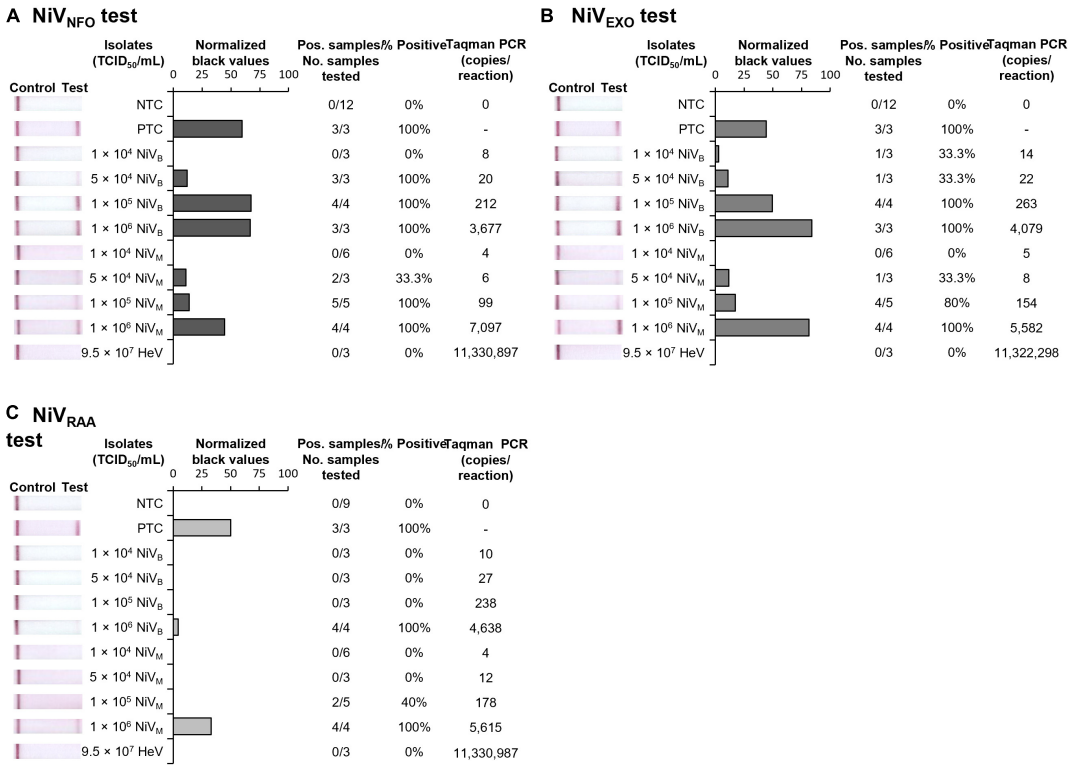

FIGURE 4
Sensitivity and specificity of three rapid NiV tests. Sensitivity testing used rapidly processed NiV_B and NiV_M strain isolates for RT-nfoRPA-LFD **(A)**, RT-exoRPA-LFD **(B)**, and RT-RAA-LFD **(C)** assays compared to $TCID_{50}$/mL determined by immunolabeling assays and copies/reaction determined by comparative Taqman PCR. Images of lateral flow strips with two bands (control and test band) indicates the sample is positive for NiV, and single control band indicates a valid reaction with negative sample. Photograph of lateral flow strips with control bands (all samples) and test bands (positive samples) compared to titer of rapidly processed serially diluted NiV isolate ($TCID_{50}$/mL) and no template control (NTC) (left). Normalized pixel density (normalized black values) from the lateral flow test strip displayed (middle). Positive samples compared to number of samples tested at that dilution was used to calculate the percentage of positive tests performed at that dilution (right).

through contaminated food, as well as *via* direct contact with animal excretions or infected humans. Human NiV incubation periods after exposure are believed to range from 4 to 14 days, with reports as long as 45 days (Chong et al., 2002). It is unclear if transmission can occur during this time, but likely begins during the incubation period, which has been demonstrated in pigs (Middleton et al., 2002). Pigs and experimentally infected cats can shed NiV in respiratory secretions and urine (Middleton et al., 2002; Mungall et al., 2007). Many other viruses in the Paramyxoviridae family (like measles virus) transmit well between people, so there is concern that a novel Nipah variant with increased transmission could arise. Our rapid NiV test could be used to rapidly detect disease at or near-POC, to enable early interventions that can reduce morbidity and mortality. It would also be interesting to consider extending this rapid test format to detect all henipaviruses (NiVB/NiVM, HeV, and Cedar virus) or all paramyxoviruses to further improve detection of these pathogens at the POC.

In conclusion, we developed three rapid Nipah tests and evaluated their potential as near-patient POC or POC diagnostic suitable for resource-limited settings. We determined the analytical sensitivity of the three recombinase-based isothermal amplification LFD tests to be at least 1,000 copies/μL, and confirmed the tests did not detect any other viruses displaying similar febrile symptoms. The rapid NiV tests demonstrated excellent diagnostic specificity and varying degrees of sensitivity (62.5–100.0%) for detection of >100,000 $TCID_{50}$/mL virus. The tests are advantageous compared to conventional methods such as RT-PCR, with improved procedural simplicity, rapid sample processing and turnaround time (30 min from sample preparation to result), minimal equipment requirements, and improved safety as the BSL-4 pathogen is inactivated in the very first step of the procedure. Our three Nipah tests represent a first step toward development of near-patient POC or POC NiV diagnostics that are affordable, appropriately sensitive for first-line screening, and sufficiently robust for adequate testing at the community level. Future research could focus on establishing operational suitability of the selected rapid NiV test, by integration of the whole testing process into a microfluidic system to facilitate a rapid, accurate, and safe testing procedure for testing at the POC level.

TABLE 2 Diagnostic test evolution of three rapid Nipah virus (NiV) tests.

Rapid NiV test	#True Pos.	True Neg.	False Pos.	False Neg.	Total tested	Sensitivity (95% CI)	Specificity (95% CI)
RT-nfoRPA-LFD	16	3	0	0	19	100.0% (79.4–100.0%)	100.0% (29.2–100.0%)
RT-exoRPA-LFD	15	3	0	1	19	93.8% (69.8–99.8%)	100.0% (29.2–100.0%)
RT-RAA-LFD	10	3	0	6	19	62.5% (35.4–84.8%)	100.0% (29.2–100.0%)

Conservative analysis included all tested henipavirus isolate samples $\geq$100,000 $TCID_{50}$/mL.

Data availability statement

The original contributions presented in this study are included in this article/supplementary material, further inquiries can be directed to the corresponding authors.

Author contributions

NP: conceptualization, data curation, formal analysis, investigation, methodology, project administration, resources, supervision, validation, visualization, writing—original draft preparation, and writing—review and editing. MO: data curation, formal analysis, investigation, methodology, validation, visualization, and writing—review and editing. GM: data curation, formal analysis, investigation, methodology, resources, validation, visualization, and writing—review and editing. JM: conceptualization, formal analysis, funding acquisition, methodology, project administration, resources, supervision, and writing—review and editing; DM: conceptualization, formal analysis, funding acquisition, methodology, project administration, resources, supervision, and writing—review and editing. All authors contributed to the article and approved the submitted version.

Funding

This project was funded by the DMTC Limited (Australia), Medical Countermeasures Program [Project 10.75], and BioCifer Pty Ltd. This work was also supported, in part, by the Bill and Melinda Gates Foundation [OPP1140133]. Under the grant conditions of the Foundation, a Creative Commons Attribution 4.0 Generic License has already been assigned to the author Accepted Manuscript version that might arise from this submission. The authors declare that this study received funding from DMTC Limited and BioCifer Pty Ltd. The funders had no involvement in the study design, collection, analysis, interpretation of data, the writing of this article, or the decision to submit it for publication.

Acknowledgments

We wish to thank Jody Hobson-Peters (Australian Infectious Diseases Research Centre and School of Chemistry and Molecular Biosciences, The University of Queensland, St Lucia, QLD Australia) for providing the dengue stocks and TRIzol samples of flaviviruses and Chikungunya virus. This manuscript includes research that was supported by the DMTC Limited (Australia). The authors have prepared this manuscript in accordance with the intellectual property rights granted to partners from the original DMTC project. DMTC Limited is a research company that runs multiparty collaborative research projects. A project has been conducted with University of Sunshine Coast and BioCifer whereby a license has been issued to BioCifer with regards to Project IP. This publication contains Project IP, and BioCifer and University of Sunshine Coast have been issued with the rights to publish the Project IP.

Conflict of interest

NP is a funded post-doctoral research scientist for DMTC Ltd., Australia. JM is a Project Leader for DMTC Ltd., Australia and co-founder, shareholder, and director of BioCifer Pty. Ltd., who has licensed the technology.

The remaining authors declare that the research was conducted in the absence of any commercial or financial relationships that could be construed as a potential conflict of interest.

The reviewer AB-B declared a past co-authorship with one of the author GM to the handling editor.

Publisher's note

References

Ahmed, J., Bouloy, M., Ergonul, O., Fooks, A., Paweska, J., Chevalier, V., et al. (2009). International network for capacity building for the control of emerging viral vector-borne zoonotic diseases: ARBO-ZOONET. *Euro Surveill.* 14:19160.

Ahmed, M., Pollak, N., Hugo, L., Van Den Hurk, A., Hobson-Peters, J., and Macdonald, J. (2022). Rapid molecular assays for the detection of the four dengue viruses in infected mosquitoes [version 1; peer review: 1 approved]. *Gates Open Res.* 6:81.

Arunkumar, G., Chandni, R., Mourya, D. T., Singh, S. K., Sadanandan, R., Sudan, P., et al. (2019). Outbreak investigation of Nipah virus disease in Kerala, India, 2018. *J. Infect. Dis.* 219, 1867–1878.

Chadha, M. S., Comer, J. A., Lowe, L., Rota, P. A., Rollin, P. E., Bellini, W. J., et al. (2006). Nipah virus-associated encephalitis outbreak, Siliguri, India. *Emerg. Infect. Dis.* 12, 235–240.

Chiang, C. F., Lo, M. K., Rota, P. A., Spiropoulou, C. F., and Rollin, P. E. (2010). Use of monoclonal antibodies against Hendra and Nipah viruses in an antigen capture ELISA. *Virol. J.* 7:115. doi: 10.1186/1743-422X-7-115

Chong, H. T., Kunjapan, S. R., Thayaparan, T., Tong, J., Petharunam, V., Jusoh, M. R., et al. (2002). Nipah encephalitis outbreak in Malaysia, clinical features in patients from Seremban. *Can. J. Neurol. Sci.* 29, 83–87. doi: 10.1017/s0317167100001785

Chua, K. B., Bellini, W. J., Rota, P. A., Harcourt, B. H., Tamin, A., Lam, S. K., et al. (2000). Nipah virus: A recently emergent deadly paramyxovirus. *Science* 288, 1432–1435.

Clayton, B. A. (2017). Nipah virus: Transmission of a zoonotic paramyxovirus. *Curr. Opin. Virol.* 22, 97–104.

Cleri, D. J., Ricketti, A. J., Porwancher, R. B., Ramos-Bonner, L. S., and Vernaleo, J. R. (2006). Viral hemorrhagic fevers: current status of endemic disease and strategies for control. *Infect. Dis. Clin. North Am.* 20, 359–393, x.

Crameri, G., Wang, L. F., Morrissy, C., White, J., and Eaton, B. T. (2002). A rapid immune plaque assay for the detection of Hendra and Nipah viruses and anti-virus antibodies. *J. Virol. Methods* 99, 41–51. doi: 10.1016/s0166-0934(01)00377-9

Drexler, J. F., Corman, V. M., Gloza-Rausch, F., Seebens, A., Annan, A., Ipsen, A., et al. (2009). Henipavirus RNA in African bats. *PLoS One* 4:e6367. doi: 10.1371/journal.pone.0006367

Drosten, C., Kummerer, B. M., Schmitz, H., and Gunther, S. (2003). Molecular diagnostics of viral hemorrhagic fevers. *Antiviral Res.* 57, 61–87.

Eaton, B. T., Broder, C. C., Middleton, D., and Wang, L. F. (2006). Hendra and Nipah viruses: Different and dangerous. *Nat. Rev. Microbiol.* 4, 23–35. doi: 10.1038/nrmicro1323

Feldman, K. S., Foord, A., Heine, H. G., Smith, I. L., Boyd, V., Marsh, G. A., et al. (2009). Design and evaluation of consensus PCR assays for henipaviruses. *J. Virol. Methods* 161, 52–57.

Fischer, K., Diederich, S., Smith, G., Reiche, S., Pinho Dos Reis, V., Stroh, E., et al. (2018). Indirect ELISA based on Hendra and Nipah virus proteins for the detection of henipavirus specific antibodies in pigs. *PLoS One* 13:e0194385. doi: 10.1371/journal.pone.0194385

Goh, K. J., Tan, C. T., Chew, N. K., Tan, P. S., Kamarulzaman, A., Sarji, S. A., et al. (2000). Clinical features of Nipah virus encephalitis among pig farmers in Malaysia. *N. Engl. J. Med.* 342, 1229–1235.

Gomez Roman, R., Wang, L. F., Lee, B., Halpin, K., De Wit, E., Broder, C. C., et al. (2020). Nipah@20: Lessons learned from another virus with pandemic potential. *mSphere* 5:e00602-20.

Guillaume, V., Lefeuvre, A., Faure, C., Marianneau, P., Buckland, R., Lam, S. K., et al. (2004). Specific detection of Nipah virus using real-time RT-PCR (TaqMan). *J. Virol. Methods* 120, 229–237. doi: 10.1016/j.jviromet.2004.05.018

Gurley, E. S., Hegde, S. T., Hossain, K., Sazzad, H. M. S., Hossain, M. J., Rahman, M., et al. (2017). Convergence of humans, bats, trees, and culture in Nipah Virus transmission, Bangladesh. *Emerg. Infect. Dis.* 23, 1446–1453. doi: 10.3201/eid2309.161922

James, A. S., Todd, S., Pollak, N. M., Marsh, G. A., and Macdonald, J. (2018). Ebolavirus diagnosis made simple, comparable and faster than molecular detection methods: preparing for the future. *Virol. J.* 15:75. doi: 10.1186/s12985-018-0985-8

Jensen, K. S., Adams, R., Bennett, R. S., Bernbaum, J., Jahrling, P. B., and Holbrook, M. R. (2018). Development of a novel real-time polymerase chain reaction assay for the quantitative detection of Nipah virus replicative viral RNA. *PLoS One* 13:e0199534. doi: 10.1371/journal.pone.0199534

Kaku, Y., Noguchi, A., Marsh, G. A., Barr, J. A., Okutani, A., Hotta, K., et al. (2012). Antigen capture ELISA system for henipaviruses using polyclonal antibodies obtained by DNA immunization. *Arch. Virol.* 157, 1605–1609. doi: 10.1007/s00705-012-1338-3

Kashiwazaki, Y., Na, Y. N., Tanimura, N., and Imada, T. (2004). A solid-phase blocking ELISA for detection of antibodies to Nipah virus. *J. Virol. Methods* 121, 259–261. doi: 10.1016/j.jviromet.2004.06.015

Kulkarni, D. D., Venkatesh, G., Tosh, C., Patel, P., Mashoria, A., Gupta, V., et al. (2016). Development and evaluation of recombinant nucleocapsid protein based diagnostic ELISA for detection of Nipah virus infection in pigs. *J. Immunoassay Immunochem.* 37, 154–166. doi: 10.1080/15321819.2015.1074922

Li, J., Macdonald, J., and Von Stetten, F. (2018). Review: a comprehensive summary of a decade development of the recombinase polymerase amplification. *Analyst* 144, 31–67.

Li, J., Macdonald, J., and Von Stetten, F. (2020). Correction: Review: A comprehensive summary of a decade development of the recombinase polymerase amplification. *Analyst* 145, 1950–1960. doi: 10.1039/c9an90127b

Li, J., Pollak, N. M., and Macdonald, J. (2019). Multiplex detection of nucleic acids using recombinase polymerase amplification and a molecular colorimetric 7-segment display. *ACS Omega* 4, 11388–11396. doi: 10.1021/acsomega.9b01097

Luby, S. P., Gurley, E. S., and Hossain, M. J. (2009). Transmission of human infection with Nipah virus. *Clin. Infect. Dis.* 49, 1743–1748.

Ma, L., Chen, Z., Guan, W., Chen, Q., and Liu, D. (2019). Rapid and specific detection of all known Nipah virus strains' sequences with reverse transcription-loop-mediated isothermal amplification. *Front. Microbiol.* 10:418. doi: 10.3389/fmicb.2019.00418

Mazzola, L. T., and Kelly-Cirino, C. (2019). Diagnostics for Nipah virus: A zoonotic pathogen endemic to Southeast Asia. *BMJ Glob. Health* 4:e001118.

Middleton, D. J., Westbury, H. A., Morrissy, C. J., Van Der Heide, B. M., Russell, G. M., Braun, M. A., et al. (2002). Experimental Nipah virus infection in pigs and cats. *J. Comp. Pathol.* 126, 124–136.

Mungall, B. A., Middleton, D., Crameri, G., Halpin, K., Bingham, J., Eaton, B. T., et al. (2007). Vertical transmission and fetal replication of Nipah virus in an experimentally infected cat. *J. Infect. Dis.* 196, 812–816. doi: 10.1086/520818

Parashar, U. D., Sunn, L. M., Ong, F., Mounts, A. W., Arif, M. T., Ksiazek, T. G., et al. (2000). Case-control study of risk factors for human infection with a new zoonotic paramyxovirus, Nipah virus, during a 1998-1999 outbreak of severe encephalitis in Malaysia. *J. Infect. Dis.* 181, 1755–1759. doi: 10.1086/315457

Paton, N. I., Leo, Y. S., Zaki, S. R., Auchus, A. P., Lee, K. E., Ling, A. E., et al. (1999). Outbreak of Nipah-virus infection among abattoir workers in Singapore. *Lancet* 354, 1253–1256.

Pernet, O., Schneider, B. S., Beaty, S. M., Lebreton, M., Yun, T. E., Park, A., et al. (2014). Evidence for henipavirus spillover into human populations in Africa. *Nat. Commun.* 5:5342.

Pernet, O., Wang, Y. E., and Lee, B. (2012). Henipavirus receptor usage and tropism. *Curr. Top. Microbiol. Immunol.* 359, 59–78.

Piepenburg, O., Williams, C. H., Stemple, D. L., and Armes, N. A. (2006). DNA detection using recombination proteins. *PLoS Biol.* 4:e204. doi: 10.1371/journal.pbio.0040204

Playford, E. G., Munro, T., Mahler, S. M., Elliott, S., Gerometta, M., Hoger, K. L., et al. (2020). Safety, tolerability, pharmacokinetics, and immunogenicity of a human monoclonal antibody targeting the G glycoprotein of henipaviruses in healthy adults: A first-in-human, randomised, controlled, phase 1 study. *Lancet Infect. Dis.* 20, 445–454. doi: 10.1016/S1473-3099(19)30634-6

Pollak, N. M., Olsson, M., Ahmed, M., Tan, J., Lim, G., Setoh, Y. X., et al. (2023). Rapid diagnostic tests for the detection of the four dengue virus serotypes in clinically relevant matrices. *Microbiol. Spectr.* doi: 10.1128/spectrum.02796-22

Qian, J., Boswell, S. A., Chidley, C., Lu, Z. X., Pettit, M. E., Gaudio, B. L., et al. (2020). An enhanced isothermal amplification assay for viral detection. *Nat. Commun.* 11:5920.

Rames, E. K., and Macdonald, J. (2019). Rapid assessment of viral water quality using a novel recombinase polymerase amplification test for human adenovirus. *Appl. Microbiol. Biotechnol.* 103, 8115–8125. doi: 10.1007/s00253-019-10077-w

Sadeghi, P., Sohrabi, H., Hejazi, M., Jahanban-Esfahlan, A., Baradaran, B., Tohidast, M., et al. (2021). Lateral flow assays (LFA) as an alternative medical diagnosis method for detection of virus species: The intertwine of nanotechnology with sensing strategies. *Trends Analyt. Chem.* 145:116460. doi: 10.1016/j.trac.2021.116460

Sazzad, H. M., Hossain, M. J., Gurley, E. S., Ameen, K. M., Parveen, S., Islam, M. S., et al. (2013). Nipah virus infection outbreak with nosocomial and corpse-to-human transmission, Bangladesh. *Emerg. Infect. Dis.* 19, 210–217. doi: 10.3201/eid1902.120971

Schulz, J. E., Seifert, S. N., Thompson, J. T., Avanzato, V., Sterling, S. L., Yan, L., et al. (2020). Serological Evidence for Henipa-like and Filo-like Viruses in Trinidad Bats. *J. Infect. Dis.* 221, S375–S382. doi: 10.1093/infdis/jiz648

Subsoontorn, P., Lohitnavy, M., and Kongkaew, C. (2020). The diagnostic accuracy of isothermal nucleic acid point-of-care tests for human coronaviruses: A systematic review and meta-analysis. *Sci. Rep.* 10:22349. doi: 10.1038/s41598-020-79237-7

TwistDx (2018). *Assay design manual, TwistAmp® DNA amplification kits*. Cambridge: TwistDx.

Wacharapluesadee, S., and Hemachudha, T. (2007). Duplex nested RT-PCR for detection of Nipah virus RNA from urine specimens of bats. *J. Virol. Methods* 141, 97–101. doi: 10.1016/j.jviromet.2006.11.023

Weber, D. J., and Rutala, W. A. (2001). Risks and prevention of nosocomial transmission of rare zoonotic diseases. *Clin. Infect. Dis.* 32, 446–456.

World Health Organization [WHO] (2018). *Nipah virus*. Available online at: https://www.who.int/news-room/fact-sheets/detail/nipah-virus (accessed September 28, 2022).

Yadav, P. D., Sahay, R. R., Balakrishnan, A., Mohandas, S., Radhakrishnan, C., Gokhale, M. D., et al. (2022). Nipah virus outbreak in Kerala state, India amidst of COVID-19 pandemic. *Front. Public Health* 10:818545. doi: 10.3389/fpubh.2022.818545

Zamani, M., Furst, A. L., and Klapperich, C. M. (2021). Strategies for engineering affordable technologies for point-of-care diagnostics of infectious diseases. *Acc. Chem. Res.* 54, 3772–3779. doi: 10.1021/acs.accounts.1c00434

Zhao, Y., Chen, F., Li, Q., Wang, L., and Fan, C. (2015). Isothermal amplification of nucleic acids. *Chem. Rev.* 115, 12491–12545. doi: 10.1021/acs.chemrev.5b00428

Zheng, C., Wang, K., Zheng, W., Cheng, Y., Li, T., Cao, B., et al. (2021). Rapid developments in lateral flow immunoassay for nucleic acid detection. *Analyst* 146, 1514–1528. doi: 10.1039/D0AN02150D

frontiers | Frontiers in Microbiology

TYPE Original Research
PUBLISHED 10 February 2023
DOI 10.3389/fmicb.2023.1116685

OPEN ACCESS

EDITED BY
Arabella Touati,
Centre Hospitalier Universitaire de Bordeaux, France

REVIEWED BY
Mariza Gonçalves Morgado,
Oswaldo Cruz Foundation (Fiocruz), Brazil
Hussein O.M. Al-Dahmoshi,
University of Babylon,
Iraq

*CORRESPONDENCE
Ayichew Seyoum
✉ ayichewseyoum@gmail.com

SPECIALTY SECTION
This article was submitted to Infectious Agents and Disease, a section of the journal Frontiers in Microbiology

RECEIVED 05 December 2022
ACCEPTED 19 January 2023
PUBLISHED 10 February 2023

CITATION
Seyoum A, Seyoum B, Gure T, Alemu A, Belachew A, Abeje D, Aseffa A, Howe R, Mulu A and Mihret A (2023) Genotype heterogeneity of high-risk human papillomavirus infection in Ethiopia. *Front. Microbiol.* 14:1116685. doi: 10.3389/fmicb.2023.1116685

Genotype heterogeneity of high-risk human papillomavirus infection in Ethiopia

Ayichew Seyoum[1,2]*, Berhanu Seyoum[2], Tadesse Gure[1], Addisu Alemu[1], Anteneh Belachew[1], Dessalegn Abeje[2], Abraham Aseffa[2], Rawleigh Howe[2], Andargachew Mulu[2] and Adane Mihret[2]

[1]College of Health and Medical Sciences, Haramaya University, Harar, Ethiopia, [2]Armauer Hansen Research Institute, Addis Ababa, Ethiopia

Cervical cancer is a vaccine-preventable sexually transmitted disease. In the year 2020, there were an estimated 604,000 new cases and 342,000 deaths worldwide. Although its incidence is global, it is much higher in sub-Saharan African countries. In Ethiopia, there is a scarcity of data about the prevalence of high-risk HPV infection and its association with cytological profiles. Therefore, this study was conducted to fill this information gap. A hospital-based cross-sectional study was conducted from April 26 to August 28, 2021, and enrolled 901 sexually active women. Socio-demographic and other relevant bio-behavioral and clinical data were collected using a standardized questionnaire. Visual inspection with acetic acid [*VIA*] was done as an initial screening method for cervical cancer. The cervical swab was then collected using L-Shaped FLOQSwabs in eNAT nucleic acid preservation and transportation medium. A Pap test was done to determine the cytological profile. Nucleic acid was extracted using STARMag 96 ProPrep Kit on SEEPREP32. A Real-time multiplex assay was performed to amplify and detect the HPV L1 gene used for genotyping. The data were entered into Epi data version 3.1 software and exported to STATA version 14 for analysis. A total of 901 (age range from 30 to 60years, mean age=34.8years, and SD± 5.8) women were screened for cervical cancer using *VIA* and 832 women had a valid co-testing (Pap test and HPV DNA testing) results for further process. The overall prevalence of hr HPV infection was 13.1%. Out of 832 women, 88% of them had normal and 12% had abnormal Pap test results. The proportion of high risk HPV was significantly higher among women with abnormal cytology (X^2=688.446, p<0.001) and younger age (X^2=15.3408, p=0.018). Among 110 women with hr HPV, 14 genotypes (HPV-16, -18, -31, -33, -35, -39, -45, -51, -52, -56, -58, -59, -66, and -68) were identified while HPV-16, -31, -52, -58, and -35 genotypes were highly prevalent. The high risk HPV infection continues to be a significant public health problem among women 30–35years old. The presence of high-risk HPV irrespective of genotypes is highly correlated with cervical cell abnormalities. Genotype heterogeneity is observed suggesting the importance of periodic geospatial genotyping surveillance for vaccine effectiveness.

KEYWORDS

human papillomavirus, cervical cancer, prevalence, genotyping, Ethiopia

1. Introduction

Cervical cancer (CC) is among the cancers caused by HPV infection and the fourth for both incidence and mortality among women (Davies-Oliveira et al., 2021). In 2020, it accounted for an estimated 604,000 new cases and 342,000 deaths (Sung et al., 2021). It was the most commonly diagnosed cancer in 23 countries and was the leading cause of cancer death in 36 countries of which the vast majority of these countries are found in sub-Saharan Africa (Pizzato et al., 2022) including Ethiopia.

The prevalence of hr HPV infection in sub-Saharan African countries is unevenly distributed, ranging from 10.7% (Domfeh et al., 2008) to 97.2% (Sahasrabuddhe et al., 2007). The pooled prevalence of hr HPV in sub-Saharan African countries is 32.3%. Similarly, the genotype distribution of hr HPV varied based on geographical location. For example, in China, HPV-52, -16, -58, -18, and -53 determined as the most prevalent genotypes (Zhang et al., 2020). However, this distribution has a different pattern among African countries. HPV-16, -18, -45, -35, and -33 were the most prevalently identified genotypes among sub-Saharan African countries (Ogembo et al., 2015) while HPV-16, -52, -18, -39, and -31 are the widely distributed in the eastern part of Africa (Seyoum et al., 2022). In Ethiopia, the distribution of hr HPV specifically HPV-16, -52, -18, -58, and -45 is almost similar to the other East African countries (Derbie et al., 2019).

Infection with human papillomavirus (HPV) is the primary cause of cervical cancer (Xing et al., 2021). Around 229 different HPV types have been listed by the International HPV Reference Centre[1], and this number continues to expand. Among them, about 40 types of HPV can infect the genitals of men and women: the skin of the genitals, the vulva (the area outside the vagina), the anus and the lining of the vagina, the cervix, and the anus. These types can also infect the lining of the mouth and throat (Sendagorta-Cudós et al., 2019).

Genital/mucosal types are of the alpha-PV genus and are classified into oncogenic (high-risk) or non-oncogenic (low-risk) types based on their involvement in malignant lesions. Genotyping of the virus defines by the genetic sequence of the protective outer shell or capsid made of a protein called the Late gene 1 (L1; Soheili et al., 2021). Accordingly, the 15 high-risk (hr) HPVs (HPV-16, -18, -31, -33, -35, -39, -45, -51, -52, -56, -58, -59, -66, -68, -73, and -82) cause dysplasia and cancer. The other 12 are low-risk types (HPV-6, -11, -40, -42, -43, -44, -54, -61, -70, -72, -81, and CP6108), which usually cause low-grade mild dysplasia, genital warts, and respiratory papillomatosis. The remaining three are probable high-risk types (HPV-26, -53, and -66; Asiaf et al., 2014; Doorbar et al., 2015).

Currently, three licensed HPV vaccines constructed using L1 capsid antigens: 9-valent HPV vaccine (Gardasil 9, 9vHPV), quadrivalent HPV vaccine (Gardasil, 4vHPV), and bivalent HPV vaccine (Cervarix, 2vHPV) are available (Gillison et al., 2008; Roden and Stern, 2018). Hence, urgent and bold action is needed to scale up and sustain implementation of the evidence-based interventions to reduce cervical cancer as a public health problem, but such action must be strategic. Since the limited cross-protection offered by the current vaccines, generating scientific data regarding the hr HPV prevalence, genotype distribution, cytological profile and associated factors among the different populations is essential in predicting the efficacy of the current vaccine and devising new vaccine strategy (Senapati et al., 2017). In eastern Ethiopia, there is no data about the prevalence and genotype distribution of the virus. Therefore, this study was conducted to fill this information gap. Therefore, we determined the prevalence of hr HPV infection and cytological profile among sexually active women in Ethiopia.

2. Materials and methods

2.1. Study settings and design

A health facility-based cross-sectional study was conducted from April 26 to August 28, 2021, in three cities (Harar- Hiwot Fana Specialized University Hospital, Dire Dawa- Dil-Chora Referral Hospital, and Jigjiga- Shiek Hassan Yabare Referral Hospital) in Ethiopia (Figure 1). These health facilities were selected mainly because of their active provision of cervical cancer screening services, and the presence of professionals who perform clinical diagnosis and cytology examinations (gynecologists and pathologists).

2.2. Population and eligibility criteria

The source populations of the study were all women who live in eastern Ethiopia and who have started heterosexual intercourse. Women between the ages of 30 and 65 years (WOH, 2021), who have lived in the study area for at least 6 months and who consented to participate in the study were included. Women who had sexual intercourse within 24 h of clinical examination, or who had abundant menstrual bleeding and found it difficult to perform appropriate presumptive screening were excluded. In addition, women with a history of hysterectomy, who were physically or mentally unfit for the interview and pelvic examination for various reasons, were excluded.

2.3. Recruitment and sample collection

2.3.1. Demographic and risk factors

Socio-demographic and other relevant bio-behavioral data [such as smoking habits, age at first sexual intercourse, sexual behavior and number of partners, contraceptive use and duration] were collected through a face-to-face interview using pre-designed and pre-tested structured questionnaire. A hospital checklist was used to collect a clinical data [such as number of parity, and history of other sexually transmitted diseases].

2.3.2. Visual inspection with acetic acid

Women who visited the selected hospitals for gynecological problems similar to the HPV virus infection, and met the inclusion criteria were initially screened with *VIA* method for cervical cancer. During *VIA* examination, women with an invisible transition zone were excluded from the study. A sterile plastic spatula was inserted into the vagina to visualize the cervix. Then, 5% acetic acid was applied to the cervix and monitored the changes for 1 min. A sharp, distinct, well-defined, dense (opaque, dull, or oyster white) aceto-white area with or without raised margins define as a positive test (Sankaranarayanan and Wesley, 2003).

1 www.hpvcenter.se, on 26/08/2022.

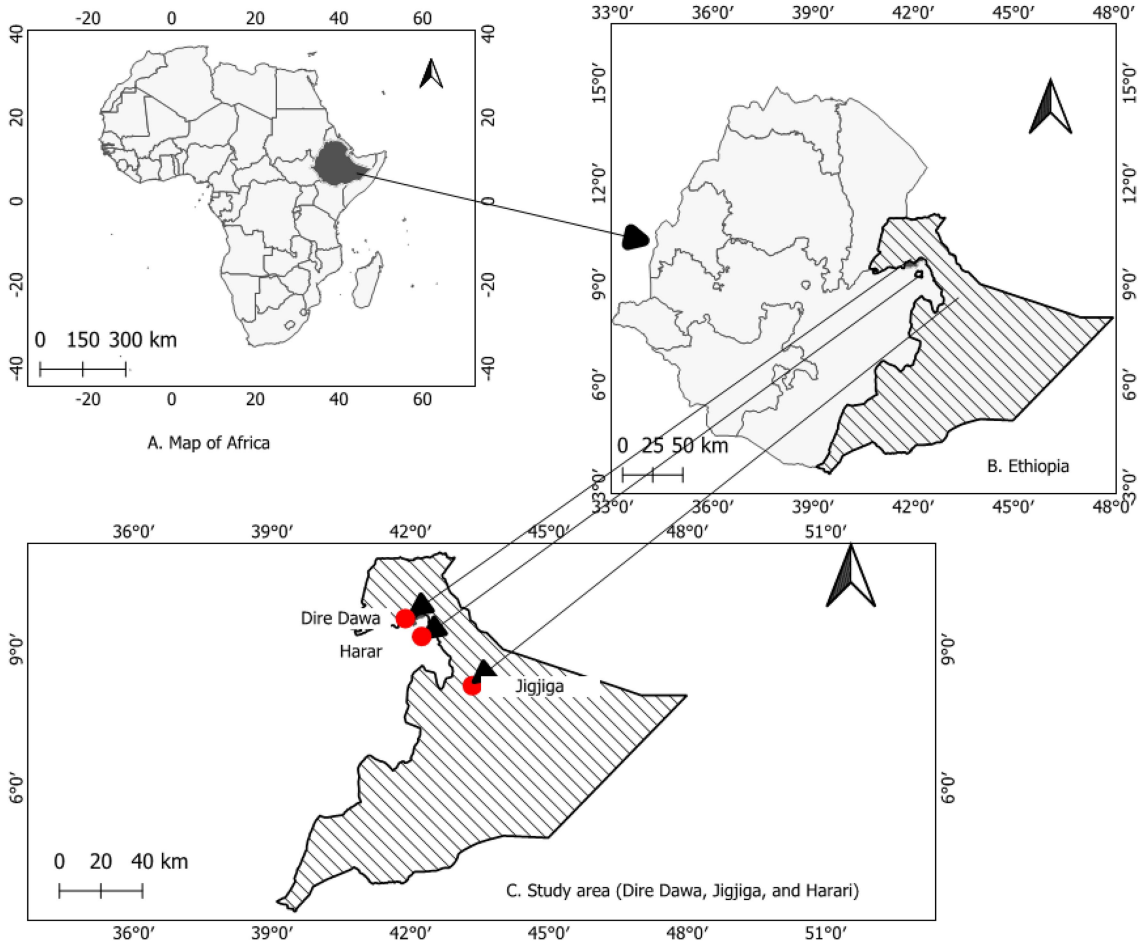

FIGURE 1
Map of study areas (Extracted using QGIS software).

2.3.3. Pap smear preparation and result interpretation

After removing the cervical mucus with a cotton swab, the exfoliated ectocervical and endocervical cells were collected using L-shaped Endo/Esocervical eNAT FLOQSwab® (Copan Italia SpA, Brescia, Italy) and make a smear on the slide. The smear was fixed on the slide using ethanol and stained according to standard protocols (Goel et al., 2020). Then, the cytological features of cells were read and results were recorded on standardized forms according to the 2015 Bethesda System which classified women with cytological findings as "normal" or more severe lesions with a positive Pap smear result (abnormal; Nayar and Wilbur, 2015). We excluded all women who had unsatisfactory results from further analysis of the study.

2.3.4. Liquid-based cervical swabs collection and storage

Endocervical and ectocervical cells were collected from the cervical canal using an L-shaped Endo/Ectocervical FLOQSwab® (Copan Italia SpA, Brescia Italy) cytobrush. The brush was then placed into a 2 ml eNAT nucleic acid collection and preservation vial (Copan Italia SpA, Brescia, Italy) for HPV DNA detection and genotyping. The collected cervical cells were transported to Child Health and Mortality Surveillance (CHAMPS) Ethiopia project, Haramaya University, and Armauer Hansen Research Institute (AHRI), Addis Ababa laboratories and stored at -80°C until further processed.

2.4. HPV DNA extraction, detection, and genotyping

An aliquot of cervical swab [200 µl] was used to extract nucleic acid using STARMag 96 ProPrep Kit (Seegene, Korea) on SEEPREP32™ (a bead transfer-based nucleic acid extraction instrument for *in vitro* diagnostics) automated Liquid Handling Workstation (Seegene, Korea). The extracted DNA was eluted with 70 µl of elution buffer. Parallel detection and genotyping of HPV was carried out using Anyplex™II HPV HR kit (Seegene, Korea) which can detect and genotype 14 h HPV (HPV-16, -18, -31, -33, -35, -39, -45, -51, -52, -56, -58, -59, -66 and -68). A multiplex Real-time assay was performed to amplify the HPV L1 gene for genotyping and Human housekeeping gene as an endogenous internal control [IC] which can ensure the purification of DNA, verification of PCR reaction, and clarification of cell adequacy from each specimen. CFX96TM Real-time PCR System (Bio-Rad) experiment setup was used for the detection of 14 types of HPV using 5 µl of template DNA in a total volume of 20 µl. The 14 HPV types detection and genotyping were done in five fluorescent channels (FAM, HEX, Cal Red 610, Quasar 670, and Quasar 705), each with individual parameters for target detection and validity; channel 1 HPV-66/-45/-58, channel 2 HPV-51/-59/-16, channel 3 HPV-33/-39/-52, channel 4 HPV-35/-18 and, channel 5 HPV-56/-68/-31.

2.5. Statistical methods

The completeness of the collected data is checked before being entered into the database. The data were then cleaned and coded and entered into Epi data version 3.1 software and exported to STATA version 14 for analysis. Frequencies, proportions, and summary statistics were used to describe the study population with relevant variables. A binary logistic regression model was used to identify factors associated with HPV infection and odds ratio with 95% CI was used to assess the degree of association. The p value < 0.05 was considered a statistically significant association and variables with $p < 0.25$ were tested for multivariable logistic regression.

2.6. Ethical considerations

The study was conducted according to the Helsinki Declaration and Ethiopian research regulations. Both, the Institutional Health Research Ethics Review Committee (IHRERC) of the College of Health and Medical Sciences, Haramaya University, Ethiopia (Reference Number: IHRERC/212/2020) and the Armauer Hansen Research Institute Ethics Committee (Reference Number: PO/20/20) approved the protocol.

3. Results

3.1. Sociodemographic characteristics

In this study, a total of 901 women (age range from 30 to 60 years, mean age = 34.8 years, and SD = ±5.8) were initially screened using *VIA* screening method. The majorities were urban residents (86.9%) and married (87.1%), while more than half of the study participants were unemployed (65.3%), unable to read and write (54.2%), and over 18 years of age at the time of their first marriage (68.4%) and first sexual intercourse (66.8%; Table 1).

TABLE 1 Socio-demographic characteristics of women who participated in the study.

Variable	Category	Residence (n=901)		
		Urban, *N* (%)	Rural, *N* (%)	Total, *N* (%)
Age (in years)	At 30	269 (34.3)	50 (43.1)	319 (35.4)
	31–35	269 (34.3)	33 (28.4)	302 (33.5)
	36–40	156 (19.9)	23 (19.8)	179 (19.9)
	41–45	48 (6.1)	4 (3.4)	52 (5.8)
	46–50	29 (3.7)	3 (2.6)	32 (3.5)
	51–55	5 (0.6)	1 (0.9)	6 (0.7)
	56–65	9 (1.1)	2 (1.7)	11 (1.2)
Marital status	Married	681 (86.7)	104 (89.7)	785 (87.1)
	Single/ Never married	17 (2.2)	1 (0.7)	18 (2)
	Widowed	27 (3.4)	3 (2.6)	30 (3.3)
	Divorced	57 (7.3)	7 (6)	64 (7.1)
	Separated	3 (0.4)	1 (0.9)	4 (0.4)
Occupational status	Full time employee	180 (22.9)	17 (14.7)	197 (21.9)
	Part-time employee	83 (10.6)	4 (3.4)	87 (9.7)
	Unemployed	503 (64.1)	85 (73.3)	588 (65.3)
	Student	6 (0.8)	2 (1.7)	8 (0.9)
	Retired	2 (0.2)	3 (2.6)	5 (0.5)
	Other	11 (1.4)	5 (4.3)	16 (1.8)
Current Educational status	Unable to read and write	410 (52.2)	78 (67.2)	488 (54.2)
	Elementary/1–8 grades	201 (25.6)	23 (19.8)	224 (24.9)
	High school/9–12 grades	78 (9.9)	6 (5.2)	84 (9.3)
	Tertiary level	96 (12.2)	9 (7.8)	105 (11.6)
Age at first marriage (in years)	<15	35 (4.5)	6 (5.2)	41 (4.5)
	15–17	189 (24.1)	55 (47.4)	244 (27.1)
	≥18	561 (71.5)	55 (47.4)	616 (68.4)
Age at first sexual intercourse (in years)	<15	41 (5.2)	9 (7.8)	50 (5.5)
	15–17	199 (25.3)	50 (43.1)	249 (27.6)
	≥18	545 (69.4)	57 (49.1)	602 (66.8)

3.2. Cytological profile of the study participants

Among 901 women who had *VIA* screening and Pap smear test, 654 (72.6%) women had negative and the remaining 247 (27.4%) positive *VIA* results. But, during the Pap smear test, 60 (6.7%) women were excluded from the study due to "unsatisfactory/unreliability test result for the evaluation of cervical epithelial cell abnormalities." Therefore, we included only 841 women who had normal (740, 88%) and abnormal (101, 12%) Pap test results for further analysis. Out of 101 women with abnormal cytology results, 98 (97%) had Low-grade squamous intraepithelial lesions (LSIL), and 3 (3%) had High-grade squamous intraepithelial lesions (HSIL; Figure 2).

3.3. Prevalence of hr HPV based on cytology outcome

Among 901 women who were diagnosed with *VIA*, 15 women had invalid PCR results due to inadequate specimen collection, processing, or the presence of inhibitors and were excluded from further analysis. However, of the remaining 886 women's samples, the hr HPV was detected on 110 (12.4%). There was also a significant difference in the proportion of hr HPV detection between the *VIA*-positive and negative women (97.3% vs. 2.7%, $p < 0.001$; Table 2).

Similarly, out of 901 women who underwent co-testing (Pap and HPV DNA test), 54 women had unsatisfactory Pap test results and 9 women had invalid HPV DNA testing results. Further, the results of 6 women for both the Pap test and HPV DNA testing were invalid. Therefore, the co-testing results of 832 women were used for further analysis. The overall proportion of hr HPV infection was 13.1%, and the rate of hr HPV detection was significantly higher in women with an abnormal Pap test result compared to women with a normal Pap test (88.1% vs. 11.9%, $p < 0.001$; Table 2).

This study also revealed that the detection rate of hr HPV infection was significantly higher in women with LSIL cytology results (86.2% vs.

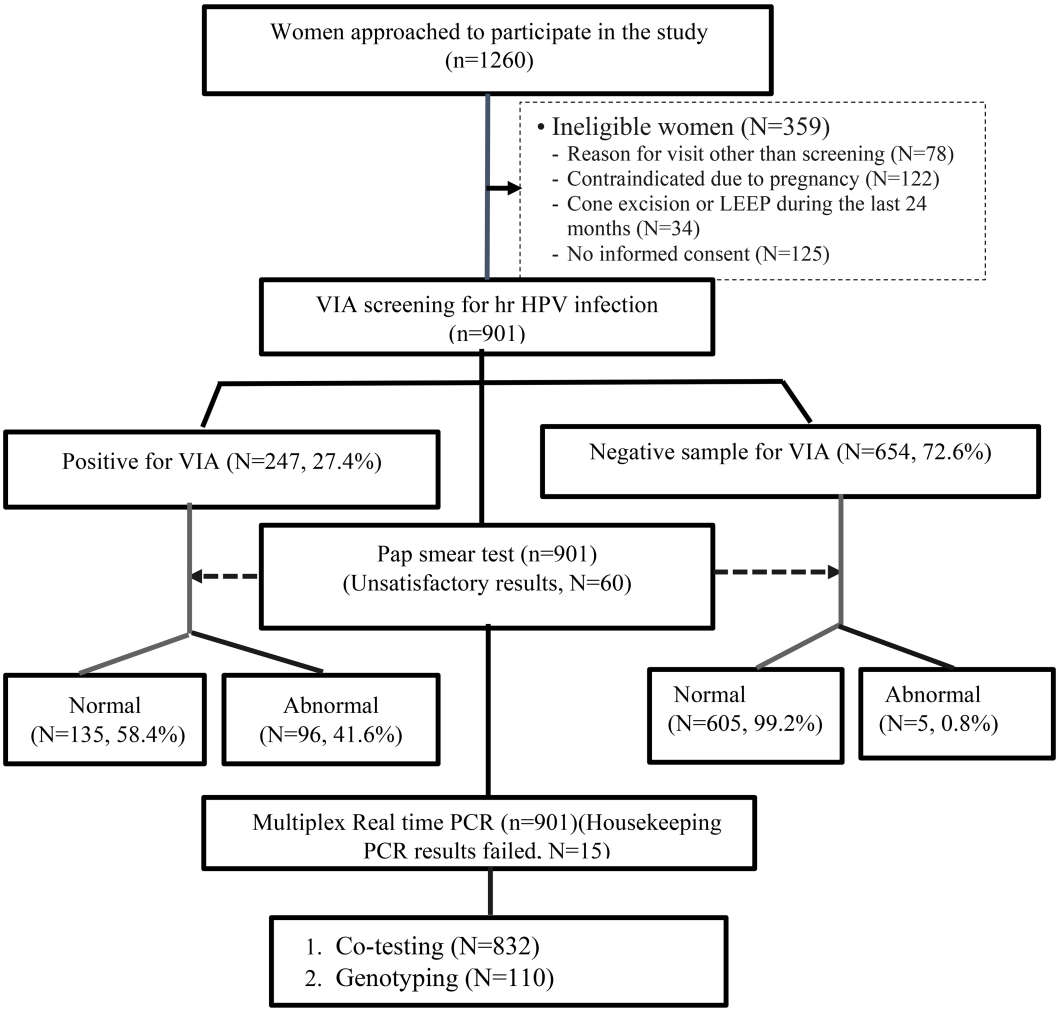

FIGURE 2
Flowchart for the liquid-based cytology and HPV DNA testing performed on the study population.

TABLE 2 Prevalence of hr HPV infection based on cytology outcome among Ethiopian women.

Cytology tests	Category	HPV DNA test			*p* value
		Not detected, *N* (%)	Detected, *N* (%)	Total, *N* (%)	
VIA (*n* = 886)	Negative	641 (82.6)	3 (2.7)*	644 (72.7)	<0.001
	Positive	135 (17.4)	107 (97.3)*	242 (27.3)	
Pap test (*n* = 832)	Normal	719 (99.4)	13 (11.9)*	732 (88)	<0.001
	Abnormal	4 (0.6)	96 (88.1)*	100 (12)	

*Statistically significant association.

0.4%, $p < 0.001$; Table 3). In addition, 8 (66.7%) of the 12 women who had a normal Pap smear result were affected by a single genotype while out of 96 who had abnormal Pap smear result, 72 (75%) women were affected by a single genotype, and the remaining 24 (25%) women were affected by more than 1 genotype (Figure 3).

Among 886 women aged 30 to 60 with valid HPV DNA results, the highest proportion of hr HPV infection (29.1%) was observed in women aged 30 to 35 years. In addition to that, the proportion of hr HPV infection decreased as the age of the women increased, and statistically, it has a significant association ($X^2 = 15.3408$, $p = 0.018$) (Figure 4).

3.4. Type-specific prevalence of hr HPV infection

In the study, 14 genotypes were identified among 110 women whose hr HPV DNA was detected. Among these, 80 (72.7%) women had a single genotype and the remaining 30 (27.3%) women had more than one (multiple) genotype. In addition, Hr HPV-16 (31.8%), -31(19.1%), -52(11.8%), 58(10.9%), and -35(10%) were the most frequently detected genotypes (Figure 5).

3.5. Factors associated with hr HPV infection on the multivariate logistic regression model

We first explored the main factors associated with hr HPV infection in this study using a binary logistic regression model. Then, we selected only associated factors with a p value <0.25 and entered them into the multivariate logistic regression model.

Accordingly, depending on their potential risk with different sex partners the odds of getting the hr HPV infection among women with single marital status is higher than married women (AOR = 8.9, 95% CI: 2.05–38.64, $p = 0.004$). Similarly, the odds of getting the hr HPV infection among women who had more than one sexual partner is higher than women who had a single sexual partner (AOR = 7.14, 95%CI: 3.08–16.54, $p < 0.001$).

The crude and adjusted effects of selected covariates obtained from logistic regression are summarized in Table 4.

4. Discussion

This study is the first hospital-based study conducted at the molecular level to determine the molecular epidemiology of hr HPV infection among sexually active women in eastern Ethiopia. The presence of high prevalence and genotype heterogeneity of hr HPV as a cause of multiple HPV infections indicates a major public health problem that requires greater attention. Additionally, it showed that the detection rate of the virus has a direct correlation with abnormal cytology.

TABLE 3 Prevalence of hr HPV infection based on Pap test results in Ethiopian women.

Pap test results (*n*=832)	PCR results (*n*=832)		Total, *N* (%)
	Detected, *N* (%)	Not detected, *N* (%)	
Normal	13 (11.9)	719 (99.4)	732 (88,0)
Low grade SIL	94 (86.2)*	3 (0.4)*	97 (11.7)
High grade SIL	2 (1.8)	1 (0.1)	3 (0.4)

*Statistically significant association.

The overall prevalence of hr HPV infection was determined to be 13.1% which is low compared to previous studies in various African countries as high as 95% for example in Benin (Tounkara et al., 2020), 83.2% in Ethiopia (Wolday et al., 2018), 76.3% in South Africa (Ebrahim et al., 2016), 57.7% in Kenya (Menon et al., 2016), 53% in Zimbabwe (Marembo et al., 2019), 48.7% in Mozambique (Omar et al., 2017), 46.2% in Swaziland (Ginindza et al., 2017), and 41.5% in Burkina Faso (Ogembo et al., 2015) and genotype heterogeneity with 14 genotypes of hr HPV were identified. The low prevalence in the current study might be explained by the differences in the occupational and health status of the study participants. The current study was conducted on women with a different type of occupations and gynecological problems (from asymptomatic to invasive stage) with normal or abnormal cytological status. This proportional inclusion of women allowed might help us to identify the high level of genotype heterogeneity of hr HPV among women. However, various studies we used for comparison were conducted on female sex workers and people living with HIV (PLWHIV). As a result, the prevalence of HPV infection was 2–3 times higher among these segments of the population.

In contrast, the hr HPV infection in this study was higher compared to the research findings of 9.4% in Iran (Malary et al., 2016) and 12% in the Gambia (Camara et al., 2018), with comparable results of 13.1 and 13.7% were found in Tunisia (Ardhaoui et al., 2016) and Ethiopia (Ali et al., 2019). This comparable result may be due to the fact that the women included in the studies we used for comparison were sexually active women, which is similar to the participants in this study. Therefore, it is important to consider the demographic and health-related aspects of a population segment in order to make appropriate comparisons and take targeted interventions.

The prevalence of hr HPV infection among women with normal cytology was 11.9% and it was very close to the global average of 11.7% (Scott-Wittenborn and Fakhry, 2021) and 12.8% in Northern Africa, but it was low compared to the average of 57.3% in the

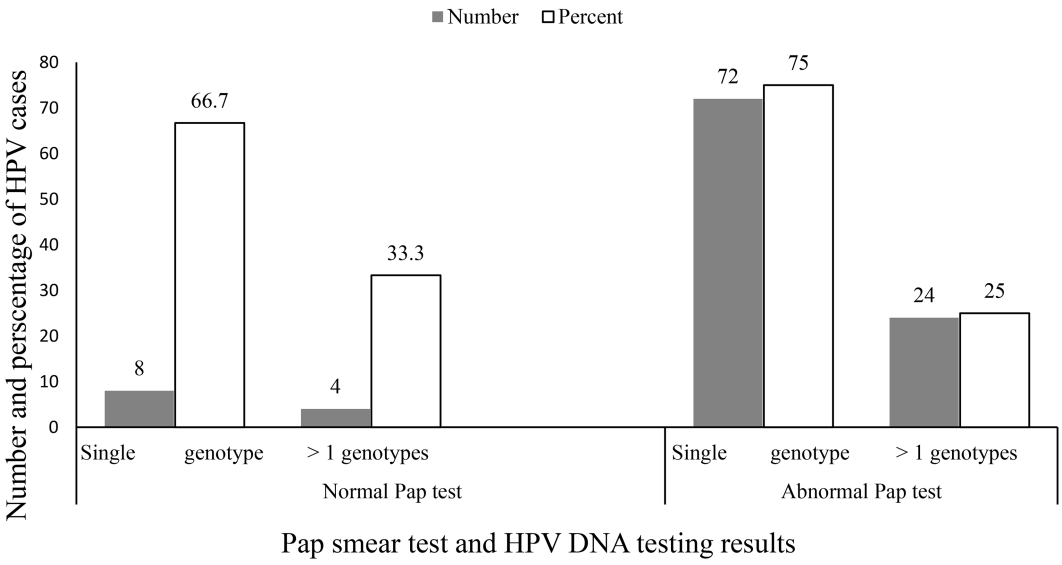

FIGURE 3
A single and co-existed genotypes of HPV within different Pap test results.

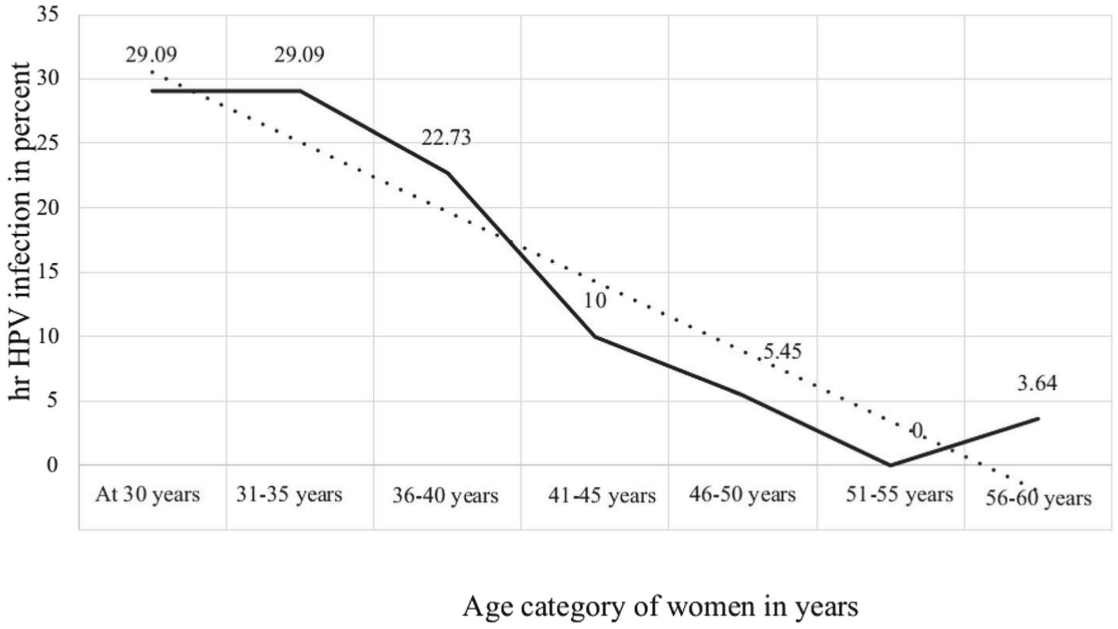

FIGURE 4
Age-specific prevalence of hr HPV infection among women in Ethiopia.

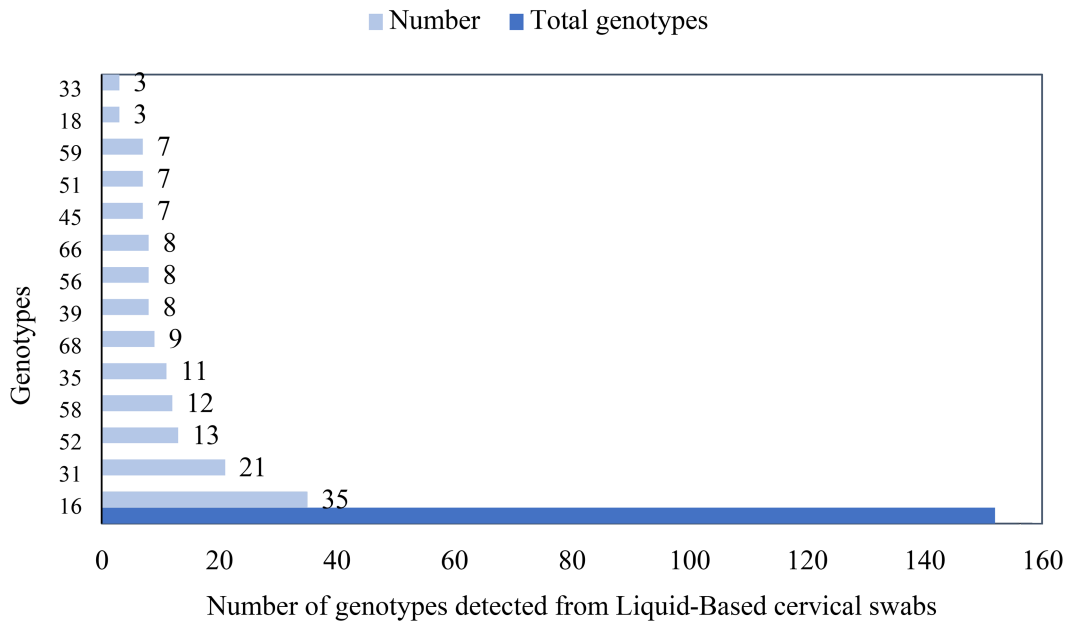

FIGURE 5
Genotypes and frequency of hr HPV among women in Ethiopia.

southern, 42.2% in eastern, and 27.8% in western Africa regions (Ogembo et al., 2015). In the current study, HPV-16, -31, -52, -39, and -45 were the top five HPV types infecting women with normal cytology. This distribution was inconsistent with the global; HPV-16, -52, -31, and -53 (Bruni et al., 2019) and eastern African countries; HPV-16, -52, -18, -51, and -58 (Ogembo et al., 2015). Contrary to normal cytology, the highest prevalence of hr HPV infection (88.1%) was determined in women with abnormal cytology. The result of the current study is inconsistent with study findings conducted in the Middle East and North Africa (MENA) where the pooled prevalence was 54% (Obeid et al., 2020). Furthermore, in the current study, HPV-16 and -31 genotypes were found to be the main cause of lesions in women with abnormal cytology. This was inconsistent with the results of a meta-analysis in East African countries where HPV-16 and -52 were the main causes of lesions with ASCUS, LSIL, and HSIL cytological results. Whereas HPV-16 and -18 were the predominant HPV genotypes found in women with ICC. Among the possible reasons for this inconsistency could be related to

TABLE 4 Shows the associated factors for hr HPV infection on the multivariate logistic regression model.

Variable name	Category	HPV DNA testing (n=886)		COR (95% CI)	AOR (95% CI)	p value
		Detected, N (%)	Not detected, N (%)			
Age (in years)	At 30	32(29.09)	283 (36.47)	*R*	*R*	
	31–35	32(29.09)	263 (33.89)	1.08 (0.64–1.81)	0.68 (0.26–1.68)	0.390
	36–40	25 (22.73)	151 (19.46)	1.46 (0.84–2.56)	0.65 (0.25–1.70)	0.380
	41–45	11(10.00)	41 (5.28)	2.37 (1.11–5.07)	0.89 (0.28–2.79)	0.845
	46–50	6 (5.5)	26 (3.4)	2.04 (0.78–5.33)	1.07 (0.24–4.83)	0.925
	51–55	–	6 (0.8)	–	–	–
	56–60	4 (3.6)	6 (0.8)	5.89 (1.58–22.00)	2.39 (0.18–31.62)	0.509
Residence	Urban	100 (90.91)	670 (86.34)	*R*	*R*	
	Rural	10 (9.09)	106 (13.66)	0.63 (0.32–1.25)	0.39 (0.08–1.93)	0.252
Marital status	Married	82 (74.55)	688 (88.66)	*R*	*R*	
	Single/Never married	9 (8.18)	9 (1.16)	8.39 (3.24–21.73)	8.90 (2.05–38.64)	0.004*
	Widowed	5 (4.55)	25 (3.22)	1.68 (0.62–4.50)	1.05 (0.24–4.61)	0.949
	Divorced	13 (11.82)	51 (6.57)	2.14 (1.11–4.09)	1.27 (0.48–3.41)	0.630
	Separated	1 (0.91)	3 (0.39)	2.80 (0.29–27.20)	2.31 (0.05–103.33)	0.666
Educational status	Unable to read and write	44 (40)	434 (55.9)	*R*	*R*	
	Elementary/1–8 grades	35 (31.8)	189 (24.4)	1.83 (1.13–2.94)	0.85 (0.34–2.16)	0.738
	High school/9–12 grades	14 (12.73)	69 (8.9)	2.00 (1.04–3.84)	1.93 (0.62–5.96)	0.253
	Tertiary level (Diploma and above)	17 (15.5)	84 (10.8)	1.99 (1.09–3.66)	1.22 (0.41–3.63)	0.720
Age at first marriage	<15 years	11 (10)	30 (3.9)	*R*	*R*	
	15–17 years	29 (26.4)	210 (27.1)	0.38 (0.17–0.83)	5.98 (0.20–176.22)	0.300
	≥18 years	70 (63.6)	536 (69.1)	0.36 (0.17–0.74)	2.37 (0.09–61.17)	0.604
Age at first sexual intercourse	<15 years	13 (11.8)	37(4.8)	*R*	*R*	
	15–17 years	28(25.5)	215(27.7)	0.37 (0.18–0.78)	0.12 (0.01–2.69)	0.185
	≥18 years	69(62.7)	524(67.5)	0.36 (0.19–0.74)	0.19 (0.01–3.96)	0.289
Sexual partners	Singe	573 (73.8)	21 (19.1)	*R*	*R*	
	Multiple	203 (26.2)	89 (80.9)	11.96 (7.24–19.76)	7.14 (3.08–16.54)	<0.001*
Long-term use of oral contraceptive (n=272)**	Yes	48 (85.1)	198 (91.7)	*R*	*R*	
	No	8 (14.3)	18 (8.3)	1.83 (0.75–4.47)	1.77 (0.64–4.89)	0.271

*Presence of statistically significant association (p < 0.05). **≥10 years. R = 1. AOR, adjusted odds ratio. CI, confidence interval. COR, crude odds ratio. R, reference.

bio-behavioral characteristics including cultural differences in age at first intercourse, lifetime number of sexual partners, and current smoking status (Lin et al., 2015). The distribution of HPV genotypes is spatially inconsistent across continents, countries, and even within a single country. This lack of uniform distribution makes the identification of HPV genotypes in every locality critical to implement vaccine-based disease preventive measures. In agreement with this conclusion, this study has a significant role in informing the HPV genotypes among women in eastern Ethiopia.

The current study also found that the hr HPV infection rate decreases as the age of the study participants' increase. The highest prevalence of hr HPV infection (29.09%) was observed in women between 30 and 35 years of age, while the prevalence of infection was comparatively lower in women over 40 years of age. The age-specific prevalence of the disease in the current study is consistent with the results of previous studies (Smith et al., 2008; Bekos et al., 2018). This is likely due to the interaction between the natural history of the disease and the genotypes that cause the lesion. Molecular studies on HPV have suggested that patient age and HPV genotypes are independent factors influencing the regression and progression rates of cervical lesions (Ho et al., 1998; Bosch and Harper, 2006). Studies show that young women generally have higher spontaneous recovery (Cox et al., 2003; Moscicki et al., 2010).

Along with women's age, the other strongest factor influencing the natural history of the disease is the presence of hr HPV (particularly HPV-16 and -18 genotypes) infection (Moscicki et al., 1998). These two genotypes increase the risk of persistent infection. In addition to these two main factors, smoking (Appleby et al., 2006), multiparity, and long-term use of oral contraceptives can double or triple the risk for progression to high-grade lesions or cervical cancer in HPV-infected women (International Collaboration of Epidemiological Studies of Cervical Cancer, 2006). If this study had been conducted using a longitudinal study design, it would have been possible to determine the viral persistence/ progression rate and assess the impact of hr HPV. However, we were forced to use a cross-sectional study design

because of insufficient financial resources to conduct a longitudinal study design. This can be considered a limitation of this study.

5. Conclusion

The hr HPV infection continues to be a major public health problem among women of 30–35 years old. Although the prevalence was high in younger women, the age-specific HPV infection prevalence declines as the age increase. The presence of hr HPV irrespective of genotypes is highly correlated with cervical cell abnormalities. Genotype heterogeneity is observed suggesting the importance of periodic geospatial genotyping surveillance for vaccine effectiveness.

Data availability statement

The original contributions presented in the study are included in the article, further inquiries can be directed to the corresponding author.

Ethics statement

The studies involving human participants were reviewed and approved by Institutional Health Research Ethics Review Committee (IHRERC) of the College of Health and Medical Sciences, Haramaya University, Ethiopia and the Armauer Hansen Research Institute Ethics Committee. The patients/participants provided their written informed consent to participate in this study.

Author contributions

AS, AdM, AnM, BS, RH, and AbA participated in proposal development, data collection, laboratory works, data analysis, and manuscript writing. TG conducted clinical examination, sample collection, and supervision of midwives during sample collection. AdA and AB participated in the cytological examination. DA participated in nucleic acid extraction, laboratory protocol review, HPV detection, and HPV genotyping. All authors contributed to the article and approved the submitted version.

Acknowledgments

First of all, we would like to thank the Armauer Hansen Research Institute (AHRI) for providing financial, laboratory and monitoring support for this study. We would also like to thank Haramaya University for providing support to conduct this research. We would like to express our gratitude to Santina Castriciano and Copan Italia, Italy, for providing free liquid-based sample collection and transportation vials and playing a major role for the successful accomplishing of this study. We would also like to extend our thanks to the management of Jugol Hospital, Harar General Hospital, Dire-Dawa Dil Chora Hospital, and Sheikh Hassan Yebere Hospital for their cooperation in collecting data from the study participants. Finally, we would like to express our gratitude to the study participants who gave their consent to participate in this study, and to Mussie Brhane, Tamrayehu Seyoum, Ashenafi Alemu, and Dawit Hailu for their professional support.

Conflict of interest

The authors declare that the research was conducted in the absence of any commercial or financial relationships that could be construed as a potential conflict of interest.

Publisher's note

References

Ali, K. E., Mohammed, I. A., Difabachew, M. N., Demeke, D. S., Haile, T., Ten Hove, R.-J., et al. (2019). Burden and genotype distribution of high-risk Human Papillomavirus infection and cervical cytology abnormalities at selected obstetrics and gynecology clinics of Addis Ababa, Ethiopia. *BMC Cancer* 19, 1–9. doi: 10.1186/s12885-019-5953-1

Appleby, P., Beral V. Berrington de González, A., Colin, D., Franceschi, S., Goodill, A., et al. (2006). Carcinoma of the cervix and tobacco smoking: collaborative reanalysis of individual data on 13,541 women with carcinoma of the cervix and 23,017 women without carcinoma of the cervix from 23 epidemiological studies. *Int. J. Cancer* 118, 1481–1495.

Ardhaoui, M., Ennaifer, E., Letaief, H., Salsabil, R., Lassili, T., Chahed, K., et al. (2016). Prevalence, genotype distribution and risk factors for cervical human papillomavirus infection in the Grand Tunis Region, Tunisia. *PLoS one* 11:e0157432. doi: 10.1371/journal.pone.0157432

Asiaf, A., Ahmad, S. T., Mohammad, S. O., and Zargar, M. A. (2014). Review of the current knowledge on the epidemiology, pathogenesis, and prevention of human papillomavirus infection. *Eur. J. Cancer Prev.* 23, 206–224. doi: 10.1097/CEJ.0b013e328364f273

Bekos, C., Schwameis, R., Heinze, G., Gaerner, M., Grimm, C., Joura, E., et al. (2018). Influence of age on histologic outcome of cervical intraepithelial neoplasia during observational management: results from large cohort, systematic review, meta-analysis. *Sci. Rep.* 8, 1–10. doi: 10.1038/s41598-018-24882-2

Bosch, X., and Harper, D. (2006). Prevention strategies of cervical cancer in the HPV vaccine era. *Gynecol. Oncol.* 103, 21–24. doi: 10.1016/j.ygyno.2006.07.019

Bruni, L., Albero, G., Serrano, B., Mena, M., Gómez, D., Muñoz, J., et al. (2019). ICO/IARC information centre on HPV and cancer (HPV information centre). Human papillomavirus and related diseases in the world. Summary Report, 17.

Camara, H. B., Anyanwu, M., Wright, E., and Kimmitt, P. T. (2018). Human papilloma virus genotype distribution and risk factor analysis amongst reproductive-age women in urban Gambia. *J. Med. Microbiol.* 67, 1645–1654. doi: 10.1099/jmm.0.000848

Cox, J. T., Schiffman, M., and Solomon, D. (2003). Prospective follow-up suggests similar risk of subsequent cervical intraepithelial neoplasia grade 2 or 3 among women with cervical intraepithelial neoplasia grade 1 or negative colposcopy and directed biopsy. *Am. J. Obstet. Gynecol.* 188, 1406–1412. doi: 10.1067/mob.2003.461

Davies-Oliveira, J., Smith, M., Grover, S., Canfell, K., and Crosbie, E. (2021). Eliminating cervical cancer: Progress and challenges for high-income countries. *Clin. Oncol.* 33, 550–559. doi: 10.1016/j.clon.2021.06.013

Derbie, A., Mekonnen, D., Yismaw, G., Biadglegne, F., Van Ostade, X., and Abebe, T. (2019). Human papillomavirus in Ethiopia. *Virus* 30, 171–179. doi: 10.1007/s13337-019-00527-4

Domfeh, A., Wiredu, E., Adjei, A., Ayeh-Kumi, P., Adiku, T., Tettey, Y., et al. (2008). Cervical human papillomavirus infection in Accra, Ghana. *Ghana Med. J.* 42, 71–78.

Doorbar, J., Egawa, N., Griffin, H., Kranjec, C., and Murakami, I. (2015). Human papillomavirus molecular biology and disease association. *Rev. Med. Virol.* 25, 2–23. doi: 10.1002/rmv.1822

Ebrahim, S., Mndende, X. K., Kharsany, A. B., Mbulawa, Z. Z., Naranbhai, V., Frohlich, J., et al. (2016). High burden of human papillomavirus (HPV) infection among young women

in KwaZulu-Natal, South Africa. *PLoS One* 11:e0146603. doi: 10.1371/journal.pone.0146603

Gillison, M. L., Chaturvedi, A. K., and Lowy, D. R. (2008). HPV prophylactic vaccines and the potential prevention of noncervical cancers in both men and women. *Cancer* 113, 3036–3046. doi: 10.1002/cncr.23764

Ginindza, T. G., Dlamini, X., Almonte, M., Herrero, R., Jolly, P. E., Tsoka-Gwegweni, J. M., et al. (2017). Prevalence of and associated risk factors for high risk human papillomavirus among sexually active women, Swaziland. *PLoS One* 12:e0170189. doi: 10.1371/journal.pone.0170189

Goel, G., Halder, A., Joshi, D., Anil, A. C., and Kapoor, N. (2020). Rapid, economic, acetic acid papanicolaou stain (REAP): an economical, rapid, and appropriate substitute to conventional pap stain for staining cervical smears. *J. Cytol.* 37:170. doi: 10.4103/JOC.JOC_89_20

Ho, G. Y., Bierman, R., Beardsley, L., Chang, C. J., and Burk, R. D. (1998). Natural history of cervicovaginal papillomavirus infection in young women. *N. Engl. J. Med.* 338, 423–428. doi: 10.1056/NEJM199802123380703

International Collaboration of Epidemiological Studies of Cervical Cancer (2006). Cervical carcinoma and reproductive factors: collaborative reanalysis of individual data on 16,563 women with cervical carcinoma and 33,542 women without cervical carcinoma from 25 epidemiological studies. *Int. J. Cancer* 119, 1108–1124. doi: 10.1002/ijc.21953

Lin, L., Benard, V. B., Greek, A., Hawkins, N. A., Roland, K. B., and Saraiya, M. (2015). Racial and ethnic differences in human papillomavirus positivity and risk factors among low-income women in federally qualified health centers in the United States. *Prev. Med.* 81, 258–261. doi: 10.1016/j.ypmed.2015.08.027

Malary, M., Moosazadeh, M., Hamzehgardeshi, Z., Afshari, M., Moghaddasifar, I., and Afsharimoghaddam, A. (2016). The prevalence of cervical human papillomavirus infection and the most at-risk genotypes among Iranian healthy women: a systematic review and meta-analysis. *Int. J. Prev. Med.* 7:70. doi: 10.4103/2008-7802.181756

Marembo, T., Mandishora, R. D., and Borok, M. (2019). Use of multiplex polymerase chain reaction for detection of high-risk human papillomavirus genotypes in women attending routine cervical cancer screening in Harare. *Intervirology* 62, 90–95. doi: 10.1159/000502206

Menon, S., Broeck, D. V., Rossi, R., Ogbe, E., Harmon, S., and Mabeya, H. (2016). Associations between vaginal infections and potential high-risk and high-risk human papillomavirus genotypes in female sex workers in western Kenya. *Clin. Ther.* 38, 2567–2577. doi: 10.1016/j.clinthera.2016.10.005

Moscicki, A.-B., Ma, Y., Wibbelsman, C., Darragh, T. M., Powers, A., Farhat, S., et al. (2010). Rate of and risks for regression of CIN-2 in adolescents and young women. *Obstet. Gynecol.* 116, 1373–1380. doi: 10.1097/AOG.0b013e3181fe777f

Moscicki, A.-B., Shiboski, S., Broering, J., Powell, K., Clayton, L., Jay, N., et al. (1998). The natural history of human papillomavirus infection as measured by repeated DNA testing in adolescent and young women. *J. Pediatr.* 132, 277–284. doi: 10.1016/S0022-3476(98)70445-7

Nayar, R., and Wilbur, D. C. (2015). *The Bethesda System for Reporting Cervical Cytology: Definitions, Criteria, and Explanatory Notes*, New York: Springer.

Obeid, D. A., Almatrrouk, S. A., Alfageeh, M. B., Al-Ahdal, M. N., and Alhamlan, F. S. (2020). Human papillomavirus epidemiology in populations with normal or abnormal cervical cytology or cervical cancer in the Middle East and North Africa: a systematic review and meta-analysis. *J. Infect. Public Health* 13, 1304–1313. doi: 10.1016/j.jiph.2020.06.012

Ogembo, R. K., Gona, P. N., Seymour, A. J., Park, H. S.-M., Bain, P. A., Maranda, L., et al. (2015). Prevalence of human papillomavirus genotypes among African women with normal cervical cytology and neoplasia: a systematic review and meta-analysis. *PLoS One* 10:e0122488. doi: 10.1371/journal.pone.0122488

Omar, V. E., Orvalho, A., Nália, I., Kaliff, M., Lillsunde-Larsson, G., Ramqvist, T., et al. (2017). Human papillomavirus prevalence and genotype distribution among young women and men in Maputo city, Mozambique. *BMJ Open* 7:e015653. doi: 10.1136/bmjopen-2016-015653

Pizzato, M., Li, M., Vignat, J., Laversanne, M., Singh, D., Vecchia, L. A., et al. (2022). The epidemiological landscape of thyroid cancer worldwide: GLOBOCAN estimates for incidence and mortality rates in 2020. *Lancet Diabet. Endocrinol.* 10, 264–272. doi: 10.1016/S2213-8587(22)00035-3

Roden, R., and Stern, P. L. (2018). Opportunities and challenges for human papillomavirus vaccination in cancer. *Nat. Rev. Cancer* 18, 240–254. doi: 10.1038/nrc.2018.13

Sahasrabuddhe, V., Mwanahamuntu, M. H., Vermund, S., Huh, W., Lyon, M., Stringer, J., et al. (2007). Prevalence and distribution of HPV genotypes among HIV-infected women in Zambia. *Br. J. Cancer* 96, 1480–1483. doi: 10.1038/sj.bjc.6603737

Sankaranarayanan, R., and Wesley, R. S. (2003). *A Practical Manual on VisualScreening for CervicalNeoplasia*. Lyon, France: International Agency for Research on Cancer, World Health Organization. 41.

Scott-Wittenborn, N., and Fakhry, C. (2021). Epidemiology of HPV related malignancies. *Semin. Radiat. Oncol.* 31, 286–296. doi: 10.1016/j.semradonc.2021.04.001

Senapati, R., Nayak, B., Kar, S. K., and Dwibedi, B. (2017). HPV genotypes distribution in Indian women with and without cervical carcinoma: implication for HPV vaccination program in Odisha, Eastern India. *BMC Infect. Dis.* 17, 1–10. doi: 10.1186/s12879-016-2136-4

Sendagorta-Cudós, E., Burgos-Cibrián, J., and Rodríguez-Iglesias, M. (2019). Genital infections due to the human papillomavirus. *Enferm. Infecc. Microbiol. Clin.* 37, 324–334. doi: 10.1016/j.eimc.2019.01.010

Seyoum, A., Assefa, N., Gure, T., Seyoum, B., Mulu, A., and Mihret, A. (2022). Prevalence and genotype distribution of high-risk human papillomavirus infection among Sub-Saharan African women: a systematic review and meta-analysis. *Front. Public Health* 10:890880. doi: 10.3389/fpubh.2022.890880

Smith, J. S., Melendy, A., Rana, R. K., and Pimenta, J. M. (2008). Age-specific prevalence of infection with human papillomavirus in females: a global review. *J. Adolesc. Health* 43:S5-25, S25.e1-41. doi: 10.1016/j.jadohealth.2008.07.009

Soheili, M., Keyvani, H., Soheili, M., and Nasseri, S. (2021). Human papilloma virus: a review study of epidemiology, carcinogenesis, diagnostic methods, and treatment of all HPV-related cancers. *Med. J. Islam Repub. Iran* 35:65. doi: 10.47176/mjiri.35.65

Sung, H., Ferlay, J., Siegel, R. L., Laversanne, M., Soerjomataram, I., Jemal, A., et al. (2021). Global cancer statistics 2020: GLOBOCAN estimates of incidence and mortality worldwide for 36 cancers in 185 countries. *CA Cancer J. Clin.* 71, 209–249. doi: 10.3322/caac.21660

Tounkara, F. K., Téguété, I., Guédou, F. A., Goma-Matsétsé, E., Koné, A., Béhanzin, L., et al. (2020). Human papillomavirus genotype distribution and factors associated among female sex workers in West Africa. *PLoS One* 15:e0242711. doi: 10.1371/journal.pone.0242711

WOH (2021). New Recommendations for Screening and Treatment to Prevent Cervical Cancer. Available at: https://www.who.int/news/item/06-07-2021-new-recommendations-for-screening-and-treatment-to-prevent-cervical-cancerac

Wolday, D., Derese, M., Gebressellassie, S., Tsegaye, B., Ergete, W., Gebrehiwot, Y., et al. (2018). HPV genotype distribution among women with normal and abnormal cervical cytology presenting in a tertiary gynecology referral Clinic in Ethiopia. *Infect. Agents Cancer* 13, 1–8. doi: 10.1186/s13027-018-0201-x

Xing, B., Guo, J., Sheng, Y., Wu, G., and Zhao, Y. (2021). Human papillomavirus-negative cervical cancer: a comprehensive review. *Front. Oncol.* 10:606335. doi: 10.3389/fonc.2020.606335

Zhang, J., Cheng, K., and Wang, Z. (2020). Prevalence and distribution of human papillomavirus genotypes in cervical intraepithelial neoplasia in China: a meta-analysis. *Arch. Gynecol. Obstet.* 302, 1329–1337.

frontiers | Frontiers in Microbiology

TYPE Correction
PUBLISHED 23 March 2023
DOI 10.3389/fmicb.2023.1178530

OPEN ACCESS

APPROVED BY
Frontiers Editorial Office,
Frontiers Media SA, Switzerland

*CORRESPONDENCE
Ayichew Seyoum
✉ ayichewseyoum@gmail.com

SPECIALTY SECTION
This article was submitted to Infectious Agents and Disease, a section of the journal Frontiers in Microbiology

RECEIVED 02 March 2023
ACCEPTED 03 March 2023
PUBLISHED 23 March 2023

CITATION
Seyoum A, Seyoum B, Gure T, Alemu A, Belachew A, Abeje D, Aseffa A, Howe R, Mulu A and Mihret A (2023) Corrigendum: Genotype heterogeneity of high-risk human papillomavirus infection in Ethiopia. *Front. Microbiol.* 14:1178530. doi: 10.3389/fmicb.2023.1178530

Corrigendum: Genotype heterogeneity of high-risk human papillomavirus infection in Ethiopia

Ayichew Seyoum[1,2]*, Berhanu Seyoum[2], Tadesse Gure[1], Addisu Alemu[1], Anteneh Belachew[1], Dessalegn Abeje[2], Abraham Aseffa[2], Rawleigh Howe[2], Andargachew Mulu[2] and Adane Mihret[2]

[1]College of Health and Medical Sciences, Haramaya University, Harar, Ethiopia, [2]Armauer Hansen Research Institute, Addis Ababa, Ethiopia

KEYWORDS

human papillomavirus, cervical cancer, prevalence, genotyping, Ethiopia

A corrigendum on

Genotype heterogeneity of high-risk human papillomavirus infection in Ethiopia

by Seyoum, A., Seyoum, B., Gure, T., Alemu, A., Belachew, A., Abeje, D., Aseffa, A., Howe, R., Mulu, A., and Mihret, A. (2023). *Front. Microbiol.* 14:1116685. doi: 10.3389/fmicb.2023.1116685

In the original article, there was an error in affiliation 3. Instead of "TDR, the Special Program for Research and Training in Tropical Diseases, WHO, Geneva, Switzerland", it should be "Armauer Hansen Research Institute, Addis Ababa, Ethiopia", which is listed as affiliation 2.

In the original article, there was a mistake in Figure 4, "Age category of women in years" and the age category on the x-axis in Figure 4. "Age-specific prevalence of hr HPV infection among women in Ethiopia" was not correctly indicated as published.

The corrected label of the x-axis of Figure 4 is "Age category of women in years" and the age category of women is listed, "at 30 years, 31–35 years, 36–40 years, 41–45 years, 46–50 years, 51–55 years, 56–60 years," as shown in the figure.

The authors apologize for these errors and state that this does not change the scientific conclusions of the article in any way. The original article has been updated.

Publisher's note

All claims expressed in this article are solely those of the authors and do not necessarily represent those of their affiliated organizations, or those of the publisher, the editors and the reviewers. Any product that may be evaluated in this article, or claim that may be made by its manufacturer, is not guaranteed or endorsed by the publisher.

10.3389/fmicb.2023.1178530

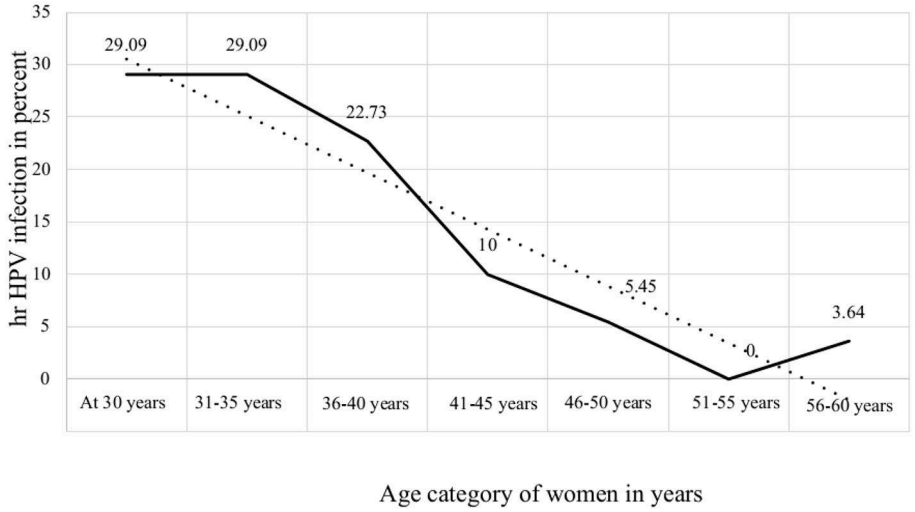

FIGURE 4
Age-specific prevalence of hr HPV infection among women in Ethiopia.

frontiers | Frontiers in Microbiology

TYPE Review
PUBLISHED 24 February 2023
DOI 10.3389/fmicb.2023.1118164

OPEN ACCESS

EDITED BY
Ons Bouchami,
Universidade Nova de Lisboa, Portugal

REVIEWED BY
Jess Vergis,
Kerala Veterinary and Animal Sciences University, India
Matthew D. Moore,
University of Massachusetts Amherst, United States
Mohamed Fethi Diouani,
Institut Pasteur de Tunis, Tunisia
Laura Cerqueira,
University of Porto, Portugal

*CORRESPONDENCE
Hamed Mirjalali
✉ hamedmirjalali@sbmu.ac.ir
Kobra Omidfar
✉ omidfar@tums.ac.ir

†These authors have contributed equally to this work

SPECIALTY SECTION
This article was submitted to Infectious Agents and Disease, a section of the journal Frontiers in Microbiology

RECEIVED 07 December 2022
ACCEPTED 30 January 2023
PUBLISHED 24 February 2023

CITATION
Nemati S, Shalileh F, Mirjalali H and Omidfar K (2023) Toward waterborne protozoa detection using sensing technologies. *Front. Microbiol.* 14:1118164. doi: 10.3389/fmicb.2023.1118164

Toward waterborne protozoa detection using sensing technologies

Sara Nemati[1], Farzaneh Shalileh[2], Hamed Mirjalali[1]*† and Kobra Omidfar[3,4]*†

[1]Foodborne and Waterborne Diseases Research Center, Research Institute for Gastroenterology and Liver Diseases, Shahid Beheshti University of Medical Sciences, Tehran, Iran, [2]Department of Life Science Engineering, Faculty of New Sciences and Technologies, University of Tehran, Tehran, Iran, [3]Biosensor Research Center, Endocrinology and Metabolism Molecular–Cellular Sciences Institute, Tehran University of Medical Sciences, Tehran, Iran, [4]Endocrinology and Metabolism Research Center, Endocrinology and Metabolism Research Institute, Tehran University of Medical Sciences, Tehran, Iran

Drought and limited sufficient water resources will be the main challenges for humankind during the coming years. The lack of water resources for washing, bathing, and drinking increases the use of contaminated water and the risk of waterborne diseases. A considerable number of waterborne outbreaks are due to protozoan parasites that may remain active/alive in harsh environmental conditions. Therefore, a regular monitoring program of water resources using sensitive techniques is needed to decrease the risk of waterborne outbreaks. Wellorganized point-of-care (POC) systems with enough sensitivity and specificity is the holy grail of research for monitoring platforms. In this review, we comprehensively gathered and discussed rapid, selective, and easy-to-use biosensor and nanobiosensor technologies, developed for the early detection of common waterborne protozoa.

KEYWORDS

waterborne protozoa, point-of-care, biosensors, microfluidic, smartphone

1. Introduction

Healthy water resources are still one of the main challenges in most countries, particularly less developed regions in dry parts of the world (WHO/UNICEF, 2014; Andrade et al., 2018). The lack of sufficient and appropriate water resources increases the use of contaminated water sources and wastewater for drinking, washing, and irrigation. Accordingly, employing contaminated water not only directly increases the risk of contamination by waterborne pathogens but also enhances the risk of contamination of vegetables with waterborne pathogens, particularly in farmlands irrigated using wastewater (Karanis et al., 2006; Javanmard et al., 2019, 2020).

Waterborne diseases include a large group of illnesses with mild to severe symptoms, which are caused by a broad spectrum of pathogens including bacteria, fungi, parasites, and viruses (Kalyoussef and Feja, 2014). Parasites, both protozoa and helminths, are important group of foodborne and waterborne pathogens, which can be transmitted from wild and domestic animals and contaminated water resources to humans (Sharma and Mutharasan, 2013; Vasilescu and Marty, 2016; Pazoki et al., 2020). The transmission route of foodborne and waterborne protozoa (FWP) is mostly oral-fecal and infection occurs when cysts or oocysts of a parasite are unintentionally ingested by a host (Kalyoussef and Feja, 2014).

Waterborne protozoa are responsible for a considerable number of outbreaks in the world. Regarding a recently published systematic review, 86.7% of eastern African countries reported at least one waterborne parasite from 1953 to 2019 (Ngowi, 2020). However, there is no periodical monitoring strategy for the detection of waterborne parasites (particularly protozoa) in less-developed regions like African countries. In contrast, outbreak surveillance in Europe between 2000 and 2007 indicated the presence of 354 and 70 outbreaks, related to drinking water and bathing water, respectively, in which protozoa were responsible for 17 (4.7%) drinking water and 38 (54.3%) bathing water outbreaks (ENHIS, 2009). Moreover, it was estimated that ~7,150,000 (95% CrI 3,880,000–12,000,000; 21.3%) illnesses in the United States in 2014 were associated with waterborne agents, of which *Giardia lamblia* and *Cryptosporidium* spp., were responsible for 415,000 (95% CrI 140,000–816,000) and 322,000 (95% CrI 61,700–993,000) illnesses, respectively (Collier et al., 2021). In addition, more than 10% of the total waterborne outbreaks from 1991 to 2008 were attributed to parasitic agents, particularly protozoa (Karanis et al., 2006; Efstratiou et al., 2017). More recently, *Cryptosporidium* spp., *G. lamblia*, *Cyclospora cayetanensis*, *Toxoplasma gondii*, *Blastocystis* sp., *Entamoeba histolytica*, microsporidia, and *Naegleria fowleri* were reported as the main causative agents detected in 251 waterborne outbreaks from 2017 to 2020 (Ma et al., 2022). Interestingly, most waterborne outbreaks due to protozoa have been reported in developed countries, indicating the importance of periodical monitoring of water resources, as well as diagnostic capabilities (Ma et al., 2022).

Significant progress has been made in recent decades in developing portable, reusable, and effective miniaturized systems or point-of-care (POC) platforms. POC tests can be performed outside a clinical laboratory setting, at or near the site of patient care. In addition, along with climate change, particularly in recent years, the risk of transmission of infectious diseases and the number of areas, which were previously unaffected by specific infectious diseases, have increased (Mora et al., 2022). In contrast, global warming, as a coming challenge in the world, decreases access to healthy water resources and increases emerging water and food safety concerns (Duchenne-Moutien and Neetoo, 2021). In fact, drought due to climate changes increases seasonal water resources, which aggregates animals and human communities in a region, recycled water resources, groundwater, and even lagoon water, and therefore, the risk of transmission of potentially pathogenic microorganisms, particularly parasites, from animals to humans (Titcomb et al., 2021). Moreover, because of the presence of a resistant stage, cyst/oocyst/egg, in the life cycle of parasites, particularly protozoa, these microorganisms endure harsh conditions such as drought much more than other microorganisms. All of these reasons highlight the importance of protozoa infections and the development of POC techniques for the detection of these parasites in the future. Guidelines, commonly needed for establishing well-organized POC systems, are presented by the World Health Organization (WHO). These guidelines are identified as ASSURED, in which the abbreviation ASSURED stands for affordable, sensitive, specific, user-friendly, rapid, equipment-free, or minimal, and delivered to those who require them (Syedmoradi et al., 2017, 2021; Omidfar et al., 2020).

This study highlights the need for rapid, selective, and easy-to-use technology for the early detection of common waterborne parasitic pathogens. The purpose of the current review is to provide a comprehensive overview of conventional methods and emerging biosensors and nanobiosensors, with a focus on recent advances in smart-based devices.

2. A brief look at the significant waterborne parasites

Although a broad spectrum of parasites is reported from waterborne outbreaks, *Cryptosporidium* spp., *G. lamblia*, *T. gondii*, and *E. histolytica* are among the most frequently detected waterborne parasites in the world (Al-Shamiri et al., 2010; Robert-Gangneux and Dardé, 2012; Plutzer and Karanis, 2016; Sarkari et al., 2016; Ma et al., 2022). Nevertheless, microsporidia, *Blastocystis* sp., *Dientamoeba fragilis*, *Balantidium coli*, *C. cayetanensis*, and *Isospora belli* are the neglected waterborne parasites (Karanis et al., 2006; Plutzer and Karanis, 2016). Regarding the worldwide waterborne outbreaks reported by Baldursson and Karanis (2011), from 2004 to 2010, *Cryptosporidium* spp., and *G. lamblia* were the major causative agents in 60.3% (120) and 35.2% (70) of 199 outbreaks, respectively, while *T. gondii*, *C. cayetanensis*, *Acanthamoeba* spp., *E. histolytica*, and *Blastocystis* sp., were the other reported agents. Recently, an update on waterborne outbreaks due to parasites from 2017 to 2020 signified the high prevalence of *Cryptosporidium* spp., and *G. lamblia* as the major reported agents, followed by *D. fragilis*, *T. gondii*, *C. cayetanensis*, *Blastocystis* sp., *E. histolytica*, *N. fowleri*, and microsporidia (Ma et al., 2022).

2.1. *Cryptosporidium* spp.

Cryptosporidium spp. are apicomplexan protozoa, with several known species that infect humans and many other vertebrates, and are transmitted *via* the fecal-oral route through ingesting oocytes in contaminated food or water (Leitch and He, 2012; Gerace et al., 2019; Zahedi and Ryan, 2020). *Cryptosporidium* spp. can infect both immunocompetent and immunocompromised individuals, of which two species, *Cryptosporidium parvum* and *Cryptosporidium hominis*, are the most prevalent species in humans (Mmbaga and Houpt, 2017).

Cryptosporidium spp. are known as the main protozoa parasite reported from waterborne outbreaks (Zahedi and Ryan, 2020; Gururajan et al., 2021; Zahedi et al., 2021). A most recent study reported that, from 251 waterborne outbreaks with parasitic agents, *Cryptosporidium* was identified among 198 outbreaks (Ma et al., 2022). *C. parvum* is a zoonotic species, which is isolated from humans and a broad spectrum of animals; therefore, there is an increased risk of contamination of water resources not only by human feces but also by excreted oocysts from free-range animals (Fernández et al., 2021; Mohammad Rahimi et al., 2022). In addition, it was documented that routine wastewater treatment processes including sedimentation, activated sludge, chlorination, and filtrations are not enough to eliminate *Cryptosporidium* oocysts

from water samples (Sroka et al., 2013; Ramo et al., 2017), which increases the concern for the contamination of downstream farmlands irrigated with treated wastewater (Javanmard et al., 2020).

2.2. *Giardia lamblia*

G. lamblia (also known as *Giardia intestinalis* and *Giardia duodenalis*) is an anaerobic-flagellated non-invasive protozoan, which can infect the small intestine and, in a few cases, the distal small bowel, cecum, stomach, and pancreas of humans and many other vertebrates (Einarsson et al., 2016; Bahramdoost et al., 2021). *G. lamblia* is more prevalent in children living in developing countries and is classified as FWP. This protozoan is transmitted *via* the fecal-oral route through ingestion of the cystic form in contaminated food or water (Bello et al., 2011).

G. lamblia is the second-most reported protozoa from waterborne outbreaks worldwide (Karanis et al., 2006; Efstratiou et al., 2017; Ma et al., 2022). Similar to *Cryptosporidium* spp., the main reason for the high prevalence of *G. lamblia* in waterborne outbreaks is the capability of this protozoan to remain viable during water treatment processes (Sroka et al., 2013; Ramo et al., 2017). Large waterborne outbreaks due to *G. lamblia* have been reported all over the world, particularly in developed countries. Nygård et al. (2006) documented a large outbreak of giardiasis among at least 1,300 cases in Norway that was linked to leakage of wastewater pipes and insufficient wastewater treatment. Recently, a large giardiasis outbreak related to tap water occurred in Bologna Province, Italy, and the presence of *G. lamblia* was documented in 228 stool samples (Resi et al., 2021). However, the number of reported outbreaks due to *G. lamblia* and *Cryptosporidium* spp., in developed countries is significantly higher than in less-developed regions, which could be due to the use of more sensitive detection technologies in developed countries (Ma et al., 2022).

2.3. *Toxoplasma gondii*

T. gondii is an obligate intracellular parasite, which infects most warm-blooded animals, and Felidae family members are its definitive hosts (Tenter et al., 2000; Mendez and Koshy, 2017). *T. gondii* is transmitted *via* several routes including vertical transmission (Kanková and Flegr, 2007; Robbins et al., 2012; Chaudhry et al., 2014), transfusion and needle stick (Foroutan-Rad et al., 2016), and fecal-oral route *via* eating or drinking oocyst-contaminated food and water (Hill and Dubey, 2002). However, *T. gondii* is considered a neglected waterborne protozoan (Baldursson and Karanis, 2011; Karanis et al., 2013; Plutzer and Karanis, 2016). Nevertheless, in an outbreak related to drinking water in the Champagne-Ardenne region, France, Villena et al. (2004) detected *T. gondii* DNA in 10/125 analyzed samples. Then, Aubert and Villena (2009) analyzed water samples, which were collected in 2001 in Champagne-Ardenne, France, and characterized *T. gondii* DNA in 37/482 environmental samples. These two studies suggested the high contamination of water samples with *T. gondii* in the studied region in France. The presence of *T. gondii* DNA in wastewater samples in Germany was as high as that reported in France. Accordingly, Gallas-Lindemann et al. (2013) scrutinized influent and effluent samples of wastewater in Germany and reported the presence of *T. gondii* DNA in 8/83 (9.6%) samples using loop-mediated isothermal amplification (LAMP). Microscopically, oocyst-like positive samples for *T. gondii* were also detected in environmental water samples collected in the Galápagos Islands, Ecuador, although molecular identification of the samples was not successful (Verant et al., 2014). *T. gondii* DNA was also identified using real-time PCR in 2/8 wastewater samples, together with *G. lamblia*, *E. coli*, *Entamoeba dispar*, *Entamoeba hartmanni*, *Blastocystis* sp., and *Acanthamoeba* spp. in Spain (Moreno-Mesonero et al., 2022). These studies, as well as a large outbreak due to the consumption of drinking water contaminated with *T. gondii*, which was reported in 2018 from Santa Maria, Brazil (Minuzzi et al., 2021), highlight the importance of waterborne toxoplasmosis and the neglected role of *T. gondii* in waterborne outbreaks due to insufficient detection techniques.

3. Available diagnostic techniques for the detection of waterborne parasites

Diagnosis plays a critical role in the discovery of new pathogens, monitoring and surveillance, the prediction of epidemics and pandemics due to emerging and re-emerging pathogens, and antibiotic resistance (Mohammad Rahimi et al., 2019). In recent decades, various methods have been developed for the diagnosis of intestinal parasites. However, conventional diagnostic methods are still employed for the detection of intestinal parasites, particularly in less-developed regions (Mohammad Rahimi et al., 2019). Accordingly, the detection of *G. lamblia*, *Cryptosporidium* spp. and *E. histolytica* is mainly based on the optical detection of cysts/oocysts and trophozoites of parasites using microscopy (Destura et al., 2015; Ricciardi and Ndao, 2015; Hooshyar et al., 2019), while the most common diagnostic method for *T. gondii* is immunoassay techniques (Elgun and Koltas, 2011; Rostami et al., 2018).

Despite the advantages of microscopic methods, there are some limitations such as the technique being time-consuming and optical skills of laboratory technicians (Laude et al., 2016; Sakamoto et al., 2018). In addition, due to the low number of FWP in a large volume of environmental samples like water, employing microscopic techniques is an important challenge. For example, the concentration of *G. lamblia* in water samples has been reported to be 0.01 to 100 cysts/L (WHO, 2014); thus, developing methods for the detection of 1 cyst/oocyst of *G. lamblia* and *Cryptosporidium* spp., in 10–100 L of water samples is desirable, particularly when we consider that *Cryptosporidium* spp., and *G. lamblia* are among the waterborne pathogens with a high priority and with infectivity dosage less than 10 oocysts/cysts (WHO, 2014). In contrast, the development of molecular techniques in recent decades has overcome the limitations of conventional methods and has provided more sensitivity and specificity for the detection of pathogens (Tavares et al., 2011).

Although progress has been made in molecular techniques, there are still some disadvantages and limitations that restrict the application of molecular techniques. Multiple steps including

TABLE 1 Comparative evaluation of conventional methods for the detection of FWP.

Technique	Detection principle	Advantages	Disadvantages	Time
Microscopy techniques	Using microscopes to screen samples	• Low cost and high feasibility • Study the structure	• Low sensitivity • Requires highly trained and experienced technician • Need for sample concentration prior to screening	30–45 min to overnight staining
Culture technique	Cultivation of parasites in a specific medium to either keep parasites alive or increase their number	• Specificity up to 100% • Availability of isolate • Providing a system to assess vaccine research • Study the biochemistry, physiology, and metabolism of the pathogens • Study of drug resistance	• Low sensitivity • High probability of contamination • Requires specific cultivation conditions • Time-consuming	3–15 days
Immunological techniques (ELISA)	Based on a specific antigen-antibody interactions and antigen or antibody detection	• Low cost • Sensitivity and specificity in the range of 93–100% • Screening a large number of samples • Providing large amounts of data about every contact to studied agent	• Cross reactions • Not suitable for real time screening of an infection • Not suitable for detection of most of intestinal parasites	15 min−5 h
Molecular techniques (PCR-based techniques)	Detection of a specific region of a target gene	• High sensitivity and specificity • Fingerprinting • Phylogenetic analysis	• High cost and need for specific equipment and instruments • Need for sample treatment before tests such as DNA/RNA extraction • The negative role of inhibitors in the amplification process • Wrong estimation of an infection due to amplification of dead microorganisms	2–4 h

DNA or RNA extraction, primer design challenges, false results due to undesirable primer interactions, and expensive equipment are the common challenges facing molecular methods (Garibyan and Avashia, 2013; Khurana and Chaudhary, 2018). Regarding the abovementioned limitations of conventional and advanced molecular methods, designing high-efficiency and field-adopted diagnostic devices with a simple user interface and a rapid protocol is the main priority (Luka et al., 2019) (Table 1).

In recent years, advanced devices have been developed to overcome the limitations of available techniques. For example, the sensitivity of microscopic techniques is not high enough, and a well-trained technician is needed to reduce the possibility of a false report. In addition, the staining procedure may take much time; these reasons are challenges at the time of outbreaks. In contrast to microscopic methods, serological and molecular techniques are not labor intensive, provide high sensitivity and specificity, and do not need a microscopist. Nevertheless, serological methods may provide cross reaction, and are not suitable for screening a population at the time of outbreaks or most intestinal FWP. In addition, due to expensive equipment and instruments for molecular methods, and the need for a well-equipped laboratory, most molecular-based approaches are not suitable for investigation of an outbreak (Mohammad Rahimi et al., 2019; Mahdavi Abhari et al., 2023). Therefore, focus has been dramatically increased on biosensors, such as POC tests, which can provide enough sensitivity and specificity, without the need for a well-trained technician or a specific facility.

4. Biosensors: Development and types

The importance of food and water safety in various industries has led to the mining and improvement of nanoscale analytical devices known as nanobiosensors. Due to the numerous advantages of these devices such as portability, low cost, rapid assay time, ease of use, and high selectivity and sensitivity (Terry et al., 2005; Ahmadi et al., 2022; Khoshfetrat et al., 2022; Saeidi et al., 2022), particularly for the detection of infectious agents and pollutants in the environment (Pejcic et al., 2006; Sin et al., 2014; Ahmadi et al., 2021c), focus on the fabrication of biosensors as a diagnostic technology for the detection of different analytes in food, water, and environmental samples has intensely increased (Terry et al., 2005; Pejcic et al., 2006; Metkar and Girigoswami, 2018; Salouti and Khadivi derakhshan, 2020) (Figure 1).

A biosensor consists of at least two functional elements, namely, a molecular recognition element (receptor), which selectively interacts with its target analyte, and a physicochemical transducer. Biological elements are generally classified into enzymes, antibodies, and nucleic acids. A transducer is a component of biosensors which plays an important role in the signal detection process, and converts biological responses into a measurable signal with high quality (Khodaei et al., 2019; Ahmadi et al., 2021a,b).

Biosensors are generally classified into label-free and labeled. The latter biosensor employs labeled molecules for the detection of a target (Proll et al., 2007; Rhouati et al., 2016). Common labeling

10.3389/fmicb.2023.1118164

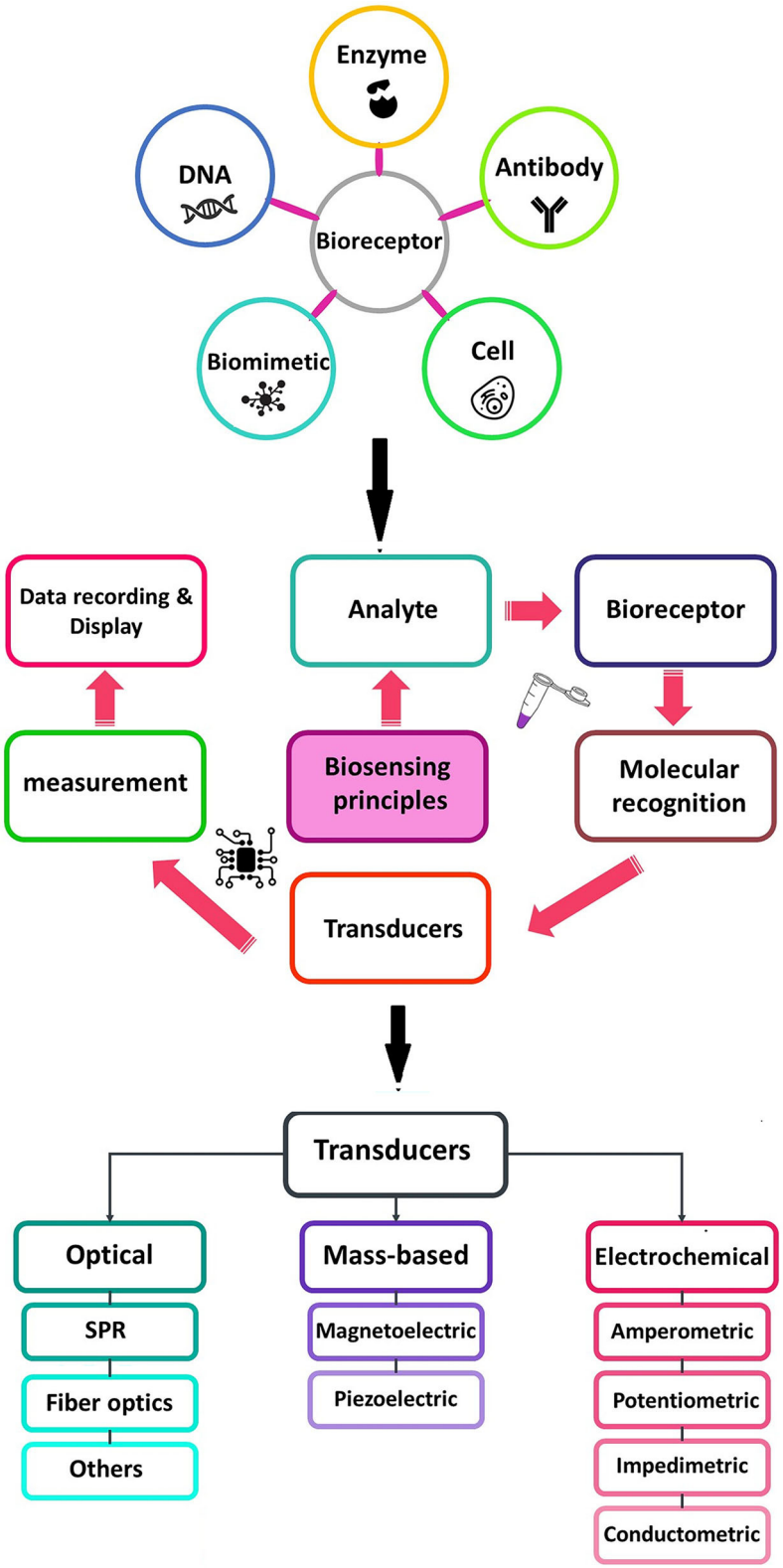

FIGURE 1
Schematic diagram of a typical biosensor consisting of various types of bioreceptors and transducers used in the biosensors.

platforms are fluorescence or luminescence labeling, radiolabeling, isotope labeling, and enzymes (Deline and Nason, 2019; Ranjbar Bahadori et al., 2021). In these procedures, the final sensor signal represents the number of labels bound to target molecules. As a drawback, label-based technologies are labor- and cost-intensive and time-consuming (Cunningham and Laing, 2008). In addition, labeling of biomolecules can block active binding sites and alter the binding properties (Schöning and Poghossian, 2018).

In contrast, label-free biosensing technologies do not employ labels to facilitate measurements and instead incorporate the intrinsic physical properties of an analyte, such as the molecular weight, size, charge, electrical impedance, dielectric permittivity, and refractive index of a sample. In recent years, label-free biosensors have been developed due to their ability for rapid and inexpensive bio-detection in small reaction volumes (Schöning and Poghossian, 2018). Moreover, they can be integrated into lab-on-a-chip platforms, allowing monitoring of target analytes in real time. Label-free biosensors are usually designed based on optical, electrical or electrochemical, and acoustic parameters (Citartan et al., 2013).

Based on the biological elements, biosensors are categorized into genosensors, immunosensors, and aptasensors (Low et al., 2012; Kokkinos et al., 2016; Campuzano et al., 2017; Mohammed et al., 2017; Felix and Angnes, 2018).

In genosensors, oligonucleotide sequences (DNA or RNA) are usually employed as bio-receptors, which are immobilized onto the transducer surface and hybridized with the single-stranded target DNA. In fact, the oligonucleotide sequences, such as a probe, recognize the analyte (sample DNA or RNA) by matching with the complementarity sequences. Genosensor-based devices are widely used for the detection of a broad spectrum of pathogens (Drummond et al., 2003; Babkina and Budnikov, 2006; Gao et al., 2010; Mohammed et al., 2017) (Figure 2A).

Immunosensors play an important role in the evaluation of specific elements in biological fluids. Currently, such assays have been extensively utilized in food safety and environmental analysis (Felix and Angnes, 2018; Hosu et al., 2018) (Figure 2B).

A single-stranded functional nucleic acid or peptide with a strong receptor property is recognized as an aptamer. Aptamers are usually constructed from combinatorial single-stranded libraries by the systematic evolution of ligands using the exponential enrichment (SELEX) method, and are applied to detect multiple target analytes (Shamah et al., 2008; Liu et al., 2020). Aptamer-based techniques have been applied for the detection of numerous pathogens such as human immunodeficiency virus (HIV), hepatitis B virus (HBV), hepatitis C virus (HCV), *Mycobacterium*, *Salmonella*, *Listeria*, *Staphylococcus*, *Clostridium*, *Bacillus*, *Escherichia*, *Aspergillus*, *Penicillium*, SARS-CoV, influenza virus, respiratory syncytial virus (RSV), *Trypanosome*, *Plasmodium*, *Cryptosporidium*, and *Leishmania* (Cho et al., 2011; Nagarkatti et al., 2012; Martín et al., 2013; Iqbal et al., 2015; Babamiri et al., 2018; Lavania et al., 2018; Li et al., 2018, 2020; Suh et al., 2018; Wei et al., 2018; Xi et al., 2018; Cai et al., 2019; Singh et al., 2019; Zou et al., 2019). The number of aptasensor-based studies for the detection of FWP is low. In this regard, Iqbal et al. (2015) developed an electrochemical nanomaterial-based aptasensor using a gold nanoparticle (NP)-modified screen-printed carbon electrode (SPCE) to detect *C. parvum* oocysts in spiked fresh fruits. In this system, 14 aptamer colons were discovered and anti-aptamer and thiolated DNA primers were mixed to produce a hybrid compound that was assembled onto the SPCE. The fabricated aptasensor recognized *C. parvum* with a wide dynamic range from 150 to 800 oocysts and a detection limit of ∼100 oocysts. This study suggested promising findings for the detection of *C. parvum* in food products (Iqbal et al., 2015) (Table 2; Figure 3).

5. A brief look at nanomaterials incorporated into sensors

Improvements in nanotechnology science have provided the opportunity for researchers to work at nanoscale levels. Nanomaterials range from 1 to 100 nm and are classified into various groups, namely, nanoparticles (NPs), quantum dots (QDs), carbon nanotubes (CNTs), graphene, graphene oxide (GO), and nanochannels (Avant et al., 2019; Saleem and Zaidi, 2020; Pandey and Chusuei, 2021). Incorporating NPs with a biosensor system is performed for modifying and improving the sensor platforms and to overcome the limitations of conventional diagnosis tools (Luo et al., 2006). NPs are employed in the main types of biosensor systems including electrochemical, calorimetric, optical, and acoustic (Malik et al., 2013). NPs have critical functions such as reducing the time of reactions, catalysis, and immobilization of biomolecules (nucleic acid, antibody, and enzymes) into the electrochemical biosensors (Luo et al., 2006). In addition, due to their large specific surface, NPs are useful for improving electron transfer between biomolecules and the surface electrode (Cho et al., 2020). Common NPs include metal NPs (Au, Ag, and Pt), oxide NPs (SiO_2, TiO_2, ZrO_2, and MnO_2), and semiconductor NPs (CdS and PbS); metal NPs are more common due to their excellent catalytic properties in catalyzing electrochemical reactions (Tang et al., 2005). Moreover, silver and gold NPs have excellent conductivity properties, which enhance electron transfer between biomolecules and electrodes (Alaqad and Saleh, 2016). Moreover, gold NPs play an important role in increasing the sensitivity of electrochemical biosensors (Saha et al., 2012).

Magnetic NPs (MNPs) are used for designing magnetic biosensors, which have been broadly applied in medical areas such as diagnostic assays, DNA or RNA isolation, magnetic resonance imaging (MRI), and drug delivery (Khoo et al., 1997; Kudr et al., 2017; Wang et al., 2017; Ali et al., 2021). MNPs are a class of nanomaterials composed of metals such as cobalt, nickel, and iron, with paramagnetic, ferromagnetic, and superparamagnetic properties (Aboul-Enein et al., 1999; Akbarzadeh et al., 2012). Magnetic iron oxide NPs are employed for biomedical applications such as magnetic separation (Wu et al., 2015). For example, immunomagnetic separation (IMS) is now employed as a standard method for the detection and separation of *Cryptosporidium* spp., and *G. lamblia* oocysts/cysts from 10 to 150 L water samples (USEPA, 2012), although several studies have been conducted to increase the recovery rate of the method using either additional concentration methods or alternative elution (Hu et al., 2004; Fradette and Charette, 2022).

Oxide NPs have several chemical properties and possess a high surface energy (Stankic et al., 2016). For example, MnO_2 NPs can directly react with biomolecules (Vukojević et al., 2018).

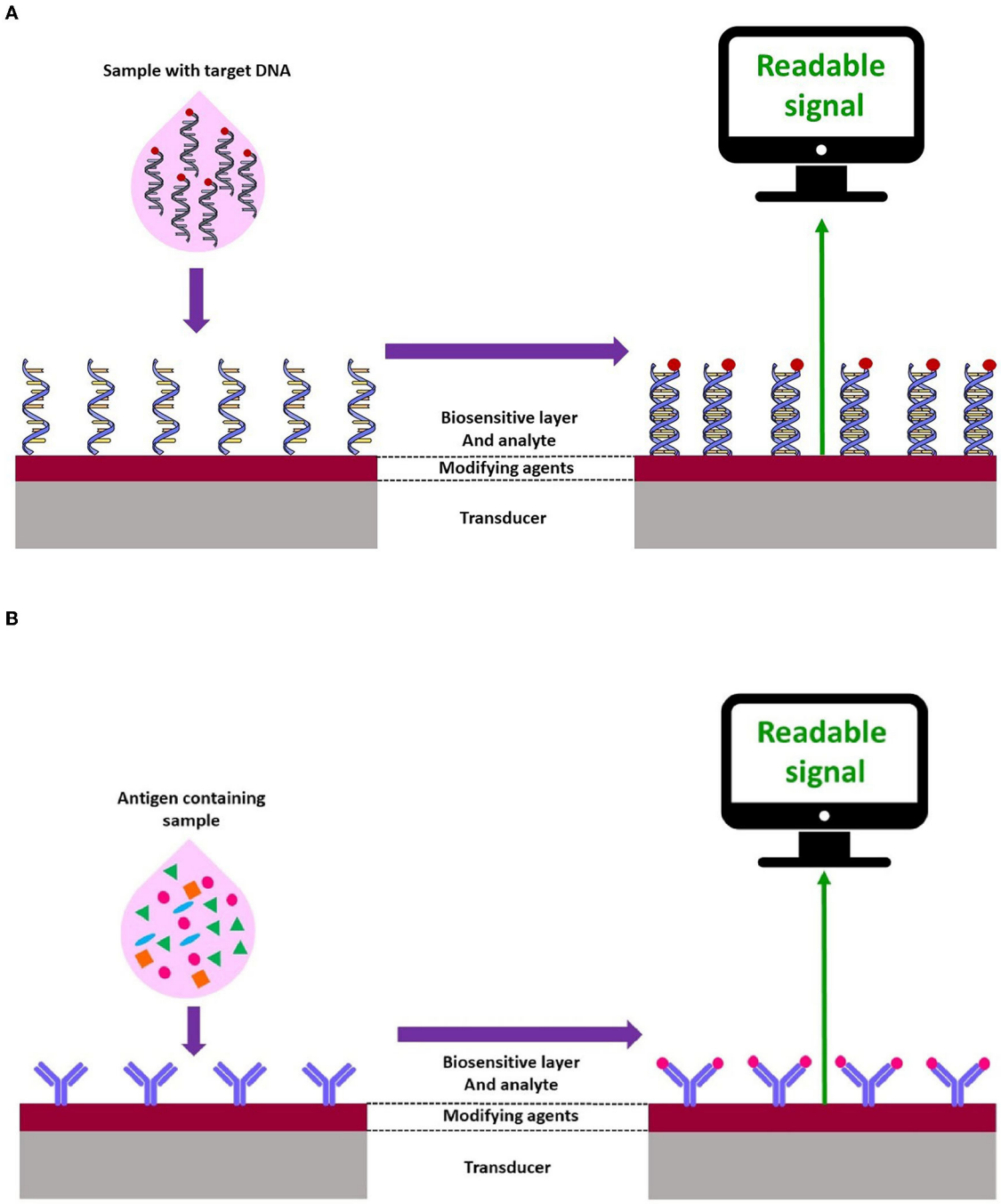

FIGURE 2
Schematic representation of electrochemical **(A)** genosensors and **(B)** immunosensor.

In addition, oxide NPs, for instance, SiO_2 NPs, can also be used as labels for biomolecules. SiO_2 NPs, as an oligonucleotide label, have been used for electrochemical sensitive detection in genosensors and immunosensors (Ma et al., 2008; Wang et al., 2013).

Quantum dots are semiconductor nanocrystals made up of a reactive core, which contains semiconductor particles such as cadmium selenide (CdSe), cadmium telluride (CdTe), indium phosphide (InP), or zinc selenide (ZnSe). However, QDs, as ideal materials, have been widely used in the development of sensing technology due to their extraordinary chemical properties such as excellent optical aspects (Ding et al., 2022).

Carbon nanotubes are the most popular advanced sensing technology, and have recently attracted interest for their unique properties such as excellent electronic conductivity features and large surface-to-volume ratios (Zaporotskova et al., 2016). Nanotubes have cylindrical structures with several hexagonal graphite planes rolled in tubes, which are divided into single-walled NTs (SWNTs) and multi-walled NTs (MWNTs), based on the number of walls (Saxena and Srivastava, 2020).

TABLE 2 Summary of selected biosensors for detection of various FWP.

Analyte	Type of sensor	Transducer	Type of chip	Limit of detection	Range (linear range)	Source	References
G. lamblia	Immunosensor	PEMC (piezoelectric excitation of millimeter cantilever)	$PbZr_{0.52}Ti_{0.48}O_3$ (PZT) films and glass layer	1–10 cysts/mL per 15 min	0.5–5.0 mL/min/10–10,000 cysts/mL	Water	Xu and Mutharasan, 2010
C. parvum	Genosensor	Chronopotentiometric (electrochemical)	Screen-printed carbon strip electrodes (SPEs)	ng/mL levels of the *Cryptosporidium* DNA target	2.0 microgram/mL to ng/mL	Untreated drinking and river water	Wang et al., 1997
C. parvum	Immunosensor (labeled)	Evanescent wave fiber (optic chemical sensor)	RAPTOR Plus 4S	10^5 oocysts/mL	10^6/mL oocysts	Water	Kramer et al., 2007
E. histolytica	Immunosensor	Electrochemical sensor (voltammetry)	Gold screen-printed electrode	10 pg/mL (588 fM).	10 pg /mL (588 fM) to 500 pg/mL (29.4 pM)	Stool samples	Grewal et al., 2014
C. parvum	Immunosensor	Colorimetric detection (non-labeling fluorescence sensor)	Polydiacetylene-based fluorescence chip	1×10^3 oocysts/mL	1×10^5 oocysts/mL *C. parvum* (in tap water) and 1×10^5 cysts/mL *G. lamblia* (in PBS buffer)	Water	Park et al., 2008
C. parvum	Immunosensor (label-free)	Electrochemical, FITc	Interdigitated gold electrodes (IDE)	40 cells/mm^2	Between 15 and 153 cells/mm^2	Water	Luka et al., 2019
T. gondii	Genosensor	Magnetic-fluorescent CdTe@Ni quantum dots (mQDs)	Not reported	2.70×10^{-9} mol/L	Not reported	*T. gondii* DNA	Xu et al., 2013
T. gondii	Immunosensor	Piezoelectric	Gold electrodes	1:5500	~1:5000–1:75	Infected rabbit serum	Wang et al., 2004
T. gondii	Genosensor	Magnetic fluorescent nanoparticles (Fe_3O_4/CdTe)	Not reported	8.339 x 10^{-9} M	$\Delta IF = 1.805c + 10.804$	*T. gondii* DNA	He et al., 2015
C. parvum	Immunosensor	Piezoelectric-excited millimeter-sized cantilever (PEMC)	PZT and glass film	100, 1000, and 10,000 oocysts/mL	100 to 10,000 oocysts/mL	Drinking water	Campbell and Mutharasan, 2006
C. parvum	Immunosensor	Electrochemical (potentiometric)	Screen printed electrode	5×10^2 oocysts/mL	10^2-10^6 oocysts/mL	Fresh bovine feces	Laczka et al., 2013
C. parvum	Immunosensor	Optical surface plasmon resonance [SPR] biosensor	Gold chip	1×10^6 oocysts/mL		*C. parvum* oocyst stock	Kang et al., 2006
C. parvum	Immunosensor	Piezoelectric electrochemical biosensor	Quartz crystal microbalance	3×10^5-1×10^7 oocysts/mL (~5 min).	3×10^5-10^7 oocysts/mL	Water	Poitras et al., 2009
C. parvum	Genosensor	Amperometric electrochemical biosensor	Interdigitated ultramicroelectrode array (IDUA) integrated with gold electrode	1 oocyst/mL	Not reported	*Cryptosporidium* oocysts DNA.	Nugen et al., 2009
C. parvum	Immunosensor (label-free)	Electrochemical impedance spectroscopy (EIS)	Biochip-based biosensing platform	<10 cells/μL	$1.43433 \times 10^{-5} \times C$ (oocysts/μl) + 7.545921×10^{-4}	Water	Houssin et al., 2010
C. parvum	Immunosensor (label-free)	EIS electrochemical biosensor	Microfabricated gold electrode	20 cells/5 μL	Up to 200 cells/5 μL	Water	Luka et al., 2022
C. parvum	Aptasensor	Square wave voltammetry electrochemical sensor	Screen-printed carbon electrode	100 oocysts/mL	200–700 oocysts/mL	Fresh fruits	Iqbal et al., 2015

10.3389/fmicb.2023.1118164

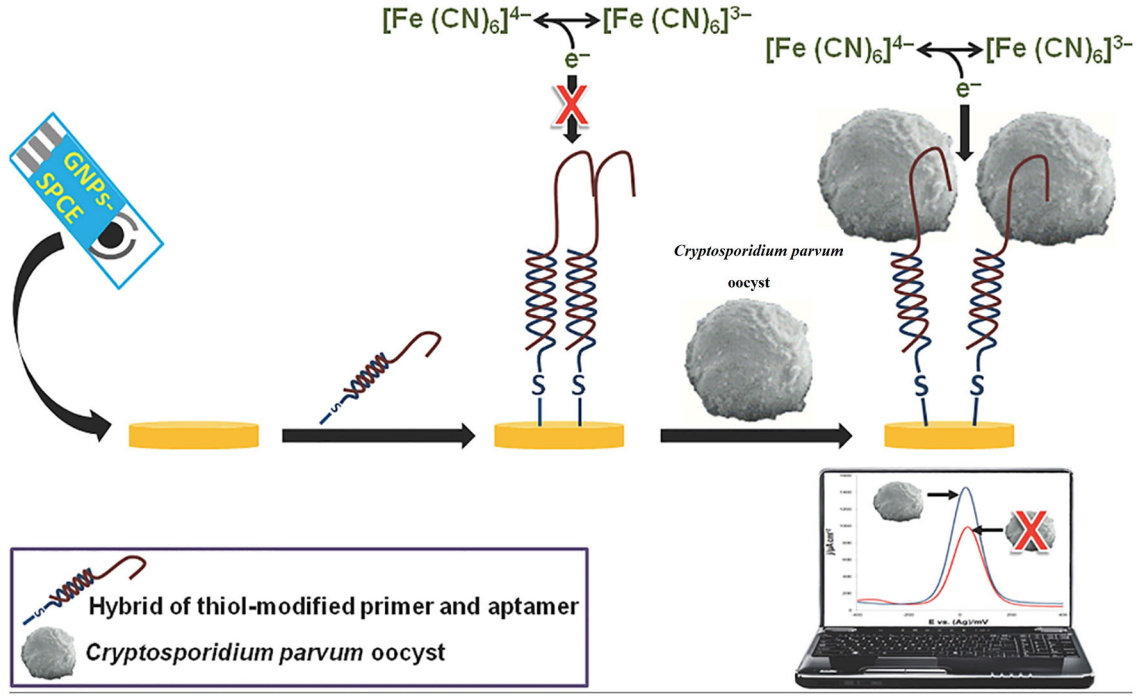

FIGURE 3
Illustration of a screen-printed aptamer-based electrochemical biosensing platform for the detection of *C. parvum* oocysts. Reproduced from Iqbal et al. (2015).

Graphene and GO nanomaterials present unique chemical and electrical features, which have highlighted them as promising materials to improve signal responses in novel sensing technologies such as electrochemical biosensors, fluorescence resonance energy biosensors transfer (FRET), laser desorption/ionization mass spectrometry (LDI-MS), and surface-enhanced Raman spectroscopy (SERS) (Chauhan et al., 2017; Janegitz et al., 2017; Morales-Narváez et al., 2017). GO possesses a hydrophobic domain structure and hydrophilic oxygen-containing functional groups, which provide good biocompatibility and water dispersibility (Ghulam et al., 2022). However, their features, including high surface area and a high affinity for a variety of biomolecules (antibodies, enzymes, DNA, cells, and proteins), have made them ideal for next-generation biosensors (Lee et al., 2016).

The recent trends are the use of both single and array nanochannels for electrical biosensing applications. Graphene and its analogs are among the emerging materials used to obtain nanochannels (de la Escosura-Muñiz and Merkoçi, 2012). The applications of nanochannels are focused on the detection of DNA, protein, virus, toxin, and other analytes (Wang et al., 2015; Sun et al., 2016; Shiohara et al., 2022).

6. Applications of biosensors based on transducer types

The biosensor system employs a sensing technique and reacts with an analyte to produce a measurable electrochemical, electrical, mechanical, optical, or thermal signal (Mehrotra, 2016; Naresh and Lee, 2021). Biosensors can also be classified as electrochemical, optical or mechanical biosensors (Cammann, 1977; Thevenot et al., 1999; Ronkainen et al., 2010; Bermejo et al., 2011; Monosik et al., 2012; Ozdemir et al., 2013).

6.1. Electrochemical

In recent years, most studies on biosensors have focused on electrochemical systems (Ronkainen et al., 2010; Low et al., 2012; Kokkinos et al., 2016). The wide practical fabrication and usage of these biosensors are based on their advantages such as feasibility, portable, rapidness, low fabrication cost, simplicity of operation, and high selectivity of this system, which make these sensors quite desirable and attractive for the POC approach. Electrodes play an important role in the performance of electrochemical cells and biosensors. The electrode structure and properties influence the cost, sensitivity, selectivity, and limit of detection (LoD) of these biosensors (Faulkner and Bard, 2002; Cesewski and Johnson, 2020). In this regard, a label-free interdigitated-based capacitive biosensor was designed on interdigitated gold electrodes for the detection of *Cryptosporidium* oocysts in water samples (Luka et al., 2019). In this study, a capture probe, anti-*Cryptosporidium* monoclonal antibodies (IgG3) and bovine serum albumin (BSA), was employed to increase the specificity and to avoid non-specific interactions. The linear detection range for this technique was 15–153 oocysts/mm^2 with a detection limit of 40 oocysts/mm^2 (Luka et al., 2019).

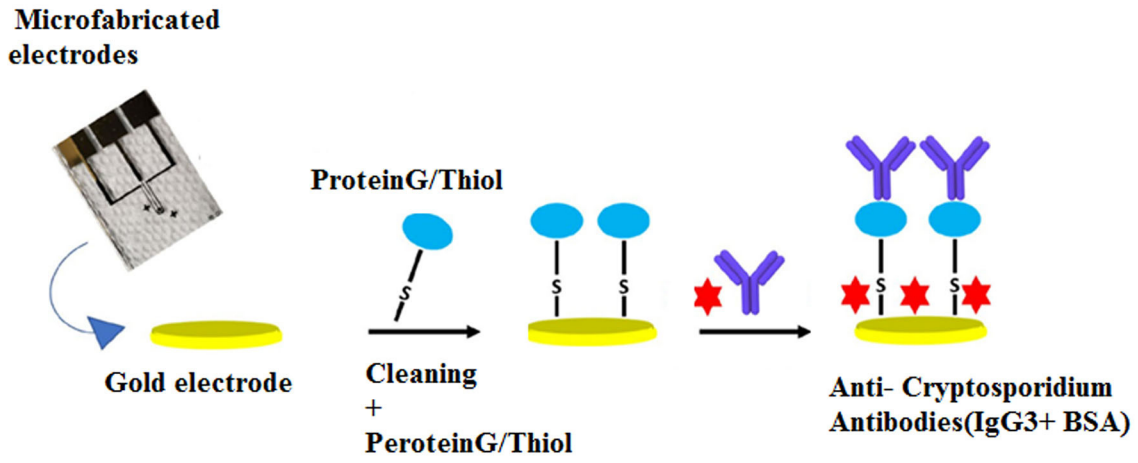

FIGURE 4
Chip-based device for label-free detection of *Cryptosporidium* oocysts in water. The figure shows the schematic process of the immobilization of anti-*Cryptosporidium* antibodies onto the Au electrode. Reproduced from Luka et al. (2022).

Potentiometric biosensors have also been used for the detection of waterborne protozoa. Laczka et al. (2013) reported a novel electrochemical approach based on a potentiometric immunosensor for the rapid detection of *C. parvum* based on (HRP)-labeled secondary antibody, which was able to detect 5 $\times$ 10^2 *Cryptosporidium* oocysts/mL in 60 min. In comparison to available ELISA techniques, Laczka et al. (2013) improved the LoD from 100- to 1,000-fold for the detection of oocysts, without the need for any specific antibody. In a study performed by Wang et al. (1997), a new electrochemical hybridization biosensor based on screen-printed carbon strip electrodes (SPEs) by the chronopotentiometry approach, as an electrochemical technique, was fabricated to detect a short specific nucleotide sequence of *Cryptosporidium* in untreated drinking and river water using the chronopotentiometric (CP) transduction method. This approach was able to discriminate *Cryptosporidium* DNA with an extremely low LoD, 50 ng/mL, and a short hybridization time of the probe, 3 min (Wang et al., 1997). Chronopotentiometry is a galvanostatic method that is used to study the mechanism and kinetics of chemical reactions with a constant level of current for a given period of time (Lingane and Peters, 1971; Kinyua Muthuri et al., 2021).

Electrochemical impedance spectroscopy (EIS) has been designed as a highly effective method based on label-free methods for the detection of biomolecules. It is used to investigate binding events that occur at the electrode surface (Magar et al., 2021). In the field of parasitology, Grewal et al. (2014) developed a nano-yeast-single-chain Fv (scFv) affinity reagents on a low-cost commercial gold screen-printed electrode for the sensitive detection of *E. histolytica* cyst antigens in stool samples at concentrations down to 10 pg/mL in buffer, with an inter-assay reproducibility of (% RSD, n = 3) 4.1%. A number of studies have also utilized this method for the detection of *Cryptosporidium* spp. A non-labeled detection system using a polydiacetylene (PDA)-based fluorescence chip based on a colorimetric detection system was developed for the detection of *C. parvum* with an LoD of 1 $\times$ 10^3 oocysts/mL (Park et al., 2008). The main advantages of this study were real-time detection of *Cryptosporidium* spp. oocysts, rapidness, simplicity, and no need for any labeling or staining for analyses (Park et al., 2008). Houssin et al. (2010) fabricated a label-free EIS biochip-based biosensing platform for the detection of *Cryptosporidium* in water samples using EIS *via* an interdigitated microelectrode array with an LoD lower than 10 cells/µL. The authors suggested that this method could be proposed as an alternative technique to current staining procedures, which was able to differentiate live and dead oocysts based on electrical impedances between 10 kHz and 100 kHz (Houssin et al., 2010). More recently, Luka et al. (2022) reported a chip-based electrochemical biosensor for the sensitive and label-free detection of *Cryptosporidium* oocysts in water samples based on anti-*Cryptosporidium* monoclonal antibodies (IgG3). This novel platform was a fast, real-time, and inexpensive tool, which was utilized to measure *C. parvum* in the range of 0–300 oocysts, with an LoD of ~20 oocysts/5 µL (Figure 4).

6.2. Optical (fluorescence, chemiluminescence-based biosensor, and surface plasmon resonance [SPR]) biosensors

The main components of an optical diagnostic device are a light source, optical transmission medium (fiber, waveguide, etc.), immobilizedm biological recognition element (enzymes, antibodies, or microbes), and optical detection system (Chen and Wang, 2020). An optical sensor converts light rays into electronic signals *via* measuring the physical quantity of light and translating it into a readable signal (Deshmukh et al., 2020). Optical sensing technologies are also divided into label-based techniques such as fluorescent labeling and label-free methods (Tang et al., 2010; Bermejo et al., 2011).

Fiber optic biosensors (FOBs), as fluorescence-based optical biosensors, are increasingly being employed for the detection of foodborne and waterborne pathogens. This technique utilizes

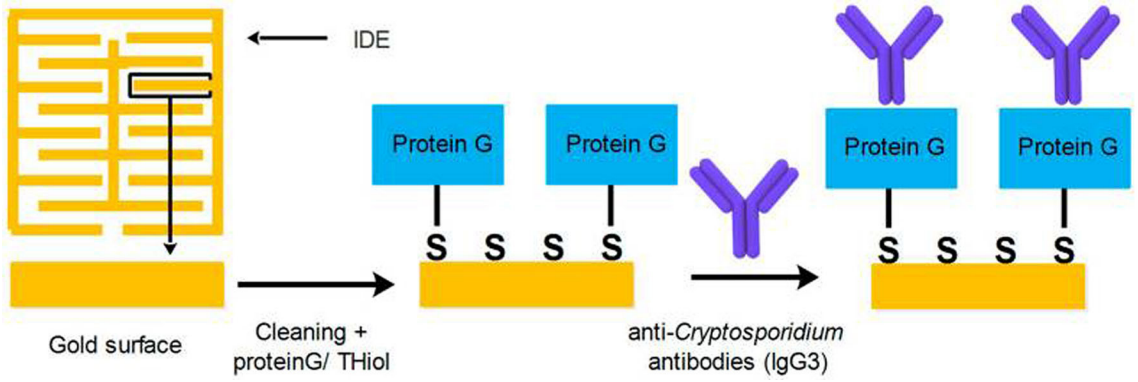

FIGURE 5
Procedure applied for covering the surface of IDE with SAM, and the attachment of anti-*Cryptosporidium* antibodies. Reproduced from Luka et al. (2019).

antibodies or other molecules to capture the target pathogen from a sample (Narayanaswamy, 2006; Hayman, 2008). In this regard, Kramer et al. (2007) developed an optical sensor (rapid automated FOB assay) based on a sandwich immunoassay using anti-*Cryptosporidium* oocyst polyclonal and monoclonal antibodies to detect the parasite in potable water. In this study, the polyclonal antibody captured the target pathogen and marked it with a cyanine 5-labeled (Cy5) detector monoclonal antibody. The LoD was 10^5 oocysts/mL, while a 10-fold increase in sensitivity was achieved using the polyclonal antibody followed by boiling samples before the detection (Kramer et al., 2007); however, owing to the low infectivity dosage of *Cryptosporidium* spp., and the low concentration of oocysts in water samples, concentration and preparation steps before employing detection techniques are still required (WHO, 2014). To overcome the short lifetime of the excited state limitation of fluorescence (Berezin and Achilefu, 2010), a luminescence process, in which a photon may be released after any time, was developed (Gaft et al., 2015). Chemiluminescence-based biosensors are another type of optical sensing device (Aboul-Enein et al., 1999), which measure the rate of photon production and generate light through a chemical reaction (Kim et al., 2021). In this optical biosensor, the analyte interacts with the immobilized biomolecule, which is marked with chemiluminescence species. Some advantages of chemiluminescence tools are high sensitivity for the detection of pathogens, fast dynamic response, and a wide calibration range (Yan et al., 2021).

As a label-free-based biosensor, Luka et al. (2019) fabricated an interdigitated-based capacitive biosensor to detect *Cryptosporidium* oocysts in water samples. In this system, the number of *Cryptosporidium* oocysts captured on the surface of the electrode was identified by means of a fluorescein isothiocyanate (FITC) immunofluorescence assay. The result of this study indicated an LoD of 40 cells/mm^2 and a linear range of detection between 15 and 153 cells/mm^2 in environmental water samples. Briefly, anti-*Cryptosporidium* monoclonal antibodies (IgG3), as the capture biomolecules, were attached to the interdigitated gold electrodes (IDE) using the protein G/thiol. Finally, upon the formation of the *Cryptosporidium*-antibody complex, changes in the capacitive/dielectric properties were detected (Figure 5).

SPR biosensors have been developed based on refractive index to increase the sensitivity of optical biosensors (Zeng et al., 2021). This system is a label-free optical phenomenon without radioactivity and fluorescence, which is recently considered a very powerful tool to study the interactions between the analyte and biorecognition molecules. This type of biosensor has remarkable advantages such as high sensitivity and specificity, label-free measurement, real-time analysis, and high-throughput capacity (Olaru et al., 2015). In addition to the common analytical applications, SPR devices are suitable for food safety monitoring and environmental applications (Olaru et al., 2015). In this regard, Kang et al. (2006) developed a flow-type SPR biosensor for the rapid detection of *Cryptosporidium* oocysts. Accordingly, an SPR biosensor was designed based on mixed self-assembled monolayers (SAMs) using 3-mercaptopropanol (3-MPOH) and 11-mercaptoundecanoic acid (11-MUA). These groups enhance the accessibility of analytes to the sensor surface using biotin–streptavidin biomolecules. This system was able to identify *C. parvum* oocysts in real time with an LoD of 1×10^6 oocyst/mL, and the sensitivity was increased to $\sim 1 \times 10^2$ oocyst/mL using biotin–streptavidin biomolecules (Figure 6).

6.3. Mechanical biosensors

Mechanical biosensors are sensitive to alterations in mechanical characteristics. These types of assays play a critical role in different bioanalytical settings (Arlett et al., 2011; Zhang and Hoshino, 2019). The functions of mechanical biosensors are mostly based on either the induced stress on the cantilever platform or the alteration in the resonant frequency of a mass-spring device (Xu et al., 2019; Chalklen et al., 2020).

The piezoelectric system is a class of mass-based biosensors, which measures changes in the oscillating crystal resonance frequency due to the interaction between bioreceptor and biological elements (antibodies, enzymes, and antigens) (Nicu et al., 2005). Various piezoelectric (like quartz crystal) (Lim et al., 2020; Wu et al., 2021) and biosensing materials have been used in piezoelectric biosensors (Skládal, 2016).

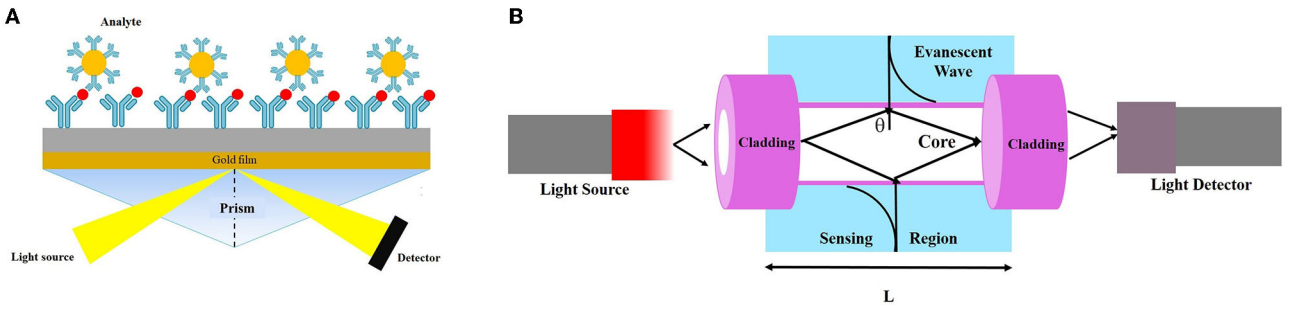

FIGURE 6
Schematic view of **(A)** evanescent wave fiber optic chemical sensor and **(B)** detection-based SPR technique.

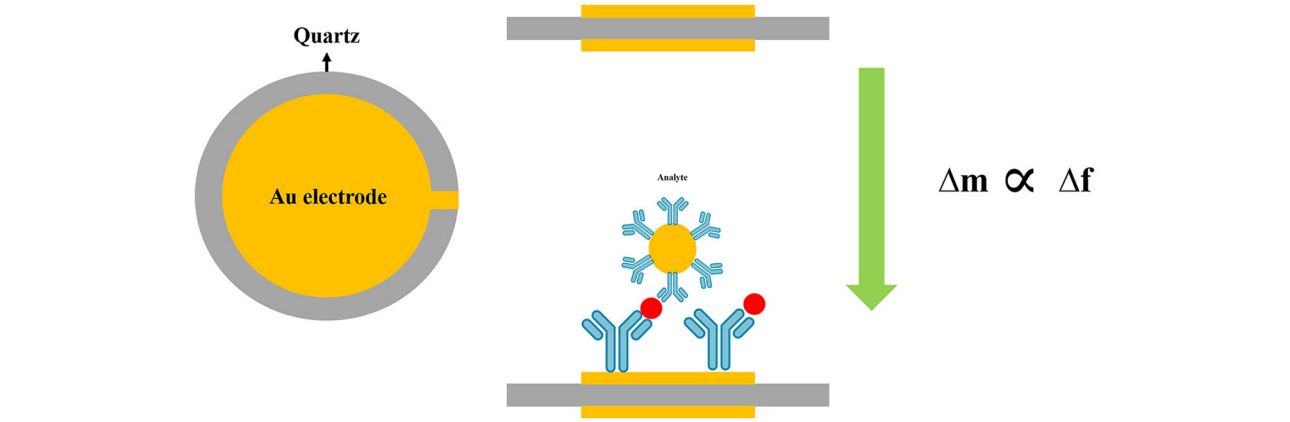

FIGURE 7
Schematic diagram of quartz crystal microbalance (QCM) technique.

Piezoelectric quartz crystal (PQC) immunosensors, as mass-sensitive devices, have been fabricated to calculate the quantification of biomolecular interactions (Bunde et al., 1998; O'Sullivan and Guilbault, 2000). Wang et al. (2004) developed a new, simple, rapid, and highly sensitive technique that was a promising alternative approach to detect anti-*T. gondii* antibodies (TgAbs) in clinical samples. The authors demonstrated that the latex piezoelectric immunoassay (LPEIA) was improved by using gold NPs, as an alternative to latex particles.

Another type of piezoelectric biosensor is a piezoelectric-excited millimeter-sized cantilever (PEMC) sensor that consists of a piezoelectric and a borosilicate glass layer with a sensing area (Zuehlke, 2022). A PEMC sensor was fabricated to detect the waterborne parasite, *G. lamblia*, in aquatic samples (Xu and Mutharasan, 2010). The resonant frequency of the sensor was continuously monitored using monoclonal antibodies against *G. lamblia* cysts, which were immobilized on PEMC sensors. In this procedure, 1–10,000 *G. lamblia* cysts/mL samples in a flow interacted with the antibody-immobilized sensor, and, upon binding cysts to the antibody, and changes in the resonant frequency of the cantilever sensor were continuously recorded. This method detected 10 cysts/mL for 15 min. Similarly, a PEMC biosensor was designed using immobilized IgM to detect *C. parvum* oocyst in a flow configuration at 1 mL/min. The PEMC detected *C. parvum* at 100, 1,000, and 10,000 oocysts/mL in less than 1 min. The resonance frequency response of the sensor was logarithmically correlated with the concentration of *C. parvum* oocysts, and due to the high sensitivity and specificity, it was employed for monitoring drinking water (Campbell and Mutharasan, 2008).

A quartz crystal microbalance (QCM) with dissipation monitoring (QCM-D) was employed to detect *Cryptosporidium* oocysts in water samples (Poitras et al., 2009). Water samples are usually contaminated by a wide range of microorganisms, including bacteria, viruses, and parasites, that may cause interference during the detection of target pathogens in the biosensing system. To overcome this limitation, the QCM-D was used as a platform for the specific binding of *C. parvum* to an antibody-covered gold-coated crystal surface to increase the specificity of the method. This technique was able to detect oocyst concentrations from 3×10^5 to 1×10^7 per mL of water with a rapid operation (~5 min) (Poitras et al., 2009) (Figure 7).

MNP-based approaches are able to rapidly detect FWP with high sensitivity and selectivity (Akbarzadeh et al., 2012). MNPs have been intensively studied due to their capability to be employed in many areas such as magnetic storage devices, optical magnetic materials, magnetic separation, and DNA-targeted diagnosis (Duguet et al., 2006; Reddy et al., 2012). In the field of parasitology, in a study developed by Xu et al. (2013), magnetic-fluorescent CdTe@Ni quantum dots (mQDs) were utilized to design a sensitive nanobiosensor based on fluorescence resonance

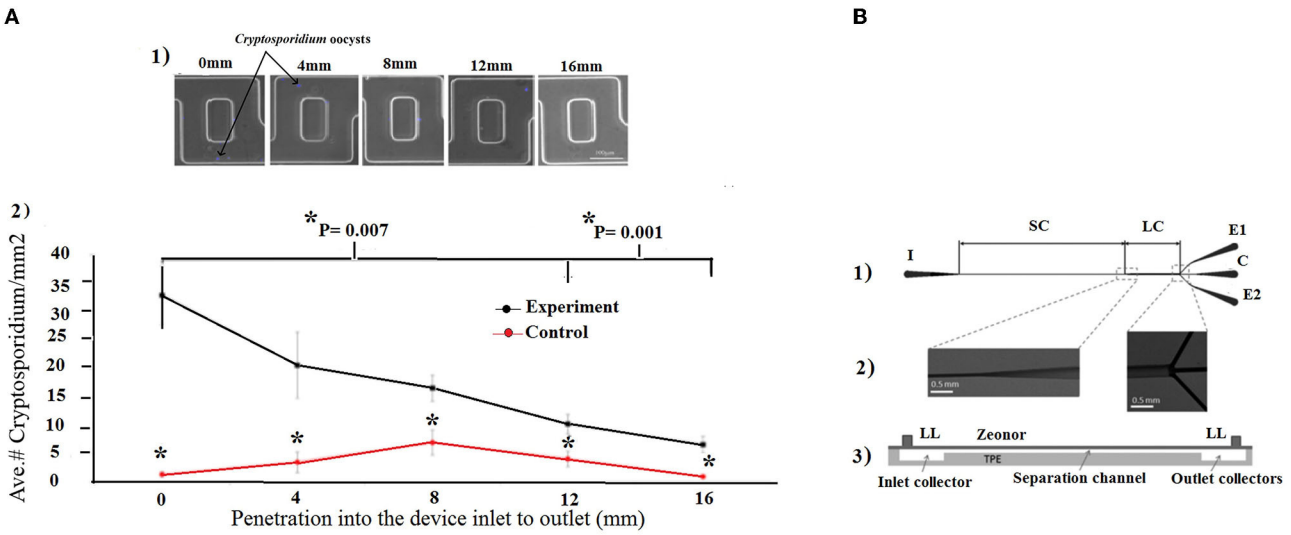

FIGURE 8
(A) Microfluidic micromixer device. (1) The captured oocysts at different lengths in the device were systematically counted randomly in 10 areas. (2) The number of oocysts per area was averaged at each length. *indicates statistical significancy. Reprinted from Diéguez et al. (2018). **(B)** Microfluidic chip. (1) The inlet (I) port allows entry into the separation channel (SC), which then widens into a large channel (LC) that splits into three outlet collectors (C, E1, and E2). (2) Scanning electron microscopy images, and (3) schematic view of a vertical section, the Zeonor-TPE chip assembly with the Luer lock (LL) ports, separation channel, and input and output collectors. Reproduced from Ganz et al. (2015) with permission from the American Society of Microbiology (ASM) publication.

energy transfer (FRET) in order to detect *T. gondii* DNA. In this study, mQDs and commercial BHQ_2 were the energy donors and acceptors, respectively. To produce a sensing probe, sCdTe@Ni mQDs and BHQ_2 were used to label a stem-loop *T. gondii* DNA oligonucleotide at the 5′ and 3′ ends, respectively. This system was able to detect the target DNA of *T. gondii* with a LoD of $\sim 2.70 \times 10^{-9}$ mol/L. In addition, a study developed by He et al. (2015) detected *T. gondii* using the quenching of magnetic fluorescence NPs (Fe_3O_4/CdTe) based on CdTe QDs, which were synthesized using 3-mercaptopropionic (MPA) capping for *T. gondii* DNA detection, with a LoD of 8.339×10^{-9} M of DNA. In this study, similar to Xu et al. (2013), a stem-loop *T. gondii* DNA oligonucleotide was employed, which was conjugated to Fe_3O_4/CdTe at the 5′ end as the energy donor and BHQ_2 at the 3′ end as the acceptor.

7. Microfluidic devices

Microfluidic systems are geometrically small scale (typically sub-millimeter) and can be incorporated with biosensor systems. Theoretically, microfluidic devices are comprised of thin grooves or small wells, channels, micro-channels, and chambers. These devices are rapid and accurate, and are increasingly employed for the detection of waterborne pathogens (Woolley and Mathies, 1994; Stone et al., 2004; Fiorini and Chiu, 2005; Chin et al., 2012).

In a biosensor-independent manner, there is a commercial microfluidic device for the detection of *Cryptosporidium* oocysts in water samples with on-chip integrated sample preparation features, named CryptoDetect CARD. This technology involves integrated immunomagnetic separation (IMS); however, the technology needs more development to specify the LoD and sensitivity, and the need for sample preparation, filtration, and concentration still limits its use (Rheonix, 2011).

As a first strategy, hydrodynamic trapping together with immunofluorescence detection was utilized (Zhu et al., 2004; Taguchi et al., 2005, 2007; Lay et al., 2008; Mudanyali et al., 2010). In this regard, Taguchi et al. (2005) developed a micro-well array strategy to capture oocysts. For trapping oocysts in wells, micro-wells with a 10 μm or 30 μm diameter and a 10 μm depth were developed to capture oocysts of *Cryptosporidium*. This technology was able to detect the oocysts in very small sample volumes and could therefore be used instead of visual inspection of microscope slides. The micro-wells were coated with streptavidin and anti-*C. parvum* antibodies, and the samples containing *C. parvum* oocysts (10^7 oocysts/mL) suspended in PBS were simply deposited onto the array. This approach was able to detect *Cryptosporidium* oocysts for 60 min at a maximum flow rate of 350 μL/min (5 mL could be processed in under 15 min), with a LoD of 36 oocysts/mL (Taguchi et al., 2005). Diéguez et al. (2018) purposed a disposable microfluidic micromixer, which was able to specifically capture, isolate, and concentrate *Cryptosporidium* from water samples. This designed device was able to analyze the quantification of captured oocysts using immunofluorescence microscopy, as well as an imaging flow cytometer. In addition, the microfluidic micromixer device provided a rapid and efficient detection method, with a capture efficiency of 96% compared to other available laboratory-scale technologies for the detection of *Cryptosporidium* oocysts (Figure 8A).

In addition, a microfluidic inertial separation chip was designed and fabricated for the separation of *Giardia* cysts from food samples

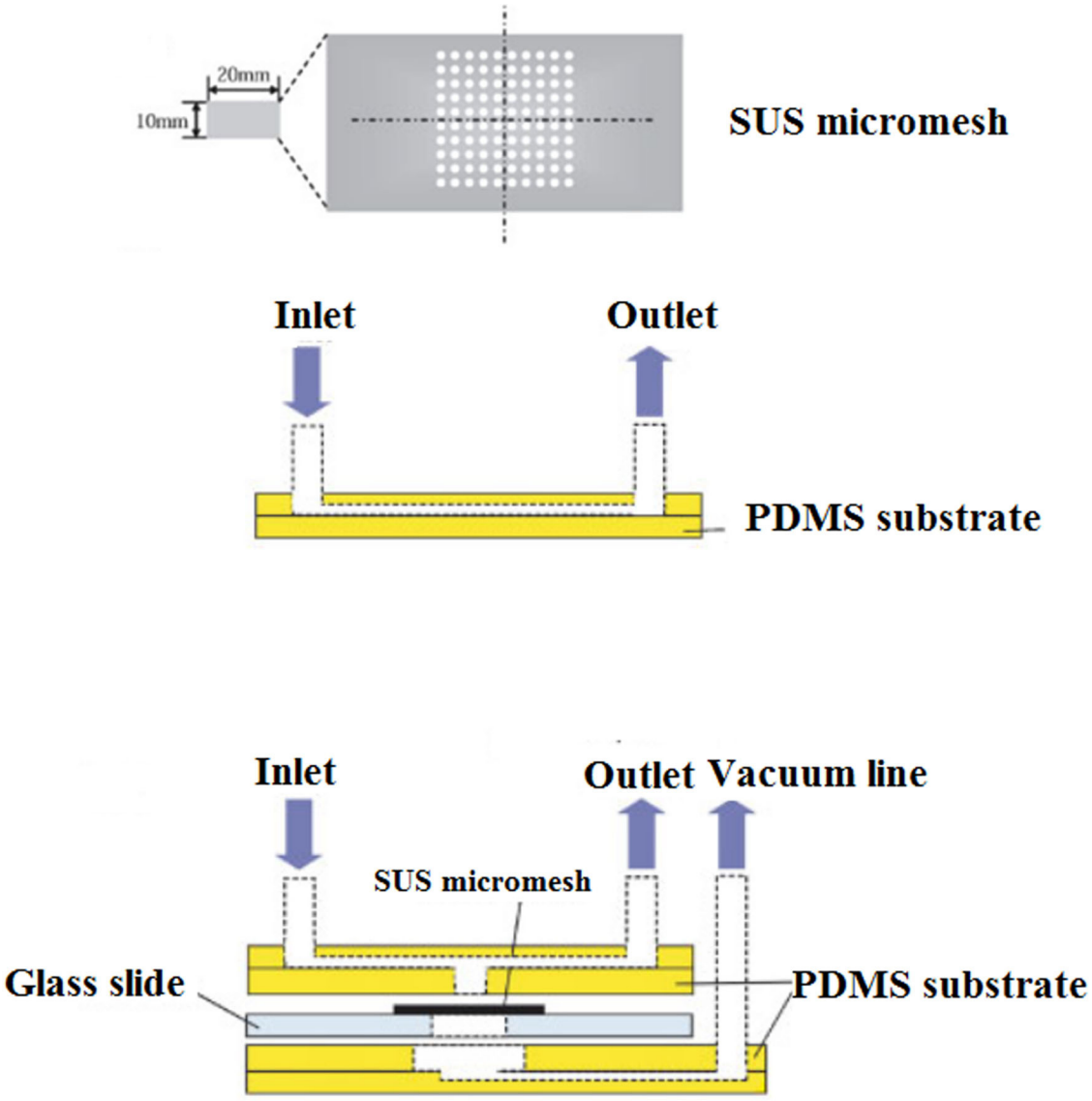

FIGURE 9
Schematic overview of the experimental setup of a micromesh microfluidic. (1) View of the SUS micromesh. (2) Side view of a PDMS microfluidic device equipped with the SUS micromesh, and (3) side view of a PDMS microfluidic device with microchannel, sample inlet, and outlet. Reproduced from Taguchi et al. (2007) with permission from Wiley & Sons.

(Ganz et al., 2015). The microfluidic chips consisted of an inlet, a main separation channel with a rectangular microfluidic channel, and a large channel, which was divided into three smaller channels connected to three output channels. The method was very efficient and specific for *G. lamblia*, and recovered an average of 68.4% of cysts, with a LoD of 38 cysts from a 25 g lettuce sample (Ganz et al., 2015) (Figure 8B).

Hydrodynamic trapping of *Cryptosporidium* oocysts, either in wells or filters, through pre-filter structures or a raindrop filter, was also developed. This microfluidic device was incorporated into a SUS micromesh to capture *C. parvum* oocysts. Trapped *C. parvum* oocysts were visualized by fluorescent staining. The concentration of added *C. parvum* oocysts and oocysts detected by the SUS micromesh was linearly correlated within the range of 18–200 oocysts/mL. The results of this technique were in agreement with the direct immunofluorescence assay coupled with the immunomagnetic separation (DFA-IMS) method, while the recovery of SUS micromesh (93%) was higher than DFA-IMS (90%), suggesting that the SUS micromesh is a promising procedure for counting *C. parvum* oocysts (Taguchi et al., 2007) (Figure 9).

As a second strategy, it was illustrated that trapping of *Cryptosporidium* oocysts using sieves or filters may increase the sensitivity of microfluidic systems (Zhu et al., 2004; Lay et al., 2008). A fully automated system consisting of a filtration unit and pumping system (1,000 L within 24 h), complemented by a microfluidic chip, Crypto-Tect bio-slide, was developed by the Shaw Water Ltd. Company, which stained and counted

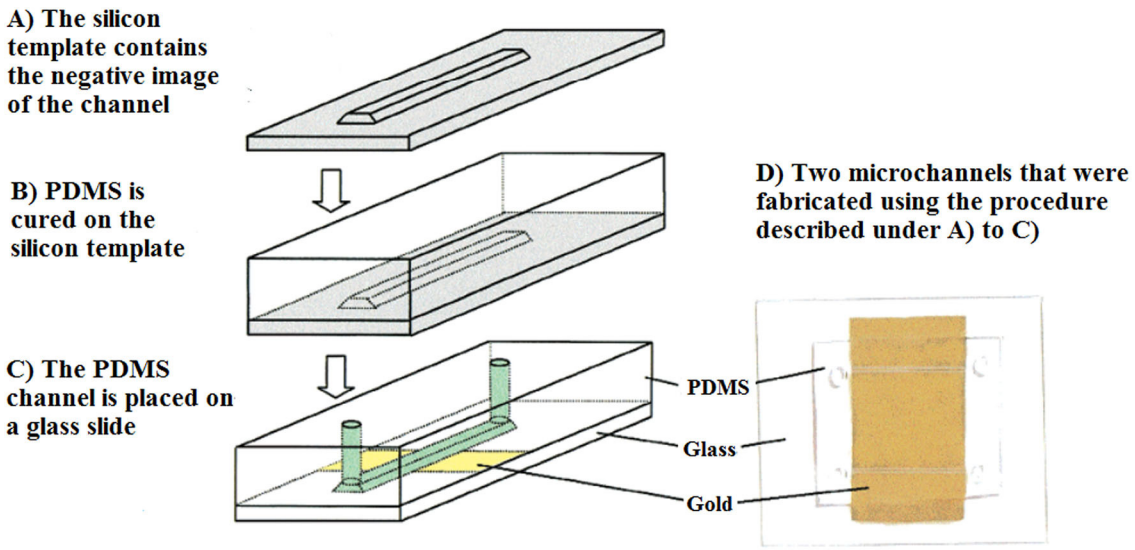

FIGURE 10
View of a PDMS microchannel. The channel was fabricated in silicon and placed on a glass slide, where gold was deposited. Reprinted with permission from Esch et al. (2001) copyright from the American Chemistry Society.

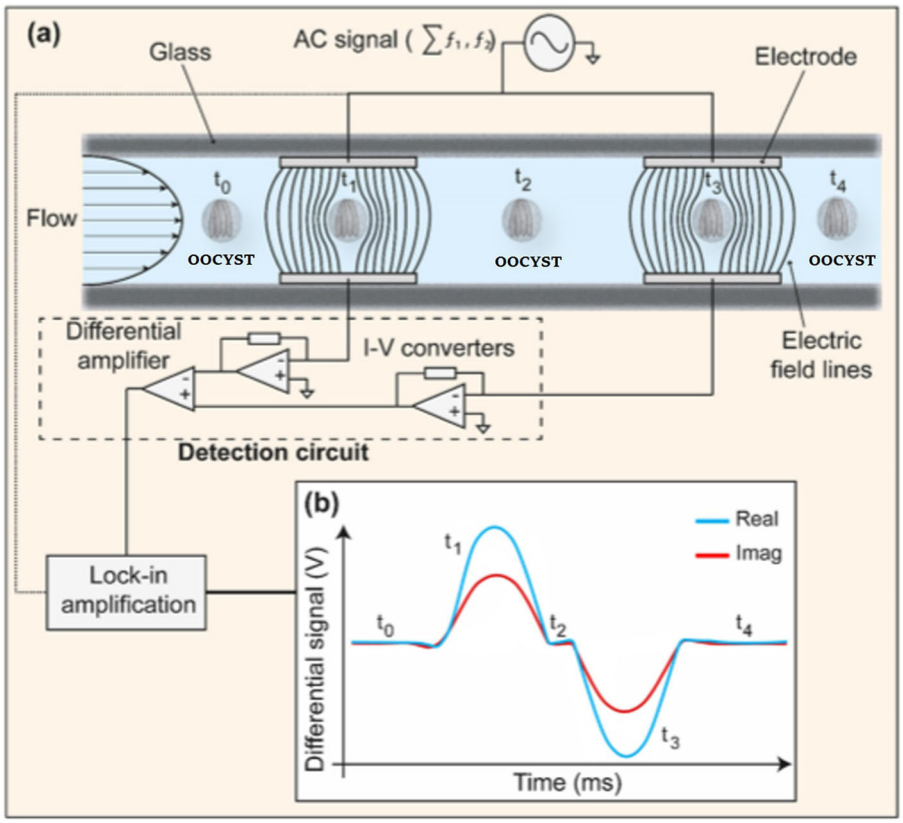

FIGURE 11
Schematic picture of a microfluidic impedance cytometer. **(a)** Two parallel facing electrodes. The electrodes were fabricated within a microfluidic channel. **(b)** The current flowing through the bottom electrodes was measured using a custom detection circuit. The circuit consists of trans-impedance amplifiers, which convert current (I) into voltage (V), and a differential amplifier. Reproduced from McGrath et al. (2017).

TABLE 3 Studies on microfluidic systems for the detection of FWP.

Type of detection	Target	Limit of Detection (LoD)	Fabrication technique	Sample source	References
Microfluidic device (micro-well array)	*C. parvum*	36 oocysts/mL in 60 min	Micro-well array strategy to trap and capture oocysts	Water	Taguchi et al., 2005
Microfluidic micromixer device	*C. parvum*	10 oocysts/L	Microfluidic micromixer to capture and isolate oocysts	Water samples	Diéguez et al., 2018
Microfluidic inertial separation chip	*Giardia*	38 cysts/mL	Microfluidic chips consists of a rectangular microfuidic channel	Food samples	Ganz et al., 2015
Microfluidic device (optical detection)	*C. parvum*	Not reported	Microfluidic device was incorporated with a SUS micromesh to trap oocysts	Water	Taguchi et al., 2007
Filter-based microfluidic device	*C. parvum* and *G. lamblia*	Not reported	Filter-based microfluidic device with immunofluorescent labeling to rapidly detect *C. parvum* and *G. lamblia*	Not reported	Zhu et al., 2004
Microfluidic chip	*C. parvum*	5 fmol of amplicon in 12.5 μL of sample solution	Detection of RNA, amplified by nucleic-acid-sequence-based amplification (NASBA) to detect viable *C. parvum*	Water	Esch et al., 2001
Microfluidic impedance cytometry (MIC) system	*C. parvum*, *C. muris* and *G. lamblia*	<10 *C. parvum* oocysts/μL	Detection of *Cryptosporidium* and *G. lamblia* based on integration of electrochemical biosensors into microfluidic systems	Not reported	McGrath et al., 2017
Optical microfluidic biosensors	*C. parvum*	1–10 oocysts/mL in 10 minutes	Microfluidic chip based on agglutination assay	Water	Angus et al., 2012

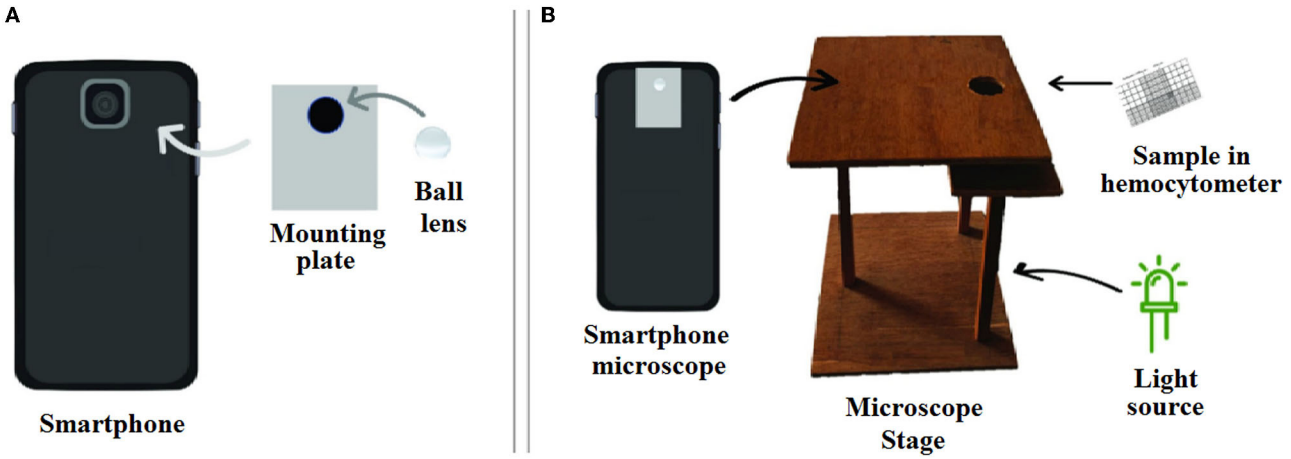

FIGURE 12
Schematic overview of a smartphone microscope setup. **(A)** Fabrication of ball lens onto mounting plate and the smartphone camera. **(B)** The set up of measurement system. Reproduced from Shrestha et al. (2020).

Cryptosporidium oocysts with a LoD slightly higher than 10 oocysts (Shaw, 2009), while 1,000 L drinking water was concentrated to a 1.5 mL sample, which was suitable for introducing to the microfluidic system. In addition, a microfluidic device based on the detection of *C. parvum* and *G. lamblia* oocysts/cysts using positive pressure was developed that identified *C. parvum* and *G. lamblia* fluorescent labels, while the staining solution was 10 to 100 times more diluted than the recommended concentration in the conventional glass method (Zhu et al., 2004).

Microfluidic trapping devices can also be integrated with on-chip molecular methods for further applications (Mahdavi Abhari et al., 2023). Molecular sensing techniques include pre-amplification of the microorganism genomic material, either *via* fluorescence or electrochemical tools. These reliable and rapid detection techniques still require genomic materials. The detection of *C. parvum* in water resources still requires the parasite to be collected and concentrated from a large water sample volume. In fact, during the analysis of water samples, the numbers of recovered parasites are usually low and cannot be detected without DNA amplification. To overcome this limitation, Esch et al. (2001), developed a microfluidic chip, which was amplified by nucleic-acid-sequence-based amplification (NASBA), using DNA-modified liposomes to detect RNA in viable *C. parvum*. A NASBA-generated amplicon was placed between the capture

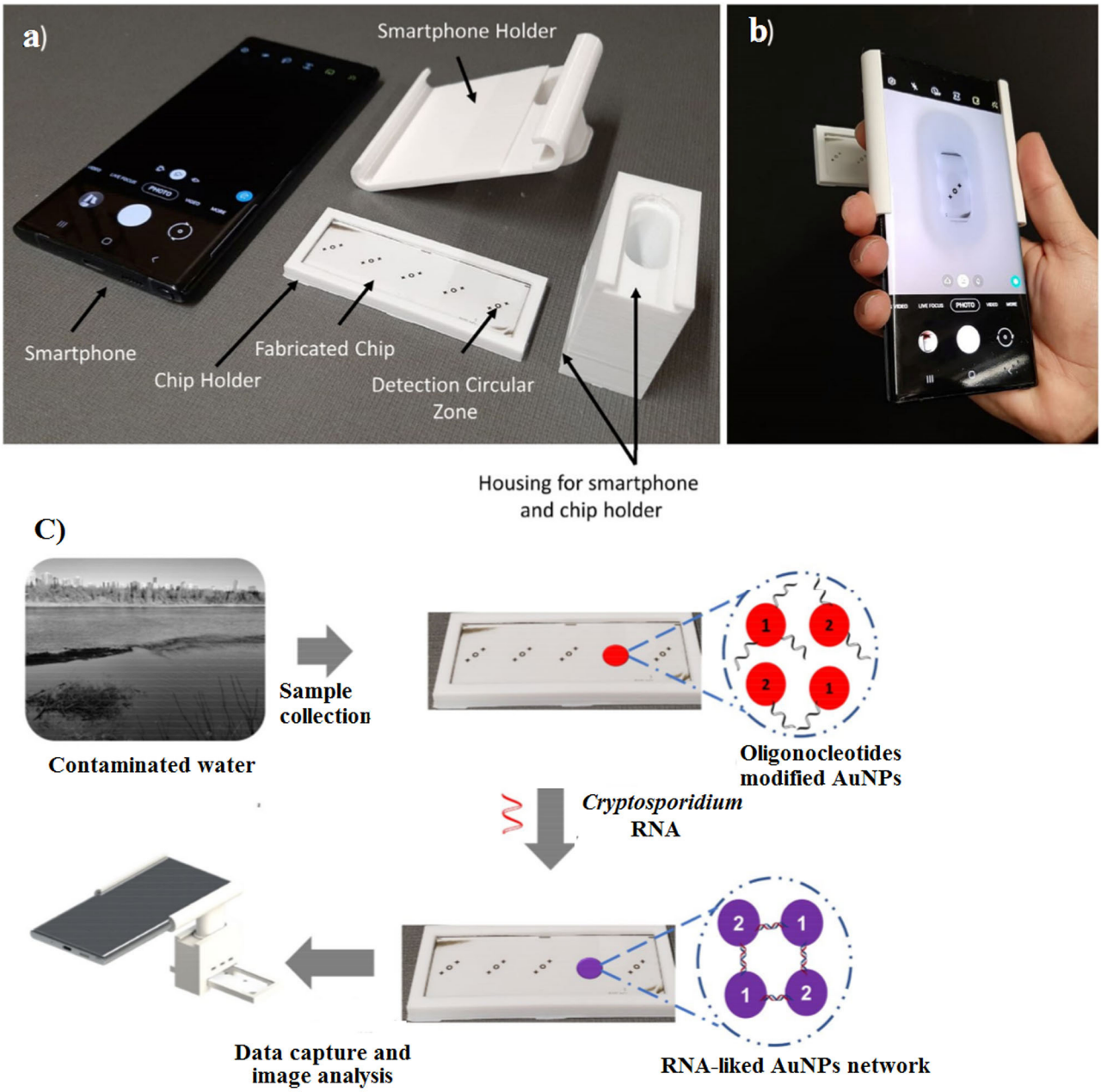

FIGURE 13
Fabricated chip and 3D portable holder assembly integrated with a smartphone. **(a)** The major components of the detection system, **(b)** the assembled detection system, and **(c)** schematic overview of sensing platform. Reproduced from Luka et al. (2021).

and reporter probes in a microfluidic channel. To generate fluorescence, reporter probes were tagged with carboxyfluorescein-filled liposomes, which increased the sensitivity of detection, even in very low concentrations of targets. The LoD of the microfluidic chip was reported to be 5 fmol of amplicon in 12.5 μL of sample solution (Figure 10).

Recent developments have been presented in novel engineering systems for the detection of *Cryptosporidium* and *G. lamblia* based on the integration of electrochemical biosensors into microfluidic systems. A microfluidic impedance cytometry (MIC) system based on the detection of viable parasites was proposed and designed by McGrath et al. (2017), which was able to rapidly discriminate live and inactive *C. parvum* oocysts with over 90% certainty, and to identify the viability of *Cryptosporidium* and *Giardia* at the single (oo)cyst level (Figure 11; Table 3).

8. Smartphone microscopic method

In recent years, smartphone microscopic methods have been described and used as an alternative platform for the detection of targeted pathogens, incorporated with traditional optical microscopic methods. The strengths of these techniques are the low cost, small size, being portable, and easy transportation to rural and remote settings. In fact, portable devices that can transmit relevant data to remote experts have a large impact on the quantity and quality of care. In addition, cell phone cameras are the most ubiquitous optical sensors in the world (Breslauer et al., 2009; Rajchgot et al., 2017).

In the field of waterborne protozoa, Shrestha et al. (2020) developed a smartphone-based microscopic assay for the simultaneous detection of oocysts/cysts of *Cryptosporidium* and *G. lamblia* in vegetable and water samples. The device consisted of a ball lens 1 mm in diameter, an aluminum mounting plate to transform a smartphone, and a white LED as an illumination source. After concentration of oocysts and staining with Lugol's iodine, oocysts were counted using the smartphone microscope. In comparison to commercial bright field and fluorescence microscopes, the smartphone-based microscopic assay was a low-cost alternative for screening oocysts/cysts of *Cryptosporidium* spp., and *G. lamblia*. The LoD of *Giardia* ranged from 24 cysts/100 g for cucumber to 73 cysts/100 g for cabbage. The LoD for *Cryptosporidium* ranged from 11 oocysts/100 g for radish to 25 oocysts/100 g for cabbage, while the LoD of *Cryptosporidium* was lower than that of *Giardia* (Shrestha et al., 2020) (Figure 12).

Recently, Luka et al. (2021) fabricated a 3D portable and smartphone-integrated on-chip colorimetric biosensor, which was invisible to the naked eye. In this regard, oligonucleotide-modified gold NPs (AuNPs) were used for the detection of *Cryptosporidium* RNA using UV–Vis spectroscopy. The color change of the AuNPs from red to blue after 5 min was an indicator for *Cryptosporidium* RNA. The advantages of these methods were the low sample volume (15 μL), short analysis time (~30 min), and high detection limit (5 μM) (Figure 13).

8.1. Future outlook

In recent years, advanced diagnostic procedures have been presented to overcome the limitations of available common techniques. Molecular biology assays, as gold standard methods, have been routinely utilized for rapid detection, identification, and differentiation of FWP. In addition, in recent decades, various studies have been conducted based on electrochemical and optical biosensors and nanobiosensors for the early detection of common waterborne pathogens. Although these methods frequently profit from good accuracy, reliability, and multiple sample processing, most of them suffer from the need for specialized expensive equipment, centralized services, infrastructure/or professional staff, and a lack of point-of-use (PoU) employment capabilities. The ASSURED criteria are an important guideline provided by the WHO for developing efficient POC devices to distinguish major human diseases (Syedmoradi et al., 2017; Ahmadi et al., 2020). Advances in digital health include mobile health, health information technology (IT), and wearable devices, and the acronym REASSURED (real-time connectivity, ease of specimen collection, affordable, sensitive, specific, user-friendly, rapid and robust, equipment-free or simple environmentally friendly, deliverable to end-users) has been offered for the development of diagnostic methods to address vital priorities such as global health emergencies (Land et al., 2019; Mahmoudi et al., 2022). Factors associated with the effective implementation of ASSURED diagnostic systems that should be considered in addressing POC diagnostic tests are real-time connectivity and ease of specimen collection (Land et al., 2019). Finally, for the successful diagnosis and management of infectious diseases, the necessity to fabricate smart biosensing systems is vital. We believe that smart biosensing platforms play an extremely significant role in diagnosing, as well as in predicting and controlling, future trends in infectious diseases, either epidemics or pandemics.

Author contributions

HM and KO: conceived, designed, reviewing, and editing the manuscript. SN: data gathering, literature review, and writing the manuscript. FS: illustrations and graphics. All authors read and approved the final version of the manuscript.

Funding

This study was financially supported by the Research Institute for Gastroenterology and Liver Diseases, Shahid Beheshti University of Medical Sciences (Grant Number: RIGLD-1126).

Acknowledgments

The authors thank all members of the Foodborne and Waterborne Diseases Research Center for their collaborations.

Conflict of interest

The authors declare that the research was conducted in the absence of any commercial or financial relationships that could be construed as a potential conflict of interest.

Publisher's note

References

Aboul-Enein, H., Stefan, R.-I., and Van Staden, J. (1999). Chemiluminescence-based (bio)sensors — an overview critical reviews in analytical chemistry. *Crit. Rev. Anal. Chem.* 29, 323–331. doi: 10.1080/10408349891199338

Ahmadi, A., Kabiri, S., and Omidfar, K. (2020). Advances in HbA1c Biosensor development based on field effect transistors: a review. *IEEE Sens. J.* 20, 8912–8921. doi: 10.1109/JSEN.2020.2987836

Ahmadi, A., Khoshfetrat, S. M., Kabiri, S., Dorraji, P. S., Larijani, B., and Omidfar, K. (2021a). Electrochemiluminescence paper-based screen-printed electrode for HbA1c detection using two-dimensional zirconium metal-organic framework/$Fe_{(3)}O_{(4)}$ nanosheet composites decorated with Au nanoclusters. *Mikrochim Acta* 188, 296. doi: 10.1007/s00604-021-04959-y

Ahmadi, A., Khoshfetrat, S. M., Kabiri, S., Fotouhi, L., Dorraji, P. S., and Omidfar, K. (2021b). Impedimetric paper-based enzymatic biosensor using electrospun cellulose acetate nanofiber and reduced graphene oxide for detection of glucose from whole blood. *IEEE Sens. J.* 21, 9210–9217. doi: 10.1109/JSEN.2021.3053033

Ahmadi, A., Khoshfetrat, S. M., Mirzaeizadeh, Z., Kabiri, S., Rezaie, J., and Omidfar, K. (2022). Electrochemical immunosensor for determination of cardiac troponin I using two-dimensional metal-organic framework/$Fe_{(3)}O_{(4)}$-COOH nanosheet composites loaded with thionine and pCTAB/DES modified electrode. *Talanta* 237, 122911. doi: 10.1016/j.talanta.2021.122911

Ahmadi, A., Mirzaeizadeh, Z., and Omidfar, K. (2021c). Simultaneous detection of SARS-CoV-2 IgG/IgM antibodies, using gold nanoparticles-based lateral flow immunoassay. *Monoclon Antibies Immunodiagn. Immunother.* 40, 210–218. doi: 10.1089/mab.2021.0027

Akbarzadeh, A., Samiei, M., and Davaran, S. (2012). Magnetic nanoparticles: preparation, physical properties, and applications in biomedicine. *Nanoscale Res. Lett.* 7, 144. doi: 10.1186/1556-276X-7-144

Alaqad, K., and Saleh, T. A. (2016). Gold and silver nanoparticles: synthesis methods, characterization routes and applications towards drugs. *J. Environ. Analyt. Toxicol.* 2016, 4. doi: 10.4172/2161-0525.1000384

Ali, A., Shah, T., Ullah, R., Zhou, P., Guo, M., Ovais, M., et al. (2021). Review on recent progress in magnetic nanoparticles: synthesis, characterization, and diverse applications. *Front. Chem.* 9, 629054. doi: 10.3389/fchem.2021.629054

Al-Shamiri, A., Al-Zubairy, A., and Al-Mamari, R. (2010). The prevalence of *Cryptosporidium* spp. in children, Taiz district, Yemen. *Iran J. Parasitol.* 5, 26–32.

Andrade, L., O'Dwyer, J., O'Neill, E., and Hynds, P. (2018). Surface water flooding, groundwater contamination, and enteric disease in developed countries: a scoping review of connections and consequences. *Environ. Pollut.* 236, 540–549. doi: 10.1016/j.envpol.2018.01.104

Angus, S., Kwon, H.-J., and Yoon, J.-Y. (2012). Low-level detection of *Cryptosporidium parvum* in field water using optical microfluidic biosensors. *Prog. Biomed. Opt. Imaging Proc. SPIE* 8229, 13. doi: 10.1117/12.909618

Arlett, J. L., Myers, E. B., and Roukes, M. L. (2011). Comparative advantages of mechanical biosensors. *Nat. Nanotechnol.* 6, 203–215. doi: 10.1038/nnano.2011.44

Aubert, D., and Villena, I. (2009). Detection of *Toxoplasma gondii* oocysts in water: proposition of a strategy and evaluation in Champagne-Ardenne region, France. *Mem. Inst. Oswaldo Cruz.* 104, 290–295. doi: 10.1590/S0074-02762009000200023

Avant, B., Bouchard, D., Chang, X., Hsieh, H. S., Acrey, B., Han, Y., et al. (2019). Environmental fate of multiwalled carbon nanotubes and graphene oxide across different aquatic ecosystems *NanoImpact* 13, 1–12. doi: 10.1016/j.impact.2018.11.001

Babamiri, B., Salimi, A., and Hallaj, R. (2018). A molecularly imprinted electrochemiluminescence sensor for ultrasensitive HIV-1 gene detection using EuS nanocrystals as luminophore. *Biosens. Bioelectron.* 117, 332–339. doi: 10.1016/j.bios.2018.06.003

Babkina, S. S., and Budnikov, G. K. (2006). Electrochemical biosensors based on nucleic acids and their use in bioaffinity assays for determining DNA and and its effectors. *J Anal Chem* 61, 728–739. doi: 10.1134/S1061934806080028

Bahramdoost, Z., Mirjalali, H., Yavari, P., and Haghighi, A. (2021). Development of HRM real-time PCR for assemblage characterization of *Giardia lamblia*. *Acta. Trop.* 224, 106109. doi: 10.1016/j.actatropica.2021.106109

Baldursson, S., and Karanis, P. (2011). Waterborne transmission of protozoan parasites: review of worldwide outbreaks - an update 2004-2010. *Water Res.* 45, 6603–6614. doi: 10.1016/j.watres.2011.10.013

Bello, J., Núñez, F. A., González, O. M., Fernández, R., Almirall, P., and Escobedo, A. A. (2011). Risk factors for *Giardia* infection among hospitalized children in Cuba. *Ann. Trop. Med. Parasitol.* 105, 57–64. doi: 10.1179/136485911X12899838413385

Berezin, M. Y., and Achilefu, S. (2010). Fluorescence lifetime measurements and biological imaging. *Chem. Rev.* 110, 2641–2684. doi: 10.1021/cr900343z

Bermejo, C., Haerizadeh, F., Takanaga, H., Chermak, D., and Frommer, W. B. (2011). Optical sensors for measuring dynamic changes of cytosolic metabolite levels in yeast. *Nat protoc* 6, 1806–1817. doi: 10.1038/nprot.2011.391

Breslauer, D. N., Maamari, R. N., Switz, N. A., Lam, W. A., and Fletcher, D. A. (2009). Mobile phone based clinical microscopy for global health applications. *PLoS One* 4, e6320. doi: 10.1371/journal.pone.0006320

Bunde, R. L., Jarvi, E. J., and Rosentreter, J. J. (1998). Piezoelectric quartz crystal biosensors. *Talanta* 46, 1223–1236. doi: 10.1016/S0039-9140(97)00392-5

Cai, R., Yin, F., Zhang, Z., Tian, Y., and Zhou, N. (2019). Functional chimera aptamer and molecular beacon based fluorescent detection of *Staphylococcus aureus* with strand displacement-target recycling amplification. *Anal. Chim. Acta.* 1075, 128–136. doi: 10.1016/j.aca.2019.05.014

Cammann, K. (1977). Bio-sensors based on ion-selective electrodes. *Fresenius' Z.Anal Chem.* 287, 1–9. doi: 10.1007/BF00539519

Campbell, G., and Mutharasan, R. (2006). Piezoelectric-excited millimeter-sized cantilever (PEMC) sensors detect *Bacillus anthracis* at 300 spores/mL. *Biosens. Bioelectron.* 21, 1684–1692. doi: 10.1016/j.bios.2005.08.001

Campbell, G. A., and Mutharasan, R. (2008). Near real-time detection of *Cryptosporidium parvum* oocyst by IgM-functionalized piezoelectric-excited millimeter-sized cantilever biosensor. *Biosens. Bioelectron.* 23, 1039–1045. doi: 10.1016/j.bios.2007.10.017

Campuzano, S., Yáñez-Sedeño, P., and Pingarrón, J. M. (2017). Electrochemical genosensing of circulating biomarkers. *Sensors* 17, 866. doi: 10.3390/s17040866

Cesewski, E., and Johnson, B. N. (2020). Electrochemical biosensors for pathogen detection. *Biosens. Bioelectron.* 159, 112214–112214. doi: 10.1016/j.bios.2020.112214

Chalklen, T., Jing, Q., and Kar-Narayan, S. (2020). Biosensors based on mechanical and electrical detection techniques. *Sensors* 20, 605. doi: 10.3390/s20195605

Chaudhry, S. A., Gad, N., and Koren, G. (2014). Toxoplasmosis and pregnancy. *Can. Fam. Physician.* 60, 334–336.

Chauhan, N., Maekawa, T., and Kumar, D. N. S. (2017). Graphene based biosensors—accelerating medical diagnostics to new-dimensions. *J. Material Res.* 32, 2860–2882. doi: 10.1557/jmr.2017.91

Chen, C., and Wang, J. (2020). Optical biosensors: an exhaustive and comprehensive review. *Analyst* 145, 1605–1628. doi: 10.1039/C9AN01998G

Chin, C. D., Linder, V., and Sia, S. K. (2012). Commercialization of microfluidic point-of-care diagnostic devices. *Lab Chip* 12, 2118–2134. doi: 10.1039/c2lc21204h

Cho, I.-H., Kim, D. H., and Park, S. (2020). Electrochemical biosensors: perspective on functional nanomaterials for on-site analysis. *Biomaterial Res.* 24, 6. doi: 10.1186/s40824-019-0181-y

Cho, S. J., Woo, H. M., Kim, K. S., Oh, J. W., and Jeong, Y. J. (2011). Novel system for detecting SARS coronavirus nucleocapsid protein using an ssDNA aptamer. *J. Biosci. Bioeng.* 112, 535–540. doi: 10.1016/j.jbiosc.2011.08.014

Citartan, M., Gopinath, S. C. B., Tominaga, J., and Tang, T.-H. (2013). Label-free methods of reporting biomolecular interactions by optical biosensors. *Analyst* 138, 3576–3592. doi: 10.1039/c3an36828a

Collier, S. A., Deng, L., Adam, E. A., Benedict, K. M., Beshearse, E. M., Blackstock, A. J., et al. (2021). Estimate of burden and direct healthcare cost of infectious waterborne disease in the United States. *Emerg. Infect. Dis.* 27, 140–149. doi: 10.3201/eid2701.190676

Cunningham, B., and Laing, L. (2008). Advantages and application of label-free detection assays in drug screening. *Expert. Opin. Drug. Discov.* 3, 891–901. doi: 10.1517/17460441.3.8.891

de la Escosura-Muñiz, A., and Merkoçi, A. (2012). Nanochannels preparation and application in biosensing. *ACS Nano*. 6, 7556–7583. doi: 10.1021/nn301368z

Deline, A., and Nason, J. (2019). Evaluation of labeling methods used for investigating the environmental behavior and toxicity of metal oxide nanoparticles. *Environ. Sci. Nano* 6, 19. doi: 10.1039/C8EN01187G

Deshmukh, K., Goel, N., and Patel, B. C. (2020). Optical sensors: overview, characteristics and applications. *Adv. Modern Sens.* 3, 27. doi: 10.1088/978-0-7503-2707-7ch3

Destura, R. V., Cena, R. B., Galarion, M. J. H., Pangilinan, C. M., Arevalo, G. M., Alba, R. O. C., et al. (2015). Advancing *Cryptosporidium* diagnostics from bench to bedside. *Curr. Trop. Med. Rep.* 2, 150–160. doi: 10.1007/s40475-015-0055-x

Diéguez, L., Winter, M., Molan, S., Monis, P., King, B., and Thierry, B. (2018). Disposable microfluidic micromixers for effective capture of *Cryptosporidium parvum* oocysts from water samples. *J. Biol. Eng.* 12, 4–4. doi: 10.1186/s13036-018-0095-6

Ding, R., Chen, Y., Wang, Q., Wu, Z., Zhang, X., Li, B., et al. (2022). Recent advances in quantum dots-based biosensors for antibiotics detection. *J. Pharm. Anal.* 12, 355–364. doi: 10.1016/j.jpha.2021.08.002

Drummond, T. G., Hill, M. G., and Barton, J. K. (2003). Electrochemical DNA sensors. *Nat. Biotechnol.* 21, 1192–1199. doi: 10.1038/nbt873

Duchenne-Moutien, R. A., and Neetoo, H. (2021). Climate change and emerging food safety issues: a review. *J. Food Prot.* 84, 1884–1897. doi: 10.4315/JFP-21-141

Duguet, E., Vasseur, S., Mornet, S., and Devoisselle, J.-M. (2006). Magnetic nanoparticles and their applications in medicine. *Nanomed.* 1, 157–168. doi: 10.2217/17435889.1.2.157

Efstratiou, A., Ongerth, J. E., and Karanis, P. (2017). Waterborne transmission of protozoan parasites: Review of worldwide outbreaks—an update 2011–2016. *Water Res.* 114, 14–22. doi: 10.1016/j.watres.2017.01.036

Einarsson, E., Ma'ayeh, S., and Svärd, S. G. (2016). An up-date on *Giardia* and giardiasis. *Curr. Opin. Microbiol.* 34, 47–52. doi: 10.1016/j.mib.2016.07.019

Elgun, G., and Koltas, I. S. (2011). Investigation of *Cryptosporidium* spp. antigen by ELISA method in stool specimens obtained from patients with diarrhea. *Parasitol. Res.* 108, 395–397. doi: 10.1007/s00436-010-2079-4

ENHIS (2009). *Outbreaks of waterborne diseases vol Fact sheet 1.1. p* 1–6.

Esch, M. B., Locascio, L. E., Tarlov, M. J., and Durst, R. A. (2001). Detection of Viable *Cryptosporidium parvum* using dna-modified liposomes in a microfluidic chip. *Anal. Chem.* 73, 2952–2958. doi: 10.1021/ac001508n

Faulkner, L. R., and Bard, A. J. (2002). *Electrochemical Methods: Fundamentals and Applications*. London: John Wiley and Sons.

Felix, F. S., and Angnes, L. (2018). Electrochemical immunosensors—a powerful tool for analytical applications. *Biosens. Bioelectron.* 102, 470–478. doi: 10.1016/j.bios.2017.11.029

Fernández, P., Navarro, E., Remesar, S., García Dios, D., Martinez, N., Prieto, A., et al. (2021). The age-related *Cryptosporidium* species distribution in asymptomatic cattle from north-western Spain. *Animals* 11, 256. doi: 10.3390/ani11020256

Fiorini, G. S., and Chiu, D. T. (2005). Disposable microfluidic devices: fabrication, function, and application. *BioTech* 38, 429–446. doi: 10.2144/05383RV02

Foroutan-Rad, M., Majidiani, H., Dalvand, S., Daryani, A., Kooti, W., Saki, J., et al. (2016). Toxoplasmosis in blood donors: a systematic review and meta-analysis. *Transfus. Med. Rev.* 30, 116–122. doi: 10.1016/j.tmrv.2016.03.002

Fradette, M. S., and Charette, S. J. (2022). Working toward improved monitoring of *Cryptosporidium* and *Giardia* (oo)cysts in water samples: testing alternatives to elution and immunomagnetic separation from USEPA Method 16231. *BMC Res. Notes*. 15, 254. doi: 10.1186/s13104-022-06118-9

Gaft, M., Reisfeld, R., and Panczer, G. (2015). *Modern Luminescence Spectroscopy of Minerals and Materials*. New York, NY: Springer.

Gallas-Lindemann, C., Sotiriadou, I., Mahmoodi, M. R., and Karanis, P. (2013). Detection of *Toxoplasma gondii* oocysts in different water resources by loop mediated isothermal amplification (LAMP). *Acta. Trop.* 125, 231–236. doi: 10.1016/j.actatropica.2012.10.007

Ganz, K. R., Clime, L., Farber, J. M., Corneau, N., Veres, T., and Dixon, B. R. (2015). Enhancing the detection of *Giardia duodenalis* cysts in foods by inertial microfluidic separation. *Appl. Environ. Microbiol.* 81, 3925–3933. doi: 10.1128/AEM.03868-14

Gao, H. W., Qin, P., Lin, C., Shang, Z. M., and Sun, W. (2010). Electrochemical DNA biosensor for the detection of *Listeria Monocytogenes* using toluidine blue as a hybridization indicator. *J. Iran Chem. Soc.* 7, 119–127. doi: 10.1007/BF03245868

Garibyan, L., and Avashia, N. (2013). Polymerase chain reaction. *J. Invest. Dermatol.* 133, 1–4. doi: 10.1038/jid.2013.1

Gerace, E., Lo Presti, V. D. M., and Biondo, C. (2019). *Cryptosporidium* infection: epidemiology, pathogenesis, and differential diagnosis. *Eur. J. Microbiol. Immunol. (Bp)* 9, 119–123. doi: 10.1556/1886.2019.00019

Ghulam, A. N., Dos Santos, O. A. L., Hazeem, L., Pizzorno Backx, B., Bououdina, M., and Bellucci, S. (2022). Graphene Oxide (GO) materials-applications and toxicity on living organisms and environment. *J. Funct. Biomater.* 13, 2. doi: 10.3390/jfb13020077

Grewal, Y. S., Shiddiky, M. J., Spadafora, L. J., Cangelosi, G. A., and Trau, M. (2014). Nano-yeast-scFv probes on screen-printed gold electrodes for detection of *Entamoeba histolytica* antigens in a biological matrix. *Biosens. Bioelectron.* 55, 417–422. doi: 10.1016/j.bios.2013.12.043

Gururajan, A., Rajkumari, N., Devi, U., and Borah, P. (2021). *Cryptosporidium* and waterborne outbreaks—a mini review. *Trop. Parasitol.* 11, 11–15. doi: 10.4103/tp.TP_68_20

Hayman, R. B. (2008). "Fiber optic biosensors for bacterial detection," in *Principles of Bacterial Detection: Biosensors, Recognition Receptors and Microsystems*, eds Zourob, M., Elwary, S., Turner, A. (New York, NY: Springer), 125–137.

He, L., Ni, L., Zhang, X., Zhang, C., Li, R., and Xu, S. (2015). Fluorescent detection of specific DNA sequences related to *Toxoplasma gondii* based on magnetic fluorescent nanoparticles Fe_3O_4/CdTe Biosensor. *Int. J. Biochem. Res. Rev.* 6, 130–139. doi: 10.9734/IJBCRR/2015/15254

Hill, D., and Dubey, J. (2002). *Toxoplasma gondii*: transmission, diagnosis and prevention. *Clin. Microbiol. Infect.* 8, 634–640. doi: 10.1046/j.1469-0691.2002.00485.x

Hooshyar, H., Rostamkhani, P., Arbabi, M., and Delavari, M. (2019). *Giardia lamblia* infection: review of current diagnostic strategies. *Gastroenterol Hepatol Bed Bench* 12, 3–12.

Hosu, O., Selvolini, G., and Marrazza, G. (2018). Recent advances of immunosensors for detecting food allergens. *Curr. Opin. Electrochem.* 10, 149–156. doi: 10.1016/j.coelec.2018.05.022

Houssin, T., Follet, J., Follet, A., Dei-Cas, E., and Senez, V. (2010). Label-free analysis of water-polluting parasite by electrochemical impedance spectroscopy. *Biosens. Bioelectron.* 25, 1122–1129. doi: 10.1016/j.bios.2009.09.039

Hu, J., Feng, Y., Ong, S. L., Ng, W. J., Song, L., Tan, X., Chu, X. (2004). Improvement of recoveries for the determination of protozoa *Cryptosporidium* and *Giardia* in water using method. *J. Microbiol. Methods.* 58, 321–325. doi: 10.1016/j.mimet.2004.04.013

Iqbal, A., Labib, M., Muharemagic, D., Sattar, S., Dixon, B., and Berezovski, M. (2015). Detection of *Cryptosporidium parvum* oocysts on fresh produce using dna aptamers. *PLoS ONE* 10, e0137455. doi: 10.1371/journal.pone.0137455

Janegitz, B. C., Silva, T. A., Wong, A., Ribovski, L., Vicentini, F. C., Taboada Sotomayor, M. D. P., et al. (2017). The application of graphene for in vitro and in vivo electrochemical biosensing. *Biosens. Bioelectron.* 89, 224–233. doi: 10.1016/j.bios.2016.03.026

Javanmard, E., Mirsamadi, E. S., Olfatifar, M., Ghasemi, E., Saki, F., Mirjalali, H., et al. (2020). Prevalence of *Cryptosporidium* and *Giardia* in vegetables in Iran: a nineteen-years meta-analysis review. *J. Environ. Health Sci. Eng.* 18, 1629–1641. doi: 10.1007/s40201-020-00493-w

Javanmard, E., Rahimi, H. M., Niyyati, M., Aghdaei, H. A., Sharifdini, M., Mirjalali, H., et al. (2019). Molecular analysis of *Blastocystis* sp. and its subtypes from treated wastewater routinely used for irrigation of vegetable farmlands in Iran. *J. Water Health* 17, 837–844. doi: 10.2166/wh.2019.045

Kalyoussef, S., and Feja, K. N. (2014). Foodborne illnesses. *Adv. Pediatr.* 61, 287–312. doi: 10.1016/j.yapd.2014.04.003

Kang, C., Lee, S., Park, T., and Sim, S. (2006). Performance enhancement of real-time detection of protozoan parasite, *Cryptosporidium* oocyst by a modified surface plasmon resonance (SPR) biosensor. *Enzyme Microb. Technol.* 39, 387–390. doi: 10.1016/j.enzmictec.2005.11.039

Kanková, S., and Flegr, J. (2007). Longer pregnancy and slower fetal development in women with latent "asymptomatic" toxoplasmosis. *BMC Infect Dis.* 7, 114. doi: 10.1186/1471-2334-7-114

Karanis, P., Aldeyarbi, H. M., Mirhashemi, M. E., and Khalil, K. M. (2013). The impact of the waterborne transmission of *Toxoplasma gondii* and analysis efforts for water detection: an overview and update. *Environ. Sci. Pollut. Res. Int.* 20, 86–99. doi: 10.1007/s11356-012-1177-5

Karanis, P., Kourenti, C., and Smith, H. (2006). Waterborne transmission of protozoan parasites: a worldwide review of outbreaks and lessons learnt. *J. Water Health* 5, 1–38. doi: 10.2166/wh.2006.002

Khodaei, R., Ahmady, A., Khoshfetrat, S. M., Kashanian, S., Tavangar, S. M., and Omidfar, K. (2019). Voltammetric immunosensor for E-cadherin promoter DNA methylation using a $Fe(_3)O(_4)$-citric acid nanocomposite and a screen-printed carbon electrode modified with poly(vinyl alcohol) and reduced graphene oxide. *Mikrochim Acta.* 186, 170. doi: 10.1007/s00604-019-3234-y

Khoo, V. S., Dearnaley, D. P., Finnigan, D. J., Padhani, A., Tanner, S. F., and Leach, M. O. (1997). Magnetic resonance imaging (MRI): considerations and applications in radiotherapy treatment planning. *Radiother. Oncol.* 42, 1–15. doi: 10.1016/S0167-8140(96)01866-X

Khoshfetrat, S. M., Seyed Dorraji, P., Shayan, M., Khatami, F., and Omidfar, K. (2022). Smartphone-based electrochemiluminescence for visual simultaneous detection of rassf1a and slc5a8 tumor suppressor gene methylation in thyroid cancer patient plasma. *Analyt Chem.* 94, 8005–8013. doi: 10.1021/acs.analchem.2c01132

Khurana, S., and Chaudhary, P. (2018). Laboratory diagnosis of cryptosporidiosis. *Trop. Parasitol.* 8, 2–7. doi: 10.4103/tp.TP_34_17

Kim, H. T., Jin, E., and Lee, M.-H. (2021). Portable chemiluminescence-based lateral flow assay platform for the detection of cortisol in human serum. *Biosensors.* 11, 21. doi: 10.3390/bios11060191

Kinyua Muthuri, L., Nagy, L., and Nagy, G. (2021). Chronopotentiometric method for assessing antioxidant activity: a reagentless measuring technique. *Electrochem. Commun.* 122, 106907. doi: 10.1016/j.elecom.2020.106907

Kokkinos, C., Economou, A., and Prodromidis, M. I. (2016). Electrochemical immunosensors: critical survey of different architectures and transduction strategies. *TrAC Trends Anal. Chem.* 79, 88–105. doi: 10.1016/j.trac.2015.11.020

Kramer, M. F., Vesey, G., Look, N. L., Herbert, B. R., Simpson-Stroot, J. M., and Lim, D. V. (2007). Development of a *Cryptosporidium* oocyst assay using an automated fiber optic-based biosensor. *J. Biol. Eng.* 1, 3–3. doi: 10.1186/1754-1611-1-3

Kudr, J., Haddad, Y., Richtera, L., Heger, Z., Cernak, M., Adam, V., et al. (2017). Magnetic nanoparticles: from design and synthesis to real world applications. *Nanomaterials (Basel)*. 7, 243. doi: 10.3390/nano7090243

Laczka, O., Skillman, L., Ditcham, W. G., Hamdorf, B., Wong, D. K., Bergquist, P., et al. (2013). Application of an ELISA-type screen printed electrode-based potentiometric assay to the detection of *Cryptosporidium parvum* oocysts. *J. Microbiol. Methods*. 95, 182–185. doi: 10.1016/j.mimet.2013.08.014

Land, K. J., Boeras, D. I., Chen, X.-S., Ramsay, A. R., and Peeling, R. W. (2019). REASSURED diagnostics to inform disease control strategies, strengthen health systems and improve patient outcomes. *Nat. Microb.* 4, 46–54. doi: 10.1038/s41564-018-0295-3

Laude, A., Valot, S., Desoubeaux, G., Argy, N., Nourrisson, C., Pomares, C., et al. (2016). Is real-time PCR-based diagnosis similar in performance to routine parasitological examination for the identification of *Giardia intestinalis*, *Cryptosporidium parvum*/*Cryptosporidium hominis* and *Entamoeba histolytica* from stool samples? Evaluation of a new commercial multiplex PCR assay and literature review. *Clin. Microbiol. Infect.* 22, 190. doi: 10.1016/j.cmi.2015.10.019

Lavania, S., Das, R., Dhiman, A., Myneedu, V. P., Verma, A., Singh, N., et al. (2018). Aptamer-based tb antigen tests for the rapid diagnosis of pulmonary tuberculosis: potential utility in screening for tuberculosis. *ACS Infect Dis.* 4, 1718–1726. doi: 10.1021/acsinfecdis.8b00201

Lay, C., Teo, C. Y., Zhu, L., Peh, X. L., Ji, H. M., Chew, B. R., et al. (2008). Enhanced microfiltration devices configured with hydrodynamic trapping and a rain drop bypass filtering architecture for microbial cells detection. *Lab Chip*. 8, 830–833. doi: 10.1039/b800015h

Lee, J., Kim, J., Kim, S., and Min, D. H. (2016). Biosensors based on graphene oxide and its biomedical application. *Adv Drug Deliv Rev.* 105, 275–287. doi: 10.1016/j.addr.2016.06.001

Leitch, G. J., and He, Q. (2012). Cryptosporidiosis-an overview. *J. Biomed. Res.* 25, 1–16. doi: 10.1016/S1674-8301(11)60001-8

Li, H. Y., Jia, W. N., Li, X. Y., Zhang, L., Liu, C., and Wu, J. (2020). Advances in detection of infectious agents by aptamer-based technologies. *Emerg. Microbes. Infect.* 9, 1671–1681. doi: 10.1080/22221751.2020.1792352

Li, L., Li, Q., Liao, Z., Sun, Y., Cheng, Q., Song, Y., et al. (2018). Magnetism-resolved separation and fluorescence quantification for near-simultaneous detection of multiple pathogens. *Anal. Chem.* 90, 9621–9628. doi: 10.1021/acs.analchem.8b02572

Lim, H. J., Saha, T., Tey, B. T., Tan, W. S., and Ooi, C. W. (2020). Quartz crystal microbalance-based biosensors as rapid diagnostic devices for infectious diseases. *Biosens. Bioelectron.* 168, 112513–112513. doi: 10.1016/j.bios.2020.112513

Lingane, P. J., and Peters, D. G. (1971). Chronopotentiometry. *C R C Crit. Rev. Anal. Chem.* 1, 587–634. doi: 10.1080/10408347108085644

Liu, Q., Zhang, W., Chen, S., Zhuang, Z., Zhang, Y., Jiang, L., et al. (2020). SELEX tool: a novel and convenient gel-based diffusion method for monitoring of aptamer-target binding. *J. Biol. Eng.* 14, 1. doi: 10.1186/s13036-019-0223-y

Low, K. F., Chuenrangsikul, K., Rijiravanich, P., Surareungchai, W., and Chan, Y. Y. (2012). Electrochemical genosensor for specific detection of the food-borne pathogen, Vibrio cholerae. *World J. Microbiol. Biotechnol.* 28, 1699–1706. doi: 10.1007/s11274-011-0978-x

Luka, G., Samiei, E., Dehghani, S., Johnson, T., Najjaran, H., and Hoorfar, M. (2019). Label-free capacitive biosensor for detection of *Cryptosporidium*. *Sensors (Basel)* 19, 21. doi: 10.3390/s19020258

Luka, G. S., Najjaran, H., and Hoorfar, M. (2022). On-chip-based electrochemical biosensor for the sensitive and label-free detection of *Cryptosporidium*. *Sci. Rep.* 12, 6957. doi: 10.1038/s41598-022-10765-0

Luka, G. S., Nowak, E., Toyata, Q. R., Tasnim, N., Najjaran, H., and Hoorfar, M. (2021). Portable on-chip colorimetric biosensing platform integrated with a smartphone for label/PCR-free detection of *Cryptosporidium* RNA. *Sci. Rep.* 11, 23192. doi: 10.1038/s41598-021-02580-w

Luo, X., Morrin, A., Killard, A. J., and Smyth, M. R. (2006). Application of nanoparticles in electrochemical sensors and biosensors. *Electroanal. Int. J. Devot. Fundam. Pract. Aspect Electroanalys.* 18, 319–326. doi: 10.1002/elan.200503415

Ma, J.-Y., Li, M.-Y., Qi, Z.-Z., Fu, M., Sun, T.-F., Elsheikha, H. M., et al. (2022). Waterborne protozoan outbreaks: An update on the global, regional, and national prevalence from 2017 to 2020 and sources of contamination. *Sci. Total Environ.* 806, 150562. doi: 10.1016/j.scitotenv.2021.150562

Ma, Y., Jiao, K., Yang, T., and Sun, D. (2008). Sensitive PAT gene sequence detection by nano-SiO_2/p-aminothiophenol self-assembled films DNA electrochemical biosensor based on impedance measurement. *Sens. Actuator B: Chem.* 131, 565–571. doi: 10.1016/j.snb.2007.12.046

Magar, H. S., Hassan, R. Y. A., and Mulchandani, A. (2021). Electrochemical impedance spectroscopy (eis): principles, construction, and biosensing applications. *Sensors (Basel)*. 21, 12. doi: 10.3390/s21196578

Mahdavi Abhari, F., Niyyati, M., Assadzadeh Aghdaei, H., and Mirjalali, H. (2023). Loop mediated isothermal amplification for detection of foodborne parasites: a journey from lab to lab-on-a-chip. *Food Control*. 143, 109251. doi: 10.1016/j.foodcont.2022.109251

Mahmoudi, T., Naghdi, T., Morales-Narváez, E., and Golmohammadi, H. (2022). Toward smart diagnosis of pandemic infectious diseases using wastewater-based epidemiology. *TrAC Trend. Anal. Chem.* 153, 116635. doi: 10.1016/j.trac.2022.116635

Malik, P., Katyal, V., Malik, V., Asatkar, A., Inwati, G., and Mukherjee, T. K. (2013). Nanobiosensors: concepts and variations. *ISRN Nanomater.* 2013, 327435. doi: 10.1155/2013/327435

Martín, M. E., García-Hernández, M., García-Recio, E. M., Gómez-Chacón, G. F., Sánchez-López, M., and González, V. M. (2013). DNA aptamers selectively target *Leishmania infantum* h2a protein. *PLOS ONE.* 8, e78886. doi: 10.1371/journal.pone.0078886

McGrath, J. S., Honrado, C., Spencer, D., Horton, B., Bridle, H. L., and Morgan, H. (2017). Analysis of parasitic protozoa at the single-cell level using microfluidic impedance cytometry. *Sci. Rep.* 7, 2601. doi: 10.1038/s41598-017-02715-y

Mehrotra, P. (2016). Biosensors and their applications—a review. *J. Oral. Biol. Craniofac. Res.* 6, 153–159. doi: 10.1016/j.jobcr.2015.12.002

Mendez, O. A., and Koshy, A. A. (2017). *Toxoplasma gondii*: Entry, association, and physiological influence on the central nervous system. *PLoS pathog.* 13, e1006351. doi: 10.1371/journal.ppat.1006351

Metkar, S., and Girigoswami, K. (2018). Diagnostic biosensors in medicine- a review. *Biocatal. Agric. Biotechnol.* 17, 32. doi: 10.1016/j.bcab.2018.11.029

Minuzzi, C. E., Fernandes, F. D., Portella, L. P., Bräunig, P., Sturza, D. A. F., Giacomini, L., et al. (2021). Contaminated water confirmed as source of infection by bioassay in an outbreak of toxoplasmosis in South Brazil. *Transbound. Emerg. Dis.* 68, 767–772. doi: 10.1111/tbed.13741

Mmbaga, B. T., and Houpt, E. R. (2017). *Cryptosporidium* and *Giardia* infections in children: a review. *Pediatr. Clin. North Am.* 64, 837–850. doi: 10.1016/j.pcl.2017.03.014

Mohammad Rahimi, H., Pourhosseingholi, M. A., Yadegar, A., Mirjalali, H., and Zali, M. R. (2019). High-resolution melt curve analysis: A real-time based multipurpose approach for diagnosis and epidemiological investigations of parasitic infections. *Comp. Immunol. Microbiol. Infect. Dis.* 67, 101364. doi: 10.1016/j.cimid.2019.101364

Mohammad Rahimi, H., Soleimani Jevinani, S., Nemati, S., Sharifdini, M., Mirjalali, H., and Zali, M. R. (2022). Molecular characterization of *Cryptosporidium skunk* genotype in raccoons (*Procyon lotor*) in Iran: concern for zoonotic transmission. *Parasitol. Res.* 121, 483–489. doi: 10.1007/s00436-021-07367-6

Mohammed, A. M., Ibraheem, I. J., Obaid, A. S., and Bououdina, M. (2017). Nanostructured ZnO-based biosensor: DNA immobilization and hybridization. *Sens. Bio-Sens. Res.* 15, 46–52. doi: 10.1016/j.sbsr.2017.07.003

Monosik, R., Stredansky, M., Tkac, J., and Sturdik, E. (2012). Application of enzyme biosensors in analysis of food and beverages. *Food Anal. Methods*. 5, 40–53. doi: 10.1007/s12161-011-9222-4

Mora, C., McKenzie, T., Gaw, I. M., Dean, J. M., von Hammerstein, H., Knudson, T. A., et al. (2022). Over half of known human pathogenic diseases can be aggravated by climate change. *Nat. Clim. Chang.* 12, 869–875. doi: 10.1038/s41558-022-01426-1

Morales-Narváez, E., Baptista-Pires, L., Zamora-Gálvez, A., and Merkoçi, A. (2017). Graphene-based biosensors: going simple. *Adv Mater.* 29, 7. doi: 10.1002/adma.201604905

Moreno-Mesonero, L., Amorós, I., Moreno, Y., and Alonso, J. L. (2022). Simultaneous detection of less frequent waterborne parasitic protozoa in reused wastewater using amplicon sequencing and qPCR techniques. *J. Environ. Manage* 314, 115029. doi: 10.1016/j.jenvman.2022.115029

Mudanyali, O., Oztoprak, C., Tseng, D., Erlinger, A., and Ozcan, A. (2010). Detection of waterborne parasites using field-portable and cost-effective lensfree microscopy. *Lab. Chip*. 10, 2419–2423. doi: 10.1039/c004829a

Nagarkatti, R., Bist, V., Sun, S., Fortes de Araujo, F., Nakhasi, H. L., and Debrabant, A. (2012). Development of an aptamer-based concentration method for the detection of *Trypanosoma cruzi* in blood. *PLoS One*. 7, e43533. doi: 10.1371/journal.pone.0043533

Narayanaswamy, R. (2006). *Optical Chemical Sensors and Biosensors for Food Safety and Security Applications*.

Naresh, V., and Lee, N. (2021). A Review on biosensors and recent development of nanostructured materials-enabled biosensors. *Sensors*. 7, 21. doi: 10.3390/s21041109

Ngowi, H. A. (2020). Prevalence and pattern of waterborne parasitic infections in eastern Africa: a systematic scoping review. *Food Waterborne Parasitol.* 20, e00089. doi: 10.1016/j.fawpar.2020.e00089

Nicu, L., Guirardel, M., Chambosse, F., Rougerie, P., Hinh, S., Trévisiol, E., et al. (2005). Resonating piezoelectric membranes for microelectromechanically based bioassay: detection of streptavidin–gold nanoparticles interaction with biotinylated DNA. *Sens. Actuat. B: Chem.* 110, 125–136. doi: 10.1016/j.snb.2005.01.021

Nugen, S. R., Asiello, P. J., Connelly, J. T., and Baeumner, A. J. (2009). PMMA biosensor for nucleic acids with integrated mixer and electrochemical detection. *Biosens. Bioelectron.* 24, 2428–2433. doi: 10.1016/j.bios.2008.12.025

Nygård, K., Schimmer, B., Søbstad, Ø., Walde, A., Tveit, I., Langeland, N., et al. (2006). A large community outbreak of waterborne giardiasis-delayed detection in a non-endemic urban area. *BMC Public Health* 6, 141. doi: 10.1186/1471-2458-6-141

Olaru, A., Bala, C., Jaffrezic-Renault, N., and Aboul-Enein, H. Y. (2015). Surface plasmon resonance (SPR) biosensors in pharmaceutical analysis. *Crit. Rev. Anal. Chem.* 45, 97–105. doi: 10.1080/10408347.2014.881250

Omidfar, K., Ahmadi, A., Syedmoradi, L., Khoshfetrat, S. M., Larijani, B. (2020). Point-of-care biosensors in medicine: a brief overview of our achievements in this field based on the conducted research in EMRI (endocrinology and metabolism research Institute of Tehran University of medical sciences) over the past fourteen years. *J. Diabet. Metab. Disord.* 2020, 1-5. doi: 10.1007/s40200-020-00668-0

O'Sullivan, C. K., and Guilbault, G. G. (2000). "Piezoelectric immunosensors: theory and applications," in *Biosensors and Their Applications*, eds Yang, V. C., Ngo, T. T. (Boston, MA: Springer), pp. 159–173.

Ozdemir, M. S., Marczak, M., Bohets, H., Bonroy, K., Roymans, D., Stuyver, L., et al. (2013). A label-free potentiometric sensor principle for the detection of antibody–antigen interactions. *Anal. Chem.* 85, 4770–4776. doi: 10.1021/ac400514u

Pandey, R. R., and Chusuei, C. C. (2021). Carbon Nanotubes, Graphene, and carbon dots as electrochemical biosensing composites. *Molecules* 26, 21. doi: 10.3390/molecules26216674

Park, C. K., Kang, C. D., and Sim, S. J. (2008). Non-labeled detection of waterborne pathogen *Cryptosporidium parvum* using a polydiacetylene-based fluorescence chip. *Biotechnol. J.* 3, 687–693. doi: 10.1002/biot.200700246

Pazoki, H., Niyyati, M., Javanmard, E., Lasjerdi, Z., Spotin, A., Mirjalali, H., et al. (2020). Isolation of *N. philippinensis and N. americana* strains from irrigation waters of farmland soils in Iran. *Environ. Sci. Pollut. Res. Int.* 27, 24568–24573. doi: 10.1007/s11356-020-08992-x

Pejcic, B., Marco, R. D., and Parkinson, G. (2006). The role of biosensors in the detection of emerging infectious diseases. *Analyst.* 131, 1079–1090. doi: 10.1039/b603402k

Plutzer, J., and Karanis, P. (2016). Neglected waterborne parasitic protozoa and their detection in water. *Water. Res.* 101, 318–332. doi: 10.1016/j.watres.2016.05.085

Poitras, C., Fatisson, J., and Tufenkji, N. (2009). Real-time microgravimetric quantification of *Cryptosporidium parvum* in the presence of potential interferents. *Water Res.* 43, 2631–2638. doi: 10.1016/j.watres.2009.03.021

Proll, G., Steinle, L., Pröll, F., Kumpf, M., Moehrle, B., Mehlmann, M., et al. (2007). Potential of label-free detection in high-content-screening applications. *J. Chromatogr. A.* 1161, 2–8. doi: 10.1016/j.chroma.2007.06.022

Rajchgot, J., Coulibaly, J. T., Keiser, J., Utzinger, J., Lo, N. C., Mondry, M. K., et al. (2017). Mobile-phone and handheld microscopy for neglected tropical diseases. *PLoS Negl. Trop. Dis.* 11, e0005550. doi: 10.1371/journal.pntd.0005550

Ramo, A., Del Cacho, E., Sánchez-Acedo, C., and Quílez, J. (2017). Occurrence and genetic diversity of *Cryptosporidium* and *Giardia* in urban wastewater treatment plants in north-eastern Spain. *Sci. Total Environ.* 598, 628–638. doi: 10.1016/j.scitotenv.2017.04.097

Ranjbar Bahadori, S., Mulgaonkar, A., Hart, R., Wu, C.-Y., Zhang, D., Pillai, A., et al. (2021). Radiolabeling strategies and pharmacokinetic studies for metal based nanotheranostics. *WIREs Nanomed. Nanobiotechnol.* 13, e1671. doi: 10.1002/wnan.1671

Reddy, L. H., Arias, J. L., Nicolas, J., and Couvreur, P. (2012). Magnetic nanoparticles: design and characterization, toxicity and biocompatibility, pharmaceutical and biomedical applications. *Chem. Rev.* 112, 5818–5878. doi: 10.1021/cr300068p

Resi, D., Varani, S., Sannella, A. R., De Pascali, A. M., Ortalli, M., Liguori, G., et al. (2021). A large outbreak of giardiasis in a municipality of the Bologna province, north-eastern Italy, November 2018 to April 2019. *Euro. Surveill.* 21, 26. doi: 10.2807/1560-7917.ES.2021.26.35.2001331

Rheonix (2011). *Rapid Detection of Waterborne Pathogens in Drinking Water*, Ithaca, NY.

Rhouati, A., Catanante, G., Nunes, G., Hayat, A., and Marty, J. (2016). Label-free aptasensors for the detection of mycotoxins. *Sensors.* 16, 2178. doi: 10.3390/s16122178

Ricciardi, A., and Ndao, M. (2015). Diagnosis of parasitic infections:what's going on? *J. Biomol. Screen.* 20, 6–21. doi: 10.1177/1087057114548065

Robbins, J. R., Zeldovich, V. B., Poukchanski, A., Boothroyd, J. C., and Bakardjiev, A. I. (2012). Tissue barriers of the human placenta to infection with *Toxoplasma gondii*. *Infect. Immun.* 80, 418–428. doi: 10.1128/IAI.05899-11

Robert-Gangneux, F., and Dardé, M. L. (2012). Epidemiology of and diagnostic strategies for toxoplasmosis. *Clin. Microbiol. Rev.* 25, 264–296. doi: 10.1128/CMR.05013-11

Ronkainen, N. J., Halsall, H. B., and Heineman, W. R. (2010). Electrochemical biosensors. *Chem. Soc. Rev.* 39, 1747–1763. doi: 10.1039/b714449k

Rostami, A., Karanis, P., and Fallahi, S. (2018). Advances in serological, imaging techniques and molecular diagnosis of *Toxoplasma gondii* infection. *Infection.* 46, 303–315. doi: 10.1007/s15010-017-1111-3

Saeidi, M., Amidian, M. A., Sheybanikashani, S., Mahdavi, H., Alimohammadi, H., Syedmoradi, L., et al. (2022). Multilayered mesoporous composite nanostructures for highly sensitive label-free quantification of cardiac troponin-I. *Biosensors (Basel)* 12, 21. doi: 10.3390/bios12050337

Saha, K., Agasti, S. S., Kim, C., Li, X., and Rotello, V. M. (2012). Gold nanoparticles in chemical and biological sensing. *Chem. Rev.* 112, 2739–2779. doi: 10.1021/cr2001178

Sakamoto, S., Putalun, W., Vimolmangkang, S., Phoolcharoen, W., Shoyama, Y., Tanaka, H., et al. (2018). Enzyme-linked immunosorbent assay for the quantitative/qualitative analysis of plant secondary metabolites. *J. Nat. Med.* 72, 32–42. doi: 10.1007/s11418-017-1144-z

Saleem, H., and Zaidi, S. J. (2020). Developments in the application of nanomaterials for water treatment and their impact on the environment. *Nanomaterials (Basel).* 10, 9. doi: 10.3390/nano10091764

Salouti, M., and Khadivi derakhshan, F. (2020). *Biosensors and Nanobiosensors in Environmental Applications*, pp. 515–591.

Sarkari, B., Hosseini, G., Motazedian, M. H., Fararouei, M., and Moshfe, A. (2016). Prevalence and risk factors of intestinal protozoan infections: a population-based study in rural areas of Boyer-Ahmad district, Southwestern Iran. *BMC Infect. Dis.* 16, 703. doi: 10.1186/s12879-016-2047-4

Saxena, S., and Srivastava, A. K. (2020). *Nano-Optics*. Thomas, S., Grohens, Y., Vignaud, G., Kalarikkal, N. and James, J. (eds), (London: Elsevier), pp. 265-291.

Schöning, M., and Poghossian, A. (2018). "Advanced materials, devices and applications," in *Label-free Biosensing*, eds Schöning, M., Poghossian, A. (Cham: Springer).

Shamah, S. M., Healy, J. M., and Cload, S. T. (2008). Complex target SELEX. *Acc. Chem. Res.* 41, 130–138. doi: 10.1021/ar700142z

Sharma, H., and Mutharasan, R. (2013). Review of biosensors for foodborne pathogens and toxins. *Sens. Actuat. B: Chem.* 183, 535–549. doi: 10.1016/j.snb.2013.03.137

Shaw, G. O. (2009). *Flow-Through Cell and Method of Use*. Google Patents.

Shiohara, A., Wojnilowicz, M., Lyu, Q., Pei, Y., Easton, C. D., Chen, Y., et al. (2022). SARS-CoV-2 virus detection via a polymeric nanochannel-based electrochemical biosensor. *Small.* 22, *e*2205281. doi: 10.1002/smll.202 205281

Shrestha, R., Duwal, R., Wagle, S., Pokhrel, S., Giri, B., and Neupane, B. B. (2020). A smartphone microscopic method for simultaneous detection of (oo)cysts of *Cryptosporidium* and *Giardia*. *PLoS Negl. Trop. Dis.* 14, e0008560–e0008560. doi: 10.1371/journal.pntd.0008560

Sin, M. L. Y., Mach, K. E., Wong, P. K., and Liao, J. C. (2014). Advances and challenges in biosensor-based diagnosis of infectious diseases. *Expert. Rev. Mol. Diagn.* 14, 225–244. doi: 10.1586/14737159.2014.888313

Singh, N. K., Jain, P., Das, S., and Goswami, P. (2019). Dye coupled aptamer-captured enzyme catalyzed reaction for detection of pan *malaria* and *P. falciparum* species in laboratory settings and instrument-free paper-based platform. *Anal Chem.* 91, 4213–4221. doi: 10.1021/acs.analchem.9b00670

Skládal, P. (2016). Piezoelectric biosensors. *TrAC Trends Analyt Chem.* 79, 127–133. doi: 10.1016/j.trac.2015.12.009

Sroka, J., Stojecki, K., Zdybel, J., Karamon, J., Cencek, T., and Dutkiewicz, J. (2013). Occurrence of *Cryptosporidium* oocysts and *Giardia* cysts in effluent from sewage treatment plant from eastern Poland. *Ann. Agric. Environ. Med. Spec.* 1, 57–62.

Stankic, S., Suman, S., Haque, F., and Vidic, J. (2016). Pure and multi metal oxide nanoparticles: synthesis, antibacterial and cytotoxic properties. *J.* 14, 73. doi: 10.1186/s12951-016-0225-6

Stone, H. A., Stroock, A. D., and Ajdari, A. (2004). Engineering flows in small devices: microfluidics toward a lab-on-a-chip. *Annu. Rev. Fluid Mech.* 36, 381–411. doi: 10.1146/annurev.fluid.36.050802.122124

Suh, S. H., Choi, S. J., Dwivedi, H. P., Moore, M. D., Escudero-Abarca, B. I., and Jaykus, L. A. (2018). Use of DNA aptamer for sandwich type detection of *Listeria monocytogenes*. *Anal. Biochem.* 557, 27–33. doi: 10.1016/j.ab.2018.04.009

Sun, X., Yasui, T., Yanagida, T., Kaji, N., Rahong, S., Kanai, M., et al. (2016). Identifying DNA methylation in a nanochannel. *Sci. Technol. Adv. Mater.* 17, 644–649. doi: 10.1080/14686996.2016.1223516

Syedmoradi, L., Daneshpour, M., Alvandipour, M., Gomez, F. A., Hajghassem, H., and Omidfar, K. (2017). Point of care testing: the impact of nanotechnology. *Biosens. Bioelectron.* 87, 373–387. doi: 10.1016/j.bios.2016.08.084

Syedmoradi, L., Norton, M. L., and Omidfar, K. (2021). Point-of-care cancer diagnostic devices: from academic research to clinical translation. *Talanta.* 225, 122002. doi: 10.1016/j.talanta.2020.122002

Taguchi, T., Arakaki, A., Takeyama, H., Haraguchi, S., Yoshino, M., Kaneko, M., et al. (2007). Detection of *Cryptosporidium parvum* oocysts using a microfluidic device equipped with the SUS micromesh and FITC-labeled antibody. *Biotechnol. Bioeng.* 96, 272–280. doi: 10.1002/bit.21104

Taguchi, T., Takeyama, H., and Matsunaga, T. (2005). Immuno-capture of *Cryptosporidium parvum* using micro-well array. *Biosens. Bioelectron.* 20, 2276–2282. doi: 10.1016/j.bios.2004.10.017

Tang, D., Yuan, R., Chai, Y., and Fu, Y. (2005). Study on electrochemical behavior of a diphtheria immunosensor based on silica/silver/gold nanoparticles and polyvinyl butyral as matrices. *Electrochem. Commun.* 7, 177–182. doi: 10.1016/j.elecom.2004.12.004

Tang, Y., Zeng, X., and Liang, J. (2010). Surface plasmon resonance: an introduction to a surface spectroscopy technique. *J. Chem. Educ.* 87, 742–746. doi: 10.1021/ed100186y

Tavares, R., Staggemeier, R., Borges, A., Rodrigues, M., Castelan, L., Vasconcelos, J., et al. (2011). Molecular techniques for the study and diagnosis of parasite infection. *J. Venomous Anim. Toxin Trop. Dis.* 17, 239–248. doi: 10.1590/S1678-91992011000300003

Tenter, A. M., Heckeroth, A. R., and Weiss, L. M. (2000). *Toxoplasma gondii*: from animals to humans. *Int. J. Parasitol.* 30, 1217–1258. doi: 10.1016/S0020-7519(00)00124-7

Terry, L. A., White, S. F., and Tigwell, L. J. (2005). The application of biosensors to fresh produce and the wider food industry. *J. Agric. Food Chem.* 53, 1309–1316. doi: 10.1021/jf040319t

Thevenot, D. R., Toth, K., Durst, R. A., and Wilson, G. S. (1999). Electrochemical biosensors: recommended definitions and classification. *Pure Appl. Chem.* 71, 2333–2348. doi: 10.1351/pac199971122333

Titcomb, G., Mantas, J. N., Hulke, J., Rodriguez, I., Branch, D., and Young, H. (2021). Water sources aggregate parasites with increasing effects in more arid conditions. *Nat. Commun.* 12, 7066. doi: 10.1038/s41467-021-27352-y

USEPA (2012). Method 1623. 1: *Cryptosporidium* and *Giardia in water by filtration/IMS/FA*.

Vasilescu, A., and Marty, J.-L. (2016). Electrochemical aptasensors for the assessment of food quality and safety. *TrAC Trends Anal. Chem.* 79, 60–70. doi: 10.1016/j.trac.2015.11.024

Verant, M. L., d'Ozouville, N., Parker, P. G., Shapiro, K., VanWormer, E., and Deem, S. L. (2014). Attempted detection of *Toxoplasma gondii* oocysts in environmental waters using a simple approach to evaluate the potential for waterborne transmission in the Galápagos Islands, Ecuador. *Ecohealth.* 11, 207–214. doi: 10.1007/s10393-013-0888-5

Villena, I., Aubert, D., Gomis, P., Ferté, H., Inglard, J. C., Denis-Bisiaux, H., et al. (2004). Evaluation of a strategy for *Toxoplasma gondii* oocyst detection in water. *Appl. Environ. Microbiol.* 70, 4035–4039. doi: 10.1128/AEM.70.7.4035-4039.2004

Vukojević, V., Djurdjić, S., Ognjanović, M., Fabián, M., Samphao, A., Kalcher, K., et al. (2018). Enzymatic glucose biosensor based on manganese dioxide nanoparticles decorated on graphene nanoribbons. *J. Electroanal. Chem.* 823, 610–616. doi: 10.1016/j.jelechem.2018.07.013

Wang, H., Zhang, Y., Yu, H., Wu, D., Ma, H., Li, H., et al. (2013). Label-free electrochemical immunosensor for prostate-specific antigen based on silver hybridized mesoporous silica nanoparticles. *Anal. Biochem.* 434, 123–127. doi: 10.1016/j.ab.2012.11.012

Wang, J., Ali, Z., Si, J., Wang, N., He, N., and Li, Z. (2017). Simultaneous extraction of DNA and RNA from hepatocellular carcinoma (Hep G2) based on silica-coated magnetic nanoparticles. *J. Nanosci. Nanotechnol.* 17, 802–806. doi: 10.1166/jnn.2017.12442

Wang, J., Rivas, G., Parrado, C., Cai, X., and Flair, M. N. (1997). Electrochemical biosensor for detecting DNA sequences from the pathogenic protozoan *Cryptosporidium parvum*. *Talanta*. 44, 2003–2010. doi: 10.1016/S0039-9140(96)02191-1

Wang, W., Lei, C., Li, J., Wu, Z., Shen, G., and Yu, R. (2004). A piezoelectric immunoagglutination assay for *Toxoplasma gondii* antibodies using gold nanoparticles. *Biosens. Bioelectron.* 19, 701–709. doi: 10.1016/S0956-5663(03)00265-3

Wang, Y., Montana, V., Grubišić, V., Stout, R. F. Jr, Parpura, V., and Gu, L. Q. (2015). Nanopore sensing of botulinum toxin type B by discriminating an enzymatically cleaved peptide from a synaptic protein synaptobrevin 2 derivative. *ACS Appl. Mater. Interfaces.* 7, 184–192. doi: 10.1021/am5056596

Wei, X., Zhou, W., Sanjay, S. T., Zhang, J., Jin, Q., Xu, F., et al. (2018). Multiplexed instrument-free bar-chart spinchip integrated with nanoparticle-mediated magnetic aptasensors for visual quantitative detection of multiple pathogens. *Anal. Chem.* 90, 9888–9896. doi: 10.1021/acs.analchem.8b02055

WHO (2014). *Guidelines for Drinking-Water Quality*. Geneva: World Health Organization, pp, 1–564.

WHO/UNICEF (2014). *Progress on Drinking Water and Sanitation: Update*. (Geneva: World Health Organization), pp. 1–78.

Woolley, A. T., and Mathies, R. A. (1994). Ultra-high-speed DNA fragment separations using microfabricated capillary array electrophoresis chips. *Proc. Natl. Acad. Sci.* 91, 11348. doi: 10.1073/pnas.91.24.11348

Wu, W., Wu, Z., Yu, T., Jiang, C., and Kim, W. S. (2015). Recent progress on magnetic iron oxide nanoparticles: synthesis, surface functional strategies and biomedical applications. *Sci. Technol. Adv. Mater.* 16, 023501doi: 10.1088/1468-6996/16/2/023501

Wu, Y., Ma, Y., Zheng, H., and Ramakrishna, S. (2021). Piezoelectric materials for flexible and wearable electronics: a review. *Mater. Des.* 211, 110164. doi: 10.1016/j.matdes.2021.110164

Xi, Z., Gong, Q., Wang, C., and Zheng, B. (2018). Highly sensitive chemiluminescent aptasensor for detecting HBV infection based on rapid magnetic separation and double-functionalized gold nanoparticles. *Sci. Rep.* 8, 9444. doi: 10.1038/s41598-018-27792-5

Xu, J., Bertke, M., Wasisto, H. S., and Peiner, E. (2019). Piezoresistive microcantilevers for humidity sensing. *J. Micromech. Microeng.* 29, 053003. doi: 10.1088/1361-6439/ab0cf5

Xu, S., and Mutharasan, R. (2010). Rapid and Sensitive Detection of *Giardia lamblia* using a piezoelectric cantilever biosensor in finished and source waters. *Environ. Sci. Technol.* 44, 1736–1741. doi: 10.1021/es9033843

Xu, S., Zhang, C., He, L., Wang, T., Ni, L., Sun, M., et al. (2013). DNA Detection of *Toxoplasma gondii* with a magnetic molecular beacon probe via CdTe@Ni quantum dots as energy donor. *J. Nanomater.* 2013, 473703. doi: 10.1155/2013/473703

Yan, X., Shu, Q., Zhao, K., Xiao, Y., Ai, F., and Zheng, X. (2021). Chemiluminescence "signal-on-off" dual signals ratio biosensor based on single-stranded DNA functions as guy wires to detect EcoR V. *Talanta.* 235, 122749. doi: 10.1016/j.talanta.2021.122749

Zahedi, A., Monis, P., Deere, D., and Ryan, U. (2021). Wastewater-based epidemiology—surveillance and early detection of waterborne pathogens with a focus on SARS-CoV-2, *Cryptosporidium* and *Giardia*. *Parasitol. Res.* 120, 4167–4188. doi: 10.1007/s00436-020-07023-5

Zahedi, A., and Ryan, U. (2020). *Cryptosporidium*—an update with an emphasis on foodborne and waterborne transmission. *Res. Vet. Sci.* 132, 500–512. doi: 10.1016/j.rvsc.2020.08.002

Zaporotskova, I. V., Boroznina, N. P., Parkhomenko, Y. N., and Kozhitov, L. V. (2016). Carbon nanotubes: sensor properties. a review. *Modern Electron. Mater.* 2, 95–105. doi: 10.1016/j.moem.2017.02.002

Zeng, Y., Zhou, J., Sang, W., Kong, W., Qu, J., Ho, H.-P., et al. (2021). High-sensitive surface plasmon resonance imaging biosensor based on dual-wavelength differential method. *Front. Chem.* 9, 21. doi: 10.3389/fchem.2021.801355

Zhang, X., and Hoshino, K. (2019). *Mechanical transducers: Cantilevers, acoustic wave sensors, and thermal sensors*, pp. 311–412.

Zhu, L., Zhang, Q., Feng, H., Ang, S., Chau, F. S., and Liu, W. T. (2004). Filter-based microfluidic device as a platform for immunofluorescent assay of microbial cells. *Lab. Chip.* 4, 337–341. doi: 10.1039/b401834f

Zou, X., Wu, J., Gu, J., Shen, L., and Mao, L. (2019). Application of aptamers in virus detection and antiviral therapy. *Front. Microbiol.* 9, 10. doi: 10.3389/fmicb.2019.01462

Zuehlke, J. (2022). *Rapid Detection of Foodborne E. coli O157: H7 using piezoelectric-excited millimeter-size cantilever Sensors*.

frontiers | Frontiers in Microbiology

TYPE Original Research
PUBLISHED 23 March 2023
DOI 10.3389/fmicb.2023.1158163

OPEN ACCESS

EDITED BY
Arabella Touati,
Centre Hospitalier Universitaire de Bordeaux, France

REVIEWED BY
Yuanshou Zhu,
Shanghai Jiao Tong University, China
Xinjie Wang,
Agricultural Genomics Institute at Shenzhen (CAAS), China

*CORRESPONDENCE
Wei Li
✉ liwei@ioz.ac.cn
Weiye Pan
✉ weiyepan@synsorbio.com

†These authors have contributed equally to this work

SPECIALTY SECTION
This article was submitted to Infectious Agents and Disease, a section of the journal Frontiers in Microbiology

RECEIVED 06 February 2023
ACCEPTED 06 March 2023
PUBLISHED 23 March 2023

CITATION
Wang X, Chen Y, Cheng X, Wang S-Q, Hu Y, Feng Y, Jin R, Zhou K, Liu T, Wang J, Pan K, Liu B, Xiang J, Wang Y, Zhou Q, Zhang Y, Pan W and Li W (2023) CDetection.v2: One-pot assay for the detection of SARS-CoV-2.
Front. Microbiol. 14:1158163.
doi: 10.3389/fmicb.2023.1158163

CDetection.v2: One-pot assay for the detection of SARS-CoV-2

Xinge Wang[1,2,3,4†], Yangcan Chen[1,2,3,4†], Xuejia Cheng[5†], Si-Qi Wang[1,2,3†], Yanping Hu[1,2,3,4], Yingmei Feng[6], Ronghua Jin[7], Kangping Zhou[8], Ti Liu[9], Jianxing Wang[9], Kai Pan[8], Bing Liu[10], Jie Xiang[11], Yanping Wang[12], Qi Zhou[1,2,3,4], Ying Zhang[1,2,3], Weiye Pan[5*] and Wei Li[1,2,3,4*]

[1]State Key Laboratory of Stem Cell and Reproductive Biology, Chinese Academy of Sciences, Institute of Zoology, Beijing, China, [2]Bejing Institute for Stem Cell and Regenerative Medicine, Beijing, China, [3]Chinese Academy of Sciences, Institute for Stem Cell and Regenerative Medicine, Beijing, China, [4]Savaid Medical School, University of Chinese Academy of Sciences, Beijing, China, [5]Beijing SynsorBio Technology Co., Ltd., Beijing, China, [6]Department of Science and Technology, Beijing Youan Hospital, Capital Medical University, Beijing, China, [7]Beijing Ditan Hospital, Capital Medical University, Beijing, China, [8]Hubei Provincial Center for Disease Control and Prevention, Wuhan, China, [9]Shandong Center for Disease Control and Prevention, Jinan, China, [10]Tonghua Central Hospital, Tonghua, Jilin, China, [11]Tongji Medical College of Huazhang, Wuhan Jinyintan Hospital, University of Science and Technology, Wuhan, China, [12]Hubei Provincial Hospital of Traditional Chinese Medicine, Wuhan, China

Introduction: The ongoing 2019 coronavirus disease pandemic (COVID-19), caused by severe acute respiratory syndrome coronavirus-2 (SARS-CoV-2) and its variants, is a global public health threat. Early diagnosis and identification of SARS-CoV-2 and its variants plays a critical role in COVID-19 prevention and control. Currently, the most widely used technique to detect SARS-CoV-2 is quantitative reverse transcription real-time quantitative PCR (RT-qPCR), which takes nearly 1 hour and should be performed by experienced personnel to ensure the accuracy of results. Therefore, the development of a nucleic acid detection kit with higher sensitivity, faster detection and greater accuracy is important.

Methods: Here, we optimized the system components and reaction conditions of our previous detection approach by using RT-RAA and Cas12b.

Results: We developed a Cas12b-assisted one-pot detection platform (CDetection.v2) that allows rapid detection of SARS-CoV-2 in 30 minutes. This platform was able to detect up to 5,000 copies/ml of SARS-CoV-2 without cross-reactivity with other viruses. Moreover, the sensitivity of this CRISPR system was comparable to that of RT-qPCR when tested on 120 clinical samples.

Discussion: The CDetection.v2 provides a novel one-pot detection approach based on the integration of RT-RAA and CRISPR/Cas12b for detecting SARS-CoV-2 and screening of large-scale clinical samples, offering a more efficient strategy for detecting various types of viruses.

KEYWORDS

CRISPR/Cas12b, SARS-CoV-2, molecular diagnosis, one-pot detection platform, clinical samples

1. Introduction

Since the outbreak of the COVID-19 pandemic, an effective strategy to prevent the spread of COVID-19 is to conduct the large-scale nucleic acid screening, followed by separating persons with confirmed or suspected COVID-19 infection from individuals who tested negative (Drain, 2022; Peeling et al., 2022). Nucleic acid detection, which relies on techniques such as sequencing, PCR, real-time quantitative PCR (RT-qPCR), and molecular switch design (Mohamadian et al., 2021; Yoo et al., 2021), is a crucial diagnostic tool to identify the viral infection at early stage. Isothermal amplification also plays an important role in COVID-19 screening due to its portability and reasonable consultation time (Yan et al., 2014; Zhao et al., 2015). However, the specificity of isothermal amplification is compromised by non-specific amplification (Schneider et al., 2019; Kaminski et al., 2021). Therefore, development of a detection platform with higher sensitivity, faster speed and greater accuracy is important.

The CRISPR/Cas system is part of the microbial adaptive immune system and is comprised of the CRISPR array and CRISPR-associated proteins (Cas) (Zhang, 2019). Since the *trans*-cleavage activity of Cas enzymes can specifically target a certain region of double strand DNA under the guidance of sgRNA (Joung et al., 2020), single CRISPR-Cas (such as Cas12 and Cas13) effector-mediated DNA *trans*-cleavage following isothermal amplification, has been used to develop portable nucleic acid detection systems with single-base resolution and high-sensitivity, such as the SHERLOCK and DETECTR technologies (Gootenberg et al., 2017, 2018; Chen et al., 2018). Despite the increased specificity of this two-step approach, its application in large-scale screening is still hampered because it does not shorten the processing time compared with isothermal amplification alone (Li et al., 2019; Guo et al., 2020). Attempts have been made to integrate amplification and CRISPR-based detection into a one-pot system that could reduce the risk of aerosol contamination caused by repeated capping and frequent exposure to the environment, thus improving portability (Huang et al., 2020; Wang et al., 2022). However, the sensitivity of these one-pot systems was reduced due to the lack of a compatible system for the isothermal amplification and CRISPR to work simultaneously (Guo et al., 2020; Joung et al., 2020). Given the high risk of COVID-19 contagion, development of a one-pot CRISPR detection system with high sensitivity, high specificity and rapid detection is necessary to control the pandemic and reduce the burden on society. In addition, these platforms can be used for portable detection in conjunction with lateral flow assays (Ding et al., 2020; Joung et al., 2020; Nguyen et al., 2020; Lu et al., 2022).

In our previous work, we developed a two-step detection system with high-sensitivity using CRISPR/Cas12b whose *trans*-cleavage activity is efficient, and enables sensitive detection at single-base resolution (Teng et al., 2018, 2019). However, this two-step detection is still complicated and time-consuming (Guo et al., 2020), prompting us to develop a one-pot approach for clinical detection by optimizing the components of the reaction system and the detection procedure. In this study, we developed a Cas12b-based one-pot platform by integrating isothermal amplification and CRISPR detection into one step, called CDetection.v2, which enables the rapid detection of SARS-CoV-2 in 30 min without compromising the sensitivity and accuracy of detection.

2. Materials and methods

2.1. Oligo preparation and synthesis

All conventional primers used in the experiments were synthesized by Sangon (Shanghai, China). RT-RAA primers were purified by high performance liquid chromatography (HPLC). The modified FAM and BHQ1 reporters were synthesized by Genscript (Nanjing, China). Standard original SARS-CoV-2 nucleic acid samples [Beijing, GBW(E)091089] and Delta (Beijing, GBW09316), Omicron (Beijing, GBW09318) variants standard nucleic acid samples were all obtained from the National Institute of Metrology. Guide RNA and RdRp RNA were generated by *in vitro* transcription using the HiScribe™ T7 Quick High Yield RNA Synthesis Kit (NEB, Ipswich, England, E2050S) according to the manufacturer's instructions. After the transcribed DNA template was digested by DNase I (RNase-free) (NEB, Ipswich, England, M0303S), the sgRNA was purified with the Monarch® RNA Cleanup Kit (NEB, Ipswich, England, T2040S) and quantified using Nanodrop. Purified sgRNA can be assessed through agarose electrophoresis and stored at −80°C.

2.2. Protein purification

The Cas12b protein was produced and purified by Genscript (Nanjing, China). The expression plasmid BPK2014-AaCas12b (Addgene, 121949) (Teng et al., 2018) was transformed into Chemically Competent BL21 (DE3) Cells (Transgene, Beijing, China, CD601-02), the bacteria were transferred to fresh LB medium with chloramphenicol and grown at 37°C until the OD_{600} was 0.6. Protein expression was induced for 16 h at 16°C. The bacteria were centrifuged and resuspended in lysis buffer (10 mM Tris-HCl, 200 mM NaCl, 10 mM Imidazole, 1 mM DTT, pH7.5). After sonication, the supernatant was passed through a 0.22 filter (Millipore, Burlington, MA, United States, SLGP033RB) and the resultant filtrate was then incubated with Ni-NTA agarose (Thermo Fisher, Waltham, MA, United States, R90115) at a temperature of 4°C for a period of 1 h. The protein was purified and washed with an imidazole gradient (included 10, 20, 50 and 100 mM imidazole). The protein was then eluted with 500 mM imidazole and subsequently desalted in the dialysate after being passed through the dialysis bag (Solarbio, Beijing, China, YA1046). The protein is ultimately concentrated utilizing Amicon® Ultra-4 Centrifugal Filter Unit (Millipore, Burlington, MA, United States, UFC8050). The concentration of the purified proteins was determined by Pierce™ BCA Protein Assay Kit (Thermo Fisher, Waltham, MA, United States, 23225). Purified protein be stored at −80°C.

2.3. Cas12b-based *trans*-cleavage assays

The Cas12b assay was performed in the presence of 50 nM AapCas12b, 30 nM sgRNA, 40 nM activator, 200 nM ssDNA FQ reporter and NEBuffer™ 2 (NEB, Ipswich, England, B7002S) in a 16 μL reaction. The activator is prepared by utilizing the synthesized 100 bp ssDNA as a template and refining the

product obtained from PCR with Q5® High-Fidelity 2X Master Mix (NEB, Ipswich, England, M0492S). The concentration of activator is determined by Nanodrop, and this is subsequently used to calculate the concentration in relation to the molecular weight. Reactions were incubated with a temperature gradient for the indicated time in an Applied Biosystems Veriti™ Thermal Cycler. The reaction was then transferred to a Corning® 384-well Polystyrene NBS Microplate (Corning, 3571) and detection was performed in a multi-detection microplate reader (BioTek Synergy 4) in the fluorescence mode (λex = 485 nm; λem = 528 nm, transmission gain = 61). The relative fluorescence unit can be analyzed directly.

2.4. CDetection.v2 assays

CDetection.v2 assays were performed by using commercial freeze-dried RT-RAA (Hangzhou ZC Bio-Sci&Tech Co., Ltd., S003ZC), according to the manufacturer's instructions. The assay system was prepared in advance and divided into three components. A total of 35 μl component A contained RT-RAA reaction buffer, 400 nM RT-RAA primer, 1200 nM FAM–BHQ1 fluorescent probe and 14 mM magnesium acetate final concentration in the final 50 μl system. Component B is the RT-RAA dry powder purchased from the manufacturer. A total of 5 μl component C consists of 200 nM sgRNA, 50 nM Cas12b protein, 200 UI RNase Inhibitor (Promega, Wisconsin, MI, United States, N2515), 50 mM NaCl, 2 mM HEPES (PH 7.4), 3 mM DTT, 10 nM EDTA and 0.001% Tween final concentration in the final 50 μl system. To perform the assay, 10 μl of the sample were added to component B, dissolved the dry powder B using the sample. Then, component A should be included to guarantee the stability of the proteins related to the amplification process in the system, followed by sequential addition of component C and gentle vortexing. It is important to pay attention to the reaction system and ensure that the sample is adequately mixed, yet not too vigorously to avoid impacting the function of enzyme. Subsequently, the only step left is to initiate the instrument to run the program for detection. The reaction was first performed at 42°C for nucleic acid template amplification for 7 min and then the temperature was increased to 52°C for *trans*-cleavage. The reaction volume was 50 μl, and the assay was performed in the Applied Biosystems QuantStudio 6 real-time PCR instrument. Rn values were exported and analyzed using GraphPad Prism 8 software.

2.5. Positive reference value determination of CDetection.v2

In three research institutions, five clinical samples were selected for throat swabs to determine the positive judgment value. Using two batches of reagents, 15 positive samples were diluted to 1×10^4 copies/ml and tested for 5 consecutive days. Each sample was tested once per day. Values obtained from each batch were analyzed for normality using SPSS 20.0 analysis software. The results showed that the data did not support the null hypothesis of normality at 5% significance level ($p = 0.018$). The results of the Kolmogorov–Smirnov test showed that the distribution of marginally positive samples was not normal. For the following calculations, a non-parametric method was used to determine the positive judgment value in the subsequent calculations, assuming a tolerable false-negative error rate of 1%.

So, rank position (1%) = 0.5 + 75 × 0.01 = 1.25

LoB = {X (1) + 0.25 × [X (2) − X (1)]}

LoB (Cutoff A) = X (0.248) + 0.25 × [X (0.254)−X (0.248)] = 0.2495

LoB (Cutoff B) = X (0.247) + 0.25 × [X (0.259)−X (0.247)] = 0.2500

To summarize, the larger data value of the two batches was chosen as the positive judgment value, so the positive judgment value must be ≥ 0.250.

Non-parametric approaches were used to ascertain reference intervals for negative samples as well. Setting the maximum acceptable false positive error rate at 1%.

Rank position (99%) = 0.5+72 × 0.99 = 71.78

LoB = {X (71) + 0.78 × [X (72)−X (71)]}

LoB (Cutoff A) = X (0.236) + 0.78 × [X (0.241)−X (0.236)] = 0.2399

LoB (Cutoff B) = X (0.238) + 0.78 × [X (0.238)−X (0.236)] = 0.2396

Thus, the negative judgment value must be < 0.24.

2.6. Analysis of clinical samples by RT-qPCR

Clinical samples were collected from the Tonghua (Jilin, China), Linyi (Shandong, China) and Wuhan (Hubei, China) CDC (Centers for disease control and prevention). Information of clinical samples are provided in the **Supplementary material**. Throat swabs of COVID-19 patients or suspected patients are used to acquire samples for the purpose of diagnosis, which are extracted with the nucleic acid extraction or purification kit (Guangzhou Magen Biotechnology Co., Ltd, IVD5412). The Ct values of the clinical samples were measured using HiScript® II U+ One Step qRT-PCR Probe Kit according to the manufacturer's instruction (Vazyme, Q223-01). Add 5 μl sample into 25 μl enzyme master mix. A 30 μl reaction included buffers, Rox, 1.5 μl One step U+ Enzyme Mix, 200 nM RdRP_SARSr-F3, 200 nM RdRP_SARSr-F3 RdRP_SARSr-R2 and 100 nM RdRP_SARSr-P2. The reaction was performed using the 7500 Fast Real-Time PCR System (Applied Biosystems) as following procedure: (1) reverse transcription at 55°C for 15 min; (2) a pre-denaturation step at 95°C for 30 s; (3) 10 s at 95°C for and 30 s at 60°C for 45 cycles.

2.7. The analysis of primers and sgRNA sequences

The SARS-CoV-2 sequence was downloaded from the virus database in NCBI.[1] We conducted a random sampling of a specific number of virus sequences from the database by country, including multiple variants. Random sequences of no more than

1 https://www.ncbi.nlm.nih.gov/

100 samples were selected from each country. We compared these sequences with the RT-RAA primers and the 20 nt spacer of the sgRNA that we utilized. The software package BLAST+2.13.0[2] was used for comparison and analysis. The samples were classified by region and time. The ratio of mismatched sequences to the total number of sequences in the region will be calculated in order to evaluate the tolerance of the primers and sgRNA of the detection system. The comparison results were analyzed using GraphPad Prism 8.

2.8. Statistical analysis

All experiments were performed in at least triplicate. Statistical analysis was carried out using GraphPad Prism 8.

3. Results

3.1. Establishment of CDetection.v2 platform

To establish a Cas12b-based SARS-CoV-2 one-pot detection platform, we selected the conserved sequence RdRp (RNA-dependent RNA polymerase) and the RT-RAA (reverse transcription recombinase-aided amplification) primers from our previous publication on Orf1ab (Guo et al., 2020), where RdRp was the target and RT-RAA primers were used for isothermal amplification (**Figure 1A**). Instead of using the previous two-step approach (Guo et al., 2020), RT-RAA and AapCas12b (Cas12b for short) were added to a single tube allowing simultaneous amplification and detection of SARS-CoV-2 in a single reaction. Because integrating of amplification and *trans*-cleavage in one reaction resulted in decreased fluorescence intensity (Guo et al., 2020), we first optimized the concentration of fluorescent probe in the reaction. The results showed that increasing the concentration of the fluorescent probe enhanced the fluorescent intensity when detecting standard RNA samples with different copy numbers (**Figure 1B**). As our previous two-step approach showed that increased sgRNA enhanced enzyme catalysis in a dose-dependent manner (Guo et al., 2020), we increased the concentration of sgRNA to improve the performance of one-pot detection assay. The results showed that a strong fluorescence signal was detected when the sgRNA concentration was increased to 200 nM (**Figure 1C**). Furthermore, we focused on increasing Cas protein *trans*-cleavage activity by optimizing the temperature because Cas12b is thermally stable and can perform extensive *trans*-cleavage at high temperature (Teng et al., 2018; Joung et al., 2020). We first examined the *trans*-cleavage activity of Cas12b in response to dsDNA activators at different temperatures and found that Cas12b exhibited a robust *trans*-cleavage activity from 25C to 65°C (**Supplementary Figure 1**). Then we tested the suitable temperature of RT-RAA from 25 to 65°C for establishing one-step reaction, while the recommended temperature for pre-amplification was 42°C. Since the components of the RT-TAA reaction were changed in one-pot system, which might affect the molecules movement and Cas enzymatic kinetics caused by increased temperature, we tested the optimal temperature for *trans*-cleavage at 42, 52, 62 and 72°C for 23 min, respectively. The result showed that 52°C was the best temperature for Cas12b-catalyzed ssDNA-cleavage (**Figure 1D**). To further increase the sensitivity, time ratio of isothermal amplification to *trans*-cleavage within 30 min was tested. Three different time ratios were evaluated and found that amplification for 7 min followed by *trans*-cleavage for 23 min gave a robust fluorescence signal. Notably, the sensitivity of RNA detection showed non-significantly improved when we prolonged the detection time (**Figure 1E** and **Supplementary Figure 2**). Collectively, our findings demonstrate that the CRISPR/Cas12b *trans*-cleavage activity and detection sensitivity can be improved by increasing the concentration of reactants, raising the reaction temperature, and optimizing the reaction process. These results show the successful establishment of one-pot detection system for SARS-CoV-2 based on RT-RAA and Cas12b with highly sensitive and rapid speed, named as CDetection.v2.

3.2. Evaluation of the detection capabilities of CDetection.v2

The sensitivity of CDetection.v2 platform was determined by detecting serial diluted standard RNA sample with designated copy number. Results showed that, compared with negative samples, the fluorescent intensity was significantly increased when the concentration of RNA sample reached to 5,000 copies/ml. Moreover, increased concentration of RNA samples produced enhanced fluorescent intensity. Compared with 1×10^{10} copies/ml sensitivity of one-pot assays from our previous publication (Guo et al., 2020), this platform exhibited a very high sensitivity and was able to detect 5,000 copies/ml RNA template within 30 min (**Figure 2A**).

In order to eliminate the influence of the initial well fluorescence on the results, the (Rn-R1)/R1 was chosen as the interpretation of the fluorescence detection results. Meanwhile, to further verify the effectiveness of this system, diluted clinical SARS-CoV-2 samples with designated copy number were used and the (Rn24-Rn1)/Rn1 value was used as the readout of CDetection.v2. To more accurately interpret and quantify the detection results, the readout standard of CDetection.v2 was first determined. Fifteen clinical SARS-CoV-2 samples were randomly selected, diluted into 1×10^4 copies/ml and analyzed at five different time points. Based on the results of these fifteen samples, models were formulated to fit the data (**Supplementary Figure 3**). Based on the requirements of "*Evaluation of Detection Capability for Clinical Laboratory Measurement Procedures, 2nd Edition*," a false positive error rate of 1% was considered as acceptable, while the sample with a value of (Rn24-Rn1)/Rn1 greater than 0.25 was considered as positive.

In order to gain a more comprehensive insight into the performance of the detection system when the form of result interpretation was clarified, it is essential to perform a systematic evaluation based on clinical samples. We first evaluated the reliability of the above detection standard: we tested a single clinical sample at three different concentrations and measured each concentration in 20 replicates (**Figure 2C**). In our study, clinical samples of up to 1×10^4 copies/ml could be detected with

2 https://ftp.ncbi.nlm.nih.gov/blast/executables/blast+/LATEST/

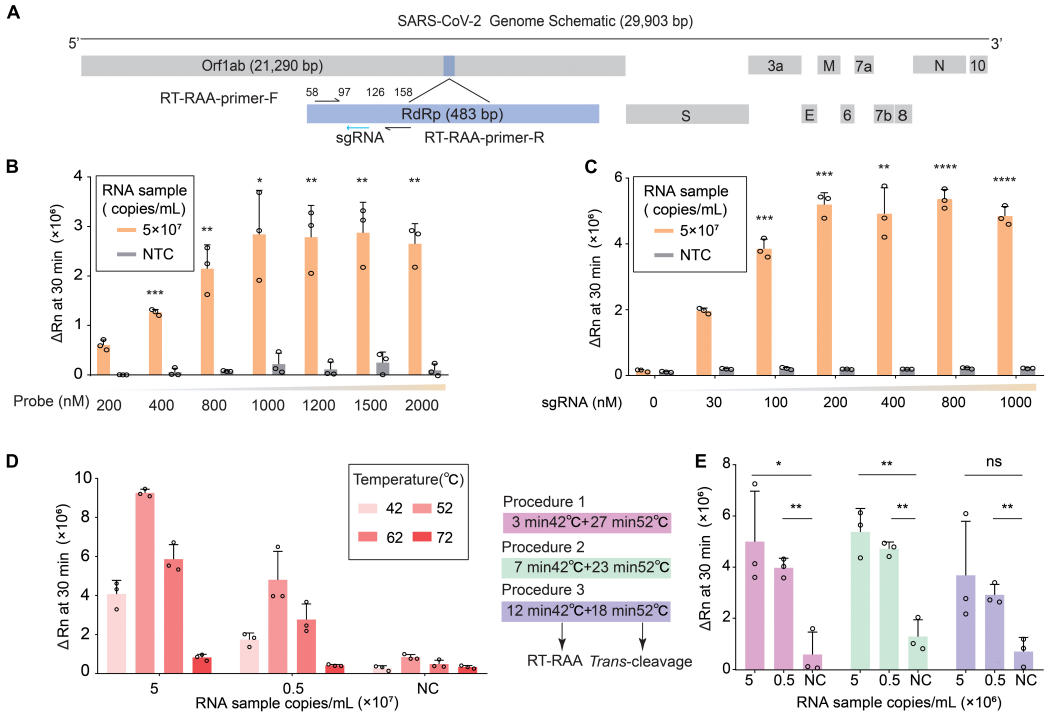

FIGURE 1
Establishment of CDetection.v2 platform. **(A)** Schematic diagram of the SARS-CoV-2 genome. RdRp segment is marked in light blue. RT-RAA primers are indicated by black arrows and sgRNAs are indicated by blue arrows. **(B)** Detection efficiency of CDetection.v2 under different concentration of ssDNA reporter. The efficiency is evaluated by delta Rn measured by real-time quantitative PCR (RT-qPCR) instrument. The delta Rn value measured at 30 min is plotted on a histogram. Error bars represent standard deviation (SD) of mean, $n = 3$ replicates. Two-tailed, unpaired Student's *t*-test, $*p < 0.05$, $**p < 0.01$, $***p < 0.001$. **(C)** Detection efficiency of CDetection.v2 under different concentration of sgRNA. The efficiency is evaluated by delta Rn measured by RT-qPCR instrument, error bars represent SD of mean, $n = 3$. Two-tailed, unpaired Student's *t*-test, $**p < 0.01$, $***p < 0.001$, $****p < 0.0001$. **(D)** Detection efficiency of CDetection.v2 under different combinations of temperatures and concentration of RNA targets. The efficiency is evaluated by delta Rn measured by RT-qPCR instrument. Different temperatures are indicated by red bars of different sizes. Error bars represent SD of mean, $n = 3$. **(E)** The analysis of the detection time ratio using two-temperature-stage procedure. The 30-minute incubation period has been divided into two stages, the amplification stage and the *trans*-cleavage stage, each with a specific temperature. These two temperature stages can be combined in different ratios to create three different conditions. The changes in delta Rn values of the RNA samples can be monitored under these three different conditions. Error bars represent SD of mean, $n = 3$. Two-tailed, unpaired Student's *t*-test, ns: not significant, $*p < 0.05$, $**p < 0.01$.

great accuracy by CDetection.v2. Meanwhile, we found that our system had good reproducibility. The specificity of the detection platform was further validated by testing other types of human coronaviruses and common viruses, as well as known viral nucleic acids that interfere with detection (Figure 2B and Supplementary Figure 4). The results of CDetection.v2 shall remain unaffected by the nucleic acid of other pathogens, medications taken by the patient, or interference from the patient themselves in the sample. That shown CDetection.v2 platform was able to sensitively detect SARS-CoV-2 without being affected by the presence of other compounds (Figure 2D). Taken together, the results indicate that CDetection.v2 has an impressive sensitivity, specificity, stability and sample inclusion in the detection of SARS-CoV-2.

3.3. The accuracy of CDetection.v2 is in agreement with that of RT-qPCR based on clinical samples

The performance of detection system is determined by the sensitivity and specificity of the clinical samples detection. Therefore, we compared the sensitivity and specificity of CDetection.v2 with those of RT-qPCR by analyzing 120 cases of clinical samples (71 positive and 49 negative samples). These clinical samples were tested by CDetection.v2, and the sensitivity and specificity of CDetection.v2 were systematically evaluated by the (Rn24-Rn1)/Rn1 ratio. The (Rn24-Rn1)/Rn1 ratio and corresponding RT-qPCR results provided by the Centers for Disease Control and Prevention (CDC) in three different cities of China was compared. The heat map showed a high consistency between CDetection.v2 and RT-qPCR method (Figure 3A). The ROC curve of the outcomes of these two methods was further calculated. The plotted Receiver Operating Characteristic (ROC) curves showed that CDetection.v2 exhibited a specificity of 100% and a sensitivity of 99.16% (Figures 3B, C). Together, our newly developed one-step CDetection.v2 displayed the similar sensitivity and specificity as RT-qPCR on clinical sample detection.

3.4. Visualization of CDetection.v2 results

In order to easily acquire the results by naked eyes which suit the specific situation such as customs, family and so forth, CDetection.v2 can be implemented without complicated

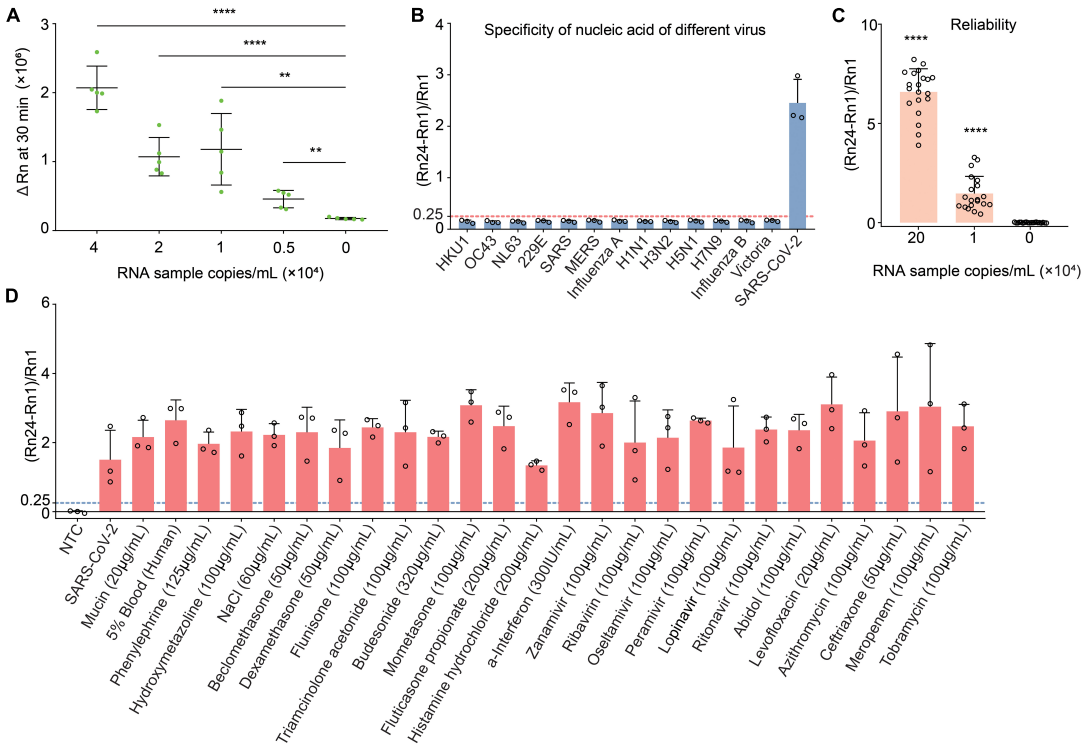

FIGURE 2
Evaluation of the detection capabilities of CDetection.v2. **(A)** The sensitivity of CDetection.v2 on gradient diluted RNA samples. The sensitivity was evaluated by delta Rn measured by real-time quantitative PCR (RT-qPCR) instrument. Error bars represent SD of mean, $n = 5$ biological replicates. Two-tailed, unpaired Student's *t*-test, $^{**}p < 0.01$, $^{****}p < 0.0001$. **(B)** Evaluation of cross reactivity of CDetection.v2. The degree of separation of nucleic acid samples containing target from 8 human epidemic viruses are serially diluted. Error bars represent SD of mean, $n = 3$. **(C)** Repeatability analysis of CDetection.v2 assay. Error bars represent SD of mean, $n = 20$ biological replicates. Two-tailed, unpaired Student's *t*-test, $^{****}p < 0.0001$. **(D)** Influence of internal and external interfering substances on CDetection.v2. The potential interferences detected include the original substances in the sample and the substances introduced during sample collection and preparation, which are mixed into the unextracted samples for interference simulation. Error bars represent SD of mean, $n = 3$.

instruments. Previous researches have utilized blue-light or ultraviolet to develop visual detection (Guo et al., 2020). The results of the CDetection.v2 platform can be directly assessed by exposing the tube containing the final reaction mixture to blue or ultraviolet light, and then interpreted directly by naked eyes. The positivity of samples with a concentration greater than 5×10^4 copies/ml can be observed using either instrumentation or the naked eye (**Figure 4A**), indicating the great potential of CDetection.v2 for point of care testing (POCT). In summary, we have developed a Cas12b-assisted one-pot detection platform based on RT-RAA and CRISPR/Cas12b that provides rapid and accurate detection of SARS-CoV-2 within 30 min (**Figure 4B**).

4. Discussion

In this study, we developed a one-pot SARS-CoV-2 detection system, named as CDetection.v2 platform, which can detect standard SARS-CoV-2 samples with a sensitivity of 5,000 copies/ml within just 30 min. Results of 120 cases of COVID-19 throat swab samples detected by CDetection.v2 platform were completely in line with the results detected by RT-qPCR, indicating the high specificity and good compatibility of this platform for complex clinical samples. Apart from these advantages, CDetection.v2 platform also displayed several other advantages in SARS-CoV-2 detection. First of all, CDetection.v2 platform can detect most current SARS-CoV-2 variants. Since SARS-CoV-2 mutates rapidly and subsequently has given rise to various variants worldwide (Scovino et al., 2022), the universality of CDetection.v2 platform was assessed by comparing and analyzing the full sequence of SARS-CoV-2 by BLAST. A total of 3,548 sequences of SARS-CoV-2 were randomly selected from the NCBI database with a maximum of 100 samples per country and further classified based on region and time of identification. Statistical analysis of the mismatch sites in the SARS-CoV-2 sequence revealed that only a very small proportion of the sequences could not be detected by our platform. The RT-RAA-Rp primers used were able to detect nearly 99% of SARS-CoV-2, and the sgRNA was able to target 99.97% of SARS-CoV-2 sequences. To further verify the efficiency of CDetection.v2 platform in detecting different variants, the standard nucleic acid of the Delta and Omicron variants were diluted into a concentration of 1×10^4 copies/ml, respectively, and further under tested by our platform. The results showed that CDetection.v2 platform could detect both variants (**Supplementary Figure 5**). Moreover, CDetection.v2 platform displays promising for POCT in the future, since we have tried to achieve the naked eye observed of the detection results. In comparison to our previous detection system, CDetection.v2 shows significantly improvement

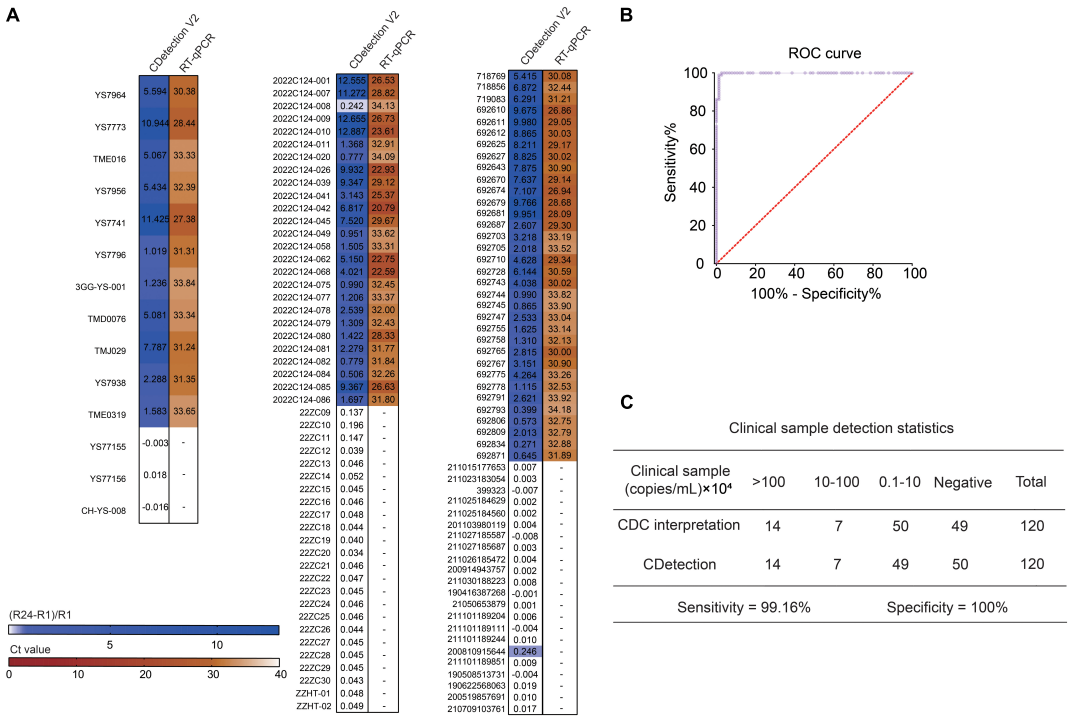

FIGURE 3
The accuracy of CDetection.v2 is in agreement with that of real-time quantitative PCR (RT-qPCR) based on clinical samples. **(A)** Clinical samples with known Ct values were detected by CDetection.v2. The (Rn24-Rn1)/Rn1 value is calculated in order to assess the conformity of the assay results. The results of the RT-qPCR are shown in brown, and CDetection.v2 in blue. **(B)** ROC curve analysis of CDetection.v2. **(C)** Statistical analysis of clinical samples. CDC, Center for Disease Control and Prevention.

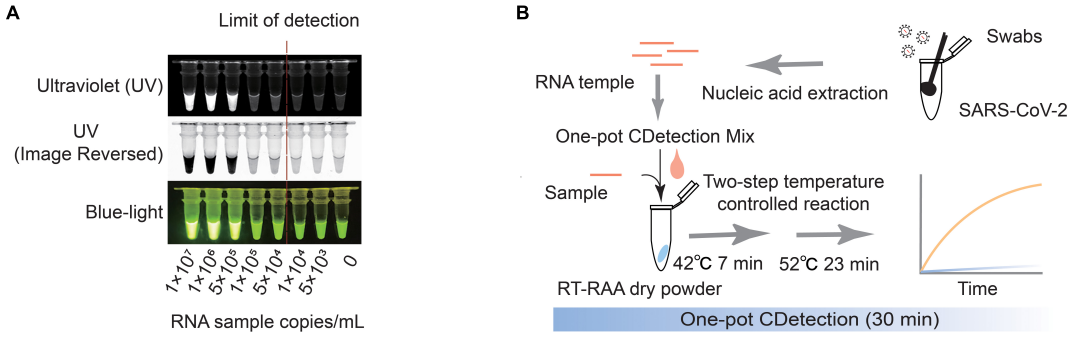

FIGURE 4
Visualization of CDetection.v2 results. **(A)** Visualization of CDetection.v2 results by exposing the samples under UV- or Blue-light. The RNA samples (5×10^3, 1×10^4, 5×10^4, 1×10^5) were all positive standard nucleic acid samples by gradient dilution, 0 copies/ml RNA sample is negative control. The dark red dotted line signifies the detection limit under visual detection. **(B)** Schematic diagram of the workflow of CDetection.v2.

on detection speed and detection procedure without compromising its adequate accuracy (**Supplementary Table 1**).

Although the CDetection.v2 platform showed satisfactory sensitivity for the detection of SARS-CoV-2, in comparison to other current detection methods, optimizations on enhancing sensitivity are still needed (**Supplementary Table 2**). Additionally, the incompatibility between isothermal amplification and CRISPR is still needed to be addressed. To date, the reasons for this incompatibility have not been well understood, several factors might affect the compatibility of two steps. For examples, competitive binding of double-stranded DNA to Cas protein in both RT-RAA and CRISPR reaction system might affect the enzyme efficiency of Cas protein during CRISPR detection (Lu et al., 2022); single-stranded DNA-binding protein (SSB),as a critical component of RT-RAA, would not only bind to the RT-RAA primers, but also could bind to the sgRNA, resulting in the reduction of the effective concentration of sgRNA in the one-pot assay (Piepenburg et al., 2006; Routsias et al., 2010; Cook et al., 2018).

With continual advancement in the fields of electron microscopy and structural biology, a detailed analysis of the structures of a variety of Cas nucleases has been conducted, from

the recognition of guide RNA, pre-processing, to the recognition and hydrolysis of target nucleic acids, including Cas12b (Yamano et al., 2016; Liu et al., 2017; Nishimasu et al., 2017; Xiao et al., 2021). Meanwhile, the mechanism of ssDNA hydrolysis also has been extensively explored. It has been demonstrated that Cas proteins can be modified to enhance nuclease activity (Chen et al., 2022; Mahas et al., 2022; Yang et al., 2022). Therefore, by utilizing rational design and directed evolution, the *trans*-cleavage activity of Cas12b, a component of the CRISPR/Cas12b system, can be further improved. On the other hand, the amplification step can also be a source of aerosols and false positives. Attention must be paid to the realization of an amplification-free, sensitive diagnostic platform based on the CRISPR system, as this will render the detection process more portable and cost-effective (Li et al., 2022). Efforts have been made within this field to integrate formats with enzyme cascade reactions or ddPCR (Liu et al., 2021; Shi et al., 2021; Xue et al., 2022). Merging multiple strategies to achieve engineering instant diagnosis *via* portable, accurate detection through the means of mini-instruments or later flow is a potential avenue for the future of this field (de Puig et al., 2021; Nguyen et al., 2021). Globally, infectious diseases such as Zika, HIV, smallpox, and Ebola virus display high mortality rates and pose a threat to human health. CRISPR/Cas12b-based systems will continue to progress and adapt to the changing needs and scenarios. Thus, the strategy underlying the CDetection.v2 system could also be used to detect these viruses and provide a sensitive, portable and rapid nucleic acid test for infectious diseases prevention and control.

Data availability statement

The datasets presented in this study can be found in online repositories. The names of the repository/repositories and accession number(s) can be found in this article/**Supplementary material**.

Ethics statement

The studies involving human participants were reviewed and approved by the Ethics Commission is QX-2022-001 the Ethics Committee of Hubei Provincial Center for Disease Control and Prevention (Hubei Academy of Preventive Medicine), 2021-73 (IRB for Preventive Medicine of Shandong Center for Disease Control and Prevention), and 2021-007-01 (the Ethics Committee for Drug Clinical Trials of Tonghua Central Hospital). Written informed consent to participate in this study was provided by the participants' legal guardian/next of kin.

Author contributions

WL, QZ, WP, and XW conceived the project and designed the experiments. XW, YC, WP, S-QW, and XC performed the experiments. WL, QZ, XW, YC, YZ, WP, XC, and YH analyzed the data. WL, QZ, YZ, XW, YC, YH, and S-QW wrote the manuscript. YF, RJ, KZ, TL, JW, KP, BL, JX, and YW provided clinical samples and ethics statements. All authors contributed to the article and approved the submitted version.

Funding

This work was supported by the National Key Research and Development Program (2020YFA0707900, 2018YFA0108400, and 2019YFA0903800), the National Natural Science Foundation of China (31621004 to QZ and WL), and the CAS Project for Young Scientists in Basic Research (YSBR-012 to WL).

Conflict of interest

XC and WP were employed by Beijing SynsorBio Technology Co., Ltd.

The remaining authors declare that the research was conducted in the absence of any commercial or financial relationships that could be construed as a potential conflict of interest.

Publisher's note

Supplementary material

The Supplementary Material for this article can be found online at: https://www.frontiersin.org/articles/10.3389/fmicb.2023.1158163/full#supplementary-material

References

Chen, J. S., Ma, E., Harrington, L. B., Da Costa, M., Tian, X., Palefsky, J. M., et al. (2018). CRISPR-Cas12a target binding unleashes indiscriminate single-stranded DNase activity. *Science* 360, 436–439. doi: 10.1126/science.aar6245

Chen, Y., Hu, Y., Wang, X., Luo, S., Yang, N., Chen, Y., et al. (2022). Synergistic engineering of CRISPR-Cas nucleases enables robust mammalian genome editing. *Innovation* 3:100264. doi: 10.1016/j.xinn.2022.100264

Cook, A., Hari-Gupta, Y., and Toseland, C. P. (2018). Application of the SSB biosensor to study in vitro transcription. *Biochem. Biophys. Res. Commun.* 496, 820–825. doi: 10.1016/j.bbrc.2018.01.147

de Puig, H., Lee, R. A., Najjar, D., Tan, X., Soeknsen, L. R., Angenent-Mari, N. M., et al. (2021). Minimally instrumented SHERLOCK (miSHERLOCK) for CRISPR-based point-of-care diagnosis of SARS-CoV-2 and emerging variants. *Sci. Adv.* 7:eabh2944. doi: 10.1126/sciadv.abh2944

Ding, X., Yin, K., Li, Z., Lalla, R. V., Ballesteros, E., Sfeir, M. M., et al. (2020). Ultrasensitive and visual detection of SARS-CoV-2 using all-in-one dual CRISPR-Cas12a assay. *Nat. Commun.* 11:4711. doi: 10.1038/s41467-020-18575-6

Drain, P. K. (2022). Rapid diagnostic testing for SARS-CoV-2. *N. Engl. J. Med.* 386, 264–272. doi: 10.1056/NEJMcp2117115

Gootenberg, J. S., Abudayyeh, O. O., Kellner, M. J., Joung, J., Collins, J. J., and Zhang, F. (2018). Multiplexed and portable nucleic acid detection platform with Cas13, Cas12a, and Csm6. *Science* 360, 439–444. doi: 10.1126/science.aaq0179

Gootenberg, J. S., Abudayyeh, O. O., Lee, J. W., Essletzbichler, P., Dy, A. J., Joung, J., et al. (2017). Nucleic acid detection with CRISPR-Cas13a/C2c2. *Science* 356, 438–442. doi: 10.1126/science.aam9321

Guo, L., Sun, X., Wang, X., Liang, C., Jiang, H., Gao, Q., et al. (2020). SARS-CoV-2 detection with CRISPR diagnostics. *Cell Discov.* 6:34. doi: 10.1038/s41421-020-0174-y

Huang, W. E., Lim, B., Hsu, C. C., Xiong, D., Wu, W., Yu, Y., et al. (2020). RT-LAMP for rapid diagnosis of coronavirus SARS-CoV-2. *Microb. Biotechnol.* 13, 950–961. doi: 10.1111/1751-7915.13586

Joung, J., Ladha, A., Saito, M., Kim, N. G., Woolley, A. E., Segel, M., et al. (2020). Detection of SARS-CoV-2 with SHERLOCK one-pot testing. *N. Engl. J. Med.* 383, 1492–1494.

Kaminski, M. M., Abudayyeh, O. O., Gootenberg, J. S., Zhang, F., and Collins, J. J. (2021). CRISPR-based diagnostics. *Nat. Biomed. Eng.* 5, 643–656.

Li, H., Xie, Y., Chen, F., Bai, H., Xiu, L., Zhou, X., et al. (2022). Amplification-free CRISPR/Cas detection technology: Challenges, strategies, and perspectives. *Chem. Soc. Rev.* 52, 361–382. doi: 10.1039/d2cs00594h

Li, L., Li, S., Wu, N., Wu, J., Wang, G., Zhao, G., et al. (2019). HOLMESv2: A CRISPR-Cas12b-assisted platform for nucleic acid detection and DNA methylation quantitation. *ACS Synth. Biol.* 8, 2228–2237. doi: 10.1021/acssynbio.9b00209

Liu, L., Chen, P., Wang, M., Li, X., Wang, J., Yin, M., et al. (2017). C2c1-sgRNA complex structure reveals RNA-Guided DNA cleavage mechanism. *Mol. Cell* 65, 310–322. doi: 10.1016/j.molcel.2016.11.040

Liu, T. Y., Knott, G. J., Smock, D. C. J., Desmarais, J. J., Son, S., Bhuiya, A., et al. (2021). Accelerated RNA detection using tandem CRISPR nucleases. *medRxiv [Preprint]* doi: 10.1101/2021.03.19.21253328

Lu, S., Tong, X., Han, Y., Zhang, K., Zhang, Y., Chen, Q., et al. (2022). Fast and sensitive detection of SARS-CoV-2 RNA using suboptimal protospacer adjacent motifs for Cas12a. *Nat. Biomed. Eng.* 6, 286–297. doi: 10.1038/s41551-022-00861-x

Mahas, A., Marsic, T., Lopez-Portillo Masson, M., Wang, Q., Aman, R., Zheng, C., et al. (2022). Characterization of a thermostable Cas13 enzyme for one-pot detection of SARS-CoV-2. *Proc. Natl. Acad. Sci. U.S.A.* 119:e2118260119. doi: 10.1073/pnas.2118260119

Mohamadian, M., Chiti, H., Shoghli, A., Biglari, S., Parsamanesh, N., and Esmaeilzadeh, A. (2021). COVID-19: Virology, biology and novel laboratory diagnosis. *J. Gene Med.* 23:e3303.

Nguyen, L. T., Smith, B. M., and Jain, P. K. (2020). Enhancement of trans-cleavage activity of Cas12a with engineered crRNA enables amplified nucleic acid detection. *Nat. Commun.* 11:4906.

Nguyen, P. Q., Soenksen, L. R., Donghia, N. M., Angenent-Mari, N. M., de Puig, H., Huang, A., et al. (2021). Wearable materials with embedded synthetic biology sensors for biomolecule detection. *Nat. Biotechnol.* 39, 1366–1374. doi: 10.1038/s41587-021-00950-3

Nishimasu, H., Yamano, T., Gao, L., Zhang, F., Ishitani, R., and Nureki, O. (2017). Structural basis for the altered PAM recognition by engineered CRISPR-Cpf1. *Mol. Cell* 67, 139.e2–147.e2. doi: 10.1016/j.molcel.2017.04.019

Peeling, R. W., Heymann, D. L., Teo, Y.-Y., and Garcia, P. J. (2022). Diagnostics for COVID-19: Moving from pandemic response to control. *Lancet* 399, 757–768.

Piepenburg, O., Williams, C. H., Stemple, D. L., and Armes, N. A. (2006). DNA detection using recombination proteins. *PLoS Biol.* 4:e204. doi: 10.1371/journal.pbio.0040204

Routsias, J. G., Kyriakidis, N., Latreille, M., and Tzioufas, A. G. (2010). RNA recognition motif (RRM) of La/SSB: The bridge for interparticle spreading of autoimmune response to U1-RNP. *Mol. Med.* 16, 19–26. doi: 10.2119/molmed.2009.00106

Schneider, L., Blakely, H., and Tripathi, A. (2019). Mathematical model to reduce loop mediated isothermal amplification (LAMP) false-positive diagnosis. *Electrophoresis* 40, 2706–2717. doi: 10.1002/elps.201900167

Scovino, A. M., Dahab, E. C., Vieira, G. F., Freire-de-Lima, L., Freire-de-Lima, C. G., and Morrot, A. (2022). SARS-CoV-2's variants of concern: A brief characterization. *Front. Immunol.* 13:834098. doi: 10.3389/fimmu.2022.834098

Shi, K., Xie, S., Tian, R., Wang, S., Lu, Q., Gao, D., et al. (2021). A CRISPR-Cas autocatalysis-driven feedback amplification network for supersensitive DNA diagnostics. *Sci. Adv.* 7:eabc7802. doi: 10.1126/sciadv.abc7802

Teng, F., Cui, T., Feng, G., Guo, L., Xu, K., Gao, Q., et al. (2018). Repurposing CRISPR-Cas12b for mammalian genome engineering. *Cell Discov.* 4:63. doi: 10.1038/s41421-018-0069-3

Teng, F., Guo, L., Cui, T., Wang, X. G., Xu, K., Gao, Q., et al. (2019). CDetection: CRISPR-Cas12b-based DNA detection with sub-attomolar sensitivity and single-base specificity. *Genome Biol.* 20:132. doi: 10.1186/s13059-019-1742-z

Wang, T., Wang, Y., Chen, P., Yin, B. C., and Ye, B. C. (2022). An ultrasensitive, one-pot RNA detection method based on rationally engineered Cas9 nickase-assisted isothermal amplification reaction. *Anal. Chem.* 94, 12461–12471. doi: 10.1021/acs.analchem.2c02617

Xiao, R., Li, Z., Wang, S., Han, R., and Chang, L. (2021). Structural basis for substrate recognition and cleavage by the dimerization-dependent CRISPR-Cas12f nuclease. *Nucleic Acids Res.* 49, 4120–4128. doi: 10.1093/nar/gkab179

Xue, Y., Luo, X., Xu, W., Wang, K., Wu, M., Chen, L., et al. (2022). PddCas: A polydisperse droplet digital CRISPR/Cas-based assay for the rapid and ultrasensitive amplification-free detection of viral DNA/RNA. *Anal. Chem.* 95, 966–975. doi: 10.1021/acs.analchem.2c03590

Yamano, T., Nishimasu, H., Zetsche, B., Hirano, H., Slaymaker, I. M., Li, Y., et al. (2016). Crystal structure of Cpf1 in complex with guide RNA and target DNA. *Cell* 165, 949–962. doi: 10.1016/j.cell.2016.04.003

Yan, L., Zhou, J., Zheng, Y., Gamson, A. S., Roembke, B. T., Nakayama, S., et al. (2014). Isothermal amplified detection of DNA and RNA. *Mol. Biosyst.* 10, 970–1003.

Yang, J., Song, Y., Deng, X., Vanegas, J. A., You, Z., Zhang, Y., et al. (2022). Engineered LwaCas13a with enhanced collateral activity for nucleic acid detection. *Nat. Chem. Biol.* 19, 45–54. doi: 10.1038/s41589-022-01135-y

Yoo, H. M., Kim, I. H., and Kim, S. (2021). Nucleic acid testing of SARS-CoV-2. *Int. J. Mol. Sci.* 22, 6150. doi: 10.3390/ijms22116150

Zhang, F. (2019). Development of CRISPR-Cas systems for genome editing and beyond. *Q. Rev. Biophys.* 52:e6. doi: 10.1017/S0033583519000052

Zhao, Y., Chen, F., Li, Q., Wang, L., and Fan, C. (2015). Isothermal amplification of nucleic acids. *Chem. Rev.* 115, 12491–12545. doi: 10.1021/acs.chemrev.5b00428

frontiers | Frontiers in Microbiology

TYPE Original Research
PUBLISHED 06 April 2023
DOI 10.3389/fmicb.2023.1161194

OPEN ACCESS

EDITED BY
Arabella Touati,
Centre Hospitalier Universitaire de Bordeaux, France

REVIEWED BY
Joseph Oliver Falkinham,
Virginia Tech,
United States
Luisa Jordao,
Instituto Nacional de Saúde Doutor Ricardo Jorge (INSA),
Portugal

*CORRESPONDENCE
Min-Kyoung Shin
✉ mkshin@gnu.ac.kr
Jung-Wan Yoo
✉ chareok-sa@daum.net

SPECIALTY SECTION
This article was submitted to Infectious Agents and Disease, a section of the journal Frontiers in Microbiology

RECEIVED 08 February 2023
ACCEPTED 17 March 2023
PUBLISHED 06 April 2023

CITATION
Shin J-I, Ha J-H, Kim K-M, Choi J-G, Park S-R, Park H-E, Park J-S, Byun J-H, Jung M, Baik S-C, Lee W-K, Kang H-L, Yoo J-W and Shin M-K (2023) A novel repeat sequence-based PCR (rep-PCR) using specific repeat sequences of *Mycobacterium intracellulare* as a DNA fingerprinting.
Front. Microbiol. 14:1161194.
doi: 10.3389/fmicb.2023.1161194

A novel repeat sequence-based PCR (rep-PCR) using specific repeat sequences of *Mycobacterium intracellulare* as a DNA fingerprinting

Jeong-Ih Shin[1,2], Jong-Hun Ha[1], Kyu-Min Kim[1,2], Jeong-Gyu Choi[1,2], Seo-Rin Park[1], Hyun-Eui Park[1], Jin-Sik Park[1], Jung-Hyun Byun[2,3], Myunghwan Jung[1,2], Seung-Chul Baik[1], Woo-Kon Lee[1,2], Hyung-Lyun Kang[1], Jung-Wan Yoo[4]* and Min-Kyoung Shin[1,2]*

[1]Department of Microbiology and Convergence Medical Sciences, Institute of Health Sciences, College of Medicine, Gyeongsang National University, Jinju, Republic of Korea, [2]Fastidious Specialized Pathogen Resources Bank, A Member of the National Culture Collection for Pathogens, Gyeongsang National University Hospital, Jinju, Republic of Korea, [3]Department of Laboratory Medicine, Gyeongsang National University Hospital, Jinju, Republic of Korea, [4]Department of Internal Medicine, Gyeongsang National University Hospital, Jinju, Republic of Korea

Repetitive sequence-based PCR (rep-PCR) is a potential epidemiological technique that can provide high-throughput genotype fingerprints of heterogeneous *Mycobacterium* strains rapidly. Previously published rep-PCR primers, which are based on nucleotide sequences of Gram-negative bacteria may have low specificity for mycobacteria. Moreover, it was difficult to ensure the continuity of the study after the commercial rep-PCR kit was discontinued. Here, we designed a novel rep-PCR for *Mycobacterium intracellulare*, a major cause of nontuberculous mycobacterial pulmonary disease with frequent recurrence. We screened the 7,645 repeat sequences for 200 fragments from the genome of *M. intracellulare* ATCC 13950 *in silico*, finally generating five primers with more than 90% identity for a total of 226 loci in the genome. The five primers could make different band patterns depending on the genome of three different *M. intracellulare* strains using an *in silico* test. The novel rep-PCR with the five primers was conducted using 34 bacterial samples of 7 species containing 25*M. intracellulare* clinical isolates, compared with previous published rep-PCRs. This shows distinguished patterns depending on species and blotting assay for 6 species implied the sequence specificity of the five primers. The Designed rep-PCR had a 95–98% of similarity value in the reproducibility test and showed 7 groups of fingerprints in *M. intracellulare* strains. Designed rep-PCR had a correlation value of 0.814 with VNTR, reference epidemiological method. This study provides a promising genotype fingerprinting method for tracing the recurrence of heterogeneous *M. intracellulare*.

KEYWORDS

***Mycobacterium intracellulre*, nontuberculous mycobacteria, repetitive sequences based-PCR (rep-PCR), mycobacterial pulmonary disease, epidemiology, diagnostics, mycobacterium strain typing, genotype fingerprinting**

1. Introduction

Mycobacterium avium complex (MAC) is a group of nontuberculous mycobacteria (NTM) responsible for MAC-pulmonary disease (MAC-PD), which has an increasing prevalence worldwide, especially in North America and East Asia (Prevots and Marras, 2015; Koh et al., 2017; Daley and Winthrop, 2020). MAC includes *M. avium, Mycobacterium intracellulare, M. arosiense, M. bouchedurhonense, M. chimaera, M. colombiense, M. marseillense, M. timonense, M. vulneris, and M. yongonense* (Parker et al., 2020; Keen et al., 2021). Among them, *M. intracellulare* has been reported to be responsible for the largest proportion of MAC-PD cases (Prevots and Marras, 2015; Chang et al., 2020; Ratnatunga et al., 2020). *Mycobacterium intracellulare* can be found in any environment, including soil, water, and air, and molecular epidemiology has revealed considerable genetic variation in its strains (Hruska and Kaevska, 2012; Parker et al., 2020; Lari and Rindi, 2022). MAC reinfection and redevelopment of MAC-PD can result from exposure to these environmental sources or regrowth of previously infected strains. The rate of the redevelopment of MAC-PD has been reported as approximately 10–48% and reinfection should be considered before deciding whether to proceed with the treatment (Kwon et al., 2019; Furuuchi et al., 2020; Kim et al., 2021).

MAC has been epidemiologically analyzed using whole genome sequencing (WGS), pulsed-field gel electrophoresis (PFGE), variable number tandem repeats (VNTR), repetitive sequence-based PCR (rep-PCR), and other molecular techniques. WGS offers comprehensive data including information of single nucleotide polymorphism (SNP) that can be used to identify allelic variation and distinguish strains. This WGS and interpretation of sequencing data requires a specialized technique for data analysis (Hatherell et al., 2016; Anyansi et al., 2020; Furuuchi et al., 2022). PFGE uses a whole-genome restriction enzyme site analysis approach that is labor-intensive and time-consuming. VNTR provides differentiated profiles of strains based on the number of copies of tandem repeats present at a specific locus in the genome, which requires at least 16 PCR reactions per *M. intracellulare* strain (Jagielski et al., 2016; Shin et al., 2020a,b). Rep-PCR is a fingerprinting method for comparing the electrophoretic patterns of PCR products of scattered repetitive sequences throughout the genome. It can reflect the site variation of the repetitive sequences in the bacterial genome, and there is economical merit that it can be conducted with a single PCR per strain (Warren et al., 2011; Rampadarath et al., 2015; Jagielski et al., 2016; Shin et al., 2020a,b). The repetitive sequences for rep-PCR are typical 'BOX' derived from *Streptococcus pneumoniae*, 'Enterobacterial intergenic consensus (ERIC)', and 'Repetitive extragenic palindromes (REP)' derived from *Escherichia coli* and *Salmonella typhimurium*. Since of their palindromic nature and capacity to form stable stem-loop structures in transcribed RNA, REP elements were first proposed as potential regulatory sequences within untranslated regions of operons. In addition, there is a similar PCR technique that detects a trinucleotide repeat sequence (TRS) that is repeated within the genome. At first, rep-PCR was used for species identification of Gram-negative intestinal bacteria and intraspecies distinction of *S. pneumoniae* (Versalovic et al., 1991; Koeuth et al., 1995; Healy et al., 2005). Rep-PCR also has been used for the classification of *M. avium*, *E. coli*, and *S. pneumoniae*, and TRS-PCR has been used to analyze MAC (Versalovic et al., 1995; Otsuka et al., 2004; Wojtasik et al., 2012). In 2003, a rep-PCR-based commercial kit was released for mycobacteria strain typing. The strain distinction in *M. avium* carried out using the kit was highly consistent with RFLP; however, the profiles of *M. intracellulare* could not be evaluated (Cangelosi et al., 2004).

To develop a new strategy for molecular fingerprinting method of *M. intracellulare*, this study seeks to explore repetitive sequences within the genome of *M. intracellulare* and develop *M. intracellulare*-based rep-PCR. We focused on the concepts from a previous study on *M. bovis*, in which repetitive sequences were searched through hybridization between genomic DNA libraries and chromosome digests, and subsequent sequencing of the identified DNA (Doran et al., 1993). As the complete genomic sequence of *M. intracellulare* ATCC 13950 is available at NCBI (Iakhiaeva et al., 2013), the The DNA library method can be modified *in silico* in this study. To evaluate this developed method, this study uses bacterial samples including *M. intracellulare* strains that had already been analyzed in their molecular epidemiologic profiles (PFGE and VNTR) in reference study (18). This evaluation can discover a correlation between novel rep-PCR and another molecular epidemiological method.

In conclusion, we hope to confirm whether the novel rep-PCR can be a potential molecular tool for disease epidemiology of *M. intracellulare* using repetitive sequences originating from the whole genome of *M. intracellulare* ATCC 13950.

2. Materials and methods

2.1. Bacterial samples

Mycobacterium intracellulare clinical isolates used in this study (n = 25) were originated from patients ($n = 23$) with pulmonary disease. Among the collection, there are isolates (n = 2) originated from a patient A on the same day (*M. intracellulare* KBN12P06800 and *M. intracellulare* KBN12P06801) and isolate ($n = 2$) from a patient B one week apart (*M. intracellulare* KBN12P06798 and *M. intracellulare* KBN12P06799). Patient labels were arbitrarily marked with letters A and B. *M. intracellulare* clinical isolates were collected between 2016 and 2017 at Gyeongsang National University Hospital (GNUH), Jinju, Korea and provided from the Fastidious Specialized Pathogen Resources Bank (a member of the National Culture Collection for Pathogens, GNUH), Jinju, Korea. For experimental control, two *M. intracellulare* reference strains (Asan 37128^T and ATCC 13950^T), two *M. avium* reference strains (MAH 101^T and MAH 104^T), *M. abscessus* KCTC 19621, *M. fortuitum* KBN12P06244, *E. coli* O157 NCCP 14541, *S. aureus* NCCP 14780, and *K. pneumoniae* NCCP 14764 were used in this study. Two *M. intracellulare* reference strains and *M. abscessus* KCTC 19621 were provided from the Korean Collection for Type Cultures (KCTC, Jeongeup, Korea). *M. fortuitum* KBN12P06244, *E. coli* O157 NCCP 14541, *S. aureus* NCCP 14780, and *K. pneumoniae* NCCP 14764 were provided from Fastidious Specialized Pathogen Resources Bank, Jinju, Korea. ^{T}: Type strain.

2.2. *In silico* analysis for the development of rep-PCR using specific repeat sequences of *Mycobacterium intracellulare*

2.2.1. Investigation of repetitive sequences and design of primers for rep-PCR

This study mimicked the method of DNA library in the reference study using 200 *E. coli* recombinants and containing approximately

3–8 kb insert DNA sequences (28, Supplementary Table S1). Experimental design has an assumption that among short fragmented genomic DNA, there are repetitive sequences of the whole genome. Two hundred recombinants of reference study (28) were modified into 200 FASTA files and 3-8 kb insert DNA sequences were modified into 5 kb-scaled fragments. A total of 200 FASTA files were generated by dividing 20% of the genome (region from 1 to 965,101) of *M. intracellulare* ATCC 13950[1] by non-overlapping 5 kb. Subsequently, the Repeats sequences finder[2] was used to search for repetitive sequences greater than 10 bp within each 5 kb-scale FASTA file (Supplementary Table S2). Using rationale of sequence-length (Figure 1C and Supplementary Table S3), candidate sequences were chosen and BLAST[3] was used to confirm whether these candidates aligned with the *M. intracellulare* ATCC 13950 genome. The alignment result was evaluated using BLAST bit score. If 16 bp matches between candidate sequences and genome without a gap, the score on BLAST was 32.2 bits. Therefore, each candidate sequence was evaluated using a frequency with a bit score of 32.2 or higher (Supplementary Table S3). Using ClustalX (version 1.8) and EditSeq (version 7.0.0), we found conserved sequences among the region with bit score ≥ 32.2 and designed a primer based on it. %Identity and matching frequency of primer candidates in the *M. intracellulare* ATCC 13950 genome were confirmed. Through this process, new primers for designed rep-PCR were generated.

2.2.2. Demonstration the designed rep-PCR using *In silico* PCR

In silico PCR amplification[4] was used to predict the PCR products amplified from genomic DNA (San Millán et al., 2013) in 45 strains, including three *M. intracellulare* strains (ATCC 13950, MOTT-02, and MOTT-64), as well as strains of *M. africanum*, *M. avium*, *M. avium* subsp. *paratuberculosis*, *M. bovis*, *M. canetti*, *M. indicus*, *M. tuberculosis*, and *M. yongonense*. The criteria were set to allow 2 mismatches between primers and template and a maximum amplicon length of 10,000 nucleotides. To investigate whether there were variations in band patterns among the three *M. intracellulare* strains, we compared the band lengths of the expected *in silico* PCR products for the five designed primers (Table 1).

2.3. Conduction of novel rep-PCR for *Mycobacterium intracellulare*

2.3.1. Experimental condition of the designed rep-PCR

Including the *M. intracellulare* clinical isolates, all bacterial samples mentioned above were used. Genomic DNA was extracted using an AccuPrep Genomic DNA Extraction Kit (Bioneer, Korea). The DNA template (120 ng per tube) and five designed primers (10 pmol/primer) per tube were simultaneously added, and the designed rep-PCR reaction was conducted as follows: initial denaturation at 95°C for 5 min; 35 cycles of 95°C for 30 s, 65°C for 1 min, and 72°C for 2 min; and a final extension at 72°C for 7 min.

2.3.2. Experimental conditions of the previous published rep-PCRs

The genomic DNA extracted above was used as a DNA template (120 ng per tube). List of primer are BOX A1R, ERIC 1R, ERIC 2, REP 1RI, REP 2I, and $(CCG)_4$ (n = 6). Set of primers were used in the PCR experiments, single primer (BOX A1R or CCG_4), in pairs (ERIC 1R + ERIC 2), or in combination (BOX A1R + ERIC 1R + ERIC 2, BOX A1R + REP 1RI + REP2I, and BOX A1R + ERIC 1R + ERIC 2 + REP 1RI + REP 2I) (Table 1). Previous published rep-PCR reaction was conducted as follows: initial denaturation at 95°C for 5 min; 30 cycles of 95°C for 30 s, 40°C for 1 min, and 72°C for 2 min; and a final extension at 72°C for 7 min (Chen et al., 2021; Jena et al., 2021; La China et al., 2021; Teixeira et al., 2021).

2.4. Validation of designed rep-PCR for *Mycobacterium intracellulare*

2.4.1. Reproducibility test

Reproducibility of the designed rep-PCR was confirmed using cultured strains of different periods of *M. intracellulare*. Four *M. intracellulare* strains (KBN12P07945, KBN12P06800, KBN12P6801, KBN12P07346) were selected randomly for the reproducibility test. DNA templates of four strains were extracted before and after subculturing, respectively. Using the extracted DNA template, the designed-PCR and the previously published rep-PCRs were performed under the conditions described in 2.3.1 and 2.3.2, respectively. We yielded %similarity (reproducibility) by comparing the band patterns before and after the subculture in each strain. The band patterns were analyzed under the conditions of Pearson coefficient, UPGMA clustering, and a tolerance value of 1.0, using the GelJ software (version 2.0), and a dendrogram was generated according to the values of the similarity calculated using the GelJ software (Arais et al., 2018; Heidari et al., 2018). In addition, the reproducibility of the designed-repPCR was confirmed using various species including *M. intracellulare*. Confirmation for % similarity between various species (Supplementary Figure S1), DNA templates were extracted before and after the subculture in each strain (Four *M. intracellulare* stains, two *M. avium* strains, one *M. fortuitum* strain, one *M. abscessus* strain, one *E. coli* strain, one *S. aureus* strain, and one *K. pneumoniae* strain). PCR such as the designed-PCR and the previously published rep-PCRs was performed under the conditions of the 2.3.1 and 2.3.2, respectively. The %similarity (reproducibility) of the band patterns were yielded under the conditions of Dice, UPGMA clustering, and a tolerance value of 1.0, using the GelJ software.

2.4.2. Confirmation of nucleotide sequence specificity of designed primers using southern blot

The electrophoretic bands of the six species (*M. intracellulare* KBN12P06800, *E. coli*, *K. pneumoniae*, *M. abscessus*, *M. fortuitum*, and *M. avium* MAH 104) using the novel rep-PCR were transferred from agarose gel to the GeneScreen Plus membrane (NEN,

1 https://www.ncbi.nlm.nih.gov/nuccore/NC_016946.1
2 https://www.novoprolabs.com/tools/repeats-sequences-finder
3 https://blast.ncbi.nlm.nih.gov/Blast.cgi
4 http://insilico.ehu.es/PCR/index.php?mo=Mycobacterium

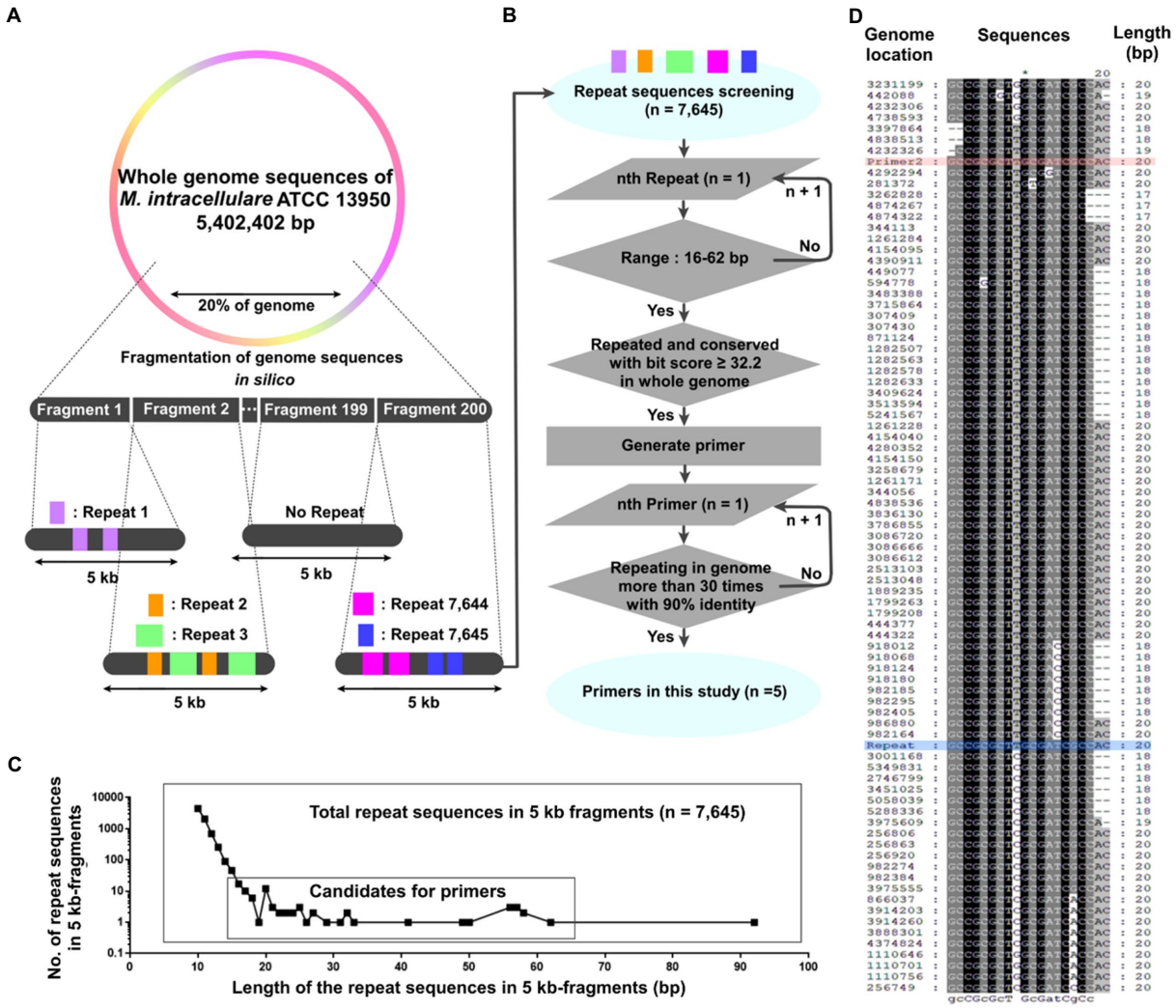

FIGURE 1
Generation of repetitive sequence-based primers across the whole genome using short 5kb fragments. **(A, B)** A schematic diagram for generating repetitive primers within a genome. **(A)** 20% of the *Mycobacterium intracellulare* ATCC 13950 genome was cut into 200 fragments (5kb-scaled). The repetitive sequences in each 5kb fragment were screened, yielding 7,645 repetitive sequences. **(B)** The 7,645 repetitive sequences were screened based on their length and the number of repeats in the genome. Primers were generated using the screened sequences, and the number of repeats and identities in the genome of the primer was evaluated. **(C)** The number of the repetitive sequences according to their length and repeats within the 5kb fragments and the range for primer candidates. Up to 19bp, the number of repetitive sequences decreased in proportion to log10, but from 20bp onwards, the number increased or stayed the same regardless of this trend. We set the range of primer screening at 16 to 62bp. **(D)** Alignment (5′ to 3′) of Primer 2 with the *M. intracellulare* ATCC 13950 genome. Genome location: the genome position annealing by primers in NCBI database. Red: Primer 2, Blue: Repeat (it means repeated sequences within each 5kb fragment).

NEF988). For instructions on transfer, we referred to the ECL Direct Labeling and Detection System (GE, RPN3000). Primers 1–5 were designed with biotin at the 5′ terminal (synthesized by Bioneer Inc., Korea) and hybridized with the membrane using hybridization and blocking buffers (GE, RPN 3000). Hybridization, washing, and detection were performed according to the instructions provided by the North2SouthChemilinescent Hybridization and Detection Kit (Thermos, 17,097). Hybridization and washing were performed at 50°C and 40°C, respectively, and streptavidin-HRP (Sigma, N100) was used for biotin detection of the probe. The absolute value of the Southern blot signal was measured in an image of the X-ray film using ImageJ (1.53e) (Gautam, 2022; Wang et al., 2022).

2.4.3. Verification of correlation with reference method

The electrophoresis results were normalized according to the reference molecular weight lanes using GelJ software (version 2.0), and the normalized rep-PCR bands were grouped based on their Pearson %similarity. For the confirmation of the correlation between designed rep-PCR and other defined epidemiological methods, we referred to data from a previous study (Shin et al., 2020a,b) that conducted PFGE and VNTR on the almost same *M. intracellulare* clinical isolates as in this study. To calculate the correlation coefficient, Cramer's V coefficient were calculated using IBM SPSS software (version 21) (Akoglu, 2018).

TABLE 1 The list of the primers used in this study.

No.	Primer	Primer sequences (5′ -3′)	Sequences origin	Reference
1	Primer 1	GATGGTGGCGACCCGCTGCG (20 bp)	*M. intracellulare* ATCC 13950	*this study*
2	Primer 2	GCCGCGCTTGCGATCGCCAC (20 bp)		*this study*
3	Primer 3	CGACGATGCAGAGCGAAGCGATG (23 bp)		*this study*
4	Primer 4	CGCCGCGCTCGCGATCGCCACT (22 bp)		*this study*
5	Primer 5	GGCGACCCGCTTCGCCCGGCTCCG (24 bp)		*this study*
6	BOX A1R	CTACGGCAAGGCGACGCTGACG (22 mer)	*Streptococcus pneumoniae*	(Rampadarath et al., 2015)
7	ERIC 1R	ATGTAAGCTCCTGGGGATTCAC (22 mer)	*E. coli* and *Salmonella typhimurium*	(Warren et al., 2011)
8	ERIC 2	AAGTAAGTGACTGGGGTGAGCG (22 mer)		(Warren et al., 2011)
9	REP 1RI	IIIICGICGICATCIGGC (11 mer)		(Warren et al., 2011)
10	REP 2I	ICGICTTATCIGGCCTAC (15 mer)		(Warren et al., 2011)
11	$(CCG)_4$	NNNNNNCCGCCGCCGCCG (18 mer)	*M. avium*	(Healy et al., 2005)

3. Results

3.1. Repetitive sequences within the genome can be identified using 5kb-scaled genomic fragments

A total of 7,645 repetitive sequences were yielded within each 5 kb-fragment, which originated from the 20% genome of *M. intracellulare* ATCC 13950 (Figure 1A and Supplementary Table S2). Among them, there are 402 duplication sequences and 7,243 unique sequences. As the length of the repetitive sequences increased from 10 bp to 19 bp, the number of repetitive sequences decreased in proportion to log10. And the number of 21 bp to 92 bp repetitive sequences remained below four (Figure 1C). We selected 51 sequences ranging from 16 bp to 62 bp, which are considered to be highly conserved in the genome relative to their length (Supplementary Table S3). 51 sequences have 2 to 95 regions with a score $\geq$ 32.2 per candidate sequence and we generated primers using these regions (Figures 1B,D). As a result, a total of 5 primers were determined for the sequences repeated throughout the genome (Table 1). Primer 1 originates from 57 bp of the sequence encoding a hypothetical protein in *M. intracellulare* ATCC 13950. The sequence of Primer 2 is shared by *M. tuberculosis*, *M. kansasii*, *M. ostraviense*, *M. avium*, *M. malmoense*, *M. ulcerans*, and *M. shottsii*, and is identical to a 20 bp sequence found in the genes that encode a hypothetical protein, ABC transporter efflux protein, DrrB family protein, and lipoprotein LpqB in *M. intracellulare* ATCC 13950. Primer 3 is derived from a 50 bp sequence in the gene encoding the PbpA protein in *M. intracellulare* ATCC 13950, and primers 4 and 5 are derived from a 62 bp sequence in the gene encoding the rfbE protein in *M. intracellulare* ATCC 13950 (Supplementary Table S4). Each primer was aligned with 90% identity in both forward and reverse orientations, at more than 31 to 63 loci in the *M. intracellulare* ATCC 13950 genome. The locations of aligned loci in the genome were investigated (Supplementary Table S5). This means that PCR polymerization is possible due to forward and reverse pairs of primers located in 31 to 63 loci per sequence in the *M. intracellulare* ATCC 13950 genome.

3.2. *In silico* PCR with designed primers demonstrate genomic variation within The *Mycobacterium intracellulare* strains

For the three *M. intracellulare* strains (ATCC 13950, MOTT-02, and MOTT-64), The amplicons of similar sizes were integrated into single band (Table 2). In the *M. intracellulare* ATCC 13950, a total of five PCR bands of approximately 4.2, 4.7, 5.5, 6.7, and 8.7 kb-lengths were yielded from eight genome positions. Likewise, a total of five PCR bands of approximately 4.2, 5.5, 6.2, 6.7, and 8.5 kb-lengths were yielded in MOTT-02, and four bands of approximately 4.7, 5.5, 6.7, and 8.5 kb-lengths were yielded in MOTT-64. Therefore, the band patterns of the *in silico* PCR amplicons for the designed five primers between the three *M. intracellulare* strains were different from each other, indicating that the designed primers can distinguish the *M. intracellulare* strains from each other. In the same way as above, the lengths of virtual PCR amplicons were predicted in various mycobacteria species registered in NCBI (Supplementary Table S6). As a result, the *in silico* PCR amplicons showed different patterns between various mycobacterial species (*M. avium*, *M. bovis*, *M. canettii*, *M. tuberculosis*, *M. yongonense*, etc.) implying the sequence specificity of primers.

3.3. The novel rep-PCR produce reproducible band patterns

First, the purpose of this test was to present the reproducibility value (% value, similarity using Pearson coefficient) of this new rep-PCR method and to use it as a criterion for the genetic clone of *M. intracellulare* strains (Yamamura et al., 2004; Healy et al., 2005; Güvenir et al., 2018; Hwang et al., 2021). In the designed rep-PCR, the *M. intracellulare* samples (4 pairs) showed reproducibility with approximately 95–98% similarity (Figure 2). Therefore, in this study, strains that shares 95 to 98% similarity are defined as a genetic clone.

Second, it was conducted to compare the results of similarity between the newly developed rep-PCR and the results of the previous published rep-PCR (Cangelosi et al., 2004). In previous published rep-PCRs (BOX-, $(CCG)_4$–, ERIC-, ERIC+BOX-, REP+BOX-, and REP+ERIC+BOX-PCR), the *M. intracellulare* samples (4 pairs) showed

TABLE 2 Different *in silico* PCR bands between the *M. intracellulare* strains using designed primers.

M. intracellulare ATCC 13950			*M. intracellulare* MOTT-02			*M. intracellulare* MOTT-64		
Primer pair	Length of *in silico* amplicon[a]	*in silico* PCR band[b]	Primer pair	Length of *in silico* amplicon	*in silico* PCR band	Primer pair	Length of *in silico* amplicon	*in silico* PCR band
Primer 1 and 4	4180	Approx.[c] 4.2kbp	Primer 1 and 2	4179	Approx. 4.2kbp	Primer 1 and 2	4663	Approx. 4.7kbp
Primer 1 and 2	4179		Primer 1 and 4	4180		Primer 2 and 3	4663	
Primer 1 and 2	4746	Approx. 4.7kbp	Primer 1 and 3	5490	Approx. 5.5kbp	Primer 2 and 5	4663	
Primer 2 and 3	4717		Primer 2 and 3	5490		Primer 2 and 4	4664	
Primer 2 and 4	4717		Primer 3 and 4	5490		Primer 1 and 3	5490	Approx. 5.5kbp
Primer 2 and 5	4717		Primer 3 and 5	5490		Primer 2 and 3	5490	
Primer 1 and 3	5490	Approx. 5.5kbp	Primer 2 and 3	6212	Approx. 6.2kbp	Primer 3 and 4	5490	
Primer 2 and 3	5490		Primer 2 and 4	6212		Primer 3 and 5	5490	
Primer 3 and 4	5490		Primer 2 and 5	6212		Primer 1 and 3	6730	Approx. 6.7kbp
Primer 3 and 5	5490		Primer 1 and 2	6241		Primer 2 and 3	6730	
Primer 1 and 3	6730	Approx. 6.7kbp	Primer 1 and 3	6730	Approx. 6.7kbp	Primer 3 and 4	6730	
Primer 2 and 3	6730		Primer 2 and 3	6730		Primer 3 and 5	6730	
Primer 3 and 4	6730		Primer 3 and 4	6730		Primer 2 and 3	8508	Approx. 8.5kbp
Primer 3 and 5	6730		Primer 3 and 5	6730		Primer 1 and 3	8538	
Primer 2 and 3	8677	Approx. 8.7kbp	Primer 1 and 3	8538	Approx. 8.5kbp	-	-	-
Primer 1 and 3	8651		Primer 2 and 3	8564		-	-	-

[a]Length of in silico amplicon: distance of sequences between pair of primer.
[b]in silico PCR band: Expected result of virtual PCR bands on agarose gel.
[c]Approx.: approximately.

reproducibility with approximately 92–96%, 91–95%, 82–95%, 92–97%, 93–96%, 86–95%, respectively. This value showed slightly lower level than Designed rep-PCR. Furthermore, the background noise of previous published rep-PCRs increases as the number of primers increases. However, the designed rep-PCR using the five primers simultaneously showed a clear background and patterns (Figure 2).

The reproducibility test results including other species (*M. abscessus*, *M. fortuitum*, *M. avium*, *S. aureus, K. penumoniae* and *E. coli*) are shown in Supplementary Figure S1. In the designed rep-PCR, 27 *M. intracellulare* strains showed bands of various patterns with a similarity of 56–90%. The band patterns between *M. intracellulare* and the other six species could be distinguished by two clusters with 50% similarity. In previous published rep-PCR, however, *M. intracellulare* and other species were difficult to distinguish. This is because the similarity between *M. intracellulare* and the other species was same or high with similarity between *M. intracellulare* strains. This test shows the reproducibility and band patterns of designed rep-PCR for bacteria that can be contaminated with *M. intracellulare*. In addition, showing different patterns between species may suggest the sequence specificity of the designed primers.

3.4. The novel rep-PCR primers can produce different bands with sequence specificity

To show the sequence specificity of the primers, Southern blot was conducted using six species (*M. intracellulare*, *E. coli*, *K. pneumoniae*, *M. abscessus*, *M. fortuitum*, and *M. avium*; denoted as MI, EC, KP, MA, MF, and MAV, respectively). MI showed 2–3 signal bands for each primer (Figure 3A). EC showed 2 signal bands for each primer, except Primer 2. KP showed 3–4 signal bands for each primer, MA showed 4–5 signal bands for each primer, MF showed 3–6 signal bands for each primer, and MAV showed 3–5 signal bands for each primer. Each strain showed a strong or weak hybridization level for the five primers as follows, using the ImageJ software: Primers 1, 4, and 5 in case of MI; Primers 1, 4, and 5 in case of EC (Primer 2 showed no signal); Primer 5 in case of KP; Primer 2 in case of MA; Primers 2 and 3 in case of MF; and Primers 1, 2, 3, and 4 in case of MAV showed signals with an absolute value of more than 15,000 (Figure 3B). In addition, while each of the five primers had similar total signals, species with high specificity were different for each of them, and the rankings were as follows (Figure 3C): Primer 1 was hybridized in the order of MAV, EC, and MI; Primer 2 was hybridized in the order of MAV, MF, and MA; Primer 3 was hybridized in the order of MAV and MF; Primer 4 was hybridized in the order of MAV, MI, and EC; Primer 5 was hybridized in the order of KP, MI, and EC (only the species with an absolute value of the signal greater than 15,000 have been mentioned). In other words, each of the five designed primers hybridized with DNA at a similar total level, and the specificity and hybridization intensity differed depending on the species. This shows that for at least six species, each primer can make different bands with sequence specificity.

3.5. The novel rep-PCR can provide molecular fingerprints alternating existing epidemiological method

As described in 3.3, strains that shares 95 to 98% similarity are defined as a genetic clone in this study. Previously analyzed epidemiological profiles were imported from the previous study (Hatherell et al., 2016) and there were 19 PFGE profiles (Supplementary Figure S2) and 27 VNTR profiles (Figure 4 and

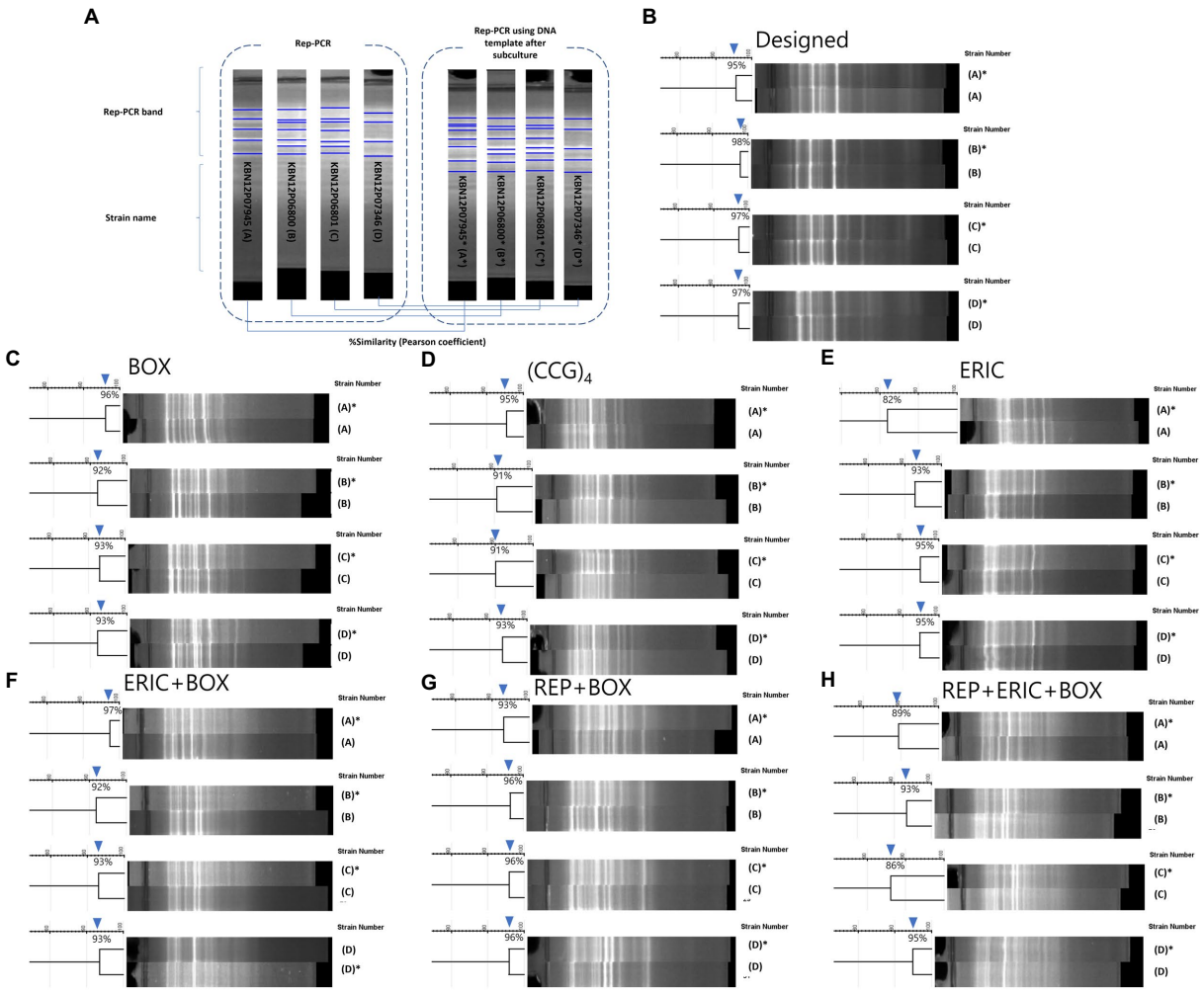

FIGURE 2
Comparison of reproducibility tests for designed and previous published rep-PCRs. **(A)** A diagram of the reproducibility test. PCR bands were compared from one *M. intracellulare* before (no asterisk) or after subculture (with an asterisk). 4*M. intracellulare* strains were used to PCR and pair of PCR bands were analyzed by the similarity of the Pearson coefficient. **(B–H)** Results of the reproducibility test for Designed, BOX, (CCG)4, ERIC, ERIC+BOX, REP+BOX, REP+ERIC+BOX rep-PCR. **(B)** The similarities of Designed rep-PCR for same clone of *M. intracellulare* (with or without subculture) were 95–98%. **(C)** The similarities of BOX-PCR for same clone of *M. intracellulare* were 92–96%. **(D)** The similarities of $(CCG)_4$-PCR for same clone of *M. intracellulare* were 91–95%. **(E)** The similarities of ERIC-PCR for same clone of *M. intracellulare* were 82–95%. **(F)** The similarities of ERIC+BOX-PCR for same clone of *M. intracellulare* were 92–97%. **(G)** The similarities of REP+BOX-PCR for same clone of *M. intracellulare* were 93–96%. **(H)** The similarities of REP+ERIC+BOX-PCR for same clone of *M. intracellulare* were 86–95%.

Supplementary Figure S2) for a correlation analysis with rep-PCR. VNTR profiles were presented by alphabet type according to the combination of copy numbers of VNTR 1 to 16 and VNTR-MIRU 3, 18, 19, 20, 22, 31, 33. Designed rep-PCR generated fingerprint groups ($n=7$) of 27 *M. intracellulare* strains, showing Cramer's V value (correlation efficient) of 0.814.

Strains from patient A ($n=2$) were included in rep-PCR group 7 (KBN12P06800 and KBN12P06801) and shared the VNTR profiles on 22/23 loci (96%) (Figure 4). Strains from patient B ($n=2$) were included in different rep-PCR groups (KBN12P06798 in group 3 and KBN12P06799 in no group) and shared VNTR profiles on 8/23 (35%). This shows the correlation between the designed rep-PCR and the VNTR method.

There is an alternative approach for determining identical clones using visual discrimination in Supplementary Figure S2. The patterns of designed rep-PCR were grouped ($n=8$) according to the visual patterns. Among the strain belonging to group 1, five strains had almost the same PFGE pattern. Some of the strains belonging to group 1 also had the same VNTR types B ($n=3$) and C (n = 5), showing Cramer's V value (correlation efficient) of 0.979 and $p=0.004$. (Their PFGE patterns were difficult to compare due to the lack of identified pattern information.) This visual discrimination can be an alternative method for researchers that omit the using gel analyzing software. For reference, the entire data of the rep-PCR band for all samples are in Supplementary Figure S3-S9.

4. Discussion

In the MAC-PD, a recurrence caused by strains having different genotypes are frequent (Koh et al., 2017; Akoglu, 2018; Heidari et al., 2018; Gautam, 2022; Wang et al., 2022), requiring a more advanced

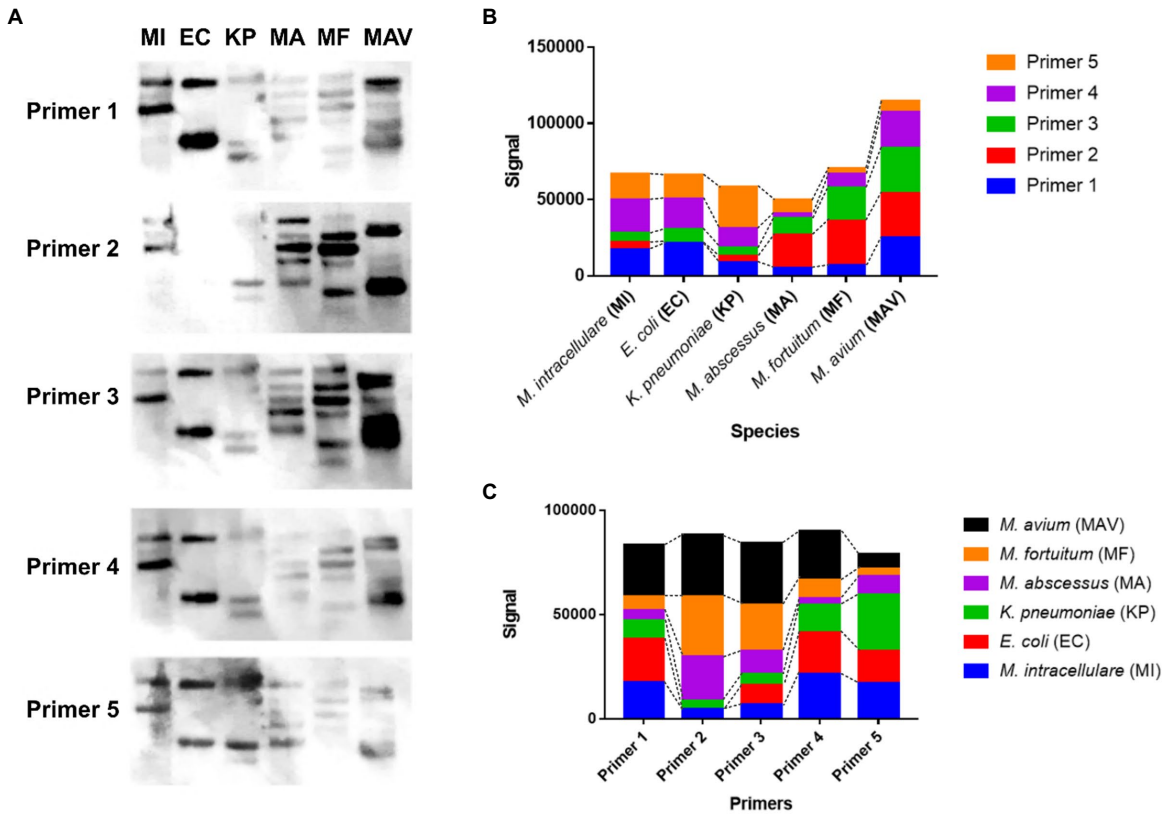

FIGURE 3
The hybridization pattern and the signal value between the designed rep-PCR product of the six species and each designed primer. **(A)** Southern blotting results of each designed primer (Primers 1 to 5) against the designed rep-PCR products of *M. intracellulare, E. coli, K. pneumoniae, M. abscessus, M. fortuitum*, and *M. avium*, denoted as MI, EC, KP, MA, MF, and MAV, respectively. **(B)** The hybridization signals of 5 primers for each species. The hybridization rate of each primer is different depending on the species. The hybridization ratio of *E. coli* is similar to that of *M. intracellulare*, but there is no hybridization with Primer 2. The total amount of signals for *M. avium* is the highest among the species with primer 2. **(C)** The hybridization signal of each species for each primer. Although the hybridization ratio is different, the total signals corresponding to one primer are similar.

approach than naïve species identification. Various studies on the efficacy of NTM treatment have employed epidemiological approaches of the intraspecies classification level using (Englund, 2003; Bussone et al., 2012; van der Zanden et al., 2012; San Millán et al., 2013; Thomson et al., 2013, 2014; Koh et al., 2017; Heidari et al., 2018; Karauz et al., 2018; van Weezep et al., 2019; Gautam, 2022; Zhao et al., 2022). Since WGS, PFGE, and VNTR require a specialized technique, labor-intensive or time-consuming approaches, several clinical studies used rep-PCR (Cangelosi et al., 2004; Jagielski et al., 2016; Jhun et al., 2018a,b; Shin et al., 2020a,b; Furuuchi et al., 2022) for diagnosis of reinfection/relapse, recurrent after latency, evaluation of antibiotics therapy in recurrent MAC-PD, and MAC bacteremia follow-up study.

In this study, we developed a novel rep-PCR intending to use it as an efficient genotype fingerprinting technique for studying the epidemiology of *M. intracellulare*. We designed five primers derived from repetitive sequences of the bacterial genome using *in silico* approach. Unlike previous published Gram-negative bacillus-derived primers, a novel rep-PCR was designed based on the mycobacterial genome. Therefore, the novel rep-PCR has sequences-based rationales for revealing fingerprinting patterns in *M. intracellulare* clinical isolates.

The designed rep-PCR showed a statistical correlation with the VNTR profiles (Cramer's V value of 0.814) (Figure 4). While the VNTR technique performed 23 PCR reactions for one test of one sample, rep-PCR performed 2 PCR reactions including reproducibility tests. Therefore, this rapid method can be an alternative to an existing epidemiologic technique that can be used to determine whether the redevelopment of MAC-PD results from relapse or re-infection of *M. intracellulare*.

In this study, the designed rep-PCR were proven to be nucleotide-specific responses. First, since the Southern blot has been used to confirm whether genetic diversity across samples can be distinguished according to the nucleotide sequence of the primer (Englund, 2003; Gautam, 2022), in this study, southern blotting was used to confirm that the nucleotide characteristics of the five primers contributed to the distinction of species, based on the hybridization intensities (Figure 3). Second, *in silico* verification can be used to monitor the usefulness of PCR diagnosis before *in vitro* experiments, and the rationale is based on the real genetic sequence (San Millán et al., 2013; van Weezep et al., 2019). Differences across strains were identified when the designed five primers were applied to three *M. intracellulare* strains using *in silico* PCR (Table 2). This reflects a shift in the position of the repetitive sequences in the genomes of the three strains, and the actual PCR also produced varied electrophoretic patterns depending on the strain. Third, since the reproducibility tests for samples before and after subculturing can reflect that the PCR is not the non-specific response (Cangelosi et al., 2004; Zhao et al., 2022), it was confirmed using samples before and after

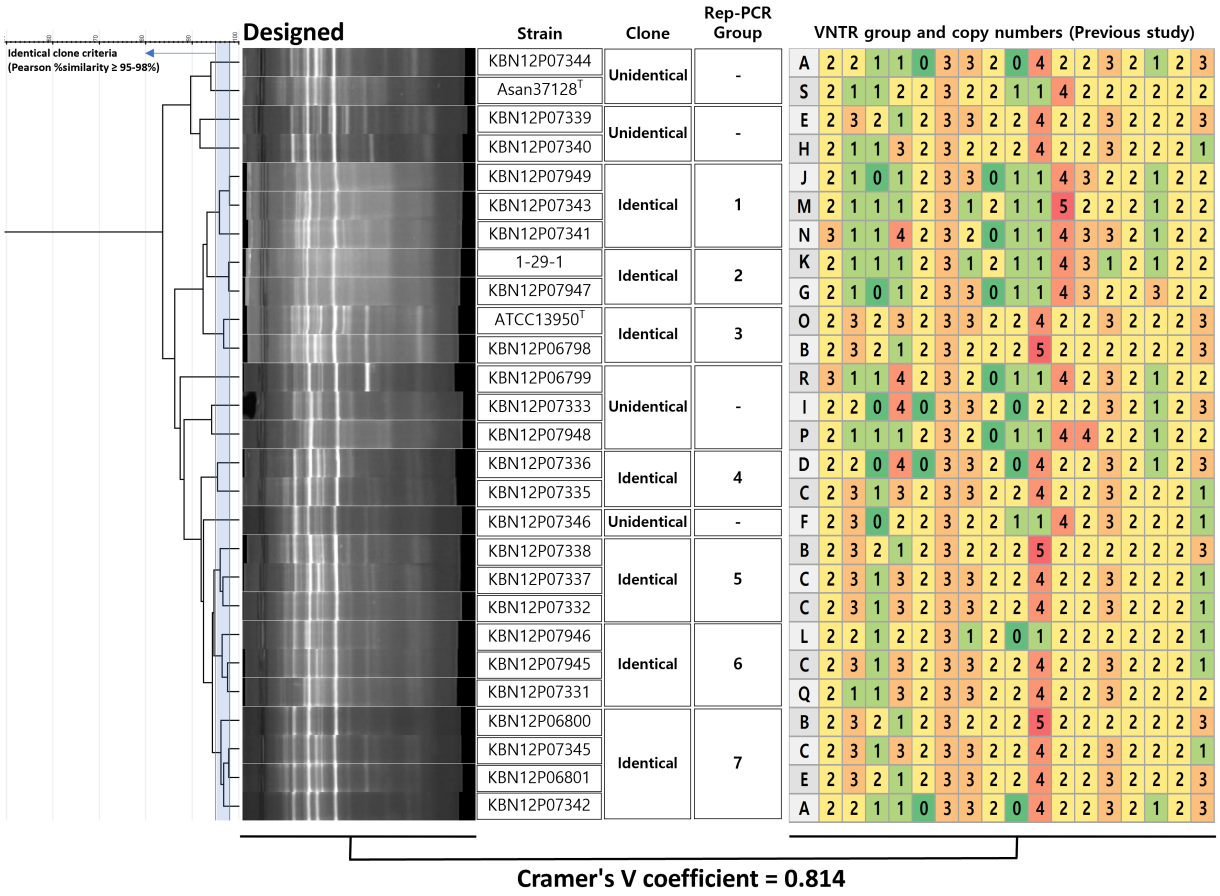

FIGURE 4
Decision of clone of *M. intracellulare* using designed rep-PCR and coefficient with VNTR method. For the decision of identical clones using designed rep-PCR, a criterion was used that Pearson similarity is 95–98%. If the similarity is higher or the same with the criterion between two or more strains, it is defined as an identical clone. The identical clone was assigned to the rep-PCR groups (n=7). The VNTR (from a previous study) type means VNTR numerical patterns (copy number of VNTR 1 to 16 and VNTR-MIRU 3, 18, 19, 20, 22, 31, 33). There was a significant correlation between the groups of designed rep-PCR and VNTR, showing Cramer's V coefficient=0.814.

subculturing that designed rep-PCR has a greater level of reproducibility (Pearson similarity 95–98%) than previous published rep-PCR (Figure 2).

In this study, designed rep-PCR showed 7 identical groups and statistical correlation with the VNTR profiles (Cramer's V value of 0.814) (Figure 4). There were two sets of serial isolated *M. intracellulare* strains; the first set (KBN12P06800 in group 7 and KBN12P06801 in group 7 from a patient A) showed same rep-PCR group and shared on 22/23 VNTR loci (96%) (Figure 4). The second set (KBN12P06798 in group 3 and KBN12P06799 in no group from patient B) showed different rep-PCR groups and shared on 8/23 VNTR loci (35%). This can emphasize correlation between designed rep-PCR and VNTR profiles. While the VNTR technique performed 23 PCR reactions for one test of one sample, rep-PCR performed only 2 PCR reactions including reproducibility tests. Therefore, this rapid method can be an alternative to an existing epidemiologic technique that can be used to determine whether the redevelopment of MAC-PD results from relapse or re-infection of *M. intracellulare*.

The discovery of *M. intracellulare*-derived highly repeated DNA sequences in this study was motivated by previously uncovered 24 bp-scaled direct repeat (DR) sequences in *M. bovis* (Doran et al., 1993). Research on *M. bovis* has indicated the possibility of searching for novel repetitive sequences and developing a new rep-PCR for *M. intracellulare* strain typing, which is expected to be more effective in classifying *M. intracellulare* than previous published rep-PCR from Gram-negative bacteria-derived sequences. The classical genomic DNA library approach of investigating the repetitive sequences in *M. bovis* was replaced by an *in silico* approach in this study and employed to identify the repetitive sequences of *M. intracellulare*. Interestingly, the sequences of the five designed primers were included in specific genes or hypothetical protein sequences within the *M. intracellulare* ATCC 13950 genome. Primer 2, which did not hybridize with the rep-PCR product from *E. coli* (Figure 3), included genomic sequences of *M. tuberculosis, M. kansasii, M. ostraviense, M. avium, M. malmoense, M. ulcerans,* and *M. shottsii.* We specified Primer 2 as a 'Mycobacteria specific sequence' in this study (Supplementary Table S4). Therefore, this study proposes an approach to explore genetically preserved repetitive sequences between specific bacterial species or highly related species, which is expected to minimize the time spent compared to the traditional DNA library methods.

Among the technologies related to rep-PCR, a commercial kit for rep-PCR-based mycobacteria strain typing was released in 2003 and has been used in many clinical epidemiological studies on the therapeutic efficiency of MAC (Bussone et al., 2012; van der Zanden et al., 2012; Thomson et al., 2013, 2014; Koh et al., 2017; Jhun et al., 2018a,b; Karauz

et al., 2018), including *M. intracellulare*. However, due to the discontinuation of the product, follow-up research is impossible. Subsequently, in 2019, a method was reported to conduct species-level identification and strain-level differentiation in real-time through a combination of nanopore sequencing and rep-PCR using Oxford Nanopore Technologies (Krych et al., 2019; Thomassen et al., 2021, 2022). Newly developed commercial DNA chips are also used to analyze the rep-PCR patterns (Bernasconi et al., 2020). These trends reveal significant interest in and necessity of clinical use of rapid epidemiological techniques for studying MAC, including *M. intracellulare*. These also suggest that the novel rep-PCR should be developed continuously for the sustainability of follow-up studies, combined with cutting-edge technologies as a rapid diagnostic tool in further study.

However, this study has some limitations. First, the *M. intracellulare* strains in this study were isolated from patients with pulmonary disease, and only 2 sets of strains derived from the same patient that could determine re-infection/reactivation were available. Based on the results of this study, a new rep-PCR was developed and validated as DNA fingerprinting for *M. intracellulare*, however, further studies are needed to diagnose relapse. Second, the NTM strains used as controls in this study were not related to pulmonary diseases, and were used to verify the specific fingerprinting for *M. intracellulare* by comparing the fingerprint patterns of each species. Third, since the method in this study distinguish the strains by reading PCR band patterns, this result may vary depending on conditions such as electrophoresis. Therefore, further study needs to be combined with advanced techniques (e.g., nanopore sequencing) (Krych et al., 2019; Thomassen et al., 2021, 2022) that can reduce differences between experimental conditions using *M. intracellulare* isolated from clinically diagnosed patients with relapse and NTM control isolated from patients with pulmonary disease.

5. Conclusion

We developed a new rep-PCR primer that enables rapid fingerprint profiling of *M. intracellulare* as an alternative to rep-PCR derived from Gram-negative bacteria. Bacterial repetitive sequences through the *M. intracellulare* genome were screened using a strategy of utilizing 5 kb-scaled genomic fragments *in silico*. The Novel designed rep-PCR can make identical clone groups ($n = 7$) in 27 *M. intracellulare* strains, with a 95–98% of reproducibility. And these clone groups had a correlation value (0.814) with the VNTR, reference epidemiological method. This method can be a promising diagnostic technique for the *M. intracellulare* clinical isolates from patients with relapsed pulmonary disease.

Data availability statement

The raw data supporting the conclusions of this article will be made available by the authors, without undue reservation.

Author contributions

J-IS analyzed, and interpreted data as well as developed study concept and wrote manuscript. J-HH, K-MK, J-GC, S-RP, H-EP, J-SP, and J-HB contributed to part of the experiments. M-HJ, S-CB, W-KL, and H-LK wrote manuscript. J-WY and M-KS developed the study concept, obtained funding and ethics, interpreted data, and wrote manuscript. All authors contributed to the article and approved the submitted version.

Funding

This research was supported by the Basic Science Research Program through the National Research Foundation (NRF) funded by the Ministry of Education (NRF-2021R1I1A2045131), and by biomedical research institute fund (GNUHBRIF-2021-0011) from the Gyeongsang National University Hospital, and by the Research Program (2022ER250300) funded by the Korea Centers for Disease Control and Prevention, the Ministry of Health and Welfare, Korea.

Acknowledgments

The clinical isolates and the pathogen resources (KBN12P06244, NCCP14541, NCCP14780, NCCP14764, KBN12P07339, KBN12P07344, KBN12P06798, KBN12P07333, KBN12P07948, KBN12P07343, KBN12P07337, KBN12P07336, KBN12P07338, KBN12P07332, KBN12P07331, KBN12P07340, KBN12P07335, KBN12P07949, KBN12P06799, KBN12P07947, KBN12P07946, KBN12P07345, KBN12P06801, KBN12P07341, KBN12P07347, KBN12P07346, KBN12P06800, and KBN12P07342) for this study were provided by the Fastidious Specialized Pathogen Resources Bank (a member of the National Culture Collection for Pathogens, Gyeongsang National University Hospital, Jinju, Korea). We thank the invaluable assistance with sample collection of two *M. avium* strains (MAH 101 and MAH 104) from Yonsei University (Seoul, Korea).

Conflict of interest

The authors declare that the research was conducted in the absence of any commercial or financial relationships that could be construed as a potential conflict of interest.

Publisher's note

Supplementary material

The Supplementary material for this article can be found online at: https://www.frontiersin.org/articles/10.3389/fmicb.2023.1161194/full#supplementary-material

References

Akoglu, H. (2018). User's guide to correlation coefficients. *Turk. J. Emerg. Med.* 18, 91–93. doi: 10.1016/j.tjem.2018.08.001

Anyansi, C., Keo, A., Walker, B. J., Straub, T. J., Manson, A. L., Earl, A. M., et al. (2020). QuantTB–a method to classify mixed *mycobacterium tuberculosis* infections within whole genome sequencing data. *BMC Genom.* 21, 1–16. doi: 10.1186/s12864-020-6486-3

Arais, L. R., Barbosa, A. V., Andrade, J. R., Gomes, T. A., Asensi, M. D., Aires, C. A., et al. (2018). Zoonotic potential of atypical enteropathogenic *Escherichia coli* (aEPEC) isolated from puppies with diarrhoea in Brazil. *Vet. Microbiol.* 227, 45–51. doi: 10.1016/j.vetmic.2018.10.023

Bernasconi, O. J., Campos-Madueno, E. I., Donà, V., Perreten, V., Carattoli, A., and Endimiani, A. (2020). Investigating the use of bacteriophages as a new decolonization strategy for intestinal carriage of CTX-M-15-producing ST131 *Escherichia coli*: an in vitro continuous culture system model. *J. Glob. Antimicrob. Resist.* 22, 664–671. doi: 10.1016/j.jgar.2020.05.018

Bussone, G., Brossier, F., Roudiere, L., Bille, E., Sekkal, N., Charlier, C., et al. (2012). Recurrent *Mycobacterium avium* infection after seven years of latency in a HIV-infected patient receiving efficient antiretroviral therapy. *J. Infect.* 64, 613–617. doi: 10.1016/j.jinf.2011.12.020

Cangelosi, G. A., Freeman, R. J., Lewis, K. N., Livingston-Rosanoff, D., Shah, K. S., Milan, S. J., et al. (2004). Evaluation of a high-throughput repetitive-sequence-based PCR system for DNA fingerprinting of *mycobacterium tuberculosis* and *Mycobacterium avium* complex strains. *J. Clin. Microbiol.* 42, 2685–2693. doi: 10.1128/JCM.42.6.2685-2693.2004

Chang, C. L., Chen, L. C., Yu, C. J., Hsueh, P. R., and Chien, J. Y. (2020). Different clinical features of patients with pulmonary disease caused by various *Mycobacterium avium-intracellulare* complex subspecies and antimicrobial susceptibility. *Int. J. Infect. Dis.* 98, 33–40. doi: 10.1016/j.ijid.2020.06.019

Chen, G., Kong, C., Yang, L., Zhuang, M., Zhang, Y., Wang, Y., et al. (2021). Genetic diversity and population structure of the *Xanthomonas campestris* pv. Campestris strains affecting cabbages in China revealed by MLST and rep-PCR based genotyping. *Plant Pathol. J.* 37, 476–488. doi: 10.5423/PPJ.OA.06.2021.0088

Daley, C. L., and Winthrop, K. L. (2020). *Mycobacterium avium* complex: addressing gaps in diagnosis and management. *J. Infect. Dis.* 222, S199–S211. doi: 10.1093/infdis/jiaa354

Doran, T., Hodgson, A., Davies, J., and Radford, A. (1993). Characterisation of a highly repeated DNA sequence from *Mycobacterium bovis*. *FEMS Microbiol. Lett.* 111, 147–152. doi: 10.1111/j.1574-6968.1993.tb06377.x

Englund, S. (2003). IS900/ERIC-PCR as a tool to distinguish *Mycobacterium avium subsp. paratuberculosis* from closely related *mycobacteria*. *Vet. Microbiol.* 96, 277–287. doi: 10.1016/j.vetmic.2003.08.004

Furuuchi, K., Morimoto, K., Kurashima, A., Fujiwara, K., Nakamoto, K., Tanaka, Y., et al. (2020). Treatment duration and disease recurrence following the successful treatment of patients with *mycobacterium avium* complex lung disease. *Chest* 157, 1442–1445. doi: 10.1016/j.chest.2019.12.016

Furuuchi, K., Seto, S., Nakamura, H., Hikichi, H., Miyabayashi, A., Wakabayashi, K., et al. (2022). Novel screening system of virulent strains for the establishment of a *mycobacterium avium* complex lung disease mouse model using whole-genome sequencing. *Microbiol. Spectr.* 10, e00451–e00422. doi: 10.1128/spectrum.00451-22

Gautam, A. *Southern and Northern Blotting. DNA and RNA Isolation Techniques for Non-experts*: Springer; (2022). p. 165–169, Germany.

Güvenir, M., Otlu, B., Tunc, E., Aktas, E., and Suer, K. (2018). High genetic diversity among *Stenotrophomonas maltophilia* isolates from single hospital: nosocomial outbreaks or genotypic profile changes during subcultures. *Malays. J. Med. Sci.* 25, 40–49. doi: 10.21315/mjms2018.25.2.5

Hatherell, H.-A., Colijn, C., Stagg, H. R., Jackson, C., Winter, J. R., and Abubakar, I. (2016). Interpreting whole genome sequencing for investigating tuberculosis transmission: A systematic review. *BMC Med.* 14, 1–13. doi: 10.1186/s12916-016-0566-x

Healy, M., Huong, J., Bittner, T., Lising, M., Frye, S., Raza, S., et al. (2005). Microbial DNA typing by automated repetitive-sequence-based PCR. *J. Clin. Microbiol.* 43, 199–207. doi: 10.1128/JCM.43.1.199-207.2005

Healy, M., Reece, K., Walton, D., Huong, J., Frye, S., Raad, I., et al. (2005). Use of the DiversiLab system for species and strain differentiation of fusarium species isolates. *J. Clin. Microbiol.* 43, 5278–5280. doi: 10.1128/JCM.43.10.5278-5280.2005

Heidari, H., Halaji, M., Taji, A., Kazemian, H., Abadi, M. S. S., Sisakht, M. T., et al. (2018). Molecular analysis of drug-resistant *Acinetobacter baumannii* isolates by ERIC-PCR. *Meta Gene.* 17, 132–135. doi: 10.1016/j.mgene.2018.06.001

Hruska, K, and Kaevska, M., (2012). Mycobacteria in water, soil, plants and air: A review. *Veterinarni Medicina*, 57, 623–79. doi: 10.17221/6558-VETMED

Hwang, S. M., Cho, H. W., Kim, T. Y., Park, J. S., Jung, J., Song, K.-H., et al. (2021). Whole-genome sequencing for investigating a health care-associated outbreak of carbapenem-resistant *Acinetobacter baumannii*. *Diagnostics* 11:201. doi: 10.3390/diagnostics11020201

Iakhiaeva, E., McNulty, S., Brown Elliott, B. A., Falkinham, J. O. 3rd, Williams, M. D., Vasireddy, R., et al. (2013). Mycobacterial interspersed repetitive-unit-variable-number tandem-repeat (MIRU-VNTR) genotyping of *Mycobacterium intracellulare* for strain comparison with establishment of a PCR-based database. *J. Clin. Microbiol.* 51, 409–416. doi: 10.1128/JCM.02443-12

Jagielski, T., Minias, A., van Ingen, J., Rastogi, N., Brzostek, A., Zaczek, A., et al. (2016). Methodological and clinical aspects of the molecular epidemiology of *mycobacterium tuberculosis* and other mycobacteria. *Clin. Microbiol. Rev.* 29, 239–290. doi: 10.1128/CMR.00055-15

Jena, R., Choudhury, P. K., Puniya, A. K., and Tomar, S. K. (2021). Efficacy of BOX-PCR fingerprinting for taxonomic discrimination of bifidobacterial species isolated from diverse sources. *3 Biotech.* 11, 1–6. doi: 10.1007/s13205-021-02765-0

Jhun, B. W., Kim, S.-Y., Moon, S. M., Jeon, K., Kwon, O. J., Huh, H. J., et al. (2018a). Development of macrolide resistance and reinfection in refractory *Mycobacterium avium* complex lung disease. *Am. J. Respir. Crit. Care Med.* 198, 1322–1330. doi: 10.1164/rccm.201802-0321OC

Jhun, B. W., Moon, S. M., Kim, S.-Y., Park, H. Y., Jeon, K., Kwon, O. J., et al. (2018b). Intermittent antibiotic therapy for recurrent nodular bronchiectatic *Mycobacterium avium* complex lung disease. *Antimicrob. Agents Chemother.* 62, e01812–e01817. doi: 10.1128/AAC.01812-17

Karauz, M., Koç, A., and Atalay, A. (2018). Identification and molecular epidemiology of mycobacterial isolates in Kayseri/Turkey. *Int. J. Respir. Pulm. Med.* 5, 092. doi: 10.23937/2378-3516/1410092

Keen, E. C., Choi, J., Wallace, M. A., Azar, M., Mejia-Chew, C. R., Mehta, S. B., et al. (2021). Comparative genomics of *Mycobacterium avium* complex reveals signatures of environment-specific adaptation and community acquisition. *Msystems.* 6, e01194–e01121. doi: 10.1128/mSystems.01194-21

Kim, O.-H., Pil Chong, Y., Shim, T. S., and Jo, K.-W. (2021). Redevelopment after spontaneous sputum conversion in noncavitary nodular bronchiectatic *Mycobacterium avium* complex lung disease. *J. Infect. Chemother.* 27, 1156–1161. doi: 10.1016/j.jiac.2021.03.006

Koeuth, T., Versalovic, J., and Lupski, J. R. (1995). Differential subsequence conservation of interspersed repetitive *Streptococcus pneumoniae* BOX elements in diverse bacteria. *Genome Res.* 5, 408–418. doi: 10.1101/gr.5.4.408

Koh, W. J., Moon, S. M., Kim, S. Y., Woo, M. A., Kim, S., Jhun, B. W., et al. (2017). Outcomes of *Mycobacterium avium complex* lung disease based on clinical phenotype. *Eur. Respir. J.* 50:1602503. doi: 10.1183/13993003.02503-2016

Krych, L., Castro-Mejia, J. L., Forero-Junco, L. M., Moesby, D. N., Mikkelsen, M. B., Rasmussen, M. A., et al. (2019). DNA enrichment and tagmentation method for species-level identification and strain-level differentiation using ON-rep-seq. *Commun. Biol.* 2:369. doi: 10.1038/s42003-019-0617-x

Kwon, B. S., Shim, T. S., and Jo, K.-W. (2019). The second recurrence of Mycobacterium avium complex lung disease after successful treatment for first recurrence. *Eur. Respir. J.* 53:1801038. doi: 10.1183/13993003.01038-2018

La China, S., De Vero, L., Anguluri, K., Brugnoli, M., Mamlouk, D., and Gullo, M. (2021). Kombucha tea as a reservoir of cellulose producing bacteria: assessing diversity among Komagataeibacter isolates. *Appl. Sci.* 11:1595. doi: 10.3390/app11041595

Lari, N., and Rindi, L. (2022). High genetic heterogeneity of *Mycobacterium intracellulare* isolated from respiratory specimens. *BMC Microbiol.* 22:5. doi: 10.1186/s12866-021-02426-5

Otsuka, Y., Parniewski, P., Zwolska, Z., Kai, M., Fujino, T., Kirikae, F., et al. (2004). Characterization of a trinucleotide repeat sequence (CGG)5 and potential use in restriction fragment length polymorphism typing of *mycobacterium tuberculosis*. *J. Clin. Microbiol.* 42, 3538–3548. doi: 10.1128/JCM.42.8.3538-3548.2004

Parker, H., Lorenc, R., Ruelas Castillo, J., and Karakousis, P. C. (2020). Mechanisms of antibiotic tolerance in *Mycobacterium avium* complex: lessons from related mycobacteria. *Front. Microbiol.* 11:573983. doi: 10.3389/fmicb.2020.573983

Prevots, D. R., and Marras, T. K. (2015). Epidemiology of human pulmonary infection with nontuberculous mycobacteria: a review. *Clin. Chest Med.* 36, 13–34. doi: 10.1016/j.ccm.2014.10.002

Rampadarath, S., Puchooa, D., and Bal, S. (2015). Repetitive element palindromic PCR (rep-PCR) as a genetic tool to study interspecific diversity in Euphorbiaceae family. *Electron. J. Biotechnol.* 18, 412–417. doi: 10.1016/j.ejbt.2015.09.003

Ratnatunga, C. N., Lutzky, V. P., Kupz, A., Doolan, D. L., Reid, D. W., Field, M., et al. (2020). The rise of non-tuberculosis mycobacterial lung disease. *Front. Immunol.* 11:303. doi: 10.3389/fimmu.2020.00303

San Millán, R. M., Martínez-Ballesteros, I., Rementeria, A., Garaizar, J., and Bikandi, J. (2013). Online exercise for the design and simulation of PCR and PCR-RFLP experiments. *BMC. Res. Notes* 6, 1–4. doi: 10.1186/1756-0500-6-513

Shin, J. I., Ha, J. H., Lee, D. H., Choi, J. G., Kim, K. M., Lee, S. J., et al. (2020a). Comparative evaluation of band-based genotyping methods for *Mycobacterium intracellulare* and its application for epidemiological analysis. *Microorganisms* 8:1315. doi: 10.3390/microorganisms8091315

Shin, J. I., Shin, S. J., and Shin, M. K. (2020b). Differential genotyping of *Mycobacterium avium* complex and its implications in clinical and environmental epidemiology. *Microorganisms* 8:98. doi: 10.3390/microorganisms8010098

Teixeira, C. G., Fusieger, A., Martins, E., de Freitas, R., Vakarelova, M., Nero, L. A., et al. (2021). Biodiversity and technological features of Weissella isolates obtained from Brazilian artisanal cheese-producing regions. *LWT.* 147:111474. doi: 10.1016/j.lwt.2021.111474

Thomassen, G. M. B., Krych, L., Knøchel, S., and Mehli, L. (2021). ON-rep-seq as a rapid and cost-effective alternative to whole-genome sequencing for species-level identification and strain-level discrimination of *listeria monocytogenes contamination* in a salmon processing plant. *Microbiology* 10:e1246. doi: 10.1002/mbo3.1246

Thomassen, G. M. B., Krych, L., Knøchel, S., and Mehli, L. (2022). Bacterial community development and diversity during the first year of production in a new salmon processing plant. *Food Microbiol.* 109:104138. doi: 10.1016/j.fm.2022.104138

Thomson, R., Tolson, C., Carter, R., Coulter, C., Huygens, F., and Hargreaves, M. (2013). Isolation of nontuberculous mycobacteria (NTM) from household water and shower aerosols in patients with pulmonary disease caused by NTM. *J. Clin. Microbiol.* 51, 3006–3011. doi: 10.1128/JCM.00899-13

Thomson, R. M., Tolson, C. E., Carter, R., Huygens, F., and Hargreaves, M. (2014). Heterogeneity of clinical and environmental isolates of *mycobacterium fortuitum* using repetitive element sequence-based PCR: municipal water an unlikely source of community-acquired infections. *Epidemiol. Infect.* 142, 2057–2064. doi: 10.1017/S0950268813003257

van der Zanden, R. J., Magis-Escurra, C., de Lange, W. C., Hoefsloot, W., Boeree, M. J., van Ingen, J., et al. (2012). Hypersensitivity pneumonitis caused by *Mycobacterium avium subsp. hominissuis* in a hot tub, as proven by IS1245 RFLP and rep-PCR typing. *Int. J. Mycobacteriol.* 1, 152–154. doi: 10.1016/j.ijmyco.2012.07.006

van Weezep, E., Kooi, E. A., and van Rijn, P. A. (2019). PCR diagnostics: in silico validation by an automated tool using freely available software programs. *J. Virol. Methods* 270, 106–112. doi: 10.1016/j.jviromet.2019.05.002

Versalovic, J., Kapur, V., Koeuth, T., Mazurek, G. H., Whittam, T. S., Musser, J. M., et al. (1995). DNA fingerprinting of pathogenic bacteria by fluorophore-enhanced repetitive sequence-based polymerase chain reaction. *Arch. Pathol. Lab. Med.* 119, 23–29.

Versalovic, J., Koeuth, T., and Lupski, R. (1991). Distribution of repetitive DNA sequences in eubacteria and application to finerpriting of bacterial enomes. *Nucleic Acids Res.* 19, 6823–6831. doi: 10.1093/nar/19.24.6823

Wang, X., Xiao, Y., Cui, Z., Li, Z., Li, L., Wu, L., et al. (2022). Cyclocytidine hydrochloride inhibits the synthesis of relaxed circular DNA of hepatitis B virus. *PeerJ.* 10:e13719. doi: 10.7717/peerj.13719

Warren, A. E., Boulianne-Larsen, C. M., Chandler, C. B., Chiotti, K., Kroll, E., Miller, S. R., et al. (2011). Genotypic and phenotypic variation in *Pseudomonas aeruginosa* reveals signatures of secondary infection and mutator activity in certain cystic fibrosis patients with chronic lung infections. *Infect. Immun.* 79, 4802–4818. doi: 10.1128/IAI.05282-11

Wojtasik, A., Kubiak, A. B., Krzyzanowska, A., Majchrzak, M., Augustynowicz-Kopec, E., and Parniewski, P. (2012). Comparison of the (CCG)4-based PCR and MIRU-VNTR for molecular typing of *Mycobacterium avium* strains. *Mol. Biol. Rep.* 39, 7681–7686. doi: 10.1007/s11033-012-1603-2

Yamamura, H., Hayakawa, M., Nakagawa, Y., and Iimura, Y. (2004). Characterization of N*ocardia asteroides* isolates from different ecological habitats on the basis of repetitive extragenic palindromic-PCR fingerprinting. *Appl. Environ. Microbiol.* 70, 3149–3151. doi: 10.1128/AEM.70.5.3149-3151.2004

Zhao, L., Zhang, D., Liu, Y., Zhang, Y.-N., Meng, D.-Q., Xu, Q., et al. (2022). Quantitative PCR assays for the strain-specific identification and enumeration of probiotic strain *Lacticaseibacillus rhamnosus* X253. *Foods* 11:2282. doi: 10.3390/foods11152282

frontiers | Frontiers in Microbiology

TYPE Original Research
PUBLISHED 17 April 2023
DOI 10.3389/fmicb.2023.1156695

OPEN ACCESS

EDITED BY
Wafa Achour,
Centre National de Greffe de la Moelle Osseuse, Tunisia

REVIEWED BY
Eileen Dunne,
Pfizer, United States
Annalisa Pantosti,
National Institute of Health (ISS), Italy

*CORRESPONDENCE
Krzysztof Trzciński
✉ k.trzcinski@umcutrecht.nl
Willem R. Miellet
✉ w.r.miellet-2@umcutrecht.nl

SPECIALTY SECTION
This article was submitted to Infectious Agents and Disease, a section of the journal Frontiers in Microbiology

RECEIVED 02 February 2023
ACCEPTED 27 March 2023
PUBLISHED 17 April 2023

CITATION
Miellet WR, van Veldhuizen J, Litt D, Mariman R, Wijmenga-Monsuur AJ, Nieuwenhuijsen T, Christopher J, Thombre R, Eletu S, Bosch T, Rots NY, van Houten MA, Miller E, Fry NK, Sanders EAM and Trzciński K (2023) A spitting image: molecular diagnostics applied to saliva enhance detection of *Streptococcus pneumoniae* and pneumococcal serotype carriage. *Front. Microbiol.* 14:1156695. doi: 10.3389/fmicb.2023.1156695

A spitting image: molecular diagnostics applied to saliva enhance detection of *Streptococcus pneumoniae* and pneumococcal serotype carriage

Willem R. Miellet[1,2]*, Janieke van Veldhuizen[2], David Litt[3], Rob Mariman[2], Alienke J. Wijmenga-Monsuur[2], Tessa Nieuwenhuijsen[1], Jennifer Christopher[3], Rebecca Thombre[3], Seyi Eletu[3], Thijs Bosch[2], Nynke Y. Rots[2], Marianne Alice van Houten[4], Elizabeth Miller[5], Norman K. Fry[3,6], Elisabeth A. M. Sanders[1,2] and Krzysztof Trzciński[1]*

[1]Department of Pediatric Immunology and Infectious Diseases, Wilhelmina Children's Hospital, University Medical Center Utrecht, Utrecht, Netherlands, [2]Centre for Infectious Disease Control, National Institute for Public Health and the Environment (RIVM), Bilthoven, Netherlands, [3]Respiratory and Vaccine Preventable Bacteria Reference Unit (RVPBRU), UK Health Security Agency, London, United Kingdom, [4]Spaarne Gasthuis, Haarlem, Netherlands, [5]Department of Infectious Disease Epidemiology, Faculty of Epidemiology and Population Health, London School of Hygiene and Tropical Medicine, London, United Kingdom, [6]Immunisation and Vaccine Preventable Diseases Division, UK Health Security Agency, London, United Kingdom

Background: Despite strong historical records on the accuracy of saliva testing, oral fluids are considered poorly suited for pneumococcal carriage detection. We evaluated an approach for carriage surveillance and vaccine studies that increases the sensitivity and specificity of pneumococcus and pneumococcal serotype detection in saliva samples.

Methods: Quantitative PCR (qPCR)-based methods were applied to detect pneumococcus and pneumococcal serotypes in 971 saliva samples collected from 653 toddlers and 318 adults. Results were compared with culture-based and qPCR-based detection in nasopharyngeal samples collected from children and in nasopharyngeal and oropharyngeal samples collected from adults. Optimal C_q cut-offs for positivity in qPCRs were determined via receiver operating characteristic curve analysis and accuracy of different approaches was assessed using a composite reference for pneumococcal and for serotype carriage based on isolation of live pneumococcus from the person or positivity of saliva samples determined with qPCR. To evaluate the inter-laboratory reproducibility of the method, 229 culture-enriched samples were tested independently in the second center.

Results: In total, 51.5% of saliva samples from children and 31.8% of saliva samples from adults were positive for pneumococcus. Detection of pneumococcus by qPCR in culture-enriched saliva exhibited enhanced sensitivity and higher agreement with a composite reference compared to diagnostic culture of nasopharyngeal samples in children (Cohen's κ: 0.69–0.79 vs. 0.61–0.73) and in adults (κ: 0.84–0.95 vs. 0.04–0.33) and culture of oropharyngeal samples in adults (κ: 0.84–0.95 vs. −0.12–0.19). Similarly, detection of serotypes with qPCR in

culture-enriched saliva exhibited enhanced sensitivity and higher agreement with a composite reference compared to nasopharyngeal culture in children (κ: 0.73–0.82 vs. 0.61–0.73) and adults (κ: 0.90–0.96 vs. 0.00–0.30) and oropharyngeal culture in adults (κ: 0.90–0.96 vs. −0.13 to 0.30). However, results of qPCRs targeting serotype 4, 5, and 17F and serogroups 9, 12, and 35 were excluded due to assays' lack of specificity. We observed excellent quantitative agreement for qPCR-based detection of pneumococcus between laboratories. After exclusion of serotype/serogroup-specific assays with insufficient specificity, moderate agreement (κ 0.68, 95% CI 0.58–0.77) was observed.

Conclusion: Molecular testing of culture-enriched saliva samples improves the sensitivity of overall surveillance of pneumococcal carriage in children and adults, but limitations of qPCR-based approaches for pneumococcal serotypes carriage detection should be considered.

KEYWORDS

***Streptococcus pneumoniae* (pneumococcus), pneumococcal serotypes, pneumococcal carriage, saliva, quantitative PCR (qPCR)**

Introduction

Streptococcus pneumoniae (pneumococcus) is an important cause of community-acquired pneumonia (CAP) and invasive bacterial disease but also a common colonizer of the human respiratory tract (Bogaert et al., 2004a; O'Brien et al., 2009; Welte et al., 2012; World Health Organization [WHO], 2019). Infants, toddlers and older adults are the age groups at highest risk of pneumococcal CAP and invasive pneumococcal disease (IPD) (Jansen et al., 2009), with young children considered to be the primary reservoir of pneumococci in the population (Bogaert et al., 2004b; Satzke et al., 2013). To reduce the burden of pneumococcal disease the World Health Organization (WHO) recommended in 2007 the implementation of pneumococcal conjugate vaccines (PCVs) (World Health Organization [WHO], 2007). Widespread introduction of PCVs into infant immunization programs has substantially reduced vaccine serotype disease (World Health Organization [WHO], 2019). Through herd immunity, PCV immunization of children has also reduced transmission of vaccine serotypes and the burden of pneumococcal disease in unvaccinated groups (Whitney et al., 2003). However, the overall impact of the PCVs implementation on pneumococcal disease has been limited by serotype replacement and aging populations (Lewnard and Hanage, 2019; van der Linden et al., 2019).

Pneumococcal carriage is now an accepted endpoint in vaccination studies (Dagan et al., 1997; van Gils et al., 2009; Flasche et al., 2011; Auranen et al., 2013), and surveillance of carriage is an important tool in monitoring the direct and indirect effects of vaccination. The laboratory protocol currently recommended by the WHO as the gold standard for pneumococcal carriage detection is the isolation of live pneumococci from culture of deep trans-nasal nasopharyngeal swab, complemented with an oropharyngeal swab for detection among adults (Satzke et al., 2013). However, this procedure lacks sensitivity when applied to highly polymicrobial samples in which pneumococcus is not a dominant bacterium (Heffron, 1939; Trzcinski et al., 2013; Krone et al., 2014; Wyllie et al., 2014, 2016a; Miellet et al., 2020; Wrobel-Pawelczyk et al., 2022) or to detect co-carriage of a secondary serotype (Huebner et al., 2000).

Pneumococcus was first described after having been isolated from saliva by both Sternberg and Pasteur separately (Pasteur, 1881; Sternberg, 1881). In early 20th century studies, saliva was also the preferred specimen for detection of pneumococcal carriers wherein high pneumococcal carriage prevalence rates across all ages were observed when saliva or oral washes were used by mouse inoculation (Heffron, 1939; Krone et al., 2014). However, with the advent of selective culture plates, nasopharyngeal swabs became the specimen of choice for pneumococcal detection and from that moment onward adult carriage rates abruptly declined in comparison with historical rates (Krone et al., 2014).

More recently, molecular diagnostic methods such as quantitative PCR (qPCR) have been proposed to improve the sensitivity of pneumococcal carriage surveillance across all ages (Carvalho et al., 2007; Trzcinski et al., 2013; Tavares et al., 2019). Studies from our group (Trzcinski et al., 2013; Wyllie et al., 2014, 2016a,b; Krone et al., 2015; Miellet et al., 2020), and others (Branche et al., 2018; Tavares et al., 2019; Almeida et al., 2020) have validated and applied pneumococcal carriage detection by qPCR in raw [minimally processed (MP)] and culture-enriched respiratory samples, demonstrating high sensitivity of *S. pneumoniae* detection (Miellet et al., 2022). Importantly, we (Wyllie et al., 2017) and others (Carvalho et al., 2012, 2013; Boelsen et al., 2020) have cautioned that assays used for molecular detection and serotyping of pneumococcus may exhibit reduced specificity in oral samples due to the presence of pneumococcal genes among commensal oral streptococci. Consequently, a robust experimental strategy is needed to maintain high specificity of pneumococcal detection in polymicrobial samples (Miellet et al., 2023). In a recent study we have described quantifying and comparing in an agreement analysis (Ranganathan et al., 2017) pneumococcal genes, *piaB* and *lytA*, and

serotype/serogroup-specific genes in nasopharyngeal samples from children, and nasopharyngeal and oropharyngeal samples from adults (Miellet et al., 2022). This dual-target (or "Two-To-Tango") approach ensures specific detection of pneumococcus by qPCR in polymicrobial samples and addresses specificity concerns of qPCR detection in oral samples. In children, the method demonstrated near-perfect agreement with conventional culture and was superior to culture when applied to samples from adults, which often exhibit low density carriage and positivity for pneumococcal carriage largely limited to oral samples (Miellet et al., 2022).

In the current study we evaluated saliva testing for carriage surveillance and vaccine studies and propose a protocol that enhances the specificity of molecular methods for the detection of live pneumococcus in oral fluids. Results from saliva were compared with results based on applying the same protocol in paired nasopharyngeal and oropharyngeal samples (Miellet et al., 2022). Inter-laboratory reproducibility of the protocol was tested independently in the second center. In conclusion, molecular testing of culture-enriched saliva samples improves the sensitivity of overall surveillance of pneumococcal carriage in children and adults, but limitations of qPCR-based approaches for pneumococcal serotypes carriage detection should be taken into account. The results highlight the importance of qPCR-based testing of oral samples.

Materials and methods

Study design and ethics statement

Pneumococcal carriage was investigated in cross-sectional prospective observational study conducted in 2015/2016 in the Netherlands (Vissers et al., 2018). The study was approved by the Medical Ethics Committee Noord Holland (NCT02522546 on clinicaltrials.gov). Written informed consent was obtained from the parent or guardian of every participating child, and adults produced written consent for their own participation. The study was conducted in accordance with the Declaration of Helsinki and Good Clinical Practice.

Sample collection and laboratory processing

The collection and laboratory processing of nasopharyngeal and oropharyngeal swabs have been previously described (Vissers et al., 2018; Miellet et al., 2022). In brief, respiratory samples were collected between October 2015 and March 2016 in a study coordinated by the National Institute of Public Health and the Environment. Nasopharyngeal samples were collected from children aged 24 months (±1 month) and 44 to 49 months, all vaccinated with 10-valent pneumococcal vaccine (PHiD-CV, GlaxoSmithKline), and from parents of 24-month-olds (one parent per child). Oropharyngeal swabs were collected exclusively from unvaccinated adults (Watt et al., 2004; Vissers et al., 2018). Nasopharyngeal and oropharyngeal swabs were collected in accordance with standard procedures recommended by the WHO (Satzke et al., 2013). In addition, saliva samples were collected from all individuals as previously described (Krone et al., 2015). In short, oral fluids were collected with sponge lollipop (Oracol Saliva Collection System Malvern Medical Developments Limited, Worcester, UK), immediately transferred to tubes pre-filled with 100 µl sterile 50% glycerol solution in water, mixed, placed on dry ice and transported to the lab. With approximately 400 µl of saliva collected per sample the final glycerol concentration was around 10%. Saliva samples were delivered to the laboratory and stored at −70°C within 8 h.

Detection of *S. pneumoniae*

Detection of *S. pneumoniae* and pneumococcal serotypes in nasopharyngeal and oropharyngeal samples, including qPCR-guided culturing, has been detailed previously (Miellet et al., 2022, 2023). Saliva samples stored frozen with 10% glycerol were thawed and diluted in an equal volume of PBS. Two-hundred microliters was used to inoculate SB7-GENT agar (Oxoid). After overnight incubation at 37°C and 5% CO_2, all growth was harvested from a plate into 10% glycerol in BHI (Oxoid) as previously described for nasopharyngeal and oropharyngeal samples (Miellet et al., 2022) and stored at −70°C. We considered these samples culture-enriched for pneumococci. DNA was extracted from 200 µl of MP saliva samples diluted in PBS using DNeasy Blood and Tissue Kit (Qiagen) and eluted with 200 µl of buffer. We consider these templates to represent MP saliva. To extract DNA from culture-enriched saliva, 100 µl of a plate harvest was centrifuged for 2 min at 14,000 × *g*, the pellet was resuspended with 90 µl of the TE buffer [20 mM Tris–HCl (pH 8.0), 2 mM EDTA] and incubated for 15 min at 95°C. Next, 90 µl of lysis buffer [20 mM Tris–HCl (pH 8.0), 2 mM EDTA, 2.4% Triton X-100 and 40 mg/ml lysozyme] was added, and the samples were processed with DNeasy Blood & Tissue Kit and eluted with 200 µl of buffer (Miellet et al., 2020). Pneumococcal DNA was detected using a dual-target approach via single-plex qPCRs with primers and probes specific for regions within genes encoding for pneumococcal iron uptake ABC transporter lipoprotein PiaB (Trzcinski et al., 2013), and for major pneumococcal autolysin LytA (Carvalho et al., 2007) by using 5.5 µl eluate from MP or 1.0 µl for culture-enriched samples in a qPCR reaction volume of 12.5 µl.

Molecular detection of pneumococcal serotypes

DNA extracts from culture-enriched samples were used to determine serotype composition of respiratory samples. We used 29 sets of primers and probes (Azzari et al., 2010, 2012; Pimenta et al., 2013; Velusamy et al., 2020) targeting 50 serotypes and including 24 vaccine serotypes covered by pneumococcal vaccines available in the Netherlands, namely ten-valent PHiD-CV, thirteen-valent PCV13 (Pfizer), and 23-valent polysaccharide vaccine PPV23 (Merck Sharp & Dohme). The panel also targeted a selection of non-vaccine serotypes, namely serotypes 6C, 6D, 7A, 9A, 9L, 10B, 11D, 12A, 12B, 15A, 15C, 15F, 18A, 18B, 18F, 16F, 21, 22A, 22F, 23A, 23B, 33A, 34, 35B, 35C, 37, and 38. With several qPCR assays it was not possible distinguish between serotypes of a serogroup,

specifically 6A and 6B; 6C and 6D; 7A and 7F; 9A, 9L, 9N and 9V; 10A and 10B; 11A and 11D; 12A, 12B and 12F; 15A, 15B, 15C and 15F; 18A, 18B, 18C and 18F; 22A and 22F; 33A, 33F and 37; and 35B and 35C. Primers and probes used in these assays and their concentrations are listed in **Supplementary Information**. We employed a sample pooling strategy as described previously (Miellet et al., 2022). Namely samples with a C_q < 40 for *piaB* or *lytA* were pooled in groups of 5 and remaining samples were pooled in groups of 10. Negative samples were used to evaluate specificity of serotype-specific qPCRs. Pooled positive samples generating a signal for a serotype-specific qPCR assay were tested individually.

Assessment of method's inter-laboratory reproducibility

Two-hundred and twenty-nine culture-enriched saliva samples were randomly selected to evaluate the inter-laboratory reproducibility of molecular methods. For this, aliquots of samples from n = 133 children and n = 96 adults were shipped to the study site in England and tested as described above. Results for paired samples were compared between centers by calculating the percent agreement and Cohen's kappa (κ). Quantitative results of both laboratories were also compared by calculating an intraclass correlation coefficient (ICC) and by comparing results in Bland–Altman plots. Carriage rates between both laboratories were compared using Cohen's kappa.

Definitions

For determination of C_q thresholds two different criteria were used for ROC curve analysis. The first criterion was based on the isolation of viable pneumococcus from primary diagnostic or qPCR-guided cultures and on quantification of *piaB* and *lytA* in saliva. Samples of $C_q \geq 40$ for either *piaB* or *lytA* were regarded as negative when calculating maximum Youden index values. The second criterion was based solely on amplification slopes considered representing viable pneumococci in saliva. Here, we disregarded samples with no increase in both *piaB* and *lytA* C_qs after culture-enrichment when compared with MP saliva. The first criterion can be applied to both MP and to culture-enriched samples. The second is applicable exclusively to culture-enriched samples yet requires MP samples to be tested.

For the evaluation of diagnostic test performance, we also used two different approaches. First, qPCR-based detection was compared with culture (primary diagnostic culture plus qPCR-guided culture) as reference standard for presence of carriage. We considered it to represent an imperfect reference (Naaktgeboren et al., 2013). The second was a composite study reference based on isolation of viable pneumococcus from a person (positivity by culture) or qPCR-based detection in saliva sample.

For evaluation of serotyping methods, qPCR-based serotyping was compared with culture (primary diagnostic culture only), and thereafter a composite reference standard with an any positive rule was also used to compare both culture (primary diagnostic culture) and qPCR-based serotyping of culture-enriched samples, including qPCR-based serotyping on nasopharyngeal samples for children and both, nasopharyngeal and oropharyngeal samples for adults. Comparisons between qPCR-based serotyping and culture were limited to qPCR-targeted serotypes. For serogroup-specific qPCR assays results were considered concordant when a serogroup detected in qPCR matched the serogroup of the serotype detected by culture.

Statistical analysis

Analysis of carriage data was performed in GraphPad Prism software version 9.3.1 and R version 4.2.2. We performed ROC curve analysis with the "cutpointr" R package. Maximum Youden index values were estimated with bootstrapping (n = 5,000) on *piaB* or *lytA* qPCR data to determine C_q thresholds for qPCR detection (Nutz et al., 2011; Miellet et al., 2022). We used Bland–Altman plots (Bland and Altman, 1986; Ranganathan et al., 2017) with the "blandr" R package and two-way mixed effects ICCs (Koo and Li, 2016) with the "irr" R package to evaluate agreement between qPCR targets (Miellet et al., 2022).

Cohen's kappa (κ) were calculated as described by McHugh (2012) and interpreted according to Landis and Koch (1977) with values of ≤0, 0.01–0.20, 0.21–0.40, 0.41–0.60, 0.61–0.80, and ≥0.81 interpreted as displaying poor, slight, fair, moderate, substantial, and near-perfect agreement, respectively (Miellet et al., 2022). The McNemar's test was used to compare carriage rates unless otherwise stated. Diagnostic test performance was conducted as described previously (Miellet et al., 2022) and we compared diagnostic accuracy estimates between methods (or subgroups) using a test of interaction (Altman and Bland, 2003). A p-value of <0.05 was regarded as significant.

Results

Samples collected from 653 children aged between 2 and 4 years and 318 adults were used to evaluate the diagnostic accuracy and added value of saliva testing for the detection of *S. pneumoniae* and pneumococcal serotypes carriage. For this, a paired comparison of saliva with nasopharyngeal samples from children, and with nasopharyngeal and oropharyngeal samples from adults was performed. Results for nasopharyngeal samples from children and adults and oropharyngeal samples from adults have previously been published (Miellet et al., 2022).

Detection of pneumococcus in saliva

The specificity of qPCR-based detection in saliva was enhanced by using a dual-target approach with *piaB* and *lytA* (**Figure 1**; Miellet et al., 2022). qPCR cycle threshold (C_q) cut-off values were determined using ROC curve analysis with as criterion individuals that were previously determined positive by nasopharyngeal culture, or also positive by oropharyngeal culture for adults, and whose paired saliva samples yielded qPCR measurements <40 C_q (**Table 1**). To ascertain that a C_q cut-off reduced relic DNA presence and was likely to improve specificity of qPCR for detection of live pneumococci, the slopes of pneumococcal abundances in paired

MP and culture-enriched samples were compared. ROC analysis was repeated with amplifying slopes as reference (**Supplementary Figure 1** and **Supplementary Table 1**). Newly derived C_q cut-offs were similar to C_q cut-offs based on culture as reference (κ 0.96, 95% CI 0.94–0.98), the latter of which were used for further analysis.

Subsequently, 336 samples from children (51.5% of 653) and 101 samples from adults (31.8% of 318) were identified as positive for pneumococcus by qPCR in either MP or culture-enriched saliva. In comparison, 368 (56.4% of 653) children and 22 (6.9% of 318) adults were positive by qPCR in either MP or culture-enriched nasopharyngeal samples. The proportions of samples positive for pneumococcus was significantly higher among culture-enriched saliva compared with MP saliva (397 or 40.9% vs. 269 or 27.7% of 971; $P < 0.0001$). Likewise, the proportions of pneumococcus positive samples were also significantly higher among children when compared with adults with MP saliva (226/653 or 34.6% vs. 43/318 or 13.5%; Fisher's exact test $P < 0.0001$) and culture-enriched saliva (306/653 or 46.9% vs. 91/318 or 28.6%; $P < 0.0001$). Positive MP and culture-enriched saliva samples exhibited significant correlation between *piaB* and *lytA* C_qs (**Figure 1**) and ICCs were indicative of excellent quantitative agreement of detection (0.93, 95% CI 0.91–0.94 and 0.95, 95% CI 0.93–0.96, respectively).

Comparison between saliva and nasopharyngeal samples collected from children

The diagnostic accuracy of qPCR-based detection of pneumococcus in saliva samples from children was evaluated using primary diagnostic and qPCR-guided culturing as reference (Miellet et al., 2022). Both MP and culture-enriched saliva exhibited limited agreement with nasopharyngeal culture (**Supplementary Table 2**). In spite of similar pneumococcal detection rates with qPCR-based testing of culture-enriched saliva and detection by nasopharyngeal culture, there was limited overlap in positive samples (**Figure 2A**). Nineteen percent and thirty-eight percent of pneumococci detected were unique to nasopharyngeal cultures and culture-enriched saliva, respectively. Importantly, culture-enriched saliva samples displayed enhanced sensitivity when compared with MP saliva samples ($P < 0.001$).

Since nasopharyngeal detection (both by culture and qPCR) can be considered an imperfect study reference, the diagnostic accuracy of saliva testing was also evaluated using a composite study reference by which a result was considered to be true positive when positive by qPCR in culture-enriched saliva or positivity by nasopharyngeal culture. Testing culture-enriched saliva exhibited increased agreement with the composite study reference and enhanced sensitivity of detection when compared with nasopharyngeal cultures ($P < 0.05$, **Table 2**). Importantly, the ICC of positive culture-enriched saliva samples for which paired nasopharyngeal samples were negative for pneumococcus exhibited excellent quantitative agreement between *piaB* and *lytA* C_qs ($n = 87$, ICC 0.93, 95% CI 0.89–0.95). Similar observations for performance of qPCR-based detection in culture-enriched saliva were made using C_q thresholds based on amplification slopes (**Supplementary Table 3**).

Comparison between saliva and nasopharyngeal and oropharyngeal samples collected from adults

When comparing saliva samples to nasopharyngeal and oropharyngeal cultures (**Figure 2B**), limited agreement was observed among adults (**Supplementary Table 4**). Overall, testing culture-enriched saliva exhibited enhanced agreement with references when compared with MP saliva samples from adults by improving sensitivity of detection. Here, a composite study reference by which a result was considered true positive when positive by qPCR in culture-enriched saliva or positivity by nasopharyngeal or oropharyngeal culture, also indicated that saliva testing improved sensitivity of pneumococcal detection ($P < 0.0001$, **Table 3**). The ICC between *piaB* and *lytA* C_qs for qPCR-positive culture-enriched saliva samples for which paired nasopharyngeal and oropharyngeal samples were negative for pneumococcus displayed good quantitative agreement ($n = 60$, ICC 0.79, 95% CI 0.68–0.87). Comparable performance of qPCR-based detection with culture-enriched saliva was made using C_q thresholds based on amplification slopes (**Supplementary Table 5**).

Molecular detection of pneumococcal serotypes in culture-enriched samples of saliva

A pooling strategy was used to test culture-enriched saliva samples in 29 serotype- or serogroup-specific qPCR assays. Using pools of samples negative for *piaB* and *lytA,* we observed that assays targeting serotypes 4, 5, 17F, and 21 and serogroups 9, 12, 33, and 35 lack specificity (**Supplementary Figure 2**). However, for qPCRs targeting serotypes 21, 23A, and serogroup 33, Bland–Altman analysis indicated that there was sufficient agreement between signal for serotype and pneumococcus to consider results reliable and include in analysis (**Supplementary Figure 3**). For qPCRs targeting serotypes 4, 5, and 17F and serogroups 9, 12, and 35, there was no such agreement and all results generated in these six assays were excluded. With this, we analyzed results generated in twenty-three qPCRs targeting thirty-eight *S. pneumoniae* serotypes. Of those 23 assays, no sample of culture-enriched saliva tested positive with qPCR for serotype 2, 23F and serogroup 18, finding in line with results reported previously for paired nasopharyngeal and oropharyngeal samples (Miellet et al., 2022). Nevertheless, the presence of one or more serotype was detected in 90.2% (358 of 397) culture-enriched saliva samples classified as positive for pneumococcus. It represented 89.5% (274/306) and 92.3% (84/91) of such a sample from children and adults, respectively.

In total 463 serotype positives were observed among culture-enriched saliva samples. Serotypes that were ranked as dominant serotype within a sample displayed good agreement (ICC 0.87, 95% CI 0.84-0.89) with *piaB* C_qs (**Figure 3**). Multiple serotype carriage was observed in 25.5% (78/306) and 13.2% (12/91)

10.3389/fmicb.2023.1156695

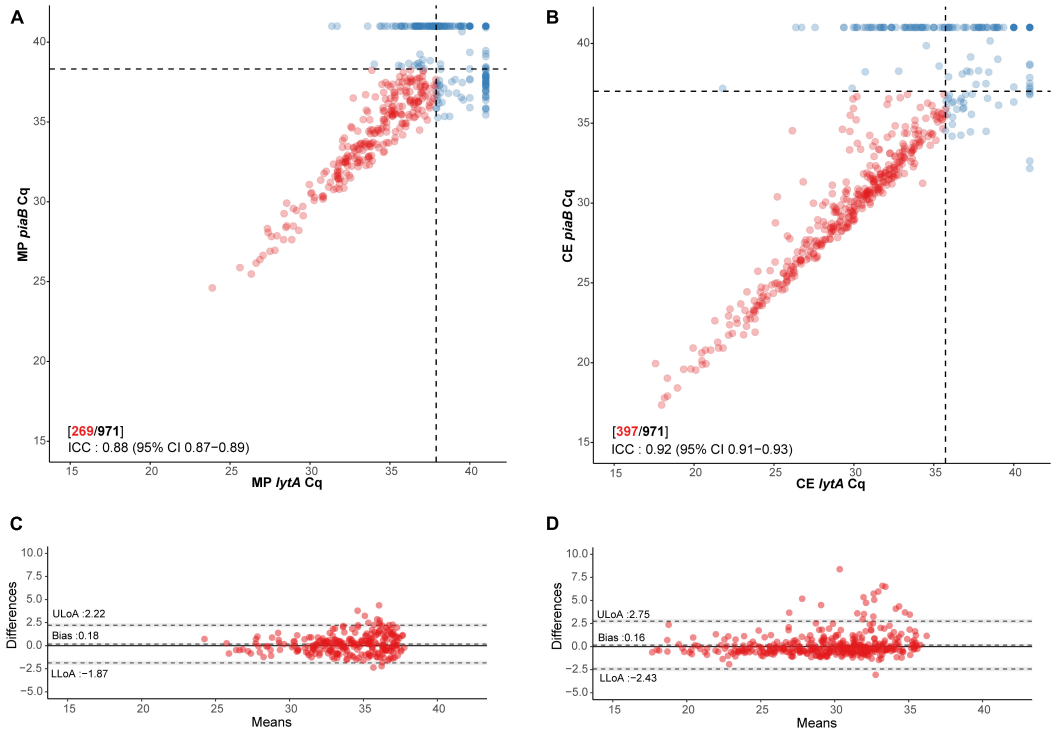

FIGURE 1
Scatter plot illustrating extent of agreement between *piaB* and *lytA* in **(A)** minimally processed and **(B)** culture-enriched saliva samples and Bland–Altman plots (**C**,**D**, respectively) displaying extent of agreement and bias among samples with C_qs < 40 for *piaB* and *lytA*. Dots colored in red depict samples with C_qs < 40 for *piaB* and *lytA*, remaining samples are colored in blue. Black dashed lines in scatter plots indicate data-driven thresholds. In Bland–Altman plots black dashed lines indicate the upper (ULoA) and lower limit of agreement (LLoA) and mean difference (bias). Shaded areas indicate 95% confidence interval. The solid black line indicates the line of equality (no bias).

TABLE 1 Optimal qPCR cycle threshold C_q for corresponding method for *Streptococcus pneumoniae* carriage detection in $n = 971$ saliva samples from children ($n = 653$) and adults ($n = 318$) samples.

Method	Criterion*	Optimal threshold *piaB* (95% CI)	Youden index *piaB*	Sensitivity *piaB*	Specificity *piaB*	Optimal threshold *lytA* (95% CI)	Youden index *lytA*	Sensitivity *lytA*	Specificity *lytA*
Minimally processed saliva	Culture and <40 C_qs in sample	38.32 (37.17–38.60)	0.77	0.97	0.80	37.90 (37.09–38.70)	0.70	0.93	0.77
Culture-enriched saliva		37.01 (34.98–38.61)	0.68	0.97	0.72	35.73 (33.47–37.69)	0.61	0.94	0.67

Results from qPCR were validated in a receiver operating characteristic curve analysis based on isolation of viable pneumococcus from primary diagnostic culture or qPCR-guided culture and quantification of *piaB* and *lytA* in saliva. *A sample was considered positive when the following criterion has been fulfilled: (I) C_qs for both *piaB* and *lytA* were <40 in the saliva sample tested with qPCR and (II) viable *S. pneumoniae* was recovered from either primary diagnostic or qPCR-guided culture of nasopharyngeal or (in case of adults) oropharyngeal samples collected from the person.

of positive culture-enriched samples from children and adults, respectively. The frequency of multiple serotype carriage was significantly higher among saliva samples when compared with nasopharyngeal samples (McNemar's test, $P < 0.0001$, 22.7 vs. 9.3% or for saliva and nasopharyngeal samples, respectively). When evaluating the diagnostic accuracy of qPCR-based serotyping of culture-enriched saliva samples from children compared to nasopharyngeal cultures (Supplementary Table 6), testing saliva exhibited limited agreement with nasopharyngeal samples (Figure 4A). Using a composite study reference, testing of saliva samples exhibited increased sensitivity of detection when compared with nasopharyngeal cultures ($P < 0.001$) and increased agreement with the reference (Table 4). Among adults testing of saliva also exhibited limited agreement (Supplementary Table 7) to nasopharyngeal samples (Figure 4B). Saliva testing among adults was associated with significantly enhanced sensitivity of detected when compared to any other method ($P < 0.0001$, Figure 4B and Table 5).

Assessment of method's inter-laboratory reproducibility

In order to evaluate the reproducibility of qPCR-based detection in culture-enriched saliva, 229 culture-enriched saliva samples were processed as part of an inter-laboratory comparison

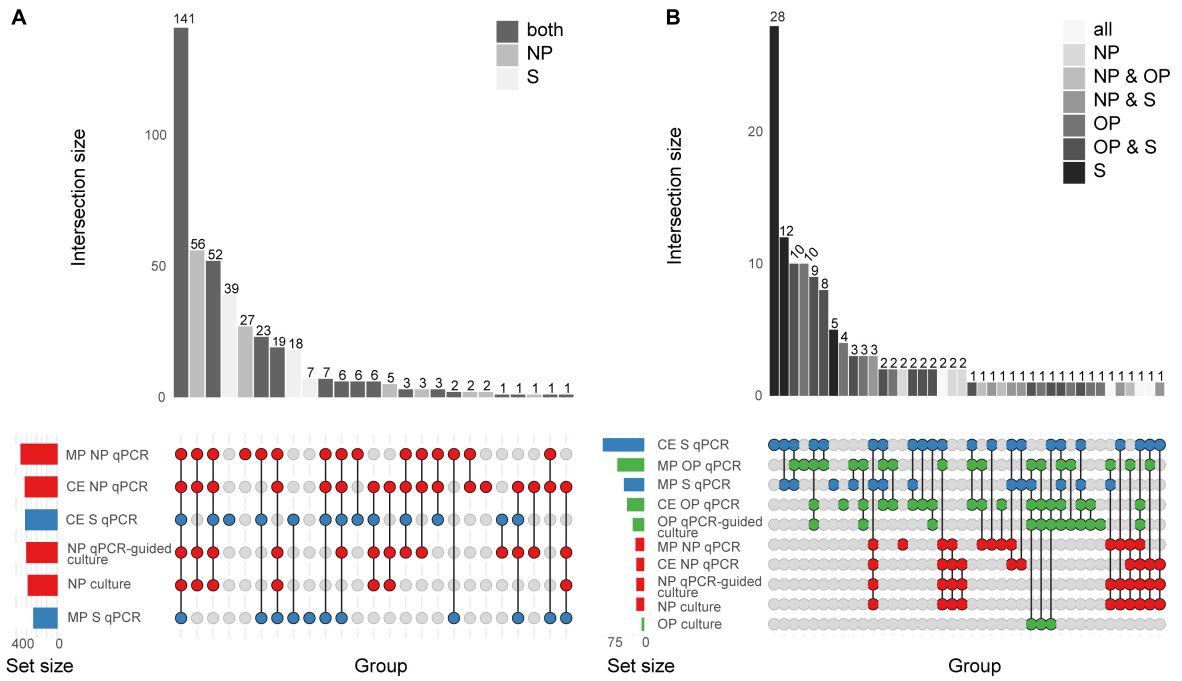

FIGURE 2
Quantitative PCR-based detection of *Streptococcus pneumoniae* among saliva and nasopharyngeal (NP) samples from **(A)** young children ($n = 653$) and **(B)** qPCR-based detection of *S. pneumoniae* among saliva (S), nasopharyngeal (NP), and oropharyngeal (OP) from adults ($n = 318$). The intersection bar diagrams display the total number of individuals positive per intersection. The matrix diagram displays intersection components (method or criterion). The set size bar diagram displays the total number of individuals positive per intersection component. Saliva, oropharyngeal, and nasopharyngeal samples are colored blue, green, and red, respectively, in the matrix diagram. "MP" stands for minimally processed, "CE" stands for culture-enrichment. "qPCR" stands for samples identified as positive for pneumococcus according with molecular method of qPCR and applying study criteria for positivity. "Culture" stands for isolation of viable *S. pneumoniae* from either primary diagnostic, or qPCR-guided culture.

TABLE 2 The accuracy of *Streptococcus pneumoniae* detection in paired nasopharyngeal and saliva samples from $n = 653$ children in the Netherlands tested using molecular methods applied to DNA extracted from minimally processed and culture-enriched samples and applying $^{ROCd}C_q$ thresholds for sample positivity in qPCRs.

Method	Reference	Percent (*n*) of positive samples (95% CI)	PPV % (95% CI)	NPV % (95% CI)	Sensitivity % (95% CI)	Specificity % (95% CI)	Concordance % (95% CI)	κ (95% CI)
Primary nasopharyngeal culture	Composite reference	42.9 (280) (39.1–46.7)	100 (98.6–100)	70.2 (65.4–74.7)	71.6 (66.9–75.9)	100 (98.6–100)	83.0 (79.9–85.7)	0.67 (0.61–0.73)
Minimally processed saliva		34.6 (226) (31.1–38.3)	95.6 (92.0–97.6)	59.0 (54.3–63.6)	55.2 (50.3–60.1)	96.2 (93.1–97.9)	71.7 (68.1–75.0)	0.47 (0.40–0.53)
Culture-enriched saliva		46.9 (306) (43.1–50.7)	100 (98.8–100)	75.5 (70.7–79.7)	78.3 (73.9–82.1)	100 (98.6–100)	87.0 (84.2–89.3)	0.74 (0.69–0.79)

Measures of diagnostic accuracy were calculated using a composite study reference consisting of positivity in either qPCR-based *S. pneumoniae* detection on culture-enriched saliva sample or based on isolation of live pneumococcus either from the primary diagnostic or qPCR-guided nasopharyngeal culture. PPV, positive predictive value; NPV, negative predictive value; 95% CI, 95% confidence interval; κ, Cohen's kappa where ≤0, 0.01–0.20, 0.21–0.40, 0.41–0.60, 0.61–0.80, and ≥0.81 are interpreted as no agreement, none to slight, fair, moderate, strong, and almost perfect agreement, respectively.

in both England and the Netherlands. We observed excellent quantitative agreement for *piaB* and *lytA* qPCRs between both laboratories, and near-perfect agreement in identifying culture-enriched saliva samples as positive for *S. pneumoniae* (κ 0.84, 95% CI 0.77–0.91). There was, however, reduced agreement between serotype/serogroup-specific assays (κ 0.40, 95% CI 0.28–0.52) that was driven by assays targeting serogroups 15A/B/C/F, 18A/B/C/F, and 33A/F/37 when performed in England. Exclusion of these assays resulted in substantial agreement between both laboratories (κ 0.68, 95% CI 0.58–0.77).

Discussion

In the current study we sought to compare *S. pneumoniae* detection methods and characterize the diagnostic accuracy of qPCR-based saliva testing for carriage surveillance and vaccine studies in children and in adults. Saliva testing was compared with results based on applying the same protocol in paired nasopharyngeal and oropharyngeal samples, and inter-laboratory reproducibility of the protocol was evaluated independently in the second laboratory. Molecular testing of culture-enriched saliva

TABLE 3 The accuracy of *Streptococcus pneumoniae* detection of serotypes in paired nasopharyngeal, oropharyngeal, and saliva samples from $n = 318$ adults in the Netherlands tested using molecular methods applied to DNA extracted from minimally processed and culture-enriched samples and applying $^{ROCd}C_q$ thresholds for sample positivity in qPCRs.

Method	Reference	Percent (*n*) of positive samples (95% CI)	PPV % (95% CI)	NPV % (95% CI)	Sensitivity % (95% CI)	Specificity % (95% CI)	Concordance % (95% CI)	κ (95% CI)
Primary nasopharyngeal culture	Composite reference	4.7 (15) (2.9–7.6)	100 (79.6–100)	70.3 (64.9–75.2)	14.3 (8.9–22.2)	100 (98.2–100)	71.7 (66.5–76.4)	0.18 (0.04–0.33)
Primary oropharyngeal culture		0.9 (3) (0.3–2.7)	100 (43.9–100)	67.6 (62.3–72.5)	2.9 (1.0–8.1)	100 (98.2–100)	67.9 (62.6–72.8)	0.04 (−0.12 to 0.19)
Either primary nasopharyngeal or primary oropharyngeal culture		5.7 (18) (3.6–8.8)	100 (82.4–100)	71.0 (65.6–75.8)	17.1 (11.1–25.5)	100 (98.2–100)	72.6 (67.5–77.2)	0.22 (0.08–0.36)
Minimally processed saliva		13.5 (43) (10.2–17.7)	81.4 (67.4–90.3)	74.5 (69.1–79.3)	33.3 (25.0–42.8)	96.2 (92.8–98.1)	75.5 (70.5–79.9)	0.35 (0.22–0.47)
Culture-enriched saliva		28.6 (91) (23.9–33.8)	100 (95.9–100)	93.8 (89.9–96.3)	86.7 (78.9–91.9)	100 (98.2–100)	95.6 (92.7–97.4)	0.90 (0.84–0.95)

Measures of diagnostic accuracy were calculated using a composite study reference consisting of positivity in either qPCR-based *S. pneumoniae* detection on culture-enriched saliva sample or based on isolation of live pneumococcus either from the primary diagnostic or qPCR-guided nasopharyngeal or oropharyngeal culture. PPV, positive predictive value; NPV, negative predictive value; 95% CI, 95% confidence interval; κ, Cohen's kappa where ≤0, 0.01–0.20, 0.21–0.40, 0.41–0.60, 0.61–0.80, and ≥0.81 are interpreted as no agreement, none to slight, fair, moderate, strong, and almost perfect agreement, respectively.

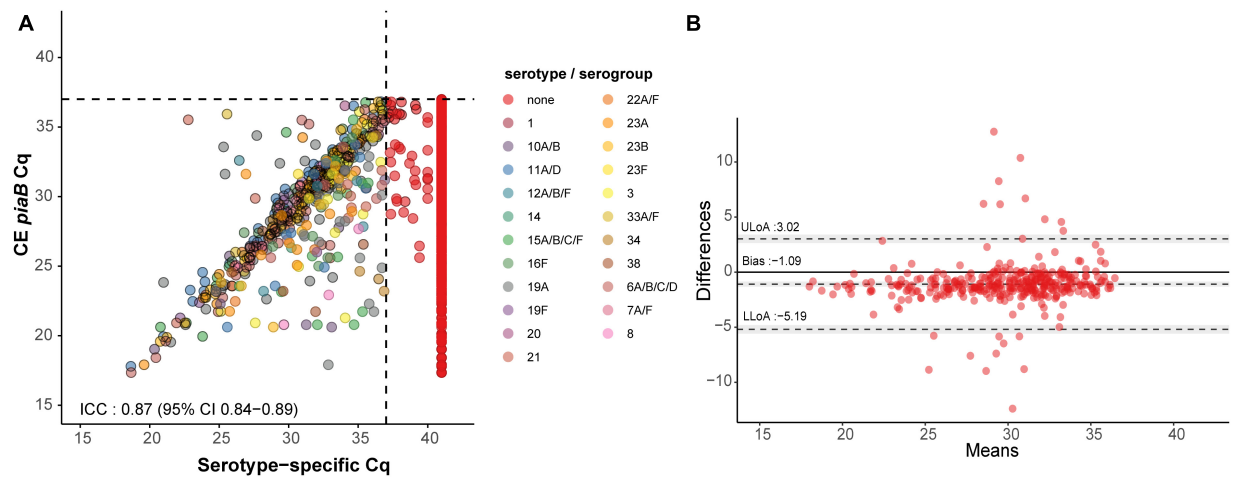

FIGURE 3
Scatter plot **(A)** illustrating extent of agreement between *piaB* and serotype/serogroup-specific detection among culture-enriched saliva samples ($n = 353$) and Bland–Altman plot **(B)** displaying extent of agreement and bias among samples with C_qs < $^{ROCd}C_q$ for *piaB* and serotype/serogroup-specific qPCR assays. In panel **(A)**, saliva samples are colored by serotype/serogroup-specific signal detected. Samples classified as negative for any of the tested serotype/serogroup-specific qPCR assays are colored in red. Black dashed lines indicate data-driven $^{ROCd}C_q$ thresholds. In panel **(B)** (Bland–Altman plot) the degree of agreement between *piaB* and *lytA* C_q measurements among positive samples is shown. The mean difference in measurements is indicated by a dashed gray line and the standard deviations of the mean, upper limit of agreement (ULoA) and lower limit of agreement (LLoA) are also shown. Shaded areas indicate the 95% confidence interval. The solid black line indicates the line of equality (no bias) and dots above this line are for samples of which *lytA* C_qs where lower than *piaB* C_qs. ICC values <0.50, 0.50–0.75, 0.75–0.90, and ≥0.90 are indicative of poor, moderate, good, and quantitative agreement, respectively.

samples improves the sensitivity of surveillance of pneumococcal carriage in children and adults, but there are also certain limitations of qPCR-based approaches for pneumococcal serotypes carriage detection to be considered. The protocol we propose enhances the specificity of molecular methods for the detection of live pneumococcus in highly polymicrobial samples.

Detection of pneumococcus by qPCR exhibited excellent quantitative agreement between *piaB* and *lytA* C_qs in MP and culture-enriched saliva, demonstrating that reliable detection of pneumococcus in saliva is feasible. To further improve the specificity of qPCR-based detection of live pneumococci, we applied ROC-derived C_q cut-offs using nasopharyngeal and oropharyngeal cultures (for adults) as criterion as previously described (Miellet et al., 2022). The application of culture-enrichment, and ROC-derived C_q cut-offs reduced the frequency of qPCR positive samples which were attributable to quantification of relic DNA. This notion was confirmed by a comparison of qPCR quantification in paired MP and culture-enriched saliva samples. A comparison with a composite study reference indicated that testing of culture-enriched saliva samples enhances the sensitivity

TABLE 4 The accuracy of *Streptococcus pneumoniae* serotypes detection in paired nasopharyngeal and saliva samples from $n = 653$ children in the Netherlands tested using molecular methods applied to DNA extracted from minimally processed and culture-enriched samples and applying $^{ROCd}C_q$ thresholds for sample positivity in qPCRs.

Method	Reference	PPV % (95% CI)	NPV % (95% CI)	Sensitivity % (95% CI)	Specificity % (95% CI)	Concordance % (95% CI)	κ (95% CI)
Nasopharyngeal culture	Serotype composite reference	100 (98.4–100)	73.5 (69.0–77.5)	68.4 (63.3–73.1)	100 (98.8–100)	83.2 (80.1–85.8)	0.67 (0.61–0.73)
Culture-enriched NP qPCR		100 (98.5–100)	77.6 (73.2–81.5)	74.7 (69.9–79.0)	100 (98.8–100)	86.5 (83.7–88.9)	0.73 (0.68–0.79)
Culture-enriched saliva qPCR		100 (98.6–100)	80.5 (76.2–84.2)	78.7 (74.1–82.7)	100 (98.8–100)	88.7 (86.0–90.9)	0.78 (0.73–0.82)

Measures of diagnostic accuracy were calculated using a composite study reference consisting of number of samples in which the dominant serotype detected with either qPCR-based serotyping in culture-enriched nasopharyngeal or saliva sample or based on isolation of live pneumococcus from primary diagnostic nasopharyngeal culture. All serotypes detected by culture are considered dominant serotypes. PPV, positive predictive value; NPV, negative predictive value; 95% CI, 95% confidence interval; κ, Cohen's kappa where ≤0, 0.01–0.20, 0.21–0.40, 0.41–0.60, 0.61–0.80, and ≥0.81 are interpreted as no agreement, none to slight, fair, moderate, strong, and almost perfect agreement, respectively.

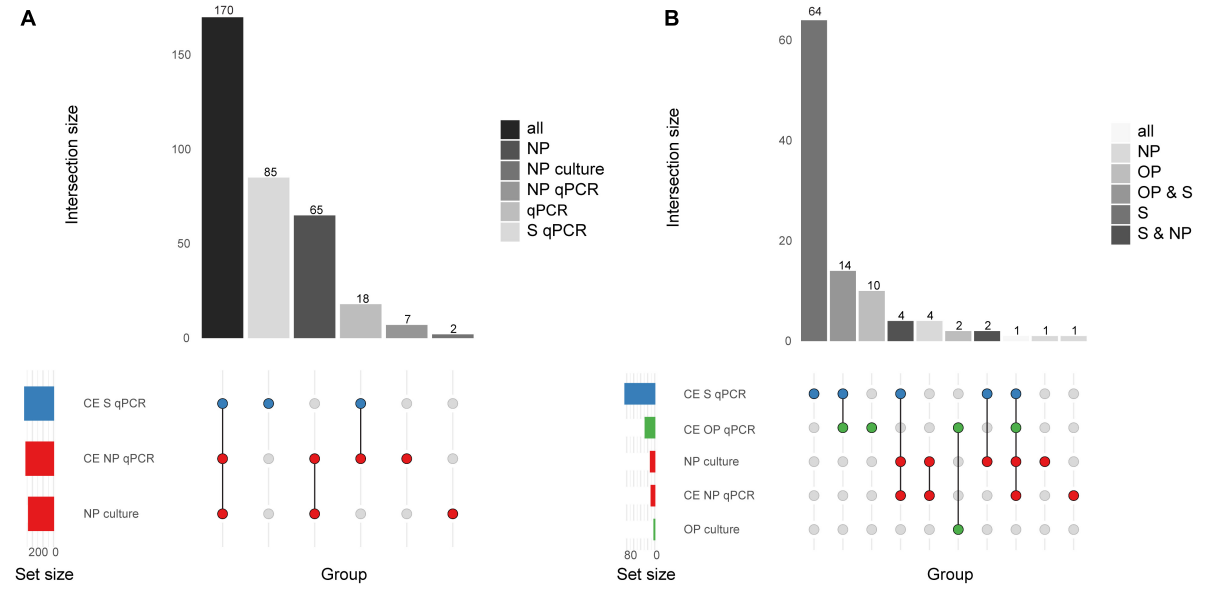

FIGURE 4
Quantitative PCR-based serotyping *Streptococcus pneumoniae* positive saliva (S) and nasopharyngeal (NP) samples from **(A)** young children ($n = 653$) and **(B)** qPCR-based serotyping of *S. pneumoniae* positive saliva, nasopharyngeal, oropharyngeal (OP) samples from adults ($n = 318$). The intersection bar diagrams display the total number of individuals positive per intersection. The matrix diagram displays intersection components (method or criterion). The set size bar diagram displays the total number of individuals positive per intersection component. Saliva, oropharyngeal, and nasopharyngeal samples are colored blue, green, and red, respectively, in the matrix diagram.

of *S. pneumoniae* detection when compared with conventional culture and nasopharyngeal sample testing. Notably, qPCR-based serotyping of saliva samples demonstrated superior sensitivity when compared with Quellung and resulted in significantly higher observed rates of multiple serotype carriage. However, we have also confirmed several constraints of the current qPCR-based approach for detection of certain serotypes due to the presence of the targeted sequences among non-pneumococcal bacterial species present in the saliva.

Adult pneumococcal carriers are seldom positive for *S. pneumoniae* in nasopharyngeal samples and are often exclusively positive for *S. pneumoniae* in oral samples. This discrepancy between nasopharyngeal and oral samples among adults was first noted Webster and Hughes (1931), and has also been observed in contemporary pneumococcal carriage studies (Trzcinski et al., 2013; Wyllie et al., 2016a; Miellet et al., 2022; Wrobel-Pawelczyk et al., 2022). Accordingly, testing of multiple sampling sites can improve the accuracy of carriage detection (Trzcinski et al., 2013; Krone et al., 2015; Wyllie et al., 2016a; Almeida et al., 2020, 2021; Miellet et al., 2022; Wrobel-Pawelczyk et al., 2022). However, contemporary carriage studies have repeatedly shown that conventional culture displays insufficient sensitivity when coupled with oral samples (Trzcinski et al., 2013; Krone et al., 2015; Wyllie et al., 2016a; Miellet et al., 2022; Wrobel-Pawelczyk et al., 2022), such as oropharyngeal swabs, as low pneumococcal abundance and commensal bacterial flora in oral samples can obscure pneumococcal presence with culture-based methods.

These limitations of conventional culture can be addressed with qPCR-based methods. We have previously evaluated qPCR-based nasopharyngeal sample testing and observed near-perfect agreement between qPCR and conventional culture

TABLE 5 The accuracy of *Streptococcus pneumoniae* serotypes detection in paired nasopharyngeal and saliva samples from $n = 318$ adults in the Netherlands tested using molecular methods applied to DNA extracted from culture-enriched samples and applying $^{ROCd}C_q$ thresholds for sample positivity in qPCRs.

Method	Reference	PPV % (95% CI)	NPV % (95% CI)	Sensitivity % (95% CI)	Specificity % (95% CI)	Concordance % (95% CI)	κ (95% CI)
NP culture	Serotype composite reference	100 (75.8–100)	70.6 (65.3–75.4)	11.8 (6.9–19.4)	100 (98.3–100)	71.7 (66.5–76.4)	0.15 (0.01–0.30)
OP culture		100 (34.2–100)	68.4 (63.0–73.2)	2.0 (0.5–6.9)	100 (98.3–100)	68.6 (63.3–73.4)	0.03 (−0.13 to 0.18)
Culture-enriched NP qPCR		100 (72.2–100)	70.1 (64.8–75.0)	9.8 (5.4–17.1)	100 (98.3–100)	71.1 (65.9–75.8)	0.13 (−0.02 to 0.28)
Culture-enriched OP qPCR		100 (87.5–100)	74.2 (68.9–78.9)	26.5 (18.9–35.8)	100 (98.3–100)	76.4 (71.5–80.7)	0.33 (0.20–0.46)
Culture-enriched saliva qPCR		100 (95.6–100)	92.3 (88.2–95.1)	82.4 (73.8–88.5)	100 (98.3–100)	94.3 (91.2–96.4)	0.86 (0.80–0.92)

Measures of diagnostic accuracy were calculated using a composite study reference consisting of samples in which the dominant serotype detected with either qPCR-based serotyping in culture-enriched nasopharyngeal, oropharyngeal or saliva sample, or based on isolation of live pneumococcus from primary diagnostic nasopharyngeal or oropharyngeal culture. All serotypes detected by culture are considered dominant serotypes. PPV, positive predictive value; NPV, negative predictive value; 95% CI, 95% confidence interval; NP, nasopharyngeal; OP, oropharyngeal; κ, Cohen's kappa where ≤0, 0.01–0.20, 0.21–0.40, 0.41–0.60, 0.61–0.80, and ≥0.81 are interpreted as no agreement, none to slight, fair, moderate, strong, and almost perfect agreement, respectively.

(Miellet et al., 2022). We also noted that complementing primary culture with qPCR-guided culturing can greatly increase the number of adults from whom live pneumococci are recovered (Trzcinski et al., 2013; Wyllie et al., 2016a; Miellet et al., 2022). Unlike conventional culture, qPCR-based methods are highly suited to oral samples. In line with previous studies (Wyllie et al., 2014; Krone et al., 2015; Miellet et al., 2020), culture-enrichment of saliva significantly enhanced the sensitivity of detection. When qPCR detection was applied to culture-enriched instead of MP saliva samples the number of child and adult carriers identified increased by 41 and 111%, respectively. It underlines the importance of testing oral samples for sensitive surveillance of pneumococcal carriage among adults (Miellet et al., 2023).

Testing of saliva samples increased the number of carriers identified among children and adults, highlighting the benefits of testing multiple sampling sites. These observations confirm previous findings (Wyllie et al., 2014; Krone et al., 2015) and mirror pneumococcal prevalence rates from the early 20th century (Webster and Hughes, 1931; Heffron, 1939). When using a composite reference to accommodate the aforementioned observations, saliva testing exhibited high diagnostic accuracy when culture-enrichment was conducted prior to qPCR-based detection. When compared with the gold standard method, qPCR applied to culture-enriched saliva samples displayed significantly enhanced sensitivity of detection for both children and adults. Application of molecular methods to saliva samples allows us to capture an image of the *S. pneumoniae* carriage that mirrors the accuracy of nasopharyngeal sample testing in children and is superior in adults (Miellet et al., 2023). However, 19 and 37% of pneumococci detected by qPCR were unique to nasopharyngeal cultures and culture-enriched saliva samples, respectively. It implies that a negative nasopharyngeal sample does not necessarily preclude a positive saliva sample, and vice versa. As such, careful interpretation of carriage detection results is important (Miellet et al., 2023).

Prior to qPCR-based serotyping of individual samples, we evaluated the specificity of the method with pooled negative samples. The analysis indicated that qPCR assays for serotypes 4, 5, and 17F, and serogroups 9A/L/N/V, 12A/B, and 35B/C exhibited insufficient specificity in saliva samples. This was further confirmed by testing samples positive for *S. pneumoniae*, in which the signals for pneumococcus and for serotype were also discordant. In addition, Bland–Altman analysis indicated reduced specificity of assays targeting serotypes 21, 23A and serogroup 33A/F/37 in saliva. However, since there was concordance between serotype-specific quantification and *piaB* or *lytA* quantification, results for these assays were still considered reliable. After testing positive culture-enriched saliva samples with serotype-specific qPCRs, 37% of samples were positive for one or more serotypes in saliva. When compared with conventional culture but not qPCR-based nasopharyngeal sample testing, qPCR-based serotyping of saliva samples displayed superior sensitivity among both children and adults. Overall, we argue that application of molecular methods captures a reliable image of pneumococcal serotypes carriage (Miellet et al., 2023).

An important part of our study was an interlaboratory assessment of qPCR-based detection and serotyping of a subset of samples conducted in two laboratories. For detection of *S. pneumoniae* in culture-enriched saliva samples we observed near-perfect agreement between results generated in both centers. This is in line with results for nasopharyngeal and oropharyngeal samples from the same study (Miellet et al., 2022). However, with qPCR-based serotyping of culture-enriched saliva samples we observed limited agreement between results from England and the Netherlands. Reproducibility was affected by poor performance of certain assays and due to overrepresentation of weakly positive results which we attribute to minor differences between the two qPCR systems in the two laboratories. These results stress the importance of intra-laboratory controls, for instance by comparing concordance between *piaB* and serotype. Furthermore, these results also highlight the need for further multicenter validation of the protocol.

Several qPCR-based serotyping assays were observed to be unreliable in saliva samples, illustrating limitations of the method

when applied to highly polymicrobial samples. Most importantly, qPCR assays targeting vaccine serotypes 4, 5, and 9V can be misinterpreted to represent circulation of VT *S. pneumoniae* in vaccinated children. However, we previously reported that assays targeting serotypes 4 and 5 were also unreliable in nasopharyngeal samples (Miellet et al., 2022), hence, this limitation of the qPCR is not unique to saliva alone. Similarly, increased richness of oral samples could impact the specificity of *lytA* and *piaB* qPCR assays. Whereas a number of studies report on *lytA* presence in non-pneumococcal streptococci (Kilian and Tettelin, 2019; Tavares et al., 2019; Gonzales-Siles et al., 2020), Tavares et al. is the only published study we are aware of to report on *piaB* detection in non-pneumococcal streptococcal strains. Importantly, neither of the two non-pneumococcal *Streptococcus* sp. strains reported by Tavares et al. (2019), to carry *piaB* (out of $n = 433$ tested), was positive for *lytA* gene. Consequently, although *lytA* and *piaB* can be simultaneously present in samples negative for *S. pneumoniae*, concordant quantification of both genes would be extremely rare. Of note, *piaB* is described by Gonzales-Siles et al. (2020) as *fepD* and by Kilian and Tettelin (2019) as SP_1033 and in both studies it is identified as one of only several genes unique to *S. pneumoniae*.

The study itself has certain limitations. First, the panel of serotype-specific and serogroup-specific qPCR did not cover all known one hundred and one pneumococcal serotypes. However, the serotypes not targeted by qPCR are rare in the Netherlands both in carriage and in IPD (Vissers et al., 2018). Secondly, with several qPCR assays targeting the serogroup rather than individual serotypes, we were not able to discern the serotype. This limitation might be of particular importance for groups that include both vaccine and non-vaccine serotypes.

Collectively, the study shows that testing of culture-enriched saliva samples improves the sensitivity of overall surveillance of pneumococcal carriage in children and adults. By ensuring the specificity of qPCR-based testing with a dual-target (or "Two-To-Tango") approach and data-driven C_q thresholds, and evaluation of quantitative measurements with Bland–Altman analysis, pneumococcal detection in saliva mirrors the sensitivity of the gold standard in children. Moreover, qPCR-based serotyping in saliva samples from children outperforms the diagnostic accuracy of nasopharyngeal sample testing. Among adults, qPCR-based testing of oral samples provides high diagnostic accuracy unlike nasopharyngeal samples. These results demonstrate the importance of testing oral samples for sensitive surveillance of pneumococcal carriage. Finally, our results illustrate the limitations of the current gold standard method and emphasize the necessity of qPCR-based approaches for pneumococcal carriage detection.

Data availability statement

The raw data supporting the conclusions of this article will be made available by the authors, without undue reservation.

Ethics statement

The studies involving human participants were reviewed and approved by the Medical Ethics Committee Noord Holland. Written informed consent to participate in this study was provided by the participants' legal guardian/next of kin.

Author contributions

ES and KT had an idea and initiated the study. EM, NF, ES, and KT conceptualized the study. TB, NR, EM, NF, ES, and KT secured the financial support. KT led the project. AW-M, NR, and MH conducted the carriage study, collected the data, and provided the study materials. WM, JV, and KT developed and validated laboratory methods, wrote the laboratory protocol, and performed the formal analysis of study data. WM, JV, DL, RM, TN, RT, and SE analyzed the samples and collected the data. WM, RM, and KT contributed to the analytical tools. WM, JV, TN, RT, SE, and DL curated the data. WM, DL, RM, AW-M, TB, NF, and KT managed the study. WM and KT visualized the presentation of the results and drafted the manuscript. All authors amended, critically reviewed, and commented on the final manuscript.

Funding

Funding for this study was provided to UMCU and UKHSA by GlaxoSmithKline Biologicals SA. GlaxoSmithKline Biologicals SA was provided the opportunity to review a preliminary version of this manuscript for factual accuracy. EM received support from the National Institute for Health Research (NIHR) Health Protection Research Unit in Immunisation at the London School of Hygiene and Tropical Medicine in partnership with UK Health Security Agency (Grant Reference NIHR200929). Other authors received no financial support or other form of compensation related to the development of the manuscript.

Conflict of interest

UKHSA provides vaccine manufacturers (GSK, Pfizer, and Sanofi) with post-marketing surveillance reports on pneumococcal infection which the companies are required to submit to the UK licensing authority in compliance with their Risk Management Strategy. A cost recovery charge is made for these reports. UKHSA has received unrestricted research grants from Pfizer to participate in pneumococcal surveillance projects. KT received funds for an unrestricted research grant from GlaxoSmithKline Biologicals SA, consultation fees, fees for participation in advisory boards, speaking fees and funds for unrestricted research grants from Pfizer, funds for an unrestricted research grant and fees for participating in advisory boards from Merck Sharp & Dohme, all paid directly to

his home institution. Except for the funds from GlaxoSmithKline Biologicals SA none was received in the relation to the work reported here.

The remaining authors declare that the research was conducted in the absence of any commercial or financial relationships that could be construed as a potential conflict of interest.

Publisher's note

Author disclaimer

The authors are solely responsible for final content and interpretation of this manuscript.

Supplementary material

The Supplementary Material for this article can be found online at: https://www.frontiersin.org/articles/10.3389/fmicb.2023.1156695/full#supplementary-material

References

Almeida, S., Paulo, A., Froes, F., de Lencastre, H., and Sa-Leao, R. (2021). Dynamics of pneumococcal carriage in adults: A new look at an old paradigm. *J. Infect. Dis.* 223, 1590–1600. doi: 10.1093/infdis/jiaa558

Almeida, S., Pedro, T., Paulo, A., de Lencastre, H., and Sa-Leao, R. (2020). Re-evaluation of *Streptococcus pneumoniae* carriage in Portuguese elderly by qPCR increases carriage estimates and unveils an expanded pool of serotypes. *Sci. Rep.* 10:8373. doi: 10.1038/s41598-020-65399-x

Altman, D., and Bland, J. (2003). Interaction revisited: The difference between two estimates. *BMJ* 326:219. doi: 10.1136/bmj.326.7382.219

Auranen, K., Rinta-Kokko, H., Goldblatt, D., Nohynek, H., O'Brien, K., Satzke, C., et al. (2013). Colonisation endpoints in *Streptococcus pneumoniae* vaccine trials. *Vaccine* 32, 153–158. doi: 10.1016/j.vaccine.2013.08.061

Azzari, C., Moriondo, M., Cortimiglia, M., Valleriani, C., Canessa, C., Indolfi, G., et al. (2012). Potential serotype coverage of three pneumococcal conjugate vaccines against invasive pneumococcal infection in Italian children. *Vaccine* 30, 2701–2705. doi: 10.1016/j.vaccine.2011.12.008

Azzari, C., Moriondo, M., Indolfi, G., Cortimiglia, M., Canessa, C., Becciolini, L., et al. (2010). Realtime PCR is more sensitive than multiplex PCR for diagnosis and serotyping in children with culture negative pneumococcal invasive disease. *PLoS One* 5:e9282. doi: 10.1371/journal.pone.0009282

Bland, J., and Altman, D. (1986). Statistical methods for assessing agreement between two methods of clinical measurement. *Lancet* 1, 307–310. doi: 10.1016/S0140-6736(86)90837-8

Boelsen, L., Dunne, E., Gould, K., Ratu, F., Vidal, J., Russell, F., et al. (2020). The challenges of using oropharyngeal samples to measure pneumococcal carriage in adults. *mSphere* 5, e00478–20. doi: 10.1128/mSphere.00478-20

Bogaert, D., De Groot, R., and Hermans, P. (2004a). *Streptococcus pneumoniae* colonisation: The key to pneumococcal disease. *Lancet Infect. Dis.* 4, 144–154. doi: 10.1016/S1473-3099(04)00938-7

Bogaert, D., van Belkum, A., Sluijter, M., Luijendijk, A., de Groot, R., Rümke, H., et al. (2004b). Colonisation by *Streptococcus pneumoniae* and *Staphylococcus aureus* in healthy children. *Lancet* 363, 1871–1872. doi: 10.1016/S0140-6736(04)16357-5

Branche, A., Yang, H., Java, J., Holden-Wiltse, J., Topham, D., Peasley, M., et al. (2018). Effect of prior vaccination on carriage rates of *Streptococcus pneumoniae* in older adults: A longitudinal surveillance study. *Vaccine* 36, 4304–4310. doi: 10.1016/j.vaccine.2018.05.107

Carvalho, M. G., Bigogo, G., Junghae, M., Pimenta, F., Moura, I., Roundtree, A., et al. (2012). Potential nonpneumococcal confounding of PCR-based determination of serotype in carriage. *J. Clin. Microbiol.* 50, 3146–3147. doi: 10.1128/JCM.01505-12

Carvalho, M. G., Pimenta, F., Moura, I., Roundtree, A., Gertz, R. Jr., Li, Z., et al. (2013). Non-pneumococcal mitis-group streptococci confound detection of pneumococcal capsular serotype-specific loci in upper respiratory tract. *PeerJ* 1:e97. doi: 10.7717/peerj.97

Carvalho, M. G., Tondella, M., McCaustland, K., Weidlich, L., McGee, L., Mayer, L., et al. (2007). Evaluation and improvement of real-time PCR assays targeting lytA, ply, and psaA genes for detection of pneumococcal DNA. *J. Clin. Microbiol.* 45, 2460–2466. doi: 10.1128/JCM.02498-06

Dagan, R., Muallem, M., Melamed, R., Leroy, O., and Yagupsky, P. (1997). Reduction of pneumococcal nasopharyngeal carriage in early infancy after immunization with tetravalent pneumococcal vaccines conjugated to either tetanus toxoid or diphtheria toxoid. *Pediatr. Infect. Dis. J.* 16, 1060–1064. doi: 10.1097/00006454-199711000-00011

Flasche, S., Van Hoek, A., Sheasby, E., Waight, P., Andrews, N., Sheppard, C., et al. (2011). Effect of pneumococcal conjugate vaccination on serotype-specific carriage and invasive disease in England: A cross-sectional study. *PLoS Med.* 8:e1001017. doi: 10.1371/journal.pmed.1001017

Gonzales-Siles, L., Karlsson, R., Schmidt, P., Salvà-Serra, F., Jaén-Luchoro, D., Skovbjerg, S., et al. (2020). A pangenome approach for discerning species-unique gene markers for identifications of *Streptococcus pneumoniae* and *Streptococcus pseudopneumoniae*. *Front. Cell. Infect. Microbiol.* 10:222. doi: 10.3389/fcimb.2020.00222

Heffron, R. (1939). *Pneumonia; with special reference to pneumococcus lobar pneumonia*. Oxford: Oxford University Press.

Huebner, R., Dagan, R., Porath, N., Wasas, A., and Klugman, K. (2000). Lack of utility of serotyping multiple colonies for detection of simultaneous nasopharyngeal carriage of different pneumococcal serotypes. *Pediatr. Infect. Dis. J.* 19, 1017–1020. doi: 10.1097/00006454-200010000-00019

Jansen, A., Rodenburg, G., de Greeff, S., Hak, E., Veenhoven, R., Spanjaard, L., et al. (2009). Invasive pneumococcal disease in the Netherlands: Syndromes, outcome and potential vaccine benefits. *Vaccine* 27, 2394–2401. doi: 10.1016/j.vaccine.2009.01.127

Kilian, M., and Tettelin, H. (2019). Identification of virulence-associated properties by comparative genome analysis of *Streptococcus pneumoniae*, *S. pseudopneumoniae*, *S. mitis*, Three *S. oralis* Subspecies, and *S. infantis*. *mBio* 10, e01985–19. doi: 10.1128/mBio.02520-19

Koo, T., and Li, M. Y. (2016). Guideline of selecting and reporting intraclass correlation coefficients for reliability research. *J. Chiropr. Med.* 15, 155–163. doi: 10.1016/j.jcm.2016.02.012

Krone, C., van de Groep, K., Trzcinski, K., Sanders, E., and Bogaert, D. (2014). Immunosenescence and pneumococcal disease: An imbalance in host-pathogen interactions. *Lancet Respir. Med.* 2, 141–153. doi: 10.1016/S2213-2600(13)70165-6

Krone, C., Wyllie, A., van Beek, J., Rots, N., Oja, A., Chu, M., et al. (2015). Carriage of *Streptococcus pneumoniae* in aged adults with influenza-like-illness. *PLoS One* 10:e0119875. doi: 10.1371/journal.pone.0119875

Landis, J., and Koch, G. (1977). The measurement of observer agreement for categorical data. *Biometrics* 33, 159–174. doi: 10.2307/2529310

Lewnard, J., and Hanage, W. (2019). Making sense of differences in pneumococcal serotype replacement. *Lancet Infect. Dis.* 19, e213–e220. doi: 10.1016/S1473-3099(18)30660-1

McHugh, M. (2012). Interrater reliability: The kappa statistic. *Biochem. Med.* 22, 276–282. doi: 10.11613/BM.2012.031

Miellet, W., Almeida, S., Trzciński, K., and Sá-Leão, R. (2023). *Streptococcus pneumoniae* carriage studies in adults: Importance, challenges, and key issues to consider when using quantitative PCR-based approaches. *Front. Microbiol.* 14:1122276. doi: 10.3389/fmicb.2023.1122276

Miellet, W., van Veldhuizen, J., Litt, D., Mariman, R., Wijmenga-Monsuur, A., Badoux, P., et al. (2022). It takes two to tango: Combining conventional culture with molecular diagnostics enhances accuracy of *Streptococcus pneumoniae* detection and pneumococcal serogroup/serotype determination in carriage. *Front. Microbiol.* 13:859736. doi: 10.3389/fmicb.2022.859736

Miellet, W., van Veldhuizen, J., Nicolaie, M., Mariman, R., Bootsma, H., Bosch, T., et al. (2020). Influenza-like illness exacerbates pneumococcal carriage in older adults. *Clin. Infect. Dis.* 73, e2680–e2689. doi: 10.1093/cid/ciaa1551

Naaktgeboren, C., Bertens, L., van Smeden, M., de Groot, J., Moons, K., and Reitsma, J. (2013). Value of composite reference standards in diagnostic research. *BMJ* 347:f5605.

Nutz, S., Doll, K., and Karlovsky, P. (2011). Determination of the LOQ in real-time PCR by receiver operating characteristic curve analysis: Application to qPCR assays for *Fusarium verticillioides* and *F. proliferatum*. *Anal. Bioanal. Chem.* 401, 717–726. doi: 10.1007/s00216-011-5089-x

O'Brien, K., Wolfson, L., Watt, J., Henkle, E., Deloria-Knoll, M., McCall, N., et al. (2009). Burden of disease caused by *Streptococcus pneumoniae* in children younger than 5 years: Global estimates. *Lancet* 374, 893–902. doi: 10.1016/S0140-6736(09)61204-6

Pasteur, L. (1881). Note sur la maladie nouvelle provoquée par la salive d'un enfant mort de la rage. *Bull. Acad. Med.* 10, 94–103.

Pimenta, F., Roundtree, A., Soysal, A., Bakir, M., du Plessis, M., Wolter, N., et al. (2013). Sequential triplex real-time PCR assay for detecting 21 pneumococcal capsular serotypes that account for a high global disease burden. *J. Clin. Microbiol.* 51, 647–652. doi: 10.1128/JCM.02927-12

Ranganathan, P., Pramesh, C., and Aggarwal, R. (2017). Common pitfalls in statistical analysis: Measures of agreement. *Perspect. Clin. Res.* 8, 187–191.

Satzke, C., Turner, P., Virolainen-Julkunen, A., Adrian, P., Antonio, M., Hare, K., et al. (2013). Standard method for detecting upper respiratory carriage of *Streptococcus pneumoniae*: Updated recommendations from the world health organization pneumococcal carriage working group. *Vaccine* 32, 165–179. doi: 10.1016/j.vaccine.2013.08.062

Sternberg, G. (1881). *A fatal form of septicaemia in the rabbit produced by the subcutaneous injection of human saliva: An experimental research*. Kentish Town: John Murphy & Company.

Tavares, D., Handem, S., Carvalho, R., Cristina Paulo, A., de Lencastre, H., Hinds, J., et al. (2019). Identification of *Streptococcus pneumoniae* by a real-time PCR assay targeting SP2020. *Sci. Rep.* 9:3285. doi: 10.1038/s41598-019-39791-1

Trzcinski, K., Bogaert, D., Wyllie, A., Chu, M. L. J. N., van der Ende, A., Bruin, J. P., et al. (2013). Superiority of trans-oral over trans-nasal sampling in detecting *Streptococcus pneumoniae* colonization in adults. *PLoS One* 8:e60520. doi: 10.1371/journal.pone.0060520

van der Linden, M., Imohl, M., and Perniciaro, S. (2019). Limited indirect effects of an infant pneumococcal vaccination program in an aging population. *PLoS One* 14:e0220453. doi: 10.1371/journal.pone.0220453

van Gils, E., Veenhoven, R., Hak, E., Rodenburg, G., Bogaert, D., Ijzerman, E., et al. (2009). Effect of reduced-dose schedules with 7-valent pneumococcal conjugate vaccine on nasopharyngeal pneumococcal carriage in children: A randomized controlled trial. *JAMA* 302, 159–167.

Velusamy, S., Tran, T., Mongkolrattanothai, T., Walker, H., McGee, L., and Beall, B. (2020). Expanded sequential quadriplex real-time polymerase chain reaction (PCR) for identifying pneumococcal serotypes, penicillin susceptibility, and resistance markers. *Diagn. Microbiol. Infect. Dis.* 97:115037. doi: 10.1016/j.diagmicrobio.2020.115037

Vissers, M., Wijmenga-Monsuur, A., Knol, M., Badoux, P., van Houten, M., van der Ende, A., et al. (2018). Increased carriage of non-vaccine serotypes with low invasive disease potential four years after switching to the 10-valent pneumococcal conjugate vaccine in The Netherlands. *PLoS One* 13:e0194823. doi: 10.1371/journal.pone.0194823

Watt, J., O'Brien, K., Katz, S., Bronsdon, M., Elliott, J., Dallas, J., et al. (2004). Nasopharyngeal versus oropharyngeal sampling for detection of pneumococcal carriage in adults. *J. Clin. Microbiol.* 42, 4974–4976.

Webster, L., and Hughes, T. (1931). The epidemiology of pneumococcus infection: The incidence and spread of pneumococci in the nasal passages and throats of healthy persons. *J. Exp. Med.* 53, 535–552. doi: 10.1084/jem.53.4.535

Welte, T., Torres, A., and Nathwani, D. (2012). Clinical and economic burden of community-acquired pneumonia among adults in Europe. *Thorax* 67, 71–79.

Whitney, C., Farley, M., Hadler, J., Harrison, L., Bennett, N., Lynfield, R., et al. (2003). Decline in invasive pneumococcal disease after the introduction of protein-polysaccharide conjugate vaccine. *N. Engl. J. Med.* 348, 1737–1746.

World Health Organization [WHO] (2007). Pneumococcal conjugate vaccine for childhood immunization–WHO position paper. *Wkly. Epidemiol. Rec.* 82, 93–104.

World Health Organization [WHO] (2019). Pneumococcal conjugate vaccines in infants and children under 5 years of age: WHO position paper. *Wkly. Epidemiol. Rec.* 94, 85–103.

Wrobel-Pawelczyk, I., Ronkiewicz, P., Wanke-Rytt, M., Rykowska, D., Górska-Kot, A., Włodkowska, A., et al. (2022). Pneumococcal carriage in unvaccinated children at the time of vaccine implementation into the national immunization program in Poland. *Sci. Rep.* 12:5858. doi: 10.1038/s41598-022-09488-z

Wyllie, A. L., Rumke, L. W., Arp, K., Bosch, A. A. T. M., Bruin, J. P., Rots, N. Y., et al. (2016a). Molecular surveillance on *Streptococcus pneumoniae* carriage in non-elderly adults; little evidence for pneumococcal circulation independent from the reservoir in children. *Sci. Rep.* 6:34888. doi: 10.1038/srep34888

Wyllie, A. L., Wijmenga-Monsuur , A. J., van Houten, M. A., Bosch, A. A., Groot, J. A., van Engelsdorp Gastelaars, J., et al. (2016b). Molecular surveillance of nasopharyngeal carriage of *Streptococcus pneumoniae* in children vaccinated with conjugated polysaccharide pneumococcal vaccines. *Sci. Rep.* 6:23809. doi: 10.1038/srep23809

Wyllie, A., Chu, M., Schellens, M., van Engelsdorp Gastelaars, J., Jansen, M., van der Ende, A., et al. (2014). *Streptococcus pneumoniae* in saliva of Dutch primary school children. *PLoS One* 9:e102045. doi: 10.1371/journal.pone.0102045

Wyllie, A., Pannekoek, Y., Bovenkerk, S., van Engelsdorp Gastelaars, J., Ferwerda, B., van de Beek, D., et al. (2017). Sequencing of the variable region of rpsB to discriminate between *Streptococcus pneumoniae* and other streptococcal species. *Open Biol.* 7:170074. doi: 10.1098/rsob.170074

frontiers | Frontiers in Microbiology

TYPE Original Research
PUBLISHED 27 April 2023
DOI 10.3389/fmicb.2023.1146322

OPEN ACCESS

EDITED BY
Ons Bouchami,
Universidade Nova de Lisboa, Portugal

REVIEWED BY
Alina Fudulu,
Stefan S. Nicolau Institute of Virology, Romania
Taro Ikegami,
University of the Ryukyus, Japan

*CORRESPONDENCE
Tipaya Ekalaksananan
✉ tipeka@kku.ac.th

RECEIVED 17 January 2023
ACCEPTED 31 March 2023
PUBLISHED 27 April 2023

CITATION
Burassakarn A, Pientong C, Tongchai P, Wongjampa W, Poosari A, Udomsin A, Sa-ngiamwibool P, Ungareewittaya P, Nutravong T and Ekalaksananan T (2023) Epidemiological evidence and association of human papillomavirus with esophageal cancer in northeastern Thailand: a case–control study. *Front. Microbiol.* 14:1146322. doi: 10.3389/fmicb.2023.1146322

Epidemiological evidence and association of human papillomavirus with esophageal cancer in northeastern Thailand: a case–control study

Ati Burassakarn[1,2], Chamsai Pientong[1,2], Panwad Tongchai[2], Weerayut Wongjampa[1,2], Arisara Poosari[1], Apiradee Udomsin[3], Prakasit Sa-ngiamwibool[4], Piti Ungareewittaya[4], Thitima Nutravong[1] and Tipaya Ekalaksananan[1,2]*

[1]Department of Microbiology, Faculty of Medicine, Khon Kaen University, Khon Kaen, Thailand, [2]HPV & EBV and Carcinogenesis Research (HEC) Group, Khon Kaen University, Khon Kaen, Thailand, [3]Ward Medic Ltd., Part., Bangkok, Thailand, [4]Department of Pathology, Faculty of Medicine, Khon Kaen University, Khon Kaen, Thailand

Recently, epidemiological evidence of high-risk human papillomavirus (hrHPV) and its association with the increasing risk of esophageal cancer (EC) have been described. However, the involvement of such a virus in the pathogenesis of EC is still inconclusive in the literature. Therefore, our objective was to clarify the epidemiology of HPV infections in primarily diagnosed EC cases and validate this correlation with hospital-based control patients using a retrospective study with a case–control model. Here, we reported that the overall prevalence of HPV DNA was statistically associated with an increased risk of EC (OR, 3.3; 95% CI, 2.5–4.3). Interestingly, a history of gastroesophageal reflux disease (GERD) was constituted and significantly associated with HPV prevalence (adjusted OR, 4.6; 95% CI, 2.2–9.5). Furthermore, our meta-analysis in public databases also indicated that the combined OR and 95% CI between HPV infection and EC risk were 3.31 and 2.53–4.34, respectively, with significant heterogeneity (I_2=78%). Variations in the geographic study, tissue type, and detection method remain potential predictors of heterogeneity. In addition, publication bias and sensitivity analysis were not observed, and the results exhibited stable outcomes. Collectively, we specify the recent epidemiological evidence in a validation of the distributed HPV, which might be statistically associated with an increased risk of EC. However, additional high-quality studies with larger sample sizes are needed to further verify the link between HPV and EC.

KEYWORDS

human papillomaviruses, esophageal neoplasms, Thailand, epidemiological characteristics, meta-analysis

1. Introduction

Esophageal cancer (EC) is the tenth most common cancer worldwide with a poor prognosis in clinical practice (Allemani et al., 2018). According to the report by the IARC, 3.1% accounts for new cases (604,100 cases of all cancers), and 5.5% accounts for impermanence (544,076 deaths in total) in 2020 (Sung et al., 2021). Based on the principle of microscopic pathology, EC

can be classified into two main histologic subtypes: adenocarcinoma (EAC, 12%) and squamous cell carcinoma (ESCC, 88%; Arnold et al., 2015). It has well-defined distinctive geographical patterns and risk factors for these diseases. Although EAC is associated with Barrett's esophagus, smoking, tobacco use, a history of gastro-esophageal reflux disease (GERD), and obesity, ESCC has been associated with alcohol consumption and smoking. In general, almost 80% of the total cases occur in the regions of developing countries (El-Serag et al., 2014; Rustgi and El-Serag, 2014; Coleman et al., 2018; Morgan et al., 2022). However, EAC has commonly been found in developed counties—particularly in Westerners due to changes in risk factor contours in these circumstances (Rumgay et al., 2021).

Human papillomaviruses (HPVs) are a type of ubiquitous double-stranded circular DNA with non-enveloped, small viruses that have been classified as the family, *Papillomaviridae*. Currently, more than 150 HPV genotypes have been identified and categorized into cutaneous and mucosal subgroups. It is well known that mucosal HPV types, specifically HPV16, 18, 31, and 33, are also recognized as high-risk HPV (hrHPV) and are the causative agents of several types of cancer in humans (Gheit, 2019). Of these, HPV16 is the most potent oncogenic genotype of the hrHPVs subgroup, according to previous epidemiologic studies (Tsikouras et al., 2016; Petrelli et al., 2021). In addition to the cancer of the genital tract (i.e., cervix, vagina, vulva, anus, and penis) and a subset of head and neck carcinomas (HNSCCs), particularly oropharyngeal cancers (OPSCCs), the pieces of evidence for the association between hrHPV infection and the increasing risk of esophageal cancers (ECs) have recently been described (Rajendra et al., 2020). In the early 1980s, the hypothesis of HPV-linked genital tract lesions and ESCC was first introduced by Syrjanen et al. (1982). The works from a pioneer group showed that the average frequency of HPVs was 29.0% (range: 15%–78%) and found the distinct prevalence of any HPV type in ESCCs (Syrjänen, 2002), while the studies using the larger scale case–control model suggested that the range rate of HPV infection was between 0% and 100% (Ludmir et al., 2015). These reports also indicated that HPV prevalence was reasonably elevated in high-burden regions of the world's EC (Petrelli et al., 2021). For example, the HPV infection rate (32.8%–63.6%) in EC cases from countries with extraordinary rates of overall EC incidence, particularly Northern China and Iran, was significantly higher than in countries with a lower incidence of EC. On the contrary, a lower percentage of HPV-infected EC was observed in regions with lower EC incidence such as Europe (15.6%) and the United States (16.6%; Hardefeldt et al., 2014). Furthermore, Rajendra et al. (2013) also exhibited the first strong evidence for the relationship between transcriptionally active hrHPV and EAC. Interestingly, a positive trend correlation between HPV16 and ESCCs as well as HPV18 and EACs was also presented by these epidemiological reports (Petrelli et al., 2021; Li et al., 2022). However, the true prevalence and contribution of HPV in EC remain to be passionately deliberated, conferring the partially unknown and capricious findings among several studies from various geographical settings (Kunzmann et al., 2017; Hošnjak and Poljak, 2018).

Esophageal cancer (EC) is one of leading cancers in Thailand (ranked 16th). Based on world ASR per 100,000, the incidence and mortality of this malignancy in Thailand were 2.9 and 2.7, respectively (Sung et al., 2021). It appears to be a considerable clinical and public health issue in Thailand. Despite well-known environmental factors, infectious agents have also affected more than one-quarter of the considerable cancer nationwide. Moreover, Thailand is situated in the high-risk flight path of esophageal cancer in Southeast Asia, where patients often do not describe the viral-related risk factors, reflecting the limitation of identified causative agents (Sunpaweravong, 2010). Even though the potentially pivotal role of HPVs, particularly high-risk types involved in the biological consequence and malignant transformation of the esophageal mucosa have been suggested and reported by the former pieces of evidence (Kunzmann et al., 2017; Hošnjak and Poljak, 2018). However, an association between HPV infection and the risk of esophageal neoplasms is not conclusive in the accumulated literature. Regarding the meta-analyzed findings, HPV infection could be an etiology that plays an important role in esophageal carcinogenesis, especially in the squamous cell carcinoma (SCC) subtype in some regions, indicating the variation in its geographical incidence, which was affected by exposure to dietary, cultural, environmental, and any specific factors. Therefore, these findings have led us to not make any decisive statements about the association between HPV infection and esophageal malignancies compared to other types of cancer, particularly oropharyngeal cancer. To this end, in this study, our objective was to highlight the frequency of HPV infections in the primary diagnosis of EC cases and validate this correlation with hospitalized control patients using a retrospective study model, accompanied by meta-analyses of published information in public databases. Corroborating this information might amend our comprehension of HPVs status in EC and provide some pieces of HPV-associated EC evidence for clinical management, improving disease outcome and prognosis.

2. Materials and methods

2.1. Ethics statement

This study was registered and approved by the Ethics Committee of the Khon Kaen University for Human Research (Reference no. HE621269). Informed consent was obtained from all volunteers who were participants in this study.

2.2. Study site

Based on the prevalence of EC cases in Thailand (Cancer in Thailand, 2022), this study was carried out at Srinagarind Hospital, a university medical teaching hospital, Faculty of Medicine, Khon Kaen University, Khon Kaen, Thailand (16°28′6″N 102°49′48″ E).

2.3. Study design and research participants

According to our previous study (Poosari et al., 2021, 2022), we dependably conducted a retrospective study with a total of 105 sample volunteers in each patient case who was diagnosed primarily with EC and the control calibrator from hospital subjects. All cases with multiple primary-diagnosed malignancies or other cancer origins, or those with a history of cancer treatment, were excluded. The healthy dependents who endured the examination of their physical body and clinical manifestation without a history

of gastric or esophageal malignancy by the hospital physician during the period of case recruitment were registered in this study as the calibrated control group. Clinico-epidemiological characteristic information on each subject including sex, age, physical height, body weight, smoking status and frequency, alcohol consumption, history of GERD, oral hygiene practices, and a family history of cancer was achieved by the structured interview questionnaire.

2.4. Tissue sample collections and processing

Formalin-fixed paraffin-embedded (FFPE) tissue samples of both EC patients and control were retrospectively retrieved from the Department of Pathology, Faculty of Medicine, Khon Kaen University, between 2015 and 2018. Based on the guidance from the International Classification of Diseases in Oncology, 3rd edition (ICD-O-3; codes: C15.3-C16.0; Fritz et al., 2013), the samples were histologically reviewed and confirmed by two independent pathologists using a histopathological report and a standard hematoxylin–eosin (H&E) staining technique (H&E), respectively. Before a step of HPV detection, 5 µm of thick serial sections were cut from each FFPE sample and placed in a sterile microcentrifuge. The tube can be stored at room temperature until used.

2.5. Determination of HPV infection using the HPV direct flow CHIP technique

As previously described by Herraez-Hernandez et al. (2013), HPV detection and genotyping in the FFPE tissue sample were carried out using the HPV Direct Flow CHIP system. In brief, the mixture of 60 µL Lysis Buffer (Master Diagnóstica, Granada, Spain) and 1.5 µL of DNA Release (Master Diagnóstica, Granada, Spain) was used to digest the three serially sectioned tissues at 60°C for 30 min, followed by inactivation at 98°C for 10 min. The extracts were then collected. In total, 4 µL of the extracts were added to a 36 µL PCR mix supplied kit (Master Diagnóstica, Granada, Spain). The product was amplified by a T 100™ Thermal Cycler (Bio-Rad, Hercules, CA, United States) using the cycling conditions at 25°C for 10 min; 94°C for 3 min; 15 cycles of denaturation at 94°C for 30 s, annealing at 42°C for 30 s, and elongation at 72°C for 30 s; 35 cycles of denaturation at 94°C for 30 s, annealing at 60°C for 30 s, and elongation at 72°C for 30 s; and final elongation at 72°C for 5 min. The PCR products were stored at −20°C until use.

For detection and genotyping, the biotinylated amplicons were first denatured at 95°C for 5 min, followed by cooling in an ice bath for 2 min. The hybridization was carried out in sets of 12 samples using the hybridSpot 12 (HS12) platforms (Master Diagnóstica, Granada, Spain), according to the manufacturer. The DNA target is primarily crossed and binds to HPV CHIP membranes containing immobilized complementary probes that are specified in the beta-globin gene, consensus, and genotype-specific sequences of HPV. The colorimetric assessment was achieved by applying NBT-BCIP substrates that detect alkaline phosphatase activity, developing insoluble purple precipitates.

2.6. Analysis of risk factors and hrHPV responsiveness in EC

The basic information on gender, age, and the well-known risk factors of EC, including status and frequency of smoking, alcohol consumption, GERD history, and a family history of cancer, was selected and analyzed. The posed data of these demographic characteristics and risk factors might be associated with infections of hrHPV. Furthermore, the answers of all participants seem to reflect their level of knowledge and overall attitudes toward the correlation between EC and potential environmental risk factors. In this study, each participant directly answered or read all the questions by trained personnel.

2.7. Systematic review and meta-analysis of HPV-associated esophageal malignancies

The depth and evenness of the existence of HPV in EC imply a hypothetically vital role for HPV infection in the oncogenesis of esophagus origin. Therefore, we conducted a meta-analysis to assess the association between them.

2.7.1. Strategy for searching the pieces of literature

The four main public databases including PubMed, SCOPUS, Excerpta Medica database (EMBASE), and Cochrane Library were restricted in English until 31 September 2022 using the combination of medical subject headings (MeSH; "esophageal neoplasms") OR the following keywords in [All Fields] of ("esophagus" AND "cancer") OR ("esophageal cancer") OR ("esophagus" AND "neoplasm") OR ("ESCC") OR ("EC") AND ("human papillomavirus") OR ("HPV"; Petrelli et al., 2021; Geng et al., 2022). In addition, the reference lists from previous systematic reviews and recovered articles were also checked.

2.7.2. Selection of the retrieved articles

The reports had to meet the following criteria to be included: (1) the studies that assessed the infection of HPV in tissue samples from healthy participants (control group) and eventually compared them with the histologically approved EC with at least 10 cases, (2) the studies with inline a case–control model were eligible, (3) any place, race, sex, age, and cancer stage was no limitation. Patients with cancer treatments were not eligible for this analysis, (4) the articles provided sufficient data to observe and/or calculate odds ratio (OR) and relative risk (RR), with a 95% confidence interval (95% CI), and (5) the most recent reports on the same population included a larger number of participants. Furthermore, studies that were implemented with preclinical models (i.e., *in vitro* or animal studies) or other types of publication including case reports, personal opinions, conference abstracts, letters, book chapters, and reviews were excluded. The notion of data overlap or duplicate articles was also not eligible for extraction and quality assessments.

2.8. Extraction and quality assessments of the retrieved data

To characterize potentially eligible reports, a recent study was conducted according to the Preferred Reporting Items for Systematic

Reviews and Meta-Analysis (PRISMA) guidelines (Page et al., 2020). Titles, abstracts, and the following information from the full main text of the retrieved articles were obtained: first author, year of publication, studied location/country, design of study model, sample number, demographic characterization of the participants, adjusted variables (i.e., confounding factors), and risk estimates (e.g., OR, RR with 95% CI) were independently investigated and assessed by three reviewers (AB, PT, and WW) accompanied with the pre-delineated criteria. The discrepancies or inconclusive results were consulted and resolved by the fourth reviewer (AP). Furthermore, the bias risk of all included studies was separately validated by the three reviewers using the Newcastle–Ottawa Scale (NOS) guidelines (Wells et al., 2014). Of these, 9 points are the maximum NOS score, and the high-quality articles had to be considered as scored 6 (Wells et al., 2014; Geng et al., 2022). All analyses were performed on previously published articles; thus, both ethical documents and the consent forms of the patients were not mandatory.

2.9. Statistical analysis

For our case–control study, descriptive statistics were used to synopsize the demographic characteristics of the participants. The categorical records and the continuous data were represented in frequencies and percentages and the numbers by mean ± standard deviation (SD), median, and minimum and maximum ranges, respectively. Bivariate analysis was performed using simple logistic regression to verify the association between EC and potential independent risk factors. While the crude odds ratio (OR_c) with 95% CI was calculated for the bivariate analysis with uncontrolled confounders, the adjusted odds ratio (OR_{adj}) with 95% CI was estimated by multivariate unconditional logistic regression for the controlling confounders (OR_c; $p < 0.25$ with EC association; Poosari et al., 2021). The backward stepwise elimination strategy was used to construct the simple and interpretable regression model. Consequently, the goodness-of-fit of the final model was evaluated by a likelihood ratio test. All HPV detection experiments were carried out in triplicate. The two-tailed test analyzed the statistical results, and a p-value of <0.05 was considered statistically significant. This analysis was performed using SPSS software version 14.0 (SPSS Inc., Chicago, IL, United States) and GraphPad Prism version 8.0 (GraphPad Software, Inc., San Diego, CA, United States).

For the meta-analysis, the pooled odds ratios (ORs) with the corresponding 95% CI were calculated from the total of EC cases and controls. Forest plots were visually constructed to determine the study's pooled effects and specificity. Using Cochran's Q test, the I statistic was performed to evaluate heterogeneity as low ($I_2 > 25\%$), moderate ($I_2 > 50\%$), and high ($I_2 > 75\%$) levels in the retrieved reports. Further analysis of heterogeneity was performed leave-one-out with a random effect model when significant articles ($p < 0.01$ or $I_2 > 50\%$) were observed (Higgins and Thompson, 2002; Higgins et al., 2003). Or else, the fixed effect model was subsequently applied (DerSimonian and Laird, 1986). After omitting heterogeneous studies, the sensitivity analysis was conducted, accompanied by the stigmatization of the new value of the OR. The possible potential effects on heterogeneity were determined by subgroup analyses based on crucial study traits including study sites, number of samples, detection methods/markers, and others. To assess the impacts of the aforementioned factors on the association between HPV infection and EC risk, the meta-regression analysis was also then applied. The potential bias of publication was examined by Begg's and Egger's tests (Begg and Mazumdar, 1994; Egger et al., 1997). Visual inspection of the asymmetry of a funnel plot was constructed to consider bias. All analyses of the statistics were performed with the Review Manager (RevMan) software version 5.4.1.,[1] SPSS software version 14.0 (SPSS Inc., Chicago, IL, United States), and GraphPad Prism version 8.0 (GraphPad Software, Inc., San Diego, CA, United States). If there is no specific mention, the statistical results were analyzed with the two-sided test, and a p-value of <0.05 was considered statistically significant.

3. Results

3.1. Clinico-demographic characteristics of patient cases and control participants

To determine the association between HPV infections and increased risk of ECs, we conducted a recent study in a case–control-dependent manner. A total of 100 EC patients and 105 hospital-based volunteers (control) group were enrolled. Of the total cases, the median age of the EC patients at diagnosis was 59.5 years (range, 38–78 years old), and male patients (64.0%) had a higher prevalence of EC than those of female (36%) patients. This group's most common histopathological diagnosis was squamous cell carcinoma (SCC; 72.0%) and tissue grading with poor differentiation (66.0%). Stage IV (66.0%) of the TNM classification was the highest frequency in registered patients. Interestingly, the difference in lifestyle behaviors between cases and controls was statistically observed. Cases had a higher prevalence of smoking (72.0% vs. 26.7%) and alcohol consumption (78.0% vs. 41.0%) than controls. Moreover, the cases also significantly diverged from the controls in a history of gastroesophageal reflux disease (GERD; 79.0% vs. 37.1%) and a family history of cancer (FHC; 73.0% vs. 41.9%). The presence of HPV DNA was subsequently found in a total of 45 (45.0%) EC cases, while 23 (21.9%) paradigms of the controls were correspondingly achieved for such viral DNA. These demographic characteristics of all participants are described in Table 1.

3.2. Frequency and distribution of HPV DNA in biological tissue samples

Although the association between HPV infection and EC risk has been postulated, the viral contribution to the pathogenesis of EC is partially unknown and capricious in the literature. To this end, the detection of HPV was subsequently performed using the HPV Direct Flow CHIP, targeting the viral genome. DNA from tissue specimens of all patient cases and control subjects was available for testing as it exhibited β-globin-positive results (Table 2). Of the 72 samples of ESCC, 32 cases (44.4%) were labeled HPV DNA-positive. Additionally, our detection illustrated a total of 11 HPV-positive paradigms (39.3%) of the 28 types of EAC tissue. On the contrary,

1 https://training.cochrane.org/online-learning/core-software/revman/revman-5-download

TABLE 1 Clinico-demographic profile of esophageal cancer patients and control participants.

Characteristics	Cases	Control	*p*-value[a]
	N =100; *n* (%)	*N* =105; *n* (%)	
Gender			
Male	64 (64.0)	51 (48.6)	0.026
Female	36 (36.0)	54 (51.4)	
Median of participant's age; year (range)	59.5 (38–78)	54 (2–86)	0.005[b]
Smoking status			
No	28 (28.0)	77 (73.3)	<0.001
Yes	72 (72.0)	28 (26.7)	
Alcohol consumption			
No	22 (22.0)	62 (59.0)	<0.001
Yes	78 (78.0)	43 (41.0)	
History of gastroesophageal reflux disease (GERD)			
No	21 (21.0)	66 (62.9)	<0.001
Yes	79 (79.0)	39 (37.1)	
Family history of cancers (FHC)			
No	27 (27.0)	61 (58.1)	<0.001
Yes	73 (73.0)	44 (41.9)	
Histopathological diagnosis			
Squamous cell carcinoma (ESCC)	72 (72.0)	–	ND
Adenocarcinoma (EAC)	28 (28.0)	–	
Histopathological grade			
Poor differentiation	66 (66.0)	–	ND
Moderate or Well differentiation	30 (30.0)	–	
Indetermination	4 (4.0)	–	
TNM stage			
Stage I, II	9 (9.0)	–	ND
Stage III	24 (24.0)	–	
Stage IV	66 (66.0)	–	
HPV detection			
Negative	55 (55.0)	82 (78.1)	<0.001
Positive	45 (45.0)	23 (21.9)	

ND, not determined the differences in *p*-values.
[a]*p*-values derived from the Chi-square test.
[b]The Kruskal–Wallis test was applied to determine the differences in *p*-values between cases and controls.

we also accounted for the viral DNA in 23 of 105 (21.9%) of the control group (Table 2; Figure 1). Fascinatingly, the presence of HPV DNA was statistically associated with an increased risk of total EC cases (OR_c, 2.9; 95% CI, 1.6–5.4; $p < 0.001$) and ESCC subtypes (OR_c, 3.2; 95% CI, 1.2–6.1; $p < 0.001$). However, our result revealed that there was no statistical difference in the association between the existing viral DNA and the EAC (OR_c, 2.3; 95% CI, 0.9–5.6; $p < 0.0651$; Table 2). Similarly, of the positive samples, HPV16 (51.0%) was the most common genotype found in ESCC, while HPV18 (49.2%) was the highest positive rate in EAC. However, HPV58 was also found in both subtypes of EC with the highest positive rate (approximately 10%–14%), as illustrated in Figure 2. Taken together, recent information suggested that the contribution of HPV infection could particularly be HPV16, HPV18, and HPV58 to the increased risk of ECs.

3.3. HPV infection could be an independent risk factor for EC

It is well known that the pieces of evidence for the involvement of various living behavior-related (environmental) factors and/or intrinsic factors on EC pathogenesis have been suggested (Morgan et al., 2022). Therefore, we consequently hypothesized whether these potential factors might be related to the risk of EC, together with HPV infection. Of those factors, a total of six potential risks, including age, gender, the status of smoking, alcohol consumption, history of GERD, and FHC, were acknowledged in the current study. Our univariate logistic analysis indicated that smoking (OR_c, 7.1; 95% CI, 3.8–13.1; $p < 0.001$), alcohol consumption (OR_c, 5.1; 95% CI, 2.8–9.4; $p < 0.001$), history of GERD (OR_c, 6.4; 95% CI, 3.4–11.9; $p < 0.001$), and FHC (OR_c, 3.7; 95% CI, 2.1–6.7; $p < 0.001$) were statistically associated with an increased risk of EC, synergizing with HPV infection (Table 3). Regardless of the promised risk factors, only smoking cases (OR_{adj}, 4.2; 95% CI, 1.8–9.8; $p < 0.001$) and patients who had a history of GERD (OR_{adj}, 4.6; 95% CI, 2.2–9.5; $p < 0.001$) were statistically dependently correlated with HPV infection (OR_{adj}, 3.7; 95% CI, 1.7–7.8; $p < 0.001$), in the EC risk context by the analysis of multivariate logistic regression (Table 3). However, our evaluations have shown that smoking (OR_{adj}, 1.2; 95% CI, 0.5–2.8; $p = 0.749$) was not statistically associated with HPV infection in patients with EC (Table 4). Compared with patients with a history of GERD, the frequency of HPV DNA was fashionably decreasing and was not statistically associated with HPV infection (OR_{adj}, 0.9; 95% CI, 0.3–2.3; $p < 0.747$; Table 4). Collectively, our contemporary evidence implied that infection with HPV could be an independent risk factor for ECs, supporting the etiologically viral agent of such disease.

3.4. The frequency of HPV DNA steadily increased in the EC tissue samples throughout the time collection

It has been reported that the occurrence of EC related to HPV infection is a favorable upward trend in the whole world, including Southeast Asia (Morgan et al., 2022). Then, we retrieved the frequency and temporal trend of HPV infection in EC tissue samples by assessing the presence of viral DNA over the collected year. The inclusive frequency of HPV-related ECs was 45.0% (Table 1). During the collection period, we observed favorable upward trends in HPV-attributable DNA frequency rates in registered EC tissue samples. The annual percentage of HPV DNA-positive cases was 18.6% in 2015, 21.2% in 2016, 24.6% in 2017, and 35.6% in 2018 (Figure 3). Altogether, our analysis provided additional information for an increasing trend of HPV-related ECs over time.

TABLE 2 Occurrence and involvement of HPVs in esophageal cancer (EC) risk.

Clinical specimen			Human papillomaviruses (HPVs)		
Participant	Type of specimen[a]	No. of available specimens[b]	Prevalence *n*, (%)	OR_c (95% CI)	*p*-value
ESCC	Tissue	72	34 (44.4)	3.2 (1.2–6.1)	<0.001
EAC	Tissue	28	11 (39.3)	2.3 (0.9–5.6)	0.0651
Total		100	45 (45.0)	2.9 (1.6–5.4)	<0.001
Control	Tissue	105	23 (21.9)	1.0 (reference)	ND
Total		105	23 (21.9)	1.0 (reference)	ND

OR_c, crude odd ratio; CI, confidence interval; ND, not determined the differences in *p*-values; ESCC, squamous cell carcinoma; EAC, adenocarcinoma.
[a]Formalin-fixed paraffin-embedded tissue.
[b]β-globin positive.

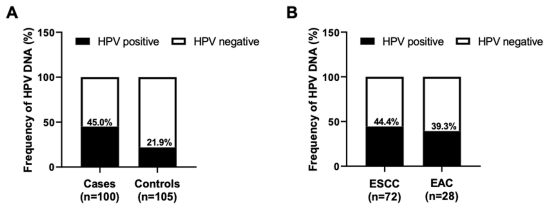

FIGURE 1
Frequency of HPV DNA in EC tissue samples. The column graph demonstrated the frequency of HPV DNA detected by the HPV Direct Flow CHIP technique in the FFPE specimens collected from EC cases and control subjects **(A)**. The infection rate of HPV in different histology subtypes of EC was also illustrated **(B)**.

3.5. Meta-analysis indicated infection with hrHPV might play a crucial role in ECs as an etiological agent

Although our recent results mentioned the association between HPV infection and the increasing risk of ECs, the evidence for this correlation is capricious in previous studies. Therefore, a recent meta-analysis was performed to clarify such a relation and verified our findings. When searching the four main public databases, a total of 51 case–control studies were selected as candidates in a recent meta-analysis (Supplementary Figure S1). Of such studies, 5,178 EC patient cases and 8,278 control participants were analyzed from 1995 to 2020. Among the registered reports, a total of 33 studies were held in the Asia continent, followed by seven from Europe, five from Africa, four from America, and two from Oceania. Interestingly, various techniques for HPV detection could be mentioned, including 34 studies that used PCR, 11 reports for antibodies (Ab), ELISA, *in situ* hybridization (ISH), and immunohistochemistry (IHC), one study for cytology, and five studies that used combination approaches. The type of biological specimens was also stated, consisting of 41 studies that collected formalin-fixed paraffin-embedded tissue (FFPE), seven reports for blood/plasma/serum, two studies for fresh frozen (FF) tissue /biopsies, and one exfoliated cell. The mean NOS score was 5.5 (Supplementary Table S1). Furthermore, the frequency of HPV DNA in ECs from enrolled studies was also described in the context of high or low EC risk (Supplementary Table S2). As shown in Figure 4, a total of 51 case–control studies were included and investigated the prevalence of HPV infection, including 5,178 EC patient cases and 8,278 control participants. The pooled prevalence of HPV in EC was 35.8% (1,855/5,178) while the rate of HPV infection was 21.9% (1,795/8,278) in the control arm. Using the random effect model ($I^2 = 78\%$; $p < 0.001$), the analytic result indicated that a significantly increased EC risk was associated with HPV infection (ORs, 3.3; 95% CI, 2.5–4.3; $p < 0.001$).

Since heterogeneity was observed in the result, we performed subgroup analyses and meta-regression on several main characteristics of registered studies, including geographic region, detection strategy, type of specimen, and risk of ECs in such countries. The presence of HPV DNA and the risk of ECs were positively correlated and consistently associated with all subgroups. Though some assessments were statistically significant, it was thought-provoking that the log ORs with 95% CIs for the relation between HPV infection and EC from different studied geographic regions were 1.29 (0.89–1.70) in Asia, 1.26 (0.27–2.24) in Europe, 0.50 (0.16–0.83) in Africa, 0.62 (−0.62–1.85) in America, and 1.32 (−1.04–3.67) in Oceania. Interestingly, we also perceived this association from the distinctive detection strategies that were 1.46 (1.14–1.77), 0.73 (0.01–1.44), and 0.83 (−1.61–3.27) in the detection of viral nucleic acid, viral protein, and combined markers, respectively, while we were unable to estimate the detection using the cytological assay. Furthermore, the log OR with 95% CI for the link between HPV infection and EC from different sample types was 1.41 (1.12–1.70) in the FFPE sample, 0.43 (−0.48–1.34) in the blood/plasma/serum sample, and 0.38 (−22.39–23.15) in the FF/biopsy sample, and not estimated in the sample obtained from exfoliated cells. Our analysis of this correlation from the variation in EC risk presented the log ORs with 95% CIs that were 1.22 (0.84–1.61) and 1.06 (0.48–1.63) in high EC risk countries and low EC risk countries, respectively. Additionally, the meta-regression unveiled that the characteristics of the enrolled studies did not significantly affect the analytic results ($p > 0.05$), except for the type of biological samples ($p = 0.015$), and moderately rationalized the source of heterogeneity. Our analyses in all subgroups and meta-regression are illustrated in Table 5. Subsequently, the sensitivity of a recent meta-analysis (Egger's test, $p < 0.05$) and publication bias (Supplementary Figure S2) were monitored, which involved the

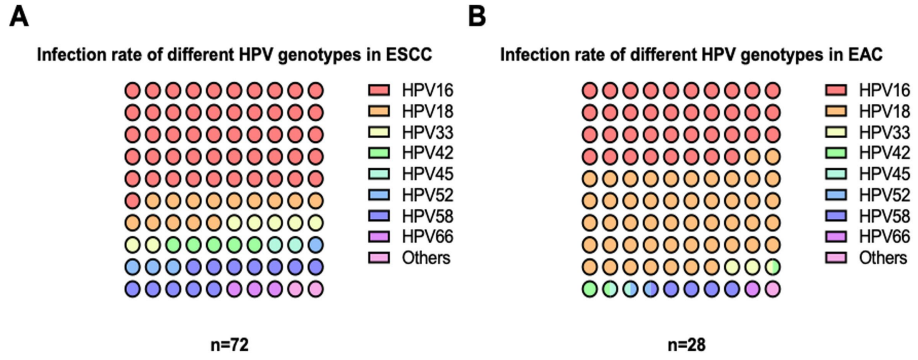

FIGURE 2
Distribution of HPV genotypes in EC tissues. The dissemination of circulated HPV genotypes in each EC subtype indicated that HPV16, HPV18, and HPV58 were the top three predominated genotypes in ESCC **(A)** and EAC **(B)**, respectively.

TABLE 3 The association between various clinicopathologic risk factors and ECs.

Characteristics	Cases	Control	OR_c (95% CI)	*p*-value	OR_{adj} (95% CI)	*p*-value[a]
	N =100; *n* (%)	*N* =105; *n* (%)				
Gender						
Male	64 (64.0)	51 (48.6)	1.9 (1.1–3.3)	0.0267	ND	ND
Female	36 (36.0)	54 (51.4)	1.0 (reference)			
Age						
≥60	50 (50.0)	38 (36.2)	1.7 (1.0–3.1)	0.047	ND	ND
<60	50 (50.0)	67 (63.8)	1.0 (reference)			
Smoking status						
Yes	72 (72.0)	28 (26.7)	7.1 (3.8–13.1)	<0.001	4.2 (1.8–9.8)	<0.001
No	28 (28.0)	77 (73.3)	1.0 (reference)		1.0 (reference)	
Alcohol consumption						
Yes	78 (78.0)	43 (41.0)	5.1 (2.8–9.4)	<0.001	1.2 (0.5–3.0)	0.619
No	22 (22.0)	62 (59.0)	1.0 (reference)		1.0 (reference)	
History of GERD						
Yes	79 (79.0)	39 (37.1)	6.4 (3.4–11.9)	<0.001	4.6 (2.2–9.5)	<0.001
No	21 (21.0)	66 (62.9)	1.0 (reference)		1.0 (reference)	
FHC						
Yes	73 (73.0)	44 (41.9)	3.7 (2.1–6.7)	<0.001	1.8 (0.9–3.6)	0.111
No	27 (27.0)	61 (58.1)	1.0 (reference)		1.0 (reference)	
HPVs detection						
Yes	45 (45.0)	23 (21.9)	2.9 (1.6–5.4)	<0.001	3.7 (1.7–7.8)	<0.001
No	55 (55.0)	82 (78.1)	1.0 (reference)		1.0 (reference)	

HPVs, human papillomaviruses; OR_c, crude odd ratio; OR_{adj}, adjusted odd ratio; CI, confidence interval; GERD, gastroesophageal reflux disease; FHC, Family history of cancers; ND, not determined.
[a]*p*-value was obtained from a multiple logistic regression model with all conditional adjusted variables.

existing risk of HPV infection in EC populations. By the leave-one-out analysis, we realized that the ORs were constantly steadily omitting any individual reports (data not shown), which statistically tested the dependability of the current meta-analysis. Taken together, our inquiries implied that HPV infection was evident in approximately 20% of totally different EC cases throughout the global studies.

3.6. HPV infection might not affect the prognosis of EC patients

To determine the involvement of HPV in the prognosis of EC, the association between HPV infection and the prognostic characteristics of EC patients was consequently performed. As shown in Table 6, $OR_{adj.}$ with 95% CI of the three potential risk

TABLE 4 The correlation of potential clinicopathologic findings and HPVs status in ECs.

Characteristics	ECs (N=100)		OR_{adj} (95% CI)	*p*-value[a]
	HPVs positive; *n* (%)	HPVs negative; *n* (%)		
Smoking status				
Yes	33 (73.3)	39 (70.9)	1.2 (0.5–2.8)	0.749
No	12 (26.7)	16 (29.1)	1.0 (reference)	
History of GERD				
Yes	35 (77.8)	44 (80.0)	0.9 (0.3 – 2.3)	0.747
No	10 (22.2)	11 (20.0)	1.0 (reference)	

HPVs, human papillomaviruses; OR_{adj}, adjusted odd ratio; CI, confidence interval; GERD, gastroesophageal reflux disease.
[a]*p*-value was obtained from a multiple logistic regression model with all conditional adjusted variables.

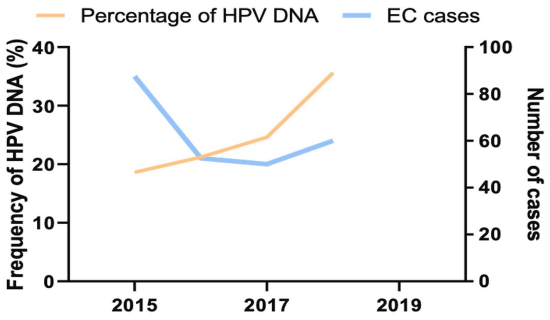

FIGURE 3
Prevalent trends for HPV-infected ECs in northeastern Thailand 2015–2018. The number of all HPV DNA-positive EC (orange) was indicated by the left y axis, while prevalent ECs (blue) were illustrated by the right y axis.

factors, including smoking, history of GERD, and HPV infection, showed a similar trend in the two different histopathological gradings (poor differentiation vs. moderate/well differentiation) of EC cases. In addition, in the analysis of the TNM stage, we observed favorable downward trends of these risk factors in the EC cases. Collectively, these results indicated that the status of HPV might not affect the survival of EC patients for better or worst prognosis context.

4. Discussions

Currently, the number of pieces of epidemiological evidence that indicated an association between hrHPV and the risk of EC has increased. However, the involvement of such a virus in EC pathogenesis is still debated. The variation in its geographical incidence, which was affected by exposure to dietary, cultural, and environmental factors, and any specific factors, is revealed to be one of the reasons that might be described as potential factors. To clarify the carcinogenic roles of hrHPV in EC pathogenesis, we, therefore, conducted a retrospective case–control study and meta-analyses of public databases to describe the relationship between hrHPV infection and the EC risk among Thai patients who lived in the northeastern part. As our hypothesis, the results indicated whether HPV infection, synergized with the history of GERD in patients, was statistically associated with an increased risk of EC, supporting that HPV may, together with the history of GERD, act as a significant etiological risk factor for EC.

Human papillomaviruses (HPVs) are double-stranded circular DNA with small, non-enveloped species-specific viruses, belonging to the *Papillomaviridae* family compartment. A total of 12 alpha-HPV genotypes from alpha-HPVs (e.g., HPV16, HPV18, and HPV33) are etiological agents of several types of cancer in humans, not only in the anogenital tract but also in a subset of the origin of the head and neck, particularly the oropharynx and oral cavity (Gheit, 2019). According to previous epidemiologic studies, infection with HPV16 and HPV18 was certified in most cases of cervical cancer, accounting for 50% and 20%, respectively (Garland, 2002; Wentzensen et al., 2009; de Sanjose et al., 2010). The malignancies that arose in the head and neck subgroups were mostly found in the base of the tongue, tonsils, and oropharynx (D'Souza et al., 2007; Gillison et al., 2012; Phusingha et al., 2017). The rate of HPV infection in oropharyngeal cancer was 11.5% for any viral genotype and 7.3% for hrHPV among men, while the prevalence of any type of HPV infection and high-risk type was 3.2% and 1.4%, respectively, among women (Sonawane et al., 2017). HPV16 is the most potent oncogenic genotype of the hrHPVs subgroup.

Infections with HPV have been implied as the oncogenic driver, implicated in the pathogenesis of ECs, particularly in ESCC by the accumulated evidence (Stoner and Gupta, 2001; Eslick, 2010; El-Zimaity et al., 2018). Recently, the correlated HPV16 and HPV18 genotypes were the most studied. However, the association between HPV infection and the increased risk of ECs has also been supposed unsettled. The previous larger scale study with go steady more than 5 years ago by using meta-data analysis indicated the range of HPV frequency between 0% and 100% with the rate of the difference in the HPV subtypes, concurring to the geographic region and the type of analytic study (Li et al., 2014; Petrick et al., 2014; Ludmir et al., 2015). As expected and consistent with previous reports, the Asian continent was the geographical area that found the highest prevalence of HPV-infected ECs. Of these, HPV16 showed the highest prevalence compared to HPV18 in the ESCC subtype. However, the report of the diverse population of both observational and case–control infection studies indicated that infections with HPV16 and HPV18 were more common in EC patients from the eastern part of the world (Europe, the Americas, and Africa) and had an ESCC connection compared to healthy subjects. Despite the

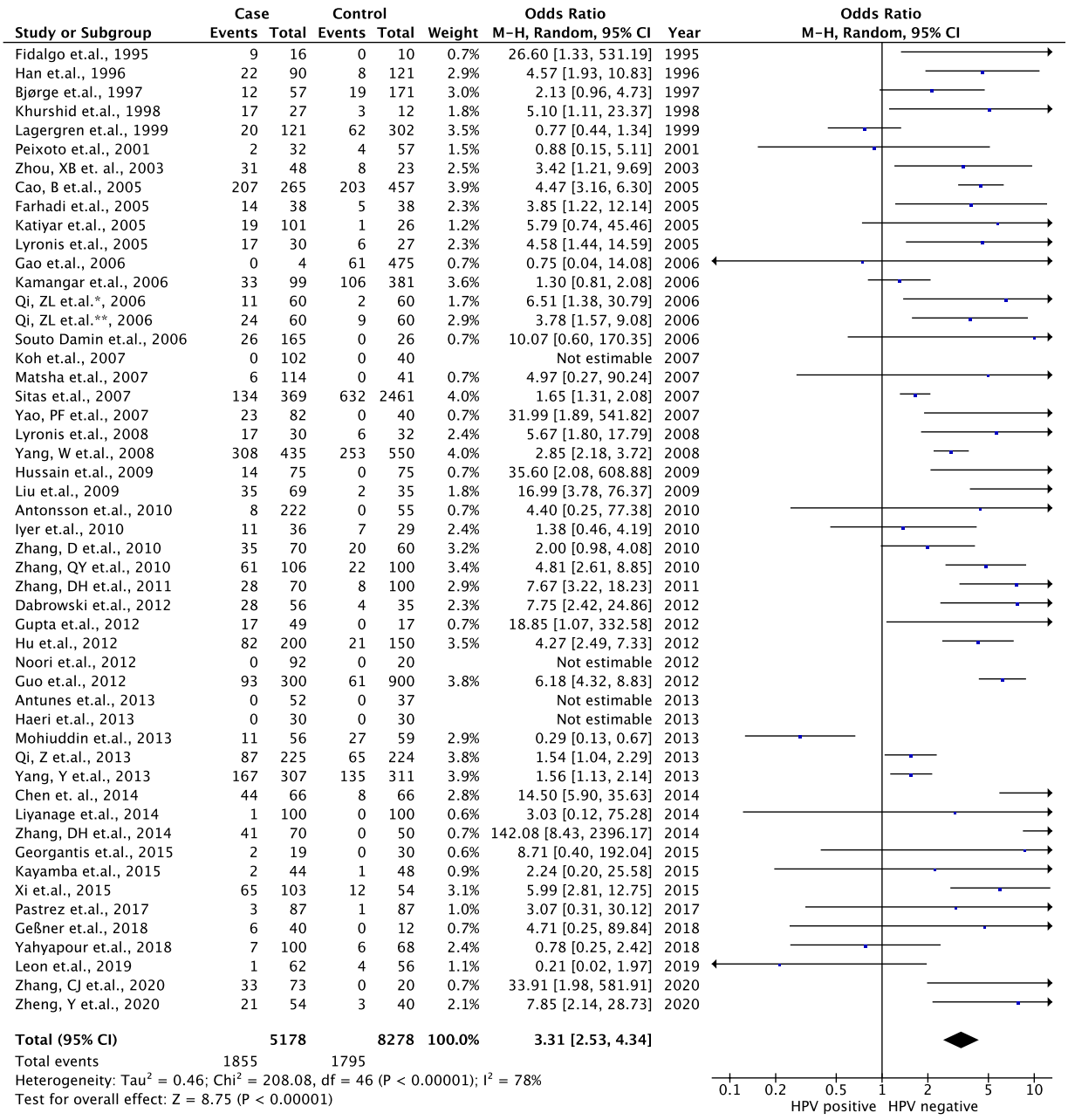

FIGURE 4
Association between HPV infection and EC risk in the meta-data analysis. Forest plots represented the pool odds ratios (ORs) and 95% CIs for the association between HPV infection and EC risk in each registered case–control study.

presence of variations across the studied types, most of the significant association was observed with less variation in the case–control model (Asian vs. non-Asian subjects). Similarly, in the multivariate regression analysis, the ORs indicated the statistical correlation between smoking, alcohol consumption, history of GERD, and FHC but were not observed in variation of age and gender of enrolled subjects. The associated results from the analysis of head and neck cancers were contrary (Gillison et al., 2008). However, the $p16^{INK4a}$ protein was the potentially promising biological marker for HPV-related malignancies and presented more precise corroboration with DNA testing using a PCR- or immunohistochemistry (IHC)-based technique for HPV diagnosis (at least in oropharyngeal carcinoma). Nevertheless, most studies targeting HPV DNA without $p16^{INK4a}$ evaluation could not be a gold standard, therefore defining the association between HPV infection and increased risk of EC in this recent meta-analysis.

It is extraordinary that the genomic landscape of ECs has been described by The Cancer Genome Atlas Research Network since 2017 (Kim et al., 2017). They illustrated three distinct existences of molecular subclassification in ESCC. Although aberrations in the Nrf2 pathway were the hallmark of the ESCC1 subtype, higher mutation rates in NOTCH1 or ZNF750 were the genomic characterization of

TABLE 5 Evaluation of the involvement of the HPV infection on EC risk in the subgroup context.

Characterization	Number of studies	Log pooled OR (95% CI)[d]	*p*-value	I^2 (%)	*p*-value for heterogeneity	Meta-regression
Overall	51	1.2 (0.89–1.49)	<0.001	81.8	<0.001	–
Geographic region						
Asia	33	1.29 (0.89–1.70)	<0.001	84.9	<0.001	0.176
Europe	7	1.26 (0.27–2.24)	0.02	72.6	<0.001	
Africa	5	0.50 (0.16–0.83)	0.02	0	0.36	
America	4	0.62 (−0.62–1.85)	0.20	0	0.56	
Oceania	2	1.32 (−1.04–3.67)	0.09	0	0.865	
Detection strategy[a]						
Nucleic acid, e.g., PCR	34	1.46 (1.14–1.77)	<0.001	65.7	<0.001	0.474
Protein, e.g., Ab, ELISA, ISH, and IHC	11	0.73 (0.01–1.44)	0.05	90.0	<0.001	
Cell, i.e., cytology	1	NE	NE	NE	NE	
Combined technique	5	0.83 (−1.61–3.27)	0.04	61.5	0.051	
Type of specimen[b]						
PE	41	1.41 (1.12–1.70)	<0.001	66.4	<0.001	0.015
Blood/plasma/serum	7	0.43 (−0.48–1.34)	0.29	90.7	<0.001	
FF/biopsies	2	0.38 (−22.39–23.15)	0.87	87.3	0.005	
Exfoliated cells	1	NE	NE	NE	NE	
Risk of ECs[c]						
High	37	1.22 (0.84–1.61)	<0.001	86.1	<0.001	0.309
Low-medium	14	1.06 (0.48–1.63)	<0.001	51.4	0.007	

OR, odd ratio; CI, confidence interval; HPVs, human papillomaviruses; EC, esophageal cancers; NE, did not estimated.
[a]PCR, polymerase chain reaction; Ab, antibodies; ISH, *in situ* hybridization; IHC, immunohistochemistry; ELISA, enzyme-linked immunosorbent assay; WB, Western blotting.
[b]PE, formalin-fixed paraffin-embedded tissue; FF, Fresh frozen tissue.
[c]Rajendra et al. (2020), Ludmir et al. (2015), and Kunzmann et al. (2017).
[d]When $I2$ <50% or *p*-value for heterogeneity > 0.10, the fixed effect model was applied.

TABLE 6 Relationship of the potential risk factors and the prognostic features for ECs.

Characteristics	Histopathological grade (*N* =96)		OR_{adj} (95% CI)	*p*-value[a]	TNM stage (*N* =100)		OR_{adj} (95% CI)	*p*-value[a]
	Poor diff.; *n* (%)	Moderate/well diff.; *n* (%)			Stage I, II; *n* (%)	Stage III, IV; *n* (%)		
Smoking								
Yes	48 (72.7)	21 (70.0)	1.1 (0.4–2.9)	0.837	7 (77.8)	65 (71.4)	0.9 (0.2–4.6)	0.872
No	18 (27.3)	9 (30.0)	1.0 (reference)		2 (22.2)	26 (28.6)	1.0 (reference)	
History of GERD								
Yes	53 (80.3)	23 (76.7)	1.3 (0.4–3.7)	0.664	9 (100.0)	70 (76.9)	0.0 (0.0)	0.998
No	13 (19.7)	7 (23.3)	1.0 (reference)		0 (0.0)	21 (23.1)	1.0 (reference)	
HPVs status								
Positive	32 (48.5)	11 (36.7)	1.6 (0.7–4.0)	0.664	5 (55.6)	40 (44.0)	0.6 (0.1–2.4)	0.470
Negative	34 (51.5)	19 (63.3)	1.0 (reference)		4 (44.4)	51 (56.0)	1.0 (reference)	

Poor diff., poor differentiation; Moderate/well diff., moderate or well differentiation; OR_{adj}, adjusted odd ratio; CI, confidence interval; GERD, gastroesophageal reflux disease; HPVs, human papillomaviruses.
[a]*p*-value was obtained from a multiple logistic regression model with all conditional adjusted variables.

ESCC2. Furthermore, this report did not indicate any evidence of cell cycle dysregulation and p53 mutations in p53 at the genomic level for ESCC3. However, the expression of p53 did not declare an association with HPV-linked ESCC, as the mutations of the p53 gene were measurable in both ESCC with and without HPV infection, implying the reciprocally inclusive consequences between p53 mutations and HPV infections. Thus, the important role of environmental carcinogens could be signified in the oncogenesis of ESCCs (Chang et al., 1994).

The overexpression of $p16^{INK4a}$ has been described as a surrogate marker for hrHPV-associated cancer of the oropharynx through the eighth edition of the American Joint Committee on Cancer Staging Manual (Lydiatt et al., 2017). However, the relationship between ECs and HPV infection is still debated. It has been proposed that anatomical and environmental causes might be allied to underlying reasons. The esophageal epithelium and squamous cell malignancy may not be more affected by the high risks of sexual behavior than EAC (Wong et al., 2018). In Asianic populations, dietary factors, including poor status nutrition, high temperature of drinking beverages, and low uptake of fruits and vegetables, might be regarded as risk rationales (Tran et al., 2005; Li et al., 2011). On the contrary, smoking and alcohol drinking were major factors in the Westerner risk (Engel et al., 2003; Freedman et al., 2007). Despite this, the raise of ECs could be augmented by HPV-positive status, intensely in patients with a history of smoking and alcohol consumption (at least in China; Qi et al., 2013) but not transpire in the countries of the Western parts as demonstrated by Georgantis et al. (2015). In the recent study, we also revealed that there is no associated evidence of HPV DNA status and prognosis in EC patients, suggesting that no significant effect of HPV infection on patient survival appears to be consistent with the previous few studies that informed the conclusion results (Petrelli et al., 2021). Similarly, the effects of HPV infection on Barrett's metaplasia and EAC were still debated, and no strong evidence could be determined in the systematic review and meta-analysis (Rajendra et al., 2020).

In harmony with the previous reports, we defined several limitations of the current analysis with a certain association. Most studies, which represent 50%, were derived from Asian people with differences in genomic landscape, mental origin, and daily life. Critically, variations in the evaluation essay, line sensitivities, and types of specimens used could have primarily shaped the summarized data. As we mentioned, FFPE tissues were supposed to be specimens of suggestive deprivation compared with FF or biopsies. Furthermore, the most enrolled studies ratified the existence of HPVs based only on PCR, despite the $p16^{INK4a}$ IHC, which was the highly sensitive standard approach to the diagnosis of HPV-associated malignancies. Consequently, there were few studies conducted with the case–control analysis, describing the risk association based on the crude information and the weight of influenced variables (e.g., smoking status and alcohol history). Additionally, the potential of hrHPVs was emphasized in squamous histology.

An aforementioned study of meta-studies indicated a positive correlation of HPV in EC patients only in the Asian population (Yong et al., 2013). However, our results overtalked this analysis and were also harmoniously observed through the moderately significant association of ECs with HPV-positive in altered geographical prevalence, especially in both Asian and Westerners, and what about our data? GERD history, smoking, and alcohol consumption seem to play a concomitant or synergistic role with HPV infection.

Despite the recent study that clarified and supported the involvement of hrHPV in EC oncogenesis, some critical points must be elucidated. Remarkably, the differences in study design and viral detection approach (e.g., the sensitivity of method) affected the quality of the OR results (i.e., adjusted and pooled OR) as well as the prevalence of HPV in EC tissue samples, respectively. We were able to analyze the clinico-demographic data only in a structured questionnaire, and the other environmental risk factors might be lost from the original patient's life. Importantly, some studies of HPV infection included inadequate sample sizes, affecting our analysis and difficult to summarize. Although more largely epidemiological studies are necessary to show the strength of this correlation, recent data have shed light on therapeutic purposes and preventive epidemiology of ECs. Furthermore, applicable studies adhere to the established procedural standards that were adhered to by other tumor articles and should be integrated into ECs to provide adequate knowledge on HPV-driven EC pathogenesis. Furthermore, the precision-treated responses and effective-prevented vaccines of HPV-associated ECs could be invented in future research.

5. Conclusion

We specify the recent epidemiologic evidence in a validation of the distributed HPV which might be statistically associated with an increased risk of EC and seems to be enhanced by GERD history, suggesting that HPV may, together with GERD history, act as a significant etiological risk factor of ECs. However, additional high-quality studies with larger sample sizes are needed to further verify the link between HPV and EC.

Data availability statement

The raw data supporting the conclusions of this article will be made available by the authors, without undue reservation.

Ethics statement

The studies involving human participants were reviewed and approved by the Khon Kaen University Ethics Committee for Human Research. The patients/participants provided their written informed consent to participate in this study.

Author contributions

AB, CP, TE, and TN designed and guided the literature. AB, PT, WW, and AP executed data acquisition, analysis, and interpretation. AB, CP, and TE wrote the review and revised the manuscript. AU, PS, PU, and TN administrated, technically, or materially supported the study. CP and TN were the study's supervisors. All authors contributed to the article and approved the submitted version.

Funding

This study was funded by a scholarship under the Post-Doctoral Training Program from Khon Kaen University, Thailand (grant no. PD2565-08) to AB. This study was supported in part by Research and Graduate Studies, Khon Kaen University, Thailand (RP65-8-001) to CP.

Acknowledgments

The authors express gratitude to all participating staff at the Srinagarind Hospital and the Department of Pathology, Faculty of Medicine, Khon Kaen University, who contributed and greatly assisted in the study.

Conflict of interest

AU was employed by Ward Medic Ltd., Part., Bangkok, Thailand.

The remaining authors declare that the research was conducted in the absence of any commercial or financial relationships that could be construed as a potential conflict of interest.

Publisher's note

All claims expressed in this article are solely those of the authors and do not necessarily represent those of their affiliated organizations, or those of the publisher, the editors and the reviewers. Any product that may be evaluated in this article, or claim that may be made by its manufacturer, is not guaranteed or endorsed by the publisher.

Supplementary material

The Supplementary material for this article can be found online at: https://www.frontiersin.org/articles/10.3389/fmicb.2023.1146322/full#supplementary-material

References

Allemani, C., Matsuda, T., Di Carlo, V., Harewood, R., Matz, M., Nikšić, M., et al. (2018). Global surveillance of trends in cancer survival 2000–14 (CONCORD-3): analysis of individual records for 37 513 025 patients diagnosed with one of 18 cancers from 322 population-based registries in 71 countries. *Lancet* 391, 1023–1075. doi: 10.1016/S0140-6736(17)33326-3

Arnold, M., Soerjomataram, I., Ferlay, J., and Forman, D. (2015). Global incidence of oesophageal cancer by histological subtype in 2012. *Gut* 64, 381–387. doi: 10.1136/gutjnl-2014-308124

Begg, C., and Mazumdar, M. (1994). Operating characteristics of a rank correlation test for publication bias. *Biometrics* 50, 1088–1101. doi: 10.2307/2533446

Cancer in Thailand. (2022). Available at: https://www.nci.go.th/e_book/cit_x/index.html

Chang, F., Syrjänen, S., Tervahauta, A., Kurvinen, K., Wang, L., and Syrjänen, S. (1994). Frequent mutations of p53 gene in oesophageal squamous cell carcinomas with and without human papillomavirus (HPV) involvement suggest the dominant role of environmental carcinogens in oesophageal carcinogenesis. *Br. J. Cancer* 70, 346–351. doi: 10.1038/bjc.1994.305

Coleman, H. G., Xie, S. H., and Lagergren, J. (2018). The epidemiology of esophageal adenocarcinoma. *Gastroenterology* 154, 390–405. doi: 10.1053/j.gastro.2017.07.046

D'Souza, G., Kreimer, A. R., Viscidi, R., Pawlita, M., Fakhry, C., Koch, W. M., et al. (2007). Case–control study of human papillomavirus and oropharyngeal cancer. *N. Engl. J. Med.* 356, 1944–1956. doi: 10.1056/NEJMoa065497

de Sanjose, S., Quint, W. G. V., Alemany, L., Geraets, D. T., Klaustermeier, J. E., Lloveras, B., et al. (2010). Human papillomavirus genotype attribution in invasive cervical cancer: a retrospective cross-sectional worldwide study. *Lancet Oncol.* 11, 1048–1056. doi: 10.1016/S1470-2045(10)70230-8

DerSimonian, R., and Laird, N. (1986). Meta-analysis in clinical trials. *Control. Clin. Trials* 7, 177–188. doi: 10.1016/0197-2456(86)90046-2

Egger, M., Smith, G. D., Schneider, M., and Minder, C. (1997). Bias in meta-analysis detected by a simple, graphical test. *BMJ* 315, 629–634. doi: 10.1136/bmj.315.7109.629

El-Serag, H. B., Hashmi, A., Garcia, J., Richardson, P., Alsarraj, A., Fitzgerald, S., et al. (2014). Visceral abdominal obesity measured by CT scan is associated with an increased risk of Barrett's esophagus: a case-control study. *Gut* 63, 220–229. doi: 10.1136/gutjnl-2012-304189

El-Zimaity, H., Di Pilato, V., Ringressi, M. N., Brcic, I., Rajendra, S., Langer, R., et al. (2018). Risk factors for esophageal cancer: emphasis on infectious agents. *Ann. N. Y. Acad. Sci.* 1434, 319–332. doi: 10.1111/nyas.13858

Engel, L. S., Chow, W. H., Vaughan, T. L., Gammon, M. D., Risch, H. A., Stanford, J. L., et al. (2003). Population attributable risks of esophageal and gastric cancers. *JNCI J. Natl. Cancer Inst.* 95, 1404–1413. doi: 10.1093/jnci/djg047

Eslick, G. D. (2010). Infectious causes of esophageal cancer. *Infect. Dis. Clin. North Am.* 24, 845–852. doi: 10.1016/j.idc.2010.08.001

Freedman, N. D., Abnet, C. C., Leitzmann, M. F., Mouw, T., Subar, A. F., Hollenbeck, A. R., et al. (2007). A prospective study of tobacco, alcohol, and the risk of esophageal and gastric cancer subtypes. *Am. J. Epidemiol.* 165, 1424–1433. doi: 10.1093/aje/kwm051

Fritz, A., Percy, C., Jack, A., Shanmugaratnam, K., Sobin, L., Parkin, M., et al. *ICD-O International Classification of Diseases for Oncology First Revision*. Geneva: WHO (2013).

Garland, S. M. (2002). Human papillomavirus update with a particular focus on cervical disease. *Pathology* 34, 213–224. doi: 10.1080/00313020212469

Geng, H., Xing, Y., Zhang, J., Cao, K., Ye, M., Wang, G., et al. (2022). Association between viral infection other than human papillomavirus and risk of esophageal carcinoma: a comprehensive meta-analysis of epidemiological studies. *Arch. Virol.* 167, 1–20. doi: 10.1007/s00705-021-05268-8

Georgantis, G., Syrakos, T., Agorastos, T., Miliaras, S., Gagalis, A., Tsoulfas, G., et al. (2015). Detection of human papillomavirus DNA in esophageal carcinoma in Greece. *World J. Gastroenterol.* 21, 2352–2357. doi: 10.3748/wjg.v21.i8.2352

Gheit, T. (2019). Mucosal and cutaneous human papillomavirus infections and cancer biology. *Front. Oncol.* 9:355. doi: 10.3389/fonc.2019.00355

Gillison, M. L., Broutian, T., Pickard, R. K. L., Tong, Z. Y., Xiao, W., Kahle, L., et al. (2012). Prevalence of oral HPV infection in the United States, 2009-2010. *JAMA* 307, 693–703. doi: 10.1001/jama.2012.101

Gillison, M. L., D'Souza, G., Westra, W., Sugar, E., Xiao, W., Begum, S., et al. (2008). Distinct risk factor profiles for human papillomavirus type 16–positive and human papillomavirus type 16–negative head and neck cancers. *JNCI J. Natl. Cancer Inst.* 100, 407–420. doi: 10.1093/jnci/djn025

Hardefeldt, H. A., Cox, M. R., and Eslick, G. D. (2014). Association between human papillomavirus (HPV) and oesophageal squamous cell carcinoma: a meta-analysis. *Epidemiol. Infect.* 142, 1119–1137. doi: 10.1017/S0950268814000016

Herraez-Hernandez, E., Alvarez-Perez, M., Navarro-Bustos, G., Esquivias, J., Alonso, S., Aneiros-Fernandez, J., et al. (2013). HPV Direct Flow CHIP: a new human papillomavirus genotyping method based on direct PCR from crude-cell extracts. *J. Virol. Methods* 193, 9–17. doi: 10.1016/j.jviromet.2013.04.018

Higgins, J. P. T., and Thompson, S. G. (2002). Quantifying heterogeneity in a meta-analysis. *Stat. Med.* 21, 1539–1558. doi: 10.1002/sim.1186

Higgins, J. P. T., Thompson, S. G., Deeks, J. J., and Altman, D. G. (2003). Measuring inconsistency in meta-analyses. *BMJ* 327, 557–560. doi: 10.1136/bmj.327.7414.557

Hošnjak, L., and Poljak, M. (2018). A systematic literature review of studies reporting human papillomavirus (HPV) prevalence in esophageal carcinoma over 36 years (1982–2017). *Acta Dermatovenerol.* 27, 127–136. doi: 10.15570/actaapa.2018.26

Kim, J., Bowlby, R., Mungall, A. J., Robertson, A. G., Odze, R. D., Cherniack, A. D., et al. (2017). Integrated genomic characterization of oesophageal carcinoma. *Nature* 541, 169–175. doi: 10.1038/nature20805

Kunzmann, A. T., Graham, S., McShane, C. M., Doyle, J., Tommasino, M., Johnston, B., et al. (2017). The prevalence of viral agents in esophageal adenocarcinoma and Barrett's esophagus: a systematic review. *Eur. J. Gastroenterol. Hepatol.* 29, 817–825. doi: 10.1097/MEG.0000000000000868

Li, X., Gao, C., Yang, Y., Zhou, F., Li, M., Jin, Q., et al. (2014). Systematic review with meta-analysis: the association between human papillomavirus infection and oesophageal cancer. *Aliment. Pharmacol. Ther.* 39, 270–281. doi: 10.1111/apt.12574

Li, S., Luk, H. Y., Xia, C., Chen, Z., Chan, P. K. S., and Boon, S. S. (2022). Oesophageal carcinoma: the prevalence of DNA tumour viruses and therapy. *Tumour Virus Res.* 13:200231. doi: 10.1016/j.tvr.2021.200231

Li, Y., Yang, H., and Cao, J. (2011). Association between alcohol consumption and cancers in the Chinese population—a systematic review and meta-analysis. *PLoS One* 6:e18776. doi: 10.1371/journal.pone.0018776

Ludmir, E. B., Stephens, S. J., Palta, M., Willett, C. G., and Czito, B. G. (2015). Human papillomavirus tumor infection in esophageal squamous cell carcinoma. *J. Gastrointest. Oncol.* 6, 287–295. doi: 10.3978/j.issn.2078-6891.2015.001

Lydiatt, W. M., Patel, S. G., O'sullivan, B., Brandwein, M. S., Ridge, J. A., Migliacci, J. C., et al. (2017). Head and neck cancers-major changes in the American joint committee on cancer eighth edition cancer staging manual. *CA Cancer J. Clin.* 67, 122–137. doi: 10.3322/caac.21389

Morgan, E., Soerjomataram, I., Rumgay, H., Coleman, H. G., Thrift, A. P., Vignat, J., et al. (2022). The global landscape of esophageal squamous cell carcinoma and esophageal adenocarcinoma incidence and mortality in 2020 and projections to 2040: new estimates from GLOBOCAN 2020. *Gastroenterology* 163, 649–658.e2. doi: 10.1053/j.gastro.2022.05.054

Page, M. J., McKenzie, J. E., Bossuyt, P. M., Boutron, I., Hoffmann, T. C., Mulrow, C. D., et al. (2020). The PRISMA Statement: an updated guideline for reporting systematic reviews. *BMJ* 2021:372. doi: 10.1136/bmj.n71

Petrelli, F., De Santi, G., Rampulla, V., Ghidini, A., Mercurio, P., Mariani, M., et al. (2021). Human papillomavirus (HPV) types 16 and 18 infection and esophageal squamous cell carcinoma: a systematic review and meta-analysis. *J. Cancer Res. Clin. Oncol.* 147, 3011–3023. doi: 10.1007/s00432-021-03738-9

Petrick, J. L., Wyss, A. B., Butler, A. M., Cummings, C., Sun, X., Poole, C., et al. (2014). Prevalence of human papillomavirus among oesophageal squamous cell carcinoma cases: systematic review and meta-analysis. *Br. J. Cancer* 110, 2369–2377. doi: 10.1038/bjc.2014.96

Phusingha, P., Ekalaksananan, T., Vatanasapt, P., Loyha, K., Promthet, S., Kongyingyoes, B., et al. (2017). Human papillomavirus (HPV) infection in a case-control study of oral squamous cell carcinoma and its increasing trend in northeastern Thailand. *J. Med. Virol.* 89, 1096–1101. doi: 10.1002/jmv.24744

Poosari, A., Nutravong, T., Namwat, W., Wasenang, W., Sa-ngiamwibool, P., and Ungareewittaya, P. (2022). The relationship between P16INK4A and TP53 promoter methylation and the risk and prognosis in patients with oesophageal cancer in Thailand. *Sci. Rep.* 12, 1–10. doi: 10.1038/s41598-022-14658-0

Poosari, A., Nutravong, T., Sa-ngiamwibool, P., Namwat, W., Chatrchaiwiwatana, S., and Ungareewittaya, P. (2021). Association between infection with campylobacter species, poor oral health and environmental risk factors on esophageal cancer: a hospital-based case-control study in Thailand. *Eur. J. Med. Res.* 26:82. doi: 10.1186/s40001-021-00561-3

Qi, Z., Jiang, Q., Yang, J., Chen, X., Wu, H., Huang, L., et al. (2013). Human papillomavirus (HPV) infection and the risk of esophageal squamous cell carcinoma. *Dis. Esophagus* 26, 61–67. doi: 10.1111/j.1442-2050.2012.01334.x

Rajendra, S., Pavey, D., McKay, O., Merrett, N., and Gautam, S. D. (2020). Human papillomavirus infection in esophageal squamous cell carcinoma and esophageal adenocarcinoma: a concise review. *Ann. N. Y. Acad. Sci.* 1482, 36–48. doi: 10.1111/nyas.14509

Rajendra, S., Wang, B., Snow, E. T., Sharma, P., Pavey, D., Merrett, N., et al. (2013). Transcriptionally active human papillomavirus is strongly associated with Barrett's dysplasia and esophageal adenocarcinoma. *Am. J. Gastroenterol.* 108, 1082–1093. doi: 10.1038/ajg.2013.94

Rumgay, H., Arnold, M., Laversanne, M., Whiteman, D. C., Thrift, A. P., Wei, W., et al. (2021). International trends in esophageal squamous cell carcinoma and adenocarcinoma incidence. *Am. J. Gastroenterol.* 116, 1072–1076. doi: 10.14309/ajg.0000000000001121

Rustgi, A. K., and El-Serag, H. B. (2014). Esophageal carcinoma. *N. Engl. J. Med.* 371, 2499–2509. doi: 10.1056/NEJMra1314530

Sonawane, K., Suk, R., Chiao, E. Y., Chhatwal, J., Qiu, P., Wilkin, T., et al. (2017). Oral human papillomavirus infection: differences in prevalence between sexes and concordance with genital human papillomavirus infection, NHANES 2011 to 2014. *Ann. Intern. Med.* 167, 714–724. doi: 10.7326/M17-1363

Stoner, G. D., and Gupta, A. (2001). Etiology and chemoprevention of esophageal squamous cell carcinoma. *Carcinogenesis* 22, 1737–1746. doi: 10.1093/carcin/22.11.1737

Sung, H., Ferlay, J., Siegel, R. L., Laversanne, M., Soerjomataram, I., Jemal, A., et al. (2021). Global cancer statistics 2020: GLOBOCAN estimates of incidence and mortality worldwide for 36 cancers in 185 countries. *CA Cancer J Clin* 71, 209–249. doi: 10.3322/caac.21660

Sunpaweravong, S. (2010). Epidemiology and risk factors of esophageal cancer. *Thai J. Surg.* 31. Available at: https://he02.tci-thaijo.org/index.php/ThaiJSurg/article/view/227597

Syrjänen, K. J. (2002). HPV infections and oesophageal cancer. *J. Clin. Pathol.* 55, 721–728. doi: 10.1136/jcp.55.10.721

Syrjanen, K., Pyrhonen, S., Aukee, S., and Koskela, E. (1982). Squamous cell papilloma of the esophagus: a tumour probably caused by human papilloma virus (HPV). *Diagn. Histopathol.* 5, 291–296.

Tran, G. D., Sun, X.-D., Abnet, C. C., Fan, J. H., Dawsey, S. M., Dong, Z. W., et al. (2005). Prospective study of risk factors for esophageal and gastric cancers in the Linxian general population trial cohort in China. *Int. J. Cancer* 113, 456–463. doi: 10.1002/ijc.20616

Tsikouras, P., Zervoudis, S., Manav, B., Tomara, E., Iatrakis, G., Romanidis, C., et al. (2016). Cervical cancer: screening, diagnosis and staging. *J. Buon.* 21, 320–325. Available at: https://www.jbuon.com/archive/21-2-320.pdf

Wells, G., Shea, B., O'Connell, D., Peterson, J., Welch, V., Losos, M., et al. (2014). The Newcastle-Ottawa scale (NOS) for assessing the quality of nonrandomised studies in meta-analyses. Available online: https://www.ohri.ca/programs/clinical_epidemiology/oxford.asp

Wentzensen, N., Schiffman, M., Dunn, T., Zuna, R. E., Gold, M. A., Allen, R. A., et al. (2009). Multiple human papillomavirus genotype infections in cervical cancer progression in the study to understand cervical cancer early endpoints and determinants. *Int. J. Cancer* 125, 2151–2158. doi: 10.1002/ijc.24528

Wong, M. Y. W., Wang, B., Yang, A., Khor, A., Xuan, W., and Rajendra, S. (2018). Human papillomavirus exposure and sexual behavior are significant risk factors for Barrett's dysplasia/esophageal adenocarcinoma. *Dis. Esophagus* 31, 1–7. doi: 10.1093/dote/doy051

Yong, F., Xudong, N., and Lijie, T. (2013). Human papillomavirus types 16 and 18 in esophagus squamous cell carcinoma: a meta-analysis. *Ann. Epidemiol.* 23, 726–734. doi: 10.1016/j.annepidem.2013.07.002

frontiers | Frontiers in Microbiology

TYPE Original Research
PUBLISHED 18 May 2023
DOI 10.3389/fmicb.2023.1181348

OPEN ACCESS

EDITED BY
Wafa Achour,
Centre National de Greffe de Moelle Osseuse, Tunisia

REVIEWED BY
Marcos Fabio DosSantos,
Federal University of Rio de Janeiro, Brazil
Hua Zhou,
Zhejiang University, China

*CORRESPONDENCE
Zida Huang
✉ huangzida@163.com
Xinyu Fang
✉ fangxinyu0417@fjmu.edu.cn

†These authors have contributed equally to this work and share first authorship

RECEIVED 08 March 2023
ACCEPTED 27 April 2023
PUBLISHED 18 May 2023

CITATION
Huang C, Huang Y, Wang Z, Lin Y, Li Y, Chen Y, Chen X, Zhang C, Li W, Zhang W, Fang X and Huang Z (2023) Multiplex PCR-based next generation sequencing as a novel, targeted and accurate molecular approach for periprosthetic joint infection diagnosis.
Front. Microbiol. 14:1181348.
doi: 10.3389/fmicb.2023.1181348

Multiplex PCR-based next generation sequencing as a novel, targeted and accurate molecular approach for periprosthetic joint infection diagnosis

Changyu Huang[1,2,3†], Ying Huang[1,2,3†], Ziwen Wang[4†], Yiming Lin[1], Yongbin Li[1], Yang Chen[1], Xiaoqing Chen[5], Chaofan Zhang[1,2,3], Wenbo Li[1,2,3], Wenming Zhang[1,2,3], Xinyu Fang[1,2,3*] and Zida Huang[1,2,3*]

[1]Department of Orthopaedic Surgery, National Regional Medical Center, Binhai Campus of the First Affiliated Hospital, Fujian Medical University, Fuzhou, China, [2]Department of Orthopedic Surgery, The First Affiliated Hospital of Fujian Medical University, Fuzhou, China, [3]Fujian Provincial Institute of Orthopedics, The First Affiliated Hospital, Fujian Medical University, Fuzhou, China, [4]Fujian Medical University, Fuzhou, China, [5]Department of Orthopedic Surgery, Quanzhou First Hospital Affiliated to Fujian Medical University, Quanzhou, China

Objectives: Periprosthetic joint infection (PJI) diagnosis remains challenging, and the identification of the causative microorganism is, by far, the most important aspect. Here, we use multiple PCR-based targeted next-generation sequencing (tNGS) to detect pathogens in PJI. To explore 1. the ability of targeted next-generation sequencing (tNGS) to detect pathogens in PJI; 2. the consistency of tNGS, metagenomic NGS (mNGS), and culture results; and 3. the ability of tNGS to detect drug resistance genes in PJI.

Methods: PJI was diagnosed according to the Musculoskeletal Infection Society (MSIS) criteria. The microorganisms were detected by culture, mNGS and tNGS to compare the diagnostic effectiveness of the three methods for PJI and to compare their consistency in detecting microorganisms. Drug resistance genes were detected using tNGS. The costs and turnaround times of mNGS and tNGS were compared.

Results: Forty-three patients with PJI, 21 patients without PJI and 10 negative control cases were included. The culture, tNGS, and mNGS sensitivities for PJI diagnosis were 74.41%, 88.37%, and 93.02%, respectively, with no significant differences. The specificities were 90.48%, 95.24%, and 95.24%, respectively, with no significant differences. tNGS detected drug resistance genes in 37.5% of culture-positive PJIs. tNGS was superior to mNGS for turnaround time (14.5 h vs. 28 h) and cost ($150 vs. $260).

Conclusions: tNGS can effectively identify PJI pathogens and may provide drug resistance information, while tNGS is superior to mNGS regarding cost and turnaround time. A multidisciplinary, multi-technology based algorithm to diagnose PJI is appropriate.

KEYWORDS

periprosthetic joint infection, targeted next-generation sequencing, metagenomic next-generation sequencing, culture, diagnostics

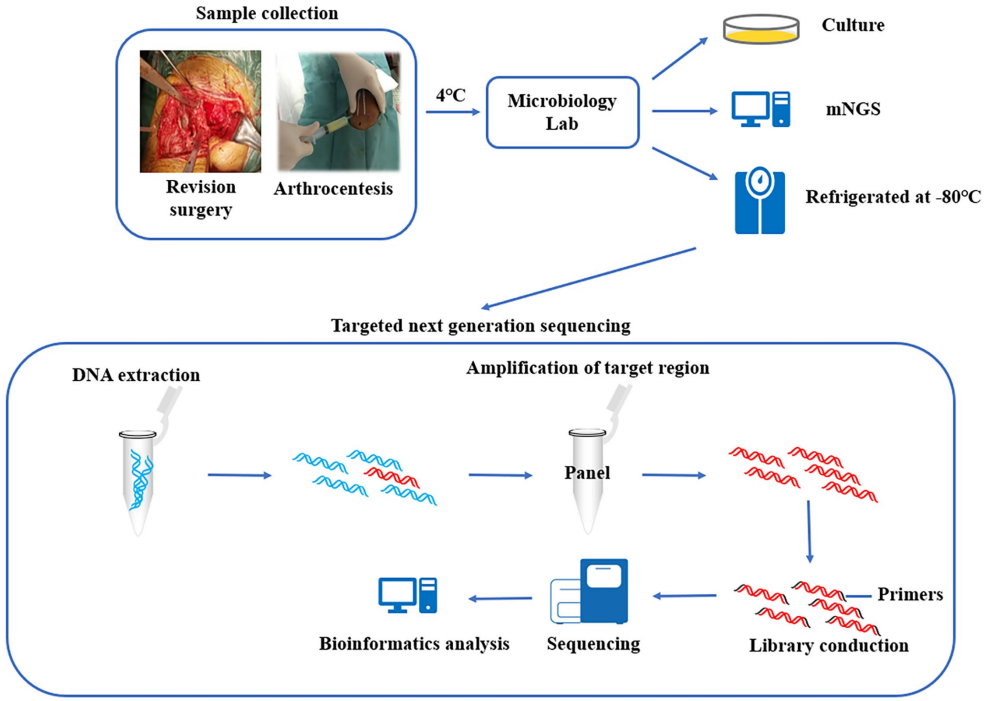

GRAPHICAL ABSTRACT
1. Synovial fluid were tested for pathogenic bacteria using culture and mNGS, and the remaining specimens were preserved in a biobank. 2. The preserved specimens were tested using multiplex PCR-based next generation sequencing. 3. Compare the diagnostic efficacy of the three methods for PJI.

Highlights

1. 298 microorganisms and 86 drug resistance genes were included in the tNGS panel.
2. Diagnostic efficacy of tNGS is not inferior to that of commonly used indicators.
3. tNGS is superior to mNGS in cost and turnaround time.

Introduction

Periprosthetic joint infection (PJI) diagnosis remains challenging. Diagnostic criteria such as those developed by the American Academy of Orthopaedic Surgeons and Musculoskeletal Infection Society (MSIS) provide good support for the diagnosis of PJI, and among these criteria, culture is considered the most critical aspect, which provides information not only on pathogenic microorganisms but also on antibiotic resistance (Workgroup Convened by the Musculoskeletal Infection Society, 2011; Parvizi et al., 2013, 2018; Tubb et al., 2020). However, biofilm formation, prior antibiotic use and fastidious pathogens contribute to the low sensitivity of conventional culture (Stoodley et al., 2011; Wouthuyzen-Bakker et al., 2017), and despite strategies such as sonication and other optimized culture protocols being used to improve detection rates (Trampuz et al., 2007; Fang et al., 2021), the rate of culture-negative PJI (CN-PJI) still ranges from 7.0 to 42.1% (Yoon et al., 2017).

In contrast with time-consuming and low-sensitivity culture, nucleic acid detection technology can detect pathogenic bacteria without culture, and based on the principle of "no preset target," the detection sensitivity of these techniques has been significantly improved. 16S ribosomal RNA gene polymerase chain reaction (PCR) can be used to detect most bacteria, but it cannot identify fungi or polymicrobial infections and cannot quantitatively distinguish contaminating bacteria (Huang et al., 2018). Metagenomic next-generation sequencing (mNGS), also known as metagenomic shotgun NGS, can overcome the shortcomings of 16S rRNA PCR and detect all known/unknown pathogens that cause bone and joint infection, including fungi, bacteria, mycoplasma, parasites, etc., and can provide multidimensional quantitative test results for the identification of polymicrobial infection and contaminating bacteria (McCombie et al., 2019). This has led to effective use of mNGS in PJI. Street et al. applied mNGS to identify pathogens in PJI with a sensitivity of 93% (Street et al., 2017). Thoendel et al. applied mNGS to detect pathogens in 94.8% of culture-positive PJIs (CP-PJIs) and identified new potential pathogens in 43.9% of CN-PJIs (Thoendel et al., 2018). However, even with continued technological advances, the unbiased sampling of mNGS makes it challenging to exclude human-derived genes from samples, and this challenge leads to waste of detection resources and a decrease in sensitivity (Chiu and Miller, 2019). Moreover,

human-derived genes result in relatively low reads of pathogen genomes, which makes it difficult for mNGS to detect drug resistance genes to inform the use of sensitive antibiotics.

Multiple PCR-based targeted NGS (tNGS) is performed by making a panel of the specific sequences of prescreened pathogens, amplifying the target genes, obtaining information about the enriched nucleic acids through a high-throughput sequencing platform, and then analyzing the results by bioinformatics to identify pathogens (Graphical abstract). Based on the predefined panel, tNGS can eliminate the interference of human-derived genes. In theory, the sensitivity of diagnosis can be high as long as the coverage of pathogens is sufficiently broad. This technique has now been used for pathogen identification in cases of pulmonary infections, brain infections, and *Mycobacterium* infections, as well as for the detection of drug resistance genes, and has been shown to have potential for clinical application (Chao et al., 2020; Gao et al., 2021; Huang et al., 2021; Li et al., 2021). Here, we design a panel of specific sequences of 298 pathogens as well as 86 drug resistance genes and applied them to the diagnosis of PJI using tNGS.

The objectives of this study are as follows: 1. to evaluate the ability of tNGS to detect pathogens from PJI; 2. to verify the consistency of the results between tNGS and mNGS and culture; and 3. to explore the ability of tNGS to detect drug resistance.

Materials and methods

This study was approved by the Ethics Committee of our institution (MTAC, ECFAH of FMU [2015] 084-2, 2018 [026]). The synovial fluid used for tNGS detection in this study were obtained from our clinical biobank, and were collected and retained with the informed consent of the patients. Synovial fluid collected between April 2020 and September 2022 were included. Inclusion criteria included the following: 1. patients undergoing joint revision surgery; 2. those who had mNGS testing during treatment and had complete microbiological data. Incomplete clinical records and potentially contaminated samples were criteria for exclusion. Clinical data of patients were obtained from the electronic medical records. The MSIS criteria was used as the gold standard to diagnose PJI (Workgroup Convened by the Musculoskeletal Infection Society, 2011). In addition, 10 patients (osteoarthritis) undergoing primary total hip/knee arthroplasty without a history of inflammatory arthritis, joint infection, or prior surgery were recruited as negative controls. The cost and turnaround time of tNGS and mNGS were defined as the cost and time incurred from the beginning of DNA extraction to the time when the result is obtained. The antibiotic regimen of all patients was determined by a multidisciplinary team based on a combination of culture and mNGS results.

Sample collection

Synovial fluid samples were obtained from patients during revision surgery, in short, the synovial fluid was aspirated with a syringe before the joint capsule was incised at the time of surgery, or if sufficient joint fluid cannot be obtained, the joint capsule was incised and then aspirated under direct vision. All surgeries were performed by the same surgical team. The collected samples were immediately transferred to the microbiology department for further processing, and the specimens were kept at 4°C during transport. The collected samples were used for conventional microbial culture and mNGS. Finally, the remaining synovial fluid (raw specimen, unprocessed) was packaged in DNase-free and RNase-free sterile cryogenic vials and stored at −80°C (Graphical abstract). Synovial fluid was retained for 12.74 months (range: 1–29 months) and tested by tNGS in September 2022.

Culture procedure

Intraoperative synovial fluid specimens were injected directly into commercial culture flasks (Becton-Dickinson GmbH, Heidelberg, Germany) within 2 h of acquisition and cultured in a specialized incubator. All the culture time was more than 7 days. Bacterial identification and drug sensitivity testing were performed using an IVD MALDI Biotyper system (Microflex LT/SH, Germany) and a Vitek II system (BioMérieux, USA).

mNGS process

The mNGS process was performed as described previously (Huang et al., 2020a). Briefly, the extracted total genomic DNA was processed to generate fragments. DNA libraries were constructed by end repair, specific adaptor ligation, purification, PCR, and cyclization reactions to generate single-stranded DNA circles. The quantitative library was sequenced on the BGISEQ-2000 platform (BGI-Wuhan, Wuhan, China) for 50 bp single-end sequencing. Finally, the raw sequencing data were analyzed using the bioinformatics pipeline (containing 32 drug resistance genes) developed by BGI.

tNGS process

This method included 298 pathogens (Supplementary Material S1) potentially associated with PJI in the panel, based on the official Chinese published National CDC Catalogue of Human Pathogenic Microorganisms, previous data from our institution, and available literature reports. The pathogens included fungi ($n = 64$), gram-positive bacteria ($n = 120$), gram-negative bacteria ($n = 82$), bacterial genera ($n = 16$), and others ($n = 16$). Eighty-six resistance genes for 13 resistance phenotypes (Supplementary Material S2) were also included in the panel. The production and testing of the panel was performed in-house by Shanghai Pathogeno Medical Technology Co., Ltd.

The method of total genome DNA extraction was consistent with that of mNGS. The DNA products were used as templates for multiplex PCR amplification using the abovementioned panel. Then, sequencing linkers and barcode sequences for sample identification were added to obtain pathogen sequencing libraries. Library concentrations were quantified using a Qubit 4.0 fluorometer (Invitrogen), requiring that the amount of data that could be fractionated to each pathogen library was no less than 0.05 M reads, and then the libraries were mixed. The concentration of the mixed libraries was accurately quantified using a Qubit 4.0 fluorometer, and the library was denatured after dilution to a final concentration of 4 nM. High-throughput sequencing was performed using an Illumina

MiSeq Reagent Nano Kit and the Illumina MiSeq sequencing platform, with an average data volume of 0.03 ~ 0.05 M reads per library and a sequencing read length of PE75. The raw data obtained were first analyzed by identifying the reads with the linker sequence, trimming the linker and the subsequent sequences, and filtering the low-quality data. The high-quality data were identified by primer sequences, and the reads with correct paired-end overlap were then compared with the pathogen sequences in RefSeq, GenBank, and other databases downloaded from NCBI to finally determine the pathogen species and content in the samples (Graphical abstract).

The interpretation of the mNGS and tNGS results was done by a multidisciplinary team (including infection physicians, microbiologists, orthopedists) based on the methods described in our previous study (Huang et al., 2020b).

Statistical analysis

Variables conforming to a normal distribution are described by the mean ± standard deviation, and variables with a nonnormal distribution are described by the median and interquartile range (IQR). Statistical significance analysis was performed with the *t* test, the chi-square test, Fisher's exact probability method or the Mann–Whitney test according to the characteristics of the variables. Statistical differences in the sensitivity and specificity of culture, tNGS, mNGS, CRP, ESR, SF-WBCs, and SF-PMNs % were analyzed using McNemar's test. p values ≤ 0.05 were considered statistically significant. Statistical analysis was performed using SPSS 26.0 (IBM, Armonk, New York, USA).

Results

Demographic characteristics

Synovial fluid from 67 patients were included, and three were excluded: two samples suspected of contamination, and one patient had incomplete clinical data. The remaining 64 patients had a mean age of 63.60 ± 12.57 years, resulting in samples from 32 females and 34 hips and 30 knees. According to the MSIS criteria, there were 43 cases of PJI (including 11 CN-PJI cases and 32 CP-PJI cases) and 21 cases of non-PJI (Non-infectious arthroplasty failure, such as: prosthesis loosening). In addition, specimens from 10 patients with primary joint arthroplasty were included as negative controls. In the latest evaluation, there were no delayed-onset infections (>1 year) in either the non-PJI or negative control groups. Clinical and laboratory data for all cases are shown in Table 1.

Microorganisms detected by culture

For the 43 cases of PJI, microorganisms were isolated using culture in 32 cases, and a single pathogen was isolated in 30 of them (Figure 1A). Two patients were diagnosed as polymicrobial infection, and they yielded 2 strains (*Streptococcus anginosus* + *Staphylococcus aureus* and *Escherichia coli* + *Streptococcus agalactiae*) in different samples. The mNGS and tNGS results of these two patients with polymicrobial infection were consistent with the culture results. In 2 of the 21 non-PJI cases, microorganisms were isolated from a single sample and were considered false positives. In these two patients, antibiotic use was not prolonged postoperatively, and no reinfection was seen at follow-up (11 and 13 months of follow-up). No microorganisms were detected in the negative control group. Detailed culture result is shown in Table 2.

Microorganisms detected by mNGS

Thirty of the 32 patients with CP-PJI tested positive by mNGS (93.8%) (Figure 1A). The mNGS results were in complete agreement (The test results were completely consistent) with the culture results for CP-PJI at the genus level in 81% of cases, at the species level in 52% of cases, in partial agreement (In addition to the same strain, there are some inconsistent results) in 13% of cases, and in complete disagreement (The test results are completely inconsistent) in 2 cases (2 cases with negative mNGS results) (Figure 1C). Among the 11 CN-PJI cases, mNGS detected microorganisms in 10 cases (90.9%), including *Staphylococcus aureus* $n = 3$, *Staphylococcus* spp. $n = 1$, *Streptococcus dysgalactiae* $n = 1$, *Candida albicans* $n = 1$, *Mycoplasma hominis* $n = 1$, *Cutibacterium acnes* $n = 1$, *Finegoldia magna* $n = 1$, and *Corynebacterium striatum* $n = 1$. Detailed mNGS result is shown in Table 2.

Microorganisms detected by tNGS

Thirty of the 32 CP-PJI patients tested positive by tNGS (93.8%) (Figure 1A). The tNGS results were in complete agreement with the culture results for CP-PJI at the genus level in 78% of cases, at the species level in 62% of cases, in partial agreement in 9% of cases, and in complete disagreement in 4 cases (3 negative tNGS results and 1 inconsistent result) (Figure 1B). Among the 11 CN-PJI cases, tNGS detected microorganisms in 10 cases (90.9%), including *Staphylococcus aureus* $n = 4$, *Streptococcus dysgalactiae* $n = 2$, *Candida albicans* $n = 1$, *Mycoplasma hominis* $n = 1$, *Cutibacterium acnes* $n = 1$, and *Corynebacterium striatum* $n = 1$. Detailed tNGS result is shown in Table 2.

For PJI, the results of tNGS and mNGS were in complete agreement at the genus level in 72% of cases, at the species level in 60% of cases, in partial agreement in 12% of cases, and in complete disagreement in 8 unmatched cases (Figure 1D). Among the 8 unmatched cases, 4 cases had negative tNGS results, 3 cases had negative mNGS results, and the last case had both mNGS and culture results for *Pseudomonas alcaligenes*, while the tNGS result was positive for *Pseudomonas aeruginosa*. For the four patients that tested negative for tNGS, the results of mNGS and culture were positive for *Staphylococcus aureus* $n = 2$, *Streptococcus gallolyticus* $n = 1$, and *Finegoldia magna* $n = 1$; *Streptococcus gallolyticus* and *Finegoldia magna* were not included in our panel of tNGS.

Antibiotic resistance detected by culture, mNGS and tNGS

Antibiotic resistance information was obtained using culture in 26 of 32 CP-PJI patients. mNGS detected the information of antibiotic

TABLE 1 Clinical and laboratory characteristic of all cases.

Characteristic	Patients (*n*=64)				Control (*n*=10)	Value of *p* (Suspected-PJI vs. Control)
	Total	Non-PJI (*n*=21)	PJI (*n*=43)	Value of *p* (non-PJI vs. PJI)		
Age (yrs), $\bar{X} \pm S$	63.60 ± 12.57	63.66 ± 10.84	63.58 ± 13.46	0.50[b]	63.40 ± 8.80	0.21[b]
Female (n)	33	15	18	0.03[a]	5	>0.99[a]
BMI (kg/m^2)	25.01 ± 1.69	24.64 ± 2.72	25.19 ± 2.68	0.84[b]	24.50 ± 2.42	0.40[b]
aCCI	2.0 (1.00,3.00)	2 (1.50,3.00)	2 (1.00,3.00)	0.51[c]	2 (1.00,2.25)	0.37[c]
Joint involved (n)						
Hip	34	13	21	0.97[a]	4	0.51[a]
Knee	30	8	22		6	
Surgical strategies						
One-stage	22	18	4	<0.01[a]		
Two-stage	40	3	37			
DAIR	2	0	2			
Interval between primary arthroplasty and revision (mths) $\bar{X} \pm S$		38.10 ± 26.48	43.30 ± 28.86	0.51[b]		
Antibiotics within 2 weeks prior to surgery (*n*)	16	4	12	0.47[a]	0	
Sinus (*n*)	17	1	16	<0.01[a]	0	
CRP (mg/L), median, IQR	15.1 (3.82,87.12)	3.81 (2.00,6.52)	39.6 (12.10,98.00)	<0.01[c]	2.98 (1.17,9.45)	<0.01[c]
ESR (mm/h), $\bar{X} \pm S$	55.79 ± 31.48	26.71 ± 14.02	65.76 ± 29.16	<0.01[b]	24.50 ± 4.35	<0.01[b]
SF-WBC (×10^6/L), median, IQR	13,123 (984,85,337)	833 (419,1,154)	64,672 (12,055,108,964)	<0.01[c]		
SF-PMN% (%), median, IQR	82.0 (49.5,90.2)	45.9 (41.2,53.0)	87.6 (78.5,91.7)	<0.01[c]		
Positive periprosthetic tissue histopathology (*n*)	32	1	31	<0.01[a]		

PJI, Prosthetic joint infection; SF-WBC, Synovial fluid white blood cell; SF-PMN, Synovial fluid polymorphonuclear; BMI, Body mass index; aCCI, age-adjusted Charlson Comorbidity Index; DAIR, Debridement, Antibiotics and Implant Retention.
[a]Chi-squared.
[b]Independent-samples *t*-test.
[c]Mann-Whitney *U* test.

resistance gene in only one sample (1/32), and the reading of specific pathogen in this patient was as high as 4,618. tNGS detected 11 different resistance genes corresponding to 8 resistance phenotypes in 37.5% of CP-PJI samples (12/32), and no resistance genes were detected in CN-PJI samples. tNGS detected resistance phenotypes consistent with drug susceptibility testing results in 75% (9/12) of cases. Penicillin resistance accounted for the highest proportion of drug resistance genes detected, with 58.3% of tNGS (7/12) and 53.8% of culture (14/26).

Diagnostic efficacy of culture, mNGS and tNGS

According to the MSIS criteria, the sensitivity of culture, tNGS and mNGS for PJI was 74.41, 88.37 and 93.02%, respectively. The sensitivity of tNGS was not significantly different from those of culture and mNGS ($p > 0.05$). The specificities of culture, tNGS and mNGS were 90.5, 95.2 and 95.2%, respectively. The specificity of tNGS was not significantly different from those of culture and mNGS ($p > 0.05$). In addition, there were mostly no significant differences in sensitivity and specificity between tNGS and CRP, ESR, SF-WBC, and SF-PMN%. Finally, the sensitivity increased to 97.7%, and the specificity decreased to 85.7% when tNGS and culture were performed in parallel. The diagnostic efficacy of each indicator is listed in Table 3.

Cost and turnaround time of tNGS and mNGS

In this study, the cost per case was approximately $150 for tNGS and $260 for mNGS. mNGS is therefore 1.73 times more expensive than tNGS. We also compared the turnaround time for the two methods. tNGS and mNGS have roughly the same overall process,

TABLE 2 Microbiology finding of culture, mNGS and tNGS in all cases.

Microorganism	Culture (*n*)	mNGS (*n*)	tNGS (*n*)
Staphylococcus aureus	15	14	17
CoNS[a]	6	11	10
Streptococcus[b]	7	8	8
Gram-negative bacilli[c]	3	4	3
Pseudomonas[d]	3	1	4
Enterococcus faecalis	0	1	0
Salmonella	2	1	2
Candida[e]	1	2	2
Mycoplasma hominis	0	1	1
Other organisms[f]	0	4	3
Total	37	47	45

mNGS, metagenomic next-generation sequencing; tNGS, targeted next-generation sequencing.
[a]Coagulase negative staphylococcus.
[b]Including *Streptococcus agalactiae*, *Streptococcus dysgalactiae*, *Streptococcus gallolyticus*, *Streptococcus anginosus*, *Streptococcus* spp.
[c]Including *Escherichia coli*, *Stenotrophomonas maltophilia*, *Enterobacter hormaechei*, *Afipia broomeae*.
[d]Including *Pseudomonas alcaligenes*, *Pseudomonas aeruginosa*, *Pseudomonas monteilii*, *Pseudomonas* spp.
[e]Including *Candida albicans*, *Candida parapsilosis*.
[f]Including *Corynebacterium striatum*, *Cutibacterium acnes*, *Finegoldia magna*, *Enterococcus casseliflavus*, *Neisseria* spp.

with tNGS requiring targeted amplification prior to library conduction, a process that takes approximately 3 h. mNGS takes more time for preprocessing, library production, and sequencing. In terms of total time, tNGS takes approximately 14.5 h per sample to generate interpretable results, while mNGS takes 28 h (Figure 2). Compared to mNGS, tNGS shortens the time by 13.5 h.

Discussion

The identification of pathogenic microorganisms is key to the diagnosis and treatment of PJI, and it can guide the development of a rational antibiotic regimen, reduce drug resistance, and improve infection control (Tande and Patel, 2014). Our institution routinely uses a comprehensive culture strategy including multiple tissue cultures, sonication culture (Trampuz et al., 2007), optimized culture protocols (Fang et al., 2021), prolonged culture time (Schäfer et al., 2008), and improved tissue homogenization protocols prior to culture (Fang et al., 2021), yet microbial culture still had a negative rate of 25.6% (11/43) in this study. Here, the sensitivity of mNGS in the diagnosis of PJI was 93.0%, and the specificity was 95.2%. Potential pathogenic bacteria were detected in 90.9% of CN-PJI cases, which was similar to previous studies (Street et al., 2017; Thoendel et al., 2018; Huang et al., 2020a), which also showed the potential of nucleic acid detection technology for PJI. In this study, a novel culture

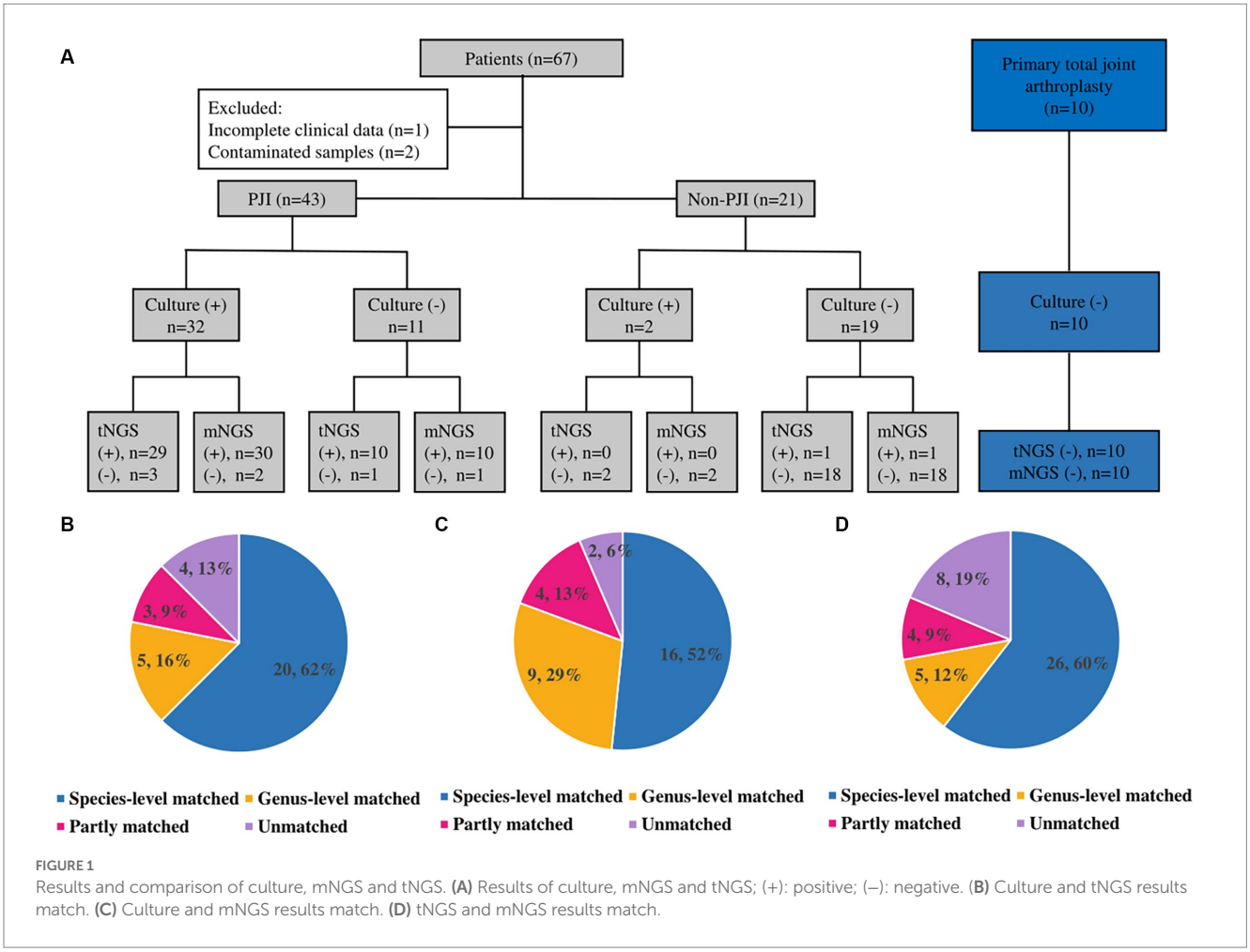

FIGURE 1
Results and comparison of culture, mNGS and tNGS. **(A)** Results of culture, mNGS and tNGS; (+): positive; (–): negative. **(B)** Culture and tNGS results match. **(C)** Culture and mNGS results match. **(D)** tNGS and mNGS results match.

10.3389/fmicb.2023.1181348

TABLE 3 Diagnostic efficiency of culture, mNGS and tNGS in PJI.

Variable	Non-PJI (n=21)	PJI (n=43)	Sensitivity	p-value[a] (VS. tNGS)	Specificity	p-value[a] (VS. tNGS)	PPA	NPA	Youden's index	PPV	NPV	LR+	LR-
tNGS	1	38	88.4%	N/A	95.2%	N/A	0.88	0.95	0.84	97.4%	80%	18.56	0.12
Culture	2	32	74.4%	0.18	90.5%	>0.99	0.74	0.90	0.65	94.1%	63.3%	7.81	0.28
mNGS	1	40	93.0%	0.73	95.2%	>0.99	0.93	0.95	0.88	97.6%	87.0%	19.53	0.07
CRP (>10 mg/L)	2	33	76.7%	0.27	90.5%	>0.99	0.77	0.90	0.67	94.3%	65.5%	8.06	0.26
ESR (>30 mm/h)	9	36	83.7%	0.74	57.1%	<0.01	0.84	0.57	0.41	80%	63.2%	1.95	0.28
SF-WBC (>3,000 × 10^6/L)	0	37	86.0%	>0.99	100%	N/A	0.86	1	0.86	100%	77.8%	N/A	0.14
SF-PMN% (>80%)	2	31	72.1%	0.12	90.5%	>0.99	0.72	0.90	0.63	93.9%	61.3%	7.57	0.31
tNGS + Culture	3	42	97.7%	0.13	85.7%	0.50	0.98	0.86	0.83	93.3%	94.7%	6.84	0.03
mNGS + Culture	3	42	97.7%	0.29	85.7%	0.63	0.98	0.86	0.83	93.3%	94.7%	6.84	0.03

Youden's index = sensitivity + specificity − 1; PJI, Prosthetic joint infection. PPA, Positive percent agreement. NPA, Negative percent agreement. LR+, Positive likelihood ratio; LR−, Negative likelihood ratio; NPV, Negative predictive value; PPV, Positive predictive value; mNGS, metagenomic next-generation sequencing; tNGS, targeted next-generation sequencing.

[a]McNemar's test.

independent pathogen detection technique was introduced, tNGS, to evaluate the diagnostic efficacy of tNGS for PJI and to compare it with mNGS and culture.

The advantage of tNGS with pre-defined targets is that the resources for detection can be focused on pre-defined targets. However, this also raises the concern of not being able to identify microorganisms outside the panel (Gaston et al., 2022). In our study, we selected specific sequences of 298 pathogens for the panels, which is probably the most pathogens incorporated into a panel in the field of PJI thus far, and this approach led to a sensitivity of 88.4% for tNGS in this study. In particular, tNGS detected 90.9% of the potentially pathogenic bacteria in CN-PJI, which shows the potential of tNGS for use in CN-PJI.

However, the detection sensitivity of mNGS in this study was still higher than that of tNGS (93.0% vs. 88.4%). One possible reason is that the samples used for the tNGS assay were not fresh samples but rather frozen samples, and prolonged freezing and rewarming may lead to degradation of DNA. Another reason is that *Streptococcus gallolyticus* and *Finegoldia magna*, which were detected by culture and mNGS, were not included in our tNGS panel. Rare pathogenic bacteria were left outside the panel, an unavoidable limitation of the targeting technique, which also occurs in multiplex PCR kits. Although some multiplex PCR kits have been shown to have good potential for PJI (Villa et al., 2017; Malandain et al., 2018), there are still concerns about the sensitivity of this approach. It is technically feasible to add new pathogens to these kits, but this requires substantial costs. Fortunately, the tNGS panel is reprogrammable, and incorporating new specific nucleic acid sequences of possible potential pathogens into the panel is not technically difficult and does not add excessive cost (Mertes et al., 2011).

The tNGS results matched the culture results at the species level better than the mNGS results matched the culture results (62% vs. 52%). A tremendous advantage of mNGS based on untargeted shotgun sequencing is the unbiased sampling of specimens, which allows mNGS to theoretically detect all pathogens, including viruses, bacteria, fungi, parasites, and undetected potential pathogens (Chiu and Miller, 2019). This also allows mNGS to detect a greater abundance of pathogens than tNGS. However, for PJI, the pathogenic microorganisms are essentially fungi and bacteria (Tande and Patel, 2014), and expending resources sequencing human-derived genes and detecting viruses and parasites increases the detection time, reduces the theoretical sensitivity, and increases costs (Chiu and Miller, 2019). In contrast, with the removal of interferences such as human-derived genes, the data volume of tNGS decreases dramatically, which makes tNGS superior to mNGS in terms of cost ($150 vs. $260) and turnaround time (14.5 h vs. 28 h), while maintaining good diagnostic efficacy, which is the advantage of targeted technologies.

For mNGS, typically less than 1% of reads are nonhuman, and the high host background in tissue samples results in a reduced number and proportion of pathogen reads (Chiu and Miller, 2019). Previous studies have found that the number of reads required for mNGS to detect pathogens in patients with PJI is much lower than that in patients with other infections, which may be related to the biased depletion of sequencing resources caused by the low concentration of planktonic pathogens and high relative human-derived nucleic acid concentrations in PJI (Trampuz et al., 2007; Huang et al., 2020a). This makes it difficult for mNGS to meet clinical requirements for the detection of antibiotic resistance. Here, we included drug resistance

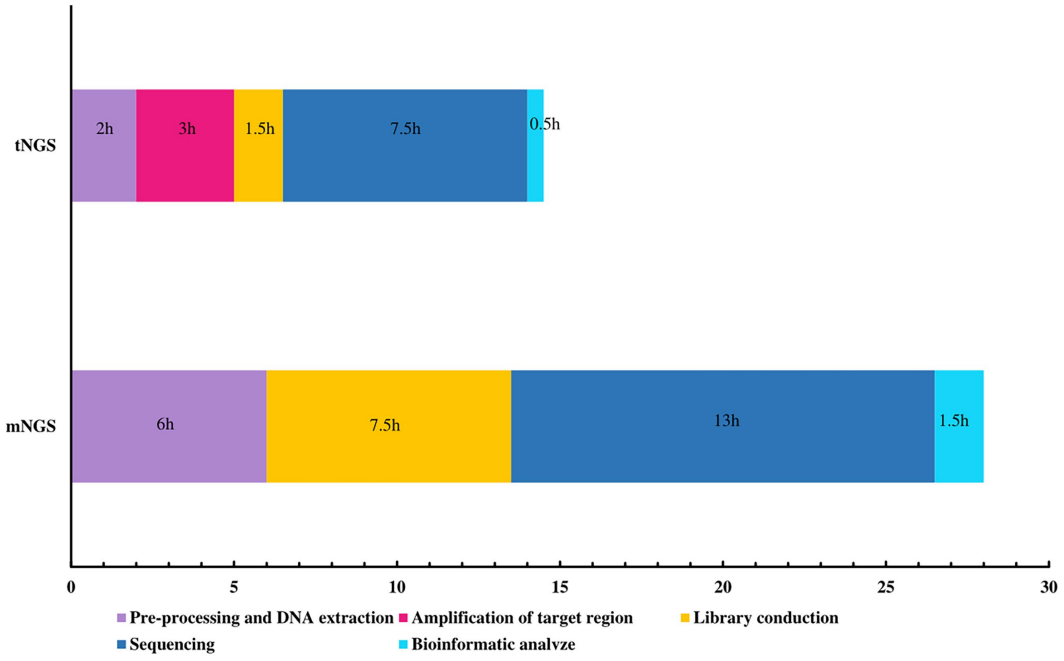

FIGURE 2
Comparison of turnaround time between mNGS and tNGS.

genes in the tNGS panel. In 37.5% of the CP-PJI cases, resistance genes were detected, and their resistance phenotypes were consistent with the culture results, with 75% being consistent. Clinically, the acquirement of resistance information by culture often takes several days, whereas tNGS results require only half a day, which allows physicians to obtain information to inform antibiotic regimen decisions more quickly. However, we must acknowledge that the ability of tNGS to detect resistance genes in PJI in this study was lower than we expected, and the low concentration of planktonic pathogens in PJI remains a possible cause; moreover, the resistance information obtained by tNGS has not been further validated, and future prospective studies are needed to confirm its accuracy.

There are some limitations of our study. 1. As mentioned earlier, the samples for tNGS were from biobank, while the data for tissue culture and mNGS were from fresh samples, which may have biased the results. Moreover, the samples used for the assay were not from consecutive cases, which may have resulted in selection bias. Future prospective studies need to be designed to improve the reliability of the study. 2. Our sample size is insufficient to determine the optimal threshold of contaminating bacteria for tNGS. Our interpretation of the tNGS results is based on our previously established criteria for mNGS. The interpretation of such results is arbitrary and subject to uncertainty. And, the microbial profile of knees versus hips in PJI potentially being different based on anatomic location, which is also a potential drawback to this study. 3. This was an exploratory study of the diagnosis of tNGS in PJI and no sample size calculations were performed prior to the study, and our sample size was limited. More samples or multicenter studies should be conducted to further validate the effectiveness of tNGS.

In summary, the advantage of tNGS over mNGS is that it excludes a range of interfering factors, including human-derived genes, and uses targeted technology to focus detection on pre-defined targets, which makes tNGS superior to mNGS in terms of cost and turnaround time. Moreover, the diagnostic efficacy of tNGS for PJI is not inferior to that of conventional diagnostic indices. The detection of drug resistance genes is one of the advantages of tNGS, which may be able to provide information on antibiotic resistance for PJI and guide the application of a more rational antibiotic regimen. However, tNGS cannot identify microorganisms outside the panel. But, the tNGS panel is reprogrammable, which allows tNGS to be readily improved. Finally, the potential for false positives exists with any microbial detection method, including culture, especially for the highly sensitive mNGS and tNGS. A multidisciplinary, multi-technology algorithm to diagnose PJI based on clinical characteristics is appropriate.

Data availability statement

The datasets presented in this study can be found in online repositories. The names of the repository/repositories and accession number(s) can be found below: CNSA (http://db.cngb.org/cnsa/) of China National GeneBank Database (CNGBdb) with accession number CNP0001047.

Ethics statement

The studies involving human participants were reviewed and approved by the Ethics Committee of First Affiliated Hospital of Fujian Medical of Fujian Medical University. The patients/participants provided their written informed consent to participate in this study.

Author contributions

CH, YH, and ZW: writing of the manuscript and original draft preparation. XF and ZH: conceptualization. YH, XC, and YoL: methodology. YiL and ZW: software. CH and YH: validation and visualization. YC and WL: formal analysis. YC and XF: investigation. WZ and ZH: resources and funding acquisition. ZH, XC, and XF: data curation. WZ, XF, and ZH: writing – review and editing. XF and WZ: supervision. ZH: project administration. All authors contributed to the article and approved the submitted version.

Funding

This work was supported by the National Natural Science Foundation Grant of China (grant number 82072458), the Foreign Cooperation Project of Science and Technology, Fujian Province, China (grant number 2019I0011), the Joint Funds for the Innovation of Science and Technology, Fujian Province, China (grant number 2019Y9301), and the Fujian Orthopaedic Bone and Joint Disease and Sports Rehabilitation Clinical Medical Research Center (grant number 2020Y2002).

Acknowledgments

The authors thank all participants that agreed to participate in this study. And thank the Department of Laboratory Medicine of The First Affiliated Hospital of Fujian Medical University and Xiamen SN Biotechnology Co., Ltd., Xiamen, China for their contribution to this study.

Conflict of interest

The authors declare that the research was conducted in the absence of any commercial or financial relationships that could be construed as a potential conflict of interest.

Publisher's note

All claims expressed in this article are solely those of the authors and do not necessarily represent those of their affiliated organizations, or those of the publisher, the editors and the reviewers. Any product that may be evaluated in this article, or claim that may be made by its manufacturer, is not guaranteed or endorsed by the publisher.

Supplementary material

The Supplementary material for this article can be found online at: https://www.frontiersin.org/articles/10.3389/fmicb.2023.1181348/full#supplementary-material

References

Chao, L., Li, J., Zhang, Y., Pu, H., and Yan, X. (2020). Application of next generation sequencing-based rapid detection platform for microbiological diagnosis and drug resistance prediction in acute lower respiratory infection. *Ann. Transl. Med.* 8:1644. doi: 10.21037/atm-20-7081

Chiu, C. Y., and Miller, S. A. (2019). Clinical metagenomics. *Nat. Rev. Genet.* 20, 341–355. doi: 10.1038/s41576-019-0113-7

Fang, X., Cai, Y., Mei, J., Huang, Z., Zhang, C., Yang, B., et al. (2021). Optimizing culture methods according to preoperative mNGS results can improve joint infection diagnosis. *Bone Joint J.* 103-B, 39–45. doi: 10.1302/0301-620X.103B1.BJJ-2020-0771.R2

Fang, X., Zhang, L., Cai, Y., Huang, Z., Li, W., Zhang, C., et al. (2021). Effects of different tissue specimen pretreatment methods on microbial culture results in the diagnosis of periprosthetic joint infection. *Bone Joint Res.* 10, 96–104. doi: 10.1302/2046-3758.102.BJR-2020-0104.R3

Gao, D., Hu, Y., Jiang, X., Pu, H., Guo, Z., and Zhang, Y. (2021). Applying the pathogen-targeted next-generation sequencing method to pathogen identification in cerebrospinal fluid. *Ann. Transl. Med.* 9:1675. doi: 10.21037/atm-21-5488

Gaston, D. C., Miller, H. B., Fissel, J. A., Jacobs, E., Gough, E., Wu, J., et al. (2022). Evaluation of metagenomic and targeted next-generation sequencing workflows for detection of respiratory pathogens from bronchoalveolar lavage fluid specimens. *J. Clin. Microbiol.* 60, e00526–e00522. doi: 10.1128/jcm.00526-22

Huang, C., Chen, H., Ding, Y., Ma, X., Zhu, H., Zhang, S., et al. (2021). A microbial world: could metagenomic next-generation sequencing be involved in acute respiratory failure? *Front. Cell. Infect. Microbiol.* 11:738074. doi: 10.3389/fcimb.2021.738074

Huang, Z., Li, W., Lee, G. C., Fang, X., Xing, L., Yang, B., et al. (2020a). Metagenomic next-generation sequencing of synovial fluid demonstrates high accuracy in prosthetic joint infection diagnostics: mNGS for diagnosing PJI. *Bone Joint Res.* 9, 440–449. doi: 10.1302/2046-3758.97.BJR-2019-0325.R2

Huang, Z., Wu, Q., Fang, X., Li, W., Zhang, C., Zeng, H., et al. (2018). Comparison of culture and broad-range polymerase chain reaction methods for diagnosing periprosthetic joint infection: analysis of joint fluid, periprosthetic tissue, and sonicated fluid. *Int. Orthop.* 42, 2035–2040. doi: 10.1007/s00264-018-3827-9

Huang, Z., Zhang, Z., Yang, B., Li, W., Zhang, C., Fang, X., et al. (2020b). Pathogenic detection by metagenomic next-generation sequencing in osteoarticular infections. *Front. Cell. Infect. Microbiol.* 10:471. doi: 10.3389/fcimb.2020.00471

Li, B., Xu, L., Guo, Q., Chen, J., Zhang, Y., Huang, W., et al. (2021). GenSeizer: a multiplex PCR-based targeted gene sequencing platform for rapid and accurate identification of major *Mycobacterium* species. *J. Clin. Microbiol.* 59, e00584–e00520. doi: 10.1128/JCM.00584-20

Malandain, D., Bémer, P., Leroy, A. G., Léger, J., Plouzeau, C., Valentin, A. S., et al. (2018). Assessment of the automated multiplex-PCR Unyvero i60 ITI® cartridge system to diagnose prosthetic joint infection: a multicentre study. *Clin. Microbiol. Infect.* 24, 83.e1–83.e6. doi: 10.1016/j.cmi.2017.05.017

McCombie, W. R., McPherson, J. D., and Mardis, E. R. (2019). Next-generation sequencing technologies. *Cold Spring Harb. Perspect. Med.* 9:a036798. doi: 10.1101/cshperspect.a036798

Mertes, F., ElSharawy, A., Sauer, S., van Helvoort, J. M. L. M., van der Zaag, P. J., Franke, A., et al. (2011). Targeted enrichment of genomic DNA regions for next-generation sequencing. *Brief. Funct. Genomics* 10, 374–386. doi: 10.1093/bfgp/elr033

Parvizi, J., Gehrke, T., and Chen, A. F. (2013). Proceedings of the international consensus on periprosthetic joint infection. *Bone Joint J.* 95-B, 1450–1452. doi: 10.1302/0301-620X.95B11.33135

Parvizi, J., Tan, T. L., Goswami, K., Higuera, C., Della Valle, C., Chen, A. F., et al. (2018). The 2018 definition of periprosthetic hip and knee infection: an evidence-based and validated criteria. *J. Arthroplast.* 33, 1309–1314.e2. doi: 10.1016/j.arth.2018.02.078

Schäfer, P., Fink, B., Sandow, D., Margull, A., Berger, I., and Frommelt, L. (2008). Prolonged bacterial culture to identify late periprosthetic joint infection: a promising strategy. *Clin. Infect. Dis.* 47, 1403–1409. doi: 10.1086/592973

Stoodley, P., Conti, S. F., DeMeo, P. J., Nistico, L., Melton-Kreft, R., Johnson, S., et al. (2011). Characterization of a mixed MRSA/MRSE biofilm in an explanted total ankle arthroplasty. *FEMS Immunol. Med. Microbiol.* 62, 66–74. doi: 10.1111/j.1574-695X.2011.00793.x

Street, T. L., Sanderson, N. D., Atkins, B. L., Brent, A. J., Cole, K., Foster, D., et al. (2017). Molecular diagnosis of orthopedic-device-related infection directly from sonication fluid by metagenomic sequencing. *J. Clin. Microbiol.* 55, 2334–2347. doi: 10.1128/JCM.00462-17

Tande, A. J., and Patel, R. (2014). Prosthetic joint infection. *Clin. Microbiol. Rev.* 27, 302–345. doi: 10.1128/CMR.00111-13

Thoendel, M. J., Jeraldo, P. R., Greenwood-Quaintance, K. E., Yao, J. Z., Chia, N., Hanssen, A. D., et al. (2018). Identification of prosthetic joint infection pathogens using

a shotgun metagenomics approach. *Clin. Infect. Dis.* 67, 1333–1338. doi: 10.1093/cid/ciy303

Trampuz, A., Piper, K. E., Jacobson, M. J., Hanssen, A. D., Unni, K. K., Osmon, D. R., et al. (2007). Sonication of removed hip and knee prostheses for diagnosis of infection. *N. Engl. J. Med.* 357, 654–663. doi: 10.1056/NEJMoa061588

Tubb, C. C., Polkowksi, G. G., and Krause, B. (2020). Diagnosis and prevention of periprosthetic joint infections. *J. Am. Acad. Orthop. Surg.* 28, e340–e348. doi: 10.5435/JAAOS-D-19-00405

Villa, F., Toscano, M., De Vecchi, E., Bortolin, M., and Drago, L. (2017). Reliability of a multiplex PCR system for diagnosis of early and late prosthetic joint infections before and after broth enrichment. *Int. J. Med. Microbiol.* 307, 363–370. doi: 10.1016/j.ijmm.2017.07.005

Workgroup Convened by the Musculoskeletal Infection Society (2011). New definition for periprosthetic joint infection. *J. Arthroplast.* 26, 1136–1138. doi: 10.1016/j.arth.2011.09.026

Wouthuyzen-Bakker, M., Benito, N., and Soriano, A. (2017). The effect of preoperative antimicrobial prophylaxis on intraoperative culture results in patients with a suspected or confirmed prosthetic joint infection: a systematic review. Patel R, editor. *J. Clin. Microbiol.* 55, 2765–2774. doi: 10.1128/JCM.00640-17

Yoon, H. K., Cho, S. H., Lee, D. Y., Kang, B. H., Lee, S. H., Moon, D. G., et al. (2017). A review of the literature on culture-negative periprosthetic joint infection: epidemiology, diagnosis and treatment. *Knee Surg. Relat. Res.* 29, 155–164. doi: 10.5792/ksrr.16.034

frontiers | Frontiers in Microbiology

TYPE Original Research
PUBLISHED 22 May 2023
DOI 10.3389/fmicb.2023.1143933

OPEN ACCESS

EDITED BY
Wafa Achour,
Centre National de Greffe de Moelle Osseuse, Tunisia

REVIEWED BY
Mick N. Mulders,
World Health Organization (Switzerland), Switzerland
Sabine Santibanez,
Robert Koch Institute, Germany

*CORRESPONDENCE
Aurora Fernández-García
✉ aurorafg@isciii.es

RECEIVED 15 January 2023
ACCEPTED 03 April 2023
PUBLISHED 22 May 2023

CITATION
Jacqueline C, Gavilán AM, López-Perea N, Penedos AR, Masa-Calles J, Echevarría JE, Fernández-García A and on behalf of the MMR Study Group (2023) Utility of MF-non coding region for measles molecular surveillance during post-elimination phase, Spain, 2017–2020.
Front. Microbiol. 14:1143933.
doi: 10.3389/fmicb.2023.1143933

Utility of MF-non coding region for measles molecular surveillance during post-elimination phase, Spain, 2017–2020

Camille Jacqueline[1,2], Ana María Gavilán[1,3], Noemí López-Perea[3,4], Ana Raquel Penedos[5], Josefa Masa-Calles[3,4], Juan E. Echevarría[1,3], Aurora Fernández-García[1,3]* and on behalf of the MMR Study Group

[1]Centro Nacional de Microbiología, Instituto de Salud Carlos III, Majadahonda, Madrid, Spain, [2]European Public Health Microbiology Training Programme (EUPHEM), European Centre for Disease Prevention and Control (ECDC), Stockholm, Sweden, [3]CIBER de Epidemiología y Salud Pública (CIBERESP), Madrid, Spain, [4]Centro Nacional de Epidemiología, Instituto de Salud Carlos III, Madrid, Spain, [5]United Kingdom Health Security Agency, London, United Kingdom

Background: In countries entering the post-elimination phase for measles, the study of variants by sequencing of 450 nucleotides of the N gene (N450) does not always allow the tracing of chains of transmission. Indeed, between 2017 and 2020, most measles virus sequences belonged to either the MVs/Dublin.IRL/8.16 (B3-Dublin) or the MVs/Gir Somnath.IND/42.16 (D8-Gir Somnath) variants. We evaluated the additional use of a non-coding region (MF-NCR) as a tool to enhance resolution and infer case origin, chains of transmission and characterize outbreaks.

Methods: We obtained 115 high-quality MF-NCR sequences from strains collected from Spanish patients infected with either B3-Dublin or D8-Gir Somnath variants between 2017 and 2020, performed epidemiological, phylogenetic and phylodynamic analyses and applied a mathematical model to determine relatedness among identified clades.

Results: Applying this model allowed us to identify phylogenetic clades potentially derived from concomitant importations of the virus rather than single chain of transmission, inferred based on only N450 and epidemiology data. In a third outbreak, we found two related clades that corresponded to two chains of transmission.

Discussion: Our results show the ability of the proposed method to improve identification of simultaneous importations in the same region which could trigger enhanced contact tracing. Moreover, the identification of further transmission chains indicates that the size of import-related outbreaks was smaller than previously found, supporting the interpretation that endemic measles transmission was absent in Spain between 2017 and 2020. We suggest considering the use of the MF-NCR region in conjunction with the study of N450 variants in future WHO recommendations for measles surveillance.

KEYWORDS

phylodynamic analyses, mathematical model, outbreaks, phylogenetic analysis, B3 genotype, D8 genotype

Introduction

Measles is caused by the measles virus (MeV) and is a major cause of morbidity worldwide. The implementation of the Global Measles and Rubella Strategic Plan 2012–2020 saw a significant reduction in measles incidence, especially through vaccination and improvements in surveillance (Wang et al., 2022). Despite this progress, the elimination targets for 2020 were not met and twice as many cases were reported globally in 2018 compared to 2017 (World Health Organization, 2020a). This upward trend was continuing in 2019 with several countries (e.g., Democratic Republic of the Congo, Ukraine, and Brazil) experiencing large outbreaks, just before the COVID-19 pandemic led to an interruption of routine vaccination in several countries and to fewer case notifications (https://www.cdc.gov/globalhealth/measles/news/covid-impact-on-measles-vaccination.html). Therefore, World Health Organization (2020b) launched a new strategic plan to eliminate measles by 2030.

Since 2014, measles presented a post-elimination profile in Spain with most cases being classified as imported or import-related and predominantly detected in adults as well as frequently associated with healthcare environments (López-Perea et al., 2021). In 2017, WHO declared measles eliminated from Spain, as endemic measles transmission had been interrupted in the country for a period of at least 36 months. Since then, measles circulation in Spain consisted of sporadic imported cases or small outbreaks linked with them. However, Spain also experienced an increase in incidence before the COVID-19 pandemic despite persistently high vaccination coverage (more than 95% received 1 dose of MMR vaccine and 91.5% received 2 doses of MMR vaccines from the 2016 cohort; Instituto de Salud Carlos III (2022)). In 2019, 287 cases were reported with an incidence of 6,1 cases per million of inhabitants [Instituto de Salud Carlos III (2020)]. One objective of the strategic plan for the elimination of measles and rubella in Spain, updated in 2021 (2021–2025), is to strengthen the surveillance system and outbreak response (Consejo Interterritorial del Sistema Nacional de Salud, 2021). Indeed, this is essential to maintain the endemic measles elimination status and requires increased efforts in data collection and interpretation (World Health Organization, 2018).

In addition to epidemiological surveillance, the use of molecular tools provides insights into the circulation of measles viruses and helps understanding whether there is endemic transmission or multiple introductions of MeV in a certain region or country (Santibanez et al., 2017). Molecular surveillance of MeV worldwide is currently based on the determination of the genotype by sequencing 450 nucleotides (nt) of the C-terminus region of the nucleoprotein gene (N450; World Health Organization, 2018). In 2018, only four MeV genotypes were circulating worldwide according to WHO (B3, D4, D8, and H1) and in Europe the vast majority of reported sequences belonged to MeV B3 and D8 genotypes (Brown et al., 2019). WHO keeps a database of MeV sequences named Measles Nucleotide Surveillance (MeaNS). Within genotypes, each set of identical N450 sequences widely detected is designated as sequence variant or "named strain" by MeaNS (World Health Organization, 2015). The study of variants inside genotypes has allowed to facilitate molecular surveillance. However, the genetic variation of N450 sequences is limited and is insufficient in the elimination phase to distinguish chains of MeV transmission and to infer the origin of cases. As a matter of fact, most reported sequences in Spain from 2017 to 2020 belonged to the MVs/Dublin.IRL/8.16 (B3-Dublin) or the MVs/Gir Somnath.IND/42.16 (D8-Gir Somnath) variants [Instituto de Salud Carlos III (2020)]. Therefore, the collection of additional genomic information was proposed as a solution to increase the resolution in molecular surveillance.

Researches have focused on the MF-NCR which is the longest non-coding region of the MeV genome, GC-rich and highly variable (Penedos et al., 2015; Harvala et al., 2016; Gil et al., 2018; Bodewes et al., 2021). However, standard protocols are still not available for the analysis of MF-NCR sequences and for the criteria used to associate sequences in order to distinguish chains of transmission. Recently, a method based on a mathematical model was validated to support the interpretation of MF-NCR sequences in relation with epidemiology data (Penedos et al., 2022).

The aim of the present study was to investigate whether the use of the MF-NCR region increases the resolution of measles surveillance by improving (i) discrimination between MeV with identical N450 sequences; and (ii) identification of chains of transmission and unknown importations. The pipeline of analyses consisted in phylogenetic and phylodynamic analyses coupled with a mathematical analysis (Figure 1). We evaluated its power to identify outbreaks and chains of transmission against two datasets containing (i) Spanish sequences available from the B3-Dublin and D8-Gir Somnath variants, and (ii) sequences from three well-described national outbreaks.

Materials and methods

Epidemiological data and analyses

In Spain, the regional public health services report measles cases to the National Epidemiological Surveillance Network (RENAVE) and complete a standardized case questionnaire *via* the Surveillance System electronic platform (SiViES in Spanish). The questionnaire includes items on demographic and clinical characteristics, complications, risk factors and laboratory results for diagnosis. For each confirmed case, we collected the following epidemiological information: date of rash onset, outbreak and chain of transmission identifier (as reported to WHO), contacts with other cases, importation status (case exposed outside of the country in the 7–21 days before symptom onset), type of exposure and molecular data including the WHO name and N450 variant or "named strain." For our analyses of chains of transmission, we focused on three national outbreaks: (i) B3-Dublin in the region of Navarra in 2017; (ii) B3-Dublin in the region of Valencia in 2017–2018 (Pampaka et al., 2023); and (iii) D8-Gir Somnath in the regions of Madrid and Castilla-La-Mancha in 2019 (González-Praetorius et al., 2021). Table 1 presents the epidemiological characteristics of each of these outbreaks. Taken into account the high number of cases reported for these outbreaks, we also obtained transmission plots and considered the following parameters: (i) a median period from MeV exposure to rash onset of 14 days (min = 7 days, max = 21 days before onset), and (ii) an infectiousness period from 4 days before to 4 days after rash onset according to the RENAVE protocol [Instituto de Salud Carlos III (ISCIII), Red Nacional de Vigilancia Epidemiológica (RENAVE), 2016]. Figures

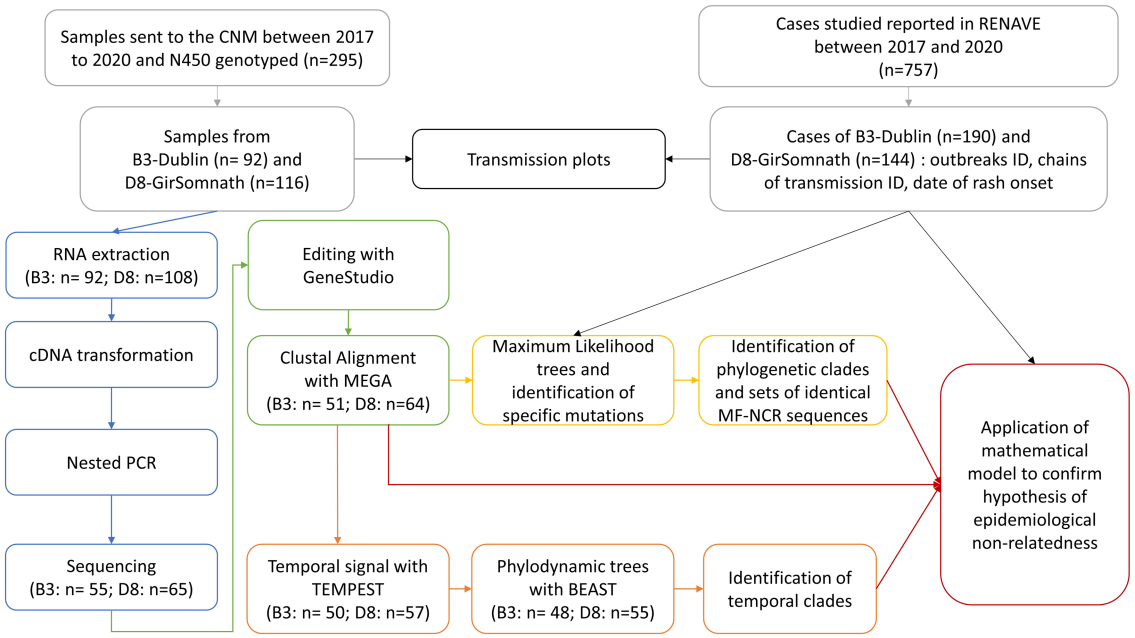

FIGURE 1
Scheme of the analysis pipeline consisting in phylogenetic and phylodynamic analyses coupled with a mathematical model.

were produced with R 4.1.2 (R Development Core Team, 2011). Networks were created using yED live[1] using the available contact-tracing information.

Clinical specimens

Between 2017 and 2020, 295 samples were received at the National Reference Laboratory for Measles and Rubella at the National Center of Microbiology (CNM) and genotyped according to WHO protocols as previously described (Mosquera et al., 2005). For our analysis, we considered 208 samples as they belonged to the Mvs/Dublin. IRL/8.16 (B3-Dublin; $n = 92$) or the MVs/Gir Somnath.IND/42.16 (D8-Gir Somnath; $n = 116$) variants. The majority of the selected samples were nasopharyngeal exudates ($n = 154$) and urines ($n = 33$).

RNA extraction, retro-transcription, PCR and sequencing

RNA was extracted from 200 µl of sample using the Quick RNA Viral kit (Zymo), according to the manufacturer's recommendations, to obtain 15 µl of final eluate. Synthesis of cDNA was performed according to the manufacturer's protocol for SuperScript IV First-Strand Synthesis System Kit (ThermoFisher) using 5 µl of the eluate.

Amplification of the MF-NCR as a single fragment was performed using primers previously described (Gil et al., 2018) with the following modifications. The first amplification was carried out using MyTaq Reaction buffer (1 ×) including 3 mM $MgCl_2$ and 1 mM dNTPs, 5 µl of cDNA as a template, 0.5 µM of each primer (MV_F1: 5′-CAAGATAGTAAGAATCCAGGCAG-3′ and MV_R1: 5′-ACTTTGTAGCTTGCACTTCC-3′) obtained from Sigma-Aldrich©, 2.5 U of MyTaq HS DNA Polymerase (Bioline) and 0.5 U of Pfu Turbo (Agilent Technologies), to a final volume of 50 µl. After a denaturation step of 2 min at 95°C, amplification was performed for 35 cycles at 95°C for 30 s, annealed at 55°C for 30 s and elongated at 72°C for 2 min, followed by a final elongation step at 72°C for 10 min. The second amplification was conducted similarly with 2 µl of PCR products as template and 0.5 µM of each primer (MV_F2: 5′-CGTGATCATAAATGATGACCAAGGAC-3′ and MV_R2: 5′-TTGTAGCTTGCACTTCCTAYYCC-3′). Amplicons were purified using Illustra ExoProStar 1-Step (GE Health Care Life Science) according to manufacturer's instructions. Amplicons were sequenced with the ABI Big Dye Terminator Cycle Sequencing Kit (Applied Biosystems) for Sanger sequencing using the MV_F2 and MV_R2 primers described above as well as the following additional primers: MV_F4 (5′-AACTTAGGGCCAAGGAAYAYAC-3′) and a newly designed primer MV_R6 (5′-GGTGTGCCTRVVTGYG-3′). All primers were prepared to 5 µM in betaine 5 M and used in a 1:5 dilution.

Sequence edition, phylogenetic analyses, and identification of sets of identical MF-NCR sequences

Sequences were assembled and edited using GeneStudio 2.2.0.0[2] to ensure that the region of the MF-NCR was supported by the

1 https://www.yworks.com/yed-live/

2 https://sourceforge.net/projects/genestudio/

TABLE 1 Characteristics of measles cases of three outbreaks in Spain.

Characteristics	2017 NAV 24	2017 VAL 2755	2019 MAD–CLM
First case	09/05/2017	01/12/2017	06/02/2019
Last case	26/06/2017	28/06/2018	25/08/2019
Total number of cases	28	154	99
Total number of chains of transmission	3 Laboral 2 (Work) Laboral 3 (Work) Hospital 1 (Nosocomial)	5 2793 (Nosocomial and Familial) 2846 (School) Carpool *UTE03-18 (Nosocomial)*	10 *670 (Imported)* 705 (Familial) 707 (Familial) 740 (Nosocomial) 783 (Familial) GU01 (Nosocomial and School and Familial) *2019GAL-01 (Nosocomial)*
Sex (%)			
Females	50.0	56.5	52.5
Males	50.0	43.5	47.5
Age group (%)			
<1	0	7.2	17.2
1–4	0	3.3	11.1
5–9	0	4.0	0
10–19	3.6	4.7	4.0
20–29	22.1	18.9	18.2
≥30	74.3	61.9	49.5
Vaccination status (%)			
Yes (at least 1 dose)	53.6	20.2	30.3
No	39.3	66.2	59.6
Unknown	7.1	13.6	10.1
Importation	Unknown	Romania	Ukraine
Travel history (%)			
Yes	7.2	8.4	7.1
No	92.8	89.0	82.8
Unknown	0	2.6	10.1

Only laboratory-confirmed cases from B3-Dublin and D8-Gir Somnath variants were included in this table. We were not able to obtain sequences for the chains of transmission shown in italic.

sequencing obtained with the two amplified DNA strands. Every consensus sequence was named in accordance with the WHO's standard nomenclature (World Health Organization, 2012). Sequences were aligned using MEGA 11's ClustalW alignment with default settings (Tamura et al., 2021). IQ-TREE v1.6.12 (Trifinopoulos et al., 2016) was used to generate a maximum likelihood (ML) tree using the best fitted nucleotide substitution model for each dataset and region previously identified using IQ-TREE's model finder. A B3 sequence from the United Kingdom in 2013 (KT732215) and a D7 sequence from United States in 2003 (JN635410) obtained from GenBank were used as outgroups as previously described (Bodewes et al., 2021). The reliability of the phylogenetic analyses at each branch node was estimated by the UltraFast bootstrap method using 1,000 replicates (Minh et al., 2013). Phylogenetic trees were edited using MEGA (Tamura et al., 2021). After multiple sequence alignment, each set of identical MF-NCR sequences was identified and named with the earliest sequence name (according to the WHO convention; Gil et al., 2018). Each group of sequences that shared a unique common ancestor were referred to as a clade (Lemey et al., 2009).

Phylodynamic analyses

Phylodynamic analyses were conducted as presented in a previous study (Penedos et al., 2022). To determine the time of divergence between samples, we estimated the time of emergence of the most recent common ancestor (MRCA) of a group of sequences using the Bayesian Markov Chain Monte Carlo (MCMC) coalescent method implemented in BEAST v1.10.4 (Bouckaert et al., 2019). First, phylogenetic trees, obtained as described above, and sample dates (defined as date of rash onset) were analyzed in TempEst v1.5.3 (Rambaut et al., 2016) using a regression of root-to-tip genetic

distances against sampling time to verify that a temporal signal is present in the dataset and to remove outliers. Then, files were prepared in BEAUti v1.10.4. (Rambaut et al., 2016) and BEAST analysis was carried out using a strict molecular clock model and the general time reversible (GTR) substitution model with ten gamma heterogeneity categories. A coalescent Bayesian Skygrid plot population growth model was used to account for variations in population size. Finally, the results of 2 runs were processed into single log and tree files which were then used to create a maximum clade credibility (MCC) tree using LogCombiner v1.10.4 and TreeAnnotator v1.10.4 (both part of the BEAST package). Convergence was assessed using Tracer v1.7.1. The consensus BEAST-inferred phylogenetic trees produced were plotted using FigTree v1.4.3[3].

Model to exclude relatedness between sample pairs

For samples belonging to different phylogenetic clades inside the same outbreak, we applied a mathematical model to exclude epidemiological relatedness as previously described (Penedos et al., 2022). We gave the model three inputs: (i) the onset dates for the two samples for which the epidemiological relatedness is being tested; (ii) the time of the earliest known case of the outbreak based on epidemiological data; and (iii) the number of substitutions between the two samples. The number of observed substitutions between two samples was calculated from the number of characters that differed between the sequences in a multiple sequence alignment. We then used the tool published by Penedos et al. (2022) to calculate Poisson probabilities and maximum expected substitutions. We used a substitution rate of 1.94×10^{-3} for B3 sequences and 2.39×10^{-3} for D8 sequences and a Poisson interval of 0.95 (Penedos et al., 2022). We considered that a sample pair was unrelated when it had higher number of substitutions than the expected maximum substitution number as calculated by the model for this time frame.

Results

Out of the 208 samples considered for our analyses, we obtained the MF-NCR sequence of 55 (60%) and 65 (56%) cases for B3-Dublin and D8-GirSomnath, respectively. Those results are comparable to what was observed previously with a OneStep RT-PCR (Penedos et al., 2015, 2022) but cDNA synthesis insure longer stability of the samples.

Confirmation of outbreaks based on the analysis of the MF-NCR

For samples belonging to the B3-Dublin variant, clean MF-NCR sequence data were obtained for 51 cases (four were excluded for poor sequence quality). Sequences were obtained from five outbreaks detected between 2017 and 2018. The three largest outbreaks were found in the regions (autonomous communities): Castilla y León (2017 VALLADOLID), Navarra (2017 NAV 24) and Valencia (2017 VAL 2755). The phylogenetic analyses and the identification of specific mutations resulted in the detection of 12 different sets of identical MF-NCR sequences (Supplementary Figure S1), most of them grouped into five phylogenetic clades (Figure 2A). While the outbreak of Valladolid (Castilla y León region) corresponded to a single set of identical MF-NCR sequences, four sets of identical MF-NCR sequences, grouped into two clades, were detected inside the outbreak of Navarra region and five sets of identical MF-NCR sequences grouped into two clades were found for the outbreak in the Valencia region. Two sequences (MVs/Cuenca.ESP/20.17 and MVs/Navarra.ESP/31.18) had a unique set of substitutions in our dataset and we could not sequence additional samples for the associated outbreaks. The analysis of the available epidemiological information also showed that the index cases of the outbreaks of Cuenca (Castilla-La Mancha region), Navarra (2018 NAV 011) and the Valencia region (2017 VAL 2755) were related to importations from Romania. The outbreak in Valladolid was also related to an importation from Romania but we could not sequence the index case.

To confirm our results, we conducted a phylodynamic analysis on the entire dataset after removing the sequence of MVs/Cuenca.ESP/20.17 as the two cases of this outbreak were related to importation. Our temporal analyses suggested that two sequences were temporal outliers (MVs/Valencia.ESP/21.18/2 and MVs/Navarra.ESP/31.18). After removing these temporal outliers, we conducted a phylodynamic analyses of the remaining 48 sequences. The results reinforced the phylogeny and supported the existence of five phylodynamic clades (defined by a node supported by posterior probability value (PP) above 0.95; Figure 2B). The estimated time of emergence of each clade was consistent with the date of rash onset of the index cases.

We apply the same methodology for MeV belonging to the D8-Gir Somnath variant. MF-NCR sequences were obtained for 64 samples (one was excluded for poor sequence quality) which correspond to eight outbreaks reported between 2018 and 2020 in Spain. We identified 15 sets of identical MF-NCR sequences, most of them grouped into five phylogenetic clades (Figure 3A; Supplementary Figure S2). Six sets of identical MF-NCR sequences, mostly grouped into three clades, were detected in the largest D8 outbreak from 2019 in the regions of Madrid and Castilla-La Mancha (2019 MAD–CLM) which was likely associated with an importation from Ukraine (the sequence of this imported case was not available). Our analyses confirmed the data from contact tracing, conducted by the public health authorities from regions, which showed that the case from Lugo (province from the region of Galicia) was part to the 2019 MAD–CLM outbreak, as it belongs to the same set of identical MF-NCR sequences than the cases of Guadalajara (Supplementary Figure S2). Eight imported cases of various origin were sequenced, two of them were the index cases of the outbreaks in the regions of Aragón (2019 ARA) and Valencia (2019 VAL 4797), and had a unique set of substitution in our dataset (Supplementary Figure S2). We could not obtain MF-NCR sequences for more cases associated with these outbreaks. In addition, the cases belonging to the outbreak of Galicia in 2020 formed a well-supported phylogenetic clade and were associated with an importation from Romania, but we could not sequence the index case. The case from Santa Cruz de Tenerife (Canary Islands) was epidemiologically linked to an imported case from Italy. A case

3 http://tree.bio.ed.ac.uk/software/figtree/

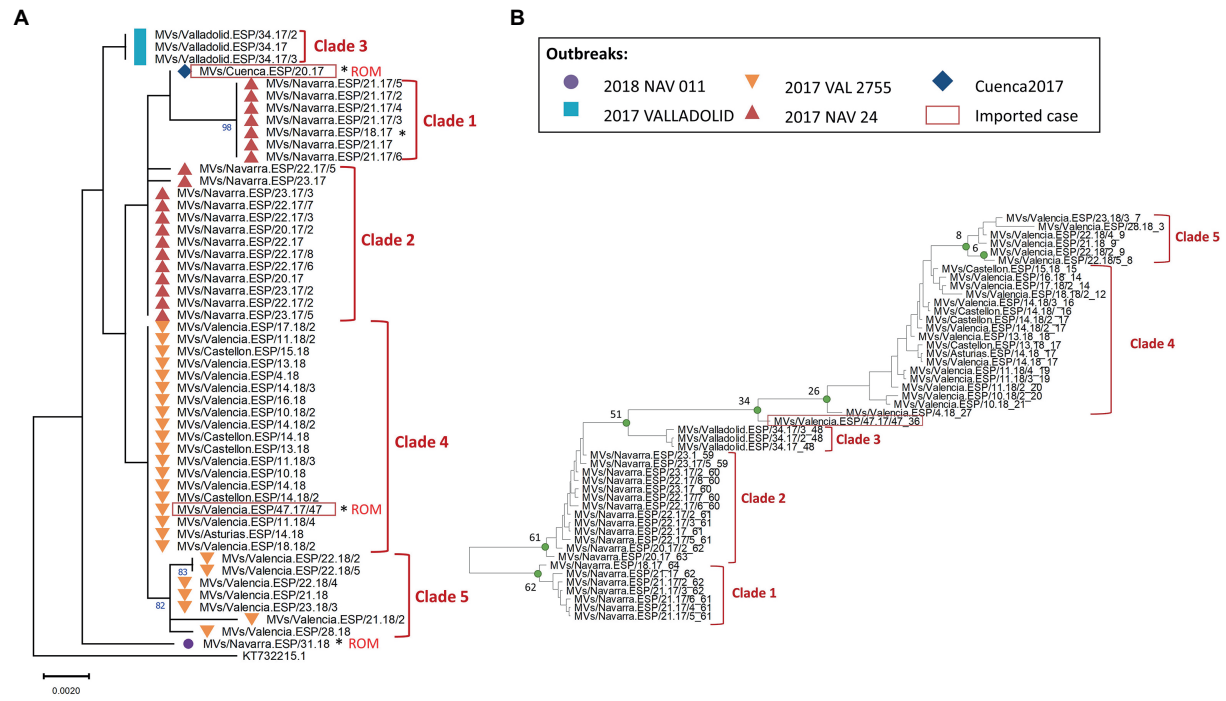

FIGURE 2
(A) Maximum likelihood tree of MeV genotype B3 strains based on the MF-NCR region using the HKY+F substitution model. Values on branches are shown as percentages based on 1,000 bootstrap replicates, only values above 80% are presented. The colored symbols represent the different outbreaks as described in the legend (NAV: Navarra, VAL: Valencia) with the codes used in SiViEs and in WHO reports. Imported cases are shown in red squares with their origin (ROM: Romania). Index cases are shown with an asterisk (*). The tree was rooted with respect to a B3 reference strain from United Kingdom in 2013 and is labeled with the accession number of GenBank. Sequences are named according to WHO convention. **(B)** BEAST maximum credibility time-scaled phylogenetic tree for MeV genotype B3 samples based on the MF-NCR region. The number of weeks since the date of onset of the last case is added to the WHO name after the underscore. Edge support values are given by the BEAST tree posterior values, well supported edges (PP>0.9) are represented by green circles. The estimated week before the date of onset of the last case of the MRCA is shown at the corresponding node for each clade. Imported cases are shown in red squares. The numbered clades are discussed in the manuscript's text.

from Madrid, that belonged to the same set of identical MF-NCR sequences, was also associated with importation from Italy. We also found that the sequences from the outbreak in the region of Valencia in 2019 (2019 VAL-4693) were not grouped into a single phylogenetic clade and two of them had an identical sequence to the ones from the outbreaks of Madrid/Castilla-La Mancha (2019 MAD–CLM) and Cataluña (2019 CAT; chain of transmission in Navarra).

Our temporal analyses showed two outliers (MVs/Guadalajara.ESP/25.19 and MVs/Valencia.ESP/12.19). After removing temporal outliers, six imported sporadic cases and the imported index case of the outbreak 2019 VAL 4797, as MF-NCR sequences could not be obtained for the two secondary cases, we performed the phylodynamic analysis on 55 sequences. The results supported the existence of five clades (posterior probability >0.95), including two inside the 2019 MAD–CLM outbreak (Figure 3B). The clade 3, based on phylogeny, was not supported by the phylodynamic analysis and only two cases (MVs/Madrid.ESP/33.19 and MVs/Madrid.ESP/34.19) formed a well-supported phylodynamic clade (Clade 3).

Deciphering chains of transmission inside the outbreaks

We then explored if (i) the MF-NCR provided sufficient resolution to identify chains of transmission inside the outbreaks; and (ii) the phylogenetic clades inside the outbreaks derived from each other by accumulation of substitutions or if there were the results of two independent importations.

The outbreak of Navarra in 2017 (2017 NAV 24) contained 28 laboratory-confirmed cases from which we obtained 20 MF-NCR sequences. First, we confirmed that MeV belonging to both phylogenetic clades were circulating simultaneously in the region in May and June 2017 (Figure 4A). Then, using epidemiological data available for the chains of transmission, we found that Clade 1 was associated with nosocomial transmission in a hospital whereas Clade 2 was associated with two chains of transmission in working places (Figure 4B). We were not able to identify a case that would link the two clades and the probabilistic model predicted that MF-NCR sequences should only differ by up to one substitution in 3–5 weeks interval since the first case of the outbreak. We found that Clade 1 differed from Clade 2 by four substitutions (A4344G, A4405G, A4406G, and A4407G; Supplementary Figure S1) and therefore it is unlikely that the two clades are related in the time frame being considered. This is in agreement with the time-scaled phylogeny obtained with BEAST (Figure 2B), which estimates that the MRCA for these clades occurred 9 weeks prior to clade 1, when there was no measles circulating in the region. The index case of Clade 1 had been visited by relatives from Portugal, however the index case of Clade 2 is unknown.

Following the same logic for the outbreak of Valencia in 2017–2018 (2017 VAL 2755), we analyzed the 27 MF-NCR sequences that

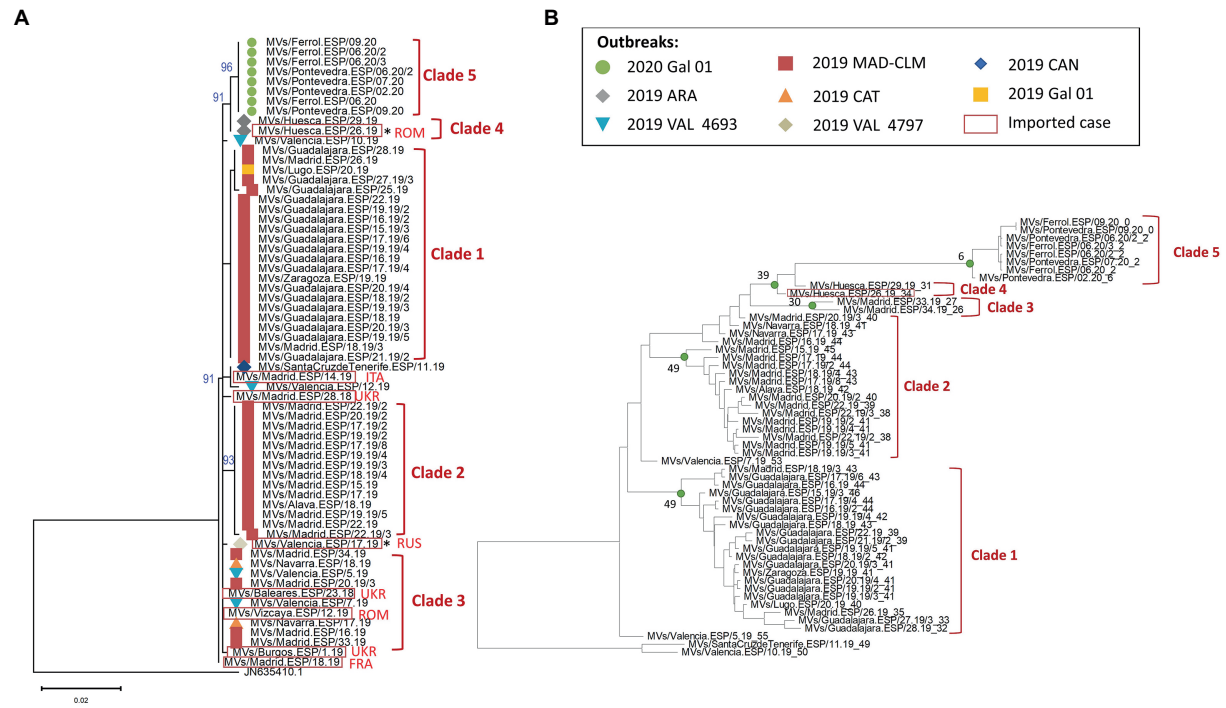

FIGURE 3
(A) Maximum likelihood tree of MeV genotype D8 strains based on the MF-NCR region using the TN+F substitution model. The colored symbols represent the different outbreak as described in the legend (Gal: Galicia, MAD: Madrid, CLM: Castilla-La Mancha, ARA: Aragón, CAT: Cataluña, CAN: Canarias, VAL: Valencia) with the codes used in SiViEs and in WHO reports. Imported cases are shown in red squares with their origin (ROM: Romania, ITA: Italia, UKR: Ukraine, RUS: Russia, FRA: France). Index cases are shown with an asterisk (*). The tree was rooted on a D7 reference strain from India in 2003 and is labeled with the accession number of GenBank. **(B)** BEAST maximum credibility time-scaled phylogenetic tree for MeV genotype D8 samples based on the MF-NCR region as presented for B3. The estimated week before the date of onset of the last case of the MRCA is shown at the corresponding node for each clade.

were representative of the 148 laboratory-confirmed cases as they uniformly covered the duration of the outbreak (Figure 5A). We observed that the cases of Clade 5 had later dates of onset in the outbreak compared to cases in Clade 4 and could have been infected by earlier cases including those for which we did not obtain a MF-NCR sequence (Figure 5A). Clade 4 consisted of cases with identical sequences from three chains of transmission in two provinces of the region of Valencia (Valencia and Castellón), and in the region of Asturias. Epidemiological information indicates that the cases from Castellón and Asturias were infected in Valencia, supporting the results of the phylogenetic analyses. The cases in Clade 5 belonged to two chains of transmission: one related to nosocomial infection, which started with cases from Clade 4, and another related to intra-familial (Family S) transmission (Figure 5B). Clade 5 share a common substitution (C5027T; Supplementary Figure S1) with Clade 4. The network analysis based on contact tracing information showed a link between one case in Clade 4 and two cases in Clade 5 as they all were exposed in the same hospital P (Figure 5C). Within Clade 5, an epidemiological link could not be identified between the cases in the hospital and the cases in the family S but the phylogenetic analysis showed two sets of identical MF-NCR sequences (MVs/Valencia.ESP/21.18 and MVs/Valencia.ESP/22.18/2) that included cases from both the family S and the hospital P. According to the mathematical model the maximum number of expected substitutions since the index case was between four and five. We observed a number of substitutions between one and four and therefore could not exclude that the cases of Clade 4 and Clade 5 were related.

Finally, we analyzed the outbreak of the regions Madrid and Castilla-La Mancha of 2019 (2019 MAD–CLM). According to the onset of rash, cases from clades 1 and 2 were circulating simultaneously from January to September 2019 (Figure 6A). Sequences from clade 1 were associated with three chains of transmission, one related to nosocomial transmission, one associated with transmission in a day care and one intra-familial. While most of the cases were reported in Guadalajara, two cases were from Madrid and one case from Zaragoza (region of Aragón; Figure 6B). Clade 2 was associated with three chains of transmission in Madrid and Álava (País Vasco), one was associated with nosocomial transmission (740), which showed identical sequence except for one case (Supplementary Figure S2). Clade 3 was associated with a single chain of transmission, but two earlier cases showed identical sequences. We did not identify an epidemiological link between the three clades. The model predicted a maximum of three substitutions between samples from Clades 1 and 2. However, we observed five substitutions suggesting the cases from the two clades were not related. While the index case of Clade 2 was associated with importation from Ukraine, we were not able to identify the index case of Clade 1.

Discussion

Since the declaration of elimination of endemic measles in Spain by the WHO in 2017, recurrent outbreaks have been sporadically reported and caused mostly by two N450 variants:

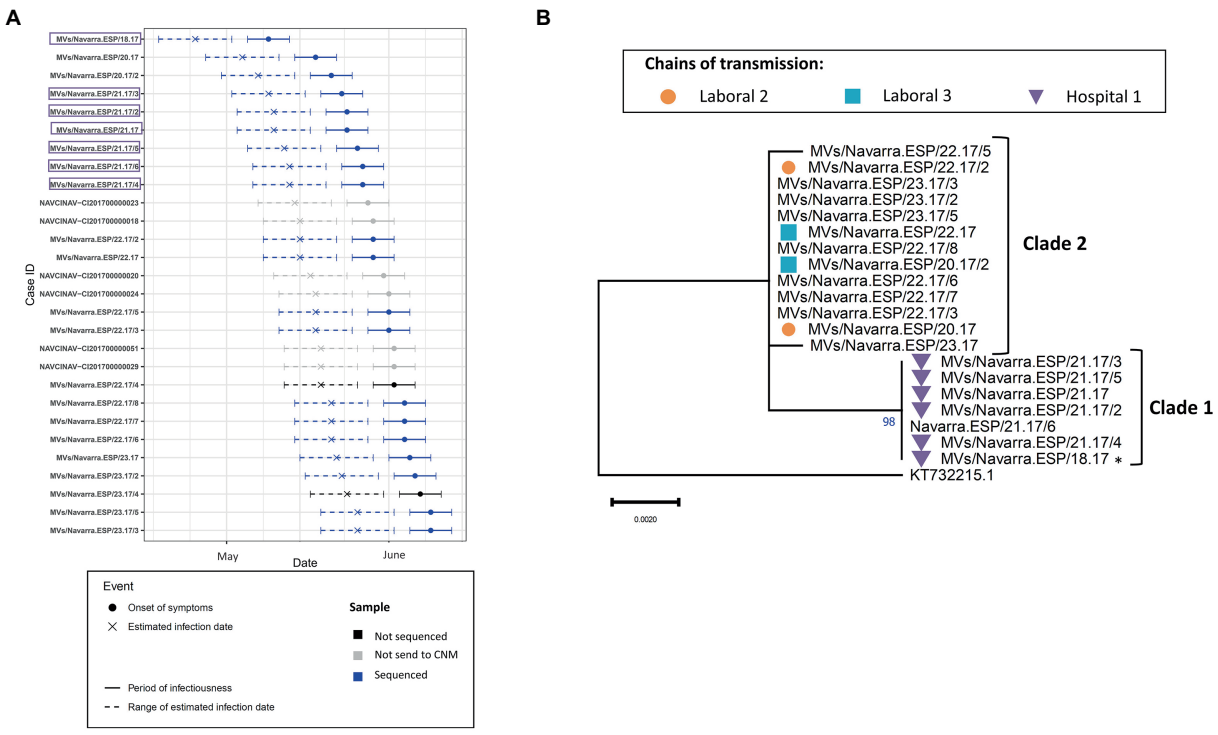

FIGURE 4
(A) Transmission plot for the outbreak of Navarra in 2017 showing the onset of symptoms, the estimated infection date, the period of infectiousness and the range of estimated infectious date as described in Material and Methods. Samples that were not send to the CNM are shown in gray, those that were sent but not sequenced for the MF-NCR (for technical reasons or because they were from other variants) are in black and the ones that were sequenced for the MF-NCR are in blue. Purple squares show the samples belonging to the clade 1. **(B)** Maximum likelihood tree of the strains belonging to the Navarra outbreak of 2017 based on the MF-NCR region using the HKY+F substitution model. The colored symbols represent the different chains of transmission as defined by contact-tracing with the codes used in SiViEs and in WHO reports. Index case is shown with an asterisk (*). The clades identified with the phylodynamic analysis are indicated in bold.

B3-Dublin and D8-Gir-Somnath. In the present study, the analysis of the MF-NCR region was evaluated as a method to increase discrimination between viruses with identical N450 sequences in order to improve the ability to infer chains of transmission and outbreaks. Using cases from multiple outbreaks, our results suggest that the MF-NCR analysis could support the outbreaks identified by contact-tracing and traditional epidemiological studies. Moreover, the probabilistic method may be useful to decipher the relatedness of samples inside outbreaks, including the identification of chains of transmission and multiple viral introductions. For example, the outbreaks of Navarra in 2017 and Madrid/Castilla-La Mancha in 2019 were probably the result of two independent introductions that were not identified by the study of N450 variants in combination with the epidemiological data. This result has two implications: (i) it shows the relevance of the method as a tool to direct contact tracing in order to identify index cases in context of simultaneous importations in the same region; (ii) it supports that endemic transmission was absent in Spain, given that the size of the importation-related outbreaks was smaller than previously found. The outbreak of Madrid/Castilla-La Mancha highlights a situation where epidemiological methods are challenged, and N450 sequencing is not sufficiently discriminative to complement them. Several contacts were established between Madrid and Guadalajara due to their geographical proximity, making the accurate attribution of individual cases to a particular outbreak impossible when based only on time and place. That is where the analyses MF-NCR showed the most added-value, as we were able to suggest two independent introductions from which one was mostly related to Guadalajara but with some cases from Madrid.

The use of the entire MF-NCR region is more cost-effective and less labor-intensive, while bringing similar resolution, than other methods such as the use of two or three different regions of the genome (Bodewes et al., 2021; Kim et al., 2021) or whole genome sequencing (WGS; Penedos et al., 2015). In addition, our protocol allows to increase stability of the samples together with high yield of MF-NCR amplifications compared to what was observed with described protocol (Penedos et al., 2022). Phylodynamic analyses showed to be a powerful tool to confirm the phylogenetic analyses, to characterize outbreaks and to support the interpretation of contact information. Nevertheless, our study shows that the relatedness model represents a good alternative, as it is faster and does not require bioinformatics analyses. Rather than assessing relatedness inside a chain of transmission, the model should be used to unlink cases when multiple introductions are suspected.

One limitation of our study is associated with the limited sampling rate as we obtained MF-NCR sequences for as little as 18% of the cases of the Valencia region outbreak. However, the sequences obtained provided a good coverage of the outbreak both temporally and

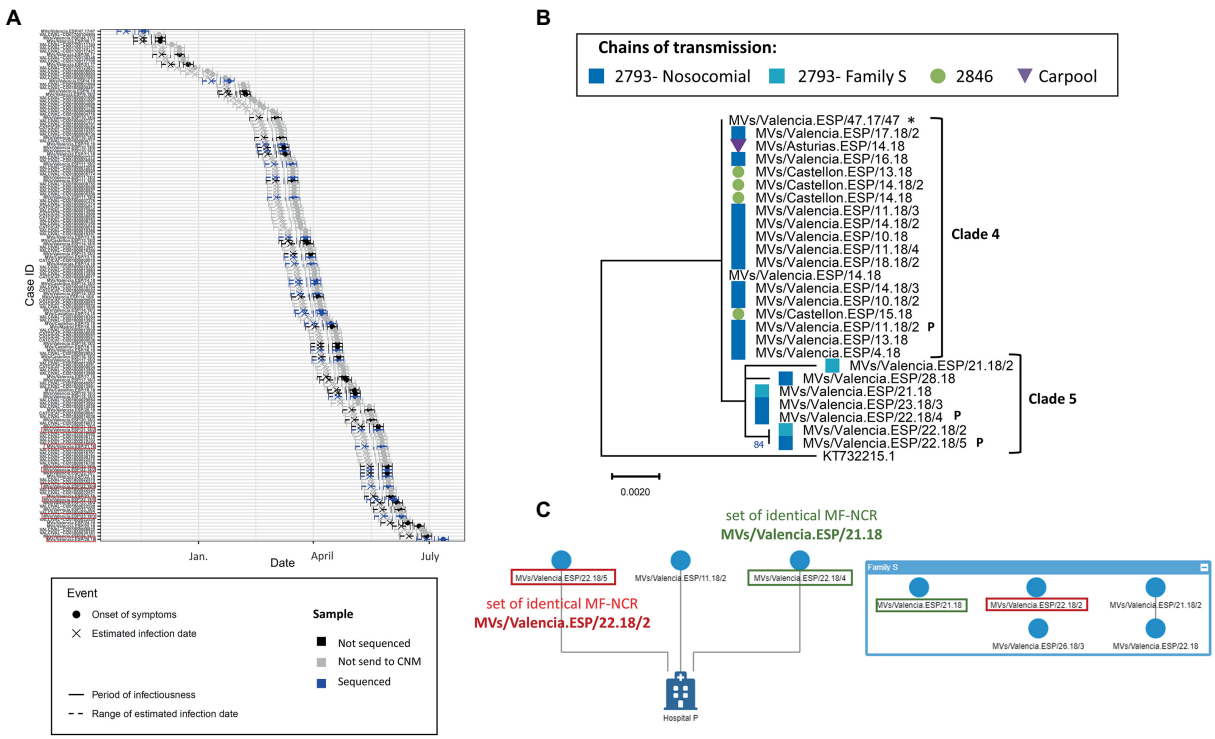

FIGURE 5
(A) Transmission plot for the outbreak of Valencia in 2017–2018. Red squares show the samples belonging to the clade 5. **(B)** Maximum likelihood tree of the strains belonging to the Valencia outbreak of 2017–2018 on MF-NCR region using the HKY+F substitution model. The colored symbols represent the different chains of transmission as defined by contact-tracing with the codes used in SiViEs and in WHO reports. Index case is shown with an asterisk (*). The clades identified with the phylodynamic analysis are indicated in bold. Sequences marked with a P belong to the cases related with the hospital P. **(C)** Network of transmission for the hospital P and the family S. Squares of color show the different sets of identical MF-NCR sequences shared by the family S and hospital P.

geographically (Figure 5A). In addition, in large outbreaks more than one N450 sets of identical MF-NCR sequences can be detected because of a substitution in the N450 region, which could occur independently of those in the MF-NCR region. We focused on the analysis of the MF-NCR sequences inside the predominant variant of the outbreak, however, future studies should include sequences from other N450 sets of identical MF-NCR sequences belonging to same outbreak to evaluate the pertinence of the MF-NCR region in those situations. Phylogeny and phylodynamic analyses could also be conducted with concatenated N450 and MF-NCR sequences to reflect changes in both genomic regions. Finally, the MF-NCR region alone is potentially not sufficient to identify all chains of transmission, even though as it has been shown to provide comparable phylogenetic resolution to that of WGS (Penedos et al., 2015). Several explanations can be proposed for samples belonging to different epidemiological chains of transmission with an identical MF-NCR sequence: (i) either cases have the same infectious origin, (ii) two separate chains of transmission may have acquired the same mutations, or (iii) the genetic diversity in circulating MeV may be insufficient, in which case WGS may help distinguishing them.

The number of measles patients surged worldwide in 2019 before the COVID-19 pandemic and the consequences that the recent conflict in Ukraine could have on the circulation of the virus in Europe are still unknown. However, the previous conflict of the Donbas region caused a sharp decline on vaccine coverage in Ukraine and a large outbreak that extended to different European countries (Lancet, 2018). In addition, with the decline in the vaccination coverage worldwide, there is an increased risk to observe sporadic outbreaks linked with importations (Durrheim et al., 2014; Lee et al., 2019). In this context, it is of primary importance to find new methods to support epidemiological evidence and increase the resolution of molecular surveillance for countries in the post-elimination phase. We showed here the added value of the MF-NCR analysis to reveal unknown importations. However, this method must be considered as a complement of the variant analysis based on recommended genotyping methods, not in place of it. It might also be a useful tool in cases where epidemiological evidence is not available, including to identify the origin of a imported cases by comparing them with reference sequences from different countries as already suggested (Kim et al., 2021). To improve this comparison, international efforts must continue for the production and sharing of genomic information on measles outbreaks, including MF-NCR sequences.

In conclusion, the multi-faceted approach described here is relevant to track importations and verify the maintenance of measles elimination status. The analysis of the MF-NCR could be added to N450 sequencing in the protocol for routine molecular surveillance to support epidemiological studies in elimination settings. In addition of phylogenetic analyses, we also propose the use of a previously described mathematical model (Penedos et al., 2022) to establish clear criteria for assessing the epidemiological relatedness between identified MeV cases.

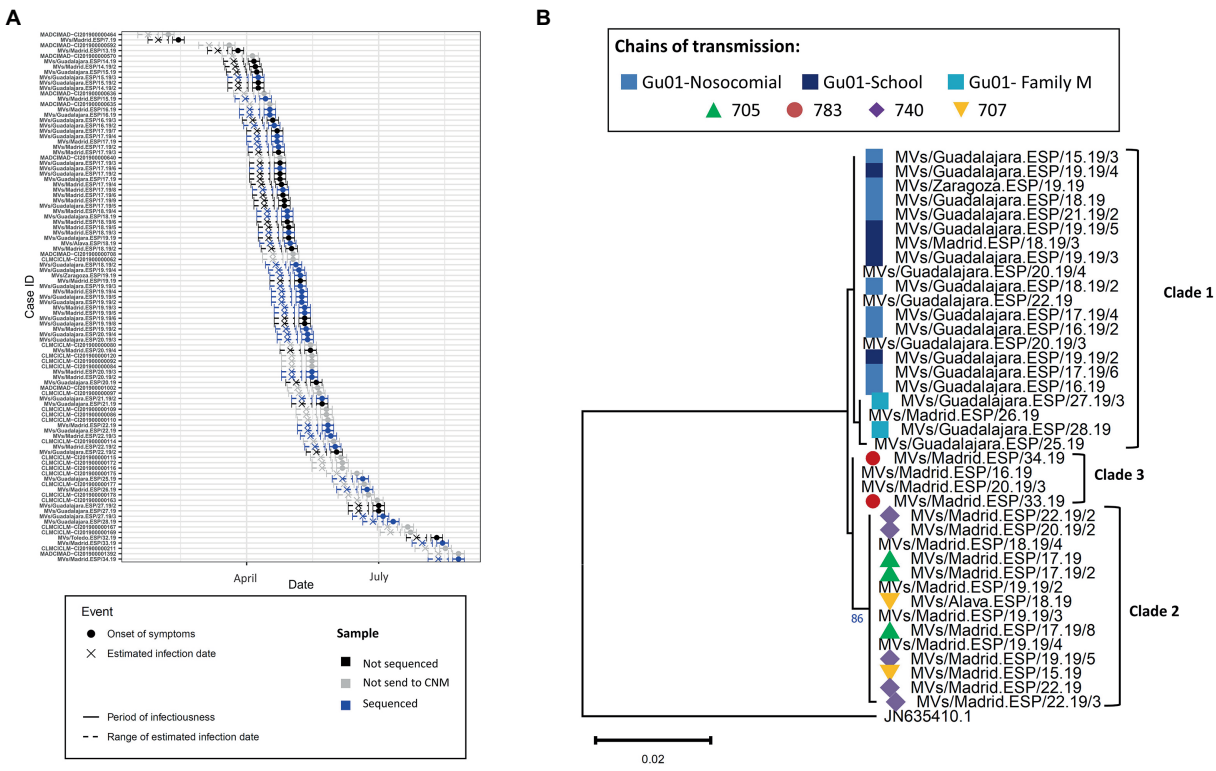

FIGURE 6
(A) Transmission plot for the outbreak of Madrid/Castilla-La Mancha 2019. **(B)** Maximum likelihood tree of the strains belonging to the outbreak based on the MF-NCR region using the HKY+F substitution model. The colored symbols represent the different chains of transmission as defined by contact-tracing with the codes used in SiViEs and in WHO reports. The clades identified with the phylodynamic analysis are indicated in bold.

Data availability statement

All the MF-NCR sequences (including the stop codon of the M gene and the start codon of the F gene, i.e., 1018 nt) included in this study were deposited in ON755137-ON755141, ON755143-ON755156, ON792426-ON792428, ON792430-ON792434 and ON792437-ON792520 and ON792522-ON792525.

Ethics statement

The samples used in this work were received by the National Reference Laboratory for Measles and Rubella at the CNM, in the context of the National Measles and Rubella Elimination Plan and used in accordance with the requirements of Spanish biomedical research law (Ley 14/2007 de Investigación Biomédica). The protocol was approved by the Comité de Ética de la Investigación of the Instituto de Salud Carlos III (approval no. CEI PI 35–2015). Written informed consent from the participants was not required to participate in this study in accordance with the national legislation and the institutional requirements.

MMR study group

Aragón.

Ana Martínez Sapiña, Servicio de Microbiología, Hospital Universitario Miguel Servet, Zaragoza, Spain.

Ana Cebollada, Dirección General de Salud Pública de Aragón, Zaragoza, Spain.

Castilla La Mancha.

Alejandro González-Praetorius, Sección de Microbiología, Hospital Universitario de Guadalajara, Guadalajara, Spain.

María Victoria García-Rivera, Servicio de Epidemiología, Dirección General de Salud Pública de Castilla-La Mancha, Toledo, Spain.

Castilla y León.

Silvia Rojo-Rello, José Mª Eiros-Bouza and Raúl Ortiz-de-Lejarazu, Servicio de Microbiología del Hospital Clínico Universitario de Valladolid, Valladolid, Spain.

Cristina Ruiz-Sopeña and Mª Jesús Rodríguez Recio, Servicio de Epidemiología. Dirección General de Salud Pública de Castilla y León. Valladolid, Spain.

Comunidad Foral de Navarra.

Ana Navascués, Servicio de Microbiología Clínica, Hospital Universitario de Navarra, Pamplona, Spain.

Manuel García-Cenoz, Instituto de Salud Pública y Laboral de Navarra, Pamplona, Spain.

Comunidad de Madrid.

Juan Carlos Sanz and Marta Pérez-Abeledo, Laboratorio Regional de Salud Pública de la Comunidad de Madrid. Dirección General de Salud Pública de la Comunidad de Madrid, Madrid, Spain.

Luis García-Comas, Inma Rodero-Garduño and Alba Nieto Juliá, Área de Vigilancia y Control de Enfermedades Transmisibles,

Dirección General de Salud Pública de la Comunidad de Madrid, Madrid, Spain.

Comunidad Valenciana.

Beatriz Acosta-Boga, Servicio de Microbiología, Hospital Universitari i Politècnic La Fe, Valencia, Spain.

María Gil, Servicio de Microbiología, Hospital General de Castellón, Castellón, Spain.

Javier Roig, Katja Villatoro, Maite Castellanos and Isabel Huertas, Servicio de Vigilancia y Control Epidemiológico de la Comunidad Valenciana, Valencia, Spain.

Juan Bellido, Centro de Salud Pública de Castellón, Castellón, Spain.

María Sanz, Centro de Salud Pública de Manises, Manises, Spain.

Galicia.

Patricia Ordoñez-Barrosa, Servicio de Microbiología, Complejo Hospitalario Universitario de Ferrol, Ferrol, Spain.

Matilde Trigo-Daporta, Servicio de Microbiología, Complejo Hospitalario Universitario de Pontevedra, Pontevedra, Spain.

Isabel Losada-Castillo, Servizo de Calidade Asistencial, Dirección Xeral de Asistencia Sanitaria de Galicia, Santiago de Compostela, Spain.

Alberto Malvar Pintos, Servizo de Epidemioloxia, Dirección Xeral de Saúde Pública, Santiago de Compostela, Spain.

Author contributions

CJ: technical work, data analysis and writing as main author. AG: technical work and data analysis. JM-C and NL-P designed the study, reviewed and assisted in the editing of the final version of the manuscript. JE, design for the study and revised the manuscript. AP assisted in the use of mathematical method and editing of the final version of the manuscript. AF-G designed the study, revised the manuscript and writing as main author. All authors contributed to the article and approved the submitted version.

Funding

This work was supported by the "Instituto de Salud Carlos III" (PI15CIII/00023, PI19ICIII/0041). AG was funded by CIBER de Epidemiología y Salud Pública (CIBERESP), ISCIII. CJ was funded by the ECDC/EUPHEM fellowship.

Acknowledgments

We would like to thank the Genomic Unit of the CNM-ISCIII for technical assistance with sequencing and Ana M. Castellanos and Sara Ruiz-Velázquez for their technical assistance.

Conflict of interest

The authors declare that the research was conducted in the absence of any commercial or financial relationships that could be construed as a potential conflict of interest.

Publisher's note

Supplementary material

The Supplementary material for this article can be found online at: https://www.frontiersin.org/articles/10.3389/fmicb.2023.1143933/full#supplementary-material

SUPPLEMENTARY FIGURE S1
Alignment of the MF-NCR region for the 12 sets of identical MF-NCR sequences found in B3. Regions without substitutions are not shown in the sake of place.

SUPPLEMENTARY FIGURE S2
Alignment of the MF-NCR region for the 15 sets of identical MF-NCR sequences found in D8. Regions without substitutions are not shown in the sake of place.

References

Bodewes, R., Reijnen, L., Zwagemaker, F., Kohl, R. H. G., Kerkhof, J., Veldhuijzen, I. K., et al. (2021). An efficient molecular approach to distinguish chains of measles virus transmission in the elimination phase. *Infect. Genet. Evol.* 91:104794. doi: 10.1016/j.meegid.2021.104794

Bouckaert, R., Vaughan, T. G., Barido-Sottani, J., Duchêne, S., Fourment, M., Gavryushkina, A., et al. (2019). BEAST 2.5: an advanced software platform for Bayesian evolutionary analysis. *PLoS Comput. Biol.* 15:e1006650. doi: 10.1371/journal.pcbi.1006650

Brown, K. E., Rota, P. A., Goodson, J. L., Williams, D., Abernathy, E., Takeda, M., et al. (2019). Genetic characterization of measles and rubella viruses detected through global measles and rubella elimination surveillance, 2016–2018. *MMWR Morb. Mortal. Wkly Rep.* 68, 587–591. doi: 10.15585/MMWR.MM6826A3

Consejo Interterritorial del Sistema Nacional de Salud (2021). Plan estratégico para la eliminación del sarampión y la rubeola en España. Ministerio de Sanidad. Available at: https://www.sanidad.gob.es/profesionales/saludPublica/prevPromocion/vacunaciones/sarampion-rubeola/docs/PlanEstrategico_SarampionyRubeola.pdf

Durrheim, D. N., Crowcroft, N. S., and Strebel, P. M. (2014). Measles - the epidemiology of elimination. *Vaccine* 32, 6880–6883. doi: 10.1016/J.VACCINE.2014.10.061

Gil, H., Fernández-García, A., Mosquera, M. M., Hübschen, J. M., Castellanos, A. M., de Ory, F., et al. (2018). Measles virus genotype D4 strains with nonstandard length M-F non-coding region circulated during the major outbreaks of 2011-2012 in Spain. *PLoS One* 13, 1–12. doi: 10.1371/journal.pone.0199975

González-Praetorius, A., Fernández-García, A., Pérez-Olmeda, M., García-Rivera, M. V., Caballero-López, B., Gilaberte-Reyzabal, S., et al. (2021). Measles outbreak in the sanitary area of Guadalajara (Spain): difficulty in microbiological diagnosis in the era of its elimination. *Enferm. Infecc. Microbiol. Clin.* 40, 532–538. doi: 10.1016/j.eimc.2021.07.011

Harvala, H., Wiman, A., Wallensten, A., Zakikhany, K., Englund, H., and Brytting, M. (2016). Role of sequencing the measles virus hemagglutinin gene and hypervariable region in the measles outbreak investigations in Sweden during 2013-2014. *J. Infect. Dis.* 213, 592–599. doi: 10.1093/infdis/jiv434

Instituto de Salud Carlos III (ISCIII), Red Nacional de Vigilancia Epidemiológica (RENAVE) (2016). Protocolo de vigilancia del sarampión. Available at: https://www.isciii.es/QueHacemos/Servicios/VigilanciaSaludPublicaRENAVE/EnfermedadesTransmisibles/Documents/archivos%20A-Z/Sarampión/Protocolo%20de%20Vigilancia%20de%20Sarampión.pdf

Instituto de Salud Carlos III (2020). Plan Nacional de Eliminación del Sarampión y de la Rubeola. Informe anual 2019. Available at: https://www.isciii.es/QueHacemos/Servicios/VigilanciaSaludPublicaRENAVE/EnfermedadesTransmisibles/Documents/archivos%20A-Z/Sarampi%C3%B3n/Informe_anual_SAR_RUB_2019_VF_Rev.pdf

Instituto de Salud Carlos III (2022). Plan estratégico para la eliminación del sarampión y la rubeola en España. Informe anual 2021. Available at: https://www.isciii.es/QueHacemos/Servicios/VigilanciaSaludPublicaRENAVE/EnfermedadesTransmisibles/Documents/archivos%20A-Z/Sarampi%C3%B3n/Informe_SAR-RUB_2021.pdf

Kim, J. M., Park, S., Kim, S., Park, K. R., Wang, J. S., and Chung, Y. S. (2021). Genetic analysis of the Measles virus from the outbreaks in South Korea, 2019. *Front. Microbiol.* 12, 1–10. doi: 10.3389/fmicb.2021.763107

Lee, A. D., Clemmons, N. S., Patel, M., and Gastanaduy, P. A. (2019). International importations of Measles virus into the United States during the post-elimination era, 2001–2016. *J. Infect. Dis.* 219, 1616–1623. doi: 10.1093/INFDIS/JIY701

Lemey, P., Salemi, M., and Vandamme, A. (Eds.) (2009). *The Phylogenetic Handbook: A Practical Approach to Phylogenetic Analysis and Hypothesis Testing*. Cambridge: Cambridge University Press 2nd Edn.

López-Perea, N., Fernandez-Garcia, A., Echevarria, J. E., de Ory, F., Pérez-Olmeda, M., and Masa-Calles, J. (2021). Measles in vaccinated people: epidemiology and challenges in. *Viruses* 13, 2014–2020. doi: 10.3390/v13101982

Minh, B. Q., Nguyen, M. A. T., and Von Haeseler, A. (2013). Ultrafast approximation for phylogenetic bootstrap. *Mol. Biol. Evol.* 30, 1188–1195. doi: 10.1093/molbev/mst024

Mosquera, M. M., De Ory, F., and Echevarría, J. E. (2005). Measles virus genotype circulation in Spain after implementation of the National Measles Elimination Plan 2001-2003. *J. Med. Virol.* 75, 137–146. doi: 10.1002/jmv.20248

Pampaka, D., López-Perea, N., Fernández-García, A., Huertas-Zarco, I., Castellanos-Martínez, M., Villatoro-Bongiorno, K., et al. (2022). An inter-regional measles outbreak in Spain with nosocomial transmission, November 2017 to July 2018. *Euro Surveill ance.* 28:pii=2200634. doi: 10.2807/1560-7917.ES.2023.28.17.2200634

Penedos, A. R., Fernández-García, A., Lazar, M., Ralh, K., Williams, D., and Brown, K. E. (2022). Mind your Ps: a probabilistic model to aid the interpretation of molecular epidemiology data. *EBioMedicine* 79:1–12:103989. doi: 10.1016/j.ebiom.2022.103989

Penedos, A. R., Myers, R., Hadef, B., Aladin, F., and Brown, K. E. (2015). Assessment of the utility of whole genome sequencing of Measles virus in the characterisation of outbreaks. *PLoS One* 10:e0143081. doi: 10.1371/JOURNAL.PONE.0143081

R Development Core Team (2011). R: A language and environment for statistical computing. R Foundation for Statistical Computing, Vienna. http://www.R-project.org

Rambaut, A., Lam, T. T., Carvalho, L. M., and Pybus, O. G. (2016). Exploring the temporal structure of heterochronous sequences using TempEst (formerly path-O-gen). *Virus Evol* 2, 1–7. doi: 10.1093/ve/vew007

Rambaut, A., and Lam, T. T.LMC and OGP (2016). Exploring the temporal structure of heterochronous sequences using TempEst. *Virus Evol* 2:vew007. doi: 10.1093/ve/vew007

Santibanez, S., Mankertz, A., Hübschen, J. M., Muller, C. P., Ben Mamou, M. C., Muscat, M., et al. (2017). Molecular surveillance of measles and rubella in the WHO European region: new challenges in the elimination phase. *Clin. Microbiol. Infect.* 23, 516–523. doi: 10.1016/j.cmi.2017.06.030

Tamura, K., Stecher, G., and Kumar, S. (2021). MEGA11: molecular evolutionary genetics analysis version 11. *Mol. Biol. Evol.* 38, 3022–3027. doi: 10.1093/molbev/msab120

The Lancet (2018). The lancet. Measles, war, and health-care reforms in Ukraine. *Lancet* 392:711. doi: 10.1016/S0140-6736(18)31984-6

Trifinopoulos, J., Nguyen, L. T., von Haeseler, A., and Minh, B. Q. (2016). W-IQ-TREE: a fast online phylogenetic tool for maximum likelihood analysis. *Nucleic Acids Res.* 44, W232–W235. doi: 10.1093/NAR/GKW256

Wang, R., Jing, W., Liu, M., and Liu, J. (2022). Trends of the global, regional, and National Incidence of Measles, vaccine coverage, and risk factors in 204 countries from 1990 to 2019. *Front. Med.* 8, 1–12. doi: 10.3389/fmed.2021.798031

World Health Organization (2012). Measles virus nomenclature update: 2012 = Nomenclature des virus rougeoleux: mise à jour 2012. *Wkly Epidemiol Rec = Relev épidémiologique Hebd* 87, 73–80. Available at: https://www.who.int/publications/i/item/WER8709

World Health Organization (2015). Genetic diversity of wildtype measles viruses and the global measles nucleotide surveillance database (MeaNS). *Wkly Epidemiol Rec = Relev épidémiologique Hebd* 30, 373–380. Available at: https://apps.who.int/iris/handle/10665/242393

World Health Organization (2018). The role of extended and whole genome sequencing for tracking transmission of measles and rubella viruses: report from the global Measles and rubella laboratory network meeting, 2017. *Wkly Epidemiol Rec* 93, 55–59.

World Health Organization. Chapter 1: manual for the laboratory-based Surveillance of Measles, rubella, and congenital rubella syndrome. (2018) Available at: https://www.who.int/publications/m/item/chapter-1-manual-for-the-laboratory-based-surveillance-of-measles-rubella-and-congenital-rubella-syndrome. Accessed June 17, 2022.

World Health Organization. Measles and rubella surveillance data. (2020a) Available at: https://www.who.int/teams/immunization-vaccines-and-biologicals/immunization-analysis-and-insights/surveillance/monitoring/provisional-monthly-measles-and-rubella-data. Accessed October 8, 2020.

World Health Organization. Measles and rubella strategic framework 2021-2030. (2020b). Available at: https://s3.amazonaws.com/wp-agility2/measles/wp-content/uploads/2020/11/measles_rubella_initiative_final_print.pdf

frontiers | Frontiers in Microbiology

TYPE Original Research
PUBLISHED 30 May 2023
DOI 10.3389/fmicb.2023.1177651

OPEN ACCESS

EDITED BY
Ons Bouchami,
Universidade Nova de Lisboa, Portugal

REVIEWED BY
Keita Matsuno,
Hokkaido University, Japan
Alexandro Guterres,
Oswaldo Cruz Foundation (Fiocruz), Brazil

*CORRESPONDENCE
Koray Ergunay
✉ ekoray@hacettepe.edu.tr

RECEIVED 01 March 2023
ACCEPTED 28 April 2023
PUBLISHED 30 May 2023

CITATION
Ergunay K, Dincer E, Justi SA, Bourke BP, Nelson SP, Liao H-M, Timurkan MO, Oguz B, Sahindokuyucu I, Gokcecik OF, Reinbold-Wasson DD, Jiang L, Achee NL, Grieco JP and Linton Y-M (2023) Impact of nanopore-based metagenome sequencing on tick-borne virus detection. *Front. Microbiol.* 14:1177651. doi: 10.3389/fmicb.2023.1177651

Impact of nanopore-based metagenome sequencing on tick-borne virus detection

Koray Ergunay[1,2,3,4]*, Ender Dincer[5], Silvia A. Justi[1,2,3], Brian P. Bourke[1,2,3], Suppaluck P. Nelson[1,2,3], Hsiao-Mei Liao[6,7], Mehmet Ozkan Timurkan[8], Bekir Oguz[9], Ismail Sahindokuyucu[10], Omer Faruk Gokcecik[10], Drew D. Reinbold-Wasson[11], Le Jiang[6,7], Nicole L. Achee[12], John P. Grieco[12] and Yvonne-Marie Linton[1,2,3]

[1]Walter Reed Biosystematics Unit (WRBU), Smithsonian Institution, Museum Support Center, Suitland, MD, United States, [2]One Health Branch, Walter Reed Army Institute of Research (WRAIR), Silver Spring, MD, United States, [3]Department of Entomology, Smithsonian Institution–National Museum of Natural History (NMNH), Washington, DC, United States, [4]Department of Medical Microbiology, Virology Unit, Faculty of Medicine, Hacettepe University, Ankara, Türkiye, [5]Department of Virology, Faculty of Veterinary Medicine, Dokuz Eylül University, Izmir, Türkiye, [6]Naval Medical Research Center (NMRC), Silver Spring, MD, United States, [7]Henry M. Jackson Foundation for the Advancement of Military Medicine, Bethesda, MD, United States, [8]Department of Virology, Faculty of Veterinary Medicine, Ataturk University, Yakutiye, Erzurum, Türkiye, [9]Department of Parasitology, Faculty of Veterinary Medicine, Van Yuzuncu Yil University, Van, Türkiye, [10]Bornova Veterinary Control Institute, Veterinary Control Institute Directorates, Ministry of Agriculture and Forestry, Izmir, Türkiye, [11]U.S. Army Medical Research Diriectorate-Georgia (USAMRD-G), Tbilisi, Georgia, [12]Department of Biological Sciences, Eck Institute for Global Health, University of Notre Dame, Notre Dame, IN, United States

Introduction: We evaluated metagenomic nanopore sequencing (NS) in field-collected ticks and compared findings from amplification-based assays.

Methods: Forty tick pools collected in Anatolia, Turkey and screened by broad-range or nested polymerase chain reaction (PCR) for Crimean-Congo Hemorrhagic Fever Virus (CCHFV) and Jingmen tick virus (JMTV) were subjected to NS using a standard, cDNA-based metagenome approach.

Results: Eleven viruses from seven genera/species were identified. Miviruses Bole tick virus 3 and Xinjiang mivirus 1 were detected in 82.5 and 2.5% of the pools, respectively. Tick phleboviruses were present in 60% of the pools, with four distinct viral variants. JMTV was identified in 60% of the pools, where only 22.5% were PCR-positive. CCHFV sequences characterized as Aigai virus were detected in 50%, where only 15% were detected by PCR. NS produced a statistically significant increase in detection of these viruses. No correlation of total virus, specific virus, or targeted segment read counts was observed between PCR-positive and PCR-negative samples. NS further enabled the initial description of Quaranjavirus sequences in ticks, where human and avian pathogenicity of particular isolates had been previously documented.

Discussion: NS was observed to surpass broad-range and nested amplification in detection and to generate sufficient genome-wide data for investigating virus diversity. It can be employed for monitoring pathogens in tick vectors or human/animal clinical samples in hot-spot regions for examining zoonotic spillover.

KEYWORDS

nanopore, tick, tick-borne, metagenome, virus, zoonoses

1. Introduction

Genomic identification of microbial pathogens has established a substantial role in the diagnosis and monitoring of infectious diseases within the One Health concept (Trinh et al., 2018). Metagenomic investigations, facilitated by the widespread use of next-generation sequencing (NGS), enable the analysis of the nucleic acid content of any sample, without prior information on pathogens. In clinical diagnosis, metagenomic testing has proven useful in infections with unconventional agents, non-specific clinical presentation, and in instances where pathogen diversity hampers targeted detection (Dulanto Chiang and Dekker, 2020). Metagenome sequencing can further be employed for environmental surveillance to identify pathogen spillover. As the majority of emerging infections originate from wildlife and adapt to domestic animals to infect humans via spillover events, identification of potential zoonotic pathogens in the animal–human interface may facilitate the description of agents with imminent public health impact (Quer et al., 2022). Another use of metagenome sequencing in emerging diseases involves bio- or xeno-surveillance where blood-sucking arthropods, such as mosquitoes, ticks, and sandflies, can be used as sentinels to screen pathogens encompassing multiple hosts (Brinkmann et al., 2016).

Sequencers based on third-generation technology including nanopore sequencing (NS) are among the most widely used NGS platforms, due to their relatively low cost and portability (Kumar et al., 2017). Based on single-molecule synthesis, NS produces longer reads and allows real-time data access, significantly reducing the time required for sequencing (Petersen et al., 2019). Despite limitations of depth and accuracy, NS holds potential as a point-of-care or field-friendly metagenomics platform due to its flexibility (Greninger et al., 2015; Quick et al., 2016; Russell et al., 2018). NS can be particularly useful in monitoring arthropod-borne viruses in vectors or reservoirs, especially in regions with probable epizootic events. Viruses involved in spillover events often carry RNA genomes and exhibit high mutation rates, requiring broad-range or high-fidelity primer sets for detection by standard amplification techniques, advocating further for an inclusive approach provided by metagenomics for surveillance. NS has been employed to characterize virus genomes in mosquito pools screened by targeted amplification (Russell et al., 2018) and has proven capable of detecting mosquito-borne viruses in a single infected sample under controlled conditions (Batovska et al., 2017). Nevertheless, it has been rarely used to identify tick-borne viruses in a clinical or surveillance setting. This study aimed to evaluate NS-based metagenome sequencing in ticks, screened by polymerase chain reaction (PCR).

2. Materials and methods

2.1. Samples

The study cohort comprised 40 tick pools, collected in Anatolia, Turkey during 2020–2021 (Supplementary Table 1) (Dinçer et al., 2022). Individual adult ticks had been collected from infested animals including cattle (*Bos taurus*), sheep (*Ovis aries*), and dogs (*Canis familiaris*). They were morphologically identified to species level using appropriate taxonomic keys (Filippova, 1997; Walker et al., 2000, 2003; Estrada-Pena et al., 2004; Apanaskevich and Horak, 2008), pooled into groups of 4–12 individuals according to the collection site and species, and then stored at −80°C. The pools were macerated by vortexing with beads in Eagle's minimum essential medium supplemented with 5% fetal bovine serum, centrifuged at 4,000 rpm for 4 min. The supernatants from the pools were subsequently collected and subjected to nucleic acid purification by High Pure Viral Nucleic Acid Kit (Roche Diagnostics, Mannheim, Germany) and complementary DNA (cDNA) synthesis with random hexamers, using the RevertAid First-Strand cDNA Synthesis Kit (Thermo Fisher Scientific, Hennigsdorf, Germany), as directed by manufacturer's protocol. The pools were screened for generic nairovirus and Jingmen tick virus (JMTV) by previously described in-house PCR assays (Honig et al., 2004; Yu et al., 2020), utilizing identical conditions. The generic nairovirus PCR targeted the central motif A of the viral replicase, encoded by the genome segment L (Honig et al., 2004), whereas viral NS5-like protein on segment 1 was targeted by the JMTV assay in a nested format (Yu et al., 2020).

2.2. Nanopore sequencing (NS)

A fresh aliquot from the processed tick pool was used for sequencing. Briefly, the aliquot was lysed in ATL-DX lysis buffer with Precellys zirconium oxide beads (Bertin Corp., Rockville, MD, USA) using Bullet Blender 24 Gold (Next Advance, Troy, NY, USA). The lysate was centrifuged, and the supernatant was extracted using the IndiMag Pathogen Kit (Indical Bioscience, Leipzig, Germany) with KingFisher™ Flex Purification System, (Thermo Fisher Scientific, Waltham, MA, USA) according to the manufacturer's protocol. Purified nucleic acids were treated with ezDNase (TFS) and subjected to cDNA synthesis using NEBNext Ultra II RNA First-Strand and Non-Directional RNA Second Strand Synthesis modules, utilizing random primer mix (New England Biolabs, Ipswich, MA, USA) according to manufacturer recommendations. Double-stranded cDNA was cleaned up using Agencourt AMPure XP reagent (Beckman Coulter Biosciences, Indianapolis, IN, USA) and quantified using the Qubit dsDNA HS Assay Kit (TFS).

A Ligation Sequencing Kit (Oxford Nanopore Technologies, Oxford, UK) and NEBNext End repair and Quick Ligation Modules (NEB) were used as directed by the manufacturer's protocol. Libraries were quantitated by Qubit (TFS). Samples were barcoded with the Rapid Barcoding Kit 96 (ONT) for combined sequencing. An epMotion 5075 (Eppendorf, Hamburg, Germany) was used for automated liquid handling. Sequencing libraries, combined as 16 and 24 barcoded pools, were loaded on GridION Mk1C (ONT) sequencer and run for 72 h.

Basecalling and demultiplexing were performed on the GridION with the MinKNOW operating software v21.11.7 (ONT) and Guppy v 5.1.13 (Wick et al., 2019). Raw reads were trimmed with Porechop to remove adapter sequences and then filtered with NanoFilt to remove reads with q-scores ≤ 9 and read lengths ≤ 100 bp (Wick et al., 2017; De Coster et al., 2018). This data was then

TABLE 1 Virus detection by NS in pooled ticks.

Viruses		Tick pools				Total
		R. bursa (n: 28, 70%)	*R. sanguineus* (n: 7, 17.5%)	*R. turanicus* (n: 3, 7.5%)	*Hae. parva* (n: 2, 5%)	
Mivirus	Bole tick virus 3	28	3	1	1	33 (82.5%)
	Xinjiang mivirus 1	0	1	0	0	1 (2.5%)
Mogiani tick virus	Jingmen tick virus	17	3	2	2	24 (60%)
Phlebovirus	Brown dog tick phlebovirus 2	12	4	1	0	17 (42.5%)
	Phlebovirus Strandja	3	0	0	0	3 (7.5%)
	Phlebovirus Anatolia	0	2	1	0	3 (7.5%)
	Lesvos virus	0	0	0	1	1 (2.5%)
Nairovirus	Crimean-Congo hemorrhagic fever virus	12	6	0	2	20 (50%)
Peribunyavirus	*Ixodes ricinus* bunyavirus-like virus 1	1	0	0	0	1 (2.5%)
Orthomyxovirus	Quaranjavirus	0	1	0	0	1 (2.5%)
Unclassified *Riboviria*	Butler's Creek virus	0	0	0	1	1 (2.5%)

cleaned by removing any tick host DNA using Minimap2 v2.24 and Samtools v1.9 (Li, 2018; Danecek et al., 2021).

2.3. Sequence data and statistical analysis

The processed reads were aligned to the National Center for Biotechnology Information (NCBI) Reference Sequence (RefSeq) database using DIAMOND v2.0.14 (Buchfink et al., 2021), visualized using MEGAN6 (v6.23.2) (Huson et al., 2016). Taxon-based read counts were obtained from MEGAN6. Sequences were handled using Geneious Prime (v2022.2.1) (Biomatters Ltd., Auckland, New Zealand). The BLASTn algorithm was used for similarity searches in the NCBI database (Altschul et al., 1990). Virus read mapping was carried out using Minimap2 plug-in for Geneious Prime, with default settings optimized for nanopore data, using BLASTn hits with highest identity scores as a reference. Optimal substitution models on individual alignments were estimated by MEGAX, which was further employed to infer evolutionary history according to the Bayesian information criterion (Kumar et al., 2018).

T-test and Wilcoxon signed rank test were used based on the F-test results to assess the variance of the groups being compared. For this purpose, the samples were separated into PCR-negative and PCR-positive groups for each virus. Within these groups, the total number of reads generated per sample by NS, total virus reads, specific virus reads (JMTV or CCHFV), and target segment reads (for each PCR) were individually recorded, and proportions relative to the total number of reads or specific virus reads were calculated. Furthermore, the samples were compared in a binomial manner, where the results were scored as either 0 (PCR/NS negative) or 1 (PCR/NS positive). The Z-statistics obtained were then compared to the critical values for 95 and 99% two-tailed tests (at 1.96 and 2.58, respectively).

3. Results

3.1. Virus detection

A total of 301 ticks were sequenced in 40 pools, which comprised *Rhipicephalus bursa* (70%), *R. sanguineus* sensu latu (17.5%), *R. turanicus* (7.5%), and *Haemaphysalis parva* (2.5%) species (Table 1). The sequencing runs produced total and virus reads in the range of 265–343,857 (mean: 37,853.2, SD: 76,767.1) and 3–19,148 (mean: 1,071.7, SD: 3,236.3), respectively (Supplementary Table 1). A total of 11 viruses from seven genera or species were identified (Table 1). Sequences from multiple viruses were observed in 31 pools (77.5%). In samples with a single detectable virus (nine pools), Bole tick virus 3 (BTV3) (genus *Mivirus*, species *Mivirus boleense*) comprised the majority of the mapped reads (7/9, 77.8%).

3.2. JMTV and CCHFV findings

Jingmen tick virus (family *Flaviviridae*, species *Mogiana tick virus*) sequences were identified in 24 pools (60%) (Table 1) (Simmonds et al., 2019). JMTV is a segmented RNA virus documented as a causative agent of febrile disease associated with tick bites in humans (Jia et al., 2019), sometimes co-detected with CCHFV in severe cases (Emmerich et al., 2018). JMTV and related viruses are widely distributed in Eurasia and

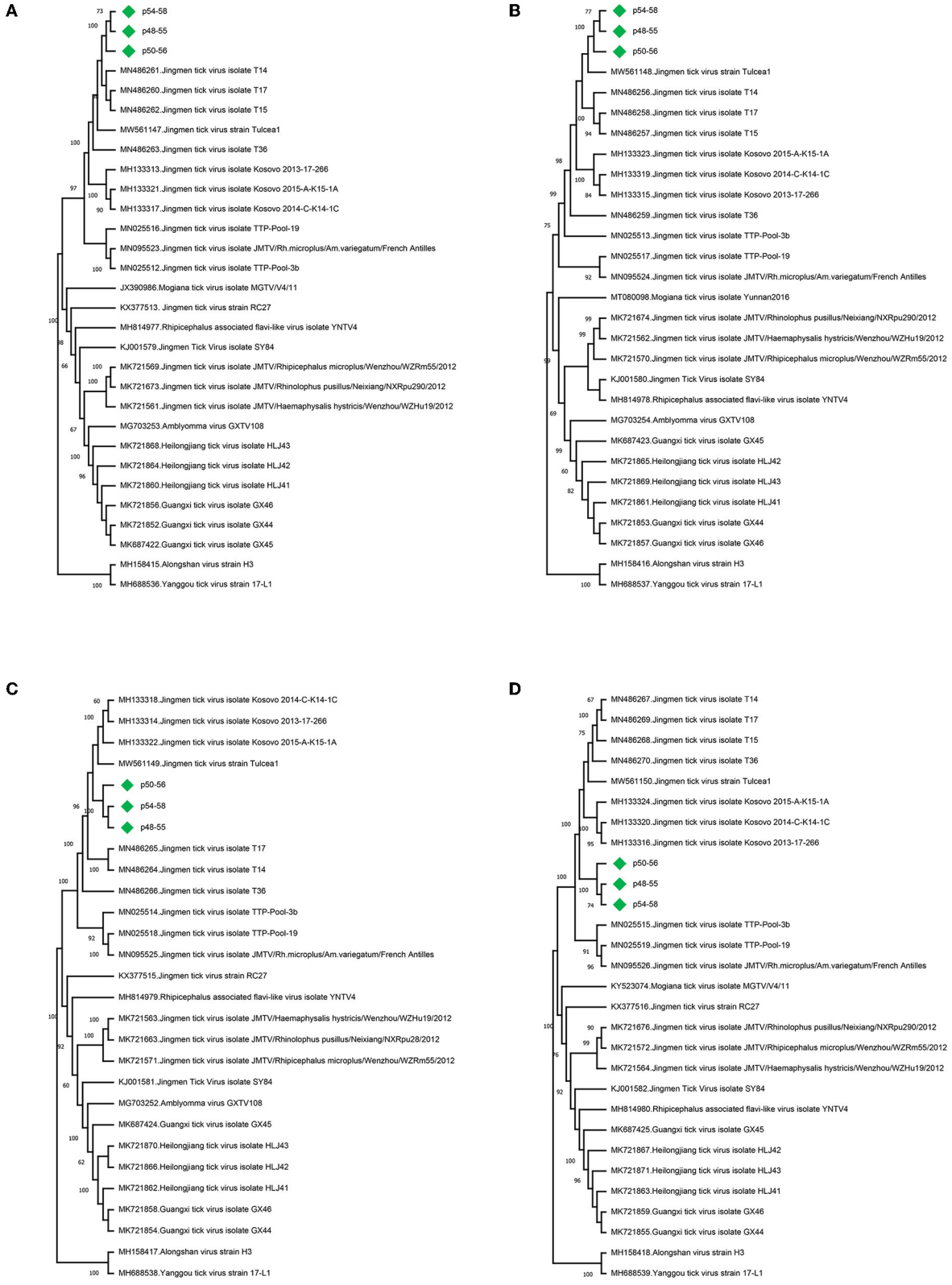

FIGURE 1
Maximum likelihood analysis of the Jingmen tick virus (JMTV) genome sequences [**(A)** segment 1,1084 bp; **(B)** segment 2, 2,325 bp; **(C)** segment 3, 1,247 bp, **(D)** segment 4, 2,293 bp]. The tree is constructed for 500 replications using the Tamura–Nei, gamma distributed with invariant sites (segments 1 and 3) or the gamma distributed, general time reversible (segments 2 and 4) models. Viruses are indicated by GenBank accession number, name, and isolate/strain identifier. The sequences obtained in the study are marked. Bootstrap values higher than 60 are provided.

TABLE 2 Crosstable of virus detection by PCR and nanopore sequencing.

PCR		Nanopore sequencing			
		Crimean-Congo hemorrhagic fever virus		Jingmen tick virus	
		Positive	Negative	Positive	Negative
Crimean-Congo hemorrhagic fever virus	Positive	6	0	4	2
	Negative	10	24	15	19
Jingmen tick virus	Positive	5	4	9	0
	Negative	11	20	10	21

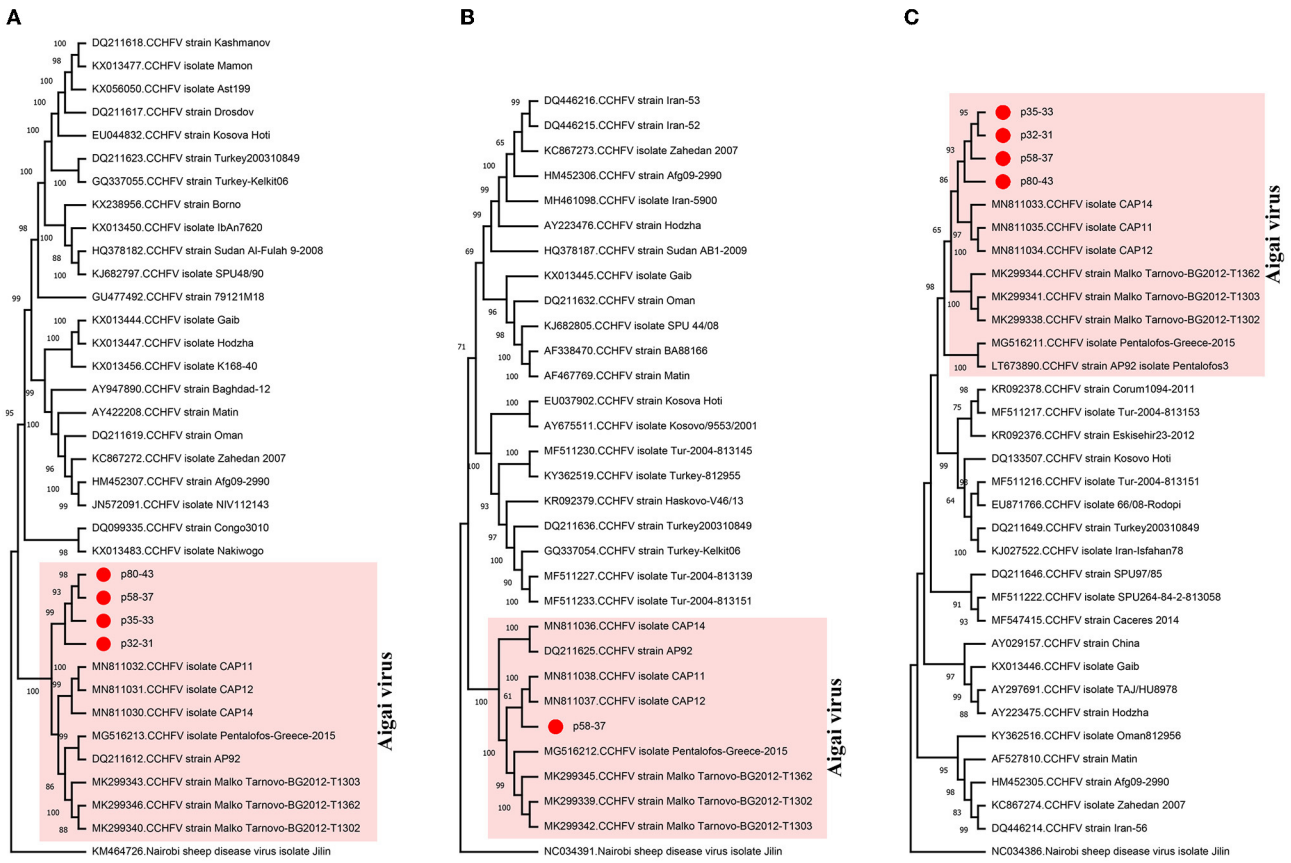

FIGURE 2
Maximum likelihood analysis of the Crimean–Congo hemorrhagic fever virus (CCHFV) genome sequences [**(A)** L segment, 12,887 bp; **(B)** M segment, 3,765 bp; **(C)** S segment, 1,361 bp]. The tree is constructed for 500 replications using the general time reversible, gamma distributed with (M segment) or without invariant sites (L segment) or Kimura 2-parameter models (S segment). Viruses are indicated by GenBank accession number, abbreviation, and isolate/strain identifier. The sequences obtained in the study are marked. Bootstrap values higher than 60 are provided. Nairobi sheep disease virus serves as an outgroup.

the Americas with virus RNA in bats, cattle, primates, and rodents, in addition to ticks and mosquitoes (Temmam et al., 2019; Guo et al., 2020). In the tick pools, we observed mapped read or contig counts of 1–10,348, with 90.2–99.4% identities to previously reported JMTV sequences (Supplementary Table 2). Near-complete open reading frame (ORF) contigs from all four genome segments were available in certain pools, where phylogenetic analysis of genome segments revealed clustering and shared ancestors with JMTVs reported from Turkey and the Balkans (Figure 1).

All nairovirus sequences obtained in the NS runs were identified as CCHFV, present in 20 (50%) of the pools (Table 1). Mapped reads or contig counts of 1–1,752 were noted, with 80.7–98.7% identities to closely related CCHFV sequences (Supplementary Table 3). We obtained near-complete coding region contigs of all CCHFV genome segments in one pool (p58–37) and L or S segment contigs in others (Supplementary Table 3). In the maximum likelihood phylogenetic analysis, the sequences clustered with CCHFV genogroup VI (Europe 2 or AP-92-like) isolates (Figure 2), which has recently been reclassified as the

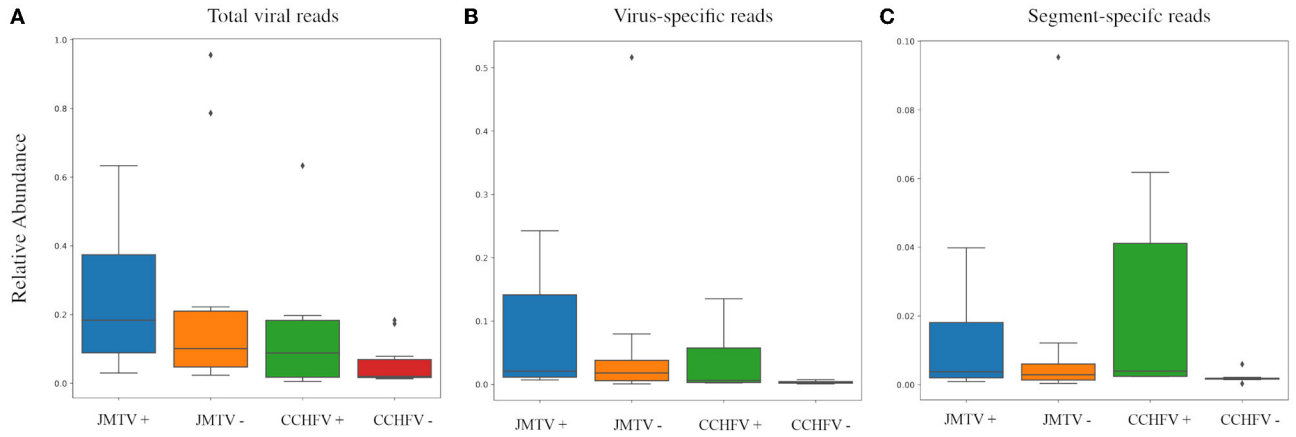

FIGURE 3
Comparison of the total virus, specific virus, and PCR-targeted segment abundances in samples with detectable JMTV and CCHFV in NS. Abundances are presented as a relative ratio to total reads **(A)** and virus reads **(B, C)**. Values in each group are given range + standard deviation, with outliers indicated with rhombuses. No statistically significant difference was observed between any PCR-positive and negative groups.

Aigai virus (AIGV) (Papa et al., 2022). Originally reported from Greece, AIGV was also reported from Albania, Bulgaria, Kosovo, and Turkey, and *R. bursa* ticks were suggested as the primary vector. Based on reports from Turkey and Iran, AIGV is a human pathogen, with the capacity to produce mild or severe CCHF-like disease (Midilli et al., 2009; Salehi-Vaziri et al., 2016).

We further compared JMTV and CCHFV detection rates by PCR and NS (Table 2). Six pools (15%) were positive using the single round generic nairovirus PCR, whereas the nested JMTV PCR identified nine pools (22.5%) as positive (Supplementary Tables 2, 3). In NS, all PCR-positive pools produced contigs of every genome segment from each virus (Table 2). Detection by NS was more frequent for both viruses with a statistical significance of 95% confidence. However, no significant difference between total virus, specific virus, or targeted segment read numbers was observed in PCR-positive and negative pools with virus detection by NS (Figure 3).

3.3. Mivirus findings

Mivirus is a recently established genus within the *Chuviridae* family (order *Jingchuvirales*) (Di Paola et al., 2022). Initially described by NGS in arthropods (Li et al., 2020), jingchuviruses are documented to be broadly distributed in major arthropod subphyla, and further associated with eucestodes, fish, helminths, mammals, nematodes, reptiles, and sea anemones. They have highly diverse, non-segmented, segmented, and/or circular genomes, varying ORF configurations and preliminary evidence of genome integration and human infections (Di Paola et al., 2022). We detected two miviruses in tick pools. BTV3 stands out as the most frequently detected virus, present in 33 (82.5%) of the pools (Table 1). In NS, read counts ranging between 1 and 468 with 83.5–99.6% BLASTN identities to the BTV3 strain previously reported from Anatolia were observed (Ergünay et al., 2020). Complete virus replicase, glycoprotein, and nucleoprotein ORF contigs could be retrieved from certain pools (Supplementary Table 4). Phylogeny construction using partial replicase, glycoprotein, and nucleoprotein contig alignments showed a clustering of the Anatolian sequences, distinct from other BTV3 strains and miviruses (Supplementary Figure 1). In addition to BTV3, a single read with 89.2% identities to Xinjiang mivirus 1 replicase was detected in a pool of *R. sanguineus* ticks (Supplementary Table 4).

3.4. Phlebovirus findings

We detected 1–18 reads or contigs mapped to phleboviruses in 24 (60%) of the tick pools (Supplementary Table 5). The sequences comprised L and S segments of the virus genome, with BLASTN identities of 90.6–99.0 and 80.1–98.8% to various phleboviruses, respectively. Tick-associated phleboviruses identified in the pools include Brown dog tick phlebovirus 2 (BDTP2), phlebovirus Strandja, tick phlebovirus Anatolia, and Lesvos virus (Table 1). Strandja and Anatolia phleboviruses were mainly reported in *Rhipicephalus* ticks from Bulgaria and Turkey (Emanet et al., 2019; Ohlendorf et al., 2019), while BDTP2 appears widespread, detected in China, and Trinidad and Tobago as well as the Balkans (Sameroff et al., 2019; Bratuleanu et al., 2022; Guo et al., 2022). Lesvos virus was originally reported from *Hae. parva* ticks from the Greek island of Lesbos (Papa et al., 2016). Vertebrate infections have not previously been documented for any of these viruses. Phylogeny construction based on partial polymerase sequences on the L genome segment revealed the grouping of the sequences with related viruses from the Balkans and Turkey (Supplementary Figure 2).

3.5. Other viruses

Finally, we detected sequences of an *Orthomyxovirus* (Quaranjavirus), a *Peribunyavirus* (*Ixodes ricinus* bunyavirus-like 1 virus), and an unclassified *Riboviria* (Butler's Creek virus) in three tick pools (Table 1). In a pool of male *R. sanguineus*

samples collected from infested canines, three reads identified as *Quaranjavirus* sp. were detected. The reads comprised 113, 171, and 244 base pairs and showed 92.37–98.2% identities to a novel Quaranjavirus PB1 sequence, recently reported in ticks from Romania (Bratuleanu et al., 2022). Quaranjaviruses are members of the *Orthomyxoviridae* family (Walker et al., 2019), and the initial isolates were described in cases of febrile diseases, with exposure in indigenous populations (Taylor et al., 1966). They have been historically documented in argasid ticks and their vertebrate hosts, primarily avian species. Some quaranjaviruses are associated with avian mortality and demonstrate pathogenicity under experimental conditions (Allison et al., 2015; Shearn-Bochsler et al., 2017; Mourya et al., 2019). Documentation of various quaranjaviruses in several hard tick species in the genera *Amblyomma*, *Haemaphysalis*, *Ixodes*, and *Rhipicephalus* including this study suggest that unrecognized tick-borne infections may be occurring (Cholleti et al., 2018; Sameroff et al., 2021; Bratuleanu et al., 2022; Kobayashi et al., 2022). Furthermore, two reads (279 and 767 base pairs) in a *Hae. parva* pool revealed 70–72.8% identity to the Butler's Creek virus, reported from pooled *Haemaphysalis bancrofti* nymphs from Australia. Finally, a single read with 70% identity to the M segment of *Ixodes ricinus* associated bunyavirus-like 1 virus reported from Croatia (Sameroff et al., 2022), was identified in a *R. bursa* pool.

4. Discussion

Our findings demonstrate that NS sequencing robustly detects tick-borne viruses in pooled ticks, with detection sensitivities significantly exceeding broad-range and nested PCR. Unlike targeted generic, specific, or multiplexed amplification, metagenome sequencing has the capability of detecting novel targets along with known pathogens without the need for prior information. However, during metagenome sequencing of field-collected arthropods, non-pathogenic microbial, host and environmental nucleic acids may mask viral sequences of interest, resulting in reduced pathogen detection sensitivity (Greninger et al., 2015; Kumar et al., 2017; Petersen et al., 2019). Sample pooling, a common practice in vector screening, is likely to increase background signal. To overcome this problem, various enrichment approaches including centrifugation/filtration, depletion of ribosomal RNA, targeted virus sequence capture, random priming, and non-specific amplification have been used (Brinkmann et al., 2016; Petersen et al., 2019). In this study, we employed a straightforward cDNA-based library preparation protocol, except for the DNase treatment of purified nucleic acids. This approach not only enabled the identification of the main targets JMTV and CCHFV, but recovered several other tick-associated viruses as well, with near-complete genome sequences obtained in samples with a sufficient number of mapped reads. Despite the relatively low number of total and virus reads due to our barcoding strategy, the longer read lengths generated by NS provided genome-wide virus sequence information, enabling reliable phylogeny construction in most of the detected viruses.

Due to the public health threat potential emergency and the lack of efficacious therapeutic or preventive measures, CCHFV is included among the pathogens targeted in the World Health Organization research and development blueprint (Mehand et al., 2018). It is widely distributed in Asia, Africa, and Southeast Europe, where the primary vector ticks of the *Hyalomma* genus are prevalent. CCHFV further exhibits a striking genome diversity, with several distinct genotypes based on viral genome segments and associated with geographic location, and with the possibility for recombination among strains (Lukashev et al., 2016). The recently reclassified AIGV was considered of low virulence, with few documented cases (Papa et al., 2022). This is further supported by the findings of a recent *in vitro* study, where diminished viral L protein expression was observed in AIGV (Pickin et al., 2022). The diagnostic or screening nucleic acid and serologic assays in current use are mostly unable to differentiate between these viruses; therefore, the impact of AIGV in CCHFV-associated disease incidence and epidemiology is hard to assess. Despite different primary hosts (*Hyalomma* vs. *Rhipicephalus*), tick species with detectable CCHFV or AIGV may overlap significantly in endemic regions, and genetic exchange resulting in altered virulence is also possible. Hence, adequate tools to diagnose and monitor AIGV are required, and our findings further indicate NS as a robust approach for this purpose.

Our NS-based metagenome approach further revealed a JMTV prevalence of 60% in the screened tick pools, and the subsequent phylogeny construction revealed clustering with those previously characterized in Anatolia and the Balkans. JMTV and related viruses (often referred to as Jingmenviruses) are included in the *Flaviviridae* family based on non-structural protein similarities, despite having segmented genomes (Simmonds et al., 2019; Temmam et al., 2019). Currently, known Jingmenvirus genomes comprise two large phylogenetic clades and are associated with tick-vertebrate or insect hosts (Colmant et al., 2022). Since its initial description in China, JMTV sequences have been detected in samples from many locations in Asia, Africa, Europe, and America (Temmam et al., 2019; Colmant et al., 2022). Reported with high prevalence in *Rhipicephalus microplus* ticks from various regions, JMTV has also been identified in many species of *Rhipicephalus*, *Amblyomma*, *Dermacentor*, *Haemaphysalis*, *Hyalomma*, and *Ixodes* ticks throughout the globe, but ecological data on transmission cycles are scant. In addition to ticks, virus RNA has been documented in bats, cattle, rodents, tortoises, individuals with febrile disease, and those co-infected with CCHFV (Emmerich et al., 2018; Jia et al., 2019; Temmam et al., 2019; Colmant et al., 2022). By antibody detection, JMTV exposure has been identified in cattle and humans from Asia and Europe. Despite its widespread presence in many regions, human JMTV infections are reported sporadically, presumably due to a common clinical presentation with well known tick-borne infections and lack of commercial diagnostic assays. Similarly, another Jingmenvirus named Alongshan virus, was detected in patients with tick-associated febrile diseases with subsequent seroconversion and evidence for exposure in domestic animals and humans (Temmam et al., 2019; Wang et al., 2019; Colmant et al., 2022). These findings demonstrate

that at least two Jingmen viruses qualify as tick-borne emerging viruses and considering their ubiquitous distribution further confirmed in this study; they must be investigated in individuals with febrile diseases of unknown etiology associated with tick bites.

The broad-range detection provided by the metagenomic approach also enabled the detection of additional viruses, including two miviruses (BTV3 and Xinjiang mivirus 1), four phleboviruses (BDTP2, Anatolia, Strandja, and Lesvos phleboviruses), and other RNA viruses (Table 1). Interestingly, BTV3 infections were observed at an unprecedented frequency of 82.5%. BTV3 and tick phleboviruses appear to be a ubiquitous virus in Anatolia, having been detected in various tick species (Dinçer et al., 2017; Brinkmann et al., 2018; Emanet et al., 2019; Ergünay et al., 2020). Tick phleboviruses are also widely distributed in Asia, Europe, and America (Ohlendorf et al., 2019; Sameroff et al., 2019; Bratuleanu et al., 2022; Guo et al., 2022). As vertebrate *in vivo* experiments failed to propagate these viruses, they are currently considered non-virulent residents of the tick virome (Emanet et al., 2019). Other RNA viruses identified in the study have also been reported in tick metagenome investigations (Pettersson et al., 2017; Sameroff et al., 2022). Despite the lack of evidence for human or veterinary health impact of these viruses, indirect effects on the replication of the pathogenic viruses in vector ticks and potential genetic exchange among strains should be considered. NS further facilitated the first documentation of Quaranjaviruses in Anatolia, Turkey—a significant finding that warrants further biosurveillance due to their potential as animal and human pathogens.

Several shortcomings of the current study should be addressed. First, information on the number of infected individuals in each pool was lacking; therefore, assessments on individual ticks or mixed infections could not be performed. We did not use a CCHFV quantitative-PCR approach, as it may not ensure accurate detection of virus genotypes including AIGV in circulation and multiple genotypes. A more informative comparison would have been possible by parallel sequencing of spiked pools with a known copy number of viral genomes. During NS, we did not carry out a real-time data interpretation for virus detection, but an end-point analysis of the sequencing data instead. NS was reported to be capable of generating 12% of the Ross River virus reads in a single infected mosquito after 10 min and 87.3% in 10 h (Batovska et al., 2017). Follow-up studies are underway to calculate timelines for reliable pathogen detection and genotyping on individual and pooled ticks. A limitation of the NS-based metagenomics for vector-borne viruses is the lack of established controls, optimized for all potential target pathogens. Moreover, assessments of detection thresholds and sensitivity, as well as the correlation of read counts with standard quantitative nucleic acid detection assays are required. Operational costs and expertise required for assay performance and data interpretation should also be considered. However, metagenome-based surveillance provided a much broader view of the viruses in circulation, as exemplified by tick pools in this study. As affordable, field-friendly sequencing platforms become widespread, many of the current limitations are likely to be circumvented.

In conclusion, this proof-of-concept study revealed that metagenomic NS with standard approaches could surpass the sensitivity of PCR amplification in tick-borne viruses and generate genome-wide data for reliable phylogeny construction. The utility of NS could be particularly useful for monitoring pathogens in tick vectors or human/animal clinical samples in hot-spot regions for zoonotic spillover.

Data availability statement

The datasets presented in this study can be found in online repositories. The names of the repository/repositories and accession number(s) can be found below: https://www.ncbi.nlm.nih.gov/genbank/, SRR21504630-SRR21504591; https://www.ncbi.nlm.nih.gov/genbank/OP432043--OP432053.

Author contributions

KE, ED, and Y-ML: conceptualization. KE and ED: data curation. KE, ED, SAJ, BPB, SPN, MOT, BO, IS, and OFG: formal analysis. NLA, JPG, and Y-ML: funding acquisition and resources. ED, SPN, MOT, BO, IS, OFG, and DDR-W: investigation. H-ML and LJ: methodology. Y-ML: project administration and supervision. KE: writing—original draft. KE and Y-ML: writing—review and editing. All authors contributed to the article and approved the submitted version.

Funding

This study was financially supported by the Armed Forces United States Army Medical Research and Development Command under contract no. W81XWH-21-C-0001 (to NLA, JPG, LJ, and Y-ML) and AFHSD-GEIS sustainment funding to the Walter Reed Biosystematics Unit (WRBU) (P0065_22_WR) and US Army Medical Detachment-Georgia (USAMRD-G) (P0008_21_GA).

Acknowledgments

This article was prepared, while KE, BPB, and SAJ held a National Research Council (NRC) Research Associateship Award at the Walter Reed Biosystematics Unit, through the Walter Reed Army Institute of Research, Silver Spring, MD.

Conflict of interest

The authors declare that the research was conducted in the absence of any commercial or financial relationships that could be construed as a potential conflict of interest.

Publisher's note

All claims expressed in this article are solely those of the authors and do not necessarily represent those of

their affiliated organizations, or those of the publisher, the editors and the reviewers. Any product that may be evaluated in this article, or claim that may be made by its manufacturer, is not guaranteed or endorsed by the publisher.

Author disclaimer

The opinions or assertions contained herein are the private views of the authors, and are not to be construed as official, or as reflecting true views of the Department of the Army, Navy or the Department of Defense. Material contained within this publication has been reviewed by the Walter Reed Army Institute of Research. There is no objection to its presentation and/or publication.

Supplementary material

The Supplementary Material for this article can be found online at: https://www.frontiersin.org/articles/10.3389/fmicb.2023.1177651/full#supplementary-material

References

Allison, A. B., Ballard, J. R., Tesh, R. B., Brown, J. D., Ruder, M. G., and Keel, M. K. (2015). Cyclic avian mass mortality in the northeastern United States is associated with a novel orthomyxovirus. *J. Virol.* 89, 1389–1403. doi: 10.1128/JVI.02019-14

Altschul, S. F., Gish, W., Miller, W., Myers, E. W., and Lipman, D. J. (1990). Basic local alignment search tool. *J. Mol. Biol.* 215, 403–410. doi: 10.1016/S0022-2836(05)80360-2

Apanaskevich, D. A., and Horak, I. G. (2008). The genus *Hyalomma* Koch, 1844: V. Reevaluation of the taxonomic rank of taxa comprising the *H. (Euhyalomma)* marginatum Koch complex of species (Acari: Ixodidae) with redescription of all parasitic stages and notes on biology. *Int. J. Acarol.* 34, 13–42. doi: 10.1080/01647950808683704

Batovska, J., Lynch, S. E., Rodoni, B. C., Sawbridge, T. I., and Cogan, N. O. (2017). Metagenomic arbovirus detection using MinION nanopore sequencing. *J. Virol. Methods.* 249, 79–84. doi: 10.1016/j.jviromet.2017.08.019

Bratuleanu, B. E., Temmam, S., Munier, S., Chretien, D., Bigot, T., and van der Werf, S. (2022). Detection of phenuiviridae, chuviridae members, and a novel quaranjavirus in hard ticks from Danube Delta. *Front. Vet. Sci.* 9, 863814. doi: 10.3389/fvets.2022.863814

Brinkmann, A., Dinçer, E., Polat, C., Hekimoglu, O., Hacioglu, S., and Földes, K. (2018). A metagenomic survey identifies Tamdy orthonairovirus as well as divergent phlebo-, rhabdo-, chu- and flavi-like viruses in Anatolia, Turkey. *Ticks. Tick. Borne Dis.* 9, 1173–1183. doi: 10.1016/j.ttbdis.2018.04.017

Brinkmann, A., Nitsche, A., and Kohl, C. (2016). Viral metagenomics on bloodfeeding arthropods as a tool for human disease surveillance. *Int. J. Mol. Sci.* 17, 1743. doi: 10.3390/ijms17101743

Buchfink, B., Reuter, K., and Drost, H. G. (2021). Sensitive protein alignments at tree-of-life scale using DIAMOND. *Nat. Methods.* 18, 366–368. doi: 10.1038/s41592-021-01101-x

Cholleti, H., Hayer, J., Mulandane, F. C., Falk, K., Fafetine, J., and Berg, M. (2018). Viral metagenomics reveals the presence of highly divergent quaranjavirus in *Rhipicephalus* ticks from Mozambique. *Infect. Ecol. Epidemiol.* 8, 1478585. doi: 10.1080/20008686.2018.1478585

Colmant, A. M. G., Charrel, R. N., and Coutard, B. (2022). Jingmenviruses: Ubiquitous, understudied, segmented flavi-like viruses. *Front. Microbiol.* 13, 997058. doi: 10.3389/fmicb.2022.997058

Danecek, P., Bonfield, J. K., Liddle, J., Marshall, J., Ohan, V., and Pollard, M. O. (2021). Twelve years of SAMtools and BCFtools. *Gigascience.* 10, giab008. doi: 10.1093/gigascience/giab008

De Coster, W., D'Hert, S., Schultz, D. T., Cruts, M., and Van Broeckhoven, C. (2018). NanoPack: visualizing and processing long-read sequencing data. *Bioinformatics.* 34, 2666–2669. doi: 10.1093/bioinformatics/bty149

Di Paola, N., Dheilly, N. M., Junglen, S., Paraskevopoulou, S., Postler, T. S., and Shi, M. (2022). Jingchuvirales: a New Taxonomical Framework for a Rapidly Expanding Order of Unusual Monjiviricete Viruses Broadly Distributed among Arthropod Subphyla. *Appl Environ Microbiol.* 88:e0195421. doi: 10.1128/aem.01954-21

Dinçer, E., Brinkmann, A., Hekimoglu, O., Hacioglu, S., Földes, K., and Karapinar, Z. (2017). Generic amplification and next generation sequencing reveal Crimean-Congo hemorrhagic fever virus AP92-like strain and distinct tick phleboviruses in Anatolia, Turkey. *Parasit Vectors.* 10, 335. doi: 10.1186/s13071-017-2279-1

Dinçer, E., Timurkan, M. Ö., Oguz, B., Sahindokuyucu, I., Sahan, A., and Ekinci, M. (2022). Several Tick-Borne Pathogenic Viruses in Circulation in Anatolia, Turkey. *Vector Borne Zoonotic Dis.* 22:148–158. doi: 10.1089/vbz.2021.0082

Dulanto Chiang, A., and Dekker, J. P. (2020). From the pipeline to the bedside: advances and challenges in clinical metagenomics. *J. Infect Dis.* 221, 331–340. doi: 10.1093/infdis/jiz151

Emanet, N., Kar, S., Dinçer, E., Brinkmann, A., Hacioglu, S., and Farzani, T. A. (2019). Novel tick phlebovirus genotypes lacking evidence for vertebrate infections in Anatolia and Thrace, Turkey. *Viruses.* 11, 703. doi: 10.3390/v11080703

Emmerich, P., Jakupi, X., von Possel, R., Berisha, L., Halili, B., and Günther, S. (2018). Viral metagenomics, genetic and evolutionary characteristics of Crimean-Congo hemorrhagic fever orthonairovirus in humans, Kosovo. *Infect. Genet. Evol.* 65, 6–11. doi: 10.1016/j.meegid.2018.07.010

Ergünay, K., Dinçer, E., Kar, S., Emanet, N., Yalçinkaya, D., Polat Dinçer, P. F., et al. (2020). Multiple orthonairoviruses including Crimean-Congo hemorrhagic fever virus, Tamdy virus and the novel Meram virus in Anatolia. *Ticks Tick. Borne. Dis.* 11, 101448. doi: 10.1016/j.ttbdis.2020.101448

Estrada-Pena, A., Bouattour, A., and Walker, C. (2004). *Ticks of Domestic Animals in the Mediterranean Region*. 1st ed. Zaragoza: University of Zaragoza Press.

Filippova, N. A. (1997). *Fauna of Russia and Neighbouring Countries, Arachnoidea, Volume IV, Issue 5, Ixodid Ticks of Subfamily Amblyomminae*. St. Petersburg: Nauka Publishing House.

Greninger, A. L., Naccache, S. N., Federman, S., Yu, G., Mbala, P., and Bres, V. (2015). Rapid metagenomic identification of viral pathogens in clinical samples by real-time nanopore sequencing analysis. *Genome Med.* 7, 99. doi: 10.1186/s13073-015-0220-9

Guo, J. J., Lin, X. D., Chen, Y. M., Hao, Z. Y., Wang, Z. X., and Yu, Z. M. (2020). Diversity and circulation of Jingmen tick virus in ticks and mammals. Virus Evol. 6:veaa051. doi: 10.1093/ve/veaa051

Guo, L., Ma, J., Lin, J., Chen, M., Liu, W., and Zha, J. (2022). Virome of *Rhipicephalus* ticks by metagenomic analysis in Guangdong, southern China. *Front. Microbiol.* 13, 966735. doi: 10.3389/fmicb.2022.966735

Honig, J. E., Osborne, J. C., and Nichol, S. T. (2004). The high genetic variation of viruses of the genus *Nairovirus* reflects the diversity of their predominant tick hosts. *Virology.* 318, 10–16. doi: 10.1016/j.virol.2003.09.021

Huson, D. H., Beier, S., Flade, I., Gorska, A., El-Hadidi, M., and Mitra, S. (2016). MEGAN community edition—interactive exploration and analysis of large-scale microbiome sequencing data. *PLoS Comput. Biol.* 12, e1004957. doi: 10.1371/journal.pcbi.1004957

Jia, N., Liu, H. B., Ni, X. B., Bell-Sakyi, L., Zheng, Y. C., Song., J. L. (2019). Emergence of human infection with Jingmen tick virus in China: a retrospective study. *EbioMedicine.* 43, 317–24. doi: 10.1016/j.ebiom.2019.04.004

Kobayashi, D., Kuwata, R., Kimura, T., Faizah, A. N., Higa, Y., and Hayashi, T. (2022). Detection of Quaranjavirus-Like Sequences from *Haemaphysalis hystricis* ticks collected in Japan. *Jpn. J. Infect. Dis.* 75, 195–198. doi: 10.7883/yoken.JJID.2021.129

Kumar, A., Murthy, S., and Kapoor, A. (2017). Evolution of selective-sequencing approaches for virus discovery and virome analysis. *Virus Res.* 239, 172–179. doi: 10.1016/j.virusres.2017.06.005

Kumar, S., Stecher, G., Li, M., Knyaz, C., and Tamura, K. (2018). MEGA X: molecular evolutionary genetics analysis across computing platforms. *Mol. Biol. Evol.* 35, 1547–1549. doi: 10.1093/molbev/msy096

Li, C. X., Shi, M., Tian, J. H., Lin, X. D., Kang, Y. J., and Chen, L. J. (2020). Unprecedented genomic diversity of RNA viruses in arthropods reveals the ancestry of negative-sense RNA viruses. *Elife.* 4, e05378. doi: 10.7554/eLife.05378

Li, H. (2018). Minimap2: pairwise alignment for nucleotide sequences. *Bioinformatics.* 34, 3094–3100. doi: 10.1093/bioinformatics/bty191

Lukashev, A. N., Klimentov, A. S., Smirnova, S. E., Dzagurova, T. K., Drexler, J. F., and Gmyl, A. P. (2016). Phylogeography of crimean congo hemorrhagic fever virus. *PLoS One*. 11, e0166744. doi: 10.1371/journal.pone.0166744

Mehand, M. S., Al-Shorbaji, F., Millett, P., and Murgue, B. (2018). The WHO RandD Blueprint: 2018 review of emerging infectious diseases requiring urgent research and development efforts. *Antiviral Res*. 159, 63–67. doi: 10.1016/j.antiviral.2018.09.009

Midilli, K., Gargili, A., Ergonul, O., and Elevli, M. (2009). The first clinical case due to AP92 like strain of Crimean-Congo Hemorrhagic Fever virus and a field survey. *BMC Infect. Dis*. 9, 90. doi: 10.1186/1471-2334-9-90

Mourya, D. T., Yadav, P. D., Nyayanit, D. A., Majumdar, T. D., Jain, S., and Sarkale, P. (2019). Characterization of a strain of quaranfil virus isolated from soft ticks in India. Is quaranfil virus an unrecognized cause of disease in human and animals. *Heliyon*. 5, e01368. doi: 10.1016/j.heliyon.2019.e01368

Ohlendorf, V., Marklewitz, M., Kopp, A., Yordanov, S., Drosten, C., and Junglen, S. (2019). Huge diversity of phleboviruses in ticks from Strandja Nature Park, Bulgaria. *Ticks. Tick. Borne. Dis*. 10, 697–703. doi: 10.1016/j.ttbdis.2019.03.001

Papa, A., Kontana, A., Tsioka, K., Saratsis, A., and Sotiraki, S. (2016). Novel phlebovirus detected in *Haemaphysalis parva* ticks in a Greek island. *Ticks. Tick. Borne. Dis*. 8, 157–160. doi: 10.1016/j.ttbdis.2016.10.012

Papa, A., Marklewitz, M., Paraskevopoulou, S., Garrison, A. R., Alkhovsky, S. V., and Avšič-Županc, T. (2022). History and classification of Aigai virus (formerly Crimean-Congo haemorrhagic fever virus genotype VI). *J. Gen. Virol*. 103, 4. doi: 10.1099/jgv.0.001734

Petersen, L. M., Martin, I. W., Moschetti, W. E., Kershaw, C. M., and Tsongalis, G. J. (2019). Third-generation sequencing in the clinical laboratory: exploring the advantages and challenges of nanopore sequencing. *J. Clin. Microbiol*. 58, e01315–e01319. doi: 10.1128/JCM.01315-19

Pettersson, J. H., Shi, M., Bohlin, J., Eldholm, V., Brynildsrud, O. B., and Paulsen, K. M. (2017). Characterizing the virome of *Ixodes ricinus* ticks from northern Europe. *Sci. Rep*. 7, 10870. doi: 10.1038/s41598-017-11439-y

Pickin, M. J., Devignot, S., Weber, F., and Groschup, M. H. (2022). Comparison of crimean-congo hemorrhagic fever virus and aigai virus in life cycle modeling systems reveals a difference in l protein activity. *J. Virol*. 96, e0059922. doi: 10.1128/jvi.00599-22

Quer, J., Colomer-Castell, S., Campos, C., Andrés, C., Piñana, M., and Cortese, M. F. (2022). Next-generation sequencing for confronting virus pandemics. *Viruses*. 14, 600. doi: 10.3390/v14030600

Quick, J., Loman, N. J., Duraffour, S., Simpson, J. T., Severi, E., and Cowley, L. (2016). Real-time, portable genome sequencing for Ebola surveillance. *Nature*. 530, 228–232. doi: 10.1038/nature16996

Russell, J. A., Campos, B., Stone, J., Blosser, E. M., Burkett-Cadena, N., and Jacobs, J. L. (2018). Unbiased strain-typing of arbovirus directly from mosquitoes using nanopore sequencing: a field-forward biosurveillance protocol. *Sci. Rep*. 8, 5417. doi: 10.1038/s41598-018-23641-7

Salehi-Vaziri, M., Baniasadi, V., Jalali, T., Mirghiasi, S. M., Azad-Manjiri, S., et al. (2016). The first fatal case of Crimean-Congo hemorrhagic fever caused by the AP92-like strain of the Crimean-Congo hemorrhagic fever virus. *Jpn. J. Infect. Dis*. 69, 344–346. doi: 10.7883/yoken.JJID.2015.533

Sameroff, S., Tokarz, R., Charles, R. A., Jain, K., Oleynik, A., and Che, X. (2019). Viral diversity of tick species parasitizing cattle and dogs in trinidad and tobago. *Sci Rep*. 9, 10421. doi: 10.1038/s41598-019-46914-1

Sameroff, S., Tokarz, R., Jain, K., Oleynik, A., Carrington, C. V. F., and Lipkin, W. I. (2021). Novel quaranjavirus and other viral sequences identified from ticks parasitizing hunted wildlife in Trinidad and Tobago. *Ticks. Tick. Borne Dis*. 12, 101730. doi: 10.1016/j.ttbdis.2021.101730

Sameroff, S., Tokarz, R., Vucelja, M., Jain, K., Oleynik, A., and Boljfeti,ć M. (2022). Virome of *Ixodes ricinus*, *Dermacentor reticulatus*, and *Haemaphysalis concinna* ticks from Croatia. *Viruses*. 14, 929. doi: 10.3390/v14050929

Shearn-Bochsler, V., Ip, H. S., Ballmann, A., Hall, J. S., Allison, A. B., and Ballard, J. (2017). Experimental Infection of Common Eider Ducklings with Wellfleet Bay Virus, a Newly Characterized Orthomyxovirus. *Emerg Infect Dis*. 23:1958–1965. doi: 10.3201/eid2312.160366

Simmonds, P., Becher, B., Bukh, J., Gould, E. A., Meyers, G., and Monath, T. (2019). ICTV virus taxonomy profile: flaviviridae. *J. Gen. Virol*. 98, 2–3. doi: 10.1099/jgv.0.000672

Taylor, R. M., Hurlbut, H. S., Work, T. H., Kingston, J. R., and Hoogstraal, H. (1966). Arboviruses isolated from *Argas* ticks in Egypt: quaranfil, chenuda, and nyamanini. *Am. J. Trop. Med. Hyg*. 15, 76–86. doi: 10.4269/ajtmh.1966.15.76

Temmam, S., Bigot, T., Chrétien, D., Gondard, M., Pérot, P., and Pommelet, V. (2019). Insights into the Host Range, Genetic Diversity, and Geographical Distribution of Jingmenviruses. *Ecol. Evol. Sci*. 4, e00645–e00619. doi: 10.1128/mSphere.00645-19

Trinh, P., Zaneveld, J. R., Safranek, S., and Rabinowitz, P. M. (2018). One health relationships between human, animal, and environmental microbiomes: a mini-review. *Front. Public Health*. 6, 235. doi: 10.3389/fpubh.2018.00235

Walker, A. R., Bouattour, A., Camicas, J. L., and Estrada-Pena, A. (2003). *Ticks of Domestic Animals in Africa: A Guide to Identification of Species, 1st ed*. Edinburgh: Bioscience Reports.

Walker, B. J., Kerians, J. E., and Horak, I. G. (2000). *The Genus Rhipicephalus (Acari, Ixodidae): A Guide to the Brown Ticks of the World, revised ed*. Cambridge: Cambridge University Press.

Walker, P. J., Siddell, S. G., Lefkowitz, E. J., Mushegian, A. R., Adriaenssens, E. M., and Alfenas-Zerbini, P. (2019). Changes to virus taxonomy and the international code of virus classification and nomenclature ratified by the international committee on taxonomy of viruses. *Arch. Virol*. 164, 2417–2429. doi: 10.1007/s00705-019-04306-w

Wang, Z. D., Wang, B., Wei, F., Han, S. Z., Zhang, L., and Yang, Z. T. (2019). A new segmented virus associated with human febrile illness in China. *N. Engl. J. Med*. 380, 2116–2125. doi: 10.1056/NEJMoa1805068

Wick, R. R., Judd, L. M., Gorrie, C. L., and Holt, K. E. (2017). Completing bacterial genome assemblies with multiplex MinION sequencing. *Microb. Genom*. 3, e000132. doi: 10.1099/mgen.0.000132

Wick, R. R., Judd, L. M., and Holt, K. E. (2019). Performance of neural network basecalling tools for Oxford Nanopore sequencing. *Genome. Biol*. 20, 129. doi: 10.1186/s13059-019-1727-y

Yu, Z. M., Chen, J. T., Qin, J., Guo, J. J., Li, K., and Xu, Q. Y. (2020). Identification and characterization of Jingmen tick virus in rodents from Xinjiang, China. *Infect Genet Evol*. 84:104411. doi: 10.1016/j.meegid.2020.104411

frontiers | Frontiers in Microbiology

TYPE Original Research
PUBLISHED 07 June 2023
DOI 10.3389/fmicb.2023.1187625

OPEN ACCESS

EDITED BY
Arabella Touati,
Centre Hospitalier Universitaire de Bordeaux, France

REVIEWED BY
Mangesh Vasant Suryavanshi,
Cleveland Clinic, United States
Beata Krawczyk,
Gdansk University of Technology, Poland

*CORRESPONDENCE
Marzena Gajecka
✉ gamar@man.poznan.pl

RECEIVED 16 March 2023
ACCEPTED 16 May 2023
PUBLISHED 07 June 2023

CITATION
Jaworska MM, Pecyna P, Jaskiewicz K, Rydzanicz M, Kaluzna M, Pawlaczyk K, Ploski R, Nowak-Malczewska DM, Karolak JA and Gajecka M (2023) Differences in the composition of the bacterial element of the urinary tract microbiome in patients undergoing dialysis and patients after kidney transplantation.
Front. Microbiol. 14:1187625.
doi: 10.3389/fmicb.2023.1187625

Differences in the composition of the bacterial element of the urinary tract microbiome in patients undergoing dialysis and patients after kidney transplantation

Marcelina M. Jaworska[1], Paulina Pecyna[1], Katarzyna Jaskiewicz[2], Małgorzata Rydzanicz[3], Malgorzata Kaluzna[4], Krzysztof Pawlaczyk[5], Rafal Ploski[3], Dorota M. Nowak-Malczewska[1], Justyna A. Karolak[1] and Marzena Gajecka[1,2]*

[1]Chair and Department of Genetics and Pharmaceutical Microbiology, Poznan University of Medical Sciences, Poznan, Poland, [2]Institute of Human Genetics, Polish Academy of Sciences, Poznan, Poland, [3]Department of Medical Genetics, Medical University of Warsaw, Warsaw, Poland, [4]Chair and Department of Endocrinology, Metabolism and Internal Diseases, Poznan University of Medical Sciences, Poznan, Poland, [5]Department of Nephrology, Transplantology and Internal Medicine, Poznan University of Medical Sciences, Poznań, Poland

Introduction: The development of molecular biology methods and their application in microbial research allowed the detection of many new pathogens that cause urinary tract infections (UTIs). Despite the advances of using new research techniques, the etiopathogenesis of UTIs, especially in patients undergoing dialysis and patients after kidney transplantation, is still not fully understood.

Methods: This study aimed to characterize and compare the composition of the bacterial element of the urinary tract microbiome between the groups of patients undergoing dialysis (n = 50) and patients after kidney transplantation (n = 50), with positive or negative urine culture, compared to healthy individuals (n = 50).

Results: Asymptomatic bacteriuria was observed in 30% of the urine cultures of patients undergoing dialysis and patients after kidney transplantation, with *Escherichia coli* as the most dominant microorganism (73%) detected with the use of classical microbiology techniques. However, differences in the bacterial composition of the urine samples between the evaluated patient groups were demonstrated using the amplicon sequencing. *Finegoldia*, *Leptotrichia*, and *Corynebacterium* were found to be discriminative bacteria genera in patients after dialysis and kidney transplantation compared to the control group. In addition, in all of urine samples, including those without bacteriuria in classical urine culture, many types of bacteria have been identified using 16S rRNA sequencing.

Discussion: The revealed microbial characteristics may form the basis in searching for new diagnostic markers in treatment of patients undergoing dialysis and patients after kidney transplantation.

KEYWORDS

urobiome, urinary tract infection, dialysis, renal transplantation, urine culture

1. Introduction

While historically urine has been considered sterile in healthy individuals, recent studies have revealed the presence of a wide variety of bacteria in the urinary tract that are usually unidentifiable by conventional microbiological techniques, but can be recognized using molecular methods, including the 16S amplicon sequencing (Wolfe et al., 2012; Lewis et al., 2013; Johnson et al., 2019).

Since the discovery of the human urobiome, which is defined as a group of microorganisms and their genomes occurring in the urinary system, some research has been done to characterize its composition and understand its relationship to human health and disease (Wolfe and Brubaker, 2019). Disturbances in the functioning of the bacterial element of the urinary tract microbiome can cause diseases of the urinary system such as overactive bladder, interstitial cystitis, or neurogenic bladder dysfunction (Pearce et al., 2014; Whiteside et al., 2015).

Urinary tract infection (UTI) is a serious problem in patients with chronic kidney disease (CKD), especially in individuals undergoing dialysis or kidney transplant (Grabe et al., 2015; Coussement et al., 2020). UTI is associated with increased risks of acute rejection, allograft dysfunction, graft loss, increased hospital stays, and mortality (Ariza-Heredia et al., 2014; Koga et al., 2022). Furthermore, a recurrent UTI, which occurs in 7% of the patients after kidney transplantation, is one of the leading causes of allograft loss and death (Britt et al., 2017). Therefore, prediction, early detection, and prevention of UTI are essential. In patients with CKD, UTI can be caused by both, opportunistic bacteria and uropathogens responsible for mixed infections (Naumnik and Myśliwiec, 2013). For many decades, knowledge about uropathogens was considered to be well-established and fairly consistent. Currently, the development of molecular biology methods and their application in research have allowed the identification of many new pathogens, also involved in the etiology of UTI (Price et al., 2018).

Knowledge about the bacterial component of the urinary tract in patients undergoing dialysis or in patients after kidney transplantation remains limited. Thus far, scarce information, including the differentiation of the bacterial element of the urinary tract microbiome depending on the gender of patients after kidney transplantation (Fricke et al., 2014) and differences in the microbiota composition between urine samples of patients after kidney transplantation and healthy individuals (Modena et al., 2017; Rani et al., 2017) have been reported. However, there is no data about differences in the urinary tract microbiome between patients undergoing dialysis and patients after kidney transplantation.

The detection of bacteria in urine samples using culturing methods is the main diagnostic criterion for UTI (Hryniewicz and Holecki, 2015). While culture-dependent techniques allow the identification of typical uropathogens, the isolation and identification of highly demanding and non-cultured microorganisms are not routinely performed in microbiological diagnostics of UTI Consequently, the role of highly demanding and non-cultured bacteria remains elusive in the etiology of UTIs (Magistro and Stief, 2019). Therefore, the molecular biology-based approach could be essential in the identification of bacteria in patients with negative urine cultures (Thomas-White et al., 2018; Wolfe and Brubaker, 2019).

Due to limited data on the bacterial component of the urinary tract microbiome in patients with kidney diseases, the aim of this research was to characterize and compare the composition of the bacterial element of the urinary tract microbiome between the groups of patients with positive or negative urine culture in classical microbiology undergoing dialysis or kidney transplant, compared to control individuals without UTI.

2. Materials and methods

2.1. Patient ascertainment and sample collection

Study individuals were recruited in the outpatient clinic and inpatient ward in the Chair and Department of Endocrinology, Metabolism, and Internal Diseases at the Poznan University of Medical Sciences (PUMS). Patients with end-stage-renal diseases (ESRD), including patients after renal transplantation and patients undergoing dialysis, as well as individuals without urinary tract dysfunction (controls), were enrolled in this study. Patients were assigned to the adequate study group based on the ESRD-treatment. The inclusion criterion for the control group was lack of active UTI. Antibiotic/antifungal treatment 3 weeks before the urine sample collection was the exclusion criterion in the subgroups of patients and controls.

A urine sample was obtained once from each study participant by a sterile mid-stream collection. Derived samples were divided into two aliquots—the first part was immediately used for the assessment by techniques of classical microbiology, while the second part was centrifuged at 800 rcf for 10 min and the pellet was stored at −80°C for the genetic testing.

The study was carried out in accordance with the research protocol approved by the Bioethics Committee at the PUMS (no. 942/14 (2014.12.04), 191/15 (2015.02.05) and 1170/19 (2019.12.05)). The possible consequences of the study were explained, and informed consent was obtained from all participants, according to the Declaration of Helsinki.

2.2. Assessment of bacterial cultures of urine samples

Urine samples were inoculated by a Hoeprich quantitative method on the chromogenic medium Chrom ID® CPS Elite (Biomerieux), then used for isolation, quantification, and presumptive identification of *Enterococcus*, *Proteeae* (*Proteus, Providencia, Morganella*), KESC group (*Klebsiella, Enterobacter, Serratia, Citrobacter*), *Staphylococcus saprophyticus,* and *Streptococcus agalactiae*. After incubation at 35–37°C for 24–48 h, the grown colonies were counted and reported as the number of colony forming units (CFUs) per 1 mL of urine sample.

2.3. DNA isolation

Genomic microbial DNA was extracted from urine pellets using Genomic Mini AX Body Fluids extraction kit (A&A Biotechnology), according to the manufacturer's protocol with one modification, in a form of adding 10 µL of each of mutanolysin (activity >10,000 U/mg),

lysostaphin (concentration: 15 U/μL), lysozyme (concentration: 10 mg/mL), and lyticase (concentration: l0 U/μL) to ensure cell lysis.

2.4. 16S rRNA amplicon sequencing

All steps were performed according to the 16S Metagenomic Sequencing Library Preparation—Preparing 16S Ribosomal RNA Gene Amplicons for the Illumina MiSeq System protocol (Illumina). Briefly, V3 and V4 hypervariable regions of the bacterial 16S rRNA gene were amplified using 515F and 806R primers. Libraries were prepared with Nextera XT Index Kit (Illumina) followed by paired-end sequencing (2×300 bp) using MiSeq System (Illumina, San Diego, CA, United States). The sequencing run was performed with 10% of reference PhiX Control v3 Library (Illumina) spike-in to improve sequencing quality of 16S rRNA amplicon low diversity libraries. The sequencing was performed at the Medical University of Warsaw in Poland.

2.5. Bioinformatic analysis and taxonomic assignment

Bioinformatic analysis of obtained 16S rRNA amplicon sequence reads was performed by the bioinformatics company, ideas4biology Sp. z o.o. in Poznan, Poland, in accordance with the previously described protocol (Katoh et al., 2002; McDonald et al., 2012; Callahan et al., 2016; Bokulich et al., 2018; Bolyen et al., 2019). Analyzes of 16Sr RNA amplicon sequencing data were performed using QIIME 2 version 2019.7 (Bolyen et al., 2019). The control and improvement of the quality of the readings (including the removal of phiX and chimeras) was based on the q2-dada2 function implementing the DADA2 algorithm (Callahan et al., 2016). The obtained amplicon sequence variants (ASVs) were aligned using the mafft algorithm (Katoh et al., 2002) implemented as part of the q2-alignment function. ASVs are generated by a *de novo* process, in which biological sequences are distinguished on the basis of more frequent repetition than sequence error, and are applied to individual DNA sequences recovered from high-throughput sequencing. The taxonomic affiliation was assigned to the ASV with the help of a naive Bayesian class fitter trained using the q2-feature-class plugin (Bokulich et al., 2018). The Greengenes 13_8 99% OTUs reference sequences database (McDonald et al., 2012) was used to teach the fi cator class, taken from the ftp address: http://qiime.org/home_static/dataFiles.html Alpha-diversity (Shannon's diversity index) and beta-diversity (Bray-Curtis distance) analyzes were carried out. The overall structural similarity and variation (beta diversity between samples) between the bacterial element of urine microbiomes from the patients undergoing dialysis, patients after kidney transplantation, and controls were then examined using the Bray–Curtis dissimilarity distance analysis with Principal Coordinates Analysis (PCoA).

2.6. Statistical analyzes

Statistical analyzes were performed using Statistica, version 13.4 (Dell Inc.). The compliance of the empirical data distributions with the normal distribution was verified with the Shapiro–Wilk W test. Due to the fact that the distribution of data was not consistent with the normal distribution, the analysis of differences between the study groups was assessed using the Kruskal-Wallis test with the post-hoc multiple comparison test (Dunn's test).

2.7. Comparison of the bacterial element of the urinary tract microbiome between patients undergoing dialysis and patients after kidney transplantation

In order to differentiate bacterial species identified in the 16S rRNA amplicon sequencing between the samples in the groups of patients undergoing dialysis and patients after kidney transplantation, with the positive or negative results of urine culture, statistical analyzes were performed using the chi square test. The analyzes were carried out in the following scheme: (i) patients undergoing dialysis with a positive urine culture vs. patients undergoing dialysis with a negative urine culture, (ii) patients after kidney transplantation with a positive urine culture vs. patients after kidney transplantation with a negative urine culture, and (iii) patients undergoing dialysis and patients after kidney transplantation with a positive urine culture vs. patients undergoing dialysis and patients after kidney transplantation with a negative urine culture.

3. Results

3.1. Characteristics of patients and controls

In total, 100 patients and 50 control individuals, with the age range of 18–80 years participated in the study. In the group of patients undergoing dialysis, 15 and 35 individuals were treated with peritoneal dialysis (DO) or hemodialysis (HD), respectively. In Table 1 demographic characteristics of study participants are compiled.

Polycystic kidney disease and glomerulonephritis were the most common indications for treatment with DO and HD, respectively. In 6% of patients, the cause of the renal dysfunction leading to the decision to apply dialysis therapy was undetermined nephropathy.

Glomerulonephritis was the most common indication for kidney transplantation. In 22% patients, the cause of the renal dysfunction remained undetermined nephropathy. Diseases identified in patients undergoing dialysis or patients after kidney transplantation are listed in Table 2.

3.2. Characteristics of microorganisms identified in urine cultures

The etiological factor responsible for UTI was identified (bacteriuria $\geq 10^5$ CFU/mL) in 30% of the samples obtained from patients undergoing dialysis and patients after kidney transplantation. Asymptomatic bacteriuria was found to be more common in women (18/43 = 42%) than in men (13/57 = 23%). In the group of patients undergoing dialysis, asymptomatic bacteriuria was recognized in 8/23 women (35%) and 7/27 men (26%), while in patients after kidney transplantation, asymptomatic bacteriuria was recognized in 10/20 women (50%) and 5/30 men (17%) *Escherichia coli* was the most common etiological factor of asymptomatic bacteriuria and was

10.3389/fmicb.2023.1187625

TABLE 1 Demographic characteristics of the studied groups.

Age ranges (years)	Patients undergoing dialysis (n =50)		Patients after kidney transplantation (n =50)		Controls (n =50)	
	Female	Male	Female	Male	Female	Male
<30	1 (2%)	1 (2%)	1 (2%)	0 (0%)	9 (18%)	0 (0%)
31–40	1 (2%)	5 (10%)	6 (12%)	10 (20%)	10 (20%)	0 (0%)
41–50	3 (6%)	3 (6%)	2 (4%)	2 (4%)	2 (4%)	3 (6%)
51–60	4 (8%)	7 (14%)	4 (8%)	11 (22%)	7 (14%)	3 (6%)
61–70	12 (24%)	6 (12%)	7 (14%)	5 (10%)	9 (18%)	3 (6%)
>70	2 (4%)	5 (10%)	0 (0%)	2 (4%)	3 (6%)	1 (2%)
Total	23 (46%)	27 (54%)	20 (40%)	30 (60%)	40 (80%)	10 (20%)

Age ranges and gender of study participants in the groups of patients undergoing dialysis, patients after kidney transplantation, and controls.

detected in 80% of patients undergoing dialysis and 67% of patients after kidney transplantation. *Staphylococcus* spp., *Enterococcus* spp., *Kocuria* spp., *Morganella morganii*, and *Enterobacter cloacae complex* were also recognized as etiological factors of asymptomatic bacteriuria in these study groups. Detailed information about bacteria identified in urine cultures is presented in Supplementary Tables S1–S3.

3.3. The composition of the bacterial element of urinary tract microbiome varies between patients undergoing dialysis and patients after renal transplantation

The bacterial DNA was extracted from all of the collected 150 urine samples. Out of them, 148 samples met the required qualitative and quantitative criteria and were subjected to the 16S rRNA amplicon sequencing.

Without taking into account the division into study groups, *Actinobacteria* (100%), *Firmicutes* (97%), *Proteobacteria* (91%), *Fusobacteria* (50%), *Cyanobacteria* (40%), *Acidobacteria* (22%), *Bacteroidetes* (16%), and *Thermi* (4%) were found as the most common types of bacteria detected in the assessed samples. The substantial difference in bacteria abundance in urine samples was detected for *Proteobacteria* between patients undergoing dialysis and controls ($p = 0.047$), and between patients undergoing dialysis and patients after renal transplantation ($p = 0.037$). The superior abundance was found in a group of patients undergoing dialysis.

Overall, at the genus level, 76 different genera were detected in the samples derived from patients. The highest number of genera were identified in patients undergoing dialysis ($n = 60$), followed by patients after renal transplantation ($n = 58$). In urine samples obtained from controls, 50 different genera were detected. The number and variability of identified bacteria genera of the bacterial element of the urinary tract microbiome between groups are presented in Figure 1.

The genera *Corynebacterium* ($p = 0.002$), *Moryella* ($p = 0.033$), *Finegoldia* ($p < 0.001$), and *Gallicola* ($p = 0.002$) were detected with increased abundance in urine samples of patients undergoing dialysis comparing to urine samples derived from controls. Representatives of the genus *Ochrobactrum* were identified more often in controls compared to patients undergoing dialysis ($p < 0.0001$).

Bacteria from genera *Mogibacterium* ($p = 0.049$) and *Sphingomonas* ($p < 0.0001$) were more often identified in the urine samples from patients after renal transplantation compared to controls. The sequences corresponding to the genus *Propionicimonas* were identified with a higher abundance in urine samples derived from controls ($p = 0.041$).

Differences in relative abundances of selected genera were also observed between urine samples obtained from patients undergoing dialysis and patients after kidney transplantation. Increased abundance of genera *Moryella* ($p = 0.033$), *Shuttleworthia* ($p = 0.003$), *Finegoldia* ($p < 0.001$), *Gallicola* ($p = 0.002$), and *Propionigenium* ($p = 0.001$) was recognized in patients undergoing dialysis. On the other hand, the genera *Ochrobactrum* ($p < 0.0001$) and *Sphingomonas* ($p < 0.0001$) were detected with higher abundance in urine samples from renal transplant patients.

The obtained values of alpha-diversity indicate heterogeneity of the samples (Figure 2). Bacterial relative abundance in samples derived from patients undergoing dialysis and patients after kidney transplantation was found to be larger as compared to control samples ($p = 0.003$ and $p = 0.004$, respectively). There was no significant difference in the relative abundance of bacteria in patients after renal transplantation compared to patients undergoing dialysis ($p = 0.68$).

The analyses of bacterial structural similarity and variation revealed substantial differences between samples were detected and the results are presented in Figure 3. Bacterial element of the urinary tract microbiome in samples from patients undergoing dialysis was the most diverse in terms of composition. On the other hand, urine samples from controls were characterized by the smallest diversity.

3.4. Composition of the urinary tract microbiome in patients with positive vs. negative urine cultures

Bacterial element of the urinary tract microbiome in patients with positive and negative urine cultures was compared (Figure 4). In urine samples derived from patients with positive urine culture in classical microbiology, lower diversity of bacterial genera comparing to samples from patients with negative urine culture was found in the 16S amplicon sequencing. In addition, bacteria from *Finegoldia*, *Leptotrichia*, and *Corynebacterium* genera were found to be discriminative in patients undergoing dialysis and patients after kidney transplantation compared to individuals without urinary tract dysfunction.

TABLE 2 Primary disease or urinary system dysfunction, treated with dialysis or resulting in a kidney transplant in studied patients.

Primary disease/ comorbidities	Classification of causes of CKD*	Studied groups		
		Patients undergoing dialysis (n =50)	Patients after kidney transplantation (n =50)	Total (n =100)
Hypertension (HT)	Vascular diseases	8 (16%)	8 (16%)	16 (16%)
HT and urinary system defects	Vascular diseases and cystic and congenital diseases	0 (0%)	1 (2%)	1 (1%)
HT and proteinuria	Vascular diseases	0 (0%)	1 (2%)	1 (1%)
Glomerulonephritis (GN)	Glomerular diseases	10 (20%)	11 (22%)	21 (21%)
GN and HT	Glomerular diseases and vascular diseases	2 (4%)	1 (2%)	3 (3%)
Obstructive nephropathy	Tubulointerstitial diseases	0 (0%)	1 (2%)	1 (1%)
Reflux nephropathy	Cystic and congenital diseases	0 (0%)	1 (2%)	1 (1%)
Chronic tubulointerstitial nephropathy	Tubulointerstitial diseases	0 (0%)	1 (2%)	1 (1%)
Chronic glomerulonephritis (cGN)	Glomerular diseases	0 (0%)	2 (4%)	2 (2%)
(cGN) and HT	Glomerular diseases and vascular diseases	0 (0%)	1 (2%)	1 (1%)
Polycystic kidney disease	Cystic and congenital diseases	9 (18%)	2 (4%)	11 (11%)
Diffuse mesangial proliferative nephritis	Glomerular diseases	0 (0%)	2 (4%)	2 (2%)
Diabetes	Glomerular diseases	0 (0%)	5 (10%)	5 (5%)
Diabetes and HT	Glomerular diseases and vascular diseases	0 (0%)	2 (4%)	2 (2%)
GN and cirrhosis of the right kidney	Glomerular diseases	1 (2%)	0 (0%)	1 (1%)
Tubulointerstitial nephropathy (TN)	Tubulointerstitial diseases	6 (12%)	0 (0%)	6 (6%)
TN and urinary system defects	Tubulointerstitial diseases and cystic and congenital diseases	2 (4%)	0 (0%)	2 (2%)
Chronic renal failure (CHF)—exact cause unknown	Unknown nephropathies	5 (10%)	0 (0%)	5 (5%)
Hypertensive nephropathy	Vascular diseases	2 (4%)	0 (0%)	2 (2%)
Wegener's granuloma	Glomerular diseases	2 (4%)	0 (0%)	2 (2%)
Cause unknown	Unknown nephropathies	3 (6%)	11 (22%)	3 (3%)
Total		50 (100%)	50 (100%)	100 (100%)

*Classification of causes of CKD according with National Kidney Foundation (https://www.kidney.org/professionals/explore-your-knowledge/how-to-classify-ckd).

In urine samples from patients undergoing dialysis, with a negative urine culture, bacteria *Leptotrichia* were identified more frequently ($p = 0.003$), and those from the genus *Finegoldia* less often ($p = 0.038$) than in the group of patients undergoing dialysis with a positive urine culture.

Corynebacterium bacteria were recognized less often in the urine samples of kidney transplant patients with negative urine culture than in positive urine culture samples from this group ($p = 0.016$).

In patients undergoing dialysis and kidney transplant patients with a negative urine culture, *Leptotrichia* was identified in the larger number of samples ($p = 0.037$) than in patients undergoing dialysis and kidney transplant patients with a culture-positive urine.

These results point to *Leptotrichia, Finegoldia* and *Corynebacterium* as potential diagnostics indicators of UTI.

4. Discussion

Chronic renal failure is a global health problem (Qiu et al., 2017) with the overall incidence of 242 people per million and an annual increase of 8% (Kim, 2019). In Poland, about 4.2 million people suffer from CKD (Gellert et al., 2020). Since the prevalence of CKD is calculated based on the number of patients with the end-stage disease only (Włodarczyk and Felcenloben, 2017–2018), the actual prevalence

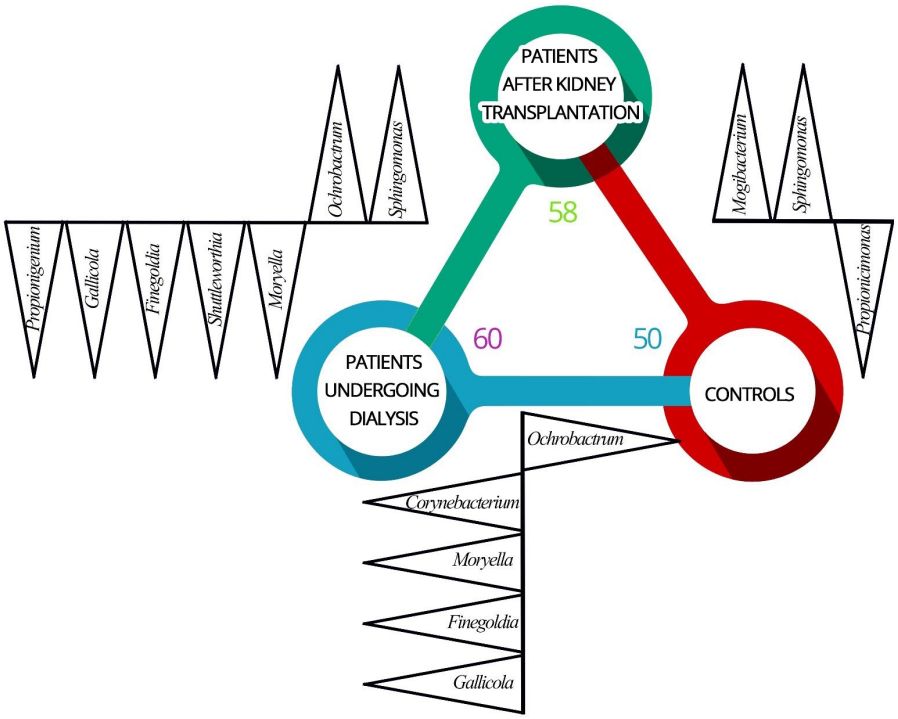

FIGURE 1
Differences in the composition of the bacterial element of urinary tract microbiome between patients undergoing dialysis (D), patients after renal transplantation (T), and control individuals (C). Identified genera (black triangles) of the bacterial element of the urinary tract microbiome varies between patients undergoing dialysis (blue circle), patients after kidney transplantation (green circle), and control individuals (red circle). Increased abundance in (D) vs. (C) were found for *Corynebacterium*, *Moryella*, *Finegoldia*, and *Gallicola*. *Ochrobactrum* was identified more often in (C) comparing to (D). *Mogibacterium* and *Sphingomonas* were more often identified in (T) comparing to (C). *Propionicimonas* was identified with a higher abundance in (C) compared to (T). Increased abundance of genera *Moryella*, *Shuttleworthia*, *Finegoldia*, *Gallicola*, and *Propionigenium* was recognized in (D) and *Ochrobactrum* and *Sphingomonas* were detected with higher abundance in (T) compared to (D).

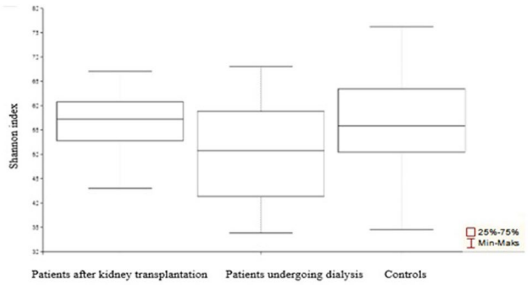

FIGURE 2
α-Diversity of the urinary tract microbiome bacterial element among patients after transplantation, undergoing dialysis, and control individuals. Compared to control samples, the most diverse was the urine microbiota composition among patients undergoing dialysis.

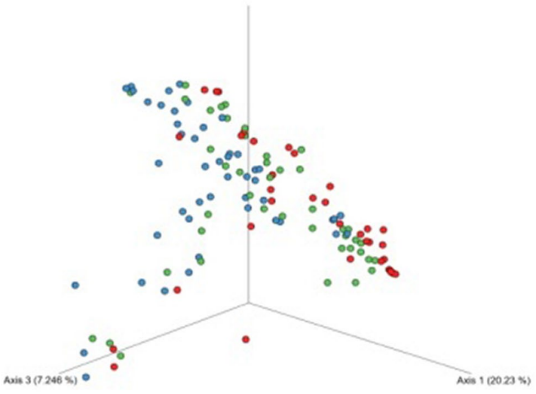

FIGURE 3
Beta-diversity assessed by the Bray–Curtis dissimilarity tests between patients undergoing dialysis (blue dots), patients after kidney transplantation (green dots), and controls (red dots) based on ASVs. The bacterial element of urine microbiota of patients undergoing dialysis was more variable in composition of microorganisms.

of CKD could be underestimated, both in Poland and worldwide (Włodarczyk and Felcenloben, 2017–2018).

UTI complication in patients undergoing dialysis is a significant problem in the process of renal replacement therapy that increases the frequency of hospitalization and the risk of death (Gołębiewska et al., 2011) Also, in the group of kidney recipients, UTI is a leading cause of post-transplant infectious complications in both men and women (Abbott et al., 2004; Tenke et al., 2008; Naber et al., 2010). In this study, asymptomatic bacteriuria, defined in accordance with the current recommendations (Hryniewicz and Holecki, 2015), was detected in 30% of patients undergoing dialysis or kidney transplantation.

Typical pathogens of the urinary tract are also most often responsible for asymptomatic bacteriuria in patients undergoing

10.3389/fmicb.2023.1187625

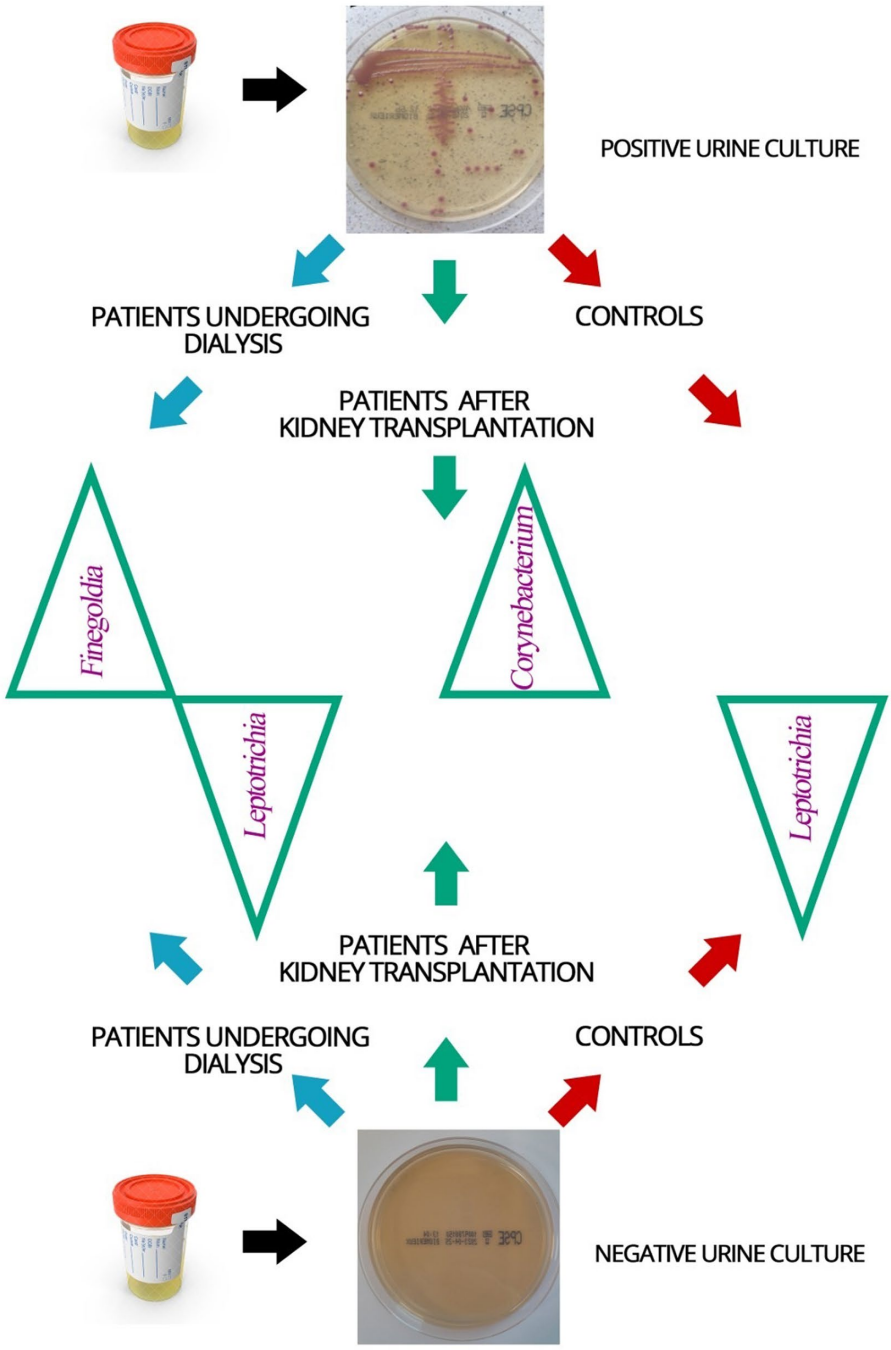

FIGURE 4
Schematic representation of the bacterial element of the urinary tract microbiome identified in the urine samples of patients and control individuals with positive and negative urine cultures. Blue arrow—dialysis patients, green arrow—patients after kidney transplantation, red arrow—controls; green triangles—names of identified bacteria genera of the bacterial element of the urinary tract microbiome that were found to be discriminative in the studied groups of patients.

dialysis and patients after kidney transplantation. Thus, the results of our study are in line with previous reports showing the presence of *Escherichia coli* in 70% (Willner et al., 2014), 72.9% (Michno et al., 2018), or 82% (Olenski et al., 2019) of the urine samples with a positive culture result.

In order to extend the knowledge about urobiome, we evaluated groups of patients rarely included in microbiome studies, namely patients undergoing dialysis and patients after kidney transplantation. Assessment of the bacterial composition using 16S amplicon sequencing revealed 60 and 58 genera in urine samples from patients undergoing dialysis and patients after kidney transplantation, respectively. In controls, 50 different genera were recognized.

Culture-based methods, compared to the 16S rRNA amplicon sequencing, are less effective in detecting bacteria in urine samples and identify a limited number of microorganisms, mainly aerobic and fast-growing bacteria such as *Escherichia coli* (García and Isenberg,

2010; Wolfe and Brubaker, 2015). Using classical microbiology techniques, four genera of microorganisms were detected in urine samples from individuals without urinary tract dysfunction, 12 genera of bacteria in urine samples from patients undergoing dialysis, and 16 genera of microbes in urine samples from patients after kidney transplantation. In contrast, using 16S rRNA sequencing, we recognized higher bacterial heterogeneity, 58 genera were recorded in urine samples from patients after kidney transplantation and 60 genera of bacteria in the group of patients undergoing dialysis. Also, 37 detected genera were found to be common to all study groups.

Since as many as 80% of the phylotypes detected by 16S rRNA sequencing correspond to bacterial species that cannot be cultured *in vitro* (Jach and Sajnaga, 2017), the differences in the number of recognized microbes identified in our study are coherent. Such large disproportion in the number of bacterial genera obtained due to classical microbiology and 16S rRNA sequencing, as well as the identification of non-cultivated microorganisms, gave the opportunity to get a more complete picture of the microbiome and highlighted the role of molecular biology methods in the clinical examination of urine samples. Therefore, a combination of 16S rRNA gene sequencing along with quantitative urine culture would provide a reliable characterization of microbial communities in the urinary tract, since culture-based approaches would allow an approximate bacterial quantification and would therefore be useful as clinically relevant indicators (Perez-Carrasco et al., 2021).

Bacteria of the genera *Corynebacterium*, *Moryella*, *Finegoldia*, and *Gallicola* were more often identified in urine samples from patients undergoing dialysis than in control individuals, in which the dominant genus was *Ochrobactrum*. It has been reported that the midstream urinary microbiomes varied in adult patients with CKD and that variability was lower in more advanced CKD (Kramer et al., 2018). In recent years, there has been an interest in rare or infrequently described *Corynebacterium* species, which are emerging opportunistic pathogens considered to be potential uropathogens due to their detection in patients with UTIs (Barberis et al., 2021). *Corynebacterium phoceense* has been isolated from the urine of a kidney transplant recipient (Cresci et al., 2016). *Ochrobactrum anthropi* is considered atypical for dialysis peritonitis, a major complication of peritoneal dialysis therapy, as well as for other human infections (Gałgowska et al., 2020). However, this bacterium is an increasingly recognized cause of infection in immunocompromised hosts such as patients with kidney failure treated by dialysis (Abbassi-Nik et al., 2022).

Also, the composition of the urobiome in patients after kidney transplantation has not been sufficiently evaluated. Rani et al. indicated that urine microbiota in kidney transplant recipients was less diverse and dominated by potentially pathogenic Gram-negative bacteria of the genus *Escherichia* or *Enterobacter*, while urine microbiome in controls showed greater diversity and a higher incidence of non-pathogenic Gram-positive organisms such as *Propionibacterium*, *Corynebacterium*, and *Mobiluncus* (Rani et al., 2017). The study showed significant differences in the presence of bacteria of the genera *Mogibacterium* and *Sphingomonas*, which were more often identified in urine samples from transplant patients than in controls (Rani et al., 2017). The results of these studies may suggest that under the multiple stressors associated with kidney transplantation (including antibiotics or immunosuppression), the urinary microbiota of kidney-transplant recipients can decrease in diversity compared to healthy controls, while the abundance of opportunistic pathogens may increase, which may favor the promotion of antibiotic resistance (Rani et al., 2017).

Mogibacterium are Gram-positive, strictly anaerobic bacilli present in the oral environment and involved in oral infections (Casarin et al., 2012). Previously, the role of these microorganisms as the cause of urolithiasis was evaluated and the study concluded that differences and interactions between gut bacteria might predict certain types of urolithiasis (Zhao et al., 2020). The genus *Sphingomonas* is comprised of more than 30 species including human pathogen, *Sphingomonas paucimobilis* (Ryan and Adley, 2010). The most *Sphingomonas* infections are nosocomial and usually occur in immunocompromised individuals, including the kidney transplant patients (Ryan and Adley, 2010; Yu et al., 2015).

In a pilot study on the urinary microbiome of 21 renal transplant recipients and nine patients with acute kidney injury, rich and differentiated microbiome was found (Gerges-Knafl et al., 2020). Also, the same study demonstrated significant differences in the certain bacterial genera profiles between renal transplant recipients and patients with acute kidney injury, but the overall diversity did not differ between the two groups (Gerges-Knafl et al., 2020). In our study, comparing the urinary microbiota of patients undergoing dialysis and patients after transplantation, genera of *Sphingomonas*, *Ochrobactrum*, and *Actinocorallia* were found with a higher frequency in patients after kidney transplantation. On the other hand, genera *Moryella*, *Shuttleworthia*, *Finegoldia*, *Gallicola,* and *Propionigenium* were identified in urine samples from patients undergoing dialysis with a significantly higher frequency than in urine samples from patients after kidney transplantation. In the future research, numerous and longitudinal sampling of the patient' urinary microbiome should be implemented to detect deviations from microbiome stability. If these changes indicate a risk of organ damage or loss, analysis of microbiome could be useful as a non-invasive method for early detection of transplanted organ failure (Campbell et al., 2020).

The genus *Ochrobactrum* includes nine species, with *Ochrobactrum anthropi*, Gram-negative oxygen-rod, increasingly recognized as a potentially problematic, opportunistic, and nosocomial pathogen (Hagiya et al., 2013). Asymptomatic bacteriuria associated with the administration of anti-thymocytic globulin contaminated with *Ochrobactrum anthropi* have been described in organ recipients (Gałgowska et al., 2020). Other complications caused by *Ochrobactrum anthropi* were associated with a superinfection of tissues implanted from deceased donors or contamination of the preservative fluid (Gałgowska et al., 2020).

Moryella indoligenes is a strictly anaerobic bacterium from the *Lachnospiraceae* family of the order *Clostridiales* (Carlier et al., 2007). Bacteria belonging to the genus *Moryella* were also detected in urine samples (Sabat et al., 2017) and the first case of bacteriemia involving this microorganism has been described in a patient with a history of prostatic hyperplasia complicated by recurrent UTI (Hansen et al., 2020).

Shuttleworthia is another discriminative type of bacteria found in our study. Previously *Shuttleworthia* has been suggested as a potential biomarker of inflammation in the urinary tract (Ling et al., 2017).

Here, the genus *Finegoldia* (formerly *Peptostreptococcus*) was identified in a high percentage in all three study groups with the highest number detected in the group of patients undergoing dialysis. *Finegoldia* are Gram-negative anaerobic opportunistic microorganisms

that colonize the skin and mucous membranes (Song and Finegold, 2007; Murphy and Frick, 2013). The representative of this genus, *Peptostreptococcus prevotii* was often identified in men with non-gonococcal urethritis, while *Peptostreptococcus magnus* was the most common anaerobic species detected in patients without urethritis (Tungland, 2018). *Finegoldia* is also present in the urine of both sexually active adult males and sexually inactive adolescents (Tungland, 2018). In another study, two specific species of *Finegoldia* found in the urine of the bladder, including *Finegoldia magna*, were associated with preoperative worsening of urinary symptoms in women undergoing stress urinary incontinence and pelvic prolapse (Fok et al., 2018).

A comparison of 16S rRNA amplicon sequencing results in mid-stream urine samples from renal transplant patients with confirmed interstitial fibrosis and tubular atrophy (IFTA) and healthy controls showed that in IFTA patients, *Streptococcus* and *Lactobacillus* were more commonly identified than in controls (Modena et al., 2017). In patients with IFTA an increase in the number of pathogenic bacteria, *Propionibacterium acnes* (formerly *Cutibacterium acnes*), *Prevotella disiens*, *Gardnerella vaginalis*, and *Finegoldia magna* was found (Modena et al., 2017). It has been suggested that as the enrichment of uropathogens increases, the immune response in IFTA patients may be enhanced. In turn, it might result in an increased risk of transplant rejection in these individuals (Modena et al., 2017).

In another study, Colas et al. identified major changes in the urinary microbiota of patients following kidney transplantation with a significant impact on recipient status (spontaneously tolerant patient—TOL; minimal immunosuppressed patient—MIS; stable patient—STA). Their results highlighted a unique and specific urinary microbiota associated with spontaneous tolerance characterized by a high diversity and a clear *Proteobacteria* profile. In addition, TOL recipients were characterized by a specific and unique increase in *Proteobacteria* phylum (*Oxalobacteraceae* [genus *Janthinobacterium*], *Caulobacteraceae, Comamonadaceae, Moraxellaceae* [*genus Acinetobacter*], *Xanthomonadaceae, Achromobacter, Yersinia*) (Colas et al., 2020).

In another study performed to identify differences in the urinary microbiome associated with chronic allograft dysfunction (CAD), *Corynebacterium* was more prevalent in female and male patients with CAD compared to non-CAD female patients. On the other hand, analysis of male CAD and female CAD patients showed greater abundance of phylum *Proteobacteria* in males (Wu et al., 2018).

In our study, 30% of patients undergoing dialysis and also 30% of patients after kidney transplantation had a positive urine culture with identification of an etiological factor indicative of UTI in classical microbiology. The impact of UTI on distant graft function is not fully understood. The predominance of pathogenic Gram-negative bacteria in urobiome of patients after kidney transplantation, indicated in some reports, highlights the problem of UTIs in recipients (Sabé et al., 2022) and a negative impact of early or late UTIs on the functioning of the transplanted kidney has been confirmed (Rani et al., 2017; Fiorentino et al., 2019; Pesce et al., 2019).

While the V3-V4 hypervariable regions of 16S rRNA are frequently used for human microbiome profiling, sequencing only two fragments of the 16S rRNA gene does not allow to narrow down the classified the bacteria to the species level due to the homology between sequences of phylogenetically related bacteria and/or issues related to bacterial nomenclature and taxonomy (Vetrovsky and Baldrian, 2013; Bukin et al., 2019; Winand et al., 2020). Many investigators have found resolution problems at the genus and/or species level with 16S rRNA gene sequencing data (Janda and Abbott, 2007; Liu et al., 2020), especially for the family Enterobacteriaceae (in particular, *Enterobacter* and *Pantoea*), *Acinetobacter baumannii—A. calcoaceticus complex, Achromobacter, Stenotrophomonas,* and *Actinomyces* (Chang et al., 2005; Janda and Abbott, 2007). In addition, 16S rRNA gene sequencing cannot distinguish between recently diverged species (Peker et al., 2019). The difference between the closest and next closest match to the unknown strain is < 0.5% divergence (>99.5% similarity) (Petti, 2007; Paul et al., 2019). In these circumstances, such small differences cannot justify choosing the closest match as a definitive identification. Since classification to the species level based on V3-V4 hypervariable regions of 16S rRNA is debatable and usually not achievable (Hiergeist et al., 2023), we performed data analysis at the bacterial genus level. Also, due to the inability to quantify microorganisms in amplicon sequencing, only qualitative assessment of microorganisms identified by this method was performed. Thus, in this study, data analysis at the level of bacterial genus has been performed. Also, due to the inability to quantify microorganisms in amplicon sequencing, only qualitative analyzes of microorganisms identified by this method were performed.

Summarizing, our study provides evidence of the diversity of bacterial composition in urine samples in patients undergoing dialysis and patients after kidney transplantation compared to unaffected individuals. The applied amplicon sequencing allowed a better characterization of the composition of urobiome than classical microbiology methods. *Leptotrichia, Finegoldia,* and *Corynebacterium* were revealed as discriminative bacteria in patients undergoing dialysis and after kidney transplantation with UTI. This latest finding may form the basis of a future diagnostic process involving these bacteria as diagnostic biomarkers or in future treatment strategies for the diseases discussed here.

Data availability statement

The datasets presented in this study can be found in online repositories. The names of the repository/repositories and accession number(s) can be found at: BioProject: PRJNA949101.

Ethics statement

The study protocol was approved by the Bioethics Committee at Poznan University of Medical Sciences (nr 942/14 (04.12.2014), nr 191/15 (05.02.2015) and 1170/19 (05.12.2019)). The possible consequences of the study were explained, and informed consent was obtained from all participants, according to the Declaration of Helsinki. The patients/participants provided their written informed consent to participate in this study.

Author contributions

MJ and MG designed the experiment. MJ and PP collected the urine samples and prepared bacterial genetic material to 16S

rRNA sequencing. KJ and MR performed the amplicon sequencing, supervised by RP. MK and KP performed medical examination and enrolled patients in this study. MJ conducted experiments using classical microbiology. DN-M performed the statistical analysis. MJ, JK, and MG participated in the data analysis. MJ and JK wrote the manuscript. MG revised the manuscript. All authors contributed to the article and approved the submitted version.

Funding

This research was funded by the National Science Centre in Poland, grant no. 2015/19/N/NZ6/01780 (to MJ).

Acknowledgments

Special thanks to colleagues at the Chair and Department of Genetics and Pharmaceutical Microbiology, PUMS, for technical assistance.

Conflict of interest

The authors declare that the research was conducted in the absence of any commercial or financial relationships that could be construed as a potential conflict of interest.

Publisher's note

All claims expressed in this article are solely those of the authors and do not necessarily represent those of their affiliated organizations, or those of the publisher, the editors and the reviewers. Any product that may be evaluated in this article, or claim that may be made by its manufacturer, is not guaranteed or endorsed by the publisher.

Supplementary material

The Supplementary material for this article can be found online at: https://www.frontiersin.org/articles/10.3389/fmicb.2023.1187625/full#supplementary-material

References

Abbassi-Nik, A., Sprenger-Mähr, H., Zitt, E., Hartmann, G., Dirschmid, H., and Lhotta, K. (2022). *Ochrobactrum anthropi* infection in dialysis patients: a case report and literature summary. *Clin. Nephrol.* 97, 188–192. doi: 10.5414/CN110692

Abbott, K. C., Swanson, S. J., Richter, E. R., Bohen, E. M., Agodoa, L. Y., Peters, T. G., et al. (2004). Late urinary tract infection after renal transplantation in the United States. *Am. J. Kidney Dis.* 44, 353–362. doi: 10.1053/j.ajkd.2004.04.040

Ariza-Heredia, E. J., Beam, E. N., Lesnick, T. G., Cosio, F. G., Kremers, W. K., and Razonable, R. R. (2014). Impact of urinary tract infection on allograft function after kidney transplantation. *Clin. Transpl.* 28, 683–690. doi: 10.1111/ctr.12366

Barberis, C. M., Traglia, G. M., Almuzara, M. N., Rocha, D. J. P. G., Santos, C. S., Aguiar, E. R. G. R., et al. (2021). Corynebacterium phoceense – a rare Corynebacterium species isolated from a urine sample. *Access Microbiol.* 3:000197. doi: 10.1099/acmi.0.000197

Bolyen, E., Rideout, J. R., Dillon, M. R., Bokulich, N. A., Abnet, C. C., al-Ghalith, G. A., et al. (2019). Reproducible, interactive, scalable and extensible microbiome data science using QIIME 2. *Nat. Biotechnol.* 37, 852–857. doi: 10.1038/s41587-019-0209-9

Bokulich, N. A., Kaehler, B. D., Rideout, J. R., Dillon, M., Bolyen, E., Knight, R., et al. (2018). Optimizing taxonomic classification of marker-gene amplicon sequences with QIIME 2's Q2-Feature-Classifier Plugin. *Microbiome* 6:90. doi: 10.1186/s40168-018-0470-z

Britt, N. S., Hagopian, J. C., Brennan, D. C., Pottebaum, A. A., Santos, C. A. Q., Gharabagi, A., et al. (2017). Effects of recurrent urinary tract infections on graft and patient outcomes after kidney transplantation. *Nephrol. Dial. Transpl.* 32, 1758–1766. doi: 10.1093/ndt/gfx237

Bukin, Y. S., Galachyants, Y. P., Morozov, I. V., Bukin, S. V., Zakharenko, A. S., and Zemskaya, T. I. (2019). The effect of 16S rRNA region choice on bacterial community metabarcoding results. *Sci. Data.* 6:190007. doi: 10.1038/sdata.2019.7

Callahan, B., McMurdie, P., Rosen, M., Han, A. W., Johnson, A. J. A., and Holmes, S. P. (2016). DADA2: high-resolution sample inference from Illumina amplicon data. *Nat. Methods* 13, 581–583. doi: 10.1038/nmeth.3869

Campbell, P. M., Humphreys, G. J., Summers, A. M., Konkel, J. E., Knight, C. G., Augustine, T., et al. (2020). Does the microbiome affect the outcome of renal transplantation? *Front. Cell. Infect. Microbiol.* 10:558644. doi: 10.3389/fcimb.2020.558644

Carlier, J. P., K'Ouas, G., and Han, X. Y. (2007). *Moryella indoligenes* gen. nov., sp. nov., an anaerobic bacterium isolated from clinical specimens. *Int. J. Syst. Evol. Microbiol.* 57, 725–729. doi: 10.1099/ijs.0.64705-0

Casarin, R. C., Saito, D., Santos, V. R., Pimentel, S. P., Duarte, P. M., Casati, M. Z., et al. (2012). Detection of *Mogibacterium timidum* in subgingival biofilm of aggressive and non-diabetic and diabetic chronic periodontitis patients. *Braz. J. Microbiol.* 43, 931–937. doi: 10.1590/S1517-83822012000300012

Chang, H. C., Wei, Y. F., Dijkshoorn, L., Vaneechoutte, M., Tang, C. T., and Chang, T. C. (2005). Species-level identification of isolates of the *Acinetobacter calcoaceticus – Acinetobacter baumannii* complex by sequence analysis of the 16S-23S rRNA gene spacer region. *J. Clin. Microbiol.* 43, 1632–1639. doi: 10.1128/JCM.43.4.1632-1639.2005

Colas, L., Mongodin, E. F., Montassier, E., Chesneau, M., Guerif, P., Hittle, L., et al. (2020). Unique and specific proteobacteria diversity in urinary microbiota of tolerant kidney transplanted recipients. *Am. J. Transplant.* 20, 145–158. doi: 10.1111/ajt.15549

Coussement, J., Kaminski, H., Scemla, A., and Manuel, O. (2020). Asymptomatic bacteriuria and urinary tract infections in kidney transplant recipients. *Curr. Opin. Infect. Dis.* 33, 419–425. doi: 10.1097/QCO.0000000000000678

Cresci, M., Ibrahima Lo, C., Khelaifia, S., Mouelhi, D., Delerce, J., di Pinto, F., et al. (2016). Corynebacterium phoceense sp. nov., strain MC1T a new bacterial species isolated from human urine. *NMNI* 14, 73–82. doi: 10.1016/j.nmni.2016.09.001

Fiorentino, M., Pesce, F., Schena, A., Simone, S., Castellano, G., and Gesualdo, L. (2019). Updates on urinary tract infections in kidney transplantation. *J. Nephrol.* 32, 751–761. doi: 10.1007/s40620-019-00585-3

Fok, C. S., Gao, X., Lin, H., Thomas-White, K. J., Mueller, E. R., Wolfe, A. J., et al. (2018). Urinary symptoms are associated with certain urinary microbes in urogynecologic surgical patients. *Int. Urogynecol. J.* 29, 1765–1771. doi: 10.1007/s00192-018-3732-1

Fricke, W. F., Maddox, C., Song, Y., and Bromberg, J. S. (2014). Human microbiota characterization in the course of renal transplantation. *Am. J. Transplant.* 14, 416–427. doi: 10.1111/ajt.12588

Gałgowska, J., Ruszkowski, J., Chmielewski, M., and Lichodziejewska-Niemierko, M. (2020). Dialysis peritonitis caused by an atypical pathogen *Ochrobactrum anthropi*. *Ochrobactrum anthropi* as an unusual cause of dialysis-associated peritonitis. *Nephrol. Forum* 13, 138–141.

García, L. S., and Isenberg, H. D., (2010) *Clinical microbiology procedures handbook. 3rd edition, Vol. 6* (Washington, DC: ASM Press)

Gellert, R., Durlik, M., and Małgorzewicz, S., (2020) Raport 2019. National Study of Nephrological Patients, Kidney Disease: a population-based polish Nationwide study, Hope for Health Foundation, nephrology forum, 13, nr 3, 149–163.

Gerges-Knafl, D., Pichler, P., Zimprich, A., Hotzy, C., Barousch, W., Lang, R. M., et al. (2020). The urinary microbiome shows different bacterial genera in renal transplant recipients and non-transplant patients at time of acute kidney injury – a pilot study. *BMC Nephrol.* 21:117. doi: 10.1186/s12882-020-01773-1

Gołębiewska, J., Dębska-Ślizień, A., and Rutkowski, B. (2011). Urinary tract infections in patients after kidney transplantation. *Nephrol. Forum* 4, 110–118.

Grabe, M., Bartoletti, R., Bjerklund Johansen, T. E., Cai, T., Çek, M., Köves, B., et al. (2015) Guideliness on urological infections. European Association of Urology 2015. Available at: http://uroweb.org/wp-content/uploads/19-Urological-infectionsLR2.pdf, 1–86.

Hagiya, H., Ohnishi, K., Maki, M., Watanabe, N., and Murase, T. (2013). Clinical characteristics of *Ochrobactrum anthropi* bacteremia. *J. Clin. Microbiol.* 51, 1330–1333. doi: 10.1128/JCM.03238-12

Hansen, S., Lřfberg, S. V., Nielsen, D. K., Kobberø, H., and Justesen, U. S. (2020). Bacteraemia with Moryella indoligenes and *Fastidiosipila sanguinis*: a case report. *Access Microbiol.* 2:acmi000108. doi: 10.1099/acmi.0.000108

Hiergeist, A., Ruelle, J., Emler, S., and Gessner, A. (2023). Reliability of species detection in 16S microbiome analysis: Comparison of five widely used pipelines and recommendations for a more standardized approach. *PLoS One* 18:e0280870.

Hryniewicz, W., and Holecki, M. (2015) Recommendations for diagnosis, therapy and prevention of urinary tract infections in adults. Publishing house financed from the funds at the disposal of the minister of health under the health program entitled: "National Program for the Protection of Antibiotics for 2011-2015", Warsaw.

Jach, M. E., and Sajnaga, E., (2017) Composition and function of the intestinal microbiome based on metagenomic studiem. Abstract-book-Metagenomy-2017.Pdf.

Janda, J. M., and Abbott, S. L. (2007). 16S rRNA gene sequencing for bacterial identification in the diagnostic laboratory: pluses, perils, and pitfalls. *J. Clin. Microbiol.* 45, 2761–2764. doi: 10.1128/JCM.01228-07

Johnson, J. S., Spakowicz, D. J., Hong, B.-Y., Petersen, L. M., Demkowicz, P., Chen, L., et al. (2019). Evaluation of 16S rRNA gene sequencing for species and strain-level microbiome analysis. *Nat. Commun.* 10:5029. doi: 10.1038/s41467-019-13036-1

Katoh, K., Misawa, K., Kuma, K. I., and Miyata, T. (2002). MAFFT: A novel method for rapid multiple sequence alignment based on fast fourier transform. *Nucleic Acids Res.* 30, 3059–3066. doi: 10.1093/nar/gkf436

Kim, G. H. (2019). Pharmacologic treatment of chronic hyperkalemia in patients with chronic kidney disease. *Electrolyte Blood Press.* 17, 1–6. doi: 10.5049/EBP.2019.17.1.1

Koga, S., Yamanaga, S., Hidaka, Y., Tanaka, K., Kaba, A., Toyoda, M., et al. (2022). Influence of graft ureter length, a donor-related factor, on urinary tract infections after living-donor kidney transplantation: a single-center analysis of 211 cases. *Transpl. Int.* 35:10754. doi: 10.3389/ti.2022.10754

Kramer, H., Kuffel, G., Thomas-White, K., Wolfe, A. J., Vellanki, K., Leehey, D. J., et al. (2018). Diversity of the midstream urine microbiome in adults with chronic kidney disease. *Int. Urol. Nephrol.* 50, 1123–1130. doi: 10.1007/s11255-018-1860-7

Lewis, D. A., Brown, R., Williams, J., White, P., Jacobson, S. K., Marchesi, J. R., et al. (2013). The human urinary microbiome; bacterial DNA in voided urine of asymptomatic adults. *Front. Cell. Infect. Microbiol.* 3:41. doi: 10.3389/fcimb.2013.00041

Ling, Z., Liu, F., Shao, L., Cheng, Y., and Li, L. (2017). Dysbiosis of the urinary microbiota associated with urine levels of proinflammatory chemokine interleukin-8 in female type 2 diabetic patients. *Front. Immunol.* 8:1032. doi: 10.3389/fimmu.2017.01032

Liu, P.-Y., Wu, W.-K., Chen, C.-C., Panyod, S., Sheen, L. Y., and Wu, M. S. (2020) Evaluation of compatibility of 16S rRNA V3V4 and V4 amplicon libraries for clinical microbiome profiling. *bioRxiv*. [Epub ahead of preprint]. doi: 10.1101/2020.08.18.256818

Magistro, G., and Stief, C. G. (2019). The urinary tract microbiome: the answer to all our open questions? *Eur. Urol. Focus* 5, 36–38. doi: 10.1016/j.euf.2018.06.011

McDonald, D., Price, M., Goodrich, J., Nawrocki, E. P., DeSantis, T. Z., Probst, A., et al. (2012). An improved Greengenes taxonomy with explicit ranks for ecological and evolutionary analyses of bacteria and archaea. *ISME J.* 6, 610–618. doi: 10.1038/ismej.2011.139

Michno, M., Sydor, A., Wałaszek, M., and Sułowicz, W. (2018). Microbiology and drug resistance of pathogens in patients hospitalized at the nephrology department in the South of Poland. *Pol. J. Microbiol.* 67, 517–524. doi: 10.21307/pjm-2018-061

Modena, B. D., Milam, R., Harrison, F., Cheeseman, J. A., Abecassis, M. M., Friedewald, J. J., et al. (2017). Changes in urinary microbiome populations correlate in kidney transplants with interstitial fibrosis and tubular atrophy documented in early surveillance biopsies. *Am. J. Transplant.* 17, 712–723. doi: 10.1111/ajt.14038

Murphy, E. C., and Frick, I. M. (2013). Gram-positive anaerobic cocci – commensals and opportunistic pathogens. *FEMS Microbiol. Rev.* 37, 520–553. doi: 10.1111/1574-6976.12005

Naber, K. G., Schaeffer, A. J., Hynes, C. F., Matsumoto, T., Shoskes, D. A., and Bjerklund Johansen, T. E.. (2010) *EAU/International Consultation on Urological Infections*. European Association of Urology. Arnhem.

Naumnik, B., and Myśliwiec, M. (2013). Dialysis: heparin-free haemodialysis-use and outcomes. *Nat. Rev. Nephrol.* 9, 381–382. doi: 10.1038/nrneph.2013.106

Olenski, S., Scuderi, C., Choo, A., Bhagat Singh, A. K., Way, M., and Jeyaseelan, L., et.al. (2019) Urinary tract infections in renal transplant recipients at a quaternary care Centre in Australia. *BMC Nephrol.*, 20,:479. doi: 10.1186/s12882-019-1666-6

Paul, B., Dixit, G., Murali, T. S., and Satyamoorthy, K. (2019). Genome-based taxonomic classification. *Genome* 62, 45–52. doi: 10.1139/gen-2018-0072

Pearce, M. M., Hilt, E. E., Rosenfeld, A. B., Zilliox, M. J., Thomas-White, K., Fok, C., et al. (2014). The female urinary microbiome: a comparison of women with and without urgency urinary incontinence. *MBio* 5, e01283–e01214. doi: 10.1128/mBio.01283-14

Peker, N., Garcia-Croes, S., Dijkhuizen, B., Wiersma, H. H., van Zanten, E., Wisselink, G., et al. (2019). A comparison of three different bioinformatics analyses of the 16S-23S rRNA encoding region for bacterial identification. *Front. Microbiol.* 10:620. doi: 10.3389/fmicb.2019.00620

Perez-Carrasco, V., Soriano-Lerma, A., Soriano, M., Gutiérrez-Fernández, J., and Garcia-Salcedo, J. A. (2021). Urinary microbiome: Yin and Yang of the urinary tract. *Front. Cell. Infect. Microbiol.* 11:617002. doi: 10.3389/fcimb.2021.617002

Pesce, F., Martino, M., Fiorentino, M., Rollo, T., Simone, S., Gallo, P., et al. (2019). Recurrent urinary tract infections in kidney transplant recipients during the first-year influence long-term graft function: a single-center retrospective cohort study. *J. Nephrol.* 32, 661–668. doi: 10.1007/s40620-019-00591-5

Petti, C. A. (2007). Detection and identification of microorganisms by gene amplification and sequencing. *Clin. Infect. Dis.* 44, 1108–1114. doi: 10.1086/512818

Price, T. K., Hilt, E. E., Dune, T. J., Mueller, E. R., Wolfe, A. J., and Brubaker, L. (2018). Urine trouble: should we think differently about UTI? *Int. Urogynecol. J. Pelvic Floor Dysfunct.* 29, 205–210. doi: 10.1007/s00192-017-3528-8

Qiu, Z., Zheng, K., Zhang, H., Feng, J., Wang, L., and Zhou, H. (2017). Physical exercise and patients with chronic renal failure: a meta-analysis. *Biomed. Res. Int.* 2017, 1–8. doi: 10.1155/2017/7191826

Rani, A., Ranjan, R., McGee, H. S., Andropolis, K. E., Panchal, D. V., Hajjiri, Z., et al. (2017). Urinary microbiome of kidney transplant patients reveals dysbiosis with potential for antibiotic resistance. *Transl. Res.* 181, 59–70. doi: 10.1016/j.trsl.2016.08.008

Ryan, M. P., and Adley, C. C. (2010). *Sphingomonas paucimobilis*: a persistent gram-negative nosocomial infectious organism. *J. Hosp. Infect.* 75, 153–157. doi: 10.1016/j.jhin.2010.03.007

Sabat, A. J., van Zanten, E., Akkerboom, V., Wisselink, G., van Slochteren, K., de Boer, R. F., et al. (2017). Targeted next-generation sequencing of the 16S-23S rRNA region for culture-independent bacterial identification – increased discrimination of closely related species. *Sci. Rep.* 7:3434. doi: 10.1038/s41598-017-03458-6

Sabé, N., Maristany, M., Tuells, M., Favà, A., Melilli, E., Tubau, F., et al. (2022). Risk factors and outcomes of acute graft pyelonephritis with bacteremia due to multidrug-resistant gram-negative Bacilli among kidney transplant recipients. *J. Clin. Med.* 11:3165. doi: 10.3390/jcm11113165

Song, Y., and Finegold, S. M. (2007). "Peptostreptococus, Finegoldia, Anaerococcus, Peptoniphilus, Veillonella, and other anaerobic cocci" in *Manual of clinical microbiology*. eds. P. R. Murray, E. J. Baron, J. H. Jorgensen, M. L. Landry and M. A. Pfaller. *9th* ed (Washington, DC: ASM Press), 862–871.

Tenke, P., Kovacs, B., Bjerklund Johansen, T. E., Matsumoto, T., Tambyah, P. A., and Naber, K. G. (2008). European and Asian guidelines on management and prevention of catheter-associated urinary tract infections. *Int. J. Antimicrob. Agents* 31, 68–78. doi: 10.1016/j.ijantimicag.2007.07.033

Thomas-White, K., Forster, S. C., Kumar, N., van Kuiken, M., Putonti, C., Stares, M. D., et al. (2018). Culturing of female bladder bacteria reveals an interconnected urogenital microbiota. *Nat. Commun.* 9:1557. doi: 10.1038/s41467-018-03968-5

Tungland, B. (2018). *Microbiota of the male urogenital tract. Human microbiota in health and disease. From pathogenesis to therapy. Chapter 14 Microbiota and the urogenital tract, pathogenesis, and therapies in human microbiota in health and disease, 14.2.1*, 605–647.

Vetrovsky, T., and Baldrian, P. (2013). The variability of the 16S rRNA gene in bacterial genomes and its consequences for bacterial community analyses. *PLoS One* 8:e57923. doi: 10.1371/journal.pone.0057923

Whiteside, S. A., Razvi, H., Dave, S., Reid, G., and Burton, J. P. (2015). The microbiome of the urinary tract–a role beyond infection. *Nat. Rev. Urol.* 12, 81–90. doi: 10.1038/nrurol.2014.361

Willner, D., Low, S., Steen, J. A., George, N., Nimmo, G. R., Schembri, M. A., et al. (2014). Single clinical isolates from acute uncomplicated urinary tract infections are representative of dominant in situ populations. *MBio* 5, e01064–e01013. doi: 10.1128/mBio.01064-13

Winand, R., Bogaerts, B., Hoffman, S., Lefevre, L., Delvoye, M., Braekel, J. V., et al. (2020). Targeting the 16S rRNA gene for bacterial identification in complex mixed samples: comparative evaluation of second (Illumina) and third (Oxford Nanopore technologies) generation sequencing technologies. *Int. J. Mol. Sci.* 21:298. doi: 10.3390/ijms21010298

Włodarczyk, E., and Felcenloben, J. (2017–2018) in cooperation with Department of the European Social Fund. Program for early detection of chronic kidney disease for residents of the Łódź Voivodeship. Available at: https://rpo.lodzkie.pl/images/2016/354-poddzialanie-x32/Zalacznik_12_Program.doc

Wolfe, A. J., and Brubaker, L. (2015). "Sterile urine" and the presence of Bacteria. *Eur. Urol.* 68, 173–174. doi: 10.1016/j.eururo.2015.02.041

Wolfe, A. J., and Brubaker, L. (2019). Urobiome updates: advances in urinary microbiome research. *Nat. Clin. Pract. Urol.* 16, 73–74. doi: 10.1038/s41585-018-0127-5

Wolfe, A. J., Toh, E., Shibata, N., Rong, R., Kenton, K., FitzGerald, M. P., et al. (2012). Evidence of uncultivated bacteria in the adult female bladder. *J. Clin. Microbiol.* 50, 1376–1383. doi: 10.1128/JCM.05852-11

Wu, J. F., Muthusamy, A., al-Ghalith, G. A., Knights, D., Guo, B., Wu, B., et al. (2018). Urinary microbiome associated with chronic allograft dysfunction in kidney transplant recipients. *Clin. Transpl.* 32:e13436. doi: 10.1111/ctr.13436

Yu, H., Meng, H., Zhou, F., Ni, X., Shen, S., and das, U. N. (2015). Urinary microbiota in patients with prostate cancer and benign prostatic hyperplasia. *Arch. Med. Sci.* 2, 385–394. doi: 10.5114/aoms.2015.50970

Zhao, E., Zhang, W., Geng, B., You, B., Wang, W., and Li, X. (2020). Intestinal dysbacteriosis leads to kidney stone disease. *Mol. Med. Rep.* 23:180. doi: 10.3892/mmr.2020.11819

frontiers | Frontiers in Microbiology

TYPE Original Research
PUBLISHED 14 June 2023
DOI 10.3389/fmicb.2023.1185216

OPEN ACCESS

EDITED BY
Wafa Achour,
Centre National de Greffe de Moelle Osseuse, Tunisia

REVIEWED BY
Marcos Fabio DosSantos,
Federal University of Rio de Janeiro, Brazil
Jozsef Soki,
University of Szeged, Hungary

*CORRESPONDENCE
Ning Sun
✉ steamsn@163.com
Xiaojun Li
✉ zxsyk_9@163.com

RECEIVED 13 March 2023
ACCEPTED 30 May 2023
PUBLISHED 14 June 2023

CITATION
Sun N, Chen Y, Zhang J, Cao J, Huang H, Wang J, Guo W and Li X (2023) Identification and characterization of pancreatic infections in severe and critical acute pancreatitis patients using *16S rRNA* gene next generation sequencing.
Front. Microbiol. 14:1185216.
doi: 10.3389/fmicb.2023.1185216

Identification and characterization of pancreatic infections in severe and critical acute pancreatitis patients using *16S rRNA* gene next generation sequencing

Ning Sun[1]*, Yong Chen[1], Jiaxun Zhang[1], Jin Cao[1], Hongjuan Huang[1], Jie Wang[2], Wentao Guo[3] and Xiaojun Li[1]*

[1]Department of Clinical Laboratory Science, Jinling Hospital, Affiliated Hospital of Medical School, Nanjing University, Nanjing, China, [2]Clinical Medicine Research Center, The Affiliated Suqian First People's Hospital of Nanjing Medical University, Suqian, China, [3]Department of Microbiology and Immunology, College of Basic Medicine, Guangdong Medical University, Dongguan, China

Objectives: This study aimed to identify the bacterial composition in the pancreatic fluid of severe and critical acute pancreatitis (SAP and CAP) patients.

Methods: A total of 78 pancreatic fluid samples were collected from 56 SAP and CAP patients and analyze using aerobic culture and *16S rRNA* gene next-generation sequencing. The clinical data of the patients were obtained from the electronic medical records.

Results: Among the total 78 samples, *16S rRNA* gene NGS identified a total of 660 bacterial taxa, belonging to 216 species in 123 genera. The dominant aerobic bacteria included *Klebsiella pneumoniae*, *Acinetobacter baumannii*, and *Enterococcus faecium*, while the dominant anaerobic bacteria included *Bacteroides*, *Dialister invisus*, and *Olsenella uli*. As compared to aerobic culturing, 95.96% (95/99) of the aerobic cultured bacteria were detected using the *16S rRNA* gene NGS.

Conclusion: The pancreatic infections in SAP and CAP patients might originate not only from the gut but also from the oral cavity and airways as well as related environments. Dynamic analysis of bacterial profile and abundance showed that some bacteria with low abundance might become the main pathogenic bacteria. There were no significant differences in the bacterial diversity between SAP and CAP.

KEYWORDS

***16S rRNA* NGS, severe acute pancreatitis, critical acute pancreatitis, infected pancreatic necrosis, bacterial profile**

1. Introduction

Acute pancreatitis (AP) is a common disease with various clinical emergency courses (Fritz et al., 2010; Dellinger et al., 2012; Banks et al., 2013). Most of the AP cases are mild and self-limited within a week. However, 15% of the cases are exacerbated to a higher level of severity known as severe or critical AP (SAP or CAP), which is associated with local complications and/or organ failure (Dellinger et al., 2012; Banks et al., 2013). Numerous studies confirmed that organ failure and infected pancreatic necrosis (IPN) were the determinants of mortality in AP patients (Dellinger et al., 2012; Banks et al., 2013). Organ failure emerges in the early and/or late phase of AP and can be assessed using a modified Marshall scoring system. Peripancreatic infections and IPN are rare during the first week (Banks et al., 2013). However, IPNs, especially multidrug-resistant microbial infections, are associated

with adverse clinical outcomes and increased mortality (Ning et al., 2019; Jiang et al., 2020). Depending on the presence and absence of organ failure and local complications, the severity of AP is classified into 4 categories based on determinants, including mild, moderate, severe, and critical AP (Dellinger et al., 2012). SAP is characterized by the presence of either IPN or persistent organ failure, while CAP is defined by the presence of both IPN and persistent organ failure. Sometimes, there is also a combination of SAP and CAP (Banks et al., 2013). Secondary infection in pancreatic necrosis can cause the development of sepsis associated with fatal outcomes, and statistical analysis indicated that the patients with IPN had a significantly higher risk of death as compared to those with no IPN (Fritz et al., 2010; Petrov et al., 2010). In summary, IPN is strongly associated with the prognosis of SAP and CAP.

Generally, bacterial translocation is considered the main infection mechanism of IPN (Fritz et al., 2010). During the early phase, pancreatic inflammation can activate cytokine cascades, resulting in systemic inflammatory response syndrome and subsequently altering intestinal permeability and motility, which leads to bacterial translocation (Liang et al., 2021). Animal studies have shown that gut microbiota can cross the mucosal barrier, reaching the pancreas or other organs in different sites (Fritz et al., 2010). In clinical microbiological laboratories, pathogenic bacteria are identified and classified using culturing. A large number of bacterial species were isolated from the pancreatic drainage fluid of SAP patients using culture (Brook and Frazier, 1996; Fan et al., 2020), among which, the predominant species included *Escherichia coli*, *Klebsiella pneumoniae*, *Pseudomonas aeruginosa, Acinetobacter baumannii*, *Bacteroides* spp., *Clostridium* spp., etc. Over the past two decades, *16S rRNA* gene sequencing technology has been used for the identification and classification of bacterial species in many infection-associated diseases (Li et al., 2017, 2018; Rogers et al., 2017; Philips et al., 2019) and microbiota-associated pancreatic diseases (Li et al., 2017; Rogers et al., 2017). The characteristic of bacteremia in AP patients could be defined and analyzed using polymerase chain reaction (PCR) (de Madaria, 2005; Bhutta and Ashley, 2013) or denaturing gradient gel electrophoresis (DGGE) (Li et al., 2013). The blood and neutrophil-associated microbiota (Li et al., 2018) as well as the gut microbiota associated with the progression of SAP (Philips et al., 2019) can be determined and analyzed using *16S rRNA* gene next-generation sequencing (NGS). However, the studies on SAP-and CAP-related gut microbiota, especially those on pancreas-associated infections, are limited. Moreover, the correlation of microbial diversity in the pancreas with the severity of AP also remains unclear. Furthermore, *16S rRNA* gene NGS has high sensitivity and specificity in identifying the composition of the microbiota, especially the anaerobic, low-abundant, fastidious, and/or slow-growing microbiota, thereby effectively implementing intervention measures to achieve better clinical outcomes (Dyrhovden et al., 2019, 2020; Stebner et al., 2021).

This study aimed to identify the composition of microbiota in the infected pancreatic fluids obtained from SAP and CAP patients using *16S rRNA* gene NGS and further analyzed their source. The results were further evaluated by comparing them to those obtained from aerobic cultures.

2. Materials and methods

2.1. Patients and clinical specimens

In this study, 56 patients, who were admitted to the general surgery department of Jinling Hospital in Nanjing, Jiangsu Province, China, from June 2020 to May 2021 and diagnosed with SAP or CAP based on the presence of organ failure and/or local determinants, were enrolled. A total of 78 pancreatic fluid samples were collected from percutaneous catheter drainage or puncture using a 10 mL tube, immediately transported to the microbiological laboratory for the detection and identification of bacteria, and then stored at −80°C. From these patients, one pancreatic fluid sample was collected from each of 41 patients, 2 samples were collected from each of 10 patients, 3 samples were collected from each of 3 patients, and 4 were collected from each of 2 patients. The demographic and clinical characteristics of all the patients were collected from the electronic medical records of the hospital and summarized.

2.2. Routine culture

A drop of pancreatic fluid was taken for smear microscopy. A 50 μL sample from each pancreatic fluid sample was then inoculated onto the plates of blood agar, chocolate agar, and MacConkey agar (Thermo Fisher Scientific Inc., Shanghai, China), respectively. The plates were incubated at 35°C in a 5% CO_2 atmosphere and observed after 72 h. Several colonies were selected by observation through the naked eye. Gram staining was performed based on the standard operation protocol of our laboratory, and biochemical identification was performed using VITEK® 2 COMPACT (bioMérieux, Marcy-l'Étoile, France). Anaerobic culturing was not performed because the samples from surgery or drainage did not guarantee an anaerobic environment.

2.3. Sample processing and DNA extraction

A 500-μl pancreatic fluid sample was centrifuged at 14,000 g for 10 min, and the supernatant was removed. Then, two 3 mm nickel beads were added to each sample tube and shaken at 3,000 rpm for 5 min. Finally, DNA was extracted using the Qiagen DNA mini kit (Qiagen, Shanghai, China) following the manufacturer's instructions, eluted with 100 μL distilled water, and stored at −80°C.

2.4. Library preparation and sequencing

The V3–V4 region of the *16S rRNA* gene was amplified using universal primers (341F, 5′-CCTAYGGGRBGCASCAG-3′ and 806R, 5′-GGACTACNNGGGTATCTAAT-3′), obtaining a product with approximately 470 bp length. PCR was performed with Phusion® High-Fidelity PCR Master Mix (New England Biolabs, Ipswich, Massachusetts, United States) reagent using a thermal cycler (Axygen MaxyGene II, Axygen Scientific, Union City, United States). The reaction mixture contained 0.2 μM of each primer, 1× Phusion Master Mix, and 10 ng DNA template. The PCR reaction conditions were as follows: initial denaturation at 98°C for 1 min; 30 cycles of denaturation at 98°C for 10 s, annealing at 50°C for 30 s, and extension at 70°C for 5 min; and final extension at 70°C for 5 min.

The PCR products were analyzed using agarose gel electrophoresis and purified using GeneJET NGS Cleanup Kit (Thermo Fisher Scientific Inc., Shanghai, China). Library preparation was performed using the TruSeq® DNA PCR-Free Sample Preparation Kit (Illumina, Redwood City, CA, United States) following the manufacturer's

instructions. The library preparation was assessed using Qubit@ 2.0 Fluorometer (Thermo Fisher Scientific Inc., United States) and Agilent Bioanalyzer 2100 system (Agilent Technologies Inc., Santa Clara, CA, United States). Finally, the pooled libraries were diluted and sequenced using the NovaSeq platform, and 2 × 250 paired-end raw sequence reads were obtained. Following the processing of each clinical sample, the sterile deionized water as a negative control was processed in parallel.

2.5. Data analysis

The quality of sequence reads was assessed using Fastp (version 0.23.2) (Chen et al., 2018), and the low-quality reads were removed. Using VSEARCH (v2.18.0) (Rognes et al., 2016), the paired sequence reads were merged after trimming the primers, and the fragments shorter than 250 bp were filtered out. Operational taxonomic unit (OTU) clustering was performed using VSEARCH with a 100% similarity. The sequences were annotated using the Basic Local Alignment Search Tool (BLAST, version 2.12.0+) against the National Center for Biotechnology Information (NCBI) *16S rRNA* database (https://ftp.ncbi.nlm.nih.gov/blast/db/16S_ribosomal_RNA.tar.gz, updated at 2022-01-08) (Camacho et al., 2009). Furthermore, each detection described as pathogens in the previous study or considered to be clinically relevant by the clinician were considered to be clinically reporting pathogens. Importantly, the detections considered to be contaminants, colonizers, and commensals were excluded.

2.6. Statistical analysis

All the data were expressed as the mean and standard deviation of the mean or as median and range between brackets as applicable. All the statistical analyses were performed using the R package (version 4.0.2) and the vegan package (version 2.5-7). The significance level was set at p-value <0.05. Alpha diversity was analyzed using Shannon's diversity index to describe the diversity of bacterial species in each sample. Shannon's diversity indices of SAP and CAP were compared using Welch's t-test. Bray–Curtis distance algorithm with an unweighted pair-group method and arithmetic means was used for the hierarchical clustering analysis of bacterial diversity in the SAP and CAP patients. Principle coordinate analysis (PCoA) was performed on the Bray-Curtis distance to analyze the differences in the bacterial compositions under various factors, such as local complications, organ failure, etc. The analysis of similarities (ANOSIM) test was used to compare the differences in bacterial composition between the patients with SAP and CAP.

3. Results

3.1. Clinical characteristics of patients

As listed in Table 1, a total of 56 patients, including 39 males and 17 females, with a mean age of 42 were enrolled in this study. Except for 2 recovering patients with SAP, all the other SAP and CAP patients were transferred from lower-level hospitals to Jinling Hospital. Based on the AP severity, the patients were divided into SAP ($n = 26$) and CAP ($n = 30$) patients. The results of statistical analysis showed that age and gender had no significant effect on the grouping. The mean durations of intensive care unit (ICU) stay were 26 days for SAP patients and 46 days for CAP patients. The CAP patients had significantly longer ICU stays than the SAP patients ($p < 0.05$). Most pancreatic fluid samples were obtained within 1–2 days after admission to the hospital (Figure 1). The etiology of AP was categorized as alcoholic, biliary, hyperlipidemia, endoscopic retrograde cholangiopancreatography (ECRP), and unknown cause. Finally, 48 patients significantly improved and were transferred to the general ward.

3.2. Workflow of *16S rRNA* gene NGS

Of the total 78 pancreatic fluid samples obtained from the patients, 56 samples including 52 aerobic culture-positive and 4 aerobic culture-negative samples, had PCR products of expected length and were sequenced. Sequencing was abandoned for 19 aerobic culture-negative samples because the PCR products of the expected length were not obtained. Three samples with no PCR products, as

TABLE 1 Demographic and clinical characteristics of all the patients.

Number of patients	56
Mean age (SD; min–max), year	42 (13; 13–68)
Gender, male	39 (69.64%)
Smoking	10 (17.86%)
History of alcoholism	17 (30.36%)
ICU stays (SD; min–max), days	37.79 (32; 2–197)
Improvement	48 (85.71%)
Severity	
Severe	26 (42.31%)
Critical	30 (57.69%)
CRP (SD; min–max)	112.37 (70.97; 0.45–385)
PCT (SD; min–max)	2.93 (6.62; 0.029–46.53)
Etiology	
Alcoholic	2 (3.57%)
Biliary	22 (39.29%)
ERCP	1 (1.79%)
Hyperlipidemia	25 (44.64%)
Unknown cause	6 (10.71%)
Local complications	
Acute necrotic collection	8 (14.29%)
Infected pancreatic necrosis	47 (83.93%)
Walled-off necrosis	1 (1.79%)
Systematic complications	
ARDS	37 (66.07%)
AKI	21 (37.5%)
Shock	7 (12.5%)
Sepsis	9 (16.07%)
Liver damage	4 (7.14%)

CRP, C-reaction protein; PCT, procalcitonin; ERCP, endoscopic retrograde cholangiopancreatography; ARDS, acute respiratory distress syndrome; AKI, acute kidney injury.

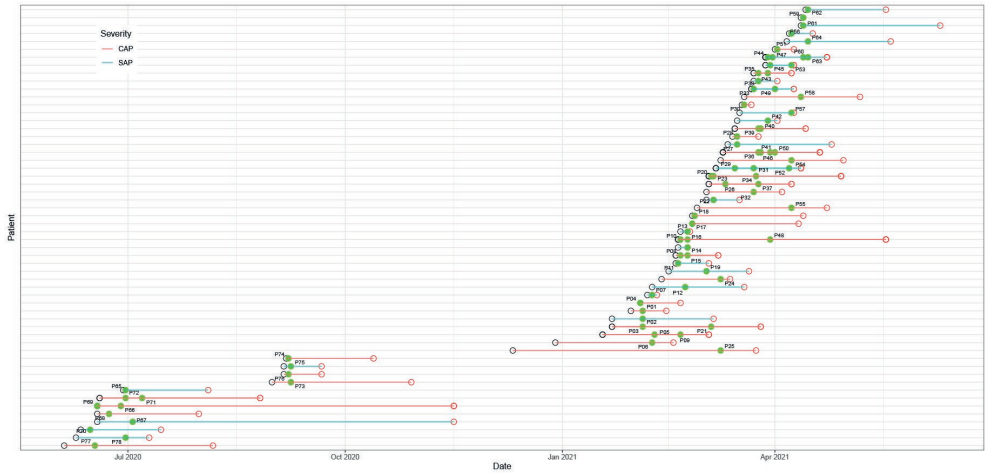

FIGURE 1
Hospitalization schedule, including hospital admission (black hollow circle), discharge (red hollow circle), and sampling (green dot). The green and red lines represent severe acute pancreatitis (SAP) and critical acute pancreatitis (CAP), respectively.

well as the sterile deionized water, were used as negative controls. The number of mean raw reads was 199,252. After quality control using Fastp, a total of 198,383 reads were reserved. For the two negative controls, the mean raw reads were 6,877, among which, 6,864 were left after quality control. Using VSEARCH, a total of 492,528 OTUs clusters with 100% similarity were obtained. The clusters were aligned against the NCBI *16S rRNA* database using BLAST with a threshold of 97% similarity. The results showed that a total of 381,718 OTUs were annotated. In the negative controls, *Romeboutsia timonensis* (84 reads) and *Akermansia muciniphila* (64 reads) had the highest number of reads. Therefore, a cut-off value of 100 reads was set, and the species emerged in negative controls as background contaminants were removed. The isolation sources of identified species were analyzed using BacDive[1] (Reimer et al., 2019), and a reference strain was selected when there were multiple strains in the database.

3.3. Composition of bacterial species identified using culturing and *16S rRNA* gene NGS

Twenty-six of the total 78 samples were aerobic culture-negative, while 99 aerobic cultures were isolated from the remaining 52 samples, which belonged to 17 species in 11 genera (Figure 2A and Supplementary Table S1). Among these species, *K. pneumoniae* complex was identified in 48.08% (25/52) of the samples. The *16S rRNA* gene NGS detected a total of 660 bacteria in 56 samples (52 aerobic culture-positive and 4 aerobic culture-negative samples; Figures 2B,C and Supplementary Table S1), which belonged to 218 species in 123 genera, including 91 aerobic species in 75 genera and 127 anaerobic species in 48 genera. Among the aerobic bacterial species, *K. pneumoniae* complex (46/56), *Acinetobacter baumannii* (37/56), *Enterococcus faecium* (35/56), *Pseudomonas aeruginosa* (34/56), *Escherichia coli* (24/56), and *Stenotrophomonas maltophilia* (20/56) were the predominant species. Among the anaerobic bacterial species, *B. fragilis* (16/56), *B. kribbi* (8/56), *B. ovatus* (7/56), *Dialister invisus* (7/56), and *Olsenella uli* (7/56) were the predominant species. Additionally, polymicrobial infections were found in 54 samples (98.21%), and only four samples had a mono-bacterial infection of *Enterococcus faecium* (sample P18, 189 reads, 51.78%), *A. baumannii* (sample P68, 120,432 reads, 99.99%), *K. pneumoniae* complex (sample P73, 13,298 reads, 99.97%), or *K. pneumoniae* complex (sample P74, 38,037 reads, 99.99%). Using the prokaryotic meta-database BacDive (see footnote 1), the isolation sources of pancreatic bacterial infections were identified as intestines (aerobes 43%; anaerobes 43%) and oral cavity and airways (aerobes 17%; anaerobes 24%; Figure 3).

16S rRNA gene NGS identified 96 bacterial species, which were also identified by aerobic culturing (Supplementary Table S1). *Stenotrophomonas maltophilia* (sample P17, 10 reads), *Pseudomonas aeruginosa* (sample P25, 81 reads), and *Escherichia coli* (sample P62, undetermined) had less than 100 reads and were considered undetermined. Among the 56 samples, *16S rRNA* gene NGS identified 660 bacterial strains, including 450 aerobic and 256 anaerobic bacterial species, while aerobic culturing identified 21.33% (96/450, excluding 3 strains, which were undetermined or had less than 100 reads).

3.4. Dynamic changes in bacterial infection in patients with SAP or CAP

Among 56 patients, multiple pancreatic fluid samples were collected from 15 patients with an average sampling interval of 7.4 days. The dynamic changes in the bacterial profile and abundance in pancreatic infection were analyzed using the *16S rRNA* gene NGS (Figure 4). When the sampling interval was less

1 https://bacdive.dsmz.de/

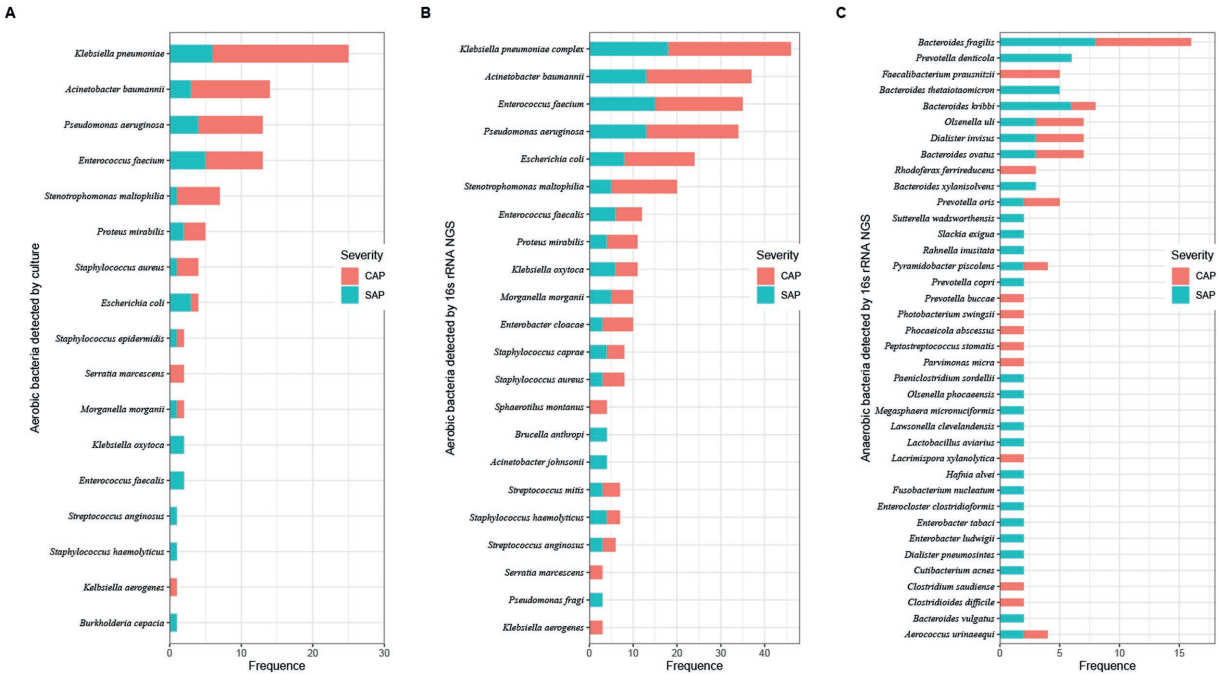

FIGURE 2
Number of bacterial taxa in pancreatic fluids identified using aerobic culturing and *16S rRNA* gene NGS. Bacterial species were identified using aerobic culturing **(A)** and using the *16S rRNA* gene NGS (aerobes: **B**; anaerobes: **C**). Colors represent the severity of AP (red, CAP; light blue, SAP).

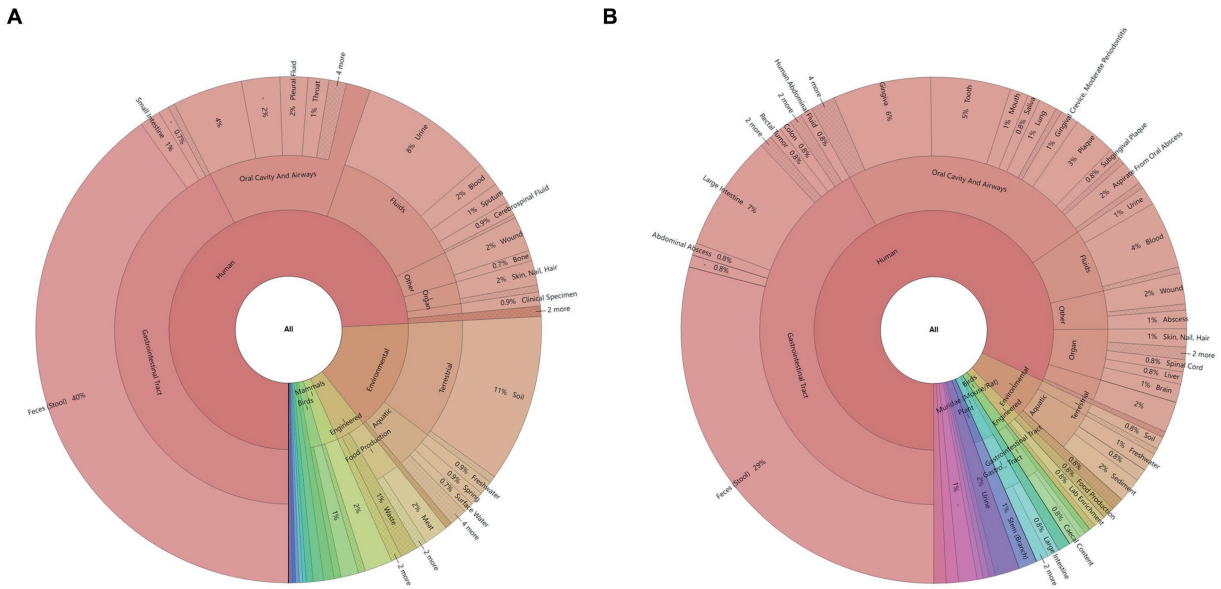

FIGURE 3
Identification of bacterial sources in the pancreatic fluid samples using the BacDive database: **(A)** aerobes and **(B)** anaerobes. The isolation sources of bacteria identified using the *16S rRNA* gene NGS were queried using the prokaryotic meta-database BacDive (see footnote 1). The reference strain was selected when multiple strains were present in the database.

than 2 weeks, the composition of bacterial species did not change much at the pancreatic site. On the other hand, when the sampling interval was more than 2 weeks later, the bacterial species in the pancreatic fluid changed greatly, which was consistent with the results of the aerobic culture. Importantly, bacteria with low abundance were often ignored in the early stage due to the limitation of culture and could become the main pathogen in the later stage (Figures 4B,H).

3.5. Comparative analysis of bacterial composition based on AP severity

The alpha diversity analysis of 56 pancreatic fluid samples (Figure 5) using Shannon's diversity index showed that the alpha diversity did not change significantly with the increase in the duration of ICU stay (Figure 5A). Welch's *t*-test also showed that there was no significant difference between SAP and CAP ($p = 0.05036$, Figure 5B). Furthermore, there was no significant difference in Shannon's diversity indices between the CAP patients who did not achieve significant treatment effects and those who achieved significant improvement. The hierarchical clustering of these samples using an unweighted pair-group method with arithmetic means (UPGMA) indicated that these samples had a similar bacterial composition (Figure 6A). PCoA was performed based on the distance matrix of Bray–Curtis dissimilarity. As shown in Figure 6B, there was no clear divergence trend in beta diversities of SAP and CAP, while considering other factors, such as etiology, prognosis, etc. The result of ANOSIM also showed no significant difference between the two groups ($R = 0.03005$, $p > 0.05$). In addition, the relative abundances of common species, such as *A. baumannii*, *Pseudomonas aeruginosa*, *K. pneumoniae* complex, and *S. maltophila*, were much higher in CAP patients than those in the SAP patients, which were mostly multidrug-resistant nosocomial bacterial species.

4. Discussion

Culture is a routine detection method for the identification of microbial species in clinical microbiological laboratories. However, it must be ensured that the microorganisms are culturable and can grow on solid or liquid media *in-vitro*. Furthermore, most clinical microbiology laboratories cannot perform anaerobic culturing due to the limitation of an oxygen-free environment, and the cultures are identified using subjective and random morphological identification methods for polymicrobial infection. As a novel method, *16S rRNA* gene NGS has great advantages as compared to culture, especially for the identification of anaerobic, low-abundant, fastidious, and/or slow-growing microorganisms. Infection is one of the risk factors, contributing to the high mortality of AP (Petrov et al., 2010; Bhutta and Ashley, 2013). The detection and identification of bacterial composition are of great significance to implement requisite interventions for AP (Mourad et al., 2017; Ning et al., 2019). This study used *16S rRNA* gene NGS to identify the bacterial composition in 78 pancreatic fluid samples in comparison to culturing. In the 52 samples, aerobic culturing identified 99 bacterial specimens, among which, *16S rRNA* gene NGS identified 96 bacterial specimens. Three patients had positive aerobic cultures with discordant *16S rRNA* gene sequencing results. This might be due to the low abundance of positive aerobic cultures and presence of more abundant bacteria in the samples, which might have interfered with the amplification and sequencing of the *16S rRNA* gene (Fida et al., 2021).

OTUs were clustered using VSEARCH and aligned with the NCBI *16S rRNA* database using BLAST in this study. Almost all the *P. aeruginosa* species were lost in clustering with 97% similarity as a threshold. A high clustering threshold might be necessary for the detection and identification of pathogenic bacteria using *16S rRNA* gene NGS, especially when multiple infections are suspected, which is different from microbiome analysis (Ikegami et al., 2021). Therefore, 100% similarity was set as a threshold. There are often DNA contaminations in the *16S rRNA* gene NGS. Dyrhovden et al. (2019, 2020, 2021) proposed a criterion for setting the threshold with the most abundant pollutant species in negative controls. Sterilized deionized water and culture-negative pancreatic fluid sample with no PCR products, was used as negative controls, and the bacterial composition was determined using the *16S rRNA* gene NGS. The number of reads with the highest abundance in negative controls was set as the threshold. In the two negative controls, *Romeboutsia*

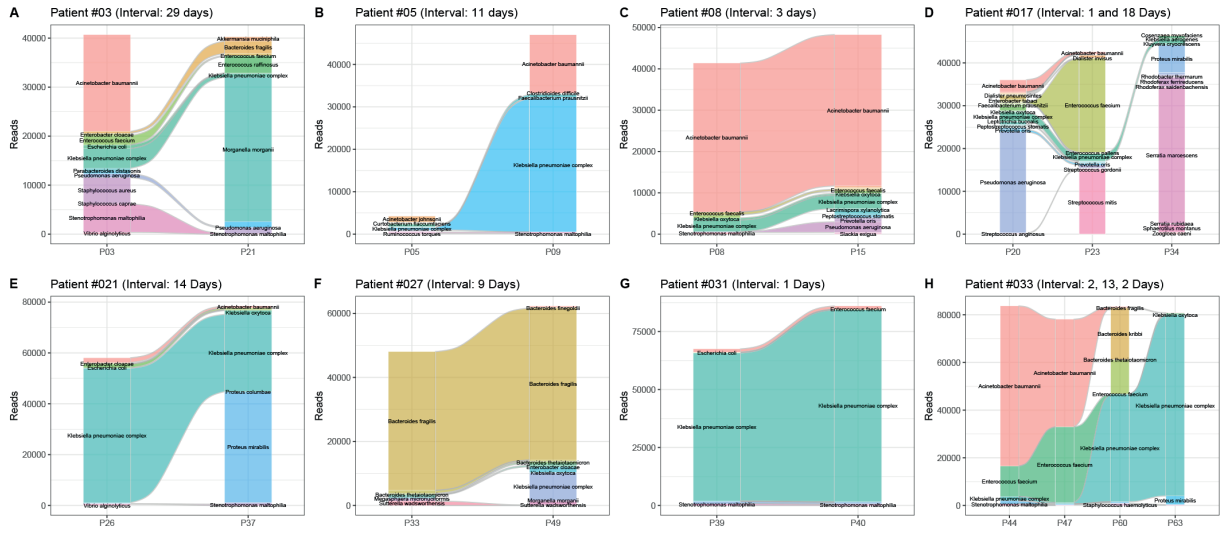

FIGURE 4
Dynamic changes in the bacterial profile and abundance in 8 patients with pancreatitis. Patient numbers and sampling intervals are marked. **(A)** Patient #03, sampling interval 29days; **(B)** patient #05, sampling interval 11days; **(C)** patient #08, sampling interval 3days; **(D)** patient #017, sampling interval 1 and 18days; **(E)** patient #21, sampling interval 14days; **(F)** patient #027, sampling interval 9days; **(G)** patient #031, two sampling interval 1day each; **(H)** patient #033, sampling intervals 2, 13, and 2days.

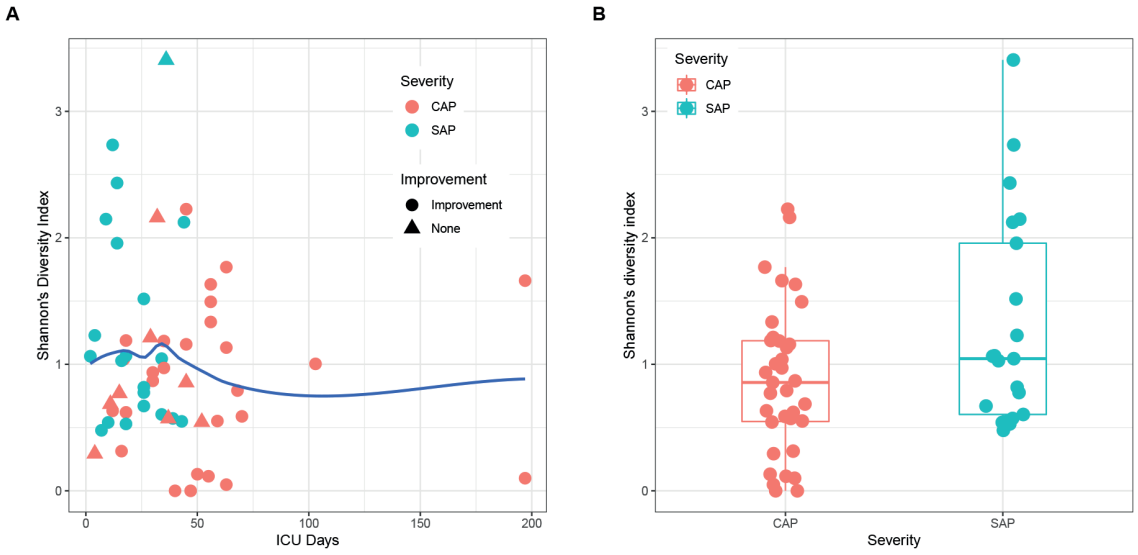

FIGURE 5
(A) Effects of ICU stay duration and improvement of patients on Shannon's diversity indices. The local regression fitting line was plotted using ggplot2 (blue line), and the dots represent the improvement of patients. **(B)** Comparison of beta diversity between SAP (light blue) and CAP (red).

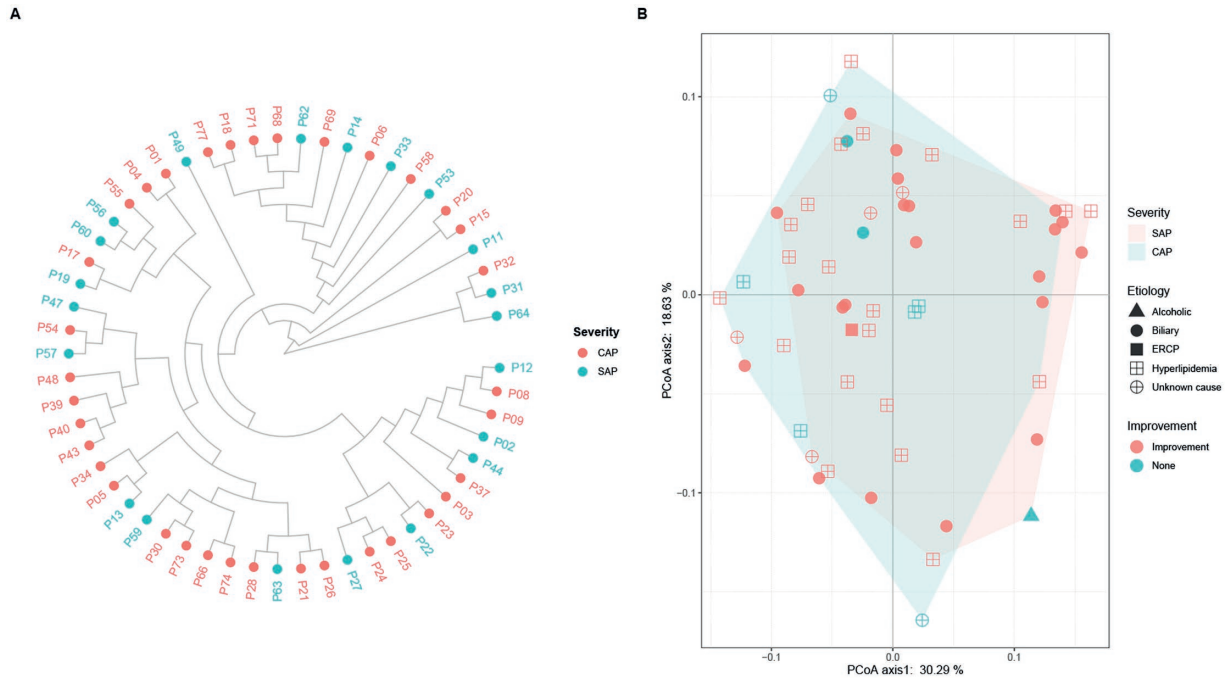

FIGURE 6
(A) Hierarchical clustering and **(B)** principal coordinate analysis (PCoA) of pancreatic fluid samples obtained from the SAP and CAP patients based on Bray–Curtis dissimilarity. **(A)** Each dot represents one pancreatic fluid sample (red, CAP; light blue, SAP). There is no clear clustering into separate groups in the comparative analysis of AP severity. **(B)** Each dot represents one sample, and the characteristics of each patient including etiology (alcoholic, biliary, ECRP, hyperlipidemia, and unknown cause) and outcome (improvement, and none) are shown. There is a large overlapping between the light red area representing SAP and the light blue area representing CAP.

timonensis and *Akermansia muciniphila* with 84 and 64 reads were detected, respectively. Therefore, 100 reads were set as the threshold, which was slightly more than the reads of the most abundant species in negative controls. However, this might have led to ignoring some low-abundance species, such as *S. maltophilia* (10 reads) in sample P17 and *P. aeruginosa* (81 reads) in sample P25.

Bacterial translocation is an important mechanism of AP infection. A previous study showed that the predominant aerobic bacteria included *E. coli*, *K. pneumoniae*, *streptococcus* group D, and *S. aureus*, while the predominant anaerobic bacteria included *Peptostreptococcus* species, *B. fragilis* group organisms, *Clostridium* species, *Prevotella* species, *Veillonella* species, and *Fusobacterium*

species (Brook and Frazier, 1996). In the current study, the results showed that the predominant aerobic bacteria were *K. pneumoniae* complex, *A. baumannii*, *E. faecium*, *P. aeruginosa*, and *E. coli*, while the predominant anaerobic bacteria were *B. fragilis*, *B. kribbi*, *B. ovatus*, *D. invisus*, and *O. uli*. The main pathogens responsible for CAP and SAP have changed somewhat as compared to those reported in previous studies. This might be related to the severity or antibiotic use in the last two decades. Approximately 42% of aerobic bacteria and 43% of anaerobic bacteria might be derived from the gut, which was different from the bacterial communities present in blood-related infections (de Madaria, 2005; Li et al., 2013, 2018). Moreover, the current study also indicated that the source of a considerable proportion of bacteria was oral and airway microbiota as well as from the environment, which was similar to the results of the pancreas-related microbial communities (Li et al., 2017). This might due to the collection of samples from the SAP and CAP patients, who were affected by long-term hospitalization, such as antibiotics, surgery, etc., and were immunocompromised, resulting in infections from various sources. Disinfection of the hospital environment and oral cleaning are necessary to prevent bacteria entering the pancreas through the gastrointestinal tract or surgical incisions from oral and environmental sources. The changes in bacterial profile and abundance in pancreatic samples were dynamically analyzed using the *16S rRNA* gene NGS. The results showed that the abundance of different bacteria varied greatly, and some low-abundance species were easily overlooked. The colonized or commensal bacteria usually do not exist in the pancreas. Some bacteria originating from the gut, respiratory tract, or environment, might appear in the pancreas and are not necessarily considered pathogenic (Blauwkamp et al., 2019; Miller et al., 2019; Fida et al., 2021; Gu et al., 2021). It is necessary to make a comprehensive and available diagnosis by combining the NGS results, clinical signs of patients, and other laboratory tests.

There were certain limitations to this study. First, all the patients were referred from other hospitals, and their previous treatment courses were unknown, while the anaerobic culturing was also not performed. Second, since all the specimens in this study came from one hospital, a larger-scale multi-center study is needed to explore the sources of all infections in order to clearly determine the type of bacterial infection in AP patients. Finally, there might be some errors in the isolation sources of bacteria; for example, although *E. coli* is generally believed to be originated from the intestine, it also appears in urinary tract infections.

In conclusion, in this study, a total of 78 pancreatic fluid samples were collected from 56 SAP and CAP patients, and the compositions of their bacterial profiles were determined using *the 16S rRNA* gene NGS. The results showed that the predominant aerobic bacteria were *K. pneumoniae*, *A. baumannii*, *E. faecium*, *P. aeruginosa*, *E. coli*, etc., while the predominant anaerobic bacteria were *B. fragilis*, *B. kribbi*, *B. ovatus*, *D. invisus*, and *O. uli*, etc. As compared to aerobic culturing, *16S rRNA* gene NGS might detect more bacteria; however, contamination and data analysis might limit its results. *16S rRNA* gene NGS can be used as an effective supplement to culturing.

Data availability statement

The datasets presented in this study can be found in online repositories. The names of the repository/repositories and accession number(s) can be found at: https://www.cncb.ac.cn/, PRJCA015500.

Ethics statement

The studies involving human participants were reviewed and approved by 2016NZGKJ-049. Written informed consent to participate in this study was provided by the participants' legal guardian/next of kin.

Author contributions

NS and XL: study design. YC, JZ, JC, and NS: data analysis. XL and NS: funding acquisition. YC, HH, and JC: resources. NS, YC, WG, and JW: experimental studies. XL: supervision. NS: writing-original draft. All authors contributed to the article and approved the submitted version.

Funding

This study was funded by the Suqian Sci&Tech Program (SY202214), National Natural Science Foundation of China (no. 81601857), and the Health Technology Development Special Foundation of Nanjing City (no. YKK18216).

Conflict of interest

The authors declare that the research was conducted in the absence of any commercial or financial relationships that could be construed as a potential conflict of interest.

Publisher's note

Supplementary material

The Supplementary material for this article can be found online at: https://www.frontiersin.org/articles/10.3389/fmicb.2023.1185216/full#supplementary-material

References

Banks, P. A., Bollen, T. L., Dervenis, C., Gooszen, H. G., Johnson, C. D., Sarr, M. G., et al. (2013). Classification of acute pancreatitis—2012: revision of the Atlanta classification and definitions by international consensus. *Gut* 62, 102–111. doi: 10.1136/gutjnl-2012-302779

Bhutta, H. Y., and Ashley, S. W. (2013). Demonstrating infection in severe acute pancreatitis: a role for polymerase chain reaction and gene sequencing?*. *Crit. Care Med.* 41, 2048–2049. doi: 10.1097/CCM.0b013e31829133aa

Blauwkamp, T. A., Thair, S., Rosen, M. J., Blair, L., Lindner, M. S., Vilfan, I. D., et al. (2019). Analytical and clinical validation of a microbial cell-free DNA sequencing test for infectious disease. *Nat. Microbiol.* 4, 663–674. doi: 10.1038/s41564-018-0349-6

Brook, I., and Frazier, E. H. (1996). Microbiological analysis of pancreatic abscess. *Clin. Infect. Dis.* 22, 384–385. doi: 10.1093/clinids/22.2.385

Camacho, C., Coulouris, G., Avagyan, V., Ma, N., Papadopoulos, J., Bealer, K., et al. (2009). BLAST+: architecture and applications. *BMC Bioinformatics* 10:421. doi: 10.1186/1471-2105-10-421

Chen, S., Zhou, Y., Chen, Y., and Gu, J. (2018). fastp: an ultra-fast all-in-one FASTQ preprocessor. *Bioinformatics* 34, i884–i890. doi: 10.1093/bioinformatics/bty560

de Madaria, E. (2005). Detection and identification of bacterial DNA in serum from patients with acute pancreatitis. *Gut* 54, 1293–1297. doi: 10.1136/gut.2004.047514

Dellinger, E. P., Forsmark, C. E., Layer, P., Lévy, P., Maraví-Poma, E., Petrov, M. S., et al. (2012). Determinant-based classification of acute pancreatitis severity: an international multidisciplinary consultation. *Ann. Surg.* 256, 875–880. doi: 10.1097/SLA.0b013e318256f778

Dyrhovden, R., Nygaard, R. M., Patel, R., Ulvestad, E., and Kommedal, Ø. (2019). The bacterial aetiology of pleural empyema. A descriptive and comparative metagenomic study. *Clin. Microbiol. Infect.* 25, 981–986. doi: 10.1016/j.cmi.2018.11.030

Dyrhovden, R., Øvrebø, K. K., Nordahl, M. V., Nygaard, R. M., Ulvestad, E., and Kommedal, Ø. (2020). Bacteria and fungi in acute cholecystitis. A prospective study comparing next generation sequencing to culture. *J. Infect.* 80, 16–23. doi: 10.1016/j.jinf.2019.09.015

Dyrhovden, R., Rippin, M., Øvrebø, K. K., Nygaard, R. M., Ulvestad, E., and Kommedal, Ø. (2021). Managing contamination and diverse bacterial loads in *16S rRNA* deep sequencing of clinical samples: implications of the law of small numbers. *mBio* 12, e00598–e00521. doi: 10.1128/mBio.00598-21

Fan, N., Hu, Y., Shen, H., Liu, S., Zhao, G., Sun, L., et al. (2020). Compositional and drug-resistance profiling of pathogens in patients with severe acute pancreatitis: a retrospective study. *BMC Gastroenterol.* 20:405. doi: 10.1186/s12876-020-01563-x

Fida, M., Wolf, M. J., Hamdi, A., Vijayvargiya, P., Esquer Garrigos, Z., Khalil, S., et al. (2021). Detection of pathogenic bacteria from septic patients using 16S ribosomal RNA gene-targeted metagenomic sequencing. *Clin. Infect. Dis.* 73, 1165–1172. doi: 10.1093/cid/ciab349

Fritz, S., Hackert, T., Hartwig, W., Rossmanith, F., Strobel, O., Schneider, L., et al. (2010). Bacterial translocation and infected pancreatic necrosis in acute necrotizing pancreatitis derives from small bowel rather than from colon. *Am. J. Surg.* 200, 111–117. doi: 10.1016/j.amjsurg.2009.08.019

Gu, W., Deng, X., Lee, M., Sucu, Y. D., Arevalo, S., Stryke, D., et al. (2021). Rapid pathogen detection by metagenomic next-generation sequencing of infected body fluids. *Nat. Med.* 27, 115–124. doi: 10.1038/s41591-020-1105-z

Ikegami, H., Noguchi, S., Fukuda, K., Akata, K., Yamasaki, K., Kawanami, T., et al. (2021). Refinement of microbiota analysis of specimens from patients with respiratory infections using next-generation sequencing. *Sci. Rep.* 11:19534. doi: 10.1038/s41598-021-98985-8

Jiang, X., Shi, J.-Y., Wang, X.-Y., Hu, Y., and Cui, Y.-F. (2020). The impacts of infectious complications on outcomes in acute pancreatitis: a retrospective study. *Mil Med Res* 7:38. doi: 10.1186/s40779-020-00265-5

Li, S., Fuhler, G. M., Bn, N., Jose, T., Bruno, M. J., Peppelenbosch, M. P., et al. (2017). Pancreatic cyst fluid harbors a unique microbiome. *Microbiome* 5:147. doi: 10.1186/s40168-017-0363-6

Li, Q., Wang, C., Tang, C., He, Q., Li, N., and Li, J. (2013). Bacteremia in patients with acute pancreatitis as revealed by 16S ribosomal RNA gene-based techniques*. *Crit. Care Med.* 41, 1938–1950. doi: 10.1097/CCM.0b013e31828a3dba

Li, Q., Wang, C., Tang, C., Zhao, X., He, Q., and Li, J. (2018). Identification and characterization of blood and neutrophil-associated microbiomes in patients with severe acute pancreatitis using next-generation sequencing. *Front. Cell. Infect. Microbiol.* 8:5. doi: 10.3389/fcimb.2018.00005

Liang, X.-Y., Jia, T.-X., and Zhang, M. (2021). Intestinal bacterial overgrowth in the early stage of severe acute pancreatitis is associated with acute respiratory distress syndrome. *World J Gastroenterol* 27, 1643–1654. doi: 10.3748/wjg.v27.i15.1643

Miller, S., Naccache, S. N., Samayoa, E., Messacar, K., Arevalo, S., Federman, S., et al. (2019). Laboratory validation of a clinical metagenomic sequencing assay for pathogen detection in cerebrospinal fluid. *Genome Res.* 29, 831–842. doi: 10.1101/gr.238170.118

Mourad, M., Evans, R., Kalidindi, V., Navaratnam, R., Dvorkin, L., and Bramhall, S. (2017). Prophylactic antibiotics in acute pancreatitis: endless debate. *Ann R Coll Surg Engl* 99, 107–112. doi: 10.1308/rcsann.2016.0355

Ning, C., Huang, G., Shen, D., Bonsu, A. A. F. K., Ji, L., Lin, C., et al. (2019). Adverse clinical outcomes associated with multidrug-resistant organisms in patients with infected pancreatic necrosis. *Pancreatology* 19, 935–940. doi: 10.1016/j.pan.2019.09.008

Petrov, M. S., Shanbhag, S., Chakraborty, M., Phillips, A. R. J., and Windsor, J. A. (2010). Organ failure and infection of pancreatic necrosis as determinants of mortality in patients with acute pancreatitis. *Gastroenterology* 139, 813–820. doi: 10.1053/j.gastro.2010.06.010

Philips, C. A., Phadke, N., Ganesan, K., Rajesh, S., Padsalgi, G., Ahamed, R., et al. (2019). Gut microbiota in alcoholic hepatitis is disparate from those in acute alcoholic pancreatitis and biliary disease. *J. Clin. Exp. Hepatol.* 9, 690–698. doi: 10.1016/j.jceh.2019.04.001

Reimer, L. C., Vetcininova, A., Carbasse, J. S., Söhngen, C., Gleim, D., Ebeling, C., et al. (2019). Bac dive in 2019: bacterial phenotypic data for high-throughput biodiversity analysis. *Nucleic Acids Res.* 47, D631–D636. doi: 10.1093/nar/gky879

Rogers, M. B., Aveson, V., Firek, B., Yeh, A., Brooks, B., Brower-Sinning, R., et al. (2017). Disturbances of the perioperative microbiome across multiple body sites in patients undergoing pancreaticoduodenectomy. *Pancreas* 46, 260–267. doi: 10.1097/MPA.0000000000000726

Rognes, T., Flouri, T., Nichols, B., Quince, C., and Mahé, F. (2016). VSEARCH: a versatile open source tool for metagenomics. *PeerJ* 4:e2584. doi: 10.7717/peerj.2584

Stebner, A., Ensser, A., Geißdörfer, W., Bozhkov, Y., and Lang, R. (2021). Molecular diagnosis of polymicrobial brain abscesses with 16S-rDNA-based next-generation sequencing. *Clin. Microbiol. Infect.* 27, 76–82. doi: 10.1016/j.cmi.2020.03.028

frontiers | Frontiers in Microbiology

TYPE Original Research
PUBLISHED 20 June 2023
DOI 10.3389/fmicb.2023.1215884

OPEN ACCESS

EDITED BY
Ons Bouchami,
Universidade NOVA de Lisboa, Portugal

REVIEWED BY
Samara Paula Mattiello,
University of Tennessee Southern, United States
Daniela Pinto,
Giuliani S.p.A., Italy

*CORRESPONDENCE
Yide Xie
✉ 13805058416@163.com
Zhihui Guo
✉ guokex@tom.com
Xiaosong Chen
✉ chenxiaosong74@163.com

†These authors have contributed equally to this work and share first authorship

RECEIVED 02 May 2023
ACCEPTED 01 June 2023
PUBLISHED 20 June 2023

CITATION
Li M, Li M, Dai Y, Li D, Yu H, Liu J, Gao H, Zhong Y, Huang M, Lin J, Xie Y, Guo Z and Chen X (2023) 16S rRNA gene sequencing reveals the correlation between the gut microbiota and the susceptibility to pathological scars.
Front. Microbiol. 14:1215884.
doi: 10.3389/fmicb.2023.1215884

16S rRNA gene sequencing reveals the correlation between the gut microbiota and the susceptibility to pathological scars

Ming Li[1,2,3†], Minghao Li[1,2,3†], Yingting Dai[1,2,3†], Dang Li[4], Han Yu[5], Jian Liu[6], Hangqi Gao[1,2,3], Yi Zhong[1,2,3], Mingquan Huang[1,2,3], Jing Lin[1,2,3], Yide Xie[1,2,3*], Zhihui Guo[1,2,3*] and Xiaosong Chen[1,2,3*]

[1]Department of Plastic Surgery and Regenerative Medicine, Fujian Medical University Union Hospital, Fuzhou, China, [2]Department of Plastic Surgery and Regenerative Medicine Institute, Fujian Medical University, Fuzhou, China, [3]Engineering Research Center of Tissue and Organ Regeneration, Fujian Province University, Fuzhou, China, [4]Nursing Department of Fujian Medical University Union Hospital, Fuzhou, China, [5]Department of Dermatology, Pingtan Comprehensive Experimental Area Hospital, Fuzhou, China, [6]Fuzhou MineButy Clinics, Fuzhou, China

The gut microbiome profile in patients with pathological scars remains rarely known, especially those patients who are susceptible to pathological scars. Previous studies demonstrated that gut microbial dysbiosis can promote the development of a series of diseases via the interaction between gut microbiota and host. The current study aimed to explore the gut microbiota of patients who are prone to suffer from pathological scars. 35 patients with pathological scars (PS group) and 40 patients with normal scars (NS group) were recruited for collection of fecal samples to sequence the 16S ribosomal RNA (16S rRNA) V3-V4 region of gut microbiota. Alpha diversity of gut microbiota showed a significant difference between NS group and PS group, and beta diversity indicated that the composition of gut microbiota in NS and PS participants was different, which implied that dysbiosis exhibits in patients who are susceptible to pathological scars. Based on phylum, genus, species levels, we demonstrated that the changing in some gut microbiota (*Firmicutes; Bacteroides; Escherichia coli*, etc.) may contribute to the occurrence or development of pathological scars. Moreover, the interaction network of gut microbiota in NS and PS group clearly revealed the different interaction model of each group. Our study has preliminary confirmed that dysbiosis exhibits in patients who are susceptible to pathological scars, and provide a new insight regarding the role of the gut microbiome in PS development and progression.

KEYWORDS

pathological scars, susceptibility, gut microbiota, 16S rRNA sequencing, dysbiosis

Introduction

Human body harbors trillions of microbial cells, which play a key role to our human life. Moreover, the highest density of these microbial cells are found in the intestinal compartment, and these microbial cells form a complex microbial community in the intestine known as gut microbiota (Lozupone et al., 2012). Numerous studies have indicated

that the gut microbiota communicate with multiple distant organs through a variety of signal transduction pathways, and they are closely related to many diseases in the human body, including Alzheimer's disease, hypertension, colon cancer (Li et al., 2017; Zheng et al., 2020; D'Argenio et al., 2022). In addition, it was reported that DNA originating from gut microbes has been found in the bloodstream of patients who are experiencing active psoriasis (Ramírez-Boscá et al., 2015). In recent years, a lot of studies have raised a concept of the gut-skin axis aiming to discover the relationship between gut microbiota and skin (Salem et al., 2018; Fang et al., 2022; Mahmud et al., 2022), previous studies revealed that there may be a positive feedback loop between dysbiosis of intestinal microbiota related to *Faecalibacterium prausnitzii* and disruption of the epithelial barrier caused by uncontrolled inflammation in the epithelium (Song et al., 2016). It was found that oral administration of *Lactobacillus plantarum HY7714* prevented ultraviolet-induced photoaging in mice by inhibiting MMP-1 expression in dermal fibroblasts (Kim et al., 2014). Moreover, De Pessemier et al. (2021) found that the gut–skin axis links the gut microbiota to skin diseases via the metabolites, gut barrier and inflammatory mediators.

Skin wound healing, a complicated pathophysiological process, is generally divided into three stages including inflammation, proliferation and reshaping phases (Martin, 1997). The formation of scar is caused by excess extracellular matrix (ECM) deposition in the place of the normal dermal tissue in the process of skin repair (Jackson et al., 2012). Pathological scars, which mainly refer to keloid and hypertrophic scars, are dermal connective-tissue disorders after dermal injury caused by inflammatory response and speed healing, and it may affect patients both esthetically and psychosocially (Lau et al., 2009; Huang et al., 2014). In addition, the treatment of pathological scars presents a significant burden for patients and has always been bothering doctors for a long term, especially those patients with multiple pathological scars (Avram et al., 2009; Pai and Cummings, 2011; Jfri et al., 2015; Ogawa, 2022). Pathological scars can be influenced by numerous local, systemic, and genetic factors that affect their characteristics and quantity (Avram et al., 2009). Most prior studies are focusing on the local lesions rather than the systemic factors in regard to scars, especially those affected by gut microbiota. Therefore, in current study, we decided to found out the relationship between gut microbiota and pathological scars.

In this study, regarding the patients who are susceptible to pathological scars, we present a pioneer work to investigate the generalizable pathological scar-associated microbial signatures and examine the relationship between the pathological scars and gut microbiota by 16S rRNA gene sequencing technology. Hence, the community composition and distribution were characterized to provide an experimental basis for future studies aimed at improving the prevention and treatment of pathological scars.

Materials and methods

Participants

In the current study, 35 patients with pathological scars (≥3 lesions throughout the body) were recruited, and 40 patients with normal scars were distributed to the control group. Participants met the following criteria were enrolled: for pathological scar (PS) group: developing lesions in the past year; with pathological scar-related symptoms such as itching, pain, etc; scar recurrence after a series of therapy resection, such as resection, local radiotherapy, drug injection, etc; for normal scar (NS) group: scar formation within 2 years after injury or surgery. Subjects who met any of the following criteria were excluded: taking antibiotics/microecological preparation/immune modulators/hormonal drugs/traditional Chinese medicine in the past month; with endocrine system disease/Inflammatory bowel disease/frequent diarrhea; digestive system surgical procedures within 3 years; with hemodialysis/cleansing enema or oral taking bowel cleansing agent within 2 weeks. This study was approved by the Ethics Committee of the Fujian Medical University Union hospital (No. 2021KJCX020), and all participants provided written informed consent.

Collection of fecal samples and DNA extraction

In all participants, the fecal samples were collected into stool specimen collection tubes containing DNA stabilizer, immediately afterward, they were flash-frozen on dry ice and stored at a temperature of −80°C until analysis. The genomic DNA of microbes was extracted from fecal samples using the E.Z.N.A.® soil DNA Kit (Omega Bio-tek, Norcross, GA, U.S.) following the manufacturer's instructions. The quality and concentration of DNA were determined using 1.0% agarose gel electrophoresis and the NanoDrop® ND-2000 spectrophotometer (Thermo Scientific Inc., USA), then the DNA samples were stored at a temperature of −80°C for further use.

16S rRNA amplicon sequencing

V3-V4, the hypervariable region of the bacterial 16S rRNA gene, were amplified with primer pairs 338F (5′-ACTC CTACGGGAGGCAGCAG-3′) and 806R(5′-GGACTACHVGGGT WTCTAAT-3′) (Liu et al., 2016) using an ABI GeneAmp® 9700 PCR thermocycler (ABI, CA, USA). The PCR reaction mixture contained 4 μL 5 × Fast Pfu buffer, 2 μL 2.5 mM dNTPs, 0.8 μL forward primer (5 μM), 0.8 μL reverse primer (5 μM), 0.4 μL Fast Pfu polymerase, 0.2 μL BSA, 10 ng of template DNA, and ddH2O was added to reach a final volume of 20 μL. The PCR amplification protocol was as follows: initial denaturation at 95°C for 3 min, followed by 30 cycles of denaturing at 95°C for 30 s, annealing at 55°C for 30 s and extension at 72°C for 45 s, and single extension at 72°C for 10 min, and end at 10°C, and all samples underwent amplification in triplicate. For all samples, the PCR product was extracted from 2% agarose gel, and purified by the AxyPrep DNA Gel Extraction Kit (Axygen Biosciences, Union City, CA, USA), following the manufacturer's instructions. The purified product was quantified using the Quantus™ Fluorometer (Promega, USA). Subsequently, the purified amplicons were combined in equimolar amounts and subjected to paired-end sequencing using an Illumina NovaSeq

PE250 platform (Illumina, San Diego, USA), following the standard protocols provided by Majorbio Bio-Pharm Technology Co., Ltd. (Shanghai, China).

Microbiome analysis and statistical analysis

The initial demultiplexing of the raw FASTQ files was performed using a custom Perl script, followed by quality filtering using fastp version 0.19.6 (Chen et al., 2018), and subsequently merging using FLASH version 1.2.7 (Magoč and Salzberg, 2011). The sequences underwent filtration and clustering to form operational taxonomic units (OTUs) using UPARSE 7.1 at a 97% similarity threshold. The taxonomy of OTU was analyzed by QIIME (Version 1.9.1) against the 16S rRNA database (Silva V138), with a confidence threshold of 70%.

The α-diversity was measured with the Ace, Chao, Shannon, Simpson and Coverage indexes using Mothur software. To identify differences in abundance in the gut microbiota between patients with NS and PS, the β-diversity was estimated by computing the Bray-Curtis (ANOSIM). Data are analyzed by wilcoxon rank-sum test with Benjamini-Hochberg false discovery rate multiple test correction. In the analysis of seeking significantly changed taxa between two groups, data were analyzed by wilcoxon rank-sum test with Benjamini-Hochberg false discovery rate multiple test correction. In LEfSe analysis, $p < 0.05$ (Kruskal–Wallis test) and log10[LDA] ≥ 3.0 were considered to indicate a significant difference in gut microbiota. $P < 0.05$ was considered statistically significant.

Results

Characteristics of participants

Based on the inclusion and exclusion criteria, fecal samples were collected from 35 patients with pathological scars and 40 patients with normal scars. In addition, the fecal samples derived from patients with pathological scars were distributed to the PS group and derived from patients with normal scars are distributed to the NS group. As seen in Table 1, there were no significant differences in gender, age, systolic blood pressure and diastolic blood pressure among the PS and NS groups. Details of the participants are shown in Table 1.

TABLE 1 Characteristics of participants.

	NS (n = 40)	PS (n = 35)	P-value
Gender, male/female	17/23	14/21	0.826
Age, years	28.92 ± 10.31	29.51 ± 11.12	0.812
BMI, kg/m^2	21.75 ± 3.69	22.45 ± 3.07	0.378
Systolic blood pressure, mmHg	121.93 ± 8.78	119.20 ± 13.53	0.298
Diastolic blood pressure, mmHg	72.40 ± 6.69	71.31 ± 8.64	0.542
Blood glucose, mmol/L	4.67 ± 0.41	4.75 ± 0.56	0.508
Ca2+, mmol/L	2.33 ± 0.10	2.33 ± 0.12	0.987
Cholesterol, mmol/L	4.67 ± 0.89	4.44 ± 0.81	0.243
Dietary habits			
Meat (%)	13 (32.5)	11 (31.43)	0.921
Dessert (%)	11 (27.5)	12 (34.29)	0.618
Spicy food (%)	6 (15)	9 (25.71)	0.386

Data were compared using the χ^2 test, or student t-test. $P > 0.05$ means no statistically significant difference.

Alpha-diversity and beta-diversity analysis

Alpha-diversity and beta-diversity analysis had been performed to compare the similarities and differences in species diversity of the gut microbiota between the NS and PS groups. According to the α-diversity analysis, the Ace, Chao, Shannon and Simpson indexes indicated that PS group showed no significant difference of community diversity compared with the NS group (Figures 1A–D). However, Coverage index demonstrated that there was a significant difference between PS and NS group (Figure 1E).

The microbiota's overall diversity was evaluated using the PCoA analysis based on the Bray-Curtis distance, and the results of the ANOSIM test indicated a significant difference between the PS and NS groups ($R = 0.5801$, $p = 0.001$, Figure 1F). The sample clustering tree and histogram combination analysis diagram (Figure 1G) clearly revealed that those with comparable β-diversity were grouped together, and the samples from the PS and NS groups could be well-clustered into two groups indicating a different composition of gut microbiota in PS and NS participants. Therefore, these findings revealed that PS patients exhibit dysbiosis, an imbalance in their gut microbial composition.

Gut microbiome composition of PS and NS groups

In our study, Venn diagram showed that PS and NS groups shared 12 phyla, with 2 and 2 phyla unique to the NS group and PS group, respectively; shared 238 genera, with 20 and 58 genera unique to the NS group and PS group, respectively; shared 425 phyla, with 64 and 149 species unique to the NS group and PS group, respectively (Supplementary Figure 1).

Subsequently, as shown in Figure 2, we conducted bar plot and Circos analyses to illustrate the differences of the microbiota composition between PS and NS. The bar plot was used to roughly indicate the relative abundance of varied gut microbiota at phylum, genera and species levels (Figures 2A–C). At phylum level (Figure 2A), in the NS group, *Bacteroidota* was the most abundant phylum, followed by *Firmicutes, Proteobacteria and Fusobacteriota*, however, in the PS group, *Firmicutes* was the most abundant phylum, followed by *Proteobacteria, Bacteroidota, Actinobacteriota* and *Fusobacteriota*. The proportion of *Bacteroides* and *Faecalibacterium* was larger, while *Escherichia-Shigella*, *Blautia*, *Bifidobacterium* and *Subdoligranulum* were smaller in the NS group than the PS group at Genus level (Figure 2B). At species level

10.3389/fmicb.2023.1215884

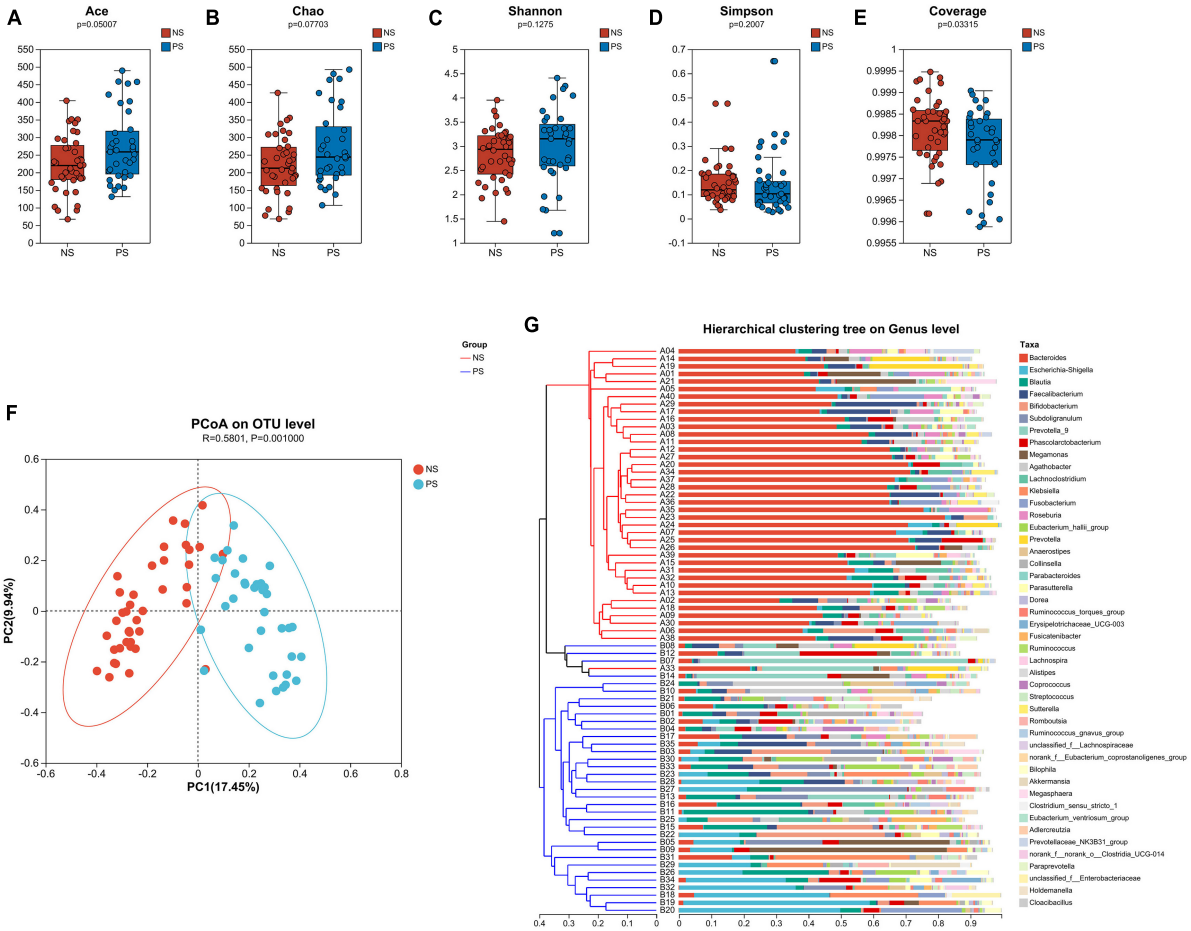

FIGURE 1
The α-diversity is analyzed by the **(A)** Ace, **(B)** Chao, **(C)** Shannon, **(D)** Simpson, **(E)** Coverage indexes. **(F)** The β-diversity is shown by principal coordinate analysis (PCoA) based on Bray–Curtis Dissimilarity index (ANOSIM, R = 0.5801, P = 0.0010). **(G)** A sample clustering tree and histogram structure analysis diagram at the genus level is shown. The hierarchical clustering analysis between samples based on community composition is on the left side and the right side indicate the histogram of a community composition of the samples.

(Figure 2C), NS patients were characterized by a higher relative abundance of *Bacteroides vulgatus* and a lower relative abundance of *Escherichia coli* compared with PS patients. The utilization of Circos analysis allowed for the depiction of the correlation in abundance of bacterial communities at the phylum (Figure 2D), genus (Figure 2E) and species (Figure 2F) levels between PS and NS, thereby corroborating the findings from the bar plot analysis.

Comparison of the relative abundance of gut microbiota between PS and NS groups

Those patients with PS displayed a relative difference of distinct gut microbiota, when compared with NS patients. The differentially abundant microbiota at the phylum, genus and species levels in PS versus NS were shown in Figure 3. At the phylum level (Figure 3A), PS showed a significant increase in *Firmicutes*, *Actinobacteriota*, *Synergistota*, *Patescibacteria* and *Cyanobacteria* but decrease in *Bacteroidota* compared with NS. At genus level (Figure 3B), the proportions of *Bacteroides* and *Parabacteroides* were significantly larger in NS, while *Escherichia-Shigella*, *Blautia*, *Bifidobacterium*, *Subdoligranulum*, *Prevotella*, *Klebsiella*, *Eubacterium hallii group*, *Anaerostipes*, *Collinsella*, *Dorea*, *Ruminococcus torques group*, *Erysipelotrichaceae UCG-003* and *Streptococcus* were significantly enriched in PS. At the species level (Figure 3C), NS showed a significant decrease in *Escherichia coli*, *unclassified Blautia*, *uncultured bacterium Subdoligranulum*, *unclassed Prevotella 9*, *Bifidobacterium pseudocatenulatum DSM 20438 = JCM 1200 = LMG 10505*, *Klebsiella variicola*, *unclassified Eubacterium hallii gourp*, *Anaerostipes hadrus*, *unclassified Ruminococcus torques group* and unclassified *Erysipelotrichaceae ucg-003*, while increase in *Bacteroides vulgatus*, *Bacteroides xylanisolvens*, *Bacteroides stercoris ATCC 43183*, *Bacteroides uniformis* and *uncultured organism Bacteroides*.

We conducted the LEfSe analysis to identify the biological taxonomic differences between PS and NS. We found 6, 31 and 43 differentially abundant taxa at the phylum level (Figure 4A), genus level (Figure 4B) and species level (Figure 4C), respectively. According to the LEfSe analysis, the PS group exhibited a predominance of *Firmicutes, Actinobacteriota*, and *Patescibacteria*, while presented a decrease in *Bacteroidota* at phylum level. At genus

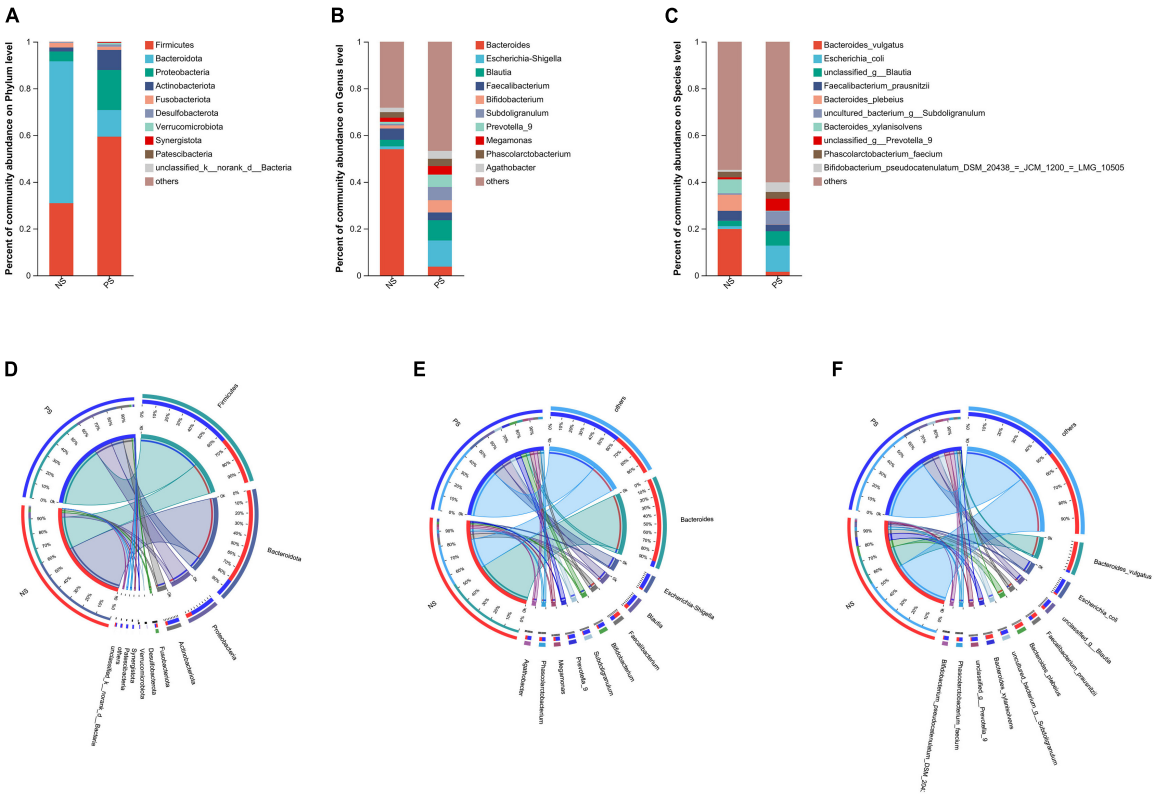

FIGURE 2
Relative abundance of microbial community at phylum, genus, species levels. **(A–C)** Bar plots show the average relative abundance of gut microbiota in NS, PS group. Circos analysis shows the corresponding abundance of fecal microbiota in NS, PS group at phylum **(D)**, genus **(E)**, species **(F)** levels.

level, the proportion of *Escherichia-Shigella*, *Blautia, Prevotella 9* were larger, but the proportion of *Bacteroides, Parabacteroides* and Lachnospiraceae UCG-004 were smaller. At species level, PS showed a significant increase in *Escherichia coli*, *uncultured bacterium Subdoligranulum* and *unclassified Prevotella 9*, but decrease in *Bacteroides vulgatus*, *Bacteroides xylanisolvens and Bacteroides stercoris ATCC 43183*. More details of the differences were shown in **Figure 4**.

Correlation network analysis

The gut microbiota forms an intricate network in which specific species are influenced not only by the host, but also by other bacteria present within the community. We performed a correlation network analysis to visualize the relationship between varied gut microbiota in PS and NS patients based on the top 50 relative abundance of OTUs. Among the 50 OTUs, 33 and 36 had associations with other OTUs in NS and PS respectively with an absolute coefficient value > 0.5, p-value < 0.05 (**Supplementary Figure 2**). Moreover, degree centrality (DC), closeness centrality (CC), and betweenness centrality (BC) centrality were performed to evaluate the taxa importance within the network (**Supplementary Table 1**).

Notably, the correlation network of NS group (**Figure 5A**) showed a simpler and similar microbial relationship, however, the PS group (**Figure 5B**) presented a substantially more complicated microbial network. These findings suggested that gut microbial dysbiosis might exist in PS patients, and implied that the interaction changing between gut microbiota might led to the occurrence of pathological scars. In addition, in the gut microbial community network of PS patients, *Firmicutes* had a higher prevalence while *Bacteroidota* had a lower prevalence. Whereas, in the group of NS, both *Bacteroidota* and *Firmicutes* played dominant role in the correlation structure of gut microbiota. These results indicated that *Bacteroidota* and *Firmicutes* might play a crucial role in maintaining scar-related gut ecosystem in patients.

Discussion

In recent years, there has been extensive research focused on the correlation between the human microbiome and various disorders. Currently, consistent evidence has demonstrated that the gut microbiota plays crucial roles in the development of skin diseases by interacting with the host system (Fang et al., 2021; Sinha et al., 2021; Moniaga et al., 2022). The current study focused on exploring the generalizable pathological scar-associated microbial signatures and determining the relationship between the gut microbiota and pathological scars using 16S rRNA gene sequencing technology with 35 PS patients and 40 NS patients' fecal samples.

Regarding PS group, we found a significant difference in microbiota alpha diversity compared with NS group, and then we performed microbial beta-diversity analysis to

10.3389/fmicb.2023.1215884

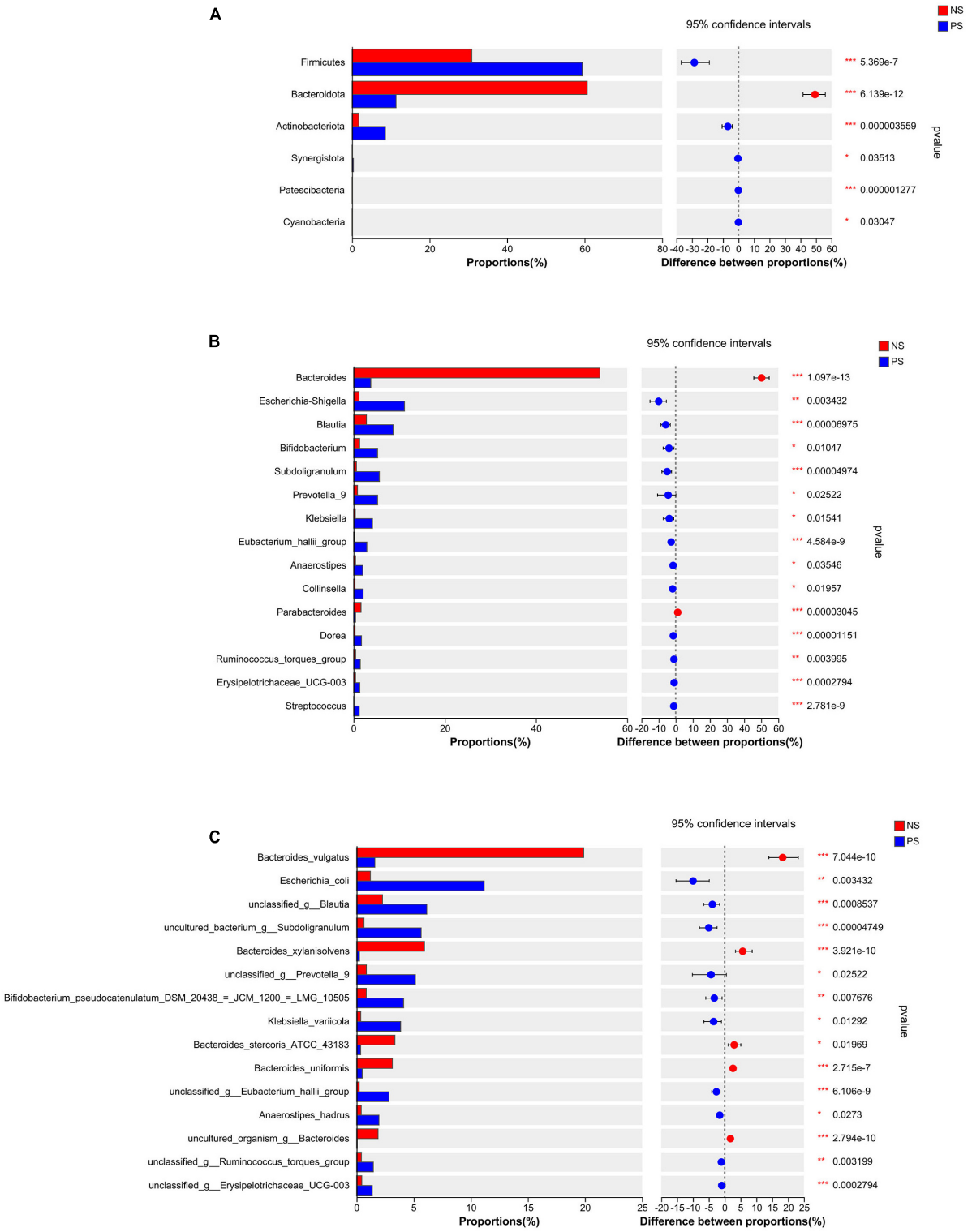

FIGURE 3
Comparison of the relative abundance of gut microbiota between NS and PS groups. Significantly changed taxa between two group at panel **(A)** phylum, **(B)** genus, **(C)** species levels. Data are analyzed by wilcoxon rank-sum test with Benjamini-Hochberg false discovery rate multiple test correction.

examine the similarity in the overall community structure between two groups, and beta-diversity revealed a significant difference in microbiota community structure between PS and NS patients. The sample clustering tree and histogram combination analysis diagram obviously demonstrated that the samples from the PS and NS groups could be well-clustered into two groups, which indicated that there was a different composition of gut microbiota in PS and NS participants.

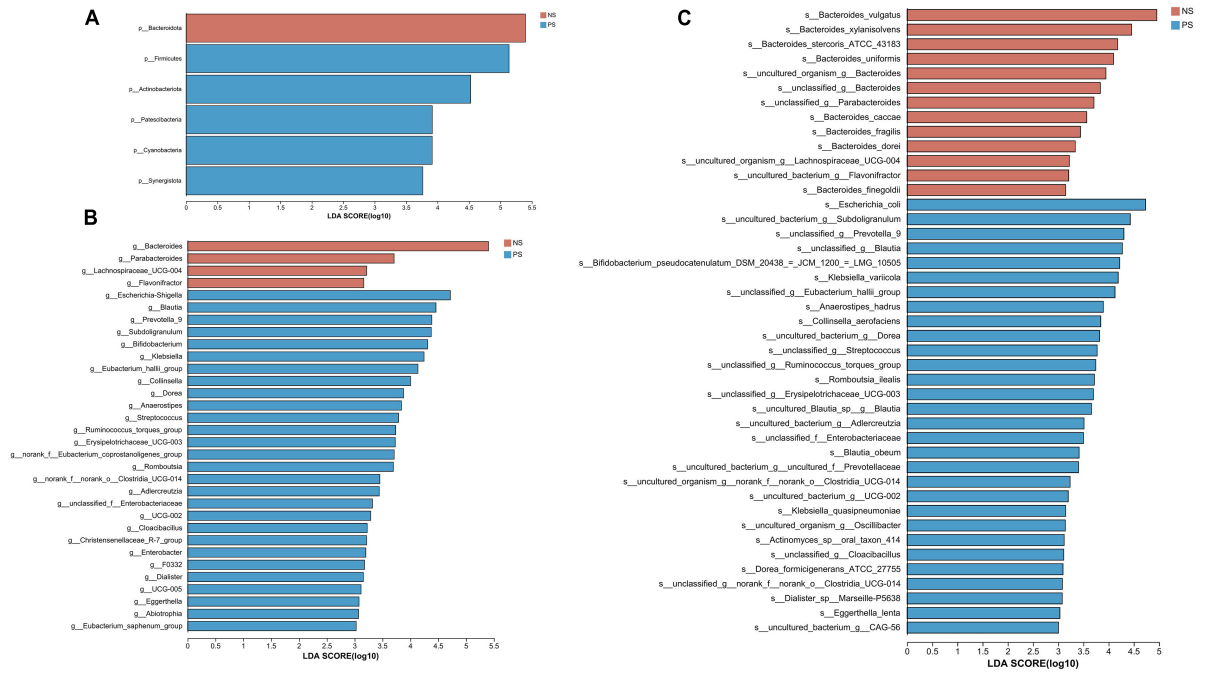

FIGURE 4
LDA diagram of LEfSe analysis at panel **(A)** phylum, **(B)** genus and **(C)** species levels. The red histogram represents NS group, and blue histogram represents PS group. The length of the histogram represents LDA score. $P < 0.05$ (Kruskal–Wallis test); log10[LDA] ≥ 3.0.

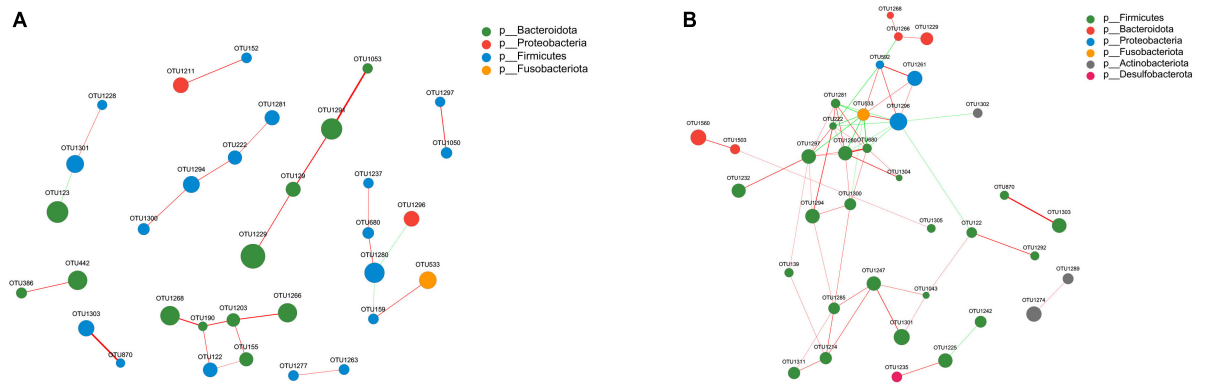

FIGURE 5
Correlation network analysis of the 50 most abundant OTUs for panel **(A)** NS and **(B)** PS. The networks display significant positive (red lines) and negative (green lines) correlations between operational taxonomic units (OTUs). The thickness of the lines represents the magnitude of the correlation coefficient, with thicker lines indicating a stronger correlation between OTUs. The size of the nodes represents the abundance of OTUs. OTUs are colored by phylum affiliation.

Moreover, these results implied that gut microbial dysbiosis exists in PS patients.

There are four primary phyla in the human gut microbiota, which are named as *Actinobacteria*, *Bacteroidetes, Firmicutes,* and *Proteobacteria* (Arumugam et al., 2011). We found that the relative abundance of *Firmicutes* was higher in PS participants compared with NS group based on our 16s rRNA gene sequencing. In previous study, it was pointed out that the abundance of *Firmicutes* was increased in old female mice compared with the young ones with higher systemic inflammation (Ma et al., 2020). According to the prior research, we found that *Firmicutes* is closely associated with inflammatory diseases. During the preclinical stage of arthritis, the intestinal microbiota is primarily dominated by *Firmicutes* (Rogier et al., 2017). Hypertrophic scars and keloids are two types of pathological scars that result from differences in the intensity and duration of inflammation present in a wound, therefore, among them, hypertrophic scars are caused by mild inflammation, while keloids are caused by severe inflammation (Berman et al., 2017). In addition, Huang et al. (2013) claimed that the systemic factors in pathological scar patients could directly influence the process of angiogenesis, local inflammation, fibrosis and pathological scars remodeling. According to the prior research, we found that *Firmicutes* is closely associated with inflammatory diseases. Hence, these results implied that *Firmicutes*

in human gut might play an important role in the occurrence of pathological scar via promoting systemic inflammatory response in the human.

At genus level, the proportion of *Bacteroides* was larger, while the ratio of *Escherichia-Shigella* was smaller in patients with NS. Previous study found that almost a quarter of the intestinal microbiota in humans is constituted by *Bacteroides*, making it a predominant genus (Ochoa-Repáraz et al., 2010). Due to their long-term existence in the host's intestinal niche and co-evolution with the host, they have established a stable mutually beneficial symbiotic relationship (Faith et al., 2013). Since *Bacteroides* is significant decreasing in patients with inflammatory bowel disease (IBD) when compared with healthy control, it is considered to have potential anti-inflammatory properties (Takahashi et al., 2016; Brown et al., 2019; Zhong et al., 2019). In the opposite, *Escherichia-Shigella* is characterized by proinflammatory properties, prior studies revealed that the reduction of blood pro-inflammatory mediators may associated with the decreasing of *Escherichia-Shigella* in gut (Chen et al., 2021; Pivari et al., 2022). *Escherichia-Shigella* showed a positive correlation with inflammatory diseases in the human gut, however, *Bacteroides* demonstrated negatively correlated with inflammatory diseases, these results indicated that the adjustment of the proportion of *Bacteroides* and *Escherichia-Shigella* in the human gut may reshape the structure of the gut microbiota and subsequently improve the patient's condition or prevent the occurrence or development of pathological scars.

On the changed species, we found that *Escherichia coli* significantly increased in PS group. An et al. (2021) demonstrated that the formation of CaOx stone in kidney can be facilitated by *Escherichia coli* through enhancing oxidative injury and inflammation. Moreover, it is found that *Escherichia coli* is responsible for the colorectal cancer susceptibility in patients by inducing inflammatory bowel disease (IBD) (Khan et al., 2017).

Franceschi et al. (2018) claimed that chronic and low-grade sterile inflammation throughout the body is an important pathogenic mechanism for various age-related diseases, including cardiovascular disease and metabolic diseases, they also demonstrate that gut microbiota plays a crucial role in both immunity and metabolism by constantly interacting with other organs and tissues throughout the body, resulting in significant effects. Pathological scars often occur after dermal injury and they are characterized by abnormal deposition of extracellular matrix and proliferation of fibroblasts (Lee et al., 2004; van der Veer et al., 2009; Huang and Ogawa, 2020). In clinical, a part of patients is prone to suffering from multiple pathological scars throughout the body for unknown reason. The delayed healing can be reversed through the use of exogenous estrogen treatment, applied either topically or systemically, via inflammation down-regulation inflammation (Ashcroft et al., 1997; Son et al., 2005). Moreover, xanthohumol and oxandrolone have been proven to accelerate wound healing by modulating the systemic inflammatory response (Costa et al., 2013; Ahmad et al., 2019). Therefore, the systemic inflammation caused by gut microbial dysbiosis may lead to the occurrence or development of pathological scars, it means that the microbiome directly or indirectly affects the balance of systemic inflammatory response in the human, and thus, perhaps, reshaping the proportion of microbiota in gut could improve the condition of patients who are susceptible to pathological scars.

Overall, based on the phylum, family, and genus levels, the current study found that the gut microbiota structure in patients who are susceptible to have pathological scars was different to that of patients with normal scars. Through their diverse biological effects, the varied gut microbiota played a crucial role on the occurrence and development of pathological scars by inducing systemic inflammation. Moreover, as shown in the correlation network, the interaction model between varied gut microbiota in patients with PS was greatly different to that of patients with normal scars.

Conclusion

We provide a valuable and complete dataset, it will be helpful for the future studies which are aiming at exploring the relationship between gut microbiota and susceptibility to pathological scars. Our findings help clarify the proportion of gut microbiota in patients with PS and NS. In conclusion, our study has preliminary confirmed that dysbiosis exhibits in patients who are susceptible to pathological scars, and provide a new insight regarding the role of the gut microbiome in PS development and progression.

Data availability statement

The datasets presented in the study are deposited in NCBI, accession number PRJNA980648.

Ethics statement

The studies involving human participants were reviewed and approved by the Ethics Committee of the Fujian Medical University Union Hospital. Written informed consent to participate in this study was provided by the participants' legal guardian/next of kin.

Author contributions

XC, ZG, YX, and ML participated in the study design and provided the financial support. ML, YD, DL, YZ, HY, JLiu, HG, and JLin participated in the data acquisition. ML and MHL analyzed the data and wrote the manuscript. MHL, YD, and MH revised the manuscript. All authors read and approved the final version.

Funding

This study was funded by the Joint Funds for the Innovation of Science and Technology, Fujian Province (grant number: 2021Y9049), Health Science and Technology Project of Fujian Province (grant number: 2022CXA008), and Special Financial Fund Project of Fujian Province (grant number: 2020CZ016).

Acknowledgments

We thank Shanghai Majorbio Bio-Pharm Technology Co., Ltd., Shanghai, China, for its technical assistance. We gratefully acknowledge the support from the nurses of Award 5 and Award 62 of Fujian Medical University Union Hospital, leaded by Guiqing Zhong and Jianling Lin, respectively.

Conflict of interest

JLiu was employed by the Fuzhou MineButy Clinics.

The remaining authors declare that the research was conducted in the absence of any commercial or financial relationships that could be construed as a potential conflict of interest.

Publisher's note

All claims expressed in this article are solely those of the authors and do not necessarily represent those of their affiliated organizations, or those of the publisher, the editors and the reviewers. Any product that may be evaluated in this article, or claim that may be made by its manufacturer, is not guaranteed or endorsed by the publisher.

Supplementary material

The Supplementary Material for this article can be found online at: https://www.frontiersin.org/articles/10.3389/fmicb.2023.1215884/full#supplementary-material

SUPPLEMENTARY FIGURE 1
OTU Venn diagram, red circle indicates the number of OTUs unique to NS, blue circle indicated the number of OTUs unique to PS, the overlap part shows the number of OTUs shared by the two groups.

SUPPLEMENTARY FIGURE 2
Heatmap of the 50 most abundant OTUs using Pearson correlation analysis. **(A)** NS group. **(B)** PS group. Correlation coefficient | r| ≥ 0.50, $P < 0.05$.

SUPPLEMENTARY TABLE 1
Network central coefficient table of NS and PS.

References

Ahmad, A., Herndon, D., and Szabo, C. (2019). Oxandrolone protects against the development of multiorgan failure, modulates the systemic inflammatory response and promotes wound healing during burn injury. *Burns* 45, 671–681. doi: 10.1016/j.burns.2018.10.006

An, L., Wu, W., Li, S., Lai, Y., Chen, D., He, Z., et al. (2021). *Escherichia coli* aggravates calcium oxalate stone formation via PPK1/flagellin-mediated renal oxidative injury and inflammation. *Oxidat. Med. Cell. Longev.* 2021:9949697. doi: 10.1155/2021/9949697

Arumugam, M., Raes, J., Pelletier, E., Le Paslier, D., Yamada, T., Mende, D., et al. (2011). Enterotypes of the human gut microbiome. *Nature* 473, 174–180.

Ashcroft, G., Dodsworth, J., van Boxtel, E., Tarnuzzer, R., Horan, M., Schultz, G., et al. (1997). Estrogen accelerates cutaneous wound healing associated with an increase in TGF-beta1 levels. *Nat. Med.* 3, 1209–1215.

Avram, M., Tope, W., Yu, T., Szachowicz, E., and Nelson, J. (2009). Hypertrophic scarring of the neck following ablative fractional carbon dioxide laser resurfacing. *Lasers Surg. Med.* 41, 185–188. doi: 10.1002/lsm.20755

Berman, B., Maderal, A., and Raphael, B. (2017). Keloids and hypertrophic scars: Pathophysiology, classification, and treatment. *Dermatol. Surg.* 43, S3–S18.

Brown, E., Ke, X., Hitchcock, D., Jeanfavre, S., Avila-Pacheco, J., Nakata, T., et al. (2019). *Bacteroides*-derived sphingolipids are critical for maintaining intestinal homeostasis and symbiosis. *Cell Host Microbe* 25, 668–680.e7. doi: 10.1016/j.chom.2019.04.002

Chen, S., Wu, X., and Yu, Z. (2021). Juglone suppresses inflammation and oxidative stress in colitis mice. *Front. Immunol.* 12:674341. doi: 10.3389/fimmu.2021.674341

Chen, S., Zhou, Y., Chen, Y., and Gu, J. (2018). Fastp: An ultra-fast all-in-one FASTQ preprocessor. *Bioinformatics* 34, i884–i890. doi: 10.1093/bioinformatics/bty560

Costa, R., Negrão, R., Valente, I., Castela, Â, Duarte, D., Guardão, L., et al. (2013). Xanthohumol modulates inflammation, oxidative stress, and angiogenesis in type 1 diabetic rat skin wound healing. *J. Nat. Prod.* 76, 2047–2053. doi: 10.1021/np4002898

D'Argenio, V., Veneruso, I., Gong, C., Cecarini, V., Bonfili, L., and Eleuteri, A. (2022). Gut microbiome and mycobiome alterations in an in vivo model of Alzheimer's disease. *Genes* 13:1564. doi: 10.3390/genes13091564

De Pessemier, B., Grine, L., Debaere, M., Maes, A., Paetzold, B., and Callewaert, C. (2021). Gut-skin axis: Current knowledge of the interrelationship between microbial dysbiosis and skin conditions. *Microorganisms* 9:353. doi: 10.3390/microorganisms9020353

Faith, J., Guruge, J., Charbonneau, M., Subramanian, S., Seedorf, H., Goodman, A., et al. (2013). The long-term stability of the human gut microbiota. *Science* 341:1237439.

Fang, Z., Li, L., Zhang, H., Zhao, J., Lu, W., and Chen, W. (2021). Gut microbiota, probiotics, and their interactions in prevention and treatment of atopic dermatitis: A review. *Front. Immunol.* 12:720393. doi: 10.3389/fimmu.2021.720393

Fang, Z., Pan, T., Li, L., Wang, H., Zhu, J., Zhang, H., et al. (2022). *Bifidobacterium longum* mediated tryptophan metabolism to improve atopic dermatitis via the gut-skin axis. *Gut Microb.* 14:2044723. doi: 10.1080/19490976.2022.2044723

Franceschi, C., Garagnani, P., Parini, P., Giuliani, C., and Santoro, A. (2018). Inflammaging: A new immune-metabolic viewpoint for age-related diseases. *Nat. Rev. Endocrinol.* 14, 576–590. doi: 10.1038/s41574-018-0059-4

Huang, C., Akaishi, S., Hyakusoku, H., and Ogawa, R. (2014). Are keloid and hypertrophic scar different forms of the same disorder? A fibroproliferative skin disorder hypothesis based on keloid findings. *Int. Wound J.* 11, 517–522. doi: 10.1111/j.1742-481X.2012.01118.x

Huang, C., Murphy, G., Akaishi, S., and Ogawa, R. (2013). Keloids and hypertrophic scars: Update and future directions. *Plastic Reconstr. Surg. Glob. Open.* 1:e25.

Huang, C., and Ogawa, R. (2020). The vascular involvement in soft tissue fibrosis-lessons learned from pathological scarring. *Int. J. Mol. Sci.* 21:2542. doi: 10.3390/ijms21072542

Jackson, W., Nesti, L., and Tuan, R. (2012). Mesenchymal stem cell therapy for attenuation of scar formation during wound healing. *Stem Cell Res. Ther.* 3:20.

Jfri, A., Rajeh, N., and Karkashan, E. A. (2015). Case of multiple spontaneous keloid scars. *Case Rep. Dermatol.* 7, 156–160.

Khan, A., Khan, Z., Malik, A., Kalam, M., Cash, P., Ashraf, M., et al. (2017). Colorectal cancer-inflammatory bowel disease nexus and felony of *Escherichia coli*. *Life Sci.* 180, 60–67. doi: 10.1016/j.lfs.2017.05.016

Kim, H., Lee, D., Park, S., Kim, Y., Kim, Y., Jeong, J., et al. (2014). Oral administration of *Lactobacillus plantarum* HY7714 protects hairless mouse against ultraviolet B-induced photoaging. *J. Microbiol. Biotechnol.* 24, 1583–1591. doi: 10.4014/jmb.1406.06038

Lau, K., Paus, R., Tiede, S., Day, P., and Bayat, A. (2009). Exploring the role of stem cells in cutaneous wound healing. *Exp. Dermatol.* 18, 921–933.

Lee, J., Yang, C., Chao, S., and Wong, T. (2004). Histopathological differential diagnosis of keloid and hypertrophic scar. *Am. J. Dermatopathol.* 26, 379–384.

Li, J., Zhao, F., Wang, Y., Chen, J., Tao, J., Tian, G., et al. (2017). Gut microbiota dysbiosis contributes to the development of hypertension. *Microbiome* 5:14. doi: 10.1186/s40168-016-0222-x

Liu, C., Zhao, D., Ma, W., Guo, Y., Wang, A., Wang, Q., et al. (2016). Denitrifying sulfide removal process on high-salinity wastewaters in the presence of *Halomonas* sp. *Appl. Microbiol. Biotechnol.* 100, 1421–1426. doi: 10.1007/s00253-015-7039-6

Lozupone, C., Stombaugh, J., Gordon, J., Jansson, J., and Knight, R. (2012). Diversity, stability and resilience of the human gut microbiota. *Nature* 489, 220–230.

Ma, J., Hong, Y., Zheng, N., Xie, G., Lyu, Y., Gu, Y., et al. (2020). Gut microbiota remodeling reverses aging-associated inflammation and dysregulation of systemic bile acid homeostasis in mice sex-specifically. *Gut Microb.* 11, 1450–1474. doi: 10.1080/19490976.2020.1763770

Magoč, T., and Salzberg, S. L. (2011). FLASH: Fast length adjustment of short reads to improve genome assemblies. *Bioinformatics* 27, 2957–2963. doi: 10.1093/bioinformatics/btr507

Mahmud, M., Akter, S., Tamanna, S., Mazumder, L., Esti, I., Banerjee, S., et al. (2022). Impact of gut microbiome on skin health: Gut-skin axis observed through the lenses of therapeutics and skin diseases. *Gut Microb.* 14:2096995. doi: 10.1080/19490976.2022.2096995

Martin, P. (1997). Wound healing–aiming for perfect skin regeneration. *Science* 276, 75–81. doi: 10.1126/science.276.5309.75

Moniaga, C., Tominaga, M., and Takamori, K. (2022). An altered skin and gut microbiota are involved in the modulation of itch in atopic dermatitis. *Cells* 11:3930. doi: 10.3390/cells11233930

Ochoa-Repáraz, J., Mielcarz, D., Wang, Y., Begum-Haque, S., Dasgupta, S., Kasper, D., et al. (2010). A polysaccharide from the human commensal *Bacteroides fragilis* protects against CNS demyelinating disease. *Mucosal Immunol.* 3, 487–495. doi: 10.1038/mi.2010.29

Ogawa, R. (2022). The most current algorithms for the treatment and prevention of hypertrophic scars and keloids: A 2020 update of the algorithms published 10 years ago. *Plastic Reconstr. Surg.* 149, 79e–94e. doi: 10.1097/PRS.0000000000008667

Pai, V., and Cummings, I. (2011). Are there any good treatments for keloid scarring after sternotomy? *Int. Cardiovasc. Thor. Surg.* 13, 415–418. doi: 10.1510/icvts.2010.264887

Pivari, F., Mingione, A., Piazzini, G., Ceccarani, C., Ottaviano, E., Brasacchio, C., et al. (2022). Curcumin supplementation (Meriva(®)) modulates inflammation, lipid peroxidation and gut microbiota composition in chronic kidney disease. *Nutrients* 14:231. doi: 10.3390/nu14010231

Ramírez-Boscá, A., Navarro-López, V., Martínez-Andrés, A., Such, J., Francés, R., Horga de la Parte, J., et al. (2015). Identification of bacterial DNA in the peripheral blood of patients with active psoriasis. *JAMA Dermatol.* 151, 670–671. doi: 10.1001/jamadermatol.2014.5585

Rogier, R., Evans-Marin, H., Manasson, J., van der Kraan, P., Walgreen, B., Helsen, M., et al. (2017). Alteration of the intestinal microbiome characterizes preclinical inflammatory arthritis in mice and its modulation attenuates established arthritis. *Sci. Rep.* 7:15613. doi: 10.1038/s41598-017-15802-x

Salem, I., Ramser, A., Isham, N., and Ghannoum, M. (2018). The gut microbiome as a major regulator of the gut-skin axis. *Front. Microbiol.* 9:1459. doi: 10.3389/fmicb.2018.01459

Sinha, S., Lin, G., and Ferenczi, K. (2021). The skin microbiome and the gut-skin axis. *Clin. Dermatol.* 39, 829–839.

Son, E. D., Lee, J., Lee, S., Kim, M., Lee, B., Chang, I., et al. (2005). Topical application of 17beta-estradiol increases extracellular matrix protein synthesis by stimulating tgf-Beta signaling in aged human skin in vivo. *J. Investig. Dermatol.* 124, 1149–1161. doi: 10.1111/j.0022-202X.2005.23736.x

Song, H., Yoo, Y., Hwang, J., Na, Y., and Kim, H. (2016). *Faecalibacterium prausnitzii* subspecies-level dysbiosis in the human gut microbiome underlying atopic dermatitis. *J. Allergy Clin. Immunol.* 137, 852–860. doi: 10.1016/j.jaci.2015.08.021

Takahashi, K., Nishida, A., Fujimoto, T., Fujii, M., Shioya, M., Imaeda, H., et al. (2016). Reduced abundance of butyrate-producing bacteria species in the fecal microbial community in Crohn's disease. *Digestion* 93, 59–65.

van der Veer, W., Bloemen, M., Ulrich, M., Molema, G., van Zuijlen, P., Middelkoop, E., et al. (2009). Potential cellular and molecular causes of hypertrophic scar formation. *Burns* 35, 15–29.

Zheng, D., Li, R., An, J., Xie, T., Han, Z., Xu, R., et al. (2020). Prebiotics-Encapsulated Probiotic Spores Regulate Gut Microbiota and Suppress Colon Cancer. *Adv. Mater.* 32:e2004529. doi: 10.1002/adma.202004529

Zhong, W., Lu, X., Shi, H., Zhao, G., Song, Y., Wang, Y., et al. (2019). Distinct microbial populations exist in the mucosa-associated microbiota of diarrhea predominant irritable bowel syndrome and ulcerative colitis. *J. Clin. Gastroenterol.* 53, 660–672. doi: 10.1097/MCG.0000000000000961

frontiers | Frontiers in Microbiology

TYPE Methods
PUBLISHED 22 June 2023
DOI 10.3389/fmicb.2023.1177273

OPEN ACCESS

EDITED BY
Arabella Touati,
Centre Hospitalier Universitaire de Bordeaux, France

REVIEWED BY
Maureen Helen Diaz,
Centers for Disease Control and Prevention (CDC), United States
Arthur H. Totten,
Stony Brook Medicine, United States
Roger Dumke,
Technical University Dresden, Germany
Wendy W. J. Unger,
Erasmus Medical Center, Netherlands

*CORRESPONDENCE
Jing Yuan
✉ yuanjing6216@163.com
Guanhua Xue
✉ xgh618@163.com

†These authors have contributed equally to this work

RECEIVED 02 March 2023
ACCEPTED 08 June 2023
PUBLISHED 22 June 2023

CITATION
Zhao H, Yan C, Feng Y, Du B, Feng J, Cui X, Cui J, Gan L, Fan Z, Xu Z, Fu T, Yu Z, Yuan J and Xue G (2023) Absolute quantification of *Mycoplasma pneumoniae* in infected patients by droplet digital PCR to track disease severity and treatment efficacy.
Front. Microbiol. 14:1177273.
doi: 10.3389/fmicb.2023.1177273

Absolute quantification of *Mycoplasma pneumoniae* in infected patients by droplet digital PCR to track disease severity and treatment efficacy

Hanqing Zhao†, Chao Yan†, Yanling Feng, Bing Du, Junxia Feng, Xiaohu Cui, Jinghua Cui, Lin Gan, Zheng Fan, Ziying Xu, Tongtong Fu, Zihui Yu, Jing Yuan* and Guanhua Xue*

Department of Bacteriology, Capital Institute of Pediatrics, Beijing, China

Mycoplasma pneumoniae is a common causative pathogen of community-acquired pneumonia. An accurate and sensitive detection method is important for evaluating disease severity and treatment efficacy. Digital droplet PCR (ddPCR) is a competent method enabling the absolute quantification of DNA copy number with high precision and sensitivity. We established ddPCR for *M. pneumoniae* detection, using clinical specimens for validation, and this showed excellent specificity for *M. pneumoniae*. The limit of detection of ddPCR was 2.9 copies/reaction, while that for real-time PCR was 10.8 copies/reaction. In total, 178 clinical samples were used to evaluate the ddPCR assay, which correctly identified and differentiated 80 positive samples, whereas the real-time PCR tested 79 samples as positive. One sample that tested negative in real-time PCR was positive in ddPCR, with a bacterial load of three copies/test. For samples that tested positive in both methods, the cycle threshold of real-time PCR was highly correlated with the copy number of ddPCR. Bacterial loads in patients with severe *M. pneumoniae* pneumonia were significantly higher than those in patients with general *M. pneumoniae* pneumonia. The ddPCR showed that bacterial loads were significantly decreased after macrolide treatment, which could have reflected the treatment efficacy. The proposed ddPCR assay was sensitive and specific for the detection of *M. pneumoniae*. Quantitative monitoring of bacterial load in clinical samples could help clinicians to evaluate treatment efficacy.

KEYWORDS

***Mycoplasma pneumoniae*, digital droplet PCR, real-time PCR, bacterial load, treatment efficiency**

Introduction

Mycoplasma pneumoniae is a causative pathogen of respiratory infections in humans. It is a small, cell-wall-deficient bacterium that belongs to the class Mollicutes. *M. pneumoniae* is a significant cause of community-acquired pneumonia, especially in children and young adults (Waites et al., 2017). The clinical manifestations of this pathogen are mostly those of atypical pneumonia, including fever, cough, sore throat, headache, and malaise. Some severe cases have extrapulmonary complications, such as cardiovascular, gastrointestinal, renal, and central

nervous system dysfunction (Atkinson et al., 2008). However, the clinical presentations of *M. pneumoniae* are indistinguishable from those of other respiratory pathogens, which also present with fever, cough, and other symptoms of respiratory tract infection. Co-infections, especially with respiratory viruses, are often observed in *M. pneumoniae* infection (Li et al., 2022). Thus, developing a precise and highly sensitive microbiological diagnosis method is important.

As a fastidious bacterium, *M. pneumoniae* is seldom routinely tested for using clinical culture. Thus, alternative molecular methods have been established for *M. pneumoniae* detection, such as real-time PCR, nucleic-acid-sequence-based amplification, loop-mediated isothermal amplification, and recombinase-aided amplification (Diaz and Winchell, 2016). These PCR-based methods all show good analytical detection performance. Real-time PCR is the mainstream diagnostic procedure used in most hospital and reference laboratories (Diaz and Winchell, 2016). The quantitative nature of this method is determining sample concentration by comparing the cycle threshold value (CT) to a standard curve. With regard to precision medicine, the accurate measurement of pathogen-related nucleic acids is becoming more important.

Digital droplet PCR (ddPCR) is an absolute quantification method that does not involve the generation of a standard curve, and it shows robust detection efficiency for various pathogens such as SARS-CoV-2, hepatitis B virus, human immunodeficiency virus, and *Mycobacterium tuberculosis* (Kuypers and Jerome, 2017; Liu et al., 2020). Several studies have shown that ddPCR has greater sensitivity than real-time PCR and is more suitable for samples with a low bacterial load (Taylor et al., 2017). Most importantly, the direct absolute quantification method is useful for evaluating disease progression and treatment efficacy.

In this study, we developed a ddPCR method for the accurate quantification of *M. pneumoniae* and compared its clinical advantages with real-time PCR. We evaluated the ability of the assay to obtain results from samples taken from different periods of *M. pneumoniae* infection, and to measure treatment efficacy based on bacterial load in infected patients.

Materials and methods

Clinical specimens and information

In total, 186 clinical respiratory specimens, including 99 sputum samples, 46 throat swabs and 41 bronchoalveolar lavage fluid, were obtained from pediatric pneumonia patients between January and December 2019. Seventy-nine specimens were collected from patients diagnosed with *M. pneumoniae* infection without any co-infection, based on a commercial real-time PCR assay (Mole Bioscience Co. Ltd., Jiangsu, China. target gene P1). The other 99 specimens were negative for *M. pneumoniae* when tested with the same kit. Six patients were sampled two- or three-times during hospital treatment, and these additional eight samples were also used to measure treatment efficacy. Clinical information was also collected, including sex, age, duration of fever, length of stay, white blood cell count, neutrophil ratio, and C-reactive protein level.

All patients were separated into a severe *M. pneumoniae* pneumonia (SMPP) group and a general *M. pneumoniae* pneumonia (GMPP) group based on the guidelines for management of pediatric community-acquired pneumonia (The Subspecialty Group of Respiratory Disease, 2013; Fan et al., 2017). The SMPP group had worsening clinical signs, persistent fever (>38.5°C), and worsening lung imaging (radiological deterioration or consolidation present in more than two-thirds of the lung) and intra- and extrapulmonary complications. The GMPP group showed improvement within 7 days of regular treatment with macrolide antibiotics. This study was approved by the Ethics Committee of the Capital Institute of pediatrics. Informed consent was obtained during admission for patient clinical records to be used in future studies. All data were analyzed anonymously.

DNA extraction

Total DNA was extracted from 200 μL of the 186 clinical samples using the QIAamp DNA Mini Kit (Qiagen, Hilden, Germany). The extracts were eluted in 150 μL of nuclease-free water and stored at −80°C until use. The concentration of nucleic acids was determined with a NanoDrop 2000 Spectrophotometer (Thermo Scientific, Waltham, MA, United States).

Principle and workflow of *Mycoplasma pneumoniae* detection with ddPCR assay

Digital PCR was conducted by dividing the samples into many droplets and counting the number of droplets in which a reaction occurred. The sample preparation in this assay was the same as for real-time PCR. The workflow of *M. pneumoniae* detection with ddPCR is shown in Figure 1 and included three steps. The samples were first loaded onto a droplet generator and divided into multiple drops. Usually, the number of drops generated was 30,000–60,000. PCR was used to process each drop. After PCR amplification, the fluorescence signal was analyzed with the droplet reader system; in this step, drops containing the target yielded a signal and were assigned as positive, otherwise they were read as negative.

Digital droplet PCR

Digital droplet PCR was performed with a TargetingOne Digital PCR System (Beijing, China). The primers and probe (Supplementary Table S1) were designed for sequences within the conserved region of the P1 gene (accession no. U00089.2) and BLASTed for *in silico* cross-reactivity. All primers showed high specificity for *M. pneumoniae*. This conserved region was cloned into vector pUC57 to obtain recombinant plasmid for further use. The master mix for the ddPCR was composed of 15 μL of reaction buffer, 6.45 μL of DNase-free water, 2.4 μL of each forward and reverse primer (10 μM), and 0.75 μL of the probe (10 μM) to form a final volume of 20 μL. A no-template control was used in every ddPCR batch. The generation of droplets was performed with a Targeting One Droplet Generator. PCR amplification was carried out using an Applied Biosystems Veriti 96-Well Thermal Cycler with the following conditions: 95°C for 10 min followed by 40 cycles of denaturation at 94°C for 30 s and 60°C for 1 min. The plate was stored at 4°C until the droplets were analyzed with a Targeting One Droplet Reader and Chip Reader R1 software.

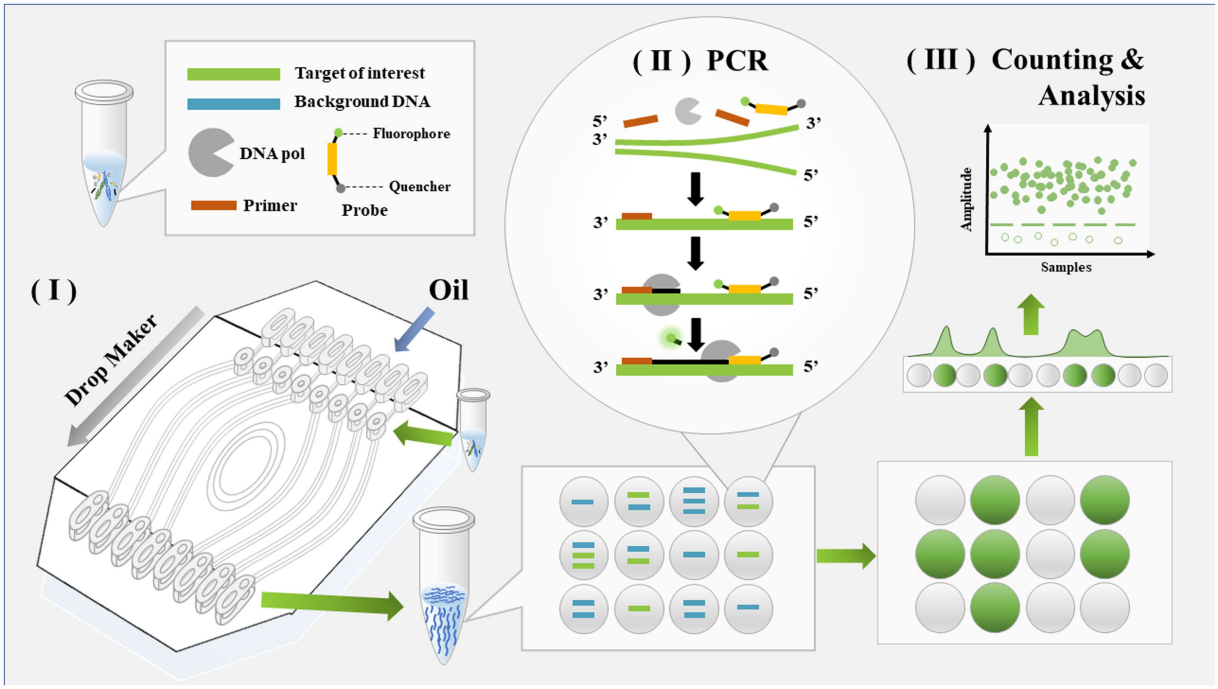

FIGURE 1
Schematic diagram of detection workflow for *Mycoplasma pneumoniae* using ddPCR. The entire workflow of ddPCR method includes three steps: droplet generation, regular PCR, and droplet analysis.

Real-time PCR

Real-time PCR was conducted in parallel with the same primers and probes used for ddPCR on ABI 7500 Software Version 2.3 (Applied Biosystems). The reaction system included 15 μL of PCR Master Mix Reagents (Tiangen Biotech Co. Ltd., Beijing, China), 0.9 μL of forward primer (10 μM), 0.9 μL of reverse primer (10 μM), 0.6 μL of probe (10 μM), and 9.6 μL of DNase-free water, and the same amount of DNA template as was used for ddPCR. The cycling conditions were as follows: 94°C for 10 min, followed by 40 cycles of denaturation at 94°C for 10 s and annealing/extension at 60°C for 45 s. The result was considered positive when the cycle threshold (Ct) for the P1 gene was ≤38 and negative when Ct was >38.

Analytical sensitivity and specificity of digital droplet PCR

The specificity was evaluated by testing for other *Mycoplasma* and common bacteria of the respiratory tract: *M. pneumoniae* type 1 strain (ATCC 29342), *M. pneumoniae* type 2 strain (ATCC 15531), *Streptococcus pneumoniae* (ATCC 49619), *Haemophilus influenzae* (ATCC 43065), *Staphylococcus aureus* (ATCC 25923), *Staphylococcus epidermidis* (ATCC 12228), *Klebsiella pneumoniae* (ATCC 27736), *Escherichia coli* (ATCC 25922), *Mycoplasma fermentans* (ATCC 19989), *Legionella pneumophila* (ATCC 33152), *Mycobacterium tuberculosis* (ATCC 25618/H37Rv), *Pseudomonas aeruginosa* (ATCC27853), *Mycoplasma genitalium* (ATCC 33530), *Ureaplasma parvum* (ATCC 27813), *Mycoplasma hominis* (ATCC 23114), adenovirus (DNA from clinical isolates), herpes simplex virus (DNA from clinical isolates), and varicella zoster virus (DNA from clinical isolates). The linear dynamic range of the ddPCR assay was determined using 10-fold serial dilutions of the recombinant plasmid. For the reproducibility of ddPCR, five independent experiments were performed with these recombinant plasmid dilutions across 5 days, then the inter-assay coefficient of variance (CV) was calculated. The limit of detection (LoD) of both real-time PCR and ddPCR was obtained using serial dilutions of spiked samples of concentrations close to the detection limits. For all concentrations, tests were performed on 20 replicates.

Performance of digital droplet PCR and real-time PCR using clinical samples

To evaluate the performance of the ddPCR assay for *M. pneumoniae* detection, 178 clinical samples were tested. The performance was compared with that of real-time PCR in parallel, using the same primers and probes.

Statistical analysis

Categorical variables (Sex) are expressed as count/percentages, and between-group comparison was done using the Chi-squared test. The distributions of continuous variables were assessed for normality using the Shapiro–Wilk W test. Continuous variables are expressed as mean (standard deviation) in the case of Gaussian distributions or median (interquartile range) in the case of skewed distributions. Comparison of continuous variables between two groups was performed using the independent samples t-test or nonparametric Mann–Whitney U test, where appropriate. Correlations between the Ct values of real-time PCR and the bacterial load determined by ddPCR were analyzed with

the Pearson correlation test. A p value <0.05 (two sided) was considered statistically significant. The above-mentioned analyses were performed using either Prism 8.0 (GraphPad, La Jolla, CA, United States) or SPSS 19.0 (College Station, TX, United States) software.

Results

Analytical performance of the *Mycoplasma pneumoniae* digital droplet PCR assay

The ddPCR assay showed excellent specificity for *M. pneumoniae* detection. Among the 12 common respiratory pathogen controls and four mollicutes species, only two *M. pneumoniae* samples (types 1 and 2) produced positive signals, while the other control samples were negative. Therefore, ddPCR showed high specificity for *M. pneumoniae*, with no cross-reaction with other pathogens (Figure 2).

The linear dynamic range was evaluated by ddPCR and compared with that of real-time PCR. Both methods showed a good linear range, and ddPCR achieved results comparable to those of real-time PCR: R^2 for ddPCR was 0.9935 and that for real-time PCR was 0.9873 when testing the 10-fold serial dilutions from 10^5 to 10 copies/μL of the recombinant plasmids (Figure 3) The inter-assay CV of different plasmid dilutions (10^5, 10^4, 10^3, 100, and 10) were 0.068, 0.094, 0.116, 0.159, and 0.197, respectively, suggesting that the ddPCR assay had good reproducibility.

LoD of *Mycoplasma pneumoniae* digital droplet PCR and real-time PCR

We used serial dilutions of the recombinant plasmid to determine the detection limit of ddPCR and compared it with that of the real-time PCR assay. The linear series DNA standards were diluted to the detection limit with cDNA from negative throat swab samples from healthy people to concentrations below the minimum detection range of ddPCR or real-time PCR. Each concentration was analyzed for 20 replicates. The LoD of ddPCR was 2.9 (95% CI: 1.8–4.4) copies/reaction while the real-time PCR was 10.8 (95% CI: 7.1–14.5) copies/reaction. The LoD of ddPCR and real-time PCR were comparable, ddPCR was probably three times below that of the real-time PCR.

Evaluation of the performance of digital droplet PCR and RT-PCR for clinical samples

In total, 178 clinical samples were tested for *M. pneumoniae* with ddPCR and real-time PCR. For ddPCR, 80 samples were positive and 98 were negative. For real-time PCR, 79 samples were positive and 99 were negative. The correlation coefficient between ddPCR and real-time PCR was 0.8784 (Figure 4A). There was one sample that showed a positive result with ddPCR and had three copy numbers but showed a negative real-time PCR result (Table 1). This sample was collected from patient A 2 days before admission, but the patient was classified as positive because the second sample was positive (data in Figure 5). The results showed that ddPCR and real-time PCR were accurate and reliable, but ddPCR was more accurate for samples with a low copy number.

Bacterial load in children with different clinical features

Among the patients diagnosed with *M. pneumoniae* infection, 25 were classified into the SMPP group and 55 into the GMPP group based on the guidelines for management of pediatric community-acquired pneumonia. The duration of fever and length of stay were longer in the SMPP group than in the GMPP group ($p < 0.001$). White blood cell count, neutrophil ratio and C-reactive protein level were higher in the SMPP group than in the GMPP group ($p < 0.001$). The bacterial loads tested by ddPCR in the SMPP group were significantly higher than those in the GMPP group ($p < 0.001$, Figure 4B). The degree of bacterial load seemed to be related to the clinical features. Information on both groups is summarized in Table 2.

Dynamic changes in bacterial load in samples of six patients

Digital droplet PCR provided accurate detection of *M. pneumoniae*; therefore, we analyzed the dynamic changes in bacterial load throughout the treatment period. Six patients (patient C and E were classified as SMPP, the rest four patient were GMPP) with macrolide antibiotic treatment were sampled two or three times before or during admission. These additional eight samples were included for testing. Detailly, three swab samples which collected at 2 days prior to admission (2d PTA), day 1 of azithromycin treatment (AZM 1d), day 3 of azithromycin treatment (AZM 3d) were from Patient A. Three swab samples collected at AZM 1d, AZM 3d and day 5 of azithromycin treatment (AZM 5d) were from Patient B. For the rest four patient, two swab samples collected at AZM 1d and AZM 3d were collected separately. When tested by ddPCR, the bacterial loads of all patients dramatically decreased after azithromycin treatment (Figure 5, $p = 0.014$), which could have reflected the efficacy of antibiotic treatment. Patient A showed fluctuation in bacterial load, which initially increased and then decreased after macrolide treatment.

Discussion

M. pneumoniae has substantially reduced its genome during its adaptive evolution, and thus it has limited metabolic capabilities and relies on its host to provide most of the nutrients it needs (Xiao et al., 2015). Hence, culturing this pathogen is difficult, and developing a fast and accurate alternative method for its clinical detection is important. Additionally, previous studies have confirmed that the severity of the clinical manifestations of respiratory infections is closely related to the copy number of the infecting bacterium or virus (Dorigo-Zetsma et al., 1999; Nilsson et al., 2010; Zhang et al., 2020); therefore, precise quantification of pathogen load is useful for assessing disease severity and progression.

Real-time PCR, a well-developed practical method for the detection of infective pathogens, has been widely used for the clinical diagnosis of *M. pneumoniae* (Dumke et al., 2007; Winchell and Mitchell, 2013; Zhao et al., 2020). However, it relies on a standard curve to calculate the DNA copy number, which differs among experiments and thus complicates the diagnostic process. Digital PCR, by contrast, quantifies nucleic acids independently of a standard curve

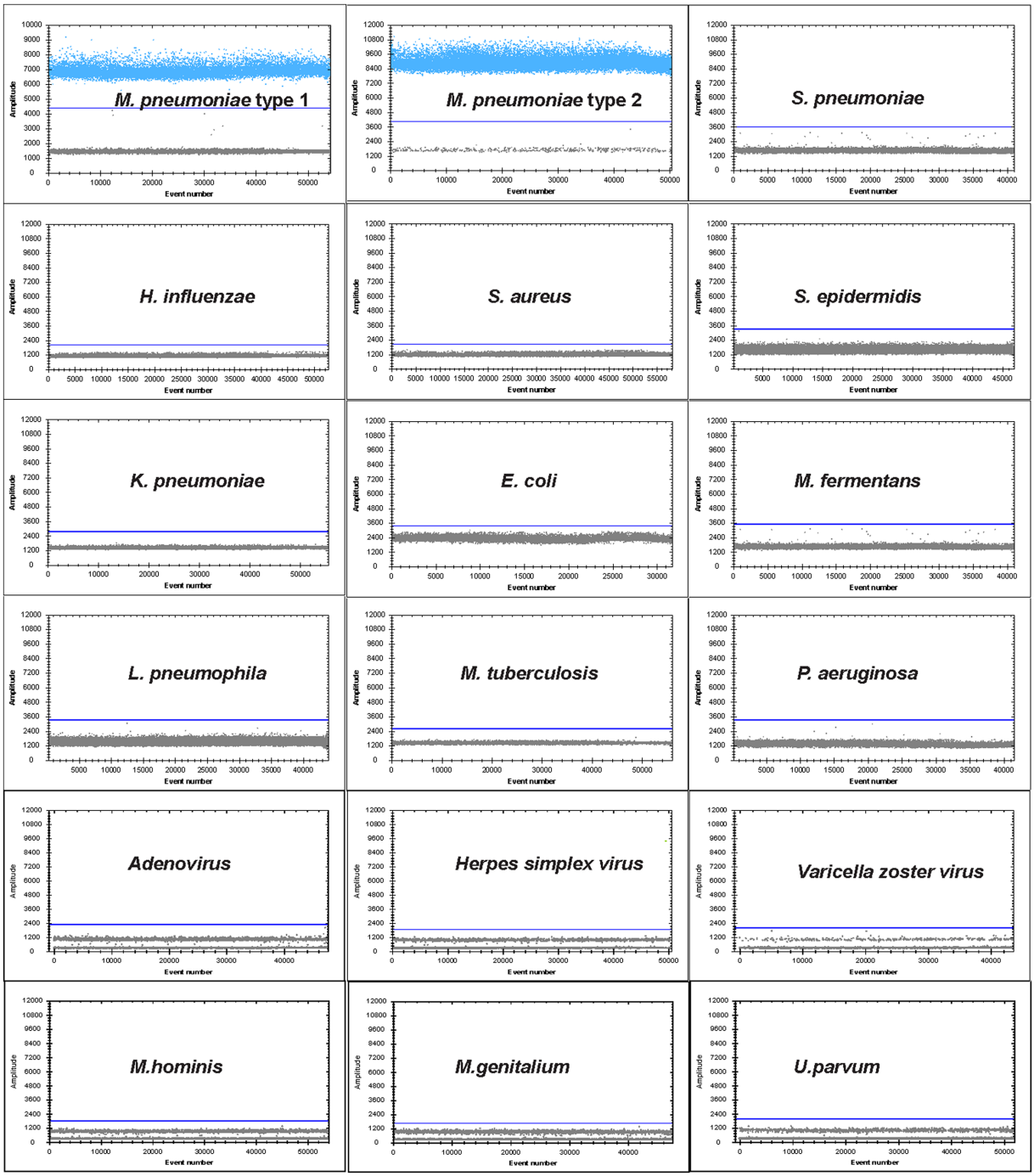

FIGURE 2
Specificity of ddPCR assay for *M. pneumoniae*. Positive droplets of *M. pneumoniae* with channel amplitude signals above 6,500. The test was negative for the other 12 pathogens of the respiratory tract: *S. pneumoniae*, *H. influenzae*, *S. aureus*, *S. epidermidis*, *K. pneumoniae*, *E. coli*, *L. pneumophila*, *M. tuberculosis*, *P. aeruginosa*, adenovirus, herpes simplex virus, varicella zoster virus and four mollicutes species *M. fermentans*, *M. genitalium*, *U. parvum* and *M. hominis*.

and is less affected by PCR efficiency (Hindson et al., 2011; Li et al., 2018). Many studies have also proved that ddPCR shows better detection efficiency for samples with a lower copy number (Sedlak et al., 2017; Li et al., 2020), which may help improve the sensitivity of detection.

In this study, we developed a ddPCR assay for the detection and quantification of *M. pneumoniae*. A conserved region of the P1 gene was selected for the target because this region has been demonstrated to provide good sensitivity and specificity in PCR amplification (Waites et al., 2017; Leal et al., 2020; Xue et al., 2020). The other reported target genes included 16S rRNA, 16S-23S rRNA spacer, CARDS toxin gene, ATPase operon, dnaK, pdhA, tuf, parE, pdhA, ptsL, repMp1, and repMp4. The sensitivity and specificity of these targets differed. Our data suggested that ddPCR of P1 gene had high specificity with no cross-reaction to other respiratory and mollicute pathogens. When we tested the linear dynamic range and compared

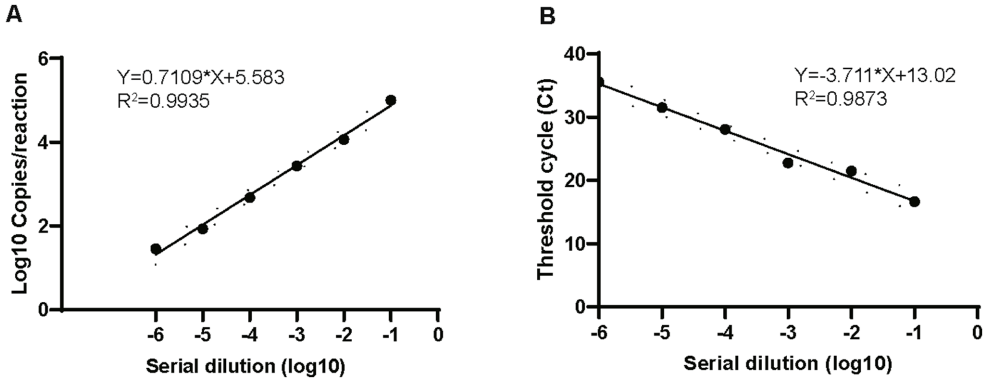

FIGURE 3
Comparison of dynamic range of ddPCR and real-time PCR. Plots of results from linearity experiment for quantification of *M. pneumoniae* with ddPCR **(A)** and real-time PCR **(B)**. Dilution multiples from 10^6 to 0 copies/μL are plotted on the *x*-axis. ddPCR (converted to log10) and real-time PCR (Ct) are plotted on the *y*-axis using GraphPad Prism 8.0.

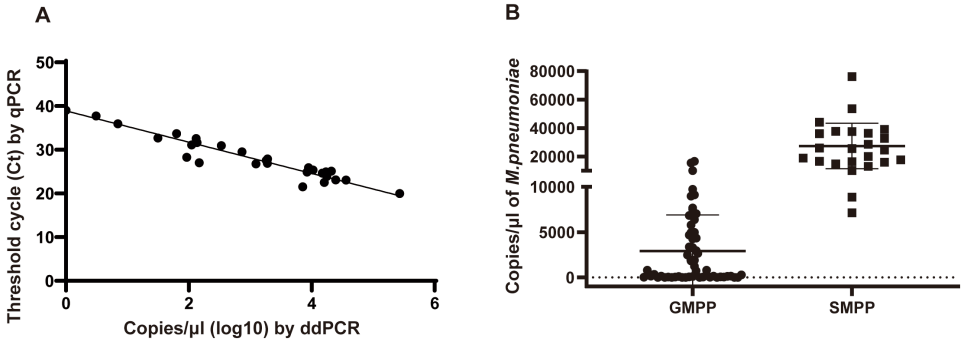

FIGURE 4
Performance of ddPCR in clinical samples. **(A)** Correlation analysis between ddPCR copies and Ct values of real-time PCR. Copies of ddPCR (converted to log10) are plotted on the *x*-axis. Ct values of real-time PCR are plotted on the y-axis using GraphPad Prism 8.0. **(B)** The copy numbers of *M. pneumoniae* positive patients in different groups. SMPP, severe *M. pneumoniae* pneumonia. GMPP, general *M. pneumoniae* pneumonia.

the results with those of real-time PCR, both methods showed excellent analytical performance. The LoD of ddPCR and real-time PCR was comparable; ddPCR was probably three times below that of the real-time PCR, which suggested that ddPCR was more suitable for detection of specimens with a low copy number, which is consistent with other studies (Jeremiah Matson et al., 2022; Milosevic et al., 2022).

In 178 patients, the results of real-time PCR and ddPCR were similar, except for one sample collected from patient A at 2 days before admission, in which the copy number detected by ddPCR was three, while that detected by qPCR was negative. Later, a second sample from this patient was positive by both methods. The two assays produced the same results for samples with a higher copy number. For patient A, even though ddPCR showed strong detection for the sample with a low copy number, we could not conclude that ddPCR was more sensitive than real-time PCR, as only one sample was tested. More samples are needed to verify the sensitivity of these two methods.

The clinical manifestations of *M. pneumoniae* infection differ among patients, and severe infection poses major therapeutic challenges (Izumikawa, 2016). At present, many research groups are exploring the clinical manifestations, laboratory examination results, and specific indicators of severe *M. pneumoniae* pneumonia. It has been shown that the load of *Mycoplasma* is positively correlated with disease severity (Wang et al., 2014). Therefore, accurate measurement of *Mycoplasma* load is important when determining disease severity, and digital PCR has advantages in this respect. In this study, we divided enrolled patients into two groups according to their clinical manifestations. After quantitative analysis of *Mycoplasma* from these patients, we found that the copy number of severe cases was generally $>10^5$, which is consistent with other studies (Zhang et al., 2020). Zhang et al. divided patients into different groups based on copy number (10^5–10^8 copies) of *M. pneumoniae* genes determined using quantitative PCR, and showed that PCR loading was associated with clinical severity and inflammatory indicators. The high bacterial load group had high fever, high thermal peak, long duration of fever, and elevated levels of C-reactive protein. Many studies have also suggested that high macrolide resistance is related to clinical features (Zhou et al., 2021). In our study, total macrolide resistance mutations were found in 93.75% of samples, and there was no significant difference between the two groups (data not shown).

Dynamic changes to the bacterial or viral load during the course of infection are closely related to treatment efficacy. Recent studies have shown that SARS-CoV-2 load increases in the early and progressive stages and decreases in the recovery stage of COVID-19 (Yu et al., 2020; Leuzinger et al., 2021). *M. pneumoniae* is difficult to

10.3389/fmicb.2023.1177273

TABLE 1 Performance of ddPCR and real-time PCR in clinical samples.

	Clinical Positive (80)	Clinical Negative (98)	Total (178)	PPV	NPV	Sensitivity	Specificity
ddPCR	80	98	178	100%	100%	100%	100%
qPCR	79	99	178	98.75%	100%	98.75%	100%

PPV, Positive predictive value; NPV, Negative predictive value.

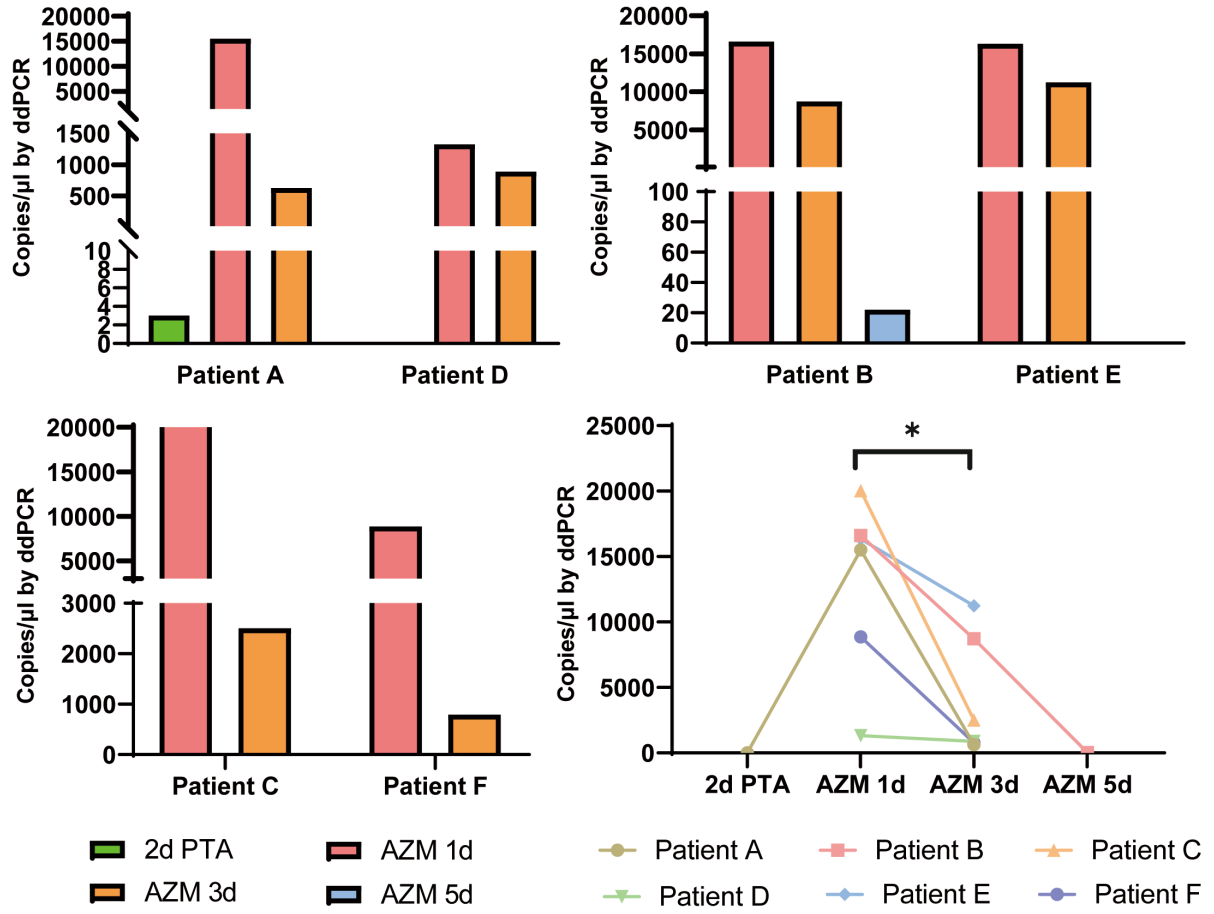

FIGURE 5
Dynamic changes of *M. pneumoniae* load in swab samples from six patients. The bacterial load numbers of six patients at different sample times were tested by ddPCR to reflect the clinical treatment efficacy. 2d PTA: 2days prior to admission; AZM 1d: day 1 of azithromycin treatment; AZM 3d: day 3 of azithromycin treatment; AZM 5d: day 5 of azithromycin treatment. *p<0.05.

TABLE 2 Clinical information for children with *M. pneumoniae* pneumonia.

Parameters	General MPP (n=55)	Severe MPP (n=25)	p value
Sex/(Male count/percentages)	29 (52.72)	15 (60%)	0.158
Age (mean month, range)	63.4 (56.6–70.2)	70.5 (59.3–81.7)	0.0086
Duration of fever after recruitment (mean day, range)	9.13 (7.85–10.41)	14.1 (12.7–15.5)	< 0.001
Length of stay (mean day, range)	7.38 (6.56–8.10)	12.64 (10.18–15.1)	< 0.001
White Blood Cells ($\times 10^9$ cells/L) (mean, range)	8.32 (7.43–9.21)	9.14 (8.59–9.69)	< 0.01
Neutrophils proportion (%) (mean, range)	58 (50–66)	65 (61–69)	< 0.001
C-reactive protein (mg/L) (mean, range)	18.3 (12.2–24.4)	41.6 (36.6–46.9)	< 0.001
Bacterial load by ddPCR (copies/μL) (mean ± SD)	2,973 ± 3,332	27,508 ± 15,946	< 0.001

grow *in vitro*, and increasing reports of high rates of resistance to azithromycin heighten the significance of clinical bacterial load detection (Zhou et al., 2014). Because ddPCR can accurately detect pathogen loads in samples with a lower copy number, it is useful for evaluation of clinical treatment efficacy. Consistent with recent studies, the bacterial load of all six patients in this study decreased 3 days after macrolide treatment, even the specimens from all these six patients were macrolide resistance, but the trend differed among the six patients. Kawai et al. also found that in macrolide-resistant patients, some demonstrated a rapid decrease in the copy number of *M. pneumoniae* after 48 h of macrolide treatment, whereas others demonstrated no or only a slow decrease (Kawai et al., 2012). The high macrolide resistance in the present study indicated that the decrease copy number after treatment may have resulted from a combination of factors. The immunomodulatory effects of the macrolide therapy, and the host immune response are potentially involved. Utilization of macrolides in the presence of macrolide resistance mutations is controversial as to the effectiveness of therapy, which is not addressed in this study. Patient A was initially deemed negative for *M. pneumoniae* infection after real-time PCR, but a second sample 3 days later showed the patient to be positive. Which may because the first sample was collected at the initial stage of infection when the bacterial load was lower. When we tested the two samples by ddPCR, both samples were positive, but the first one showed only three copy numbers. This also demonstrated that ddPCR had higher sensitivity than real-time PCR.

Increasing test sensitivity, such as ddPCR, could help screen samples with low copy numbers, but that does not indicate true infection. Asymptomatic carriers of *M. pneumoniae* should also be considered (Spuesens et al., 2013). In that circumstance, the laboratory test results need to be confirmed with clinical symptoms, and resampling is necessary for diagnosis. If the patient is indeed infected, the copy number of the second sample usually increases with disease progression, as was the case in patient A in our study.

There were some limitations to this study. First, the clinical sample size was small. A larger size will give more accurate information, especially in terms of sensitivity, specificity and treatment efficiency. Second, only five *Mycoplasma* species were applied for specificity test. The other species which relevant to human disease should also be included. Last, different specimen types was related with bacterial load, only one sample type was collected from each patient, the difference between sample types was not observed in this study.

In conclusion, ddPCR was demonstrated to be a sensitive and accurate assay for *M. pneumoniae* detection, especially for low bacterial load samples, and showed a comparable detection efficiency to that of real-time PCR. ddPCR enabled absolute quantification of nucleic acids, without the need for a standard curve or reference sample each time; therefore, its performance in evaluating disease severity and treatment efficacy was excellent. However, ddPCR needs expensive equipment, complex operation, and experienced staff for evaluation of the results, which limit its widespread clinical application (Diaz and Winchell, 2016).

Data availability statement

The original contributions presented in the study are included in the article/Supplementary material, further inquiries can be directed to the corresponding authors.

Ethics statement

The studies involving human participants were reviewed and approved by the Ethics Committee of Capital Institute of Pediatrics. Written informed consent to participate in this study was provided by the participants' legal guardian/next of kin.

Author contributions

GX and JY designed and supervised the study. GX, HZ, and CY created the study methodology. HZ, CY, and YF collected clinical samples clinical data. HZ, JF, CY, BD, YF, XC, JC, LG, ZF, ZX, TF, and ZY processed samples and generated experimental data. GX, JY, HZ, and CY drafted and revised the manuscript. JY and GX obtained funding. All authors have confirmed that they have read and approved the final version of the manuscript.

Funding

This work was supported by grants from the National Natural Science Foundation of China (32170201 and 82002191), National Natural Science Foundation for Key Programs of China Grants (82130065), Beijing Natural Science Foundation (7222014), FENG foundation (FFBR 202103), the Research Foundation of Capital Institute of Pediatrics (CXYJ-2021-04), and Beijing high-level public health technical talent project-02-08.

Acknowledgments

The authors thank Suzanne Leech and Cathel Kerr from Liwen Bianji (Edanz; www.liwenbianji.cn) for basic language editing of a draft of this manuscript.

Conflict of interest

The authors declare that the research was conducted in the absence of any commercial or financial relationships that could be construed as a potential conflict of interest.

Publisher's note

Supplementary material

The Supplementary material for this article can be found online at: https://www.frontiersin.org/articles/10.3389/fmicb.2023.1177273/full#supplementary-material

References

Atkinson, T. P., Balish, M. F., and Waites, K. B. (2008). Epidemiology, clinical manifestations, pathogenesis and laboratory detection of *Mycoplasma pneumoniae* infections. *FEMS Microbiol. Rev.* 32, 956–973. doi: 10.1111/j.1574-6976.2008.00129.x

Diaz, M. H., and Winchell, J. M. (2016). The evolution of advanced molecular diagnostics for the detection and characterization of *Mycoplasma pneumoniae*. *Front. Microbiol.* 7:232. doi: 10.3389/fmicb.2016.00232

Dorigo-Zetsma, J. W., Zaat, S. A. J., Vriesema, A. J. M., and Dankert, J. (1999). Demonstration by a nested PCR for *Mycoplasma pneumoniae* that *M. pneumoniae* load in the throat is higher in patients hospitalised for *M.pneumoniae* infection than in non-hospitalised subjects. *J. Med. Microbiol.* 48, 1115–1122. doi: 10.1099/00222615-48-12-1115

Dumke, R., Schurwanz, N., Lenz, M., Schuppler, M., Lück, C., and Jacobs, E. (2007). Sensitive detection of *Mycoplasma pneumoniae* in human respiratory tract samples by optimized real-time PCR approach. *J. Clin. Microbiol.* 45, 2726–2730. doi: 10.1128/JCM.00321-07

Fan, L., Li, D., Zhang, L., Hao, C., Sun, H., Shao, X., et al. (2017). Pediatric clinical features of *Mycoplasma pneumoniae* infection are associated with bacterial P1 genotype. *Exp. Ther. Med.* 14, 1892–1898. doi: 10.3892/etm.2017.4721

Hindson, B. J., Ness, K. D., Masquelier, D. A., Belgrader, P., Heredia, N. J., Makarewicz, A. J., et al. (2011). High-throughput droplet digital PCR system for absolute quantitation of DNA copy number. *Anal. Chem.* 83, 8604–8610. doi: 10.1021/ac202028g

Izumikawa, K. (2016). Clinical features of severe or fatal *Mycoplasma pneumoniae* pneumonia. *Front. Microbiol.* 7:800. doi: 10.3389/fmicb.2016.00800

Jeremiah Matson, M., Ricotta, E., Feldmann, F., Massaquoi, M., Sprecher, A., Giuliani, R., et al. (2022). Evaluation of viral load in patients with Ebola virus disease in Liberia: a retrospective observational study. *Lancet Microbe* 3, e533–e542. doi: 10.1016/S2666-5247(22)00065-9

Kawai, Y., Miyashita, N., Yamaguchi, T., Saitoh, A., Kondoh, E., Fujimoto, H., et al. (2012). Clinical efficacy of macrolide antibiotics against genetically determined macrolide-resistant *Mycoplasma pneumoniae* pneumonia in paediatric patients. *Respirology* 17, 354–362. doi: 10.1111/j.1440-1843.2011.02102.x

Kuypers, J., and Jerome, K. R. (2017). Applications of digital PCR for clinical microbiology. *J. Clin. Microbiol.* 55, 1621–1628. doi: 10.1128/JCM.00211-17

Leal, S. M., Totten, A. H., Xiao, L., Crabb, D. M., Ratliff, A., Duffy, L. B., et al. (2020). Evaluation of commercial molecular diagnostic methods for detection and determination of macrolide resistance in *Mycoplasma pneumoniae*. *J. Clin. Microbiol.* 58, e00242–e00220. doi: 10.1128/JCM.00242-20

Leuzinger, K., Gosert, R., Søgaard, K. K., Naegele, K., Bielicki, J., Roloff, T., et al. (2021). Epidemiology and precision of SARS-CoV-2 detection following lockdown and relaxation measures. *J. Med. Virol.* 93, 2374–2384. doi: 10.1002/jmv.26731

Li, H., Bai, R., Zhao, Z., Tao, L., Ma, M., Ji, Z., et al. (2018). Application of droplet digital PCR to detect the pathogens of infectious diseases. *Biosci. Rep.* 38:20181170. doi: 10.1042/BSR20181170

Li, Z., Pan, L., Lyu, L., Li, J., Jia, H., du, B., et al. (2020). Diagnostic accuracy of droplet digital PCR analysis of cerebrospinal fluid for tuberculous meningitis in adult patients. *Clin. Microbiol. Infect.* 26, 213–219. doi: 10.1016/j.cmi.2019.07.015

Li, F., Zhang, Y., Shi, P., Cao, L., Su, L., Fu, P., et al. (2022). Mycoplasma pneumoniae and adenovirus coinfection cause pediatric severe community-acquired pneumonia. *Microbiol. Spectr.* 10:e0002622. doi: 10.1128/spectrum.00026-22

Liu, X., Feng, J., Zhang, Q., Guo, D., Zhang, L., Suo, T., et al. (2020). Analytical comparisons of SARS-COV-2 detection by qRT-PCR and ddPCR with multiple primer/probe sets. *Emerg. Microb. Infect.* 9, 1175–1179. doi: 10.1080/22221751.2020.1772679

Milosevic, D., Moyer, A. M., Majumdar, R., Kipp, B. R., and Yao, J. D. (2022). A reverse-transcription droplet digital PCR assay to detect and quantify SARS-CoV-2 RNA in upper respiratory tract specimens. *J. Clin. Virol.* 153:105216. doi: 10.1016/j.jcv.2022.105216

Nilsson, A. C., Björkman, P., Welinder-Olsson, C., Widell, A., and Persson, K. (2010). Clinical severity of *Mycoplasma pneumoniae* (MP) infection is associated with bacterial load in oropharyngeal secretions but not with MP genotype. *BMC Infect. Dis.* 10:39. doi: 10.1186/1471-2334-10-39

Sedlak, R. H., Nguyen, T., Palileo, I., Jerome, K. R., and Kuypers, J. (2017). Superiority of digital reverse transcription-PCR (RT-PCR) over real-time RT-PCR for quantitation of highly divergent human rhinoviruses. *J. Clin. Microbiol.* 55, 442–449. doi: 10.1128/JCM.01970-16

Spuesens, E. B., Fraaij, P. L., Visser, E. G., Hoogenboezem, T., Hop, W. C., van Adrichem, L. N., et al. (2013). Carriage of *Mycoplasma pneumoniae* in the upper respiratory tract of symptomatic and asymptomatic children: an observational study. *PLoS Med.* 10:e1001444. doi: 10.1371/journal.pmed.1001444

Taylor, S. C., Laperriere, G., and Germain, H. (2017). Droplet digital PCR versus qPCR for gene expression analysis with low abundant targets: from variable nonsense to publication quality data. *Sci. Rep.* 7:2409. doi: 10.1038/s41598-017-02217-x

The Subspecialty Group of Respiratory Disease (2013). The Society of Pediatrics, Chinese Medical Association, the editorial board, Chinese journal of pediatrics. Guidelines for management of community acquired pneumonia in children (the revised edition of 2013) (I). *Chin J Pediatr* 51, 745–799.

Waites, K. B., Xiao, L., Liu, Y., Balish, M. F., and Atkinson, T. P. (2017). *Mycoplasma pneumoniae* from the respiratory tract and beyond. *Clin. Microbiol. Rev.* 30, 747–809. doi: 10.1128/CMR.00114-16

Wang, M., Wang, Y., Yan, Y., Zhu, C., Huang, L., Shao, X., et al. (2014). Clinical and laboratory profiles of refractory *Mycoplasma pneumoniae* pneumonia in children. *Int. J. Infect. Dis.* 29, 18–23. doi: 10.1016/j.ijid.2014.07.020

Winchell, J. M., and Mitchell, S. L. (2013). Detection of *Mycoplasma pneumoniae* by real-time PCR. *Methods Mol. Biol.* 943, 149–158. doi: 10.1007/978-1-60327-353-4_10

Xiao, L., Ptacek, T., Osborne, J. D., Crabb, D. M., Simmons, W. L., Lefkowitz, E. J., et al. (2015). Comparative genome analysis of *Mycoplasma pneumoniae*. *BMC Genomics* 16:610. doi: 10.1186/s12864-015-1801-0

Xue, G., Li, S., Zhao, H., et al. (2020). Use of a rapid recombinase-aided amplification assay for *Mycoplasma pneumoniae* detection. *BMC Infect. Dis.* 20:79. doi: 10.1186/s12879-019-4750-4

Yu, F., Yan, L., Wang, N., Yang, S., Wang, L., Tang, Y., et al. (2020). Quantitative detection and viral load analysis of SARS-CoV-2 in infected patients. *Clin. Infect. Dis.* 71, 793–798. doi: 10.1093/cid/ciaa345

Zhang, C., Zhang, Q., Du, J. L., Deng, D., Gao, Y. L., Wang, C. L., et al. (2020). Correlation between the clinical severity, bacterial load, and inflammatory reaction in children with *Mycoplasma Pneumoniae* pneumonia. *Curr. Med. Sci.* 40, 822–828. doi: 10.1007/s11596-020-2261-6

Zhao, F., Guan, X., Li, J., Liu, L., Gong, J., He, L., et al. (2020). Real-time PCR and quantitative culture for *Mycoplasma pneumoniae* load in pharyngeal swabs from children at preliminary diagnosis and discharge. *Biomed. Res. Int.* 2020, 1–8. doi: 10.1155/2020/9814916

Zhou, Y., Shan, Y., Cui, Y., Shi, J., Wang, F., Miao, H., et al. (2021). Characteristics and outcome of severe *Mycoplasma pneumoniae* pneumonia admitted to PICU in Shanghai: a retrospective cohort study. *Crit. Care Explor.* 3:e0366. doi: 10.1097/CCE.0000000000000366

Zhou, Y., Zhang, Y., Sheng, Y., Zhang, L., Shen, Z., and Chen, Z. (2014). More complications occur in macrolide-resistant than in macrolide-sensitive *Mycoplasma pneumoniae* pneumonia. *Antimicrob. Agents Chemother.* 58, 1034–1038. doi: 10.1128/AAC.01806-13

frontiers | Frontiers in Microbiology

TYPE Original Research
PUBLISHED 06 July 2023
DOI 10.3389/fmicb.2023.1181912

OPEN ACCESS

EDITED BY
Wafa Achour,
Centre National de Greffe de Moelle Osseuse, Tunisia

REVIEWED BY
Indu Kumari,
Regional Centre for Biotechnology (RCB), India
Takashi Kato,
Yasuda Women's University, Japan

*CORRESPONDENCE
Ming-Ming Shao
✉ michelle_0913@163.com
Huan-Zhong Shi
✉ shihuanzhong@sina.com

†These authors have contributed equally to this work

RECEIVED 08 March 2023
ACCEPTED 19 June 2023
PUBLISHED 06 July 2023

CITATION
Zheng S-C, Huang Z-Y, Zhai K, Shi H-Z and Shao M-M (2023) Hepatocyte growth factor combined with adenosine deaminase as biomarker for diagnosis of tuberculous pleural effusion.
Front. Microbiol. 14:1181912.
doi: 10.3389/fmicb.2023.1181912

Hepatocyte growth factor combined with adenosine deaminase as biomarker for diagnosis of tuberculous pleural effusion

Sheng-Cai Zheng[1,2†], Zhong-Yin Huang[1,2†], Kan Zhai[1,2], Huan-Zhong Shi[1,2*] and Ming-Ming Shao[1,2*]

[1]Department of Respiratory and Critical Care Medicine, Beijing Institute of Respiratory Medicine and Beijing Chao-Yang Hospital, Capital Medical University, Beijing, China, [2]Clinical Center for Pleural Diseases, Capital Medical University, Beijing, China

Background: The simple, rapid, and accurate diagnosis of tuberculous pleural effusion (TPE) remains difficult. This study aimed to determine the accuracy of hepatocyte growth factor (HGF) in the diagnosis of TPE.

Methods: We quantified the expression of HGF, adenosine deaminase (ADA), and interferon gamma (IFN-γ) in pleural effusion (PE) in 97 TPE subjects and 116 non-TPE subjects using an enzyme-linked immunosorbent assay (ELISA) or a fully automatic biochemical analyzer. The diagnostic performance of these three biomarkers was evaluated using a receiver operating characteristic (ROC) curve of subjects by age and gender.

Results: We discovered that the TPE group had much higher levels of HGF than the non-TPE group, regardless of age or gender, and that there was no statistically significant difference between the two groups' levels of HGF expression in peripheral plasma. In female TPE patients aged ≤65 years, the AUCs of TPE and non-TPE diagnosed by HGF, ADA or IFN-γ were 0.988, 0.964, and 0.827, respectively. HGF plus ADA had the highest diagnostic efficacy in female TPE patients aged ≤65 years. With HGF plus ADA having a cut-off value of 0.219 for distinguishing TPE from non-TPE, the area under the curve (AUC), sensitivity (SEN), specificity (SPE), positive predictive value (PPV), and negative predictive value (NPV) were, respectively, 0.998 (95% confidence interval [CI], 0.993–1.000), 100 (95% CI, 89.997–100.000), 96.667 (95% CI, 82.783–99.916), 97.222 (95% CI, 83.594–99.586), and 100.

Conclusion: This study confirmed that HGF plus ADA has high diagnostic efficacy in younger female TPE patients and has the potential to be an excellent biomarker.

KEYWORDS

tuberculous pleural effusion, HGF, ADA, diagnostic efficacy, biomarkers

Introduction

Tuberculosis (TB) is by far the leading cause of death from infectious disease worldwide, disproportionately affecting immunosuppressed patients and socioeconomically vulnerable populations (Chakaya et al., 2022). Tuberculous pleural effusion (TPE) is not uncommon clinically, but its diagnosis is difficult (Baumann et al., 2007; Pang et al., 2019; Kang et al., 2020).

In the diagnosis of TPE, the available gold standards are as follows: (1) microscopic examination of Ziehl–Neelsen staining smear; (2) *Mycobacterium tuberculosis* (*Mtb*) culture detection in pleural effusion (PE); and (3) pleural biopsy (PB), followed by pathological microscopy. However, the detection rates of the first two methods are often low, while the last is an invasive examination with certain surgical risks and complications that has low patient acceptance. Biomarkers are a fast, simple diagnostic method (Porcel, 2016; Zhang et al., 2020); therefore, it is important to find reliable biomarkers of TPE such as adenosine deaminase (ADA). Originally, hepatocyte growth factor (HGF) was identified as a liver-regenerative circulatory factor and named for its increased protein expression levels after liver injury or hepatectomy (Nakamura et al., 1989; Sonnenberg et al., 1993; Zhao et al., 2022). Many studies have demonstrated that HGF has a variety of activities, including mitosis, morphogenesis, and motor effects in different tissues (Stoker et al., 1987; Montesano et al., 1991; Ebens et al., 1996). HGF is a cytokine that plays a pleiotropic role in inflammatory response and immune regulation (Li et al., 2022). Increasing evidence from *in vivo* animal experiments also supports the protective role of HGF in various immune inflammatory diseases, including classic autoimmune diseases such as rheumatoid arthritis (RA) and autoimmune neuroinflammation, and typical inflammatory diseases such as inflammatory bowel disease (IBD) and asthma. Taken together, this evidence suggests that HGF might play an important anti-inflammatory role (Wang M. et al., 2018).

Studies have also reported that HGF levels in PBMCs are significantly downregulated in TB patients compared with LTBI patients or healthy subjects (He et al., 2020). In addition, the expression of HGF in the serum of TB patients has been found to be higher than that in healthy subjects but lower than that in bacterial-pneumonia patients (Huang et al., 1999). One study found that HGF expression in the cerebrospinal fluid (CSF) of Alzheimer disease (AD) patients was higher than in that of patients with other neurological diseases; the AUC for the diagnosis of AD reached 0.802 (Gaetani et al., 2021). Other studies have shown that the level of HGF in the plasma of cirrhosis patients was higher than that in patients with liver fibrosis, with an AUC of 0.71 (Andersen et al., 2011). However, the expression of HGF in TPE and its diagnostic value have not been reported to date. In addition, research suggests that age and gender might play important roles in immune regulation (Markle and Fish, 2014; Giefing-Kröll et al., 2015; Jiang et al., 2020). Therefore, in this study, we analyzed subgroups using age and gender as criteria to determine the diagnostic efficacy of HGF in distinguishing TB patients with TPE from those non-TPE patients.

Materials and methods

Study populations and sample collection

The patients included in this study were admitted to the Department of Respiratory and Critical Care Medicine, Beijing Chaoyang Hospital, Capital Medical University (CMU; Beijing, China) from June 2019 to June 2022. The exclusion criteria were as follows: (1) any invasive pleural surgery or thoracic trauma within 3 months prior to hospitalization; (2) any anti-tubercular chemotherapy, antitumor therapy, glucocorticoids, or other nonsteroidal anti-inflammatory treatment; (3) diabetes; and (4) COVID-19, HIV or latent TB infection. Given that activation of HGF is related to glucose abnormalities or the pathogenesis of diabetes and can affect HGF expression in PEs, we excluded patients with abnormal glucose metabolism or diabetes (Oliveira et al., 2018). Patients with confirmed TPE were included in this study; non-TPE cases included patients with malignant PE (MPE) and parapneumonic PE (PPE).

Clinically, TPE is confirmed if the PE or PB specimen is positive for *Mtb* culture, Ziehl–Neelsen staining is positive, or granuloma is found in pleural biopsy specimens. MPE is confirmed when malignant cells are found in PE and/or PB specimens. PPE is defined as being associated with pulmonary infections such as bacterial pneumonia, lung abscess, and bronchiectasis and as featuring the presence of PE.

In this study, we collected PEs and peripheral blood samples and centrifuged them at 400 g for 10 min. The supernatant was separated and stored at −80°C for subsequent detection of HGF, ADA, and interferon gamma (IFN-γ).

This study was approved by the Ethics Committee of Beijing Chao-Yang Hospital of CMU. All participants were fully informed about this study and signed informed-consent forms.

Determination of HGF, ADA, and IFN-γ protein concentrations

We measured the levels of HGF and IFN-γ in PE using enzyme-linked immunosorbent assay (ELISA) kits (Thermo Fisher Scientific, Waltham, MA, USA) as per manufacturer's instructions. The expression of ADA in PE was detected using a fully automatic biochemical analyzer (Toshiba Corp., Tokyo, Japan) as per manufacturer's instructions. All samples were assessed in duplicate.

Statistical analysis

Continuous statistics in this study are expressed as medians (25th–75th percentiles). Categorical data are described by frequency. If data did not conform to a normal distribution, we used the Mann–Whitney *U* test to compare differences in continuous statistics between groups and the χ^2 test to compare categorical data. Receiver operating characteristic (ROC) analysis was used to determine the ability of HGF, ADA, and IFN-γ to distinguish TPE from non-TPE, expressed as the area under the curve (AUC) (Hanley and McNeil, 1982; Zweig and Campbell, 1993). We used GraphPad Prism version 8.0 (GraphPad Software, Inc., San Diego, CA, USA) and MedCalc 20.0.4 (MedCalc Software Ltd., Ostend, Belgium) for statistical analysis. $p < 0.05$ was considered statistically significant.

Results

Clinical and demographic characteristics of patients with pleural effusion

Some data on diagnostic types, complications, and demographics for TPE and non-TPE patient groups are shown in Table 1. Based on our preliminary results, we used 65 years as the cut-off value for the age subgroups: the younger group was ≤65 years of age, and the

TABLE 1 Baseline characteristics according to study population.

Variable	Total population	TPE (n=97)	Non-TPE (n=116)	*p*-value
Gender, male/female, n	131/82	58/39	73/43	0.639
Age, years	50 (35, 65)	35 (31, 45)	63 (52, 67)	<0.0001
Diagnosis				
tuberculosis		97	0	-
lung cancer		0	95	-
mesothelioma		0	1	-
pneumonia		0	20	-
Complication				
Chronic obstructive pulmonary disease		0	1	-
hypertension		0	7	-
hyperlipidemia		0	1	-

Data are presented as median (25th–75th centile). Differences of continuous data between groups were compared using Mann–Whitney U-test, and χ2-test was used for comparisons of categorical data. TPE, tuberculous pleural effusion; non-TPE, non-tuberculous pleural effusion.

elderly group was >65 years of age. In this study, patients with TPE were younger overall than those without TPE ($p < 0.0001$).

Expression of HGF, ADA, and IFN-γ in pleural effusion

Regardless of age or gender, the expression of HGF in the PE of the TPE group was higher than that in the non-TPE group, to a statistically significant degree ($p < 0.0001$; Table 2; Figure 1A). In addition, we found no statistically significant difference in HGF expression in peripheral plasma between the two groups ($p > 0.05$; Supplementary Figure 1A). Other indicators such as ADA and IFN-γ were similar in their differences between age and gender subgroups in the TPE and non-TPE groups (Table 2; Supplementary Figure 1).

Diagnostic value of HGF in pleural effusion

In the overall cohort, with a cut-off value of 9314.84 pg./mL, the AUC, sensitivity (SEN), specificity (SPE), positive likelihood ratio (PLR), negative likelihood ratio (NLR), positive predictive value (PPV), and negative predictive value (NPV) of HGF expression in PE to discriminate between TPE and non-TPE cases were 0.835 (95% confidence interval [CI], 0.780–0.890; $p < 0.001$), 85.567, 71.552%, 3.008, 0.202, 71.552, and 85.567, respectively (Table 3; Figure 1B). Meanwhile, the AUCs of ADA and IFN-γ were 0.932 and 0.833, respectively (Supplementary Figures 1B,D).

We also measured the diagnostic accuracy of HGF in the PE of different subgroups. With a cut-off value of 7023.44 pg./mL, the AUC of HGF in the younger female group to differentiate between TPE and non-TPE cases was 0.988 (95% CI, 0.966–1.000; $p < 0.001$), while its Sen,

TABLE 2 Concentrations of HGF, ADA, and IFN-γ in PF according to age and/or gender.

Variable	TPE	non-TPE	*p*-value
HGF, pg./mL			
All ages	13715.00 (10433.00, 17998.00)	6511.30 (3082.50, 9948.80)	<0.0001
M	13905.00 (10938.00, 18018.00)	7214.00 (2686.00, 9935.00)	<0.0001
F	13476.00 (9991.00, 18049.00)	6012.00 (3787.00, 10856.00)	<0.0001
Age ≤ 65 y	13834.00 (10458.00, 18291.00)	4392.00 (2497.00, 6930.00)	<0.0001
M	14007.00 (10726.00, 19253.00)	4051.00 (1840.00, 7492.00)	<0.0001
F	13587.00 (9991.00, 18049.00)	4901.00 (2822.00, 6447.00)	<0.0001
Age > 65 y	13476.00 (10284.00, 16098.00)	10695.00 (8805.00, 17920.00)	0.2569
ADA, U/L			
All ages	36.10 (28.40, 41.45)	8.60 (6.33, 12.80)	<0.0001
M	38.40 (28.45, 44.45)	9.60 (6.450, 13.00)	<0.0001
F	34.40 (27.50, 38.00)	7.30 (5.90, 12.80)	<0.0001
Age ≤ 65 y	36.80 (30.58, 42.10)	9.00 (7.00, 14.00)	<0.0001
M	39.60 (34.00, 46.50)	10.60 (7.30, 14.80)	<0.0001
F	34.40 (29.00, 38.00)	6.90 (5.99, 13.28)	<0.0001
Age > 65 y	24.00 (16.00, 30.00)	8.00 (5.50, 12.50)	0.0002
IFN-γ, pg./mL			
All ages	2346.00 (819.30, 5066.00)	2.12 (0.00, 6.78)	<0.0001
M	2027.00 (725.60, 42,670)	1.40 (0.00, 6.125)	<0.0001
F	2371.00 (883.70, 5875.00)	3.45 (0.00, 11.95)	<0.0001
Age ≤ 65 y	2510.00 (1126.00, 5269.00)	2.12 (0.00, 6.54)	<0.0001
M	2445.00 (1138.00, 5268.00)	1.76 (0.00, 4.44)	<0.0001
F	2575.00 (1088.00, 5875.00)	3.45 (0.78, 152.80)	<0.0001
Age > 65 y	592.20 (0.00, 1222.00)	1.58 (0.00, 7.15)	0.106

Data are presented as median (25th–75th centile). Differences between groups were compared using Mann–Whitney U-test for HGF, ADA, and IFN-γ. TPE, tuberculous pleural effusion; non-TPE, non-tuberculous pleural effusion. HGF, hepatocyte growth factor; ADA, adenosine deaminase; IFN-γ, interferon gamma. M, male; F, female.

SPC, PLR, NLR, PPV, and NPV were 97.143, 93.333%, 14.571, 0.031, 94.444, and 96.552, respectively (Table 4; Figure 1F). The male group, female group, younger group, and younger male group had AUCs of 0.847 (95% CI, 0.781–0.913; Table 3; Supplementary Figure 1F), 0.811 (95% CI, 0.711–0.911; Table 3; Supplementary Figure 1L), 0.967 (95% CI, 0.942–0.991; Table 3; Supplementary Figure 2D), and 0.950 (95% CI, 0.910–0.990; Table 3; Supplementary Figure 2J), respectively. The diagnostic-accuracy parameters of ADA and IFN-γ in different subgroups are shown in Tables 4, 5 and in Supplementary Figure 2.

Diagnostic value of HGF plus ADA, HGF plus IFN-γ and ADA plus IFN-γ in pleural effusion

In the age ≤65 years group, the AUC values of HGF combined with ADA, HGF combined with IFN-γ, and ADA combined with IFN-γ were 0.982, 0.974, and 0.952, respectively (Table 6; Figures 2A–C). In the males aged ≤65 years group, the AUCs of HGF plus ADA, HGF plus IFN-γ, and ADA plus IFN-γ were 0.972, 0.966, and 0.946, respectively (Table 7; Figures 2D–F). In the females aged ≤65 years group, the AUCs of HGF plus ADA, HGF plus IFN-γ, and ADA plus IFN-γ were 0.998, 0.990, and 0.970, respectively (Table 8; Figures 2G–I). In different subgroups, the AUCs of HGF plus ADA and of HGF plus IFN-γ were higher than those of each of HGF, ADA, and IFN-γ alone. In addition, the AUC of HGF plus ADA was higher than that of HGF plus IFN-γ or of ADA plus IFN-γ, especially in the females aged ≤65 years group, where we found that the AUC of HGF plus ADA peaked at 0.998 (Figure 2G). With a cut-off of 0.219, the

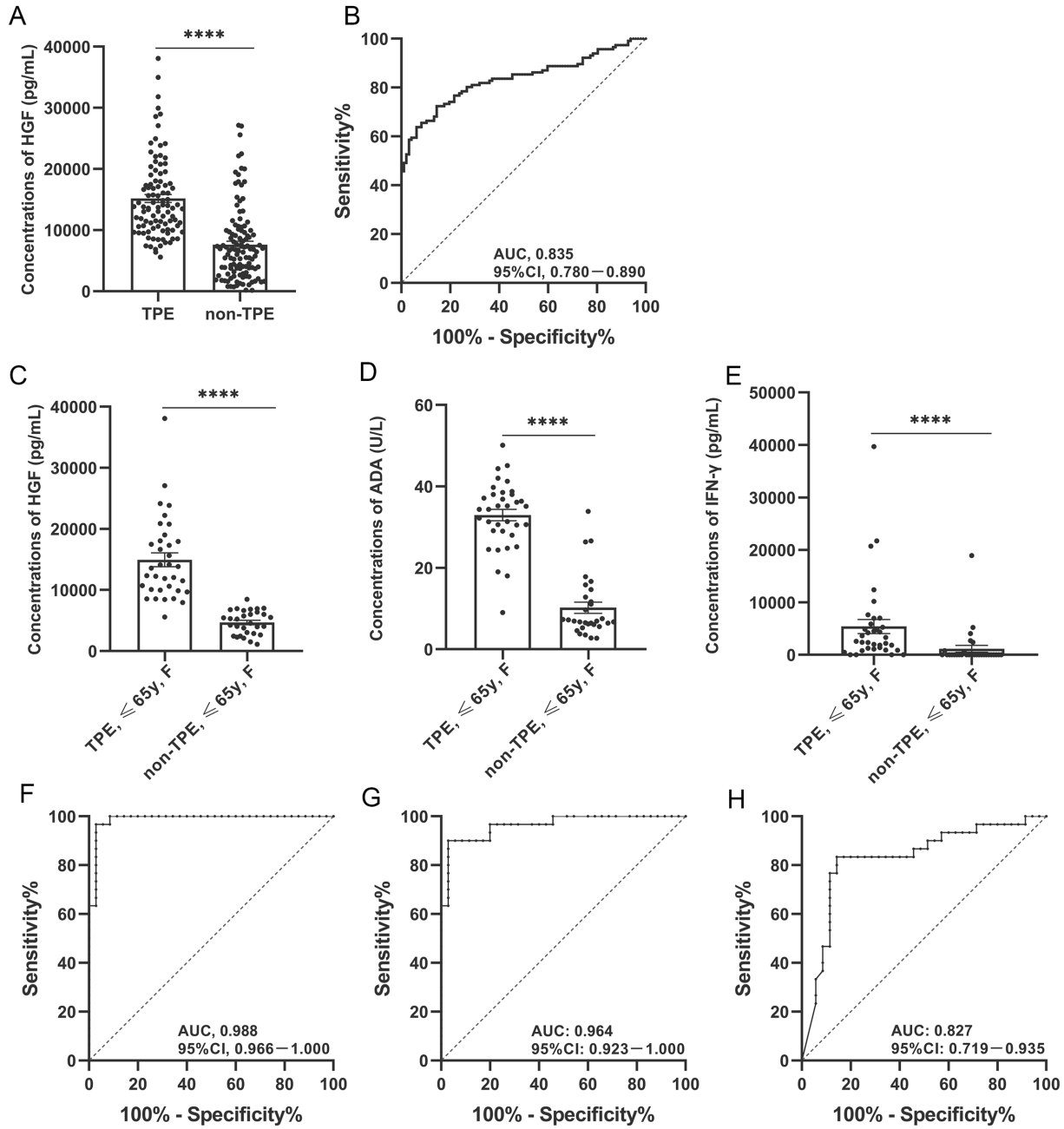

FIGURE 1
Diagnostic accuracy of HGF, ADA, and IFN-γ in PE for TPE overall or by gender. Expression of HGF in PE from TPE and non-TPE patients **(A)**; expression of HGF, ADA, and IFN-γ in PE from female TPE and non-TPE patients aged ≤65years, respectively **(C–E)**. ROC curves show the diagnostic value of HGF in TPE and non-TPE patients **(B)**. ROC curves show the diagnostic value of HGF, ADA, and IFN-γ in female TPE and non-TPE patients aged ≤65years **(F–H)**. *p<0.05, **p<0.01, ***p<0.001, ****p<0.0001. TPE, tuberculous pleural effusion; non-TPE, non-tuberculous pleural effusion. HGF, hepatocyte growth factor; ADA, adenosine deaminase; IFN-γ, interferon gamma. F, female.

TABLE 3 Diagnostic performance of HGF in PF in differentiating between patients with TPE and those with non-TPE according to age or/and gender.

Variable	Cut-off value (pg/mL)	AUC (95% CI)	Sensitivity (%)	Specificity (%)	PLR	NLR	PPV (%)	NPV (%)
HGF, all ages	>9314.84	0.835	85.567	71.552	3.008	0.202	71.552	85.567
			(76.971–91.879)	(62.429–79.541)	(2.228–4.060)	(0.123–0.332)	(65.076–77.247)	(78.276–90.702)
M	>10695.41	0.847	77.586	82.192	4.357	0.273	77.586	82.192
			(64.728–87.491)	(71.475–90.163)	(2.611–7.269)	(0.167–0.445)	(67.477–85.240)	(73.862–88.288)
F	>7023.44	0.811	97.436	67.442	2.993	0.038	73.077	96.667
			(86.524–99.935)	(51.456–80.924)	(1.941–4.615)	(0.005–0.266)	(63.769–80.717)	(80.557–99.510)
HGF, age ≤ 65 y	>8224.00	0.967	91.860	91.781	11.176	0.089	92.941	90.541
			(83.946–96.665)	(82.964–96.924)	(5.179–24.118)	(0.043–0.181)	(85.918–96.600)	(82.426–95.130)
M	>9223.83	0.950	86.275	90.698	9.275	0.151	91.667	84.783
			(73.745–94.299)	(77.865–97.407)	(3.624–23.736)	(0.076–0.303)	(81.126–96.570)	(73.554–91.777)
F	>7023.44	0.988	97.143	93.333	14.571	0.031	94.444	96.552
			(85.083–99.928)	(77.926–99.182)	(3.815–55.657)	(0.004–0.212)	(81.654–98.483)	(80.187–99.486)

AUC, area under the curve; PLR, positive likelihood ratio; NLR, negative likelihood ratio; PPV, positive predictive value; NPV, negative predictive value. TPE, tuberculous pleural effusion; non-TPE, non-tuberculous pleural effusion. HGF, hepatocyte growth factor; ADA, adenosine deaminase; IFN-γ, interferon gamma. M, male; F, female.

TABLE 4 Diagnostic performance of ADA in PF in differentiating between patients with TPE and those with non-TPE according to age or/and gender.

Variable	Cut-off value (U/L)	AUC (95% CI)	Sensitivity (%)	Specificity (%)	PLR	NLR	PPV (%)	NPV (%)
ADA, all ages	>17.80	0.932	93.814	84.483	6.046	0.073	83.486	94.231
			(87.022–97.696)	(76.589–90.536)	(3.942–9.273)	(0.034–0.160)	(76.724–88.576)	(88.229–97.267)
M	>20.60	0.922	89.655	86.301	6.545	0.120	83.871	91.304
			(78.831–96.108)	(76.247–93.231)	(3.656–11.717)	(0.056–0.257)	(74.389–90.300)	(83.037–95.749)
F	>17.80	0.951	94.872	88.372	8.159	0.058	88.095	95.000
			(82.676–99.373)	(74.917–96.115)	(3.568–18.659)	(0.015–0.225)	(76.391–94.421)	(83.064–98.660)
ADA, age ≤ 65 y	>23.00	0.938	93.023	86.301	6.791	0.081	88.889	91.304
			(85.431–97.397)	(76.247–93.231)	(3.807–12.113)	(0.037–0.176)	(81.769–93.451)	(82.839–95.805)
M	>23.10	0.927	94.118	86.047	6.745	0.068	88.889	92.500
			(83.758–98.770)	(72.068–94.702)	(3.201–14.214)	(0.023–0.206)	(79.151–94.400)	(80.344–97.383)
F	>17.80	0.964	97.143	90.000	9.714	0.032	91.892	96.429
			(85.083–99.928)	(73.471–97.888)	(3.315–28.464)	(0.005–0.220)	(79.457–97.077)	(79.582–99.468)

AUC, area under the curve; PLR, positive likelihood ratio; NLR, negative likelihood ratio; PPV, positive predictive value; NPV, negative predictive value. TPE, tuberculous pleural effusion; non-TPE, non-tuberculous pleural effusion. HGF, hepatocyte growth factor; ADA, adenosine deaminase; IFN-γ, interferon gamma. M, male; F, female.

SEN, SPE, PLR, NLR, PPV, and NPV of HGF plus ADA in the younger female group to differentiate between TPE and non-TPE cases were 100, 96.667%, 30, 0, 97.222, and 100%, respectively (Table 8).

Discussion

The World Health Organization (WHO)'s *Global tuberculosis report 2021* paints a rather grim picture of the trajectory of the global TB epidemic: a slow decline in incidence, but an increase in deaths due to TB. Not all of the objectives stated at the 2018 UN High Level Meeting on TB have been achieved (Chakaya et al., 2022). In addition, the pleura is a common locus of extrapulmonary TB (EPTB), with tuberculous pleurisy occurring in about 50% of EPTB patients (Kang et al., 2020; Shaw and Koegelenberg, 2021). Early animal investigations imply that delayed hypersensitivity brought on by *Mtb* infiltrating into the chest cavity, rather than a direct infection-induced local inflammatory response, is what causes tuberculous pleurisy (Chakrabarti and Davies, 2006; Shaw et al., 2019; Shaw and Koegelenberg, 2021). In addition, the bacterial load of *Mtb* in PE is often low, making the diagnosis of TPE more difficult and often requiring invasive surgery to obtain sufficient pleural tissue for histological and microbiological examination to confirm the diagnosis (Wang et al., 2015; Carlucci et al., 2019). Considering that invasive chest examination causes some harm to patients, it is valuable to explore soluble biomarkers for the diagnosis of TPE (Wang et al., 2015; Wang W. et al., 2018; Zhang et al., 2020).

TABLE 5 Diagnostic performance of IFN-γ in PF in differentiating between patients with TPE and those with non-TPE according to age or/and gender.

Variable	Cut-off value (pg/mL)	AUC (95% CI)	Sensitivity (%)	Specificity (%)	PLR	NLR	PPV (%)	NPV (%)
IFN-γ, all ages	>159.48	0.833	87.629	85.345	5.979	0.145	83.333	89.189
			(79.387–93.441)	(77.576–91.225)	(3.830–9.335)	(0.085–0.248)	(76.205–88.644)	(82.853–93.371)
M	>159.48	0.823	86.207	87.671	6.992	0.157	84.746	88.889
			(74.619–93.852)	(77.882–94.205)	(3.760–13.003)	(0.082–0.301)	(74.922–91.175)	(80.695–93.869)
F	>34.12	0.844	89.744	81.395	4.824	0.126	81.395	89.744
			(75.779–97.134)	(66.599–91.609)	(2.558–9.095)	(0.049–0.322)	(69.884–89.187)	(77.377–95.724)
IFN-γ, age ≤ 65 y	>149.60	0.852	90.698	82.192	5.093	0.113	85.714	88.235
			(82.491–95.898)	(71.475–90.163)	(3.097–8.376)	(0.058–0.221)	(78.487–90.798)	(79.354–93.604)
M	>149.60	0.869	92.157	86.047	6.605	0.091	88.679	90.244
			(81.119–97.822)	(72.068–94.702)	(3.131–13.934)	(0.035–0.235)	(78.782–94.294)	(78.180–95.981)
F	>793.66	0.827	85.714	80.000	4.286	0.179	83.333	82.759
			(69.743–95.194)	(61.433–92.286)	(2.069–8.879)	(0.078–0.410)	(70.705–91.196)	(67.647–91.680)

TPE, tuberculous pleural effusion; non-TPE, non-tuberculous pleural effusion. HGF, hepatocyte growth factor; ADA, adenosine deaminase; IFN-γ, interferon gamma. M, male; F, female. AUC, area under the curve; PLR, positive likelihood ratio; NLR, negative likelihood ratio; PPV, positive predictive value; NPV, negative predictive value.

TABLE 6 Diagnostic performance of HGF+ADA, HGF+IFN-γ, and ADA+IFN-γ in PF in differentiating between patients with TPE and those with non-TPE according to no more than 65years.

	Variable	Cut-off value	AUC (95% CI)	Sensitivity (%)	Specificity (%)	PLR	NLR	PPV (%)	NPV (%)
Age ≤ 65 y	HGF + ADA	>0.319	0.982	96.512	91.781	11.742	0.038	93.258	95.714
			(0.965–0.999)	(90.14–99.28)	(82.96–96.92)	(5.450–25.300)	(0.012–0.116)	(86.523–96.754)	(88.00–98.55)
	HGF + IFN-γ	>0.397	0.974	95.349	91.781	11.601	0.051	93.182	94.366
			(0.952–0.995)	(88.517–98.718)	(82.964–96.924)	(5.382–25.005)	(0.019–0.132)	(86.377–96.717)	(86.518–97.764)
	ADA + IFN-γ	>0.652	0.952	89.535	91.781	10.893	0.114	92.771	88.158
			(0.916–0.988)	(81.061–95.102)	(82.964–96.924)	(5.044–23.527)	(0.061–0.212)	(85.595–96.518)	(79.987–93.273)

TPE, tuberculous pleural effusion; non-TPE, non-tuberculous pleural effusion. HGF, hepatocyte growth factor; ADA, adenosine deaminase; IFN-γ, interferon gamma. M, male; F, female. AUC, area under the curve; PLR, positive likelihood ratio; NLR, negative likelihood ratio; PPV, positive predictive value; NPV, negative predictive value.

In this study, we found that HGF expression was significantly increased in TPE. Further subgrouping by age and gender showed that it had better diagnostic efficacy in distinguishing TPE from non-TPE in female patients aged ≤65 years, with an AUC of 0.988, which was better than the diagnostic efficacy of either ADA or IFN-γ.

We also found that the expression of HGF in the pleural fluid from the TPE group was significantly higher than that of the non-TPE group, suggesting that HGF could play an important regulatory role. Previous studies have reported that age and gender might be independent factors strongly influencing the occurrence and development of diseases. Therefore, we divided TPE and non-TPE patients into age subgroups of ≤65 years and > 65 years. We found that HGF expression in the age ≤ 65 years TPE subgroup was higher than that in the corresponding non-TPE subgroup, and in ROC analysis, the AUC of HGF was higher in the TPE group than in the age > 65 years non-TPE subgroup. Meanwhile, in female TPE patients aged ≤65 years, the AUCs of TPE and non-TPE diagnosed by ADA or IFN-γ were 0.964 and 0.827, respectively. In TPE patients aged ≤65 years, male TPE patients aged ≤65 years or female TPE patients aged ≤65 years, the AUCs of ADA or IFN-γ did not differ significantly, fluctuating between 0.927–0.964 and 0.827–0.869, respectively. In particular, the AUC of female TPE patients aged ≤65 years reached 0.988, which was also higher than those of the corresponding ADA and IFN-γ subgroups.

According to our data, HGF in the PE of younger female patients had a PLR of 14.571, indicating that the probability of positive HGF was 13.571-fold higher in TPE patients than in non-TPE patients, which was high enough for diagnosis. Moreover, an NLR of 0.031 suggested that if the HGF result was negative, the probability of the patient being confirmed to have TPE was 3.1%, which was an acceptable value for ruling out TPE. The high PPV

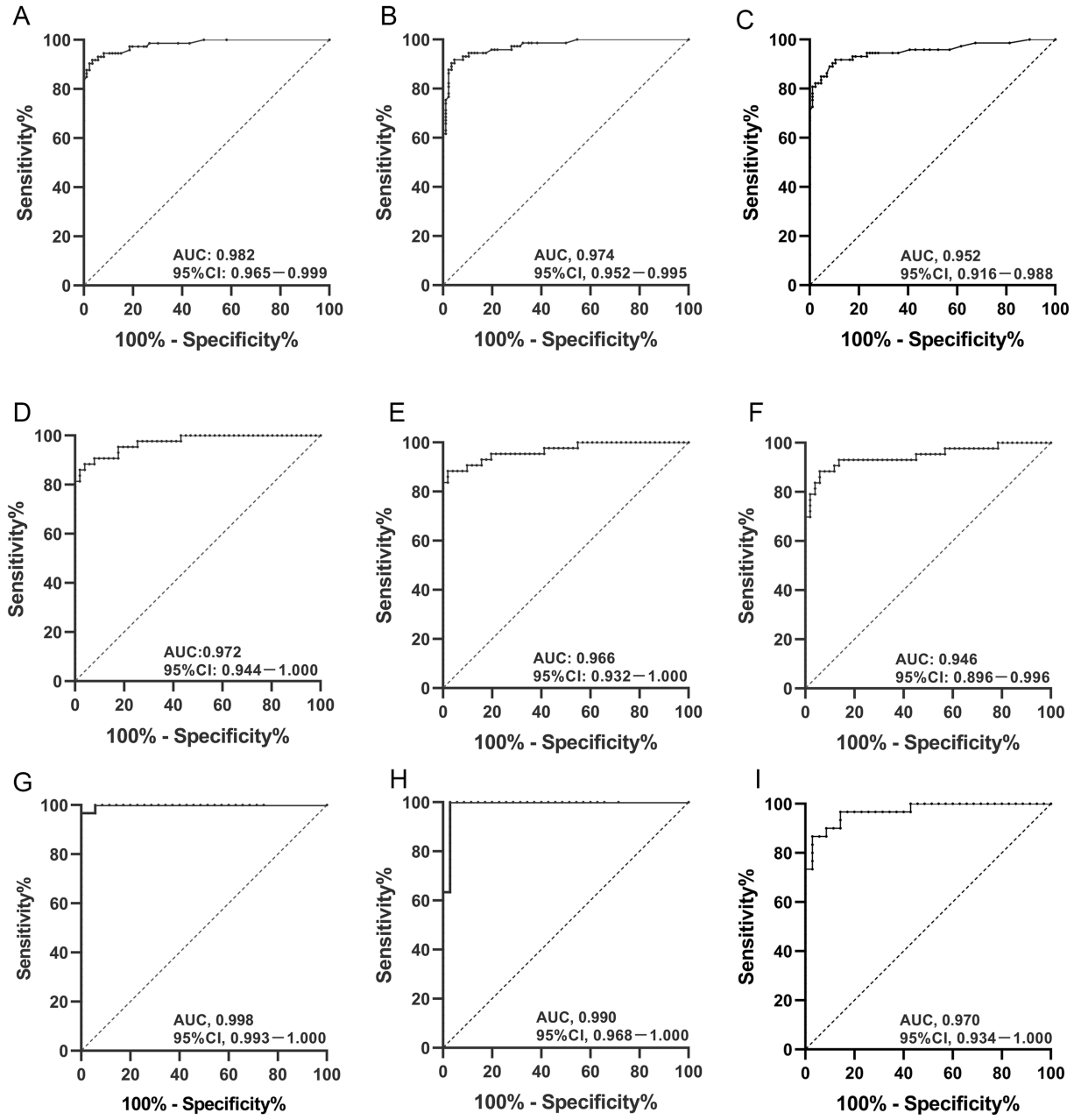

FIGURE 2
Diagnostic accuracy of HGF plus ADA, HGF plus IFN-γ, and ADA plus IFN-γ in PE for TPE by gender or age. AUC values of HGF plus ADA, HGF plus IFN-γ, and ADA plus IFN-γ in PE from TPE patients aged ≤65years **(A–C)**; AUC values of HGF plus ADA, HGF plus IFN-γ, and ADA plus IFN-γ in PE from male TPE patients aged ≤65years **(D–F)**; AUC values of HGF plus ADA, HGF plus IFN-γ, and ADA plus IFN-γ in PE from female TPE patients aged ≤65years **(G–I)**. TPE, tuberculous pleural effusion. HGF, hepatocyte growth factor; ADA, adenosine deaminase; IFN-γ, interferon gamma.

(94.444) and NPV (96.552) of HGF found in this study further indicated that both the false-negative and false-positive rates were low. However, the PLR, NLR, PPV, and NPV of ADA and IFN-γ in PE were less effective than those of HGF, suggesting that HGF had better diagnostic efficacy than ADA or IFN-γ in female TPE patients aged ≤65 years.

In our research, we found that combining multiple factors for diagnosis could improve diagnostic efficacy and help improve differential diagnosis between TPE and non-TPE. Our previous studies showed that the AUC of ADA plus interleukin-32 (IL-32) for the diagnosis of TPE was 0.994, and its SEN, SPE, PLR, NLR, PPV, and NPV were 93.0, 98.4%, 56.7, 0.1, 97.6, and 95.2%, respectively (Du et al., 2022). The SEN, SPE, PLR, NLR, PPV, and NPV of ADA plus IL-27 in the diagnosis of TPE were 91.3, 100%, 140.5, 0.09, 100, and 87.1%, respectively (Wu et al., 2013). In all subgroups, the diagnostic efficacy of HGF plus ADA or HGF plus IFN-γ was significantly higher; in the females aged ≤65 years group, the AUC of HGF plus ADA was the best, reaching 0.998. The AUC of HGF plus ADA in the diagnosis of TPE, meanwhile, was comparable to that of IL-27 plus ADA or IL-32 plus ADA.

TABLE 7 Diagnostic performance of HGF+ADA, HGF+IFN-γ, and ADA+IFN-γ in PF in differentiating between patients with TPE and those with non-TPE according to male with no more than 65years.

	Variable	Cut-off value	AUC (95% CI)	Sensitivity (%)	Specificity (%)	PLR	NLR	PPV (%)	NPV (%)
Age ≤ 65 y, M	HGF + ADA	>0.404	0.972	96.078	88.372	8.263	0.044	90.741	95
			(0.944–1.000)	(86.541–99.522)	(74.917–96.115)	(3.618–18.871)	(0.011–0.173)	(81.100–95.723)	(82.944–98.671)
	HGF + IFN-γ	>0.267	0.966	98.039	86.047	7.026	0.023	89.286	97.368
			(0.932–1.000)	(89.553–99.950)	(72.068–94.702)	(3.341–14.774)	(0.003–0.159)	(79.851–94.601)	(84.111–99.615)
	ADA + IFN-γ	>0.497	0.946	94.118	88.372	8.094	0.067	90.566	92.683
			(0.896–0.996)	(83.758–98.770)	(74.917–96.115)	(3.541–18.504)	(0.022–0.201)	(80.766–95.642)	(80.781–97.447)

TPE, tuberculous pleural effusion; non-TPE, non-tuberculous pleural effusion. HGF, hepatocyte growth factor; ADA, adenosine deaminase; IFN-γ, interferon gamma. M, male; F, female. AUC, area under the curve; PLR, positive likelihood ratio; NLR, negative likelihood ratio; PPV, positive predictive value; NPV, negative predictive value.

TABLE 8 Diagnostic performance of HGF+ADA, HGF+IFN-γ, and ADA+IFN-γ in PF in differentiating between patients with TPE and those with non-TPE according to female with no more than 65years.

	Variable	Cut-off value	AUC (95% CI)	Sensitivity (%)	Specificity (%)	PLR	NLR	PPV (%)	NPV (%)
Age ≤ 65 y, F	HGF + ADA	>0.219	0.998	100	96.667	30	0	97.222	100
			(0.993–1.000)	(89.997–100.000)	(82.783–99.916)	(4.367–206.078)	-	(83.594–99.586)	-
	HGF + IFN-γ	>0.692	0.990	97.143	100	-	0.029	100	96.774
			(0.968–1.000)	(85.083–99.928)	(88.430–100.000)	-	(0.004–0.197)	-	(81.297–99.519)
	ADA + IFN-γ	>0.215	0.970	97.143	86.667	7.286	0.033	89.474	96.296
			(0.934–1.000)	(85.083–99.928)	(69.278–96.245)	(2.921–18.174)	(0.005–0.229)	(77.311–95.496)	(78.938–99.449)

TPE, tuberculous pleural effusion; non-TPE, non-tuberculous pleural effusion. HGF, hepatocyte growth factor; ADA, adenosine deaminase; IFN-γ, interferon gamma. M, male; F, female. AUC, area under the curve; PLR, positive likelihood ratio; NLR, negative likelihood ratio; PPV, positive predictive value; NPV, negative predictive value.

Research has shown that age and sex play significant roles in immune system regulation (Markle and Fish, 2014; Giefing-Kröll et al., 2015). In addition, immune cells such as liver-derived macrophages can massively express and secrete HGF, thereby regulating hepatocytic regeneration and repair (Dong et al., 2019; Huang et al., 2022). These findings suggest that age or sex might help regulate the expression and secretion of HGF. In this study, HGF showed differential-diagnostic efficacy between TPE and non-TPE in different age and gender subgroups. In female patients aged ≤65 years, HGF or HGF plus ADA had markedly greater diagnostic efficacy, indicating that in TPE, HGF expression was also affected by gender and age. The specific mechanism of age and/or gender in regulating the expression of HGF needs further study.

This study has some limitations. First, the numbers of older patients with TPE and younger patients with non-TPE we included were too small, which was likely to have led to selection bias. Second, non-TPE subjects were mainly patients with malignant tumors, some benign tumors, and pneumonia; our sample lacked patients with PE caused by autoimmune diseases. In future studies, we will consider increasing the sample size, especially to include older TPE and younger non-TPE patients, so that our results will be more consistent with real-world statistics.

In conclusion, our study showed that the expression of HGF in PE was significantly higher in TPE patients than in non-TPE patients and that it had favorable diagnostic efficacy in female TPE patients aged ≤65 years, even better than that of ADA or IFN-γ.

Data availability statement

The raw data supporting the conclusions of this article will be made available by the authors, without undue reservation.

Ethics statement

The studies involving human participants were reviewed and approved by the Ethics Committee of Beijing Chao-Yang Hospital of CMU (2019-ke-37). The patients/participants provided their written informed consent to participate in this study. Written informed consent was obtained from the individual (s) for the publication of any potentially identifiable images or data included in this article.

Author contributions

KZ: conceptualization. S-CZ, Z-YH, H-ZS, and M-MS: data curation, formal analysis, methodology, and validation. H-ZS: funding acquisition, investigation, and supervision. H-ZS and M-MS: project administration. S-CZ and M-MS: software and visualization. S-CZ: writing – original draft. S-CZ and KZ: writing – review and editing. All authors contributed to the article and approved the submitted version.

Funding

This work was supported in part by grants from the National Natural Science Foundation of China (No. 81970088) and the Beijing Scholars Program (No. 048).

Acknowledgments

We thank LetPub (www.letpub.com) for its linguistic assistance during the preparation of this manuscript.

Conflict of interest

The authors declare that the research was conducted in the absence of any commercial or financial relationships that could be construed as a potential conflict of interest.

Publisher's note

Supplementary material

The Supplementary material for this article can be found online at: https://www.frontiersin.org/articles/10.3389/fmicb.2023.1181912/full#supplementary-material

References

Andersen, E. S., Ruhwald, M., Moessner, B., Christensen, P. B., Andersen, O., Eugen-Olsen, J., et al. (2011). Twelve potential fibrosis markers to differentiate mild liver fibrosis from cirrhosis in patients infected with chronic hepatitis C genotype 1. *Eur. J. Clin. Microbiol. Infect. Dis.* 30, 761–766. doi: 10.1007/s10096-010-1149-y

Baumann, M. H., Nolan, R., Petrini, M., Lee, Y. C., Light, R. W., and Schneider, E. (2007). Pleural tuberculosis in the United States: incidence and drug resistance. *Chest* 131, 1125–1132. doi: 10.1378/chest.06-2352

Carlucci, P., Trigiani, M., Mori, P. A., Mondoni, M., Pinelli, V., Casalini, A. G., et al. (2019). Competence in pleural procedures. *Panminerva Med.* 61, 326–343. doi: 10.23736/S0031-0808.18.03564-4

Chakaya, J., Petersen, E., Nantanda, R., Mungai, B. N., Migliori, G. B., Amanullah, F., et al. (2022). The WHO Global Tuberculosis 2021 Report - not so good news and turning the tide back to End TB. *Int. J. Infect. Dis.* 124, S26–s29. doi: 10.1016/j.ijid.2022.03.011

Chakrabarti, B., and Davies, P. D. (2006). Pleural tuberculosis. *Monaldi Arch. Chest Dis.* 65, 26–33. doi: 10.4081/monaldi.2006.582

Dong, N., Shi, X., Wang, S., Gao, Y., Kuang, Z., Xie, Q., et al. (2019). M2 macrophages mediate sorafenib resistance by secreting HGF in a feed-forward manner in hepatocellular carcinoma. *Br. J. Cancer* 121, 22–33. doi: 10.1038/s41416-019-0482-x

Du, J., Shao, M. M., Yi, F. S., Huang, Z. Y., Qiao, X., Chen, Q. Y., et al. (2022). Interleukin 32 as a Potential Marker for Diagnosis of Tuberculous Pleural Effusion. *Microbiol. Spectr.* 10:e0255321. doi: 10.1128/spectrum.02553-21

Ebens, A., Brose, K., Leonardo, E. D., Hanson, M. G. Jr., Bladt, F., Birchmeier, C., et al. (1996). Hepatocyte growth factor/scatter factor is an axonal chemoattractant and a neurotrophic factor for spinal motor neurons. *Neuron* 17, 1157–1172. doi: 10.1016/S0896-6273(00)80247-0

Gaetani, L., Bellomo, G., Parnetti, L., Blennow, K., Zetterberg, H., and Di Filippo, M. (2021). Neuroinflammation and Alzheimer's Disease: A Machine Learning Approach to CSF Proteomics. *Cells* 10:1930. doi: 10.3390/cells10081930

Giefing-Kröll, C., Berger, P., Lepperdinger, G., and Grubeck-Loebenstein, B. (2015). How sex and age affect immune responses, susceptibility to infections, and response to vaccination. *Aging Cell* 14, 309–321. doi: 10.1111/acel.12326

Hanley, J. A., and McNeil, B. J. (1982). The meaning and use of the area under a receiver operating characteristic (ROC) curve. *Radiology* 143, 29–36. doi: 10.1148/radiology.143.1.7063747

He, J., Fan, Y., Shen, D., Yu, M., Shi, L., Ding, S., et al. (2020). Characterization of cytokine profile to distinguish latent tuberculosis from active tuberculosis and healthy controls. *Cytokine* 135:155218. doi: 10.1016/j.cyto.2020.155218

Huang, M., Jiao, J., Cai, H., Zhang, Y., Xia, Y., Lin, J., et al. (2022). C-C motif chemokine ligand 5 confines liver regeneration by down-regulating reparative macrophage-derived hepatocyte growth factor in a forkhead box O 3a-dependent manner. *Hepatology* 76, 1706–1722. doi: 10.1002/hep.32458

Huang, M. S., Tsai, M. S., Wang, T. H., Chong, I. W., Hou, J. J., Lin, Y. J., et al. (1999). Serum hepatocyte growth factor levels in patients with inflammatory lung diseases. *Kaohsiung J. Med. Sci.* 15, 195–201.

Jiang, C. G., Wang, W., Zhou, Q., Wu, X. Z., Wang, X. J., Wang, Z., et al. (2020). Influence of age on the diagnostic accuracy of soluble biomarkers for tuberculous pleural effusion: a post hoc analysis. *BMC Pulm. Med.* 20:178. doi: 10.1186/s12890-020-01219-2

Kang, W., Yu, J., Du, J., Yang, S., Chen, H., Liu, J., et al. (2020). The epidemiology of extrapulmonary tuberculosis in China: A large-scale multi-center observational study. *PLoS One* 15:e0237753. doi: 10.1371/journal.pone.0237753

Li, Y., Sheng, Y., Liu, J., Xu, G., Yu, W., Cui, Q., et al. (2022). Hair-growth promoting effect and anti-inflammatory mechanism of *Ginkgo biloba* polysaccharides. *Carbohydr. Polym.* 278:118811. doi: 10.1016/j.carbpol.2021.118811

Markle, J. G., and Fish, E. N. (2014). SeXX matters in immunity. *Trends Immunol.* 35, 97–104. doi: 10.1016/j.it.2013.10.006

Montesano, R., Matsumoto, K., Nakamura, T., and Orci, L. (1991). Identification of a fibroblast-derived epithelial morphogen as hepatocyte growth factor. *Cells* 67, 901–908. doi: 10.1016/0092-8674(91)90363-4

Nakamura, T., Nishizawa, T., Hagiya, M., Seki, T., Shimonishi, M., Sugimura, A., et al. (1989). Molecular cloning and expression of human hepatocyte growth factor. *Nature* 342, 440–443. doi: 10.1038/342440a0

Oliveira, A. G., Araújo, T. G., Carvalho, B. M., Rocha, G. Z., Santos, A., and Saad, M. J. A. (2018). The Role of Hepatocyte Growth Factor (HGF) in Insulin Resistance and Diabetes. *Front. Endocrinol.* 9:503. doi: 10.3389/fendo.2018.00503

Pang, Y., An, J., Shu, W., Huo, F., Chu, N., Gao, M., et al. (2019). Epidemiology of Extrapulmonary Tuberculosis among Inpatients, China, 2008-2017. *Emerg. Infect. Dis.* 25, 457–464. doi: 10.3201/eid2503.180572

Porcel, J. M. (2016). Advances in the diagnosis of tuberculous pleuritis. *Ann. Transl. Med.* 4:282. doi: 10.21037/atm.2016.07.23

Shaw, J. A., Diacon, A. H., and Koegelenberg, C. F. N. (2019). Tuberculous pleural effusion. *Respirology* 24, 962–971. doi: 10.1111/resp.13673

Shaw, J. A., and Koegelenberg, C. F. N. (2021). Pleural Tuberculosis. *Clin. Chest Med.* 42, 649–666. doi: 10.1016/j.ccm.2021.08.002

Sonnenberg, E., Meyer, D., Weidner, K. M., and Birchmeier, C. (1993). Scatter factor/hepatocyte growth factor and its receptor, the c-met tyrosine kinase, can mediate a signal exchange between mesenchyme and epithelia during mouse development. *J. Cell Biol.* 123, 223–235. doi: 10.1083/jcb.123.1.223

Stoker, M., Gherardi, E., Perryman, M., and Gray, J. (1987). Scatter factor is a fibroblast-derived modulator of epithelial cell mobility. *Nature* 327, 239–242. doi: 10.1038/327239a0

Wang, M., Song, L., Strange, C., Dong, X., and Wang, H. (2018). Therapeutic Effects of Adipose Stem Cells from Diabetic Mice for the Treatment of Type 2 Diabetes. *Mol. Ther.* 26, 1921–1930. doi: 10.1016/j.ymthe.2018.06.013

Wang, X. J., Yang, Y., Wang, Z., Xu, L. L., Wu, Y. B., Zhang, J., et al. (2015). Efficacy and safety of diagnostic thoracoscopy in undiagnosed pleural effusions. *Respiration* 90, 251–255. doi: 10.1159/000435962

Wang, W., Zhou, Q., Zhai, K., Wang, Y., Liu, J. Y., Wang, X. J., et al. (2018). Diagnostic accuracy of interleukin 27 for tuberculous pleural effusion: two prospective studies and one meta-analysis. *Thorax* 73, 240–247. doi: 10.1136/thoraxjnl-2016-209718

Wu, Y. B., Ye, Z. J., Qin, S. M., Wu, C., Chen, Y. Q., and Shi, H. Z. (2013). Combined detections of interleukin 27, interferon-γ, and adenosine deaminase in pleural effusion for diagnosis of tuberculous pleurisy. *Chin. Med. J.* 126, 3215–3221. doi: 10.3760/cma.j.issn.0366-6999.20130020

Zhang, M., Li, D., Hu, Z. D., and Huang, Y. L. (2020). The diagnostic utility of pleural markers for tuberculosis pleural effusion. *Ann. Transl. Med.* 8:607. doi: 10.21037/atm.2019.09.110

Zhao, Y., Ye, W., Wang, Y. D., and Chen, W. D. (2022). HGF/c-Met: A Key Promoter in Liver Regeneration. *Front. Pharmacol.* 13:808855. doi: 10.3389/fphar.2022.808855

Zweig, M. H., and Campbell, G. (1993). Receiver-operating characteristic (ROC) plots: a fundamental evaluation tool in clinical medicine. *Clin. Chem.* 39, 561–577. doi: 10.1093/clinchem/39.4.561

frontiers | Frontiers in Microbiology

TYPE Original Research
PUBLISHED 12 July 2023
DOI 10.3389/fmicb.2023.1230533

OPEN ACCESS

EDITED BY
Arabella Touati,
Centre Hospitalier Universitaire de Bordeaux, France

REVIEWED BY
Shaoqiang Wu,
Chinese Academy of Inspection and Quarantine (CAIQ), China
Sheng-ce Tao,
Shanghai Jiao Tong University, China
Guido van Marle,
University of Calgary, Canada

*CORRESPONDENCE
Wei Yuan
✉ yuanwei181@126.com
Jun He
✉ gzgyhjjj@163.com
Xu Chen
✉ xuchen1220@126.com

†These authors have contributed equally to this work

RECEIVED 29 May 2023
ACCEPTED 27 June 2023
PUBLISHED 12 July 2023

CITATION
Chen X, Du C, Zhao Q, Zhao Q, Wan Y, He J and Yuan W (2023) Rapid and visual identification of HIV-1 using reverse transcription loop-mediated isothermal amplification integrated with a gold nanoparticle-based lateral flow assay platform.
Front. Microbiol. 14:1230533.
doi: 10.3389/fmicb.2023.1230533

Rapid and visual identification of HIV-1 using reverse transcription loop-mediated isothermal amplification integrated with a gold nanoparticle-based lateral flow assay platform

Xu Chen[1,2*†], Cheng Du[3†], Qiang Zhao[4], Qi Zhao[5], Yonghu Wan[6], Jun He[4*] and Wei Yuan[7*]

[1]The Second Clinical College, Guizhou University of Traditional Chinese Medicine, Guiyang, Guizhou, China, [2]Clinical Medical Laboratory of the Second Affiliated Hospital, Guizhou University of Traditional Chinese Medicine, Guiyang, Guizhou, China, [3]Department of Anesthesiology, The Second Affiliated Hospital, Guizhou University of Traditional Chinese Medicine, Guiyang, Guizhou, China, [4]Clinical Laboratory, Guizhou Provincial Center for Clinical Laboratory, Guiyang, Guizhou, China, [5]Gastroenterology of the Second Affiliated Hospital, Guizhou University of Traditional Chinese Medicine, Guiyang, Guizhou, China, [6]Experiment Center, Guizhou Provincial Centre for Disease Control and Prevention, Guiyang, Guizhou, China, [7]Department of Quality Control, Guizhou Provincial Center for Clinical Laboratory, Guiyang, Guizhou, China

Human immunodeficiency virus type one (HIV-1) infection remains a major public health problem worldwide. Early diagnosis of HIV-1 is crucial to treat and control this infection effectively. Here, for the first time, we reported a novel molecular diagnostic assay called reverse transcription loop-mediated isothermal amplification combined with a visual gold nanoparticle-based lateral flow assay (RT-LAMP-AuNPs-LFA), which we devised for rapid, specific, sensitive, and visual identification of HIV-1. The unique LAMP primers were successfully designed based on the *pol* gene from the major HIV-1 genotypes CRF01_AE, CRF07_BC, CRF08_BC, and subtype B, which are prevalent in China. The optimal HIV-1-RT-LAMP-AuNPs-LFA reaction conditions were determined to be 68°C for 35 min. The detection procedure, including crude genomic RNA isolation (approximately 5 min), RT-LAMP amplification (35 min), and visual result readout (<2 min), can be completed within 45 min. Our assay has a detection limit of 20 copies per test, and we did not observe any cross-reactivity with any other pathogen in our testing. Hence, our preliminary results indicated that the HIV-1-RT-LAMP-AuNPs-LFA assay can potentially serve as a useful point-of-care diagnostic tool for HIV-1 detection in a clinical setting.

KEYWORDS

human immunodeficiency virus type one, loop-mediated isothermal amplification, gold nanoparticle-based lateral flow assay, point-of-care platform, limit of detection

Introduction

Human immunodeficiency virus type one (HIV-1) is an important agent that is responsible for acquired immunodeficiency syndrome (AIDS): approximately 38 million people globally live with this virus, and nearly 650,000 people died from AIDS-related illnesses in 2021, according to the Joint United Nations Programme on HIV/AIDS (UNAIDS) (Bernstein and Wegman, 2018; Eisinger and Fauci, 2018; UNAIDS, 2022). HIV-1 infection remains a global public health concern, the UNAIDS initiated the global project termed "95-95-95" to end the global HIV/AIDS epidemic by 2030, stressing the importance of diagnostic tests and aiming for 95% of people living with HIV-1 to know their status, 95% of people with diagnosed HIV-1 infection to receive sustained treatment, and 95% of people on treatment to achieve viral load suppression (Rojas-Celis et al., 2019; Kin-On et al., 2022). Developing an advanced testing system is crucial to meet these goals and timely control the transmission of the disease.

Diagnosis of HIV-1 agent is critical for both the prevention of its transmission and the improvement of antiretroviral therapy efficacy. However, traditional immunoassays may not be suit for detecting acute HIV-1 infection due to having a long window period (3–6 weeks) (Curtis et al., 2012). During this stage, HIV-1-specific antibodies are not yet generated in patients (Feinberg and Keeshin, 2022). Moreover, sero-conversion may be much later than 3–6 week, even when viral loads may have dropped. Real-time polymerase chain reaction (RT–PCR) has been regarded as a major breakthrough and has been most widely used for the early detection of HIV-1 infection (Zhao et al., 2021). However, RT–PCR limits the application of point-of-care (POC) techniques because it requires a relatively sophisticated thermocycler, trained technical personnel, and extended reaction times (approximately 2.5 h) (Li et al., 2021; Zhao et al., 2021). In addition, these tests need to be carried out in specialized and often centralized laboratories. Hence, devising an easy-to-operate, cost-effective, rapid, sensitive, and specific POC assay system is necessary for the prevention and follow-up treatment of HIV-1 infection.

Loop-mediated isothermal amplification (LAMP) is a promising nucleic acid isothermal amplification method that has enormous potential to transform POC molecular diagnostics due to its easy operation, high specificity, sensitivity, and lack of specialized equipment (i.e., PCR machines) (Notomi et al., 2000; Park, 2022; Shirshikov and Bespyatykh, 2022). In principle, LAMP requires a *Bst* DNA polymerase with strand displacement activity and a set of four to six specific primers that recognize different fragments in the target sequence (Notomi et al., 2000). In particular, the amount of amplicon generated from LAMP amplification is usually 100-fold greater than that generated from traditional PCR-based reactions (Avendaño and Patarroyo, 2020; Chaouch, 2021). The LAMP assay has previously been used for the detection of pathogens such as human influenza virus, severe acute respiratory syndrome coronavirus 2, and Zika virus (Ahn et al., 2019; Silva et al., 2019; Li et al., 2022). Moreover, LAMP has already been applied to detect HIV-1. Curtis et al. (2008) combined reverse-transcription LAMP with agarose gel electrophoresis for the identification of HIV-1. Curtis et al. (2008), Li et al. (2022), and Zhang et al. (2022) combined LAMP with a fluorescence reader for the detection of HIV-1. However, these assays require specific facilities for the analysis of LAMP products.

Gold nanoparticle-based lateral flow assay (AuNPs-LFA) has shown great potential as an ideal POC diagnostic platform due to their superior portability, usability by non-technical personnel, visual interpretation by the naked eye, and rapid detection (Campuzano et al., 2019; Gumus et al., 2023). AuNPs-LFA strips have been widely used to identify various analytes, such as nucleic acids, proteins, and infectious pathogens (Quesada-González and Merkoçi, 2015; Ince and Sezgintürk, 2022; Sohrabi et al., 2022). In the current study, the RT-LAMP reaction was combined with a AuNPs-based LFB detector (RT-LAMP-AuNPs-LFA) to develop an advanced assay for specific, sensitive, rapid, visual, and cost-saving identification of HIV-1 by targeting its *pol* gene (Zhao et al., 2021), which showed has no homology to other pathogen genomes in BLAST searches of the GenBank database. The RT-LAMP-AuNPs-LFA principle and workflow are shown in **Figures 1**, **2**, respectively. The feasibility of our assay was verified through clinical serum samples from suspected HIV-1-infected patients.

Materials and methods

Reagents

AuNPs-LFA-related materials, including crimson red dye streptavidin-coated AuNPs (SA-AuNPs; 40 ± 5 nm, 10 mg/mL), were obtained from Bangs Laboratories Inc. (Fishers, IN, USA), rabbit anti-fluorescein antibody (anti-FAM; 0.2 mg/mL) and biotinylated bovine serum albumin (biotin-BSA; 4 mg/mL) were obtained from Abcam Co., Ltd. (Shanghai, China), and nitrocellulose membrane (NC) was obtained from Merck Millipore Co., Ltd. (Darmstadt, Germany). Four components of the AuNPs-LFA, including the sample, conjugate, absorption pads, and nitrocellulose membranes, were manufactured and laminated on plastic adhesive backing by HuiDeXin Biotech. Co., Ltd. (Tianjin, China) according to our design scheme (**Figure 2**). Nucleic acid releasing agents were obtained from GenDx Biotech Co., Ltd. (Suzhou, China). LAMP amplification kits and colorimetric indicator (Leuco-hydroxynaphthol blue, L-HNB) were obtained from HaiGene Biotech Co., Ltd. (Harbin, China). Commercial RT–qPCR diagnostic kits for HIV-1 were obtained from DaAn Gene Co., Ltd. (Guangzhou, China).

Clinical specimens and target gene preparation

In this study, 65 clinical serum specimens were collected from suspected HIV-infected patients from Guizhou Provincial Center for Clinical Laboratory between January 2023 and April 2023. Genomic RNA was isolated using Nucleic Acid Releasing Agent (GenDx Biotech Co., Ltd.) in accordance with the manufacturer's instructions.

The full-length *pol* gene sequences of the representative genotypes of all known HIV-1 prevalent genotypes, including CRF01_AE, CRF07_BC, CRF08_BC, and subtype B, in China were downloaded from the GenBank database (genotype CRF01_AE:

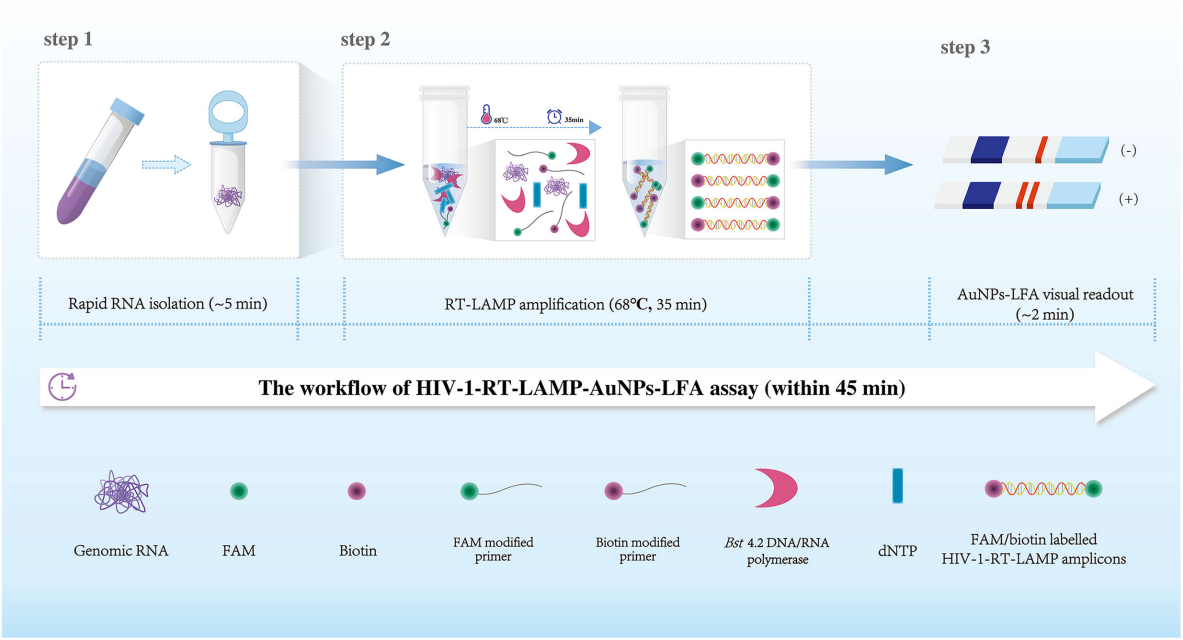

FIGURE 1
Human immunodeficiency virus type one (HIV-1)-RT-LAMP-AuNPs-LFA assay workflow. The HIV-1-RT-LAMP-AuNPs-LFA assay's workflow includes genomic RNA isolation (within 5 min), HIV-1-RT-LAMP amplification (35 min), and AuNPs-LFA visual interpretation (<2 min) and can be completed within 45 min. HIV-1, human immunodeficiency virus type one; RT-LAMP, reverse transcription loop-mediated isothermal amplification; AuNPs-LFA, gold nanoparticles-based lateral flow assay.

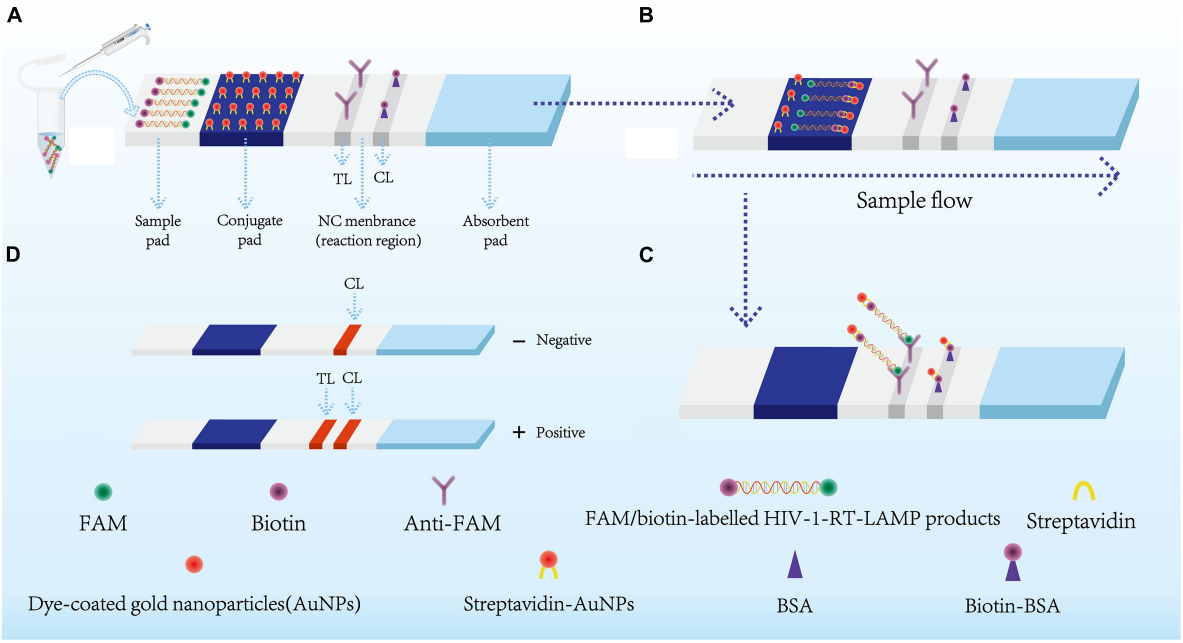

FIGURE 2
Schematic diagram showing AuNPs-LFA principles for visual HIV-1-RT-LAMP products interpretation. **(A)** HIV-1-RT-LAMP amplification products (2 μl) and running buffer (100 μl) were added simultaneously on the sample pad. **(B)** The FAM/biotin-labeled HIV-1-LAMP products flowing to the conjugate pad through capillary forces. Meanwhile, the streptavidin-AuNPs were hydrated and integrated with HIV-1-RT-LAMP products. **(C)** FAM/biotin-labeled HIV-1-RT-LAMP products were captured with anti-FAM at TL, and streptavidin-AuNPs were captured through biotin-BSA at CL. **(D)** Interpretation of the HIV-1-RT-LAMP-AuNPs-LFA assay. HIV-1 positive results were indicated by CL and TL bands on the AuNPs-LFA, Negative results were indicated when only the CL band appears on the AuNPs-LFA. HIV-1, human immunodeficiency virus type one; RT-LAMP, reverse transcription loop-mediated isothermal amplification; streptavidin-AuNPs, crimson red dye streptavidin-coated gold nanoparticles. AuNPs-LFA, gold nanoparticles-based lateral flow assay. CL, control line; TL, test line.

GenBank Accession No. U54771.1; genotype CRF07_BC: GenBank Accession No. U54771.1; genotype CRF08_BC: GenBank Accession No. AY008715.1; genotype subtype B: GenBank Accession No. GU647198.1) (He et al., 2012; Zhao et al., 2018). The four genomic sequences were synthesized and cloned into the pUC57 vector by Tsingke Biotech (Beijing, China). The initial concentration of each plasmid was 1×10^8 copies per milliliter, and the HIV-1 genotype CRF01_AE plasmid was used as a positive control.

AuNPs-based LFB construction

A schematic of the AuNPs-based LFA used in this study is shown in **Figure 2**. Briefly, the AuNPs-LFA (60 mm × 4 mm) is composed of four sections, including the sample pad, conjugate pad, detection region (nitrocellulose membrane), and absorption pad. Crimson red dye streptavidin-coated gold nanoparticles (SA-AuNPs) were deposited on the conjugate pad. Rabbit anti-FAM (0.2 mg/mL) and biotin-BSA (4 mg/mL) were fixed onto the nitrocellulose membrane of the test line (TL) and control line (CL), respectively, and the two lines were separated by 5 mm. In the end, the four separate sections were combined together on a plastic card through adhesive backing. The AuNPs-based LFA was kept dry and at room temperature until use.

LAMP primer design

The HIV-1 *pol* gene was selected as the amplification target for the RT-LAMP-AuNPs-LFA assay. The *pol* gene sequences from representative genotypes of all known HIV-1 prevalent genotypes (CRF01_AE, CRF07_BC, CRF08_BC, and subtype B) in China were aligned with DNASTAR software (DNASTAR Inc., Madison, WI, USA) (**Supplementary Figure 1**). The conserved sequences were used for HIV-1 RT-LAMP primers design through Primer Explorer v.5[1] and Primer Premier v.5.0 software. The specificity of the primer set was verified with the BLAST analysis tool. The primer sequences and alterations designed in this study are summarized in **Table 1**, and the primer locations are shown in **Supplementary Figure 1**. All primers were synthesized and purified via high-performance liquid chromatography at TsingKe Biotech Co., Ltd. (Beijing, China).

Standard HIV-1-RT-LAMP-AuNPs-LFA reaction

The RT-LAMP reaction for HIV-1 was performed in 25 μl volumes containing 2.5 μl of 10 × *Bst* 4.2 Buffer (Mg^{2+} free); 1.5 μl of 100 mM Mg^{2+}; 3 μl of dNTP Mixture (10 mM each); 0.1 μM of F3 and B3 primers; 0.4 μM of FIP or FIP* (for AuNPs-LFA only) and BIP primers; 0.2 μM of LF or LF* (for AuNPs-LFA only) and LB; 1 μl of *Bst* 4.2 DNA/RNA polymerase (8 U); 1.5 μl of L-HNB (for colorimetry only); and 1 μl of plasmid DNA (5 μl of clinical sample template); with double-distilled water added to bring the volume to 25 μl. The reactions were carried out at a constant temperature (reaction conditions were optimized as outlined below).

The LAMP products were tracked through agarose gel electrophoresis, real-time turbidity, colorimetry (L-HNB), and AuNPs-LFA. Briefly, for positive results, the agarose gel presented ladder-like bands, while there have no bands in negative outcomes. A turbidity value of >0.1 indicated a successful outcome. A reaction mixture that turned from deep violet to light green indicated successful L-HNB visual detection, and the mixture that remained deep violet throughout the reaction indicated a negative result. For AuNP-LFB detection, the simultaneous appearance of CL and TL on the AuNPs-LFA indicated a positive HIV-1-LAMP result or a negative outcome with only CL present on the AuNPs-LFA.

HIV-1-RT-LAMP-AuNPs-LFA assay condition optimization

RT-LAMP reaction temperatures from 63 to 70°C (in 1°C increments) were tested to confirm the optimal temperature under the standard HIV-1-RT-LAMP reaction system, and the amplification results were assessed using real-time turbidity. Then, the optimal reaction time was determined by incubating the HIV-1-RT-LAMP reactions at 15 to 45 min (in 10 min increments) and detecting their amplification results through AuNPs-LFA and L-HNB visual reagent. Each test was performed in triplicate.

HIV-1-RT-LAMP-AuNPs-LFA assay sensitivity

The *pol* plasmids were produced and serially diluted 10-fold (2.0×10^4 to 2.0×10^{-1} copies) to confirm the limit of detection (LoD) of the HIV-1-RT-LAMP-AuNPs-LFA assay. The HIV-1-RT-LAMP reactions were performed under optimum conditions, and the amplification results were assayed using AuNPs-LFA and L-HNB. Each test was repeated three times.

HIV-1-RT-LAMP-AuNPs-LFA assay specificity

Four synthetic *pol*-plasmid DNA templates (HIV-1 genotypes CRF01_AE, CRF07_BC, CRF08_BC, and subtype B) and other bacterial, viral, and fungal nucleic acid templates at $\geq 1.0 \times 10^4$ copies were used to evaluate the HIV-1-RT-LAMP-AuNPs-LFA assay's specificity (**Table 2**). Distilled water (DW) served as a negative control, and the amplification results were tested using AuNPs-LFA. Each assay was performed in triplicate.

1 http://primerexplorer.jp/e/

TABLE 1 The HIV-1-RT-LAMP-AuNPs-LFA primers used in this study.

Primer name	Sequence and modifications	Length	Gene
F3	5′-ATGGCAGTATTCAT(T/C)CACAAT-3′	21 nt	*pol*
B3	5′-CTACTGCCCCTTCACCT-3′	17 nt	
FIP	5′-GTATGTCTGTTGCTATTAT(G/A)TCTA(T/C)-TAAAAGAAAAGGGGGGATTGG-3′	46 mer	
FIP*	5′-FAM-GTATGTCTGTTGCTATTAT(G/A)TCTA(T/C)-TAAAAGAAAAGGGGGGATTGG-3′	46 mer	
BIP	5′-TCAAAATTTTCGGGTTTATTACAG(G/A)-AG(T/G)AG(T/C)TT(T/)GCTGGTCCTT-3′	44 mer	
LF	5′-TCTTTCCCCTGCACTGTAC-3′	19 nt	
LF*	5′-Biotin-TCTTTCCCCTGCACTGTAC-3′	19 nt	
LB	5′-ACAGCAGAGA(C/T)CC(A/C)(A/C)(T/G)TTG-3′	19 nt	

pol-FIP*, 5′-labeled with FAM, *pol*-LF*, 5′-labeled with biotin, when used for the AuNPs-LFA assay. FAM, 6-carboxy-fluorescein; nt, nucleotide; mer, monomeric unit.

Feasibility of HIV-1-RT-LAMP-AuNPs-LFA for clinical samples

Serum specimens were collected from 65 suspected HIV-1-infected patients at Guizhou Provincial Center for Clinical Laboratory. Genomic RNA templates were obtained rapidly with Nucleic Acid Releasing Agents (GenDx Biotech Co., Ltd; Suzhou, China; Cat No. NR202) according to the manufacturer's guidelines. Briefly, 150 μl of serum specimens were added into 1.5 ml EP tube, then the nucleic acid releasing agent RNA LB1 (120 μl) and RNA BB2 (500 μl) were added into the specimens for 20 s to release nucleic acid, and then the nucleic acids were collected through centrifuge absorption column. After washing steps, the nucleic acids were eluted in to 30 μl nuclease free H_2O. the genomic RNA was stored at −80°C before use. The Human Ethics Committee of Guizhou Provincial Center for Clinical Laboratory approved the lawful and ethical collection and analyses. All the samples were detected with RT–qPCR and our HIV-1-LAMP-AuNPs-LFA assay. HIV-1 RT–qPCR detection was performed using HIV-1 Nucleic Acid Assay Kits (DaAn Gene Co., Ltd.; Guangzhou, China) on an Applied Biosystems™ 7500 Real-Time PCR System (Life Technologies; Singapore). The limit of detection (LoD) of this assay was 50 IU/ml (approximately 30 copies/ml), and the basis for determining the copy number of the samples according to the corresponding standard curve. The negative and positive accordance rate of this assay was 97.76 and 99.80%, respectively, according to the manufacturer's guidelines. In addition, the HIV-1-positive samples were amplified with nested PCR by targeting the *pol* gene, and then the nucleotide sequences were aligned with reference sequences in HIV databases[2] for HIV-1 subtyping (Njouom et al., 2003; Zhao et al., 2018). The HIV-1-RT-LAMP-AuNPs-LFA assay was performed as previously described. The identification investigations were performed at biosafety level 2 based on the WHO Biosafety Manual (3rd Edition). The HIV-1-LAMP-AuNPs-LFA data were compared with RT–qPCR results. The statistical parameters were calculated using online tool from MedCalc[3] (Jevtuševskaja et al., 2016).

2 http://www.hiv.lanl.gov/content/index

3 http://www.medcalc.org/calc/diagnostic_test.php

Results

Schematic mechanism of the HIV-1-RT-LAMP-AuNPs-LFA assay

A representative schematic and workflow of the HIV-1-RT-LAMP-AuNPs-LFA assay is shown in Figure 1. In brief, genomic RNA templates were rapidly extracted within 5 min (Figure 1, step 1). The RT-LAMP technique was performed to rapidly and specifically amplify the target gene at a constant temperature (68°C) within 35 min.

The RT-LAMP method amplified the target sequence by using only a *Bst* 4.2 DNA/RNA polymerase with strand displacement activity and a set of 6 primers, including two outer primers (F3 and B3), two inner primers (FIP and BIP), and two loop primers (LF and LB). The FIP* and LF* primers were 5′-labeled with fluorescein (FAM) and biotin, respectively. The RT-LAMP products were labeled with FAM and biotin (Figure 1, step 2). Finally, the HIV-1-RT-LAMP products were visually interpreted with an AuNPs-LFA within 2 min (Figure 1, step 3). The whole assay can be completed within 45 min.

The principle of AuNPs-LFA analysis of HIV-1-RT-LAMP amplification products is presented in Figure 2. Briefly, HIV-1-RT-LAMP products (2.0 μl) and running buffer (100 μL; 100 mM phosphate-buffered saline with 1% Tween 20 [pH 7.4]) were dripped concurrently into the sample pad of AuNPs-LFA (Figure 2A). Capillary action carries the RT-LAMP product-containing running buffer move along the AuNPs-LFA platform, then the streptavidin-dye coated gold nanoparticles (streptavidin-AuNPs) were rehydrated and combined with FAM/biotin-labeled HIV-1-RT-LAMP products at the conjugate pad (Figure 2B). In the reaction region, the anti-FAM was anchored at test line (TL) and used to arrest FAM/biotin-labeled HIV-1-RT-LAMP products, the biotin-BSA was fixed at control line (CL) and used to capture streptavidin-AuNPs (Figure 2C). The interpretation of the HIV-1-RT-LAMP-AuNPs-LFA assay is outlined in Figure 2D. In a positive result, both CL and TL appeared simultaneously on the

TABLE 2 Pathogens used in this study.

No.	Pathogen	Source of pathogens[a]	No. of strains	HIV-1-LAMP- AuNPs LFB result[b]
1	HIV-1 CRF01_AE *pol*-plasmid	Constructed by Tsingke Biotech (Beijing, China)	1	P
2	HIV-1 CRF07_BC *pol*-plasmid	Constructed by Tsingke Biotech (Beijing, China)	1	P
3	HIV-1 CRF08_BC *pol*-plasmid	Constructed by Tsingke Biotech (Beijing, China)	1	P
4	HIV-1 subtype B *pol*-plasmid	Constructed by Tsingke Biotech (Beijing, China)	1	P
5	HIV-1 clinical samples	GZCCL	7	P
6	Hepatitis B virus	2nd GZUTCM	1	N
7	Hepatitis C virus	2nd GZUTCM	1	N
8	Influenza A virus	GZCDC	1	N
9	Influenza B virus	GZCDC	1	N
10	Coxsackie virus CAV16	GZCDC	1	N
11	Human enterovirus EV71	GZCDC	1	N
12	Human papillomavirus	2nd GZUTCM	1	N
13	Epstein-Barr virus	2nd GZUTCM	1	N
14	*Mycobacterium tuberculosis*	GZCDC	1	N
15	*Streptococcus pneumoniae*	2nd GZUTCM	1	N
16	*Pseudomonas aeruginosa*	ATCC27853	1	N
17	*Chlamydia trachomatis*	2nd GZUTCM	1	N
18	*Neisseria gonorrhoeae*	2nd GZUTCM	1	N
19	*Ureaplasma urealyticum*	2nd GZUTCM	1	N
20	*Staphylococcus aureus*	ATCC25923	1	N
21	*Escherichia coli*	ATCC25922	1	N
22	*Enterococcus faecalis*	2nd GZUTCM	1	N
23	*Cryptococcus neoformans*	ATCC 13690	1	N
24	*Shigella boydii*	2nd GZUTCM	1	N
25	*Streptococcus glabra*	2nd GZUTCM	1	N
26	*Haemophilus influenzae*	ATCC49247	1	N
27	*Streptococcus albus*	2nd GZUTCM	1	N
28	*Stenotrophomonas maltophilia*	2nd GZUTCM	1	N
29	*Salmonella typhimurium*	2nd GZUTCM	1	N
30	*Salmonella enteritidis*	2nd GZUTCM	1	N
31	*Acinetobacter lwoffii*	2nd GZUTCM	1	N
32	*Enterobacter aerogenes*	2nd GZUTCM	1	N
33	*Brucella*	GZCDC	1	N

[a]ATCC, American Type Culture Collection; 2nd GZUTCM, the Second Affiliated Hospital, Guizhou University of Traditional Chinese Medicine; GZCCL, Guizhou Provincial Center for Clinical Laboratory; GZCDC, Guizhou Provincial Center for Disease Control and Prevention.
[b]P, positive; N, negative.

biosensor, and the result was negative when only CL was present on the biosensor.

HIV-1-RT-LAMP-AuNPs-LFA assay confirmation

To confirm the feasibility of the HIV-1-RT-LAMP-AuNPs-LFA assay, the HIV-1-RT-LAMP-amplification mixes were incubated at a constant temperature (65°C) for 1 h, and then, the amplification products were analyzed using 2% agarose gel electrophoresis, real-time turbidity, colorimetric indicator (visual detection reagent, L-HNB) and AuNPs-LFA. For agarose gel electrophoresis identification, only the agarose gel of HIV-1-LAMP presented ladder-like bands, and the negative and blank controls have no bands were observed (Figure 3A). The turbidity of HIV-1-LAMP at the positive control was >0.1 and regarded as a positive outcome, while the negative and blank controls were <0.1 and considered negative reactions (Figure 3B). For colorimetric indicator (L-HNB) detection, the positive HIV-1-LAMP reaction

10.3389/fmicb.2023.1230533

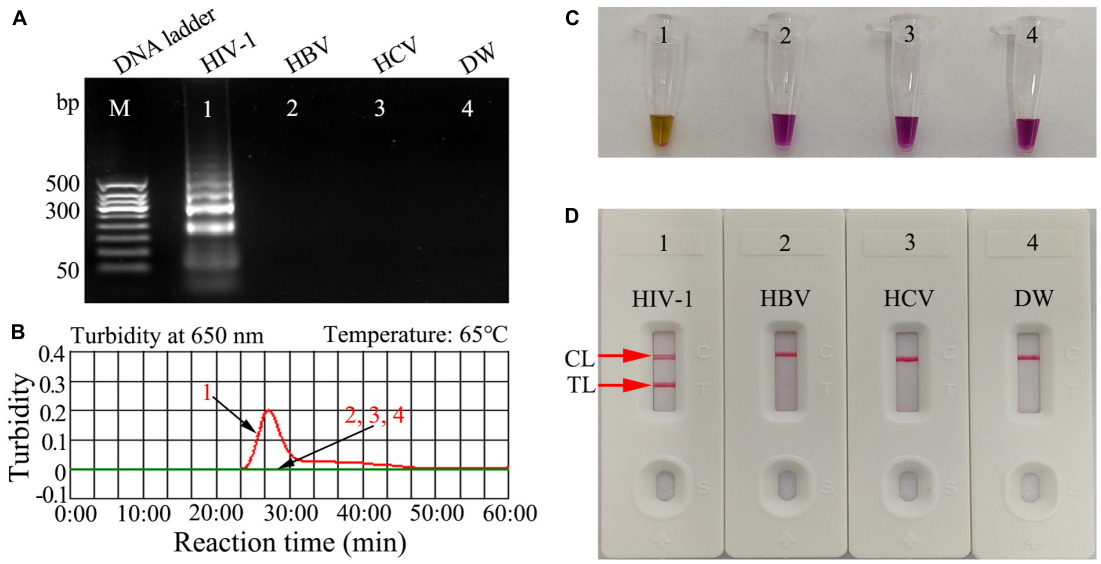

FIGURE 3
Human immunodeficiency virus type one (HIV-1)-RT-LAMP products verification. The HIV-1-RT-LAMP products were identified simultaneously using **(A)** 2% agarose gel electrophoresis, **(B)** real-time turbidity, **(C)** color change (L-HNB), and **(D)** AuNPs-LFA. Templates of A1/B1/C1/D1 -A4/B4/C4/D4 were the HIV-1-plasmid (positive), HBV (negative), HCV (negative), and DW (blank control), respectively. HIV-1, human immunodeficiency virus type one; HBV, hepatitis B virus; HCV, hepatitis C virus; DW, distilled water; L-HNB, Leuco-hydroxynaphthol blue; CL, control line; TL, test line.

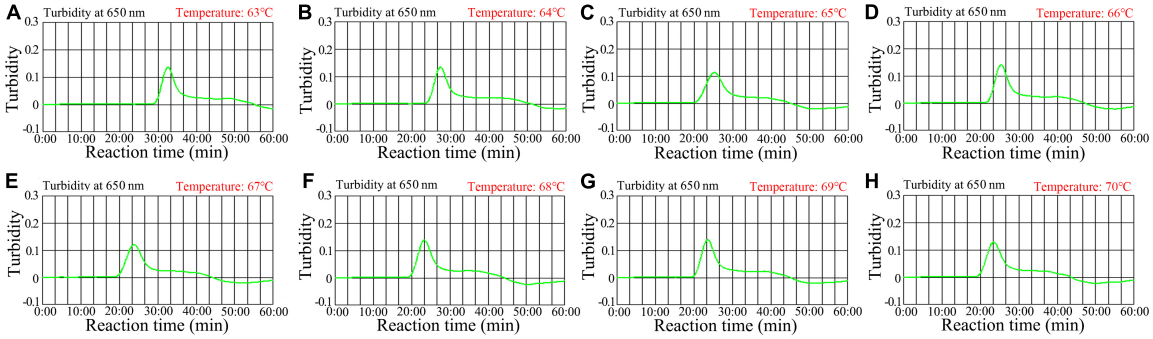

FIGURE 4
Temperature optimization for the HIV-1-RT-LAMP amplification. RT-LAMP amplifications for HIV-1 were monitored using real-time turbidity, and their corresponding amplicon curves are shown as graphs, a turbidity > 0.1 indicated a positive result. Eight kinetic graphs were obtained at different temperatures (63°C–70°C in 1°C increments) with 2×10^3 target gene copies **(A–H)**. Graphs **(F–H)** (68–70C) showed robust amplification.

changed from deep violet to light green, and the negative and blank controls remained deep violet (Figure 3C). More importantly, two clearly visible crimson-red bands (TL and CL) were observed in the AuNPs-LFA, indicating a positive HIV-1-RT-LAMP reaction, while only the CL was observed in the negative and blank controls (Figure 3D). These data indicated that the LAMP primer set designed for HIV-1 detection was an appropriate candidate for the development of the HIV-1-RT-LAMP-AuNPs-LFA assay.

HIV-1-RT-LAMP amplification temperature optimization

Optimizing the reaction temperature is critical for high-efficiency LAMP amplification. In this study, we used a standard *pol*-plasmid copy number (2.0×10^3) to test reaction temperatures from 63 to 70°C with 1°C increments. The HIV-1-RT-LAMP reactions were tracked by means of real-time turbidity measurement, and the kinetic graph was generated from each reaction temperature. The results indicated that robust HIV-1-RT-LAMP amplification was observed at 68 to 70°C (Figure 4). Therefore, 68°C was considered the optimal reaction temperature for our assay.

HIV-1-RT-LAMP-AuNPs-LFA assay sensitivity

Serial dilutions of *pol* plasmid with 2.0×10^4 to 2.0×10^{-1} copies were used as templates to determine the LoD of our assay. HIV-1-RT-LAMP reactions were carried out at 68°C for 1 h, and the results were monitored using a colorimetric indicator

(L-HNB) and AuNPs-LFA. The results obtained via the AuNPs-LFA platform were in accordance with those obtained through the L-HNB method (Figures 5A, B), and the LoD of our assay was 20 copies per test based on HIV-1 DNA.

HIV-1-RT-LAMP-AuNPs-LFA assay reaction time optimization

The optimal reaction time required for our assay at the HIV-1-RT-LAMP amplification stage was evaluated by testing times from 15 to 45 min in 10 min increments at the optimal amplification temperature (68°C), and the LAMP products were analyzed through a colorimetric indicator (L-HNB) and the AuNPs-LFA platform. The results showed that the LoD of the *pol* plasmid (20 copies) was detected when the reaction time was 35 min (Figure 6). Hence, an HIV-1-RT-LAMP reaction time of 35 min was recommended for our assay. As a result, the whole detection procedure for the HIV-1-RT-LAMP-AuNPs-LFA assay, including rapid template isolation (approximately 5 min), LAMP reaction (35 min), and result visual reporting with AuNPs-LFA (within 2 min), can be completed within 45 min.

HIV-1-RT-LAMP-AuNPs-LFA assay specificity

The specificity of our assay was evaluated using four *pol* plasmids of HIV-1 genotypes (CRF01_AE, CRF07_BC, CRF08_BC, and subtype B) prevalent in China, positive HIV-1 clinical samples (confirmed by RT-qPCR), and 28 other pathogens (Table 2). The HIV-1-RT-LAMP-AuNPs-LFA reactions were performed under optimal conditions, and the results were monitored using the AuNPs-LFA platform. The nucleic acid isolated from HIV-1 samples presented positive results, while other pathogens and blank control groups showed negative results (Table 2 and Figure 7). These data demonstrated that our assay had excellent specificity and no cross-reactivity with non-HIV-1 pathogens.

Feasibility of HIV-1-RT-LAMP-AuNPs-LFA assay in clinical specimens

To further evaluate the suitability of our assay as a valuable tool for HIV-1 detection, the HIV-1-RT-LAMP-AuNPs-LFA system was tested using 65 suspected HIV-1-infected serum specimens collected from the Guizhou Provincial Center for Clinical Laboratory (Guiyang, China), and the Human Ethics Committee of Guizhou Provincial Center for Clinical Laboratory approved the lawful and ethical collection and analyses. All clinical specimens were tested simultaneously using RT–qPCR and our assay. The results showed that 38 of 65 samples were diagnosed as HIV-1 positive with RT–qPCR (>30 copies). We also analyzed the genotypes of HIV-1-positive samples through nested PCR and sequencing.

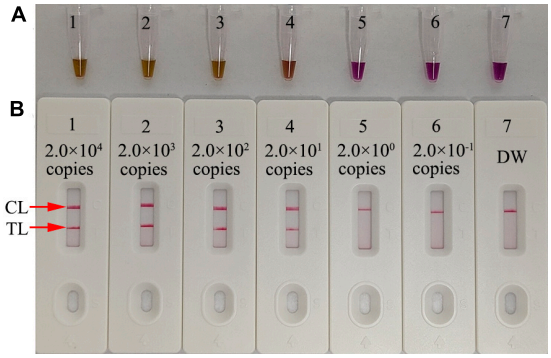

FIGURE 5
Serial dilutions (2.0×10^4, 2.0×10^3, 2.0×10^2, 2.0×10^1, 2.0×10^0, and 2.0×10^{-1} copies) of HIV-1 plasmids were used as templates, and DW was used as the blank control. Results were simultaneously analyzed through visual reagent L-HNB **(A)** and the AuNPs-LFA **(B)**. A sensitivity analysis of the HIV-1-LAMP assay indicated its LoD was 20 copies per test. DW, distilled water; CL, control line; TL, test line.

The results showed that the HIV-1-LAMP-AuNPs-LFA assay was consistent with traditional RT–qPCR testing outcomes (Table 3 and Supplementary Table 1). Comparing with the RT–qPCR technology, the HIV-1-RT-LAMP-AuNPs-LFA sensitivity and specificity was 100% (95% CI: 90.75 to 100.00%) and 100% (95% CI: 87.23 to 100.00%), respectively (Table 3). These data indicated that our assay developed in the current study is a valuable clinical diagnostic tool for HIV-1.

Discussion

In this study, we successfully developed and verified a novel HIV-1-RT-LAMP-AuNPs-LFA POC testing system to identify HIV-1, which dexterously integrated HIV-1 specific and rapid RT-LAMP amplification with a visual and sensitive AuNPs-LFA readout platform. The feasibility of our novel assay was confirmed through clinical sera from individuals with suspected HIV-1 infection, and its results were compared with a valuable commercial RT–qPCR assay.

Human immunodeficiency virus type one is one of the major human viruses that can affect the ability of the immune system to defend against life-threatening infections (Inamdar et al., 2019; Pedro et al., 2019; Gandhi et al., 2023). The clinical symptoms are often difficult to distinguish from those associated with the common fevers, muscle pains, and rash at the early stage of HIV-1 infection (Bernstein and Wegman, 2018; Rhee et al., 2022). A rapid, sensitive, specific, easy-to-operate, and cost-saving diagnosis system that can provide early viral detection is critical for prescribing more effective antiretroviral treatments (ARTs) and preventing HIV-1 transmission. Here, Our HIV-1-RT-LAMP-AuNPs-LFA assay only requires basic facilities, such as a heating block, metal bath, water bath, or even a thermos cup, that can hold the reaction temperature at 68°C for the HIV-1-RT-LAMP preamplification step. In our detection system, crude nucleic acid is sufficient for LAMP amplification because the *Bst* 4.2

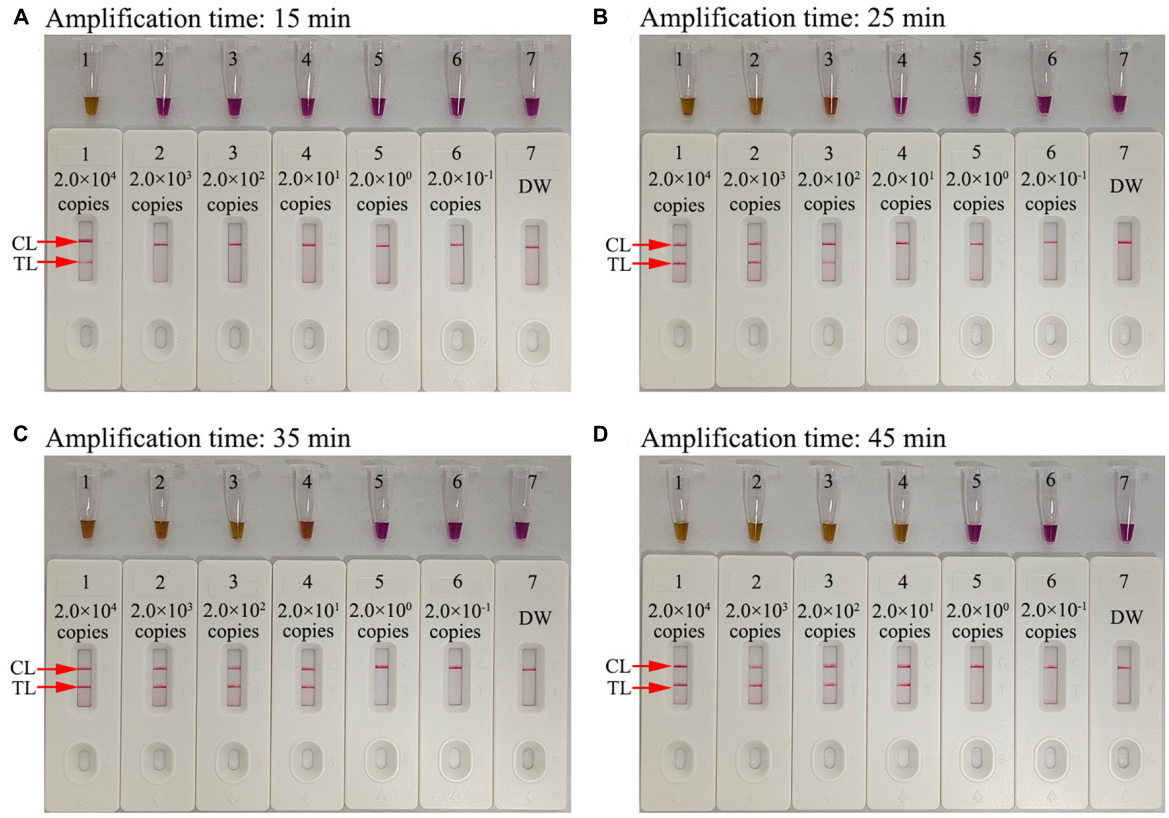

FIGURE 6
Amplification time optimization for the HIV-1-RT-LAMP-AuNPs-LFA assay. Four RT-LAMP reaction times were evaluated at 68°C: **(A)** 15 min, **(B)** 25 min, **(C)** 35 min, and **(D)** 45 min. Tube/biosensor 1-7 represent nucleic acid template levels 2.0×10^4, 2.0×10^3, 2.0×10^2, 2.0×10^1, 2.0×10^0, and 2.0×10^{-1} copies and blank control (DW), respectively. Results were analyzed using visual reagent L-HNB and AuNPs-LFA. The optimal LoD occurred with a 35 min reaction time. DW, distilled water; CL, control line; TL, test line.

DNA/RNA polymerase is used for LAMP amplification, which has fewer inhibitors than the *Taq* DNA polymerase used in traditional PCR (Somboonna et al., 2018). Hence, our assay is time-saving, and the entire procedure, including crude genomic RNA isolation (~5 min), RT-LAMP amplification (35 min), and AuNPs-LFA visual result interpretation (<2 min), can be completed within 45 min.

In our study, the target gene HIV-1 *pol* was amplified using the RT-LAMP technique, which can robustly amplify amplicons at a constant temperature and provide 100-fold greater detection capability than traditional PCR (Avendaño and Patarroyo, 2020; Chaouch, 2021). The specific amplicons were generated in the LAMP reaction system through the *Bst* 4.2 DNA/RNA polymerase with six specific primers that span eight unique segments of the target gene. Here, we successfully designed a set of unique primers based on the four main prevalent HIV-1 genotypes (CRF07_BC, CRF01_AE, CRF08_BC and subtype B) in China for specific amplification of the HIV-1 *pol* gene (He et al., 2012; Zhao et al., 2018). The primer set included two outer primers (F3 and B3), two inner primers (FIP and BIP), and two loop primers (LF and LB). The specificity of the HIV-1-RT-LAMP-AuNPs-LFA assay was verified with HIV-1 strain and 28 other pathogens. Our results confirmed that our assay can correctly identify the target pathogen HIV-1 and has no cross-reaction with non-HIV-1 strains (**Table 2** and **Figure 7**). In addition, the LoD of our assay was as low as 20 copies based on HIV-1 DNA (**Figure 5**). To further verify the feasibility of our assay in clinical practice, 65 genomic RNA specimens were extracted from suspected HIV-1-infected patients and then analyzed simultaneously using RT–qPCR and our assay. The data confirmed that our assay can effectively identify clinical samples. Furthermore, a next trial should test more clinical samples with significantly lower viral loads with our assay to better reflect its clinical applications.

For a visual and convenient readout of the HIV-1-RT-LAMP amplification results, a AuNPs-LFA platform was constructed and applied in our assay. AuNPs-LFA, as a paper-based biosensor, fits the requirements of POC testing owing to its good selectivity, high sensitivity, low limit of detection, quick assay performance, low cost, and low sample volume (Henderson et al., 2018; Bishop et al., 2019; Boehringer and O'Farrell, 2021). More importantly, AuNPs are the most suitable nanomaterial for use as an optical label in biosensors due to their biocompatibility, ease of synthesis, size-tunability, and intense red color, which is easy to detect by the naked eye (Quesada-González and Merkoçi, 2015; Li et al., 2023). The AuNPs-LFA can readout visually the HIV-1-RT-LAMP results for anchoring anti-FAM and BSA-biotin on the NC membrane. If HIV-1-RT-LAMP positive products presented in the sample, they will be integrated with streptavidin-AuNPs at the conjugate

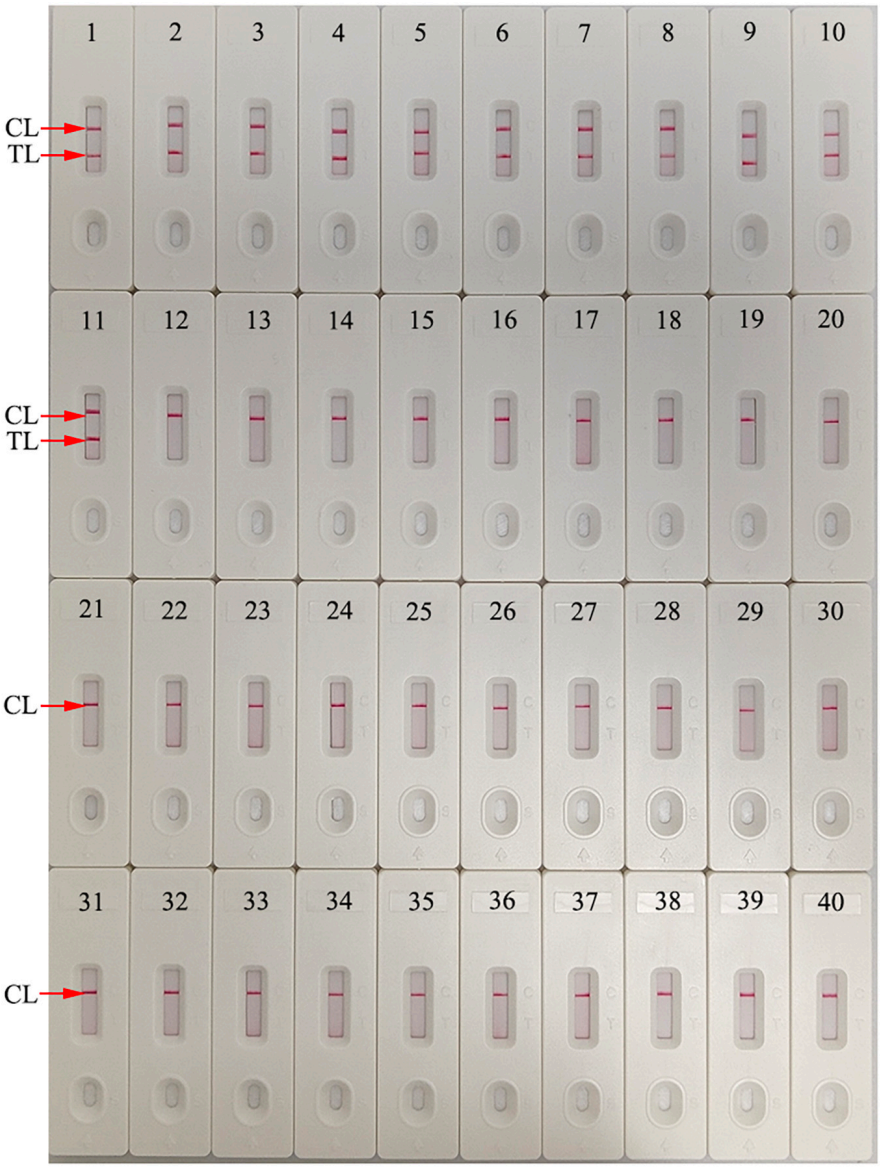

FIGURE 7
Human immunodeficiency virus type one (HIV-1)-RT-LAMP-AuNPs-LFA assay specificity with different strains. Assay specificity was evaluated using different nucleic acid templates. Amplification products were tested using AuNPs-LFA: 1–4, HIV-1 CRF01_AE, CRF07_BC, CRF08_BC, and subtype B pol plasmids; 5-11, HIV-1 clinical samples; 12, hepatitis B virus; 13, hepatitis C virus; 14, influenza A virus; 15, influenza B virus; 16, Coxsackie virus CAV16; 17, human enterovirus EV71; 18, human papillomavirus; 19, Epstein-Barr virus; 20, *Mycobacterium tuberculosis*; 21, *Streptococcus pneumoniae*; 22, *Pseudomonas aeruginosa*; 23, *Chlamydia trachomatis*; 24, *Neisseria gonorrhoeae*; 25, *Ureaplasma urealyticum*; 26, *Staphylococcus aureus*; 27, *Escherichia coli*; 28, *Enterococcus faecalis*; 29, *Cryptococcus neoformans*; 30, *Shigella boydii*; 31, *Streptococcus glabra*; 32, *Haemophilus influenzae*; 33, *Streptococcus albus*; 34, *Stenotrophomonas maltophilia*; 35, *Salmonella typhimurium*; 36, *Salmonella enteritidis*; 37, *Acinetobacter lwoffii*; 38, *Enterobacter aerogenes*; 39, *Brucella*; 40, distilled water (Blank control). CL, control line; TL, test line.

pad. And then, passing through the NC membrance, FAM/biotin-labeled HIV-1-RT-LAMP products will be captured at TL. And to the CL, being always captured for evidence that the streptavidin-AuNPs biosensor works (**Figure 2**).

In previous studies, RT-LAMP-based methods have already been used to identify HIV-1 strain. Curtis et al. (2012) combined RT-LAMP with agarose gel electrophoresis for HIV-1 detection (Curtis et al., 2012). Hosaka et al. (2009) integrated with RT-LAMP with turbidimeter for HIV-1 identification, Ocwieja et al. (2015) and Zhang et al. (2022) combined RT-LAMP with fluorescence detector for HIV-1 identification. However, these techniques require special equipment for HIV-1-RT-LAMP results interpretation. Khan et al. (2023) integrated RT-LAMP with visual reagent for detection of HIV-1 through the naked eye. Nevertheless, the results were ambiguous when the RT-LAMP product concentrations were low. Their advantages/disadvantages were shown in **Table 4**. In our study, we first ingenious integrated RT-LAMP amplification with the AuNPs-LFA platform for the identification of HIV-1. Our AuNPs-LFA is easy to operate and cost-saving (~US$2.0 per test). Therefore, the total cost of each HIV-1-RT-LAMP-AuNPs-LFA detection, including genomic RNA

TABLE 3 Comparing HIV-1 levels in clinical samples using RT-qPCR and our HIV-1-RT-LAMP-AuNPs-LFA methods.

HIV-1-LAMP-AuNPs-LFA	HIV-1 RT-qRCR (reference method)			Sensitivity		Specificity	
	Positive	Negative	Total	Value	95% CI	Value	95% CI
Positive	38 (CRF01_AE, 16; CRF07_BC, 14; CRF08_BC, 4; Subtype B, 4)	0	38	100%	90.75–100.00%	100%	87.23–100.00%
Negative	0	27	27				
Total	38	27	65				

TABLE 4 Comparisons of the commonly used RT-LAMP-based methods for detection of HIV-1.

Results detection technique	Advantages	Disadvantages	References
Agarose gel electrophoresis	High specificity and sensitivity	Require special equipment for agarose gel electrophoresis; time-consuming; need open the reaction tube for results identification	Curtis et al., 2012 Current study
Turbidity	High specificity; without opening the reaction tubes for results identification	Require special equipment for turbidity measurement	Hosaka et al., 2009 Current study
Fluorescence probe	High specificity and sensitivity; without opening the reaction tubes for results identification	Require expensive equipment for fluorescence signal detection	Ocwieja et al., 2015; Zhang et al., 2022
Visual reagent	High specificity; without opening the reaction tubes for results identification	The results are ambiguous when the LAMP product concentrations are low	Khan et al., 2023 Current study
AuNPs-LFA	High sensitivity and specificity; accurate and visual interpretation; easy to operate and cost-saving	Need open the reaction tube for results identification	Current study

isolation (∼US$0.5), RT-LAMP reactions (∼US$1.5), and AuNPs-LFA readout (∼US$2.0), was approximately US$4.0.

Our HIV-1-RT-LAMP-AuNPs-LFA assay also has some shortcomings. First, because HIV-1 has very high heterogeneity and many genotypes, our degenerate LAMP primers specifically identify only HIV-1 genotypes (CRF01_AE, CRF07_BC, CRF08_BC, and subtype B) prevalent in China, and there is still a need to further refine the LAMP primers for detecting many more HIV-1 genotypes. Second, the outcomes obtained from the AuNPs-LFA platform with the naked eye are qualitative but not quantitative. Quantitative measurements with the HIV-1-RT-LAMP-AuNPs-LFA assay require further study. Finally, the HIV-1-RT-LAMP amplification tube must be opened to be read by the AuNPs-LFA, which will increase the risk of carry-over contamination. In our laboratory, spraying nucleic acid contamination scavenger soon after completing each AuNPs-LFA assay is an effective way to avoid nucleic acid contamination. For adaptation to clinical application, it is necessary to refine the HIV-1-RT-LAMP-AuNPs-LFA assay system and design a device that avoids the tube opening procedure to prevent aerosol contamination.

Conclusion

Here, we integrated RT-LAMP isothermal amplification with the AuNPs-LFA platform to create a novel HIV-1-RT-LAMP-AuNPs-LFA assay system for high-sensitivity, high-specificity, rapid identification of HIV-1 by visual readout in clinical settings. Our assay had a 20-copy LoD and showed no cross-reactivity with other pathogens. The entire detection procedure can be accomplished within 45 min and with no need for any expensive facilities. Hence, our assay can meet the WHO-recommended ASSURED criteria (affordable, sensitive, specific, user-friendly, rapid and robust, equipment-free and deliverable to end users) for POC testing requirements.

Data availability statement

The original contributions presented in the study are included in the article/**Supplementary material**, further inquiries can be directed to the corresponding authors.

Author contributions

XC, WY, and JH involved in study conceptualization, supervision, and project administration. XC, CD, QiaZ, QiZ, YW, and JH performed experiments and data curation. XC and CD involved in study funding acquisition and methodology. XC, QiaZ, and YW collected clinical samples. CD, QiaZ, and QiZ involved in

validation studies and visualization. XC involved in writing–original draft. JH and WY involved in writing–review and editing. All authors contributed to the article and approved the submitted version.

Funding

This work was supported by the Guizhou Provincial Key Technology R&D Program [Grant No. Qian Ke He support (2023) General 242], the Program of Science and Technology of Guizhou Provincial Health Commission (gzwjkj2022-1-497).

Acknowledgments

We thank the medical personnel at the Second Affiliated Hospital, Guizhou University of Traditional Chinese Medicine, and Guizhou Provincial Center for Clinical Laboratory for their cooperation in this study. We also thank the patients who provided samples.

Conflict of interest

The authors declare that the research was conducted in the absence of any commercial or financial relationships that could be construed as a potential conflict of interest.

Publisher's note

Supplementary material

The Supplementary Material for this article can be found online at: https://www.frontiersin.org/articles/10.3389/fmicb.2023.1230533/full#supplementary-material

References

Ahn, S. J., Baek, Y. H., Lloren, K., Choi, W. S., Jeong, J. H., Antigua, K., et al. (2019). Rapid and simple colorimetric detection of multiple influenza viruses infecting humans using a reverse transcriptional loop-mediated isothermal amplification (RT-LAMP) diagnostic platform. *BMC Infect. Dis.* 19:676. doi: 10.1186/s12879-019-4277-8

Avendaño, C., and Patarroyo, M. A. (2020). Loop-mediated isothermal amplification as point-of-care diagnosis for neglected parasitic infections. *Int. J. Mol. Sci.* 21:7981. doi: 10.3390/ijms21217981

Bernstein, H. B., and Wegman, A. D. (2018). HIV infection: antepartum treatment and management. *Clin. Obstet. Gynecol.* 61, 122–136. doi: 10.1097/GRF.0000000000000330

Bishop, J. D., Hsieh, H. V., Gasperino, D. J., and Weigl, B. H. (2019). Sensitivity enhancement in lateral flow assays: a systems perspective. *Lab Chip*. 19, 2486–2499. doi: 10.1039/c9lc00104b

Boehringer, H. R., and O'Farrell, B. J. (2021). Lateral flow assays in infectious disease diagnosis. *Clin. Chem.* 68, 52–58. doi: 10.1093/clinchem/hvab194

Campuzano, S., Yáñez-Sedeño, P., and Pingarron, J. M. (2019). Nanoparticles for nucleic-acid-based biosensing: opportunities, challenges, and prospects. *Anal. Bioanal. Chem.* 411, 1791–1806. doi: 10.1007/s00216-018-1273-6

Chaouch, M. (2021). Loop-mediated isothermal amplification (LAMP): an effective molecular point-of-care technique for the rapid diagnosis of coronavirus SARS-CoV-2. *Rev. Med. Virol.* 31:e2215. doi: 10.1002/rmv.2215

Curtis, K. A., Rudolph, D. L., and Owen, S. M. (2008). Rapid detection of HIV-1 by reverse-transcription, loop-mediated isothermal amplification (RT-LAMP). *J. Virol. Methods* 151, 264–270. doi: 10.1016/j.jviromet.2008.04.011

Curtis, K. A., Rudolph, D. L., Nejad, I., Singleton, J., Beddoe, A., Weigl, B., et al. (2012). Isothermal amplification using a chemical heating device for point-of-care detection of HIV-1. *PLoS One* 7:e31432. doi: 10.1371/journal.pone.0031432

Eisinger, R. W., and Fauci, A. S. (2018). Ending the hiv/aids pandemic. *Emerg. Infect. Dis.* 24, 413–416. doi: 10.3201/eid2403.171797

Feinberg, J., and Keeshin, S. (2022). Prevention and initial management of HIV infection. *Ann. Intern. Med.* 175, ITC81–ITC96. doi: 10.7326/AITC202206210

Gandhi, R. T., Bedimo, R., Hoy, J. F., Landovitz, R. J., Smith, D. M., Eaton, E. F., et al. (2023). Antiretroviral drugs for treatment and prevention of hiv infection in adults: 2022 recommendations of the international antiviral society-USA panel. *JAMA* 329, 63–84. doi: 10.1001/jama.2022.22246

Gumus, E., Bingol, H., and Zor, E. (2023). Lateral flow assays for detection of disease biomarkers. *J. Pharm. Biomed. Anal.* 225:115206. doi: 10.1016/j.jpba.2022.115206

He, X., Xing, H., Ruan, Y., Hong, K., Cheng, C., Hu, Y., et al. (2012). A comprehensive mapping of hiv-1 genotypes in various risk groups and regions across China based on a nationwide molecular epidemiologic survey. *PLoS One* 7:e47289. doi: 10.1371/journal.pone.0047289

Henderson, W. A., Xiang, L., Fourie, N. H., Abey, S. K., Ferguson, E. G., Diallo, A. F., et al. (2018). Simple lateral flow assays for microbial detection in stool. *Anal. Methods* 10, 5358–5363. doi: 10.1039/c8ay01475b

Hosaka, N., Ndembi, N., Ishizaki, A., Kageyama, S., Numazaki, K., and Ichimura, H. (2009). Rapid detection of human immunodeficiency virus type 1 group M by a reverse transcription-loop-mediated isothermal amplification assay. *J. Virol. Methods* 157, 195–199. doi: 10.1016/j.jviromet.2009.01.004

Inamdar, K., Floderer, C., Favard, C., and Muriaux, D. (2019). Monitoring HIV-1 assembly in living cells: insights from dynamic and single molecule microscopy. *Viruses* 11:72. doi: 10.3390/v11010072

Ince, B., and Sezgintürk, M. K. (2022). Lateral flow assays for viruses diagnosis: up-to-date technology and future prospects. *Trends Analyt. Chem.* 157:116725. doi: 10.1016/j.trac.2022.116725

Jevtuševskaja, J., Uusna, J., Andresen, L., Krõlov, K., Laanpere, M., Grellier, T., et al. (2016). Combination with antimicrobial peptide lyses improves loop-mediated isothermal amplification based method for Chlamydia trachomatis detection directly in urine sample. *BMC Infect. Dis.* 16:329. doi: 10.1186/s12879-016-1674-0

Khan, M. J. R., Bhuiyan, M. A., Tabassum, S., and Munshi, S. U. (2023). Use of whole blood and dried blood spot for detection of HIV-1 nucleic acids using reverse transcription loop-mediated isothermal amplification. *J. Virol. Methods*. 312:114642. doi: 10.1016/j.jviromet.2022.114642

Kin-On, L. J., Murdock, N., Murray, J., Justman, J., Parkin, N., and Miller, V. (2022). A systematic review of limiting antigen avidity enzyme immunoassay for detection of recent hiv-1 infection to expand supported applications. *J. Virus Erad.* 8:100085. doi: 10.1016/j.jve.2022.100085

Li, C. H., Chan, M. H., Chang, Y. C., and Hsiao, M. (2023). Gold nanoparticles as a biosensor for cancer biomarker determination. *Molecules* 28:364. doi: 10.3390/molecules28010364

Li, M., Ge, H., Sun, Z., Fu, J., Cao, L., Feng, X., et al. (2022). A loop-mediated isothermal amplification-enabled analytical assay for the detection of SARS-CoV-2: a review. *Front. Cell. Infect. Microbiol.* 12:1068015. doi: 10.3389/fcimb.2022.1068015

Li, Y., Chen, X., Zhao, Y., Wan, Z., Zeng, Y., Ma, Y., et al. (2021). A rapid variant-tolerant reverse transcription loop-mediated isothermal amplification assay for the point of care detection of HIV-1. *Analyst* 146, 5347–5356. doi: 10.1039/d1an00598g

Njouom, R., Pasquier, C., Sandres-Saune, K., Harter, A., Souyris, C., and Izopet, J. (2003). Assessment of hiv-1 subtyping for cameroon strains using phylogenetic analysis of *pol* gene sequences. *J. Virol. Methods* 110, 1–8. doi: 10.1016/s0166-0934(03)00080-6

Notomi, T., Okayama, H., Masubuchi, H., Yonekawa, T., Watanabe, K., Amino, N., et al. (2000). Loop-mediated isothermal amplification of DNA. *Nucleic Acids Res.* 28:E63. doi: 10.1093/nar/28.12.e63

Ocwieja, K. E., Sherrill-Mix, S., Liu, C., Song, J., Bau, H., and Bushman, F. D. (2015). A reverse transcription loop-mediated isothermal amplification assay optimized to detect multiple HIV subtypes. *PLoS One* 10:e0117852. doi: 10.1371/journal.pone.0117852

Park, J. W. (2022). Principles and applications of loop-mediated isothermal amplification to point-of-care tests. *Biosens. Basel.* 12:857. doi: 10.3390/bios12100857

Pedro, K. D., Henderson, A. J., and Agosto, L. M. (2019). Mechanisms of hiv-1 cell-to-cell transmission and the establishment of the latent reservoir. *Virus Res.* 265, 115–121. doi: 10.1016/j.virusres.2019.03.014

Quesada-González, D., and Merkoçi, A. (2015). Nanoparticle-based lateral flow biosensors. *Biosens. Bioelectron.* 73, 47–63. doi: 10.1016/j.bios.2015.05.050

Rhee, S., Kassaye, S. G., Jordan, M. R., Kouamou, V., Katzenstein, D., and Shafer, R. W. (2022). Public availability of HIV-1 drug resistance sequence and treatment data: a systematic review. *Lancet Microbe* 3, e392–e398. doi: 10.1016/S2666-5247(21)00250-0

Rojas-Celis, V., Valiente-Echeverria, F., Soto-Rifo, R., and Toro-Ascuy, D. (2019). New challenges of HIV-1 infection: how HIV-1 attacks and resides in the central nervous system. *Cells* 8:1245. doi: 10.3390/cells8101245

Shirshikov, F. V., and Bespyatykh, J. A. (2022). Loop-mediated isothermal amplification: from theory to practice. *Russ. J. Bioorg. Chem.* 48, 1159–1174. doi: 10.1134/S106816202206022X

Silva, S., Pardee, K., and Pena, L. (2019). Loop-mediated isothermal amplification (LAMP) for the diagnosis of zika virus: a review. *Viruse* 12:19. doi: 10.3390/v12010019

Sohrabi, H., Majidi, M. R., Khaki, P., Jahanban-Esfahlan, A., de la Guardia, M., and Mokhtarzadeh, A. (2022). State of the art: lateral flow assays toward the point-of-care foodborne pathogenic bacteria detection in food samples. *Compr. Rev. Food Sci. Food Saf.* 21, 1868–1912. doi: 10.1111/1541-4337.12913

Somboonna, N., Choopara, I., Arunrut, N., Sukhonpan, K., Sayasathid, J., Dean, D., et al. (2018). Rapid and sensitive detection of chlamydia trachomatis sexually transmitted infections in resource-constrained settings in Thailand at the point-of-care. *PLoS Neglect. Trop. Dis.* 12:e0006900. doi: 10.1371/journal.pntd.0006900

UNAIDS, (2022). *Global HIV & AIDS statistics — Fact sheet*. Geneva: UNAIDS.

Zhang, X., Li, H., Liu, Z., Zhao, Y., Zeng, Y., Dong, Y., et al. (2022). An HFman probe-based reverse transcription loop-mediated isothermal amplification (RT-LAMP) assay for HIV-1 detection. *Mol. Cell. Probes* 64:101834. doi: 10.1016/j.mcp.2022.101834

Zhao, J., Ao, C., Wan, Z., Dzakah, E. E., Liang, Y., Lin, H., et al. (2021). A point-of-care rapid HIV-1 test using an isothermal recombinase-aided amplification and CRISPR Cas12a-mediated detection. *Virus Res.* 303:198505. doi: 10.1016/j.virusres.2021.198505

Zhao, S., Feng, Y., Hu, J., Li, Y., Zuo, Z., Yan, J., et al. (2018). Prevalence of transmitted HIV drug resistance in antiretroviral treatment naive newly diagnosed individuals in China. *Sci. Rep.* 8:12273. doi: 10.1038/s41598-018-29202-2

frontiers | Frontiers in Microbiology

TYPE Original Research
PUBLISHED 16 August 2023
DOI 10.3389/fmicb.2023.1238666

OPEN ACCESS

EDITED BY
Ons Bouchami,
Universidade Nova de Lisboa, Portugal

REVIEWED BY
Aijun Pan,
University of Science and Technology of China, China
Xiaogang Xu,
Fudan University, China

*CORRESPONDENCE
Wenfang Xia
✉ rm000982@whu.edu.cn

†These authors have contributed equally to this work and share first authorship

RECEIVED 12 June 2023
ACCEPTED 03 August 2023
PUBLISHED 16 August 2023

CITATION
Yao Z, Liu Y, Zhan L, Qiu T, Li G, Chen Z, Fang X, Liu Z, Wu W, Liao Z and Xia W (2023) The utilization of nanopore targeted sequencing proves to be advantageous in the identification of infections present in deceased donors.
Front. Microbiol. 14:1238666.
doi: 10.3389/fmicb.2023.1238666

The utilization of nanopore targeted sequencing proves to be advantageous in the identification of infections present in deceased donors

Zhiyuan Yao[1†], Yu Liu[2,3,4†], Liying Zhan[1], Tao Qiu[5], Guang Li[1], Zhongbao Chen[5], Xiaoyu Fang[1], Zhou Liu[1], Wei Wu[1], Zhaomin Liao[1] and Wenfang Xia[1*]

[1]Department of Critical Care Medicine, Renmin Hospital of Wuhan University, Wuhan, Hubei, China, [2]Department of Cardiology, Renmin Hospital of Wuhan University, Wuhan, Hubei, China, [3]Cardiovascular Research Institute of Wuhan University, Wuhan, Hubei, China, [4]Hubei Key Laboratory of Cardiology, Wuhan, Hubei, China, [5]Department of Organ Transplantation, Renmin Hospital of Wuhan University, Wuhan, Hubei, China

Background: Nanopore Target Sequencing (NTS) represents a novel iteration of gene sequencing technology; however, its potential utility in the detection of infection in deceased donors has yet to be documented. The present study endeavors to assess the applicability of NTS in this domain.

Methods: This retrospective study comprised a cohort of 71 patients who were under intensive care at Renmin Hospital of Wuhan University between June 2020 and January 2022. The specimens were subjected to microbiological tests utilizing NTS, culture, and other techniques, and subsequently, the diagnostic accuracy of NTS was compared with conventional methods.

Results: Blood NTS exhibited a better agreement rate of 52.11% and a greater positive rate of pathogen detection than blood culture (50.70% vs. 5.63%, $p < 0.001$). In NTS of deceased donors, *Klebsiella pneumoniae*, *Escherichia coli*, and *Acinetobacter baumannii* were the most frequently found bacteria, and *Candida* was the most frequently found fungus. Blood NTS had a considerably better sensitivity for detecting clinical bloodstream infection than blood culture (62.50%: 7.14%, $p < 0.001$). These findings were supported by comparisons between blood NTS and conventional microbial detection methods (such as blood culture, glucan testing, galactomannan testing, T cell spot testing for tuberculosis infection, smear, etc.).

Conclusion: The pathogen detection technology NTS has a high sensitivity and positive rate. It can more accurately and earlier detect infection in deceased donors, which could be very important for raising the donation conversion rate.

KEYWORDS

Chinese donation after citizen's death, deceased donors, nanopore targeted sequencing, blood culture, third-generation sequencing

1. Introduction

An important form of treatment for advanced organ failure is organ transplantation. The number of organ transplants worldwide has dramatically increased despite the effects of COVID-19. The second-largest country in the world for organ transplant surgery is now China (Home, n.d.; Shi et al., 2020). One of China's primary sources of transplantable organs at the moment is deceased donors. In recent years, the number of organ donors has increased (Home, n.d.; Shi et al., 2020). Many variables, including the experience level of the surgeons and the age of the donors, influence the outcomes of organ transplantation. One of the main reasons why recipients of transplants develop malignant outcomes is infection after the procedure (Wang et al., 2018). According to studies, infections account for 30.9% of the causes of death among kidney transplant recipients within a year (Begaj et al., 2013). Studies have revealed that 5% of donated organs had sepsis (Wolfe et al., 2019). Anti-infective therapy is advised by the guidelines for all donors who may be infected (Wolfe et al., 2019), however many donors' infection statuses cannot be determined in a timely manner. Additionally, infections in organ donors may make it more difficult to use transplantable organs effectively (Choi et al., 2021). Therefore, early detection of illness in organ donors may aid in increasing the rate of donation.

The gold standard for diagnosing bloodstream infection is blood culture (Allerberger and Kern, 2020), but it has drawbacks such a long waiting period, a narrow detection range, and a low detection efficiency for specific bacteria and fungi. To maintain the survival of transplantable organs, deceased donors must be screened for infection within 4–12 h and some donors must undertake organ removal operations within hours or 1–2 days. Blood culture is currently unable to match the demands, thus doctors urgently require effective and quick diagnostic technologies. The third generation of gene sequencing technology is called nanopore target sequencing (NTS). It can identify DNA sequences by the current changes brought on when DNA strands are compelled to pass through membrane-encased nanopores (Tyler et al., 2018). Small size, low cost, and portability are its benefits. NTS can identify large gene sequences (Ciuffreda et al., 2021), does not rely on polymerase chain reaction technology, and requires little effort to prepare a gene library. Endophthalmitis (Huang et al., 2021), lower respiratory tract infections (Wirth et al., 2012; Charalampous et al., 2019; Chan et al., 2020), surgical site infections (Whittle et al., 2022), new coronaviruses, and respiratory viruses (Wang et al., 2020b) have all been diagnosed using NTS. There is no information available, though, about the use of NTS to check for infection in deceased donors. Therefore, in order to assess the viability and effectiveness of NTS in quickly screening for infection in such individuals, this study retrospectively assessed the NTS test results of blood samples from deceased donors.

2. Materials and methods

2.1. Design of the study and participants

From June 2020 to January 2022, deceased donors who were being cared for in the intensive care unit (ICU) at Renmin Hospital of Wuhan University (Wuhan, China) were included in this retrospective investigation. The Renmin Hospital of Wuhan University's Ethics Committee of Clinical Research accepted this study, which complies with the Helsinki Declaration. The family of every participant gave their signed, informed consent. The organ donation procedure used in this study complies with the rules and procedures used when Chinese citizens pass away (Huang et al., 2015). Patients who did not have blood samples subjected to NTS detection met the exclusion criteria.

2.2. Data collection

Clinical information was retrieved from the examined medical records of deceased donors, including demographic information, medical history, results of laboratory tests, and a treatment plan. To maintain secrecy, each participant uses a predetermined number.

2.3. Sample collection

Peripheral venous blood samples: Within 24 h after being admitted to the intensive care unit, clinical nurses with experience took peripheral venous blood samples under stringent aseptic guidelines. (1) Collection of blood culture samples: Each time, 2 sets of blood cultures were obtained, each set from a separate puncture location. Each set contained 8–10 mL of blood that was injected into both aerobic and anaerobic bottles. (2) Collection of the NTS sample: Blood samples of at least 2 mL were taken and preserved in a specialized container.

2.4. Culture

After collection, peripheral venous blood samples were sent right away for culture and NTS. Using the BACTEC 9120 culture system (BD Diagnostics, Sparks, MD), the specimens were initially inoculated on Columbia blood agar basal medium (bacteria) and Sabouraud's glucose agar medium (fungi). The isolated fungi or/and bacteria in the positive instances were identified using the MALDI Biotyper mass spectrometer (Bruker, Madison, WI) and the Vitek 2 Compact automatic identification system (BioMérieux, Marcy l'Etoile, 106 France).

2.5. Nanopore targeted sequencing

NTS was carried out utilizing Wang et al.'s method (Wang et al., 2020a). The QIAamp UCP Pathogen Mini Kit (Qiagen, Venlo, Netherlands) was used to extract DNA. The same sample's 16 s rRNA, ITS1/2, and rpoB genes were amplified, and the combined barcode products were mixed at a mass ratio of 10:3:1. The 1D Lliging Kit (SQK-LSK109; Oxford Nanopore Technologies, Oxford, UK) was used to mix the combined products of the several samples in equal parts. The Min ION or Grid ION system (Oxford Nanopore Technologies, Oxford, UK) was used to sequence the library. Each batch included TE buffer measurement as a negative control. If any set threshold is met after bioinformatics analysis of the material, positive identification of bacteria or fungi is carried out.

2.6. The principles for identifying microbial infections and contamination

According to clinical guidelines and previous studies, pathogenic microorganisms were divided into: (1) Absolute pathogenic bacteria, such as *Salmonella* spp., *Mycobacterium tuberculosis*, *Corynebacterium diphtheriae*, etc. (2) Common opportunistic pathogens, such as *Staphylococcus aureus*, *Enterococcus* spp., *Escherichia coli*, *Pseudomonas* spp., *Klebsiella* spp., *Acinetobacter* spp. and *Candida* spp. (3) Common contaminated bacteria: such as Coagulase negative *Staphylococcus*, *Corynebacterium* spp., *Propionibacterium* spp., *Streptococcus viridans*, *Aeromonas* spp., *Bacillus* spp., and *Micrococcus* spp., etc. (Horan et al., 2008; Byrd et al., 2018; Timsit et al., 2020; Sommerstein et al., 2021; Gouel-Cheron et al., 2022).

For absolute pathogenic bacteria and common opportunistic pathogens, when one or more blood cultures were positive and NTS was positive, the pathogen was considered to be causative pathogens. For common contaminated bacteria, (1) When two or more blood cultures are positive and have infection-related symptoms (such as fever, chills, and hypotension, etc.), the pathogen is considered to be a causative pathogens; (2) When NTS is positive, the patient has infection-related symptoms and laboratory test results and cannot be explained by other reasons, and the antibiotic treatment is effective, the pathogen is considered to be a causative pathogens (Horan et al., 2008).

2.7. Statistical analysis

The mean and standard deviation (SD) were used to characterize data with normal distribution, the median (interquartile range, IQR), and the count (%), for non-normal distribution. For difference analysis, the T test, variance analysis, non-parametric test, and chi-square test were utilized. The effectiveness of NTS and blood culture as diagnostic tools was compared using the McNemar chi-square test. The 95% confidence interval (95% CI) and the sensitivity, specificity, positive predictive value (PPV), and negative predictive value (NPV) were provided. Statistics were judged significant at $p < 0.05$. Excel 2019 was used to gather the data, and IBM SPSS Statistics 26 Windows (Armonk, NY, USA) was utilized for the statistical analysis.

3. Results

3.1. Clinical and demographic characteristics

We looked at the medical files of 75 deceased donors. 71 patients were eventually included after four patients who refused NTS were eliminated. Table 1 displays the demographic and medical traits of the patients. The median age was 55 (46,62) years, the median length of stay in the ICU was 4 (2,5) days, and the median acute physiology and chronic health evaluation II (APACHE II) score was 20 (16,23). There were 64 men and 7 women in the study. Cerebral hemorrhage (70.42%) was the most prevalent underlying condition, followed by lung infection (61.97%) and hypertension (54.93%). When the patient entered the ICU, the white blood cell (WBC), neutrophil ratio, C-reactive protein (CRP), and procalcitonin (PCT) levels were all greater than the standard reference value. Following ICU admission, all patients received empirical anti-infective therapy, with meropenem, teicoplanin, and voriconazole being the most frequently prescribed antibiotics.

TABLE 1 Clinical and demographic characteristics of deceased donors.

Items	Deceased donors
Sex (Male)	64 (90.14%)
Age (years)	55 (46, 62)
Days in ICU	4 (2, 5)
Acute physiology and chronic health evaluation II	20 (16, 23)
Primary disease	
Cerebral hemorrhage	50 (70.42%)
Pulmonary infection	44 (61.97%)
Hypertensive	39 (54.93%)
Mechanical ventilation	71 (100.00%)
Extracorporeal membrane oxygenation	7 (9.86%)
White blood cell ($\times 10^9$/L)	12.06 (9.58, 15.86)
Neutrophils (%)	83.21 ± 8.51
C-reactive protein (mg/L)	111.84 ± 71.42
Procalcitonin (ng/ml)	0.92 (0.15, 2.94)
Antibiotic	
Teicoplanin	70 (98.59%)
Meropenem	64 (90.14%)
Polymyxin B sulfate	22 (30.99%)
Imipenem and Cilastatin sodium	14 (19.72%)
Antifungal	
Voriconazole	65 (91.55%)
Micafungin Sodium	13 (18.31%)

Data are expressed as $\bar{x} \pm$ SD, M (IQR) or n (%).

3.2. Pathogen detection in blood using NTS and blood culture comparison

Blood cultures from four patients (5.63%) were positive. In blood culture, three bacteria (*Klebsiella pneumoniae*, *Enterococcus faecalis*, and *Acinetobacter baumannii*) and one fungus (*Candida tropicalis*) were found. 36 patients (50.70%) showed positive blood NTS; 21 (58.33%) had just one pathogen, and 15 (41.67%) had two or more. Blood culture was unable to detect four individuals who had bacterial and fungal co-infections according to NTS. 32 (86.49%) bacteria and 5 (13.51%) fungus at the species level were found in blood NTS. Gram-negative bacteria made up 62.50% of the identified bacteria, with *Escherichia coli* accounting for the majority (11 instances), followed by *Pseudomonas stutzeri* and *Enterobacter cloacae* (Figure 1). Supplementary Table S1 provides specific information on pathogens identified by blood culture, blood NTS, and other microbial detection techniques.

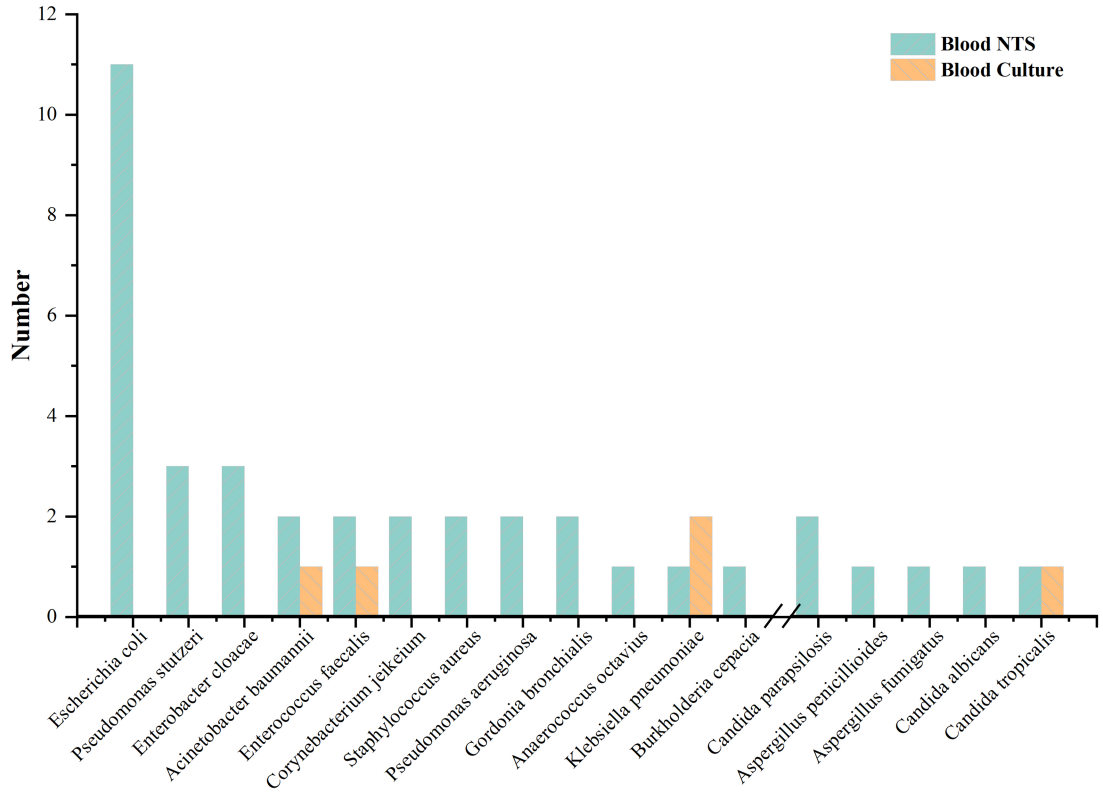

FIGURE 1
Blood nanopore target sequencing (NTS) and blood culture pathogen identification.

TABLE 2 Blood nanopore target sequencing (NTS) and blood culture agreement rate.

		Blood culture		Sensitivity% (95%CI)	Specificity% (95%CI)	PPV% (95%CI)	NPV% (95%CI)
		+	–				
Blood NTS	+	3	33	75.00 (21.94, 98.68)	50.75(38.36, 63.05)	8.33 (2.17, 23.59)	97.14(83.38, 99.85)
	–	1	34				

PPV, Positive Predictive Value; NPV, Negative Predictive Value.

3.3. Blood culture and blood NTS consistency comparison

We begin by contrasting the agreement rate between blood NTS and blood culture (Table 2), as blood culture is now the gold standard for the diagnosis of bloodstream infections (Allerberger and Kern, 2020). The agreement rate was 52.11 percent, and blood NTS had a positive rate that was substantially higher than blood culture (50.70 percent vs. 5.63 percent, $p < 0.001$). According to the findings, there is a strong correlation between NTS and blood cultures, and when NTS is negative, blood cultures are more likely to turn out negatively.

3.4. Comparison of blood NTS and blood culture's diagnostic effectiveness in individuals who are infected and those who are not

After being admitted to the intensive care unit, 71 deceased donors received broad-spectrum antibiotic treatment to avoid infection. In the infection group, there were 56 patients, while in the non-infected group, there were only 15. After a thorough examination of clinical symptoms, signs (such as increased body temperature, decreased blood pressure, increased heart rate or increased respiratory rate, etc.), laboratory results (white blood cell count, neutrophil count, procalcitonin and C-reactive protein, etc.), imaging results, treatment choices, and outcomes, three skilled doctors made the infection diagnosis (Horan et al., 2008; Cui et al., 2022, 2010–2019). Only 4 of the 56 sick patients were found by blood culture; 35 were found by NTS. A blood culture revealed no false positives, however one of the 15 non-infected patients tested positive for NTS and had erroneous positives. The sensitivity of blood NTS was substantially higher than that of blood culture (62.50%: 7.14%, P<0.001) and was 55.36% higher than that of blood culture. Blood NTS's specificity was 93.33%, while its PPV and NPV values were 97.22 and 40.00%, respectively. Blood culture's specificity was 100%, its PPV and NPV were 100% and 22.39%, respectively (Table 3). Additionally, when we compared the outcomes of blood NTS with all other conventional methods for detecting pathogenic microorganisms (such as blood cultures, glucan tests, galactomannan tests, T cell spot tests for tuberculosis infection,

smears, etc.), we discovered that blood NTS had a higher diagnostic effectiveness (see Supplementary Table S2).

3.5. Effect of blood NTS test results

The blood NTS of patient NO.18# revealed the presence of *Staphylococcus aureus*, while patient NO.37# revealed the presence of *Escherichia coli*, *Pseudomonas stutzeri*, and *Acinetobacter gilrohlii*. The two patients' anti-infective regimens were modified in light of the NTS results (Table 4). The two patients' subsequent blood culture results were negative, demonstrating that NTS can more quickly provide recommendations for therapeutic therapy.

3.6. The role of NTS in predicting receptor infection

In this study, we collected the pathogenic microbial test results of kidney recipients matching deceased donors in order to assess the role of NTS in predicting infection in organ transplant recipients (since the donor kidney is mainly distributed to our hospital, and other organs are distributed throughout the country, the data of the kidney recipients we obtained are the most complete.). There were 128 renal recipients in all, 86 of whom were men (87.2%) and 42 of whom were women (32.8%), with an average age of 44.98 ± 11.42 years. After surgery, 111 (86.7%) patients had blood cultures performed (positive rate: 2.7%), 121 (94.5%) patients had urine cultures performed (positive rate: 3.3%), 48 (37.5%) patients had blood NTS performed (positive rate: 77.1%), 32 (25.0%) patients had urine NTS performed (positive rate: 31.3%), and 112 (87.5%) patients had surgical site secretion cultures performed (positive rate: 1.8%). The aforementioned findings demonstrated that NTS had a considerably greater positive rate than culture ($p < 0.001$). Comparing the results of pathogenic microorganism detection between donors and recipients, we discovered that 12 recipients and their corresponding 7 donors both had the same pathogenic bacteria (all *Escherichia coli*), all of which were detected by NTS but not by culture (Table 5). As a result, NTS may be superior to culture in predicting postoperative infection in recipients. Additionally, we discovered that the diagnosis of donor-derived infection (DDI) coincided in five groups of patients (group meaning donor and its corresponding recipient) (Wolfe et al., 2019), which may suggest that NTS also has promise in screening DDI. Supplementary Table S1 of the Supplementary Material displays the complete results.

4. Discussion

Renal artery rupture and thrombosis are just two of the harmful outcomes that can result from DDI (Wang et al., 2018; Liu et al., 2019; Tong et al., 2020), and the attributable mortality of recipients with DDI is as high as 25–33%(Benamu et al., 2017). Infection in deceased donors is not a strict prohibition against organ donation, according to earlier research (Kieslichova et al., 2019). The safe performance of liver and kidney transplantation with the prophylactic use of antibiotics is possible even if the donor has a systemic illness (even a multidrug-resistant bacterial infection) (Yuan et al., 2016), and positive transplantation outcomes are possible (Ye et al., 2017). The majority of patients, however, do not receive particular antibacterial treatment prior to organ removal surgery since the illness of deceased donors is frequently not recognized in a timely and efficient manner (Yuan et al., 2016). The majority of patients suffer from lung infections or other organ damage brought on by underlying disorders, and the majority of deceased donors have terrible underlying diseases. According to the study's findings, cerebral hemorrhage, lung infection, and hypertension were the primary basic disorders affecting the patients. Organ removal surgery might begin at different times for deceased donors with varied circumstances. It has been challenging for doctors to maintain the organ function of such individuals because of this hazy node. Although empirical antibiotic therapy will be administered to dead donors after ICU admission, clinicians hope to get quicker, more concrete results to help them decide how to employ antimicrobial medications. Blood culture requires a lot of time and has a limited detection area, which is insufficient. Due to its broad detection range and quick detection, third-generation gene detection technology NTS has been used in a variety of industries. Its use in checking for infection in deceased donors has not, however, been documented. The effectiveness of NTS in the diagnosis of infection in such patients was therefore investigated in this study.

In this investigation, 71 individuals were included, and 37 pathogens, mostly Gram-negative bacteria (62.50%), were found in peripheral blood samples from 36 (50.70%) NTS-positive patients. A Gram-negative bacterial infection in the donor has been linked to an increased risk of DDI, according to earlier research [5]. According to this study, *Candida* was the fungus and *Klebsiella pneumoniae*, *Escherichia coli*, and *Acinetobacter baumannii* were the most prevalent infectious bacteria found in deceased donors. Pathogens that blood culture could not reliably identify, such as *Pseudomonas stutzeri*, *Enterobacter cloacae*, and *Aspergillus*, were found by blood NTS. The difference between the number of fungus found in blood NTS and blood culture—7 fungi were found in blood NTS, compared to none in blood culture—showed that NTS was more effective in detecting fungal infection and had a wider detection range. There are two sides

TABLE 3 Blood nanopore target sequencing (NTS) and culture performance in clinical infectious disease diagnosis.

		Infection (56)	Non-infection (15)	Sensitivity% (95%CI)	Specificity% (95%CI)	PPV% (95%CI)	NPV% (95%CI)
Blood NTS	+	35	1	62.50 (48.52, 74.77)	93.33 (66.03, 99.65)	97.22 (83.80, 99.85)	40.00 (24.35, 57.79)
	–	21	14				
Blood culture	+	4	0	7.14 (2.31, 18.13)	100.00 (74.65, 100.00)	100.00 (39.58, 100.00)	22.39 (13.47, 34.52)
	–	52	15				

PPV, Positive Predictive Value; NPV, Negative Predictive Value.

TABLE 4 Based on the findings of nanopore target sequencing (NTS), treatment changes.

Patient ID	Putative pathogens detected by blood NTS (reads)	Changes in antibiotic
NO.18#	*Staphylococcus aureus* (96)	Teicoplanin added
NO.37#	*Escherichia coli* (572), *Pseudomonas stutzeri* (293), *Acinetobacter guillouiae* (116)	Ceftazidime upgraded to meropenem

to this NTS feature. The benefit is that it can locate suspected infectious pathogens to the greatest extent possible, particularly unique diseases that cannot be found by culture or other techniques. It may be challenging to discern between important pathogens, conditional pathogens, and normal non-pathogenic symbiotic microbes, which is a drawback. Despite the fact that NTS can provide a reference based on the detection data, physicians' clinical expertise is ultimately what determines if the pathogen is a critical pathogen.

When we first evaluated the consistency of blood NTS and blood culture, we discovered that there was a 52.11% agreement between the two. The effectiveness of the two techniques in diagnosing clinical bloodstream infections was also contrasted. According to results of earlier studies (Wang et al., 2020a; Huang et al., 2021; Fu et al., 2022), it was discovered that the positive rate of blood NTS was significantly higher than that of blood culture (50.70%: 5.63%, $p < 0.001$), the sensitivity was also significantly higher than that of blood culture (62.50%: 7.14%, $p < 0.001$), and the NPV was also significantly higher than that of blood culture (40.00%: 22.39%). When we compare the overall outcomes of blood NTS and conventional pathogenic microbe identification (including blood culture, glucan test, galactomannan test, T cell spot test of tuberculosis infection, smear, etc.), the aforementioned conclusions are likewise drawn. One benefit of NTS is that it is almost unaffected to antibiotics, and the positive rate of culture changes significantly before and after antibiotic use (Cheng et al., 2019; Li et al., 2019). Culture detects living microorganisms, whereas NTS is based on microbial DNA detection. Some bacteria may be difficult to grow on conventional media, which may explain why NTS and culture are affected by antibiotics to varying degrees and also partially explains the difference in sensitivity between the two. This also suggests that NTS has a high false positive rate, which somewhat restricts its application, however its larger negative predictive value may be more useful. The findings of this study suggest that, particularly following empirical antibiotic treatment or the identification of specific pathogens, NTS has a greater diagnostic effectiveness than culture for clinical infections. Rapid detection is another benefit of NTS, with an initial report coming in 6 h after sample and a full report in 16 h (Wang et al., 2020a). In this investigation, 5 peripheral blood samples were collected from 5 individuals who took two NTS examinations. NTS can more quickly and precisely detect the alterations caused by infected strains in patients. When the No. 54 patients entered the intensive care unit, *Staphylococcus aureus* and *Acinetobacter baumannii* infections were found. NTS was negative after 3 days of therapy, and other indications including WBC, PCT, and others also indicated a decreased trend. When evaluating NTS, it was discovered that the infectious bacteria in the No. 37, No. 39, and No. 46 patients had changed, but the blood culture study findings did not reveal this change. This demonstrates that the use of NTS can reflect the clinical therapy impact more promptly. However, the pathogen load in the sample affects NTS detection. Wrong detection results may be produced when sample collection, processing, and storage are not uniform, there are technological faults, sample confusion, or insufficient initial sample concentration.

The main DDI organisms were Gram-negative bacteria, such as *Stenotrophomonas maltophilia*, *Pseudomonas aeruginosa*, methicillin-resistant *Staphylococcus aureus*, *Escherichia coli*, *Klebsiella pneumoniae*, and *Acinetobacter baumannii* (Bunsow et al., 2020). The presence of DDI in organ transplantation has a great impact on the prognosis of recipients. NTS was used in this investigation to identify 11 instances of *Escherichia coli* infection, 2 cases each of *Staphylococcus aureus* and *Pseudomonas aeruginosa*, and 1 case each of *Klebsiella pneumoniae*. However, one of the limitations of NTS was that it was unable to establish whether the identified bacteria were multidrug-resistant bacteria because it was unable to detect the drug sensitivity of the bacteria. However, NTS can preliminarily determine whether the bacteria are multidrug-resistant by comparing them to the published genome of multidrug-resistant bacteria. This can allow clinicians modify their usage of antibiotics and do target bacterial culture once more. Two NTS tests were performed on No. 69# patients on the same day, but only one result was positive, indicating some level of NTS error (van Dijk et al., 2018). Based on the patient's clinical symptoms and other relevant investigations, doctors must evaluate the NTS results. In this study, it was discovered that NTS revealed that 12 recipients and their matching 7 donors both had the same pathogen infection, but culture did not reveal this phenomenon. This finding suggests that NTS may be more accurate than culture for predicting postoperative infection in recipients. These 12 recipients may have DDI, as defined by the term (Wolfe et al., 2019). Additionally, the infections were Gram-negative bacilli (*Escherichia coli*), which was consistent with earlier research (Ison et al., 2013). However, because we were unable to obtain the recipient's pathogenic microorganisms' test results before the organ transplant operation (no pathogenic microorganisms were tested prior to the operation) and the results of these pathogens' drug sensitivity tests, it could not to definitively diagnose DDI, but may be NTS can be used as a powerful screening method and help to give timely treatment. In this study, the recipients included in the evaluation of the role of donor NTS results in predicting recipient infection were all renal recipients, which may be biased. In the future, a more thorough comparative analysis will be required to confirm this advantage.

This research contains some flaws. First off, the sample population in this study is limited and only originates from one center, which could have an impact on how well NTS can be detected. Second, all of the study subjects were deceased donors. Single patients made up the patient types, and they were all seriously ill. Therefore, it was not assessed if NTS might detect infections in other mild individuals. Thirdly, because this study was not retrospective cross-sectional, it was unable to determine how antibiotic therapy affected NTS outcomes. Fourthly, because the patients in this study had empirical anti-infective therapy before they were admitted to the intensive care unit, they might have some influence over the outcomes of the blood culture. Fifth, because this study only examined bacteria, fungus, mycoplasma, chlamydia, and other pathogens and did not compare viruses and spirochetes due to the lack of clinical case data, it was not feasible to assess the detection effectiveness of NTS for additional

10.3389/fmicb.2023.1238666

TABLE 5 The results of pathogenic microorganism examination of deceased donors and their corresponding renal recipients.

Deceased donors			Renal recipients					
Patient ID	Blood NTS results (reads)	Blood Culture results	Patient ID	Blood Culture results	Urine culture	Blood NTS results (reads)	Urine NTS results (reads)	Surgical site secretion culture results
NO.32	*Escherichia coli* (492), *Burkholderia vietnamiensis* (73)	Negative	NO.55	Negative	Negative	*Escherichia coli* (2395)	Non-implementation	Negative
			NO.56	Negative	Negative	*Escherichia coli* (5151), *Pseudomonas stutzeri* (72)	Non-implementation	*Escherichia coli*
NO.34	*Escherichia coli* (434)	Negative	NO.59	Negative	Negative	*Escherichia coli* (324), *Burkholderia cepacia* (1277), *Acinetobacter johnsonii* (4434)	Negative	Negative
			NO.60	Negative	Negative	*Escherichia coli* (89), *Streptococcus oralis* (111)	Negative	Negative
NO.36	*Pseudomonas fluorescens* (209), *Escherichia coli* (59)	Negative	NO.62	Negative	Negative	*Pseudomonas aeruginosa* (127), *Escherichia coli* (4227)	*Enterococcus gallinarum* (16)	Negative
			NO.63	Negative	Negative	*Staphylococcus aureus* (664), *Escherichia coli* (1297) , *Pseudomonas stutzeri* (228)	Negative	Negative
NO.37	*Escherichia coli* (973), *Acinetobacter guillouiae* (293), *Pseudomonas stutzeri* (116), *Corynebacterium mucifaciens* (4948)	Negative	NO.64	Negative	Negative	*Escherichia coli* (2352)	Non-implementation	Non-implementation
NO.39	*Escherichia coli* (256), *Anaerococcus octavius* (1481), *Acinetobacter haemolyticus* (218)	Negative	NO.68	Negative	Negative	*Escherichia coli* (132), *Pseudomonas luteola* (309)	Negative	Non-implementation
			NO.69	Negative	Negative	*Escherichia coli* (134), *Streptococcus oralis* (293), *Pseudomonas stutzeri* (270), *Malassezia.restricta* (361)	Negative	Negative
NO.50	*Escherichia coli* (548), *Pseudomonas hibiscicola* (203)	Negative	NO.88	non-implementation	Negative	*Pseudomonas stutzeri* (78), *Escherichia coli* (20)	Non-implementation	Negative
			NO.89	non-implementation	Negative	*Pseudomonas stutzeri* (364), *Escherichia coli* (169), *Pseudomonas oryzihabitans* (250)	Non-implementation	Negative
NO.51	*Escherichia coli* (156)	Negative	NO.90	Negative	Negative	*Escherichia coli* (67)	Non-implementation	Negative

NTS, Nanopore Target Sequencing.

diseases. The NTS results were debated among the multidisciplinary group's members, however there is no commonly agreed quantitative standard for the diagnosis of pathogenic microorganisms, thus there may be some bias due to possible false positives.

5. Conclusion

This study demonstrates the effectiveness of NTS for detecting possible bloodstream infections in deceased donors. It is not just an improvement over microbial culture methods; it also outperforms them. In terms of detection speed, positive rate, sensitivity, and identification of rare pathogens, it is superior than conventional microbiological detection. In addition, NTS may have an advantage in predicting recipient infection.

Data availability statement

The datasets presented in this study can be found in online repositories. The names of the repository/repositories and accession number(s) can be found at: National Genomics Data Center - 'CRA011898' (https://www.cncb.ac.cn).

Ethics statement

The studies involving humans were approved by the Renmin Hospital of Wuhan University's Ethics Committee of Clinical Research. The studies were conducted in accordance with the local legislation and institutional requirements. Written informed consent for participation was not required from the participants or the participants' legal guardians/next of kin in accordance with the national legislation and institutional requirements.

Author contributions

ZY and YL: responsible for data collection, data statistics, data analysis, and paper writing. LZ, TQ, GL, ZC, XF, ZhoL, WW, and ZhaL: responsible for data collection. WX: responsible for data collection and research guidance. All authors contributed to the article and approved the submitted version.

Acknowledgments

The authors express great respect to the patients who donated organs and thank them for their contribution to this study.

Conflict of interest

The authors declare that the research was conducted in the absence of any commercial or financial relationships that could be construed as a potential conflict of interest.

Publisher's note

Supplementary material

The Supplementary material for this article can be found online at: https://www.frontiersin.org/articles/10.3389/fmicb.2023.1238666/full#supplementary-material

References

Allerberger, F., and Kern, W. V. (2020). Bacterial bloodstream infection. *Clin. Microbiol. Infect.* 26, 140–141. doi: 10.1016/j.cmi.2019.10.004

Begaj, I., Khosla, S., Ray, D., and Sharif, A. (2013). Socioeconomic deprivation is independently associated with mortality post kidney transplantation. *Kidney Int.* 84, 803–809. doi: 10.1038/ki.2013.176

Benamu, E., Wolfe, C. R., and Montoya, J. G. (2017). Donor-derived infections in solid organ transplant patients: toward a holistic approach. *Curr. Opin. Infect. Dis.* 30, 329–339. doi: 10.1097/QCO.0000000000000377

Bunsow, E., Los-Arcos, I., Martin-Gómez, M. T., Bello, I., Pont, T., Berastegui, C., et al. (2020). Donor-derived bacterial infections in lung transplant recipients in the era of multidrug resistance. *J. Infect.* 80, 190–196. doi: 10.1016/j.jinf.2019.12.006

Byrd, A. L., Belkaid, Y., and Segre, J. A. (2018). The human skin microbiome. *Nat. Rev. Microbiol.* 16, 143–155. doi: 10.1038/nrmicro.2017.157

Chan, W. S., Au, C. H., Leung, S. M., Ho, D. N., Wong, E. Y. L., To, M. Y., et al. (2020). Potential utility of targeted nanopore sequencing for improving etiologic diagnosis of bacterial and fungal respiratory infection. *Diagn. Pathol.* 15:41. doi: 10.1186/s13000-020-00960-w

Charalampous, T., Kay, G. L., Richardson, H., Aydin, A., Baldan, R., Jeanes, C., et al. (2019). Nanopore metagenomics enables rapid clinical diagnosis of bacterial lower respiratory infection. *Nat. Biotechnol.* 37, 783–792. doi: 10.1038/s41587-019-0156-5

Cheng, M. P., Stenstrom, R., Paquette, K., Stabler, S. N., Akhter, M., Davidson, A. C., et al. (2019). Blood culture results before and after antimicrobial administration in patients with severe manifestations of sepsis: a diagnostic study. *Ann. Intern. Med.* 171:547. doi: 10.7326/M19-1696

Choi, A. Y., Jawitz, O. K., Raman, V., Mulvihill, M. S., Halpern, S. E., Barac, Y. D., et al. (2021). Predictors of nonuse of donation after circulatory death lung allografts. *J. Thorac. Cardiovasc. Surg.* 161, 458–466.e3. doi: 10.1016/j.jtcvs.2020.04.111

Ciuffreda, L., Rodríguez-Pérez, H., and Flores, C. (2021). Nanopore sequencing and its application to the study of microbial communities. *Comput. Struct. Biotechnol. J.* 19, 1497–1511. doi: 10.1016/j.csbj.2021.02.020

Cui, J., Li, M., Cui, J., Wang, J., Qiang, X., and Liang, Z. (2022). The proportion, species distribution and dynamic trends of bloodstream infection cases in a tertiary hospital in China, 2010–2019. *Infection* 50, 121–130. doi: 10.1007/s15010-021-01649-y

Fu, Y., Chen, Q., Xiong, M., Zhao, J., Shen, S., Chen, L., et al. (2022). Clinical performance of nanopore targeted sequencing for diagnosing infectious diseases. *Microbiol. Spectr.* 10, e00270–e00222. doi: 10.1128/spectrum.00270-22

Gouel-Cheron, A., Swihart, B. J., Warner, S., Mathew, L., Strich, J. R., Mancera, A., et al. (2022). Epidemiology of ICU-Onset Bloodstream Infection: Prevalence, Pathogens, and Risk Factors Among 150, 948 ICU Patients at 85 U.S. Hospitals*. *Crit. Care Med.* 50, 1725–1736. doi: 10.1097/CCM.0000000000005662

Home (n.d.). *GODT*. Available at: https://www.transplant-observatory.org/ (Accessed February 24, 2023).

Horan, T. C., Andrus, M., and Dudeck, M. A. (2008). CDC/NHSN surveillance definition of health care–associated infection and criteria for specific types of infections in the acute care setting. *Am. J. Infect. Control* 36, 309–332. doi: 10.1016/j.ajic.2008.03.002

Huang, Q., Fu, A., Wang, Y., Zhang, J., Zhao, W., and Cheng, Y. (2021). Microbiological diagnosis of endophthalmitis using nanopore targeted sequencing. *Clin. Exp. Ophthalmol.* 49, 1060–1068. doi: 10.1111/ceo.13992

Huang, J., Millis, J. M., Mao, Y., Millis, M. A., Sang, X., and Zhong, S. (2015). Voluntary organ donation system adapted to Chinese cultural values and social reality. *Liver Transpl.* 21, 419–422. doi: 10.1002/lt.24069

Ison, M. G., and Grossi, P.AST Infectious Diseases Community of Practice (2013). Donor-derived infections in solid organ transplantation. *Am. J. Transplant.* 13, 22–30. doi: 10.1111/ajt.12095

Kieslichova, E., Protus, M., Nemcova, D., and Uchytilova, E. (2019). Single mutidrug resistant enterobacteriacae donor-derived infection in four solid organ transplant recipients: a case report. *BMC Surg.* 19:111. doi: 10.1186/s12893-019-0574-9

Li, G., Sun, J., Pan, S., Li, W., Zhang, S., Wang, Y., et al. (2019). Comparison of the performance of three blood culture systems in a Chinese tertiary-care hospital. *Front. Cell. Infect. Microbiol.* 9:285. doi: 10.3389/fcimb.2019.00285

Liu, G., Wang, X., Wu, J., Peng, W., Wang, R., Huang, H., et al. (2019). Successful repair of kidney graft artery rupture secondary to infection using a preprocessed homologous "Y"-shaped iliac artery. *Clin. Transpl.* 33:e13493. doi: 10.1111/ctr.13493

Shi, B.-Y., Liu, Z.-J., and Yu, T. (2020). Development of the organ donation and transplantation system in China. *Chin. Med. J.* 133, 760–765. doi: 10.1097/CM9.0000000000000779

Sommerstein, R., Damonti, L., Marschall, J., Harbarth, S., Gasser, M., Kronenberg, A., et al. (2021). Distribution of pathogens and antimicrobial resistance in ICU-bloodstream infections during hospitalization: a nationwide surveillance study. *Sci. Rep.* 11:16876. doi: 10.1038/s41598-021-95873-z

Timsit, J.-F., Ruppé, E., Barbier, F., Tabah, A., and Bassetti, M. (2020). Bloodstream infections in critically ill patients: an expert statement. *Intensive Care Med.* 46, 266–284. doi: 10.1007/s00134-020-05950-6

Tong, L., Hu, X.-G., Huang, F., Huang, S.-W., Li, L.-F., Tang, Z.-X., et al. (2020). Clinical impacts and outcomes with possible donor-derived infection in infected donor liver transplantation: a single-center retrospective study in China. *J. Infect. Dis.* 221, S164–S173. doi: 10.1093/infdis/jiz591

Tyler, A. D., Mataseje, L., Urfano, C. J., Schmidt, L., Antonation, K. S., Mulvey, M. R., et al. (2018). Evaluation of oxford nanopore's MinION sequencing device for microbial whole genome sequencing applications. *Sci. Rep.* 8:10931. doi: 10.1038/s41598-018-29334-5

van Dijk, E. L., Jaszczyszyn, Y., Naquin, D., and Thermes, C. (2018). The third revolution in sequencing technology. *Trends Genet.* 34, 666–681. doi: 10.1016/j.tig.2018.05.008

Wang, M., Fu, A., Hu, B., Shen, G., Liu, R., Zhao, W., et al. (2020a). Same-day simultaneous diagnosis of bacterial and fungal infections in clinical practice by nanopore targeted sequencing. infectious diseases (except HIV/AIDS). *medRxiv*. doi: 10.1101/2020.04.08.20057604

Wang, M., Fu, A., Hu, B., Tong, Y., Liu, R., Liu, Z., et al. (2020b). Nanopore targeted sequencing for the accurate and comprehensive detection of SARS-CoV-2 and other respiratory viruses. *Small* 16:2002169. doi: 10.1002/smll.202002169

Wang, Y., Lei, H., Zhang, Y., Yang, Q., Wang, Y., Wang, J., et al. (2018). Epidemiology of carbapenem-resistant *Klebsiella pneumoniae* bloodstream infections after renal transplantation from donation after cardiac death in a Chinese hospital: a case series analysis. *Antimicrob. Resist. Infect. Control* 7:66. doi: 10.1186/s13756-018-0355-8

Whittle, E., Yonkus, J. A., Jeraldo, P., Alva-Ruiz, R., Nelson, H., Kendrick, M. L., et al. (2022). Optimizing nanopore sequencing for rapid detection of microbial species and antimicrobial resistance in patients at risk of surgical site infections. *mSphere* 7, e00964–e00921. doi: 10.1128/msphere.00964-21

Wirth, S. E., Ayala-del-Río, H. L., Cole, J. A., Kohlerschmidt, D. J., Musser, K. A., Sepúlveda-Torres, L. D. C., et al. (2012). *Psychrobacter sanguinis* sp. nov., recovered from four clinical specimens over a 4-year period. *Int. J. Syst. Evol. Microbiol.* 62, 49–54. doi: 10.1099/ijs.0.029058-0

Wolfe, C. R., and Ison, M. G.AST Infectious Diseases Community of Practice (2019). Donor-derived infections: guidelines from the American society of transplantation infectious diseases community of practice. *Clin. Transpl.* 33:e13547. doi: 10.1111/ctr.13547

Ye, Q.-F., Zhou, W., and Wan, Q.-Q. (2017). Donor-derived infections among Chinese donation after cardiac death liver recipients. *World J. Gastroenterol.* 23:5809. doi: 10.3748/wjg.v23.i31.5809

Yuan, X., Chen, C., Zhou, J., Han, M., Wang, X., Wang, C., et al. (2016). Organ donation and transplantation from donors with systemic infection: a single-center experience. *Transplant. Proc.* 48, 2454–2457. doi: 10.1016/j.transproceed.2016.02.092

frontiers | Frontiers in Microbiology

TYPE Review
PUBLISHED 28 August 2023
DOI 10.3389/fmicb.2023.1202752

OPEN ACCESS

EDITED BY
Arabella Touati,
Centre Hospitalier Universitaire de Bordeaux, France

REVIEWED BY
Megha Sharma,
AIIMS BILASPUR, India
Aliabbas A. Husain,
Central India Institute of Medical Sciences, India

*CORRESPONDENCE
An Wen
✉ wenan666@sina.com

RECEIVED 10 April 2023
ACCEPTED 21 July 2023
PUBLISHED 28 August 2023

CITATION
Cao W-F, Leng E-L, Liu S-M, Zhou Y-L, Luo C-Q, Xiang Z-B, Cai W, Rao W, Hu F, Zhang P and Wen A (2023) Recent advances in microbiological and molecular biological detection techniques of tuberculous meningitis.
Front. Microbiol. 14:1202752.
doi: 10.3389/fmicb.2023.1202752

Recent advances in microbiological and molecular biological detection techniques of tuberculous meningitis

Wen-Feng Cao[1,2], Er-Ling Leng[3], Shi-Min Liu[1,2], Yong-Liang Zhou[1,2], Chao-Qun Luo[1,2], Zheng-Bing Xiang[1,2], Wen Cai[1,2], Wei Rao[1,2], Fan Hu[1,2], Ping Zhang[1,2] and An Wen[1,2]*

[1]Department of Neurology, Jiangxi Provincial People's Hospital (The First Affiliated Hospital of Nanchang Medical College), Nanchang, Jiangxi, China, [2]Department of neurology, Xiangya Hospital, Central South University, Jiangxi Hospital, National Regional Center for Neurological Diseases, Nanchang, Jiangxi, China, [3]Department of Pediatrics, Jiangxi Provincial People's Hospital (The First Affiliated Hospital of Nanchang Medical College), Nanchang, Jiangxi, China

Tuberculous meningitis (TBM) is the most common type of central nervous system tuberculosis (TB) and has the highest mortality and disability rate. Early diagnosis is key to improving the prognosis and survival rate of patients. However, laboratory diagnosis of TBM is often difficult due to its paucibacillary nature and sub optimal sensitivity of conventional microbiology and molecular tools which often fails to detect the pathogen. The gold standard for TBM diagnosis is the presence of MTB in the CSF. The recognised methods for the identification of MTB are acid-fast bacilli (AFB) detected under CSF smear microscopy, MTB cultured in CSF, and MTB detected by polymerase chain reaction (PCR). Currently, many studies consider that all diagnostic techniques for TBM are not perfect, and no single technique is considered simple, fast, cheap, and efficient. A definite diagnosis of TBM is still difficult in current clinical practice. In this review, we summarise the current state of microbiological and molecular biological diagnostics for TBM, the latest advances in research, and discuss the advantages of these techniques, as well as the issues and challenges faced in terms of diagnostic effectiveness, laboratory infrastructure, testing costs, and clinical expertise, for clinicians to select appropriate testing methods.

KEYWORDS

tuberculous meningitis, *Mycobacterium tuberculosis*, microbiology, molecular biology, research progress

1. Introduction

Tuberculosis (TB) is a chronic infectious disease caused by *Mycobacterium tuberculosis* (MTB) that can affect many organs of the human body and is a serious public health problem. Tuberculous meningitis (TBM) is a subacute or chronic inflammation of the meningeal membrane caused by MTB invasion of the subarachnoid space. TBM is the most serious form of extrapulmonary TB and accounts for approximately 1% of TB cases worldwide (Foppiano Palacios and Saleeb, 2020). It has an average mortality rate of 30–40% (Pormohammad et al., 2019; Foppiano Palacios and Saleeb, 2020); the mortality rate is 10% in the first week, rising to

80% in the fifth week (Thwaites, 2013). Most survivors suffer long-term sequelae and even permanent disabilities (Thwaites et al., 2013).

TBM usually involves the pia mater, arachnoid, cerebral parenchyma, and cerebral vessels. The most common symptoms include headache, fever, night sweats, anorexia, nausea, vomiting, and seizures. A typical neurological examination is usually characterised by neck stiffness, fundus abnormalities, an altered level of consciousness, focal neurological deficits, and cranial nerve palsy (Marais et al., 2010). However, TBM is characterised by occult onset, varying clinical symptoms, and poor specificity of early clinical manifestations, which are similar to cryptococcal meningitis (Vidal et al., 2017) and partially treated bacterial meningitis (Wen et al., 2022); therefore, clinical diagnosis is difficult.

The cerebrospinal fluid (CSF) is colourless, transparent, or yellowish. The protein level is moderately elevated, and the sugar and chloride levels were decreased. Dynamic observation of the changes in the CSF is helpful for assisting diagnosis and evaluation of therapeutic effects (Marais et al., 2010). It is believed that in the acute phase of TBM, the CSF is neutrophilic and undergoes a mixed-cell cytological reaction in the subacute phase. After treatment with effective anti-TB drugs, the white blood cell count in the CSF decreases significantly, and neutrophils decrease gradually and disappear completely in the recovery period (Thwaites et al., 2004). Brain imaging examinations of patients with TBM can show hydrocephalus, meningeal enhancement, tuberculoma, cerebral infarction, and skull base enhancement. In addition, pulmonary TB (miliary TB) can be seen on lung scans (Marais et al., 2010; Wen et al., 2023). Typical blood, CSF, and cranial imaging changes improve the reliability of diagnosis, but cannot be used as a definitive diagnostic basis. In recent years, much progress has been made in the diagnosis of TBM using laboratory confirmation. Therefore, this article reviews the current situation of TBM diagnosis in microbiological and molecular biology and discusses the problems and challenges, providing a reference for clinicians.

2. Microbiological diagnostic tests

2.1. Smear microscopy

The 130-year-old Ziehl-Neelsen (Z-N) staining is a rapid and affordable diagnostic test widely available. Z-N staining uses microscopy to visualise acid-fast bacilli (AFB) in CSF, and remains the cornerstone of laboratory TBM diagnosis (Mai and Thwaites, 2017; Garg, 2019). However, this test usually requires >10,000 organisms to obtain a positive result. As most cases of CSF specimens are paucibacillary, the TBM diagnostic sensitivity is only approximately 10–20% (Thwaites et al., 2000; Wang and Xie, 2018; Stadelman et al., 2022). In recent years, the processing methods of CSF and the staining and microscopy techniques have improved, resulting in a significant improvement in the smear detection rate in some laboratories (Table 1).

2.1.1. CSF collection modifications

One study showed that 58% TBM sensitivity was achieved by obtaining a large volume of CSF (>6 mL) and analysing for >30 min (Thwaites et al., 2004). However, another study argued that taking ≥6 mL CSF may be dangerous for children and prolonged slide examination time > 30 min is not feasible for busy laboratory technicians (Yasuda et al., 2002; Wilkinson et al., 2017; Heemskerk et al., 2018). Kennedy and Fallon (1979) used multiple lumbar punctures to collect CSF for 52 patients with TBM. The Z-N staining results showed that the AFB detection rate was 37% after one lumbar puncture and 83% after four. However, this requires repeated lumbar puncture, which increases the burden on physicians and potential risk of complications, and is usually unacceptable to the patient. Another study showed that sensitivity decreases significantly with prolonged treatment time (Thwaites et al., 2004).

2.1.2. Modified Z-N staining of CSF (triton processing)

Recently, Chen et al. modified the conventional Z-N staining by adopting two additional key steps: centrifugation and separation of CSF samples by cytospin (1,000 ×*g* for 5–10 min) and permeabilisation by Triton X-100 (0.3% for 30 min) (Chen et al., 2012). A pilot study by Chen et al. included 29 patients with culture-confirmed TBM (0.5–1 mL CSF was required); the modified Z-N staining was positive in all patients, while conventional Z-N staining was only 22.9% (Chen et al., 2012). Subsequently, the method was assessed in a larger study of 280 individuals clinically diagnosed with TBM. In this study, the sensitivity of the modified Z-N staining was significantly higher than that of conventional Z-N staining (82.9% vs. 3.3%, respectively), using the clinical diagnosis as the gold standard (Feng et al., 2014). This modified technique significantly improved the detection rate of extracellular mycobacteria and enhanced the intracellular staining of bacilli. In addition, these simple modifications can be applied in most laboratories.

In 2018, the Thwaites team conducted a prospective, international, multicentre study involving 618 individuals with suspected TBM from Vietnam, South Africa, and Indonesia. Conventional and modified Z-N staining with cytospin methods were compared (Heemskerk et al., 2018). Unexpectedly, the sensitivities of the two methods were 66.4 and 67.5%, respectively, when using culture as the reference. This shows that the modified Z-N staining still lacks sensitivity and could not improve the diagnostic performance of TBM. The results of this study are inconsistent with those reported by a Chinese team. Further studies are needed to confirm the performance of the modified Z-N staining for TBM diagnosis.

2.1.3. Microscopy technique improvements

A meta-analysis found that fluorescence microscopy not only improves the sensitivity of sputum smear analysis compared with conventional light microscopy, but also enables slide evaluation in the same microscopic field with a higher efficiency and lower workload (Steingart et al., 2006). However, in addition to needing experienced technicians (Wilkinson et al., 2017; Garg et al., 2018), fluorescence microscopy often requires the use of toxic and carcinogenic dyes, such as auramine-rhodamine or acridine, which are relatively expensive and quench fluorescence quickly (Zou et al., 2016).

A study from China compared the practicality of conventional and modified Z-N staining for CSF specimens and found that the combination of modified Z-N staining and auramine O-free fluorescence microscopy showed significantly higher sensitivity (sensitivity of 96.2% and specificity of 89.3%) (Zou et al., 2016). Compared with light microscopy, the examination time with fluorescence microscopy was halved and the sensitivity increased by

TABLE 1 The diagnostic performance for selected tests for tuberculous meningitis (TBM) performed in CSF specimens.

Diagnostic tests for TBM (references)	Limit of detection (cfu/mL)	Sensitivity (%)	Specificity (%)	Role in current practice in TBM & Key points	
Ziehl-Neelsen staining	>10,000	8–20	100	**Used in routine practice**	
Wang and Xie (2018), Garg et al. (2019), Stadelman et al. (2022), and Ssebambulidde et al. (2022)				• Rapid test & inexpensive • Simple operation • High specificity	• Poor sensitivity •Exposure to toxic substances •Fail to differentiate between MTB & NTM
MTB culture	< 10 (Liquid medium) 10–100 (Solid medium)	50–70	100	**Used in routine practice**	
van Zyl-Smit et al. (2011), Bahr et al. (2019), Ahlawat et al. (2020), and Bhasin et al. (2020)				• High specificity (100% gold standard) • MTB detection & DST •Provide a vibrant pure culture	• Variable and low sensitivity • Time consuming • High requirements (biosafety Level III) on the laboratory
LAMP	Not available	43–88	80–100	**Conditional recommendation**	
Nagdev et al. (2011), Modi et al. (2016), Sun W. W. et al. (2017), and Yu et al. (2018)				• Rapid test & inexpensive • No special instruments are needed • High biosecurity •Its results are easy to identify	•Variable sensitivity and specificity • CSF specimens required further evaluation •High dependent on primer design
Xpert	~ 110	27–85	94.8–100	**WHO recommended for initial diagnosis**	
Rufai et al. (2017), Sharma et al. (2018), Hernandez et al. (2021), and Wakode et al. (2022)				• Rapid test • High specificity • MTB & RIF resistance detection • Semi-quantification of bacillary load	• Poor sensitivity & expensive •Poor diagnosis in EPTB and HIV+ and children • Unable to differentiate between dead and live bacteria
Xpert ultra	~ 10–15	44.19–92.9	93.9–100	**WHO recommended for initial diagnosis**	
Halliday et al. (2019), Wang G. et al. (2019), Cresswell et al. (2020), and Huang et al. (2021)				**Compared with Xpert**	
				• Lower LOD • Higher sensitivity	• Variable sensitivity • Cannot rule out TBM
mNGS	Not available	44–88.9	86.7–100	**Not recommended as a first-line diagnosis**	
Wang S. et al. (2019), Yan et al. (2020), and Ramachandran et al. (2022)				• Broad-coverage pathogen • Conducive to precision therapy	•Expensive •Difficult to detect intracellular bacteria/fungi •Prone to cross contamination •Affected by non-pathogenic microorganisms

MTB, *Mycobacterium tuberculosis*; NTM, non-tuberculous mycobacteria; DST, drug sensitive test; EPTB, extra-pulmonary; LOD, limit of detection.

10%, which was supported by the studies of Xia et al. (2013) and Steingart et al. (2006). Moreover, this method reduces harm to technicians and can be performed in a general laboratory.

Light-emitting diode (LED) fluorescence microscopy is cheaper than conventional fluorescence microscopy, using the culture method as a reference standard. Its sensitivity for diagnosing TB is 84%, with a specificity of 98%, a 6% increase in sensitivity compared to traditional Z-N microscopy (Marais et al., 2008; WHO Guidelines Approved by the Guidelines Review Committee, 2011). To compare the performances of the two microscopies in terms of examination

time, fading of fluorescently stained slides, and average unit cost, Xia et al. examined 11,276 slides from peripheral laboratories in China. LED fluorescence microscopy was found to have a higher smear-positive detection rate, shorter test time, and lower unit test costs. LED fluorescence microscopy may be an alternative to Z-N as a cost-effective method for detecting MTB (Xia et al., 2013). A review suggested that LED is inexpensive and has many advantages over conventional Z-N-based bright-field microscopy, and has become increasingly popular and is widely used as an alternative light source for fluorescence microscopy in recent years (Ojha et al., 2020).

These studies underscore that the differences in laboratory operator expertise, volume of CSF used, and time spent per sample can vary greatly and significantly affect results. Generally, the diagnostic efficiency of Z-N staining can be improved by increasing the volume of CSF (>6 mL), prolonging slide examination (>30 min), recruiting experienced technicians, adopting a modified Z-N staining method, and examining multiple specimens. However, in most low-resource clinical settings, the performance of this test remains unsatisfactory (Table 1).

2.2. Culture

Generally, the sensitivity of MTB CSF culture is slightly superior to that of the AFB smear (Thwaites et al., 2004). In addition, this method can be used to perform drug sensitivity tests and provide strains for other laboratory tests (such as molecular biological examination and strain identification) in the later stage, which is beneficial for TBM diagnosis and treatment. However, this technique is slow and cumbersome, and the extremely low bacterial load means it has variable and low sensitivities in patients with TBM, which makes diagnosis confirmation difficult (Wong et al., 2016, Ahlawat et al., 2020) (Table 1).

2.2.1. Solid culture

Traditional solid media includes Ogawa and Lowenstein-Jensen (L-J). There are many kinds of drug sensitivity tests, which are convenient to guide the selection of clinical anti-tuberculosis drugs and are widely used in developing countries. However, this method is time-consuming; under optimal conditions it takes up to 2–3 weeks to generate results and 3–4 weeks to show drug susceptibility (Caviedes et al., 2000). In addition, L-J culture has approximately 50–70% sensitivity compared to the case definitions (Thwaites et al., 2004).

2.2.2. Liquid culture

Owing to the rapid growth rate of MTB and the shortened drug sensitivity test time, liquid culture is currently superior to solid culture and has gradually replaced traditional L-J culture (Cheng et al., 1994; Caviedes et al., 2000). At present, BACTEC, mycobacteria growth indicator tubes (MGITs), and microscopic observation broth drug susceptibility (MODS) methods are widely used.

2.2.2.1. BACTEC culture system

In a study from India (Baveja et al., 2009), the CSF of 100 children with TBM was tested using BACTEC culture, Z-N staining, L-J culture, and polymerase chain reaction (PCR). The results showed that 22 cases were positive using BACTEC culture and PCR; the coincidence rate between BACTEC culture and PCR for TBM diagnosis was 100%. Among the 22 cases, only two were positive using Z-N staining and six using L-J culture. In another study examining 2,325 CSF samples, the positive rate of the BACTEC 460 TB culture system was 61%, while that of L-J culture was only 7% (Venkataswamy et al., 2007). These results indicate that BACTEC culture has a better sensitivity than traditional L-J culture for TBM.

2.2.2.2. Mycobacteria growth indicator tubes

Compared with L-J culture, MGITs are slightly more sensitive and the detection time is usually 2 weeks (Thwaites et al., 2004; Ssebambulidde et al., 2022). As a liquid culture, it has been indicated that the MGIT 960 has a high specificity in diagnosing TBM, but its sensitivity is only 30–60% (Bhasin et al., 2020). Richard et al. analysed the detection thresholds of four mycobacterium load determination techniques, and the results showed that the limit of detection (LOD) of MGIT was approximately 10 colony forming units (CFU)/mL (1 CFU = 1 organism), L-J culture was 10–100 CFU/mL, and the PCR method Xpert-MTB/RIF was approximately 100 CFU/mL (van Zyl-Smit et al., 2011).

2.2.2.3. Microscopic observation drug susceptibility

The MODS assay, established by Caviedes et al., is a drug susceptibility test based on the liquid culture method by microscopic observation. This assay is inexpensive, reliable, and can be used to simultaneously culture MTB and detect drug susceptibility in a short time (Caviedes et al., 2000). Based on Caws et al. (2007) compared the practicality of MODS to other techniques in the diagnosis of 156 patients with clinically suspected TBM. The positivity rates were 64.9% by MODS, 70.2% by MGIT, 70.2% by L-J culture, and 52.6% by Z-N staining. The MODS assay had low costs ($0.53 per specimen), and the median time to a positive test was significantly reduced to 10 days (Caws et al., 2007). Another study by Sanogo et al. found that the median time for MODS testing was 8 days (Sanogo et al., 2017).

MODS-Wayne is a convenient and sensitive test developed in recent years that can assess pyrazinamide (PZA) resistance by rapidly detecting pyrazinoic acid (a hydrolysed product of PZA), with a sensitivity of 92.7% and specificity of 99.3%. It is a very promising assay and there will be a large market in countries with a high TB burden and limited resources (Alcántara et al., 2019).

2.2.2.4. Other liquid culture methods

To shorten culture time, Bhattacharya et al. developed a novel bilayered medium and compared it with L-J, Middlebrook 7H10 medium, and Kirchner's medium. After 7 days of culture, the isolation rate of MTB by the bilayered medium was 81.7%, and the earliest positive time was 48 h. The isolation rate of this assay was significantly increased compared to the other methods tested, and the positive detection time was shortened (Bhattacharya et al., 2009). Another study further improved the sensitivity by using a 0.45 μm sterile filter to filter CSF and then culture the membrane (Kumar et al., 2008).

Researchers centrifuged and filtrated CSF from 112 children. Among them, 11 CSF samples were culture-positive after the centrifugation, and 13 CSF samples were culture-positive after filtration; among the samples that were treated with these two methods simultaneously, 17 (15.2%) were culture-positive (Selvakumar et al., 1996). This method improved the culture rate. CSF filtration is simple and inexpensive and can be performed even in

hospitals with poor medical conditions. The filtered membranes can be transported to a laboratory with conditions for cultivating MTB.

Compared with the traditional solid culture, the liquid culture system significantly increases the sensitivity, shortens the positive reporting time, and is simple to perform. However, CSF culture is often time-consuming and it is impossible to provide information for clinical diagnosis during the acute phase of TBM. In practice, most patients with TBM have complex and dangerous conditions and cannot wait for culture results before treatment. To ensure the safety of the laboratory environment, the culture of MTB should be performed in a biosafety Level III laboratory, which indirectly increases the cost of testing samples. Nevertheless, when the culture is positive, it plays an important role in subsequent drug susceptibility tests (Table 1).

3. Nucleic acid amplification tests

As there are few bacteria in the CSF with TBM, the application of microbial methods such as AFB staining and culture is limited, while molecular biological techniques are advantageous. The molecular detection of pathogens in CSF helps to diagnose TB and anti-TB drug resistance by detecting the MTB genome through NAATs. These are significantly more sensitive than smear assays and take less time diagnose than culture methods (Pormohammad et al., 2019). Furthermore, NAATs can detect TB DNA even after short-term anti-TB treatment (5–15 day) (Thwaites et al., 2004).

In 2019, a systematic review and meta-analysis of NAATs showed that the pooled sensitivity and specificity of NAATs were 82 and 99%, respectively, compared with the reference standard of culture. Compared with clinical case definitions, the sensitivity and specificity of NAAT were 68 and 98%, respectively (Pormohammad et al., 2019) (Table 1).

3.1. Multiplex polymerase chain reaction

Multiplex PCR can simultaneously amplify multiple target DNA fragments in a single test. It has been suggested that multiplex PCR can help distinguish MTB from non-tuberculous mycobacterial (NTM) species (Kumar et al., 2014). Kusum et al. used multiplex PCR with three primers, MPB64, IS6110, and protein b, in 210 CSF specimens. The sensitivity and specificity of TBM reached 94.4 and 100%, respectively (Kusum et al., 2011). In addition, researchers from Nepal used IS6110 and MPB64 as primers to diagnose TBM, with a sensitivity of 91.8% and specificity of 100% (Lekhak et al., 2016).

3.2. Nested PCR

Nested PCR uses two pairs of PCR primers to amplify a fragment of a target gene, which significantly increases the number of cycles compared to conventional PCR, allowing for easier detection and increased sensitivity (Rios-Sarabia et al., 2016; Garg, 2019). Huang et al. evaluated the efficacy of *rpo*B nested PCR, and the detection of MTB in CSF reached a sensitivity of 86% and specificity of 100% (Huang et al., 2009). Nora et al. obtained a sensitivity of 98% and specificity of 92% using nested PCR in TBM cases (Rios-Sarabia et al., 2016).

In recent years, Chinese researchers have developed a one-tube nested PCR-lateral flow strip test (OTNPCR-LFST) technique, which is fast, sensitive, and simple to operate. It maintains the sensitivity of traditional two-step nested PCR and reduces the chance of cross-contamination and the analysis time. The modification yielded a sensitivity of 89% and a specificity of 100% (Sun Y. et al., 2017).

Real-time PCR (RT-PCR) has been widely used because of quantitative detection, simple operation, small errors, and high automation. It can provide results within 2 h after the DNA extraction process (Ahlawat et al., 2020). Sharma et al. reported that RT-PCR using *rpo*B and MPB64 as targets simultaneously detected drug resistance and MTB in TBM, with a sensitivity of 83.63%, and rifampicin resistance was detected in three out of 110 TBM cases. The results were better than the 1.8 and 10.9% detection rates of smears and cultures, respectively (Sharma et al., 2015). Quantitative real-time PCR (qRT-PCR) was used to detect CSF "filtrates" and "sediments" to diagnose TBM with a sensitivity of 87.6 and 53.1%, respectively. Similar results were obtained using gel-based devR-and IS6110-PCR, suggesting that using filtrates instead of sediments provided more reliable results (Haldar et al., 2009). Additionally, other studies have indicated that the average sensitivity of RT-PCR for TBM diagnosis is 86%, which is superior to that of conventional PCR assays targeting the IS6110 and devR genes (Paverd, 1988; de Almeida et al., 2019; Ahlawat et al., 2020).

3.3. Loop-mediated isothermal amplification

Developed in 2000, LAMP is mainly used for DNA amplification of MTB genes IS6110, MPB64, and HspX. A meta-analysis by Chinese researchers showed that LAMP had a pooled sensitivity of 77% and specificity of 99% in extrapulmonary TB (Yu et al., 2018). A multitargeted LAMP assay has also been used for CSF samples. A study from India involving 250 patients (150 patients with TBM) yielded a pooled sensitivity of 88% and specificity of 100% for diagnosing TBM (Modi et al., 2016). In contrast, a study from China showed a sensitivity of 43.0% and specificity of 92.9% for diagnosing TBM using IS6110-based LAMP (Sun Y. et al., 2017). Nagdev et al. retrospectively evaluated the diagnostic value of LAMP in 27 CSF specimens (17 patients with TBM) and this assay yielded a sensitivity of 88% and a specificity of 80% (Nagdev et al., 2011). In one study, IS6110 loop-mediated isothermal amplification had a sensitivity of 88.23% and specificity of 80%, whereas nested PCR had a sensitivity of 52.9% and specificity of 90% (Sun W. W. et al., 2017).

This method does not require sophisticated laboratory infrastructure or strict conditions, can achieve specific and efficient amplification of target DNA at a constant temperature, and results can be read directly with the naked eye. In addition, it is a simple method with high biosecurity. Therefore, it is better suited for widespread implementation in resource-poor, TB-endemic countries (Seki et al., 2018). Currently, LAMP is used in pulmonary TB, and its diagnostic efficacy in extrapulmonary TB is still unclear. It is unclear whether LAMP can be a rule-out test for TB diagnosis in the Xpert MTB/RIF and the new Xpert MTB/RIF Ultra era (Modi et al., 2016). Accuracy

is highly dependent on primer design; therefore, its clinical application value needs to be further evaluated (Tables 1, 2).

3.4. Xpert MTB/RIF (Xpert)

Xpert is a real-time, fully automated, hemi-nested PCR assay developed by Cepheid (United States). Using *rpoB* as the target gene, Xpert can directly detect the MTB bacilli complex and RIF resistance in CSF and other clinical specimens simultaneously (Committee, WHO Guidelines Approved by the Guidelines Review, 2013; Kay et al., 2022). Xpert was endorsed by the World Health Organization (WHO) for the diagnosis of TB and has been widely used to detect MTB in sputum samples since 2010. In 2013, its utility was further expanded, and it was recommended for all forms of extrapulmonary TB, including TBM (Committee, WHO Guidelines Approved by the Guidelines Review, 2013, 2014).

However, studies have reported that Xpert's diagnostic performance for TBM is suboptimal (Patel et al., 2023), with a pooled sensitivity of 24–86% and a pooled specificity of 94.8–98.6% against microbially confirmed cases (Boyles and Thwaites, 2015; Rufai et al., 2017; Dorman et al., 2018; Sharma et al., 2018). Two studies from South Africa suggested that increasing the CSF volume tested can increase the diagnostic sensitivity (Patel et al., 2013; Bahr et al., 2015). Similarly, recent studies have shown that testing a large volume (at least 8–10 mL) of centrifuged CSF improves the performance of TBM diagnosis. However, this large volume is not always available in routine testing, especially in children and patients with low cranial pressure (Nhu et al., 2014; Bahr et al., 2016; Khonga and Nicol, 2018). Many studies have also shown that Xpert is highly effective in diagnosing MTB in CSF samples. Results are quick, with a turn-around time within 2 h compared to 2–3 weeks with culture methods (Kohli et al., 2018; Cresswell et al., 2020). In this regard, as a clinical reference standard, culture alone is not sufficient for the confirmation of TBM.

Xpert is rapid and highly automated, with higher biosafety than smear microscopy and lower cross-contamination risk than culture (Cresswell et al., 2018; Dorman et al., 2018; Shapiro et al., 2021). Although Xpert has high specificity for diagnosing TBM, its sensitivity is relatively low in clinical practice (especially in HIV-associated and smear-negative TB patients). While sensitivity can be improved by centrifuging CSF samples, it is necessary to combine it with other highly sensitive detection techniques to improve the early TBM diagnosis (Chen et al., 2022, Patel et al., 2023) (Tables 1, 2).

3.5. Xpert MTB/RIF ultra (Xpert ultra)

To reduce the limitations, Cepheid has developed a next-generation Xpert assay called Xpert Ultra, which uses the original reaction system and equipment while doubling the specimen volume. The detection technique was changed from semi-nested to nested PCR. At the same time, two DNA targets (IS6110 and IS1081) were added for more accurate identification of MTB and RIF resistance (Bahr et al., 2018, 2019; Kay et al., 2020). Some studies have confirmed that the LOD is lower for Xpert Ultra (16 cfu/mL) compared with Xpert (114 cfu/mL) (Chakravorty et al., 2017; Committee, WHO Guidelines Approved by the Guidelines Review, 2020). In theory, this means that Xpert Ultra can detect MTB in clinical specimens that contain a small amount of MTB, yielding more positive results (Kohli et al., 2021).

Multiple studies have demonstrated the efficacy of this technique in TBM diagnosis. In 2018, Bahr et al. evaluated the diagnostic value

TABLE 2 Comparison of various molecular biological detection tests for the diagnosis of tuberculous meningitis (TBM).

Tests	Technique Used	Testing purpose	Target gene	Report time (h)	Sensitivity (%)	Specificity (%)	References
LAMP	Thermostatic amplification technique	Etiology	IS6110, MPB64 and HspX etc.	1	43–88	80–100	Nagdev et al. (2011), Modi et al. (2016), and Sun W. W. et al. (2017)
Xpert MTB/RIF	Real-time fluorescence quantitative PCR	Etiology and drug resistance	rpoB	2	27–85	94.8–100	Rufai et al. (2017), Hernandez et al. (2021), and Wakode et al. (2022)
Xpert MTB/RIF Ultra	High resolution melting	Etiology and drug resistance	rpoB, IS6110, IS1081	1.5	44.19–92.9	93.9–100	Wang G. et al. (2019), Cresswell et al. (2020), and Huang et al. (2021)
mNGS	Gene sequencing	Etiology	Standard sequences in the database	24–48	44–88.9	86.7–100	Zhou et al. (2019), Yan et al. (2020), and Ramachandran et al. (2022)
GenoType MTB DRplus	Molecular line probe assay	Etiology and drug resistance	rpoB, inhA, and katG	24	33–76.3	98	Gupta et al. (2015), Solomons et al. (2015), and Mitha et al. (2020)

of Xpert Ultra in 23 HIV-positive patients with definite and probable TBM. Xpert Ultra had a 70% sensitivity compared to 43% with MGIT or 43% with Xpert (Bahr et al., 2018). In 2019, Xpert Ultra was shown to be more sensitive than Xpert (44.2% vs. 18.6%, respectively) in 43 HIV-negative patients clinically diagnosed with TBM (Wang G. et al., 2019). Similar results were also obtained in a Chinese study where Xpert Ultra sensitivity was higher than that of Xpert (45% vs. 28%, respectively) in 76 HIV-negative clinical patients diagnosed with TBM (Huang et al., 2021). In 2020, Cresswell et al. further confirmed that the sensitivity of Xpert Ultra was higher than that of Xpert and MGIT in a prospective study that enrolled TBM patients with HIV (Cresswell et al., 2020).

Despite the higher sensitivity of Xpert Ultra, its negative predictive value is inadequate, varying from 61.1–92.7%; a negative result cannot exclude TBM. Therefore, further MGIT 960 culture is recommended for Xpert Ultra negative samples; it is a rule in testing, but not a confidently rule-out test (Cresswell et al., 2020; Donovan et al., 2020a,b). Other studies have noted that Xpert Ultra's performance is characterised by low LOD and detection of dead bacteria after starting anti-TB or HIV treatment. Therefore, it can detect MTB in cases missed by culture or Xpert (Bahr et al., 2018; Khonga and Nicol, 2018). Although the assay thresholds for both Xpert Ultra and culture were similar, the former had a small number of false-positive results in patients with a history of TB, which could be due to the presence of inactive bacilli or MTB DNA in clinical samples (Arend and van Soolingen, 2018; Dorman et al., 2018; Opota et al., 2019).

Recent research has shown that Xpert Ultra is a potential gamechanger with more advantages than Xpert in TBM diagnosis. Xpert Ultra has increased sensitivity (including accuracy of RIF resistance testing), and detection of MTB in smear-negative, paucibacillary, paediatric, CSF, and other specimens of extrapulmonary TB (Kaswala et al., 2022; Signorino et al., 2022; Sun et al., 2022). In 2017, WHO recommended the use of Xpert Ultra to replace Xpert in diagnosing TBM (Bahr et al., 2018; Rindi, 2022). Despite this, a larger sample size (especially in HIV-negative patients) or more prospective studies are needed to evaluate its diagnostic performance (Tables 1, 2).

3.6. Metagenomic next-generation sequencing

mNGS does not rely on traditional microbial culture and can conduct high-throughput sequencing of nucleic acids in clinical samples, rapidly detecting pathogens at the genome level. Theoretically, it can detect all pathogens (viruses, fungi, bacteria, and parasites), providing exact diagnosis for difficult diseases and rare pathogen infections when other testing techniques fail. The development of mNGS may provide a new method for the diagnosis of TBM.

A retrospective study in 2019 reported that the sensitivity of mNGS was 66.7%, which was significantly higher than that of traditional methods such as smear (33.3%), PCR (25.0%), and culture (8.3%), using definite TBM as the reference standard (Wang S. et al., 2019). Analysis by Yan et al. showed the sensitivity of mNGS for TBM in 51 inpatient cases (45 patients with TBM) was significantly higher than that of AFB, MGIT960, MTB PCR, and Xpert (84.4, 0, 22.2, 24.4 and 40.0%, respectively) (Yan et al., 2020). Another retrospective, multi-centre study from China had similar results, indicating that mNGS combined with modified Z-N staining or Xpert could improve TBM diagnosis sensitivity (Chen et al., 2022). A meta-analysis from China evaluating the TBM diagnostic accuracy of mNGS found that mNGS sensitivity was moderate, whereas the specificity was high. Due to the high heterogeneity of the included literature, the conclusions should be treated with caution (Yu et al., 2020). A large prospective study from Uganda involving 368 HIV-infected adults with subacute meningitis showed a sensitivity of 88.9% and specificity of 86.7% by integrating CSF mNGS with a machine learning classifier (MLC) based on host gene expression (Ramachandran et al., 2022). mNGS requires a large volume of CSF (at least 3–5 mL), relatively long detection time (24–48 h), and high cost, which limits wide clinical application. In terms of pathogen detection, mNGS is advantageous for providing a large amount of information that can be searched for clues. From this perspective, mNGS is undoubtedly an important tool. However, mNGS is characterised by a relatively complex detection process, easy contamination by exogenous nucleic acids, long detection time, high professional requirements for result interpretation, difficulty in determining whether the TBM is resistant, and high detection cost.

As the clinical application time of mNGS is low, the clinical significance of mNGS detection remains unclear. The number of sequences of mNGS detection has diagnostic value in which pathogens are clinically significant, and the types of reliable specimens require further research. In summary, mNGS is not recommended as a first-line detection method. It can be considered when traditional tests fail to provide clear etiological results, affecting the accurate diagnosis and treatment, or in emergency situations, where it can used for detection simultaneously with the conventional method (Tables 1, 2).

3.7. Other molecular biological detection techniques

GenoType MTB DRplus is a commercially available molecular line probe assay to assess isoniazid and rifampicin resistance by identifying mutations in the *inhA*, *katG*, and *rpoB* genes in MTB isolates. A multicentre prospective study from India examined MTB isolates in CSF specimens from patients diagnosed with TBM. Using the BACTEC MGIT drug sensitivity test as the gold standard, the sensitivity and specificity of this assay to isoniazid resistance was 93 and 97%, and rifampicin resistance was 80 and 98.8%, respectively (Gupta et al., 2015). A small sample study from South Africa found that GenoType MTB DRplus had a sensitivity of only 33% and specificity of 98% (Solomons et al., 2015). Owing to its low sensitivity, complex operation, and high price, it is not widely used in the clinic (Table 2).

High-resolution melting curve analysis (HRM) is a new gene analysis technique based on the different melting temperatures of single nucleotides and the formation of varying melting curves (Sharma et al., 2017). A study evaluated the role of real-time PCR targeting *rpo*B, IS6110, and MPB64 in diagnosing patients with TBM, followed by HRM curve analysis of rpoB gene amplicons to screen for drug resistance. The sensitivity of RT-PCR was much higher than those of culture and smears (83.63, 10.9, and 1.8%, respectively). *rpo*B HRM analysis revealed that rifampicin resistance was detected in three of 110 TBM cases (3.33%) (Sharma et al., 2015). This study indicates that *rpo*B HRM can rapidly diagnose and screen for drug

resistance in patients with TBM within 90 min, which is simple and fast, and is more suitable for clinical promotion (Sharma et al., 2015).

In a study of 46 patients with clinically diagnosed TBM by Li et al., the sensitivity of detecting MTB cell-free DNA (cfDNA) (56.5%) in CSF was significantly higher than that of smear (2.2%), culture (13.0%), and Xpert (23.9%) methods (Li X. et al., 2020). A multi-centre prospective study conducted at three TB-specialised hospitals in China found that the cfDNA technique sensitivity was 93.3%, consistent with Xpert Ultra and higher than that of culture methods (13.3%) (Shao et al., 2020).

Matrix-assisted laser desorption ionization-time of flight mass spectrometry (MALDI-TOF MS) is a rapidly developed bioassay with high-throughput characteristics that can be used to identify TB and non-TB bacteria strains. It has the advantages of high resolution, speed, and accuracy and requires fewer bacteria. A previous study showed that the overall detection sensitivity and specificity of MALDI-TOF MS were 92.2 and 100.0% for rifampicin, 90.9 and 98.6% for isoniazid, 71.4 and 81.2% for ethambutol, and 85.1 and 93.1% for streptomycin. This suggests that MALDI-TOF MS has a good performance in predicting the drug resistance of TB bacteria (Wu et al., 2022). Other studies have shown some limitations to the type of drugs that MALDI-TOF MS screens for TB resistance, and drugs with less than 45% of the relevant resistance gene mutations may reduce the sensitivity of this approach (Shi et al., 2022). This technology has some limitations: expensive testing equipment and high technical requirements difficult its promotion in many TB control institutions.

Researchers have used targeted next-generation sequencing (tNGS) to simultaneously detect MTB in bronchoalveolar lavage fluid from patients with TB and to detect resistance to first-line anti-TB drugs, such as rifampicin, isoniazid, ethambutol, and pyrazinamide. Finally, the MTB detection rate of tNGS was 63.1%, which was significantly higher than that of acid-fast bacilli smears (32.3%), cultures (32.3%), and immunological tests (48.6%). Simultaneously, tNGS showed similar sensitivity to Xpert MTB/RIF, using clinical diagnosis as the reference standard. Of the 130 patients, Xpert identified four RIF resistance cases, and phenotypic drug susceptibility testing (pDST) confirmed one as a false positive. All false positive cases were found to be INH resistant using tNGS and pDST. Using pDST as the reference standard, the sensitivity and specificity of tNGS for detecting RIF resistance were 100%, and the sensitivity and specificity for detecting INH resistance were 80 and 100%, respectively (Wu et al., 2023).

Li et al. used digital PCR (dPCR) to detect MTB in 101 HIV-negative patients with TBM, using IS6110 as the target gene, with a higher sensitivity than that of Xpert (70% vs. 30%, respectively) (Li Z. et al., 2020). Ai et al. used a Clustered regularly interspaced short palindromic repeat (CRISPR)-based assay to detect the CSF of 27 patients clinically diagnosed with TBM, with a sensitivity of 73%, which was significantly higher than that of Xpert (54%) and culture (25%) (Ai et al., 2019).

Drug-resistant TB is increasing, and a 5-year retrospective study from India showed that 17.5% of TBM cases are multidrug-resistant (MDR), defined as resistance to both rifampicin and isoniazid (Nagarathna et al., 2008). The Xpert MTB/XDR automated molecular assay (Xpert XDR) is an Xpert Ultra's next-generation test that can be used to detect mutations in resistance genes for isoniazid, fluoroquinolones, ethionamide, and second-line injectable drugs (amikacin, kanamycin, and capreomycin). In a prospective multicenter diagnostic accuracy study, Xpert XDR showed a sensitivity of 94, 94, 73, 86, and 61% for isoniazid resistance, fluoroquinolones, amikacin, kanamycin, and capreomycin, respectively, with a specificity of 98–100% for all drugs. Its diagnostic efficacy was comparable to that of linear probe analysis. The results showed that Xpert XDR technology has high diagnostic accuracy, quickly and accurately diagnoses drug-resistant tuberculosis, and provides the best treatment plan (Penn-Nicholson et al., 2022). Although Xpert XDR is a promising diagnostic method, further evaluation of its efficacy in clinical specimens from different sources, including special populations such as people with human immunodeficiency virus and children, is needed. BD MAX MDR-TB is a new automated molecular diagnostic platform for detecting MTB in clinical extrapulmonary and pulmonary specimens and its resistance to rifampicin and isoniazid (Sağıroğlu and Atalay, 2021). The system can simultaneously test up to 24 samples and produce results within 4 h (Hofmann-Thiel et al., 2020). The sensitivity and specificity of this assay for detecting rifampicin resistance in MTB were 90 and 95%, respectively, and those for detecting isoniazid resistance in MTB were 82 and 100%, respectively, compared to the drug sensitivity test (Shah et al., 2020).

Recently, India has introduced the Truenat system, which is more suitable for use in low-income countries with high TB prevalence, with high test efficiency and low test cost. Truenat MTB, MTB Plus, and MTB-RIF Dx assays just-in-time test platforms are available (Chakaya et al., 2021; WHO Guidelines Approved by the Guidelines Review Committee, 2021). Several studies have shown that the overall sensitivities of Truenat MTB and MTB Plus reached 83 and 89%, respectively, and the overall specificities reached 99 and 98%, respectively. The overall sensitivity and specificity of Truenat MTB-RiF Dx for the diagnosis of rifampicin resistance were 93 and 95%, respectively. Its diagnostic performance was similar to those of Xpert and Xpert Ultra (Meaza et al., 2021; Penn-Nicholson et al., 2021; Ngangue et al., 2022; Sharma et al., 2022). Moreover, an Indian study of 148 CSF samples with 76 confirmed, 32 probable, and 40 non-TBM controls found that the Truenat assay performed as well as the Xpert Ultra assay in diagnosing TBM (Sharma et al., 2021). However, it is inferior to the Xpert Ultra in determining rifampicin resistance. Nevertheless, compared with GeneXpert, Truenat MTB requires less specimen volume (from 1 mL for GeneXpert to 0.5 mL for Truenat MTB). The Truenat technology only takes 1 h to complete the entire test process. The advantage of Truenat technology is that the rifampicin resistance is tested only when the specimen test results are positive for TB, which significantly reduces the cost of reagents and testing (Acharya et al., 2020; Meaza et al., 2021).

Results of these studies need to be taken with caution as the sample sizes were small. In the future, more cases from different populations will be required to determine the precise role of these methods in TBM diagnosis.

Recently, the continuous development of molecular biotechnology has become a rapid and effective means to improve the etiological detection rate of MTB and realize early and rapid diagnosis of TB and drug-resistant TB. Conventional NAATs are easy to pollute and cumbersome to operate; usually, only qualitative analysis, medium sensitivity, and non-specific amplification are used, but their international standards are complete, the cost of the required instruments and reagents is low, and PCR products can be recycled for other molecular biology experiments and cannot be completely

replaced. Conventional and novel NAATs should be a reasonable choice according to the specific situation and their respective advantages and cannot blindly pursue expensive technology. Our understanding of many novel NAATs is insufficient, and their clinical significance remains unclear. Large-scale prospective multicenter clinical studies are needed to accumulate more data.

4. Proteomics

In 2011, Kataria et al. applied CSF proteomics to the study of TBM and found that the expression levels of 11 human and eight mycobacterial proteins changed using 2-dimensional difference gel electrophoresis and mass spectrometry. Further screening indicated that arachidonate 5-lipoxygenase has a potential diagnostic value in TBM (Kataria et al., 2011). Ou et al. found differences between the calcium-binding protein A8 (S100A8) and lipoprotein B-100 in the TBM group compared with cryptococcal meningitis and healthy control groups (Mu et al., 2015). Simultaneously, Mu et al. found that the lipoprotein B-100 is a diagnostic protein marker for TBM (Mu et al., 2015). In 2022, Huang et al. identified eight different proteins, which were further verified using enzyme-linked immunosorbent assay (ELISA), and found that a combination of three biomarkers (APOE, APOAl, and S100A8) was a diagnostic protein marker for TBM (Huang et al., 2022).

However, these studies screened only one or two candidate proteins for western blotting or ELISA verification. The study sample size was small, and the individuals in the control group had only one disease and were mainly healthy. Therefore, expanding the sample size and increasing the number of disease types in the control group is necessary for independent verification of the screened proteins.

5. Discussion

TBM is a serious threat to human life, and rapid diagnosis and timely treatment are key factors in determining patient prognosis (Wilkinson et al., 2017). However, the sensitivity of existing laboratory tests is low, and sometimes all test results are negative or only one is positive. Therefore, combining multiple tests is necessary to improve the MTB detection rate. In addition, any diagnosis that considers TBM should be examined for the presence of TB foci outside the central nervous system, particularly in the lungs (Galimi, 2011; Donovan et al., 2020c).

Microbiological examination of the CSF is the traditional TBM diagnostic method. However, as MTB concentration in CSF rarely exceeds 100–1,000 colonies/mL (Davis and Wilkinson, 2020), the results of CSF microbiological detection methods are unsatisfactory. MTB culture in CSF is a conventional method for TBM diagnosis, which plays a decisive role. However, this method is time-consuming. Recently, the detection efficiency of MTB has been improved owing to the wide application of liquid culture medium, but rapid TBM diagnosis in the early stage is still difficult (Mai and Thwaites, 2017). AFB staining of CSF smears is the most widely used detection method. It is simple, rapid, and inexpensive, but the sensitivity is poor, so it is necessary to repeat the test and increase the number of smears to improve MTB detection rate (Kennedy and Fallon, 1979). In recent years, improvements have been made in the CSF collection and treatment methods, and in staining and microscopy techniques, resulting in a significant increase in the positive rate of smears in some laboratories. However, the conclusions are not widely verified, and repeated testing and refining of multi-centre, large sample, randomised controlled clinical trials are needed to guide clinical medical strategies accurately, reliably, and effectively.

In recent years, the continuous development of molecular biological techniques has improved MTB detection from the cellular to molecular level. These detection techniques have the advantages of rapidity, repeatability, and high throughput. They have become a rapid and effective means to improve MTB and drug resistance detection rates (Pormohammad et al., 2019). However, these emerging technologies also have limitations. The requirements for laboratory equipment and trained technical operators are higher. Additionally, false-negative results can occur, and a negative result does not rule out TBM even with Xpert Ultra, which is currently the most sensitive diagnostic tool (Cresswell et al., 2020; Donovan et al., 2020a,b). This emphasises that a clear understanding of these detection techniques is needed by clinicians, otherwise they may cause treatment delays or misdiagnosis, greatly increasing the economic burden on patients.

Research on the microbiology and molecular biology of TBM still faces many challenges. First, the inclusion criteria for patients with TBM are inconsistent, making parallel comparisons difficult. According to the Marais score criteria (in 2010), TBM is classified as definite, probable, and possible (Marais et al., 2010). Some studies included only confirmed TBM, while others included confirmed and probable TBM or all suspected TBM, as well as some studies including people with HIV, making direct comparisons difficult between the few published studies. Second, including CSF specimens in assessing the diagnostic value of the test is difficult. CSF is obtained through an invasive lumbar puncture, and only a limited number of CSF samples can be taken for testing at a time. Due to the relatively low incidence of TBM, many studies have small sample sizes, and the reliability of the diagnostic value assessed is not high. Third, control groups are often inconsistent from study to study; therefore, caution is needed when comparing and evaluating the results. Studies with a greater number of control groups are more difficult, but the conclusions are more reliable. Fourth, molecular biological technologies are more expensive than traditional microbiological tests for MTB, making it difficult for these technologies to be utilised in low-and medium-developed countries where a larger proportion of patients have TBM. In future research, it is particularly important to develop molecular detection technology suitable for regions with limited medical conditions on the basis of comprehensive measurement of technical performance and economic affordability.

6. Conclusion

In conclusion, although great progress has been made in the laboratory diagnosis of TBM, challenges remain. With the advent of precision diagnosis and treatment, molecular biology has been widely studied and applied. However, we must emphasize that classical microbiology technology should not be ignored, and the two should be combined to complement each other. Clinicians need to understand the characteristics of various diagnostic methods and choose the most reasonable and economical detection methods according to different patient conditions, instead of blindly seeking new methods and casting nets.

Author contributions

AW, W-FC, and E-LL designed the study. AW wrote the manuscript. S-ML, Y-LZ, and C-QL did the data searches and study selection. Z-BX and WC did the data synthesis. WR, FH, and PZ created the tables. All authors contributed to the article and approved the submitted version.

Funding

This work was supported by grant from Jiangxi Provincial Health Commission Foundation (no. 202310122).

Conflict of interest

The authors declare that the research was conducted in the absence of any commercial or financial relationships that could be construed as a potential conflict of interest.

Publisher's note

All claims expressed in this article are solely those of the authors and do not necessarily represent those of their affiliated organizations, or those of the publisher, the editors and the reviewers. Any product that may be evaluated in this article, or claim that may be made by its manufacturer, is not guaranteed or endorsed by the publisher.

References

Acharya, B., Acharya, A., Gautam, S., Ghimire, S. P., Mishra, G., Parajuli, N., et al. (2020). Advances in diagnosis of tuberculosis: an update into molecular diagnosis of *Mycobacterium tuberculosis*. *Mol. Biol. Rep.* 47, 4065–4075. doi: 10.1007/s11033-020-05413-7

Ahlawat, S., Chaudhary, R., Dangi, M., Bala, K., Singh, M., and Chhillar, A. K. (2020). Advances in tuberculous meningitis diagnosis. *Expert. Rev. Mol. Diagn.* 20, 1229–1241. doi: 10.1080/14737159.2020.1858805

Ai, J. W., Zhou, X., Xu, T., Yang, M., Chen, Y., He, G. Q., et al. (2019). CRISPR-based rapid and ultra-sensitive diagnostic test for *Mycobacterium tuberculosis*. *Emerg Microbes Infect.* 8, 1361–1369. doi: 10.1080/22221751.2019.1664939

Alcántara, R., Fuentes, P., Antiparra, R., Santos, M., Gilman, R. H., Kirwan, D. E., et al. (2019). MODS-Wayne, a colorimetric adaptation of the microscopic-observation drug susceptibility (MODS) assay for detection of *Mycobacterium tuberculosis* pyrazinamide resistance from sputum samples. *J. Clin. Microbiol.* 57, e01162–e01118. doi: 10.1128/jcm.01162-18

Arend, S. M., and van Soolingen, D. (2018). Performance of Xpert MTB/RIF ultra: a matter of dead or alive. *Lancet Infect. Dis.* 18, 8–10. doi: 10.1016/S1473-3099(17)30695-3

Bahr, N. C., Marais, S., Caws, M., van Crevel, R., Wilkinson, R. J., Tyagi, J. S., et al. (2016). Gene Xpert MTB/Rif to diagnose tuberculous meningitis: perhaps the first test but not the last. *Clin. Infect. Dis.* 62, 1133–1135. doi: 10.1093/cid/ciw083

Bahr, N. C., Meintjes, G., and Boulware, D. R. (2019). Inadequate diagnostics: the case to move beyond the bacilli for detection of meningitis due to *Mycobacterium tuberculosis*. *J. Med. Microbiol.* 68, 755–760. doi: 10.1099/jmm.0.000975

Bahr, N. C., Nuwagira, E., Evans, E. E., Cresswell, F. V., Bystrom, P. V., Byamukama, A., et al. (2018). Diagnostic accuracy of Xpert MTB/RIF ultra for tuberculous meningitis in HIV-infected adults: a prospective cohort study. *Lancet Infect. Dis.* 18, 68–75. doi: 10.1016/S1473-3099(17)30474-7

Bahr, N. C., Tugume, L., Rajasingham, R., Kiggundu, R., Williams, D. A., Morawski, B., et al. (2015). Improved diagnostic sensitivity for tuberculous meningitis with Xpert(®) MTB/RIF of centrifuged CSF. *Int. J. Tuberc. Lung Dis.* 19, 1209–1215. doi: 10.5588/ijtld.15.0253

Baveja, C. P., Gumma, V., Jain, M., Choudhary, M., Talukdar, B., and Sharma, V. K. (2009). Newer methods over the conventional diagnostic tests for tuberculous meningitis: do they really help? *Trop. Dr.* 39, 18–20. doi: 10.1258/td.2008.080082

Bhasin, H., Goyal, M., and Sharma, S. (2020). Advances in the diagnosis and Management of Tubercular Meningitis in children. *Indian J. Pediatr.* 87, 26–33. doi: 10.1007/s12098-019-03089-x

Bhattacharya, S., Roy, R., Chowdhury, N. R., Dasgupta, A., and Dastidar, S. G. (2009). Comparison of a novel bilayered medium with the conventional media for cultivation of *Mycobacterium tuberculosis*. *Indian J. Med. Res.* 130, 561–566.

Boyles, T. H., and Thwaites, G. E. (2015). Appropriate use of the Xpert® MTB/RIF assay in suspected tuberculous meningitis. *Int. J. Tuberc. Lung Dis.* 19, 276–277. doi: 10.5588/ijtld.14.0805

Caviedes, L., Lee, T. S., Gilman, R. H., Sheen, P., Spellman, E., Lee, E. H., et al. (2000). Rapid, efficient detection and drug susceptibility testing of *Mycobacterium tuberculosis* in sputum by microscopic observation of broth cultures. The tuberculosis working Group in Peru. *J. Clin. Microbiol.* 38, 1203–1208. doi: 10.1128/JCM.38.3.1203-1208.2000

Caws, M., Dang, T. M., Torok, E., Campbell, J., Do, D. A., Tran, T. H., et al. (2007). Evaluation of the MODS culture technique for the diagnosis of tuberculous meningitis. *PLoS One* 2:e1173. doi: 10.1371/journal.pone.0001173

Chakaya, J., Khan, M., Ntoumi, F., Aklillu, E., Fatima, R., Mwaba, P., et al. (2021). Global tuberculosis report 2020- reflections on the global TB burden, treatment and prevention efforts. *Int. J. Infect. Dis.* 113, S7–S12. doi: 10.1016/j.ijid.2021.02.107

Chakravorty, S., Simmons, A. M., Rowneki, M., Parmar, H., Cao, Y., Ryan, J., et al. (2017). The new Xpert MTB/RIF ultra: improving detection of *Mycobacterium tuberculosis* and resistance to Rifampin in an assay suitable for point-of-care testing. *MBio* 8, e00812–e00817. doi: 10.1128/mBio.00812-17

Chen, P., Shi, M., Feng, G. D., Liu, J. Y., Wang, B. J., Shi, X. D., et al. (2012). A highly efficient Ziehl-Neelsen stain: identifying de novo intracellular *Mycobacterium tuberculosis* and improving detection of extracellular *M. tuberculosis* in cerebrospinal fluid. *J. Clin. Microbiol.* 50, 1166–1170. doi: 10.1128/JCM.05756-11

Chen, Y., Wang, Y., Liu, X., Li, W., Fu, H., Liu, X., et al. (2022). Comparative diagnostic utility of metagenomic next-generation sequencing, gene Xpert, modified Ziehl-Neelsen staining, and culture using cerebrospinal fluid for tuberculous meningitis: a multi-center, retrospective study in China. *J. Clin. Lab. Anal.* 36:e24307. doi: 10.1002/jcla.24307

Cheng, A. F., Li, M. S., Chan, C. Y., Chan, C. H., Lyon, D., Wise, R., et al. (1994). Evaluation of three culture media and their combinations for the isolation of *Mycobacterium tuberculosis* from pleural aspirates of patients with tuberculous pleurisy. *J Trop Med Hyg* 97, 249–253.

Committee, WHO Guidelines Approved by the Guidelines Review. (2013). *Automated Real-Time Nucleic Acid Amplification Technology for Rapid and Simultaneous Detection of Tuberculosis and Rifampicin Resistance: Xpert MTB/RIF Assay for the Diagnosis of Pulmonary and Extrapulmonary TB in Adults and Children: Policy Update*. Geneva: World Health Organization

Committee, WHO Guidelines Approved by the Guidelines Review. (2014). *Xpert MTB/RIF Implementation Manual: Technical and Operational 'How-To'; Practical Considerations*. Geneva: World Health Organization

Committee, WHO Guidelines Approved by the Guidelines Review. (2020). *WHO Consolidated Guidelines on Tuberculosis: Module 3: Diagnosis – Rapid Diagnostics for Tuberculosis Detection*. Geneva: World Health Organization

Cresswell, F. V., Bangdiwala, A. S., Bahr, N. C., Trautner, E., Nuwagira, E., Ellis, J., et al. (2018). Can improved diagnostics reduce mortality from tuberculous meningitis? Findings from a 6.5-year cohort in Uganda. *Wellcome Open Res.* 3:64. doi: 10.12688/wellcomeopenres.14610.2

Cresswell, F. V., Tugume, L., Bahr, N. C., Kwizera, R., Bangdiwala, A. S., Musubire, A. K., et al. (2020). Xpert MTB/RIF ultra for the diagnosis of HIV-associated tuberculous meningitis: a prospective validation study. *Lancet Infect. Dis.* 20, 308–317. doi: 10.1016/S1473-3099(19)30550-X

Davis, A. G., and Wilkinson, R. J. (2020). Diagnostic tests for tuberculous meningitis. *Lancet Infect. Dis.* 20, 262–263. doi: 10.1016/S1473-3099(19)30718-2

de Almeida, S. M., Borges, C. M., Santana, L. B., Golin, G., Correa, L., Kussen, G. B., et al. (2019). Validation of *Mycobacterium tuberculosis* real-time polymerase chain reaction for diagnosis of tuberculous meningitis using cerebrospinal fluid samples: a pilot study. *Clin. Chem. Lab. Med.* 57, 556–564. doi: 10.1515/cclm-2018-0524

Donovan, J., Cresswell, F. V., Thuong, N. T. T., Boulware, D. R., Thwaites, G. E., and Bahr, N. C. (2020a). Xpert MTB/RIF ultra for the diagnosis of tuberculous meningitis: a small step forward. *Clin. Infect. Dis.* 71, 2002–2005. doi: 10.1093/cid/ciaa473

Donovan, J., Thu, D. D. A., Phu, N. H., Dung, V. T. M., Quang, T. P., Nghia, H. D. T., et al. (2020b). Xpert MTB/RIF ultra versus Xpert MTB/RIF for the diagnosis of tuberculous meningitis: a prospective, randomised, diagnostic accuracy study. *Lancet Infect. Dis.* 20, 299–307. doi: 10.1016/S1473-3099(19)30649-8

Donovan, J., Thwaites, G. E., and Huynh, J. (2020c). Tuberculous meningitis: where to from here? *Curr. Opin. Infect. Dis.* 33, 259–266. doi: 10.1097/QCO.0000000000000648

Dorman, S. E., Schumacher, S. G., Alland, D., Nabeta, P., Armstrong, D. T., King, B., et al. (2018). Xpert MTB/RIF ultra for detection of *Mycobacterium tuberculosis* and rifampicin resistance: a prospective multicentre diagnostic accuracy study. *Lancet Infect. Dis.* 18, 76–84. doi: 10.1016/S1473-3099(17)30691-6

Feng, G. D., Shi, M., Ma, L., Chen, P., Wang, B. J., Zhang, M., et al. (2014). Diagnostic accuracy of intracellular *Mycobacterium tuberculosis* detection for tuberculous meningitis. *Am. J. Respir. Crit. Care Med.* 189, 475–481. doi: 10.1164/rccm.201309-1686OC

Foppiano Palacios, C., and Saleeb, P. G. (2020). Challenges in the diagnosis of tuberculous meningitis. *J Clin Tuberc Other Mycobact Dis.* 20:100164. doi: 10.1016/j.jctube.2020.100164

Galimi, R. (2011). Extrapulmonary tuberculosis: tuberculous meningitis new developments. *Eur. Rev. Med. Pharmacol. Sci.* 15, 365–386.

Garg, R. K. (2019). Microbiological diagnosis of tuberculous meningitis: phenotype to genotype. *Indian J. Med. Res.* 150, 448–457. doi: 10.4103/ijmr.IJMR_1145_19

Garg, R. K., Rizvi, I., Malhotra, H. S., Uniyal, R., and Kumar, N. (2018). Management of complex tuberculosis cases: a focus on drug-resistant tuberculous meningitis. *Expert Rev. Anti-Infect. Ther.* 16, 813–831. doi: 10.1080/14787210.2018.1540930

Gupta, R., Thakur, R., Gupta, P., Jalan, N., Kushwaha, S., Gupta, M., et al. (2015). Evaluation of Geno type MTBDRplus line probe assay for early detection of drug resistance in tuberculous meningitis patients in India. *J Glob Infect Dis.* 7, 5–10. doi: 10.4103/0974-777X.150882

Haldar, S., Sharma, N., Gupta, V. K., and Tyagi, J. S. (2009). Efficient diagnosis of tuberculous meningitis by detection of *Mycobacterium tuberculosis* DNA in cerebrospinal fluid filtrates using PCR. *J. Med. Microbiol.* 58, 616–624. doi: 10.1099/jmm.0.006015-0

Halliday, A., Masonou, T., Tolosa-Wright, M., and Mandagere, V. (2019). Immunodiagnosis of active tuberculosis. *Expert Rev. Respir. Med.* 13, 521–532. doi: 10.1080/17476348.2019.1615888

Heemskerk, A. D., Donovan, J., Thu, D. D. A., Marais, S., Chaidir, L., Dung, V. T. M., et al. (2018). Improving the microbiological diagnosis of tuberculous meningitis: a prospective, international, multicentre comparison of conventional and modified Ziehl-Neelsen stain, gene Xpert, and culture of cerebrospinal fluid. *J. Infect.* 77, 509–515. doi: 10.1016/j.jinf.2018.09.003

Hernandez, A. V., de Laurentis, L., Souza, I., Pessanha, M., Thota, P., et al. (2021). Diagnostic accuracy of Xpert MTB/RIF for tuberculous meningitis: systematic review and meta-analysis. Tropical medicine & international health: *TM & IH.* 26, 122–132. doi: 10.1111/tmi.13525

Hofmann-Thiel, S., Plesnik, S., Mihalic, M., Heiß-Neumann, M., Avsar, K., Beutler, M., et al. (2020). Clinical evaluation of BD MAX MDR-TB assay for direct detection of *Mycobacterium tuberculosis* complex and resistance markers. *J. Mol. Diagn.* 22, 1280–1286. doi: 10.1016/j.jmoldx.2020.06.013

Huang, M., Ding, Z., Li, W., Chen, W., Du, Y., Jia, H., et al. (2022). Identification of protein biomarkers in host cerebrospinal fluid for differential diagnosis of tuberculous meningitis and other meningitis. *Front. Neurol.* 13:886040. doi: 10.3389/fneur.2022.886040

Huang, M., Wang, G., Sun, Q., Jiang, G., Li, W., Ding, Z., et al. (2021). Diagnostic accuracy of Xpert MTB/RIF ultra for tuberculous meningitis in a clinical practice setting of China. *Diagn. Microbiol. Infect. Dis.* 100:115306. doi: 10.1016/j.diagmicrobio.2020.115306

Huang, H. J., Xiang, D. R., Sheng, J. F., Li, J., Pan, X. P., Yu, H. Y., et al. (2009). Rpo B nested PCR and sequencing for the early diagnosis of tuberculous meningitis and rifampicin resistance. *Int. J. Tuberc. Lung Dis.* 13, 749–754.

Kaswala, C., Schmiedel, Y., Kundu, D., George, M. M., Dayanand, D., Devasagayam, E., et al. (2022). Accuracy of Xpert MTB/RIF ultra for the diagnosis of tuberculosis in adult patients: a retrospective cohort study. *Int. J. Infect. Dis.* 122, 566–568. doi: 10.1016/j.ijid.2022.07.016

Kataria, J., Rukmangadachar, L. A., Hariprasad, G., Tripathi, M., and Srinivasan, A. (2011). Two dimensional difference gel electrophoresis analysis of cerebrospinal fluid in tuberculous meningitis patients. *J. Proteome* 74, 2194–2203. doi: 10.1016/j.jprot.2011.06.020

Kay, A. W., González Fernández, L., Takwoingi, Y., Eisenhut, M., Detjen, A. K., Steingart, K. R., et al. (2020). Xpert MTB/RIF and Xpert MTB/RIF ultra assays for active tuberculosis and rifampicin resistance in children. *Cochrane Database Syst. Rev.* 8:CD013359. doi: 10.1002/14651858.CD013359.pub2

Kay, A. W., Ness, T., Verkuijl, S. E., Viney, K., Brands, A., Masini, T., et al. (2022). Xpert MTB/RIF ultra assay for tuberculosis disease and rifampicin resistance in children. *Cochrane Database Syst. Rev.* 9:Cd013359. doi: 10.1002/14651858.CD013359.pub3

Kennedy, D. H., and Fallon, R. J. (1979). Tuberculous meningitis. *JAMA* 241, 264–268. doi: 10.1001/jama.1979.03290290032021

Khonga, M., and Nicol, M. P. (2018). Xpert MTB/RIF ultra: a gamechanger for tuberculous meningitis? *Lancet Infect. Dis.* 18, 6–8. doi: 10.1016/S1473-3099(17)30536-4

Kohli, M., Schiller, I., Dendukuri, N., Dheda, K., Denkinger, C. M., Schumacher, S. G., et al. (2018). Xpert(®) MTB/RIF assay for extrapulmonary tuberculosis and rifampicin resistance. *Cochrane Database Syst. Rev.* 8:CD012768. doi: 10.1002/14651858.CD012768.pub2

Kohli, M., Schiller, I., Dendukuri, N., Yao, M., Dheda, K., Denkinger, C. M., et al. (2021). Xpert MTB/RIF ultra and Xpert MTB/RIF assays for extrapulmonary tuberculosis and rifampicin resistance in adults. *Cochrane Database Syst. Rev.* 1:Cd012768. doi: 10.1002/14651858.CD012768.pub3

Kumar, P., Benny, P., Jain, M., and Singh, S. (2014). Comparison of an in-house multiplex PCR with two commercial immuno-chromatographic tests for rapid identification and differentiation of MTB from NTM isolates. *Int J Mycobacteriol.* 3, 50–56. doi: 10.1016/j.ijmyco.2013.12.001

Kumar, P., Srivatsava, M. V., Singh, S., and Prasad, H. K. (2008). Filtration of cerebrospinal fluid improves isolation of mycobacteria. *J. Clin. Microbiol.* 46, 2824–2825. doi: 10.1128/JCM.00210-08

Kusum, S., Aman, S., Pallab, R., Kumar, S. S., Manish, M., Sudesh, P., et al. (2011). Multiplex PCR for rapid diagnosis of tuberculous meningitis. *J. Neurol.* 258, 1781–1787. doi: 10.1007/s00415-011-6010-4

Lekhak, S. P., Sharma, L., Rajbhandari, R., Rajbhandari, P., Shrestha, R., and Pant, B. (2016). Evaluation of multiplex PCR using MPB64 and IS6110 primers for rapid diagnosis of tuberculous meningitis. *Tuberculosis (Edinb.)* 100, 1–4. doi: 10.1016/j.tube.2016.05.016

Li, X., Du, W., Wang, Y., Liu, Z., Li, K., Chen, H., et al. (2020). Rapid diagnosis of tuberculosis meningitis by detecting *Mycobacterium tuberculosis* cell-free DNA in cerebrospinal fluid. *Am. J. Clin. Pathol.* 153, 126–130. doi: 10.1093/ajcp/aqz135

Li, Z., Pan, L., Lyu, L., Li, J., Jia, H., Du, B., et al. (2020). Diagnostic accuracy of droplet digital PCR analysis of cerebrospinal fluid for tuberculous meningitis in adult patients. *Clin. Microbiol. Infect.* 26, 213–219. doi: 10.1016/j.cmi.2019.07.015

Mai, N. T., and Thwaites, G. E. (2017). Recent advances in the diagnosis and management of tuberculous meningitis. *Curr. Opin. Infect. Dis.* 30, 123–128. doi: 10.1097/QCO.0000000000000331

Marais, B. J., Brittle, W., Painczyk, K., Hesseling, A. C., Beyers, N., Wasserman, E., et al. (2008). Use of light-emitting diode fluorescence microscopy to detect acid-fast bacilli in sputum. *Clin. Infect. Dis.* 47, 203–207. doi: 10.1086/589248

Marais, S., Thwaites, G., Schoeman, J. F., Török, M. E., Misra, U. K., Prasad, K., et al. (2010). Tuberculous meningitis: a uniform case definition for use in clinical research. *Lancet Infect. Dis.* 10, 803–812. doi: 10.1016/S1473-3099(10)70138-9

Meaza, A., Tesfaye, E., Mohamed, Z., Zerihun, B., Seid, G., Eshetu, K., et al. (2021). Diagnostic accuracy of Truenat tuberculosis and rifampicin-resistance assays in Addis Ababa, Ethiopia. *PLoS One.* 16:e0261084. doi: 10.1371/journal.pone.0261084

Mitha, M., Pillay, M., Moodley, J. Y., Balakrishna, Y., Abbai, N., Bhagwan, S., et al. (2020). Laboratory diagnosis of tuberculous meningitis in human immunodeficiency virus-seropositive patients: correlation with the uniform case definition. *S. Afr. J. Infect. Dis.* 35:135. doi: 10.4102/sajid.v35i1.135

Modi, M., Sharma, K., Sharma, M., Sharma, A., Sharma, N., Sharma, S., et al. (2016). Multitargeted loop-mediated isothermal amplification for rapid diagnosis of tuberculous meningitis. *Int. J. Tuberc. Lung Dis.* 20, 625–630. doi: 10.5588/ijtld.15.0741

Mu, J., Yang, Y., Chen, J., Cheng, K., Li, Q., Wei, Y., et al. (2015). Elevated host lipid metabolism revealed by iTRAQ-based quantitative proteomic analysis of cerebrospinal fluid of tuberculous meningitis patients. *Biochem. Biophys. Res. Commun.* 466, 689–695. doi: 10.1016/j.bbrc.2015.08.036

Nagarathna, S., Rafi, W., Veenakumari, H. B., Mani, R., Satishchandra, P., and Chandramuki, A. (2008). Drug susceptibility profiling of tuberculous meningitis. *Int. J. Tuberc. Lung Dis.* 12, 105–107.

Nagdev, K. J., Kashyap, R. S., Parida, M. M., Kapgate, R. C., Purohit, H. J., Taori, G. M., et al. (2011). Loop-mediated isothermal amplification for rapid and reliable diagnosis of tuberculous meningitis. *J. Clin. Microbiol.* 49, 1861–1865. doi: 10.1128/JCM.00824-10

Ngangue, Y. R., Mbuli, C., Neh, A., Nshom, E., Koudjou, A., Palmer, D., et al. (2022). Diagnostic accuracy of the Truenat MTB plus assay and comparison with the Xpert MTB/RIF assay to detect tuberculosis among hospital outpatients in Cameroon. *J. Clin. Microbiol.* 60:e0015522. doi: 10.1128/jcm.00155-22

Nhu, N. T., Heemskerk, D., Do, D. A. T., Chau, T. T., Mai, N. T., Nghia, H. D., et al. (2014). Evaluation of gene Xpert MTB/RIF for diagnosis of tuberculous meningitis. *J. Clin. Microbiol.* 52, 226–233. doi: 10.1128/JCM.01834-13

Ojha, A., Banik, S., Melanthota, S. K., and Mazumder, N. (2020). Light emitting diode (LED) based fluorescence microscopy for tuberculosis detection: a review. *Lasers Med. Sci.* 35, 1431–1437. doi: 10.1007/s10103-019-02947-6

Opota, O., Mazza-Stalder, J., Greub, G., and Jaton, K. (2019). The rapid molecular test Xpert MTB/RIF ultra: towards improved tuberculosis diagnosis and rifampicin resistance detection. *Clin. Microbiol. Infect.* 25, 1370–1376. doi: 10.1016/j.cmi.2019.03.021

Patel, S., Dadheech, M., Maurya, A. K., Singh, J., Purwar, S., Rai, N., et al. (2023). Assessment of the diagnostic utility of gene Xpert *Mycobacterium tuberculosis*/rifampicin (MTB/RIF) assay in the suspected cases of tuberculous meningitis. *Cureus.* 15:e37761. doi: 10.7759/cureus.37761

Patel, V. B., Theron, G., Lenders, L., Matinyena, B., Connolly, C., Singh, R., et al. (2013). Diagnostic accuracy of quantitative PCR (Xpert MTB/RIF) for tuberculous meningitis in a high burden setting: a prospective study. *PLoS Med.* 10:e1001536. doi: 10.1371/journal.pmed.1001536

Paverd, N. (1988). Crimean-Congo haemorrhagic fever. A protocol for control and containment in a health care facility--part III. *Nurs. RSA* 3, 33–37.

Penn-Nicholson, A., Georghiou, S. B., Ciobanu, N., Kazi, M., Bhalla, M., David, A., et al. (2022). Detection of isoniazid, fluoroquinolone, ethionamide, amikacin, kanamycin, and capreomycin resistance by the Xpert MTB/XDR assay: a cross-sectional multicentre diagnostic accuracy study. *Lancet Infect. Dis.* 22, 242–249. doi: 10.1016/S1473-3099(21)00452-7

Penn-Nicholson, A., Gomathi, S. N., Ugarte-Gil, C., Meaza, A., Lavu, E., Patel, P., et al. (2021). A prospective multicentre diagnostic accuracy study for the Truenat tuberculosis assays. *Eur. Respir. J.* 58:2100526. doi: 10.1183/13993003.00526-2021

Pormohammad, A., Nasiri, M. J., McHugh, T. D., Riahi, S. M., and Bahr, N. C. (2019). A systematic review and meta-analysis of the diagnostic accuracy of nucleic acid amplification tests for tuberculous meningitis. *J. Clin. Microbiol.* 57, e01113–e01118. doi: 10.1128/jcm.01113-18

Ramachandran, P. S., Ramesh, A., Creswell, F. V., Wapniarski, A., Narendra, R., Quinn, C. M., et al. (2022). Integrating central nervous system metagenomics and host response for diagnosis of tuberculosis meningitis and its mimics. *Nat. Commun.* 13:1675. doi: 10.1038/s41467-022-29353-x

Rindi, L. (2022). Rapid molecular diagnosis of extra-pulmonary tuberculosis by Xpert/RIF ultra. *Front. Microbiol.* 13:817661. doi: 10.3389/fmicb.2022.817661

Rios-Sarabia, N., Hernández-González, O., Merchand, J., González, G., Gordillo, G., Vázquez-Rosales, G., et al. (2016). Identification of *Mycobacterium tuberculosis* in the cerebrospinal fluid of patients with meningitis using nested PCR. *Int. J. Mol. Med.* 38, 1289–1295. doi: 10.3892/ijmm.2016.2698

Rufai, S. B., Singh, A., Singh, J., Kumar, P., Sankar, M. M., and Singh, S. (2017). Diagnostic usefulness of Xpert MTB/RIF assay for detection of tuberculous meningitis using cerebrospinal fluid. *J. Infect.* 75, 125–131. doi: 10.1016/j.jinf.2017.04.010

Sağıroğlu, P., and Atalay, M. A. (2021). Evaluation of the performance of the BD MAX MDR-TB test in the diagnosis of *Mycobacterium tuberculosis* complex in extrapulmonary and pulmonary samples. *Expert. Rev. Mol. Diagn.* 21, 1361–1367. doi: 10.1080/14737159.2021.1997594

Sanogo, M., Kone, B., Diarra, B., Maiga, M., Baya, B., Somboro, A. M., et al. (2017). Performance of microscopic observation drug susceptibility for the rapid diagnosis of tuberculosis and detection of drug resistance in Bamako, Mali. *Clin. Microbiol. Infect.* 23, 408 e1–408 e6. doi: 10.1016/j.cmi.2017.01.004

Seki, M., Kilgore, P. E., Kim, E. J., Ohnishi, M., Hayakawa, S., and Kim, D. W. (2018). Loop-mediated isothermal amplification methods for diagnosis of bacterial meningitis. *Front. Pediatr.* 6:57. doi: 10.3389/fped.2018.00057

Selvakumar, N., Vanajakumar, N. T., and Paramasivan, C. N. (1996). Isolation of *Mycobacterium tuberculosis* from cerebrospinal fluid by the centrifugation & filtration methods. *Indian J. Med. Res.* 103, 250–252.

Shah, M., Paradis, S., Betz, J., Beylis, N., Bharadwaj, R., Caceres, T., et al. (2020). Multicenter study of the accuracy of the BD MAX multidrug-resistant tuberculosis assay for detection of *Mycobacterium tuberculosis* complex and mutations associated with resistance to Rifampin and isoniazid. *Clin. Infect. Dis.* 71, 1161–1167. doi: 10.1093/cid/ciz932

Shao, L., Qiu, C., Zheng, L., Yang, Y., Yang, X., Liang, Q., et al. (2020). Comparison of diagnostic accuracy of the gene Xpert ultra and cell-free nucleic acid assay for tuberculous meningitis: a multicentre prospective study. *Int. J. Infect. Dis.* 98, 441–446. doi: 10.1016/j.ijid.2020.06.076

Shapiro, A. E., Ross, J. M., Yao, M., Schiller, I., Kohli, M., Dendukuri, N., et al. (2021). Xpert MTB/RIF and Xpert ultra assays for screening for pulmonary tuberculosis and rifampicin resistance in adults, irrespective of signs or symptoms. *Cochrane Database Syst. Rev.* 3:CD013694. doi: 10.1002/14651858.CD013694.pub2

Sharma, K., Modi, M., Kaur, H., Sharma, A., Ray, P., and Varma, S. (2015). Rpo B gene high-resolution melt curve analysis: a rapid approach for diagnosis and screening of drug resistance in tuberculous meningitis. *Diagn. Microbiol. Infect. Dis.* 83, 144–149. doi: 10.1016/j.diagmicrobio.2015.06.010

Sharma, K., Sharma, M., Chaudhary, L., Modi, M., Goyal, M., Sharma, N., et al. (2018). Comparative evaluation of Xpert MTB/RIF assay with multiplex polymerase chain reaction for the diagnosis of tuberculous meningitis. *Tuberculosis (Edinb.)* 113, 38–42. doi: 10.1016/j.tube.2018.09.002

Sharma, K., Sharma, M., Modi, M., Singla, N., Sharma, A., Sharma, A., et al. (2021). Comparative analysis of Truenat™ MTB plus and Xpert(®) ultra in diagnosing tuberculous meningitis. *Int. J. Tuberc. Lung Dis.* 25, 626–631. doi: 10.5588/ijtld.21.0156

Sharma, K., Sharma, M., Sharma, V., Sharma, M., Samanta, J., Sharma, A., et al. (2022). Evaluating diagnostic performance of Truenat MTB plus for gastrointestinal tuberculosis. *J. Gastroenterol. Hepatol.* 37, 1571–1578. doi: 10.1111/jgh.15878

Sharma, K., Sharma, M., Singh, S., Modi, M., Sharma, A., Ray, P., et al. (2017). Real-time PCR followed by high-resolution melting curve analysis: a rapid and pragmatic approach for screening of multidrug-resistant extrapulmonary tuberculosis. *Tuberculosis (Edinb.)* 106, 56–61. doi: 10.1016/j.tube.2017.07.002

Shi, J., He, G., Ning, H., Wu, L., Wu, Z., Ye, X., et al. (2022). Application of matrix-assisted laser desorption ionization time-of-flight mass spectrometry (MALDI-TOF MS) in the detection of drug resistance of *Mycobacterium tuberculosis* in re-treated patients. *Tuberculosis (Edinb.)* 135:102209. doi: 10.1016/j.tube.2022.102209

Signorino, C., Votto, M., De Filippo, M., Marseglia, G. L., Galli, L., and Chiappini, E. (2022). Diagnostic accuracy of Xpert ultra for childhood tuberculosis: a preliminary systematic review and meta-analysis. *Pediatr. Allergy Immunol.* 33, 80–82. doi: 10.1111/pai.13637

Solomons, R. S., Visser, D. H., Friedrich, S. O., Diacon, A. H., Hoek, K. G., Marais, B. J., et al. (2015). Improved diagnosis of childhood tuberculous meningitis using more than one nucleic acid amplification test. *Int. J. Tuberc. Lung Dis.* 19, 74–80. doi: 10.5588/ijtld.14.0394

Ssebambulidde, K., Gakuru, J., Ellis, J., Cresswell, F. V., and Bahr, N. C. (2022). Improving technology to diagnose tuberculous meningitis: are we there yet? *Front. Neurol.* 13:892224. doi: 10.3389/fneur.2022.892224

Stadelman, A. M., Ssebambulidde, K., Buller, A., Tugume, L., Yuquimpo, K., Bakker, C. J., et al. (2022). Cerebrospinal fluid AFB smear in adults with tuberculous meningitis: a systematic review and diagnostic test accuracy meta-analysis. *Tuberculosis (Edinb.)* 135:102230. doi: 10.1016/j.tube.2022.102230

Steingart, K. R., Henry, M., Ng, V., Hopewell, P. C., Ramsay, A., Cunningham, J., et al. (2006). Fluorescence versus conventional sputum smear microscopy for tuberculosis: a systematic review. *Lancet Infect. Dis.* 6, 570–581. doi: 10.1016/S1473-3099(06)70578-3

Sun, Y., Chen, J., Li, J., Xu, Y., Jin, H., Xu, N., et al. (2017). Novel approach based on one-tube nested PCR and a lateral flow strip for highly sensitive diagnosis of tuberculous meningitis. *PLoS One* 12:e0186985. doi: 10.1371/journal.pone.0186985

Sun, L., Liu, Y., Fang, M., Chen, Y., Zhu, Y., Xia, C., et al. (2022). Use of Xpert MTB/RIF ultra assay on stool and gastric aspirate samples to diagnose pulmonary tuberculosis in children in a high-tuberculosis-burden but resource-limited area of China. *Int. J. Infect. Dis.* 114, 236–243. doi: 10.1016/j.ijid.2021.11.012

Sun, W. W., Sun, Q., Yan, L. P., and Zhang, Q. (2017). The application of IS6110-baced loop-mediated isothermal amplification (LAMP) in the early diagnosis of tuberculous meningitis. *Oncotarget* 8, 57537–57542. doi: 10.18632/oncotarget.15734

Thwaites, G. (2013). Tuberculous meningitis. *Medicine* 41, 683–685. doi: 10.1016/j.mpmed.2013.09.006

Thwaites, G. E., Caws, M., Chau, T. T., Dung, N. T., Campbell, J. I., Phu, N. H., et al. (2004). Comparison of conventional bacteriology with nucleic acid amplification (amplified mycobacterium direct test) for diagnosis of tuberculous meningitis before and after inception of antituberculosis chemotherapy. *J. Clin. Microbiol.* 42, 996–1002. doi: 10.1128/JCM.42.3.996-1002.2004

Thwaites, G. E., Chau, T. T., and Farrar, J. J. (2004). Improving the bacteriological diagnosis of tuberculous meningitis. *J. Clin. Microbiol.* 42, 378–379. doi: 10.1128/JCM.42.1.378-379.2004

Thwaites, G., Chau, T. T., Mai, N. T., Drobniewski, F., McAdam, K., and Farrar, J. (2000). Tuberculous meningitis. *J. Neurol. Neurosurg. Psychiatry* 68, 289–299. doi: 10.1136/jnnp.68.3.289

Thwaites, G. E., van Toorn, R., and Schoeman, J. (2013). Tuberculous meningitis: more questions, still too few answers. *Lancet Neurol.* 12, 999–1010. doi: 10.1016/S1474-4422(13)70168-6

van Zyl-Smit, R. N., Binder, A., Meldau, R., Mishra, H., Semple, P. L., Theron, G., et al. (2011). Comparison of quantitative techniques including Xpert MTB/RIF to evaluate mycobacterial burden. *PLoS One* 6:e28815. doi: 10.1371/journal.pone.0028815

Venkataswamy, M. M., Rafi, W., Nagarathna, S., Ravi, V., and Chandramuki, A. (2007). Comparative evaluation of BACTEC 460TB system and Lowenstein-Jensen medium for the isolation of *M. tuberculosis* from cerebrospinal fluid samples of tuberculous meningitis patients. *Indian J. Med. Microbiol.* 25, 236–240. doi: 10.1016/S0255-0857(21)02112-5

Vidal, J. E., Peixoto de Miranda, E. J., Gerhardt, J., Croda, M., and Boulware, D. R. (2017). Is it possible to differentiate tuberculous and cryptococcal meningitis in HIV-infected patients using only clinical and basic cerebrospinal fluid characteristics? *S. Afr. Med. J.* 107, 156–159. doi: 10.7196/SAMJ.2017.v107i2.11162

Wakode, P., Siddaiah, N., Manjunath, N., and Bahubali, V. K. H. (2022). Genexpert: a rapid and supplementary diagnostic tool for tuberculous meningitis, experience from tertiary neurocenter. *J. Neurosci. Rural Pract.* 13, 204–210. doi: 10.1055/s0041-1742138

Wang, S., Chen, Y., Wang, D., Wu, Y., Zhao, D., Zhang, J., et al. (2019). The feasibility of metagenomic next-generation sequencing to identify pathogens causing tuberculous meningitis in cerebrospinal fluid. *Front. Microbiol.* 10:1993. doi: 10.3389/fmicb.2019.01993

Wang, G., Wang, S., Jiang, G., Yang, X., Huang, M., Huo, F., et al. (2019). Xpert MTB/RIF ultra improved the diagnosis of paucibacillary tuberculosis: a prospective cohort study. *J. Infect.* 78, 311–316. doi: 10.1016/j.jinf.2019.02.010

Wang, Y. Y., and Xie, B. D. (2018). Progress on diagnosis of tuberculous meningitis. *Methods Mol. Biol.* 1754, 375–386. doi: 10.1007/978-1-4939-7717-8_20

Wen, A., Cao, W. F., Liu, S. M., Zhou, Y. L., Xiang, Z. B., Hu, F., et al. (2023). Incidence and risk factors of cranial nerve palsy in patients with tuberculous meningitis: a retrospective evaluation. *Infect Drug Resist.* 16, 829–841. doi: 10.2147/idr.s396022

Wen, A., Liu, S. M., Cao, W. F., Zhou, Y. L., Luo, C. Q., Xiang, Z. B., et al. (2022). A new scoring system to differentially diagnose and distinguish tuberculous meningitis and bacterial meningitis in South China. *Front. Neurol.* 13:830969. doi: 10.3389/fneur.2022.830969

WHO Guidelines Approved by the Guidelines Review Committee (2011). *Fluorescent Light-Emitting Diode (LED) Microscopy for Diagnosis of Tuberculosis: Policy Statement*. Geneva: World Health Organization.

WHO Guidelines Approved by the Guidelines Review Committee (2021) *WHO Consolidated Guidelines on Tuberculosis: Module 3: Diagnosis – Rapid Diagnostics for Tuberculosis Detection*. Geneva: World Health Organization

Wilkinson, R. J., Rohlwink, U., Misra, U. K., van Crevel, R., Mai, N. T. H., Dooley, K. E., et al. (2017). Tuberculous meningitis. *Nat. Rev. Neurol.* 13, 581–598. doi: 10.1038/nrneurol.2017.120

Wong, C., Ha, N. P., Pawlowski, M. E., Graviss, E. A., and Tkaczyk, T. S. (2016). Differentiating between live and dead *Mycobacterium smegmatis* using autofluorescence. *Tuberculosis (Edinb.)* 101S, S119–S123. doi: 10.1016/j.tube.2016.09.010

Wu, X., Liang, R., Xiao, Y., Liu, H., Zhang, Y., Jiang, Y., et al. (2023). Application of targeted next generation sequencing technology in the diagnosis of *mycobacterium tuberculosis* and first line drugs resistance directly from cell-free DNA of bronchoalveolar lavage fluid. *J. Infect.* 86, 399–401. doi: 10.1016/j.jinf.2023.01.031

Wu, X., Tan, G., Yang, J., Guo, Y., Huang, C., Sha, W., et al. (2022). Prediction of *Mycobacterium tuberculosis* drug resistance by nucleotide MALDI-TOF-MS. *Int. J. Infect. Dis.* 121, 47–54. doi: 10.1016/j.ijid.2022.04.061

Xia, H., Song, Y. Y., Zhao, B., Kam, K. M., O'Brien, R. J., Zhang, Z. Y., et al. (2013). Multicentre evaluation of Ziehl-Neelsen and light-emitting diode fluorescence microscopy in China. *Int. J. Tuberc. Lung Dis.* 17, 107–112. doi: 10.5588/ijtld.12.0184

Yan, L., Sun, W., Lu, Z., and Fan, L. (2020). Metagenomic next-generation sequencing (mNGS) in cerebrospinal fluid for rapid diagnosis of tuberculosis meningitis in HIV-negative population. *Int. J. Infect. Dis.* 96, 270–275. doi: 10.1016/j.ijid.2020.04.048

Yasuda, T., Tomita, T., McLone, D. G., and Donovan, M. (2002). Measurement of cerebrospinal fluid output through external ventricular drainage in one hundred infants and children: correlation with cerebrospinal fluid production. *Pediatr. Neurosurg.* 36, 22–28. doi: 10.1159/000048344

Yu, G., Shen, Y., Zhong, F., Ye, B., Yang, J., and Chen, G. (2018). Diagnostic accuracy of the loop-mediated isothermal amplification assay for extrapulmonary tuberculosis: a meta-analysis. *PLoS One* 13:e0199290. doi: 10.1371/journal.pone.0199290

Yu, G., Zhao, W., Shen, Y., Zhu, P., and Zheng, H. (2020). Metagenomic next generation sequencing for the diagnosis of tuberculosis meningitis: a systematic review and meta-analysis. *PLoS One* 15:e0243161. doi: 10.1371/journal.pone.0243161

Zhou, X., Wu, H., Ruan, Q., Jiang, N., Chen, X., Shen, Y., et al. (2019). Clinical evaluation of diagnosis efficacy of active mycobacterium tuberculosis complex infection via metagenomic next-generation sequencing of direct clinical samples. *Front. cell. infect.* 9:351. doi: 10.3389/fcimb.2019.00351

Zou, Y., Bu, H., Guo, L., Liu, Y., He, J., and Feng, X. (2016). Staining with two observational methods for the diagnosis of tuberculous meningitis. *Exp. Ther. Med.* 12, 3934–3940. doi: 10.3892/etm.2016.3859

frontiers | Frontiers in Immunology

TYPE Review
PUBLISHED 26 September 2023
DOI 10.3389/fimmu.2023.1223675

OPEN ACCESS

EDITED BY
Wafa Achour,
Centre National de Greffe de Moelle Osseuse, Tunisia

REVIEWED BY
Jialin Jin,
Fudan University, China
Yubao Wang,
Tianjin Medical University General Hospital, China
Hua Gao,
Peking University People's Hospital, China

*CORRESPONDENCE
An Wen
wenan666@sina.com

RECEIVED 26 May 2023
ACCEPTED 05 September 2023
PUBLISHED 26 September 2023

CITATION
Xiang Z-B, Leng E-L, Cao W-F, Liu S-M, Zhou Y-L, Luo C-Q, Hu F and Wen A (2023) A systematic review and meta-analysis of the diagnostic accuracy of metagenomic next-generation sequencing for diagnosing tuberculous meningitis. *Front. Immunol.* 14:1223675. doi: 10.3389/fimmu.2023.1223675

A systematic review and meta-analysis of the diagnostic accuracy of metagenomic next-generation sequencing for diagnosing tuberculous meningitis

Zheng-Bing Xiang[1,2], Er-Ling Leng[3], Wen-Feng Cao[1,2], Shi-Min Liu[1,2], Yong-Liang Zhou[1,2], Chao-Qun Luo[1,2], Fan Hu[1,2] and An Wen[1,2]*

[1]Department of Neurology, Jiangxi Provincial People's Hospital (The First Affiliated Hospital of Nanchang Medical College), Nanchang, Jiangxi, China, [2]Department of Neurology, Xiangya Hospital, Central South University, Jiangxi Hospital, National Regional Center for Neurological Diseases, Nanchang, Jiangxi, China, [3]Department of Pediatrics, Jiangxi Provincial People's Hospital (The First Affiliated Hospital of Nanchang Medical College), Nanchang, Jiangxi, China

Objective: The utility of metagenomic next-generation sequencing (mNGS) in the diagnosis of tuberculous meningitis (TBM) remains uncertain. We performed a meta-analysis to comprehensively evaluate its diagnostic accuracy for the early diagnosis of TBM.

Methods: English (PubMed, Medline, Web of Science, Cochrane Library, and Embase) and Chinese (CNKI, Wanfang, and CBM) databases were searched for relevant studies assessing the diagnostic accuracy of mNGS for TBM. Review Manager was used to evaluate the quality of the included studies, and Stata was used to perform the statistical analysis.

Results: Of 495 relevant articles retrieved, eight studies involving 693 participants (348 with and 345 without TBM) met the inclusion criteria and were included in the meta-analysis. The pooled sensitivity, specificity, positive likelihood ratio, negative likelihood ratio, diagnostic odds ratio, and area under the summary receiver-operating characteristic curve of mNGS for diagnosing TBM were 62% (95% confidence interval [CI]: 0.46–0.76), 99% (95% CI: 0.94–1.00), 139.08 (95% CI: 8.54–2266), 0.38 (95% CI: 0.25–0.58), 364.89 (95% CI: 18.39–7239), and 0.97 (95% CI: 0.95–0.98), respectively.

Conclusions: mNGS showed good specificity but moderate sensitivity; therefore, a more sensitive test should be developed to assist in the diagnosis of TBM.

KEYWORDS

tuberculous meningitis, cerebrospinal fluid, metagenomic next-generation sequencing, diagnosis, meta-analysis

1 Introduction

Tuberculous meningitis (TBM) is a type of central nervous system (CNS) infection caused by *Mycobacterium tuberculosis* (MTB) invading meninges and spinal membranes. TBM is associated with high disability and mortality rates (1). It is the most severe type of extrapulmonary tuberculosis (EPTB) with the worst prognosis, and is a serious health threat causing a high economic burden to society worldwide (2–4). The onset of TBM is often insidious and its clinical manifestations have variable severity and lack specificity (5). Diagnosis of TBM depends on the detection of MTB in the cerebrospinal fluid (CSF) (6). Owing to the low load of MTB in the CSF, the detection rate of conventional MTB assays is unsatisfactory, leading to difficulty in making an early microbiological diagnosis (7).

Timely and accurate diagnosis at an early stage and initiation of antituberculosis therapy is key to improving the survival rate and prognosis of patients with TBM (8, 9). Recently, attention has been paid to the role of molecular diagnostics in precision diagnosis and treatment. Among them, metagenomic next-generation sequencing (mNGS) is a revolutionary technology that has emerged in recent years and can be used to conduct high-throughput sequencing of microbial nucleic acid in clinical samples and identify pathogens through comparison and analysis with standard sequences in the database (10, 11). This technique has played an increasingly important clinical role in the diagnosis of CNS infections (12–14).

A literature search revealed that no systematic quantitative analysis has been conducted of current studies on the use of mNGS in the diagnosis of TBM. Most studies of the diagnostic accuracy of mNGS for diagnosing TBM are case-control studies with a small sample size, and the reported sensitivity varies greatly; therefore the diagnostic value of mNGS for diagnosing TBM is still unclear. Hence, we conducted a systematic literature review and meta-analysis to systematically and objectively assess the value of mNGS in the diagnosis of TBM.

2 Methods

2.1 Search strategy

We conducted a comprehensive computerized search of English (PubMed, Medline, Web of Science, Cochrane Library, and Embase), and Chinese (CNKI, Wanfang, and CBM) databases for studies on the use of mNGS for TBM diagnosis. We also manually searched the list of included references to identify additional relevant studies. The target keywords that we used were various combinations of "tuberculosis", "TB", "*Mycobacterium*", "MTB", "tuberculous meningitis", "TBM", "extrapulmonary tuberculosis", "EPTB", "cerebrospinal fluid", "CSF", "metagenomic next-generation sequencing", "mNGS", "next-generation sequencing", "accuracy", "sensitivity", and "specificity". The retrieval period was from the establishment of each database until February 1, 2023.

2.2 Study selection

Studies were included if they met all the following criteria:

(i) Published prospective or retrospective studies of mNGS technique for diagnosing TBM;

(ii) Reference standard for the diagnosis of TBM (test group) was acid-fast staining, culture, or nucleic acid amplification tests (NAATs) of the CSF, or a composite reference standard (CRS);

(iii) The control group included patients with diseases that are clinically confused with TBM, including suppurative meningitis, fungal meningitis, viral meningitis, and other CNS infections;

(iv) The specimen used for mNGS was CSF;

(v) Access to the full text.

Studies were excluded if they met any of the following criteria:

(i) Duplicate studies;

(ii) No non-TBM control group was included, or the control group included only healthy individuals;

(iii) The research question was inconsistent with that of this study;

(iv) Animal experiments;

(v)Reviews, systematic reviews, or meta-analyses;

(vi) Case reports, abstracts, conference abstracts, comments, or letters;

(vii) The 2×2 table data could not be extracted directly or indirectly.

2.3 Data extraction

Two investigators independently conducted literature searches according to pre-established criteria, and screening was conducted according to the inclusion and exclusion criteria. The data extracted from the included studies included the author, publication year, study site, study design (prospective or retrospective), age of study participants, reference standard, sample size, sample condition (fresh or frozen), patient selection method, pretreatment of CSF specimens, and 2×2 table data. For the screening of the above studies and the extraction of relevant materials and data, any discrepancies were resolved through open discussion and consultation with a third researcher.

2.4 Quality assessment

The quality of the studies was independently assessed by two reviewers using Review Manager software (version 5.3). Quality

Assessment of Diagnostic Accuracy Studies-2 (QUADAS-2) was used to evaluate the risk of bias and applicability concerns of all the included studies (15), and a literature quality evaluation chart was drawn.

2.5 Statistical analysis

Statistical analyses were performed using STATA 15.0, and *P* values < 0.05 were considered to be statistically significant. The pooled sensitivity, specificity, positive likelihood ratio (PLR), negative likelihood ratio (NLR), and diagnostic odds ratio (DOR) were calculated for the included studies with 95% confidence intervals (CIs). Cochran's Q test was used to test heterogeneity among the selected studies, and heterogeneity was measured by *I*-square (I^2) statistics. The appropriate statistical analysis model was selected for the meta-analysis based on the heterogeneity test results. A summary receiver-operating characteristic (SROC) curve was drawn and the area under the curve (AUC) was calculated. Deeks' funnel plot was drawn to detect publication bias (16), with the level of statistical significance set at $\alpha = 0.05$. To evaluate the role of mNGS in the diagnosis of TBM, Fagan's nomogram was used to compare pre- and post-test probabilities.

3 Results

3.1 Literature search results and the characteristics of the included studies

A total of 495 candidate articles were retrieved. According to the inclusion criteria, eight studies published between 2019 and 2022 were included in the final meta-analysis (17–24). The selection process is shown in Figure 1. A total of 693 participants were included in the eight studies, including 348 patients with TBM and 345 non-TBM controls. Of these studies, three were prospective (18, 19, 21) and five were retrospective (17, 20, 22–24) in design. The patients were randomly selected in three studies (18, 21, 22) and consecutively selected in five studies (17, 19, 20, 23, 24). Fresh CSF samples were used for testing in three studies (20, 22, 24), frozen CSF was used in three studies (17, 19, 21), both fresh and frozen CSF were used in one study (18), and samples were not described in detail in one study (23). All studies used a CRS as a diagnostic reference standard. In two studies, ultrasonication was used (18, 22); in five studies, bead beating was used (17, 19–21, 24); and in one study, the sample pretreatment method was not described in detail (23). The characteristics and relevant data of the included studies are shown in Tables 1, 2.

3.2 Study quality

The QUADAS-2 tool was used to assess the quality of all eligible studies in terms of four aspects: patient selection, index test, reference standard, and flow and timing (Figure 2). As the selected studies included consecutive or randomly selected patients, the risk of bias in terms of patient selection was assessed as low. The risk of bias in the index test was unclear in one study, and the applicability of the index test was unclear in four studies. All studies used CRS as the reference standard for diagnosing TBM, which could correctly distinguish the target disease and the risk of bias in the reference standard was assessed as low.

3.3 Meta-analysis results

3.3.1 Diagnostic accuracy of mNGS for TBM

The I^2 value and Cochrane Q test results showed significant heterogeneity between studies in terms of sensitivity (I^2 = 86.3%, P < 0.01), specificity (I^2 = 64.27%, P = 0.01), and DOR (I^2 = 100%, P < 0.01); therefore the random-effects model was used in the meta-analysis. The pooled sensitivity, specificity, PLR, NLR, DOR and AUC of the SROC of mNGS for diagnosing TBM was 62% (95% CI: 0.46–0.76), 99% (95% CI: 0.94–1.00), 139.08 (95% CI: 8.54–2266), 0.38 (95% CI: 0.25–0.58), 364.89 (95% CI: 18.39–7239) and 0.97 (95% CI: 0.95–0.98), respectively (Figures 3, 4).

3.3.2 Publication bias analysis

The Deeks' funnel plot showed no significant publication bias (P = 0.372) (Figure 5).

3.3.3 Post-test probability of TBM

Fagan's nomogram showed that the pre-test probability of TBM was 20%, and the post-test probability increased to 97% if a patient tested positive using mNGS. If the mNGS test result was negative, the likelihood of the patient having TBM decreased to 9% (Figure 6).

4 Discussion

Identification of MTB in the CSF is the key to diagnosing TBM. As MTB is an intracellular bacterium, the pathogen content in CSF is extremely low, and its concentration rarely exceeds 100–1000 colonies per mL(7), whereas acid-fast staining requires that the MTB load in CSF be >10,000 organisms, resulting in a positive result acquired by acid-fast staining for TBM diagnosis of only 10–40% (25, 26). Even though some studies have shown that the modified acid-fast staining method improves the sensitivity for diagnosing TBM (27, 28), other studies have shown that the sensitivity of this method is inadequate for clinical application (25). Compared with acid-fast staining, CSF culture improved the probability of MTB detection; the sensitivity reached 50–70% (26, 29), and the drug sensitivity test could be carried out simultaneously (30). Nevertheless, this method is time-consuming and often causes delays that make the early diagnosis of TBM difficult. Additionally, MTB culture should be performed in a biosafety level III laboratory, which indirectly increases the cost of testing samples (5) (Table 3).

TBM is a type of paucibacillary EPTB (7), which limits the application of traditional etiological detection methods. With the development of modern precision medicine technology, molecular

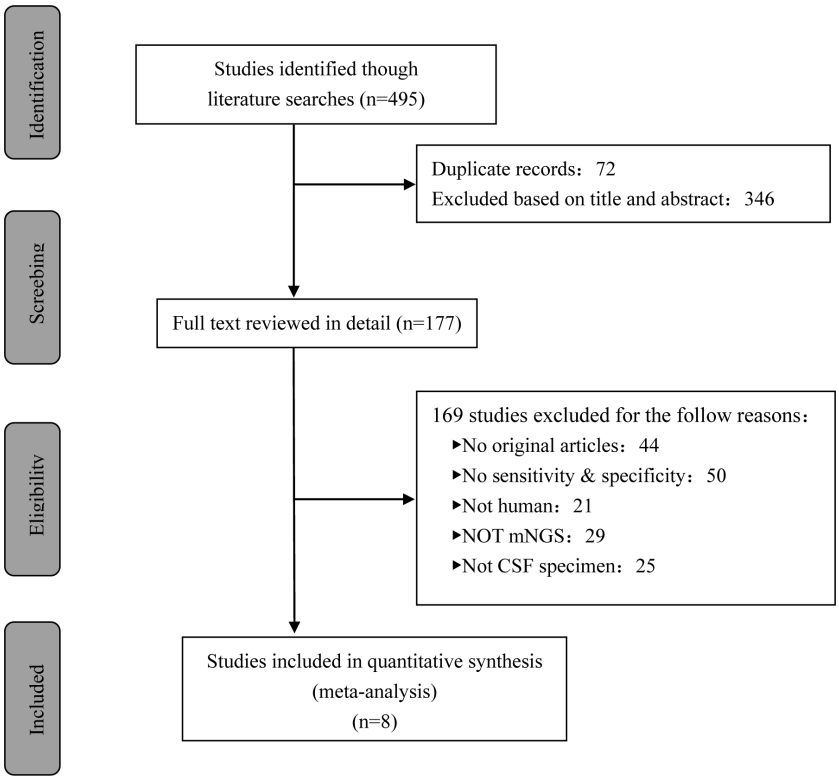

FIGURE 1
The study selection process flowchart.

diagnostics has been widely paid attention to and applied. Xpert MTB/RIF Ultra (Xpert Ultra) is a novel NAAT that can be used to detect MTB genes and rifampicin resistance in 1.5–2 hours (32, 37). Xpert Ultra is rapid and highly automated, with higher biosafety than smear microscopy and lower cross-contamination risk than culture (32, 38, 39). In 2017, the World Health Organization recommended Xpert Ultra as the initial test for TBM diagnosis (40). Although Xpert Ultra has advantages over other classical microbiological methods (31), its sensitivity is still unsatisfactory (41, 42), and a negative result cannot rule out TBM (32, 43).

TABLE 1 Baseline characteristics of the studies that were included.

Study	Sample size(n/N)	Age(years)	Study design	QUADUS score	Specimen condition	Specimen pretreatment	Patient selection
Zhou2019	16/33	49.3/46.3 [†#]	Prospective	11	Fresh/Frozen	Ultrasonication	Consecutive
Wang2019	23/6	37 [†]	Retrospective	11	Frozen	Bead beating	Random
Xing2020	44/169	41 (14-76) [$&]	Prospective	12	Frozen	Bead beating	Random
Yan2020	45/6	34 (19-80)/34.5(24-55) [¶]	Retrospective	11	Fresh	Bead beating	Random
Sun2021	45/3	29.6 ± 18.1[‡*]	Retrospective	11	Fresh	Ultrasonication	Consecutive
Lin2021	34/16	35.67 ± 6.89 [‡]	Prospective	12	Frozen	Bead beating	Consecutive
Yu2021	24/13	59/60.5 [¶]	Retrospective	10	unclear	unclear	Random
Chen2022	117/99	40 (25-53) [¶]	Retrospective	11	Fresh	Bead beating	Random

n, TBM group.
N, Non TBM group.
[†] Mean.
[‡] Mean ± SD.
[$]Mean (range).
[¶] Median or Median (IQR).
[#]Tuberculosis/Non- tuberculosis group.
[&] Tuberculous meningitis.
[*] Extrapulmonary tuberculosis.

TABLE 2 Principal data characteristics of included studies.

Author	Year	Country	Patients	Diagnostic methods (N)	Reference standard	Test result			
						TP	FP	FN	TN
Zhou	2019	China	49	Culture, Xpert	CRS	7	1	9	32
Wang	2019	China	29	Culture (1), AFB (8), PCR (3)	CRS	18	0	5	6
Xing	2020	China	213	Xpert (5), AFB (1)	CRS	12	6	32	163
Yan	2020	China	51	AFB (0), MGIT960 (10), RT-PCR (11), Xpert (18)	CRS	38	0	7	6
Sun	2021	China	48	MGIT960, Xpert	CRS	38	0	7	3
Lin	2021	China	50	MGIT960 (6), FQ-PCR (5), Xpert (13)	CRS	20	0	14	16
Yu	2021	China	37	AFB (2), Culture (4), Xpert (8)	CRS	10	0	14	13
Chen	2022	China	216	Modified Z-N (67), MGIT960 (22), Xpert (65)	CRS	74	0	43	99

AFB, acid fast bacilli.
Z-N, Ziehl-Neelsen staining.
MGITs, mycobacteria growth indicator tubes.
PCR, polymerase chain reaction.
RT-PCR, real-time fluorescence quantitative RCR.
FQ-PCR, Real-time fluorescent quantitative PCR.
TP, true-positive.
FP, false-positive.
FN, false-negative.
TN, true-negative.
CRS, composite reference standard.

However, its high requirements for sample size and bacterial load, and unsatisfactory performance in EPTB, HIV coinfection, and children limit its application in clinical practice (32, 40) (Table 3).

Adenosine deaminase (ADA) detection has the advantages of being simple, rapid, and stable, which makes it useful as a reference test for the diagnosis of TBM. A meta-analysis showed that ADA had a sensitivity of 89% and specificity of 91% for diagnosing TBM (33). However, there is no clear cutoff for the diagnosis of TBM, and it is difficult to distinguish TBM from suppurative meningitis and viral meningitis (33, 34). Clinical manifestations and other relevant diagnostic tests are required for the diagnosis of TBM. Interferon-gamma release assays (IGRAs) are used to detect the presence of MTB infection by measuring the amount of interferon (IFN)-gamma released by T cells after stimulation with MTB-specific antigens and the number of T cells releasing IFN-gamma (44). A meta-analysis showed that the overall sensitivity and specificity of IGRA 74% and 79%, respectively, in blood, and 78% and 95%, respectively, in CSF, suggesting moderate accuracy in the diagnosis of TBM (35, 36). However, IGRA is not effective at distinguishing between latent and active TB (45, 46). CSF IGRAs also has the disadvantages of requiring a large volume of CSF (> 4 mL) and an uncertain critical value (32, 47–49) (Table 3).

More recently, the CSF mNGS has been gradually adopted for the diagnosis of infectious diseases of the CNS (13, 50–52). Although research on the diagnosis of TBM is still in its infancy, some progress has been made. In 2020, Yu et al. conducted the first meta-analysis of mNGS diagnosis of TBM (a total of four studies were included) and found that the sensitivity of mNGS detection was 62%, while the specificity was as high as 98% (53). However, owing to the small number of studies included in this meta-analysis (<5 studies) and the small sample size of the included studies (342 patients), the results and conclusions should be interpreted with caution. Eight studies were included in this meta-analysis. Comprehensive analysis showed that the pooled sensitivity and specificity of mNGS for the diagnosis of TBM was 62% and 99% (i.e., the missed diagnosis and misdiagnosis rates were 38% and 1%, respectively), and the pooled DOR and SROC areas were 364.89 and 0.97, respectively. The results of this study are similar to the sensitivity and specificity of mNGS obtained by Yu et al., which further validates the diagnostic efficacy of mNGS. Compared with Yu et al.'s study, this study included more studies and sample sizes, and established more detailed and strict inclusion and exclusion criteria. By integrating all relevant studies, this meta-analysis could more accurately evaluate the diagnostic efficacy of mNGS.

In 2020, a prospective multicenter randomized controlled study conducted by Donovan et al. found that the sensitivities of Xpert Ultra and Xpert in diagnosing TBM were 47.2% and 39.6%, respectively, with a specificity of 100.0% (43). In the same year, a meta-analysis of 14 articles found that Xpert had a pooled sensitivity of 63% and specificity of 98.1% for diagnosing TBM (54). In 2021, Shen et al. conducted a meta-analysis using Xpert Ultra and Xpert for the diagnosis of TBM, and the results suggested that the sensitivity of Xpert Ultra (68%) was higher than that of Xpert (37%), but the specificity of both was up to 100% (42). Comprehensive analysis showed that mNGS had no significant advantage in diagnosing TBM sensitivity compared to Xpert Ultra and Xpert. However, the specificity of all three methods was >95%, indicating a low misdiagnosis rate. According to relevant studies, mNGS has moderate sensitivity, good specificity, and high accuracy for diagnosing TBM. In addition, mNGS can detect almost all pathogens, including viruses, bacteria, fungi, and parasites, is rapid, and has a high throughput (11, 24, 55) (Table 3).

The emergence of mNGS provides a novel approach to the diagnosis of TBM; however, many problems and challenges remain. First, the operation process of mNGS is complicated and it requires high levels of laboratory infrastructure and technical proficiency of

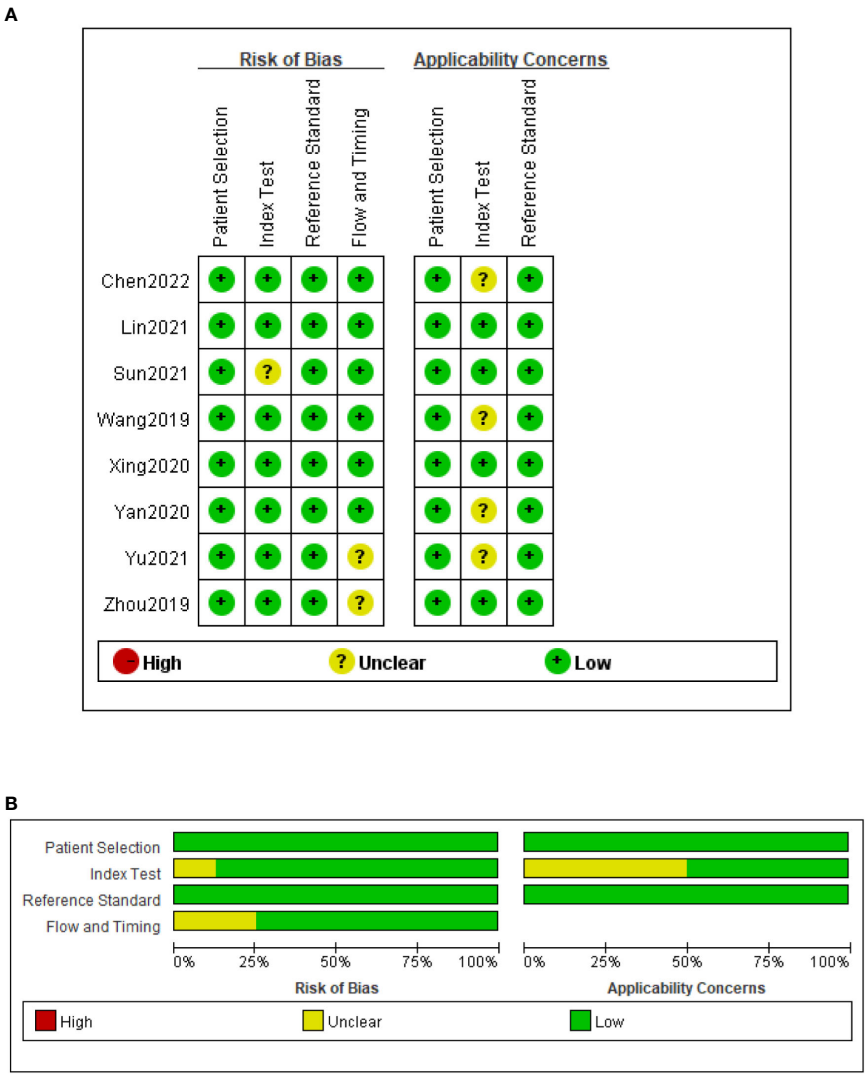

FIGURE 2
Risk of bias and applicability concerns summary **(A)**; risk of bias and applicability concerns graph **(B)**.

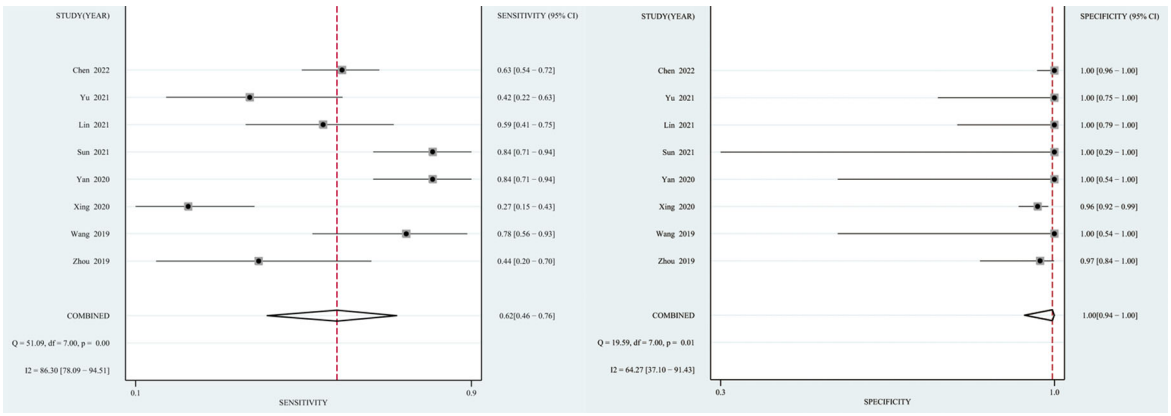

FIGURE 3
Forest plot of the sensitivity and specificity of pooled testing for mNGS.

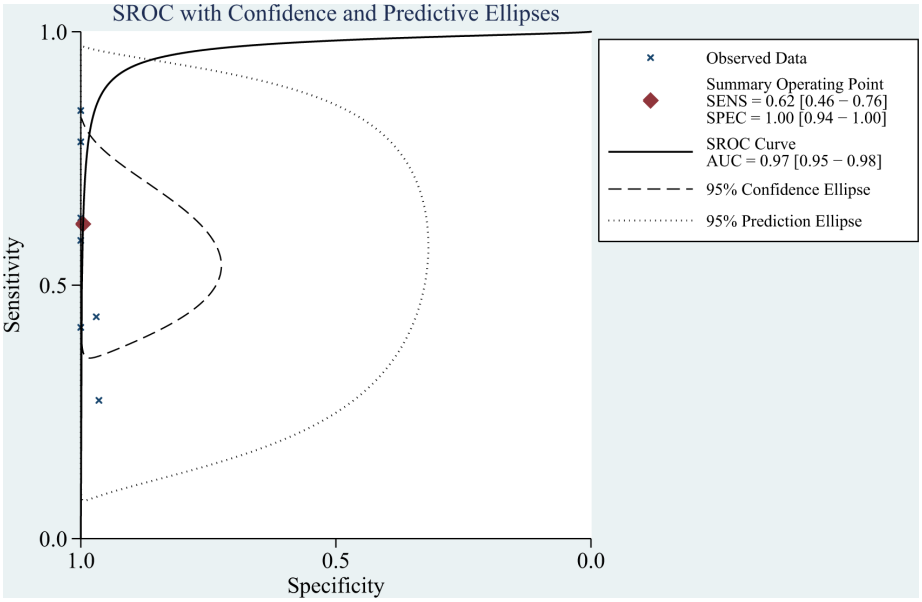

FIGURE 4
Receiver-operating characteristic curve of mNGS for diagnosing TBM.

operators (55). Second, the test results are subject to many factors, and their interpretation depends on the professional knowledge and clinical experience of the clinician (11). Third, owing to the relatively high testing cost of mNGS, its clinical use is limited, particularly in low- and middle-income countries (11). Fourth, the etiological database is inadequate. Finally, mNGS cannot directly detect drug sensitivity, which limits its use as a guide to antituberculosis therapy (56). The present analysis has several limitations: First, the search scope was limited to published literature, and unpublished studies and gray literature may have been missed, so potential publication bias cannot be ruled out. Second, microbiological confirmation was not achieved in all TBM cases, which may have affected the reliability of the results. Third, among the eight eligible studies, all were conducted in China, and most involved adult patients. Studies on patients in low-burden areas and children are lacking. Four, the duration of anti-tuberculosis treatment in the included literature is unknown; and anti-tuberculosis treatment before mNGS detection may affect their diagnostic sensitivity, which will also cause heterogeneity among the included studies. Finally, the number of studies and the amount of clinical data were relatively limited, and the sample conditions and pretreatment methods differed among the studies.

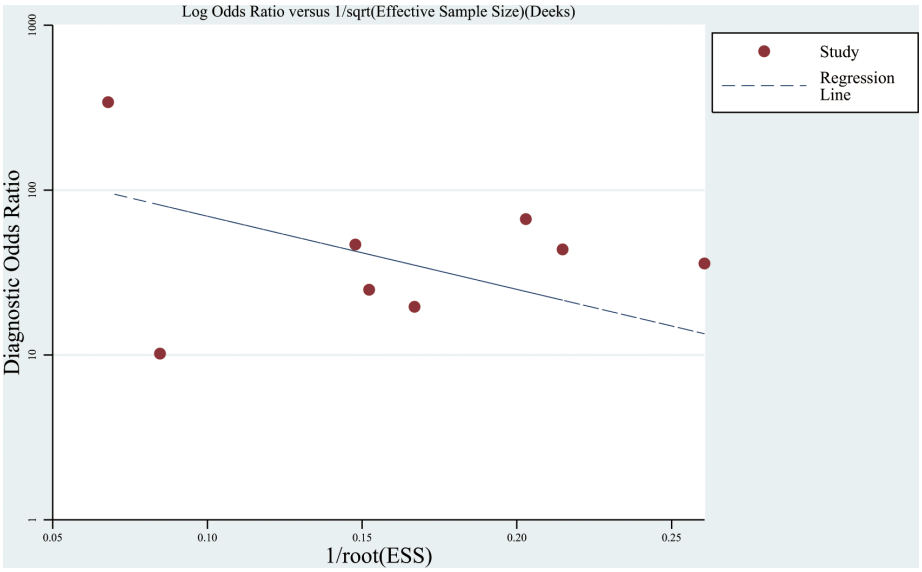

FIGURE 5
Deeks' funnel plot of the included studies.

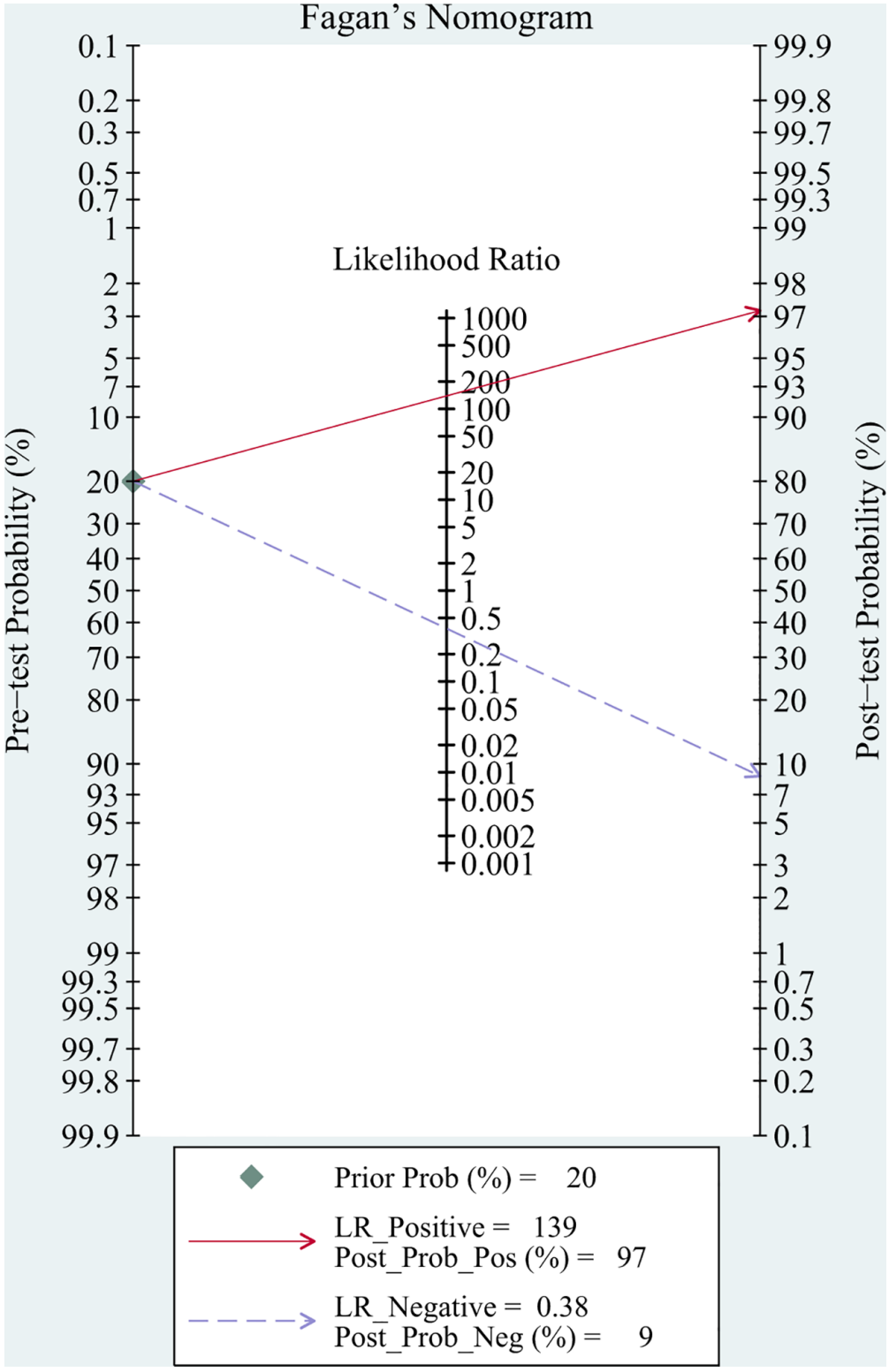

FIGURE 6
Post-test probabilities of TBM for CSF mNGS.

5 Conclusion

In summary, current evidence shows that mNGS has good specificity for the diagnosis of TBM; however, its sensitivity is moderate. The high requirements for laboratory infrastructure and high cost, make mNGS unsuitable for use as an initial test for TBM in the short term. However, it should be used as an effective pathogen-screening method to diagnose patients with negative

TABLE 3 Comparison of mNGS and conventional/novel diagnostic tests for tuberculous meningitis performed on CSF specimens.

Tests for TBM diagnosis	Sensitivity (%)	Specificity (%)	Key points	References
Ziehl-Neelsen staining	10-40	100	Sensitivity substantially improved by increasing the volume of CSF(>6mL), prolonging slide examination(>30min) and examining multiple specimens.	Bahr et al. (26) Heemskerk et al. (25)
Mycobacterial culture • Solid culture • Liquid culture	50-70 (L-J culture) Improve the MTB detection rate up to 10% than solid format (Liquid media)	100	High requirements (biosafety Level III) on the laboratory. Long time to result (3-5 weeks for solid medium; within 2 weeks for liquid medium), and impossible to provide information for clinical diagnosis during the acute phase of TBM.	Thwaites et al. (30) Bahr et al. (26) Ahlawat et al. (29)
Xpert MTB/ RIF Ultra	44-93	94-100	A potential gamechanger. It is a rule-in testing, but not a confidently rule-out test. Requires further evaluation.	Wang et al. (31) Cresswell et al. (32)
ADA	60-90	80-90	Provide variable results. Fail to differentiate between purulent meningitis and TBM.	Pormohammad et al. (33) Ekermans et al. (34)
CSF IGRAS	79-81	89-95	Cut-off range and incubation cell numbers across the studies were inconsistent. Fail to differentiate between active and latent TB.	Wen et al. (35) Lan et al. (36)
mNGS	62% (95% CI: 0.46–0.76)	99% (95% CI: 0.94–1.00)	Prone to contamination. Its specificity is extremely high, but its sensitivity is moderate. Requires a large volume of CSF, relatively long detection time and high cost. Very few studies, small subject numbers.	Present

L-J, Lowenstein-Jensen.
mNGS, metagenomic next-generation sequencing.
CSF, cerebrospinal fluid.
ADA, adenosine deaminase.
IGRA, interferon-gamma release assay.
TB, tuberculosis.

results to microbiological tests, failure of empirical therapy, and critical illness. Owing to the limited quality and quantity of the included studies, these conclusions need to be interpreted with caution. Additional high-quality prospective, large, multicenter studies are required to confirm the diagnostic value of mNGS for TBM in a more comprehensive, systematic, scientific, and objective manner.

Author contributions

Z-BX and AW had the original idea of this study. E-LL and W-FC designed the research. The article was written by AW and Z-BX. S-ML and Y-LZ contributed to the data searches and study selection. C-QL and FH analyzed data and created the tables and figures. All authors contributed to the article and approved the submitted version.

Funding

This work was supported by grant from Jiangxi Province Traditional Chinese medicine science and technology Project (no. 2023A0174).

Acknowledgments

The authors thank the staffs from the Neurology ward of Jiangxi Provincial People' s Hospital for technical assistance as well as *Editage* (www.editage.cn) for English language editing.

Conflict of interest

The authors declare that the research was conducted in the absence of any commercial or financial relationships that could be construed as a potential conflict of interest.

Publisher's note

References

1. Donovan J, Thwaites GE, Huynh. J. Tuberculous meningitis: where to from here? *Curr Opin Infect Dis* (2020) 33:259–66. doi: 10.1097/qco.0000000000000648

2. Brancusi F, Farrar J, Heemskerk. D. Tuberculous meningitis in adults: a review of a decade of developments focusing on prognostic factors for outcome. *Future Microbiol* (2012) 7:1101–16. doi: 10.2217/fmb.12.86

3. Török ME. Tuberculous meningitis: advances in diagnosis and treatment. *Br Med Bull* (2015) 113:117–31. doi: 10.1093/bmb/ldv003

4. Manyelo CM, Solomons RS, Walzl G, Chegou. NN. Tuberculous meningitis: pathogenesis, immune responses, diagnostic challenges, and the potential of biomarker-based approaches. *J Clin Microbiol* (2021) 59:e01771–20. doi: 10.1128/jcm.01771-20

5. Ssebambulidde K, Gakuru J, Ellis J, Cresswell FV, Bahr NC. Improving technology to diagnose tuberculous meningitis: are we there yet? *Front Neurol* (2022) 13:892224. doi: 10.3389/fneur.2022.892224

6. Marais S, Thwaites G, Schoeman JF, Török ME, Misra UK, Prasad. K, et al. Tuberculous meningitis: a uniform case definition for use in clinical research. *Lancet Infect Dis* (2010) 10:803–12. doi: 10.1016/s1473-3099(10)70138-9

7. Davis AG, Wilkinson RJ. Diagnostic tests for tuberculous meningitis. *Lancet Infect Dis* (2020) 20:262–3. doi: 10.1016/s1473-3099(19)30718-2

8. Sheu JJ, Yuan RY, Yang. CC. Predictors for outcome and treatment delay in patients with tuberculous meningitis. *Am J Med Sci* (2009) 338:134–9. doi: 10.1097/MAJ.0b013e3181a590f1

9. Thao LTP, Heemskerk AD, Geskus RB, Mai NTH, Ha DTM, Chau. TTH, et al. Prognostic models for 9-month mortality in tuberculous meningitis. *Clin Infect Dis* (2018) 66:523–32. doi: 10.1093/cid/cix849

10. Miao Q, Ma Y, Wang Q, Pan J, Zhang Y, Jin. W, et al. Microbiological diagnostic performance of metagenomic next-generation sequencing when applied to clinical practice. *Clin Infect Dis* (2018) 67(suppl_2):S231–s240. doi: 10.1093/cid/ciy693

11. Gu W, Miller S, Chiu. CY. Clinical metagenomic next-generation sequencing for pathogen detection. *Annu Rev Pathol* (2019) 14:319–38. doi: 10.1146/annurev-pathmechdis-012418-012751

12. Miller S, Naccache SN, Samayoa E, Messacar K, Arevalo S, Federman. S, et al. Laboratory validation of a clinical metagenomic sequencing assay for pathogen detection in cerebrospinal fluid. *Genome Res* (2019) 29:831–42. doi: 10.1101/gr.238170.118

13. Wilson MR, Sample HA, Zorn KC, Arevalo S, Yu G, Neuhaus. J, et al. Clinical metagenomic sequencing for diagnosis of meningitis and encephalitis. *N Engl J Med* (2019) 380:2327–40. doi: 10.1056/NEJMoa1803396

14. Zhang Y, Cui P, Zhang HC, Wu HL, Ye MZ, Zhu. YM, et al. Clinical application and evaluation of metagenomic next-generation sequencing in suspected adult central nervous system infection. *J Transl Med* (2020) 18:199. doi: 10.1186/s12967-020-02360-6

15. Whiting PF, Rutjes AW, Westwood ME, Mallett S, Deeks. JJ. QUADAS-2: a revised tool for the quality assessment of diagnostic accuracy studies. *Ann Intern Med* (2011) 155:529–36. doi: 10.7326/0003-4819-155-8-201110180-00009

16. Deeks JJ, Macaskill P, Irwig. L. The performance of tests of publication bias and other sample size effects in systematic reviews of diagnostic test accuracy was assessed. *J Clin Epidemiol* (2005) 58:882–93. doi: 10.1016/j.jclinepi.2005.01.016

17. Wang S, Chen Y, Wang D, Wu Y, Zhao D, Zhang. J, et al. The feasibility of metagenomic next-generation sequencing to identify pathogens causing tuberculous meningitis in cerebrospinal fluid. *Front Microbiol* (2019) 10:1993. doi: 10.3389/fmicb.2019.01993

18. Zhou X, Wu H, Ruan Q, Jiang N, Chen X, Shen. Y, et al. Clinical Evaluation of Diagnosis Efficacy of Active Mycobacterium tuberculosis Complex Infection via Metagenomic Next-Generation Sequencing of Direct Clinical Samples. *Front Cell Infect Microbiol* (2019) 9:351. doi: 10.3389/fcimb.2019.00351

19. Xing XW, Zhang JT, Ma YB, He MW, Yao GE, Wang. W, et al. Metagenomic next-generation sequencing for diagnosis of infectious encephalitis and meningitis: A large, prospective case series of 213 patients. *Front Cell Infect Microbiol* (2020) 10:88. doi: 10.3389/fcimb.2020.00088

20. Yan L, Sun W, Lu Z, Fan. L. Metagenomic Next-Generation Sequencing (mNGS) in cerebrospinal fluid for rapid diagnosis of Tuberculosis meningitis in HIV-negative population. *Int J Infect Dis* (2020) 96:270–5. doi: 10.1016/j.ijid.2020.04.048

21. Lin A, Cheng B, Han X, Zhang H, Liu X, Liu. X. Value of next-generation sequencing in early diagnosis of patients with tuberculous meningitis. *J Neurol Sci* (2021) 422:117310. doi: 10.1016/j.jns.2021.117310

22. Sun W, Lu Z, Yan. L. Clinical efficacy of metagenomic next-generation sequencing for rapid detection of Mycobacterium tuberculosis in smear-negative extrapulmonary specimens in a high tuberculosis burden area. *Int J Infect Dis* (2021) 103:91–6. doi: 10.1016/j.ijid.2020.11.165

23. Yu G, Wang X, Zhu P, Shen Y, Zhao W, Zhou. L. Comparison of the efficacy of metagenomic next-generation sequencing and Xpert MTB/RIF in the diagnosis of tuberculous meningitis. *J Microbiol Methods* (2021) 180:106124. doi: 10.1016/j.mimet.2020.106124

24. Chen Y, Wang Y, Liu X, Li W, Fu H, Liu. X, et al. Comparative diagnostic utility of metagenomic next-generation sequencing, GeneXpert, modified Ziehl-Neelsen staining, and culture using cerebrospinal fluid for tuberculous meningitis: A multi-center, retrospective study in China. *J Clin Lab Anal* (2022) 36:e24307. doi: 10.1002/jcla.24307

25. Heemskerk AD, Donovan J, Thu DDA, Marais S, Chaidir L, Dung. VTM, et al. Improving the microbiological diagnosis of tuberculous meningitis: A prospective, international, multicentre comparison of conventional and modified Ziehl-Neelsen stain, GeneXpert, and culture of cerebrospinal fluid. *J Infect* (2018) 77:509–15. doi: 10.1016/j.jinf.2018.09.003

26. Bahr NC, Meintjes G, Boulware DR. Inadequate diagnostics: the case to move beyond the bacilli for detection of meningitis due to Mycobacterium tuberculosis. *J Med Microbiol* (2019) 68:755–60. doi: 10.1099/jmm.0.000975

27. Chen P, Shi M, Feng GD, Liu JY, Wang BJ, Shi. XD, et al. A highly efficient Ziehl-Neelsen stain: identifying *de novo* intracellular Mycobacterium tuberculosis and improving detection of extracellular M. tuberculosis in cerebrospinal fluid. *J Clin Microbiol* (2012) 50:1166–70. doi: 10.1128/jcm.05756-11

28. Feng GD, Shi M, Ma L, Chen P, Wang BJ, Zhang. M, et al. Diagnostic accuracy of intracellular mycobacterium tuberculosis detection for tuberculous meningitis. *Am J Respir Crit Care Med* (2014) 189:475–81. doi: 10.1164/rccm.201309-1686OC

29. Ahlawat S, Chaudhary R, Dangi M, Bala K, Singh M, Chhillar AK. Advances in tuberculous meningitis diagnosis. *Expert Rev Mol Diagn* (2020) 20:1229–41. doi: 10.1080/14737159.2020.1858805

30. Thwaites GE, Chau TT, Farrar. JJ. Improving the bacteriological diagnosis of tuberculous meningitis. *J Clin Microbiol* (2004) 42:378–9. doi: 10.1128/jcm.42.1.378-379.2004

31. Wang G, Wang S, Jiang G, Yang X, Huang M, Huo. F, et al. Xpert MTB/RIF Ultra improved the diagnosis of paucibacillary tuberculosis: A prospective cohort study. *J Infect* (2019) 78:311–6. doi: 10.1016/j.jinf.2019.02.010

32. Cresswell FV, Tugume L, Bahr NC, Kwizera R, Bangdiwala AS, Musubire. AK, et al. Xpert MTB/RIF Ultra for the diagnosis of HIV-associated tuberculous meningitis: a prospective validation study. *Lancet Infect Dis* (2020) 20:308–17. doi: 10.1016/s1473-3099(19)30550-x

33. Pormohammad A, Riahi SM, Nasiri MJ, Fallah F, Aghazadeh M, Doustdar. F. Diagnostic test accuracy of adenosine deaminase for tuberculous meningitis: A systematic review and meta-analysis. *J Infect* (2017) 74:545–54. doi: 10.1016/j.jinf.2017.02.012

34. Ekermans P, Dusé A, George J. The dubious value of cerebrospinal fluid adenosine deaminase measurement for the diagnosis of tuberculous meningitis. *BMC Infect Dis* (2017) 17:104. doi: 10.1186/s12879-017-2221-3

35. Wen A, Leng EL, Liu SM, Zhou YL, Cao WF, Yao. DY. Diagnostic accuracy of interferon-gamma release assays for tuberculous meningitis: A systematic review and meta-analysis. *Front Cell Infect Microbiol* (2022) 12:788692. doi: 10.3389/fcimb.2022.788692

36. Lan Y, Chen W, Yan Q, Liu. W. Interferon-γ release assays for tuberculous meningitis diagnosis: a meta-analysis. *Arch Med Sci* (2021) 17:1241–50. doi: 10.5114/aoms.2019.86994

37. Huang M, Wang G, Sun Q, Jiang G, Li W, Ding. Z, et al. Diagnostic accuracy of Xpert MTB/RIF Ultra for tuberculous meningitis in a clinical practice setting of China. *Diagn Microbiol Infect Dis* (2021) 100:115306. doi: 10.1016/j.diagmicrobio.2020.115306

38. Dorman SE, Schumacher SG, Alland D, Nabeta P, Armstrong DT, King. B, et al. Xpert MTB/RIF Ultra for detection of Mycobacterium tuberculosis and rifampicin resistance: a prospective multicentre diagnostic accuracy study. *Lancet Infect Dis* (2018) 18:76–84. doi: 10.1016/s1473-3099(17)30691-6

39. Shapiro AE, Ross JM, Yao M, Schiller I, Kohli M, Dendukuri. N, et al. Xpert MTB/RIF and Xpert Ultra assays for screening for pulmonary tuberculosis and rifampicin resistance in adults, irrespective of signs or symptoms. *Cochrane Database Syst Rev* (2021) 3:Cd013694. doi: 10.1002/14651858.CD013694.pub2

40. Bahr NC, Nuwagira E, Evans EE, Cresswell FV, Bystrom PV, Byamukama A, et al. Diagnostic accuracy of Xpert MTB/RIF Ultra for tuberculous meningitis in HIV-infected adults: a prospective cohort study. *Lancet Infect Dis* (2018) 18:68–75. doi: 10.1016/s1473-3099(17)30474-7

41. Bahr NC, Marais S, Caws M, van Crevel R, Wilkinson RJ, Tyagi JS, et al. GeneXpert MTB/Rif to Diagnose Tuberculous Meningitis: Perhaps the First Test but not the Last. *Clin Infect Dis* (2016) 62:1133–5. doi: 10.1093/cid/ciw083

42. Chen YZ, Sun LC, Wen YH, Li ZW, Fan SJ, Tan. HK, et al. Pooled analysis of the Xpert MTB/RIF assay for diagnosing tuberculous meningitis. *Biosci Rep* (2020) 40:BSR20191312. doi: 10.1042/bsr20191312

43. Donovan J, Thu DDA, Phu NH, Dung VTM, Quang TP, Nghia. HDT, et al. Xpert MTB/RIF Ultra versus Xpert MTB/RIF for the diagnosis of tuberculous meningitis: a prospective, randomised, diagnostic accuracy study. *Lancet Infect Dis* (2020) 20:299–307. doi: 10.1016/s1473-3099(19)30649-8

44. Pai M, Kalantri S, Dheda. K. New tools and emerging technologies for the diagnosis of tuberculosis: part I. Latent tuberculosis. *Expert Rev Mol Diagn* (2006) 6:413–22. doi: 10.1586/14737159.6.3.413

45. Pai M, Riley LW, Colford JM Jr. Interferon-gamma assays in the immunodiagnosis of tuberculosis: a systematic review. *Lancet Infect Dis* (2004) 4:761–76. doi: 10.1016/s1473-3099(04)01206-x

46. Gao L, Li X, Liu J, Wang X, Lu W, Bai. L, et al. Incidence of active tuberculosis in individuals with latent tuberculosis infection in rural China: follow-up results of a population-based, multicentre, prospective cohort study. *Lancet Infect Dis* (2017) 17:1053–61. doi: 10.1016/s1473-3099(17)30402-4

47. Park KH, Cho OH, Lee EM, Lee SO, Choi SH, Kim. YS, et al. T-cell-based assays on cerebrospinal fluid and PBMCs for rapid diagnosis of TB meningitis in non-HIV patients. *Eur Respir J* (2012) 39:768–70. doi: 10.1183/09031936.00098111

48. Qin L, Zhang L, Zhang Y, Shi X, Zhang Y, Liu. X. Diagnostic value of T-cell interferon-γ Release assays on cerebrospinal fluid for tuberculous meningitis. *PloS One* (2015) 10:e0141814. doi: 10.1371/journal.pone.0141814

49. Pan L, Liu F, Zhang J, Yang X, Zheng S, Li. J, et al. Interferon-gamma release assay performance of cerebrospinal fluid and peripheral blood in tuberculous meningitis in China. *BioMed Res Int* (2017) 2017:8198505. doi: 10.1155/2017/8198505

50. Brown JR, Bharucha T, Breuer. J. Encephalitis diagnosis using metagenomics: application of next generation sequencing for undiagnosed cases. *J Infect* (2018) 76:225–40. doi: 10.1016/j.jinf.2017.12.014

51. Ramachandran PS, Wilson MR. Metagenomics for neurological infections - expanding our imagination. *Nat Rev Neurol* (2020) 16:547–56. doi: 10.1038/s41582-020-0374-y

52. Graff K, Dominguez SR, Messacar. K. Metagenomic next-generation sequencing for diagnosis of pediatric meningitis and encephalitis: A review. *J Pediatr Infect Dis Soc* (2021) 10(Supplement_4):S78–s87. doi: 10.1093/jpids/piab067

53. Yu G, Zhao W, Shen Y, Zhu P, Zheng. H. Metagenomic next generation sequencing for the diagnosis of tuberculosis meningitis: A systematic review and meta-analysis. *PloS One* (2020) 15:e0243161. doi: 10.1371/journal.pone.0243161

54. Shen Y, Yu G, Zhao W, Lang. Y. Efficacy of Xpert MTB/RIF Ultra in diagnosing tuberculosis meningitis: A systematic review and meta-analysis. *Med (Baltimore)* (2021) 100:e26778. doi: 10.1097/md.0000000000026778

55. Schlaberg R, Chiu CY, Miller S, Procop GW, Weinstock. G. Validation of metagenomic next-generation sequencing tests for universal pathogen detection. *Arch Pathol Lab Med* (2017) 141:776–86. doi: 10.5858/arpa.2016-0539-RA

56. Tan J, Liu Y, Ehnert S, Nüssler AK, Yu Y, Xu J, et al. The effectiveness of metagenomic next-generation sequencing in the diagnosis of prosthetic joint infection: A systematic review and meta-analysis. *Front Cell Infect Microbiol* (2022) 12:875822. doi: 10.3389/fcimb.2022.875822

Frontiers in Microbiology

Explores the habitable world and the potential of microbial life

The largest and most cited microbiology journal which advances our understanding of the role microbes play in addressing global challenges such as healthcare, food security, and climate change.

Discover the latest Research Topics

See more →

Frontiers

Avenue du Tribunal-Fédéral 34
1005 Lausanne, Switzerland
frontiersin.org

Contact us

+41 (0)21 510 17 00
frontiersin.org/about/contact